# FACTORS AFFECTING THE INITIAL STIFFNESS AND STIFFNESS DEGRADATION OF COHESIVE SOILS

by

**Maria Caterina Santagata**

Laurea in Ingegneria Civile, December 1990
Universita' di Ancona, Ancona, Italia

Master of Science in Civil and Environmental Engineering, May 1994
Massachusetts Institute of Technology, Cambridge, Massachusetts

Submitted to the
Department of Civil and Environmental Engineering
in partial fulfillment of the requirements for the Degree of

Doctor of Philosophy in Geotechnical and Geoenvironmental Engineering

at the

MASSACHUSETTS INSTITUTE OF TECHNOLOGY

December, 1998
[February, 1999]

© Massachusetts Institute of Technology
All rights reserved.

Signature of Author.....
Department of Civil and Environmental Engineering
December 17, 1998

Certified by .....
Dr. John T. Germaine, Thesis Co-Supervisor

Certified by .....
Professor Charles C. Ladd, Thesis Co-Supervisor

Accepted by .....
Professor Andrew J. Whittle
Chairman, Departmental Committee on Graduate Studies

MASSACHUSETTS INSTITUTE OF TECHNOLOGY
FEB 1 0 1999
LIBRARIES

ARCHIVES

# FACTORS AFFECTING THE INITIAL STIFFNESS AND STIFFNESS DEGRADATION OF COHESIVE SOILS

by

**Maria Caterina Santagata**

Submitted to the Department of Civil and Environmental Engineering on December 19, 1998
in partial fulfillment of the requirements for the degree of
Doctor of Philosophy in Geotechnical and Geoenvironmental and Engineering

## ABSTRACT

This research investigated the pre-failure stress-strain behavior of cohesive soils through an extensive testing program conducted on Resedimented Boston Blue Clay (RBBC). The uniformity and reproducibility in the behavior of this soil permitted a detailed study of the role of the following factors on both initial stiffness and small strain ($\varepsilon_a$<0.1%) non-linearity in undrained triaxial compression: consolidation stress level (0.5-12 ksc), overconsolidation ratio (1,2,4,8), pre-shear consolidation stress path (loading vs. unloading), pre-shear lateral stress ratio ($K_0$-1), rate of shear (0.05-4%/hr), and duration of laboratory aging (1-2 cycles).

Pre-failure stress-strain behavior was evaluated using a novel device specifically designed to perform on-specimen measurements of axial strains. The device makes use of two miniature submersible LVDT's mounted on a pair of yokes which clamp onto the soil specimen. This measuring system is capable of resolving displacements of less than 0.1 microns, corresponding to less than 0.0001% strain, over a 10% strain range.

A multi-stage (i.e., a series of undrained shear and consolidation phases) testing approach was developed to minimize specimen variability, reduce testing time and conserve soil. The testing program, which comprises more than 100 phases of undrained shear, isolated parameters (initial stiffness, linear threshold [$\varepsilon_a$ at 0.98 $E_uMAX$], coefficient of non-linearity [$E_{0.001\%}$/ $E_{0.01\%}$], plastic strain at 0.1% total strain, axial strain since most recent load reversal) that provide a consistent and concise description of the small strain behavior of cohesive soils. These parameters were used to develop a framework describing the dependence of the small strain ($10^{-4}$%-$10^{-1}$%) behavior of soft clays on the above six factors.

Experimental results indicate that the initial stiffness, $E_uMAX$, of RBBC ($K_c$=$K_0$ to 1, $d\varepsilon/dt$=0.1-4%/hr) is governed by both the vertical consolidation and the void ratio through a double exponential function ($E_uMAX$ =1014 $e^{-2.45}\sigma'_{vc}{}^{0.43}$ [ksc]). Laboratory aging leads to an increase of the initial stiffness by approximately 20-25% per log cycle of time. The stiffness of OC RBBC is slightly affected by load reversals.

The small strain non-linearity of RBBC is virtually independent of void ratio or stress level and is controlled primarily by the direction of loading prior to shear. Normally consolidated RBBC presents the smallest linear region and the most rapid stiffness degradation. Unloading to the OC state results in the most dramatic increase in the linear threshold and decrease in the non-linearity. Subsequent reloading leads to an increase in the non-linearity that is proportional to the reloading strain. Increases in K, strain rate and aging all contribute to a reduction in the small strain non-linearity of the soil. These effects can be interpreted in terms of the level of shear stress mobilized at any given strain level, and the capacity to override/reduce viscous deformation of the soil.

Thesis Co-Supervisor: Dr. John T. Germaine
Title: Principal Research Associate

Thesis Co-Supervisor: Professor Charles C. Ladd
Title: Professor of Civil and Environmental Engineering

# ACKNOWLEDGEMENTS

Many years, several projects, many great friends, a wonderful husband later, as I turn in my thesis, my MIT adventure is over. While I recognize it is going to be hard ceasing to call these halls home, I am grateful for all that I have learned and especially for the opportunity I have had to be part of this special place.

Everything I am as a researcher I owe to *Dr. Jack Germaine* (Dr.G[1]) and *Professor Charles Ladd*. Dr. Germaine has supervised both my Master's and Doctoral work. Through his continuous guidance he has taught me about thoroughness, honesty, dedication and method in research. I am grateful to Professor Ladd for teaching me all I know about soil behavior, for his meticulous review of my thesis and for taking the time to encourage me and praise my work ... it made a difference.

I am also indebted to *Professor Lorna Gibson* for agreeing to be part of my doctoral committee and for providing an example of what a great (woman) scientist should be.

I owe thanks to other faculty in the department, in particular: *Professor Trish Culligan*, for her generous financial support during part of the last year of work, and for kindly offering advice on my professional future; and *Professor Herbert Einstein* for his daily kind words, his continuous encouragement and for always being available to listen.

I am forever grateful to *Stephen Rudolph* for his friendship and for always being available to build, fix, create what I needed, often at 3:50 p.m.

I am thankful also for my interaction with *Professor Jamiolkowski* and his group at the Technical University of Turin, in particular *Professor Diego Lo Presti*. I have gained many insights from our conversations on (small strain) soil behavior. I thank Professor Jamiolkowski also for first motivating me to come to MIT and for pushing me to come back and finish. With his dedication to research and his profound knowledge of soil mechanics he has set an example that I can only hope to emulate.

As always, when one is lucky enough to be surrounded by motivated and bright individuals, much is learned from the daily interaction and conversations. So thank you to *Joe Sinfield, Lucy Jen, Niell Elvin, Samir Chauhan, John Sutabutr* for allowing me to brainstorm on soil behavior, instrumentation, and modeling, and for providing advice on several technical issues. A truly special recognition goes to my very good friend and CSSD co-developer, *Greg Da Re*, a gifted experimentalist with whom I shared electronic noise frustrations, as well as beautiful-data induced highs. If our friendship has survived the signal conditioning nightmares... it is destined to last forever.

---

During the long nights spent completing this thesis my mind often wandered off to think of the many people that, particularly over the last year and a half had, often without knowing it, made a difference, and provided motivation or encouragement to complete this goal. This appears to be a good moment to recognize them all. So.....thanks to:

many of the friends who have left MIT, but who have continued to support me and demonstrate their friendship, in particular *Achilles Papadimitriou, Muriel Mora, Lucy Jen, Mike Geer, Niell Elvin, Samir Chauhan, Jordina Vidal, Antonio Bobet*, and *Violeta Ivanova*.

the current students in the department, in particular my running partner *Catalina Marulanda*, who has helped me stay (pseudo) healthy during the last grueling months of work, and my office mates *Greg Da Re* and *Thoma(s) Meyer*. Our long conversations have provided much necessary distraction and many many laughs.

my first roommate at MIT, *Holly Yanco*, with whom I have shared so many moments, as our paths have proceeded, almost always, on parallel tracks. Her morning calls and her continuous reminders that there is life beyond research have, particularly during the last year of work, kept me going.

*Carolyn Jundzillo, Alise Kalemkiarian, Mary Elliff, Cynthia Stewart* and *Karen Joss* who have been good friends and in doing their job with dedication and joy have contributed to create a lighthearted atmosphere in our group.

the friends at home who, on my rare visits, made me feel like I had never left. Thanks in particular to my once ski-racing companion *Michele Bernetti* for the many phone calls and the frequent visits ..... now we can head back to the mountains.

Having spent so many years at MIT, there are many people that I am bound to forget at this point. It seems to me anybody with whom I have shared good memories must have played at least one game with the *Dirtballs* (one word!). So as the senior dirtball player and only founding member still at MIT..... thanks to all of you. Some of the best moments of these years were undoubtedly spent out in the fields, under the sun, waiting for our pitches.....

---

I owe everything I am to my family, the most wonderful there ever was. Thanks to *Mamma, Papà, Ezio, Leandra* and *zia Lilli* for encouraging me, for being by my side in the good and the less good times, for taking a plane to come to see me with 24 hours notice, for never letting me feel lonely, for being proud of me always.
I also owe much inspiration to the two most beautiful boys in the world, my nephews *Edoardo* and *Lorenzo*, who have provided the greatest incentive to complete my work and head back to the best country in the world.

Finally, I am thankful for having met at MIT my husband *Joe*, who has patiently waited for me to finish, always believing in me more than I did. I learned a lot from him and I made it through many difficult moments only thanks to his love and support. As I realize that I have shared my time here with the brightest of experimentalists, the most creative researcher, as well as a truly generous and beautiful man, I look forward to a wonderful life together, and I know I leave MIT taking with me the very best!


---

[1] © Santagata 1992

This thesis is dedicated to my grandmother who taught me about commitment, sense of duty, the importance of education and dedication to family.

## Table of Contents


| | Page |
|---|---|
| **Abstract** | **3** |
| **Acknowledgments** | **5** |
| **Dedication** | **7** |
| **Table of Contents** | **9** |
| **List of Tables** | **15** |
| **List of Figures** | **19** |
| **List of Symbols** | **33** |
| **1. INTRODUCTION** | **37** |
| 1.1 PROBLEM STATEMENT | 37 |
| 1.2 RESEARCH OBJECTIVES | 41 |
| 1.3 ORGANIZATION OF THE THESIS | 42 |
| 1.4 REFERENCES | 44 |
| **2. PRE-FAILURE BEHAVIOR OF COHESIVE SOILS** | **47** |
| 2.1 INTRODUCTION | 47 |
| 2.2 MEASUREMENT OF SMALL STRAIN BEHAVIOR IN THE LABORATORY | 49<br>46 |
| 2.3 PRE-FAILURE BEHAVIOR OF COHESIVE SOILS | 53 |
| 2.3.1 Introduction | 53 |

2.3.2 The Small Strain Linear Region 55
*2.3.2.1 Factors Affecting the Magnitude of the Stiffness in the Linear Region* 57
*2.3.2.2 Factors Affecting the Size of the Linear Region* 65
2.3.3 The Pre-Failure Non-Linear Region 69
*2.3.3.1 Overview* 69
*2.3.3.2 Factors affecting the stiffness in the non-linear region* 71

2.4 REFERENCES 76

**3. RESEDIMENTED BOSTON BLUE CLAY 83**

3.1 INTRODUCTION 83

3.2 RESEDIMENTATION PROCEDURE 88

3.3 INDEX PROPERTIES 92

3.3.1 Introduction 92
3.3.2 Series IV RBBC 94

3.4 BEHAVIOR OF RBBC 96

3.4.1 Introduction 96
3.4.2 Compression Behavior 96
*3.4.2.1 Introduction* 96
*3.4.2.2 Compression Curves and Compressibility Parameters* 97
*3.4.2.3 Lateral Stress Ratio* 99
*3.4.2.4 Secondary Compression* 102
*3.4.2.5 Coefficient of Consolidation* 102
3.4.3 Overview of Behavior in Undrained Shear 103
3.4.4 Behavior in Undrained Triaxial Compression 105
*3.4.4.1 Introduction* 105
*3.4.4.2 General Behavior* 105
*3.4.4.3 Undrained Strength Ratio* 108
*3.4.4.4 Effective Stress Failure Envelope* 109
*3.4.4.5 Strain at Failure* 110
*3.4.4.6 Stiffness* 111
*3.4.4.7 Strain Rate Sensitivity* 112

3.4.5 Comparison with Natural Boston Blue Clay 116
*3.4.5.1 Introduction* 116
*3.4.5.2 Index Properties* 116
*3.4.5.3 Compression Behavior* 117
*3.4.5.4 Triaxial Compression Undrained Shear Behavior* 117

3.5 REFERENCES 119

**4. EQUIPMENT 125**

4.1 INTRODUCTION 125

4.2 MIT AUTOMATED STRESS PATH TRIAXIAL CELLS 126

4.2.1 General Overview 126
4.2.2 Recent Modifications for Small Strain Measurements 131

4.3 SMALL STRAIN MEASURING SYSTEM 134

4.3.1 Design Criteria 134
4.3.2 Mechanical Configuration 136
4.3.3 Signal Conditioning Unit 138
4.3.4 Mounting of the Small Strain System on the Triaxial Specimen 140
4.3.5 Electrical Performance 141
*4.3.5.1 Stability Characteristics* 141
*4.3.5.2 Effect of Temperature on LVDT Output* 143
4.3.6 Proof Testing on Aluminum and PMMA 144
4.3.7 Validation/Evaluation of Technology 146
4.3.7.1 Tests on Resedimented Boston Blue Clay 146
4.3.7.2 Tests on Frozen Manchester Fine Sand 151

4.4 REFERENCES 153

**5. RESEARCH METHODOLOGY 155**

5.1 INTRODUCTION 155

5.2 VARIABLES INVESTIGATED 155

5.2.1 Introduction 155
5.2.2 OCR 156
5.2.3 Consolidation Stress Level 157
5.2.4 Lateral Stress Ratio 158
5.2.5 Pre-Shear Stress Path 161
5.2.6 Strain Rate 163
5.2.7 Duration of Pre-Shear Aging 165

5.3 MULTI-STAGE TESTING APPROACH 165

5.3.1 Description and Procedures 165
5.3.2 Applications and Advantages 169
5.3.3 Validation 171

5.4 SUMMARY OF EXPERIMENTAL PROGRAM 177

5.5 DATA REDUCTION AND EVALUATION 177

5.6 REFERENCES 185

**6. RESULTS 187**

6.1 INTRODUCTION 187

6.2 OVERVIEW OF BEHAVIOR FOR $K_0$-CONSOLIDATED NC RBBC 187

6.3 EFFECT OF STRESS LEVEL 194

6.3.1 Introduction 194
6.3.2 Initial Stiffness 198
6.3.3 Non-Linear Region 201

6.4 EFFECT OF OVERCONSOLIDATION RATIO 206

6.4.1 Introduction 206
6.4.2 Initial Stiffness 206
6.4.3 Non-Linear Region 212

6.5 EFFECT OF LATERAL STRESS RATIO 218

6.5.1 Normally Consolidated Clay 218
*6.5.1.1 Introduction* 218
*6.5.1.2 Initial Stiffness* 219
*6.5.1.3 Non-Linear Behavior* 222
6.5.2 Overconsolidated Clay 225

6.6 EFFECT OF PRE-SHEAR STRESS PATH –NC RBBC 228

6.6.1 Introduction 228
6.6.2 Initial Stiffness 229
6.6.3 Non-Linear Behavior 231

6.7 EFFECT OF PRE-SHEAR STRESS PATH: OC RBBC 233

6.7.1 Unloading and Loading Paths 233
*6.7.1.1 Introduction* 233
*6.7.1.2 Initial Stiffness* 235
*6.7.1.3 Non-linear Behavior* 240
6.7.2 Additional Paths for OCR2 RBBC 247

6.8 EFFECT OF STRAIN RATE 252

6.8.1 Introduction 252
6.8.2 NC RBBC 252
*6.8.2.1 Introduction* 252
*6.8.2.2 Initial Stiffness* 253
*6.8.2.3 Non-linear Behavior* 257
6.8.3 OC RBBC 260
*6.8.3.1 Introduction* 260
*6.8.3.2 Initial Stiffness* 260
*6.8.3.3 Non-linear Behavior* 263

6.9 EFFECT OF LABORATORY AGING 276

6.10 REFERENCES 285

**7. INTERPRETATION OF RESULTS 287**

7.1 INTRODUCTION 287

7.2 INITIAL STIFFNESS 289

7.3 NON-LINEAR BEHAVIOR 299

7.4 REFERENCES 315

**8. CONCLUSIONS AND RECOMMENDATIONS 317**

8.1 OVERVIEW 317

8.2 RESULTS AND CONCLUSIONS 318

8.2.1 Introduction 318
8.2.2 Review of Effects of Variables 319
*8.2.2.1 Reference Behavior* 319
*8.2.2.2 Effect of Stress Level - NC RBBC* 319
*8.2.2.3 Effect of Overconsolidation Ratio* 320
*8.2.2.4 Effect of Lateral Stress Ratio* 321
*8.2.2.5 Effect of Pre-Shear Stress Path - NC RBBC* 322
*8.2.2.6 Effect of Pre-Shear Stress Path - OC RBBC* 322
*8.2.2.7 Effect of Strain Rate* 324
*8.2.2.8 Effect of Laboratory Aging* 324
8.2.3 Conclusions on Initial Stiffness 325
8.2.4 Conclusions on Stiffness Degradation Behavior 326

8.3 RECOMMENDATIONS FOR FUTURE RESEARCH 327

8.3.1 Equipment Enhancement 327
8.3.2 Further Investigations 328

8.4 REFERENCES 331

**Appendix A 333**

## List of Tables


| | | Page |
|---|---|---|
| Table 1.1: | Factors affecting ground movements induced by engineering structures (adapted from Jardine 1994). | 38 |
| Table 2.1: | Apparatuses employed in the laboratory to measure stiffness: a) static, b.) dynamic. | 50 |
| Table 2.2: | Summary of data for the stress level exponent, n. | 59 |
| Table 2.3: | Values of the $N_G$ coefficient for sands and clays (Lo Presti et. al. 1996). | 63 |
| Table 3.1: | Overview of studies performed employing RBBC. | 84 |
| Table 3.2: | Index properties of RBBC. | 93 |
| Table 3.3: | Overview of database on one-dimensional compression behavior of RBBC Series III and IV. | 97 |
| Table 3.4: | Effect of strain rate on SHANSEP parameters for $CK_0U$ triaxial compression (Sheahan 1996). | 115 |
| Table 4.1: | Resolution and stability of transducer signals as measured by the central data acquisition system (adapted from Sheahan 1991). | 130 |
| Table 5.1: | Number of tests conducted on RBBC at each investigated OCR. | 156 |
| Table 5.2: | Ranges in stress level investigated. | 157 |
| Table 5.3: | Values of K investigated for each OCR. | 159 |
| Table 5.4: | Strain rates examined for NC and OC RBBC. | 164 |
| Table 5.5: | Duration of a multi-stage test (*TX406*). | 171 |
| Table 5.6: | Summary of Tests Performed. | 178 |
| Table 6.1: | Tests performed on NC RBBC at $\sigma'_{vc}$ equal to 1.7 ksc. | 192 |

Table 6.2: Linear threshold and coefficient of non-linearity for four tests performed on NC RBBC at $\sigma'_{vc}$ equal to 1.7 ksc. 194

Table 6.3: Tests performed at each of the stress levels examined. 194

Table 6.4: Total and residual strains measured in NC RBBC after unloading from 0.1% axial strain. 205

Table 6.5: Tests performed on OC RBBC ("standard" conditions only). 206

Table 6.6: Tests performed to investigate the effect of the lateral stress ratio. 218

Table 6.7: Pre-shear conditions and initial stiffness results for $K_0$ and hydrostatically consolidated OCR2 RBBC. 226

Table 6.8: Tests conducted to investigate the effect of the pre-shear stress path on the pre-failure behavior of NC RBBC. 229

Table 6.9: Tests performed to investigate the effect of unloading versus loading pre-shear stress path on the pre-failure behavior of OC RBBC. , 235

Table 6.10: Pre-shear conditions and initial stiffness results after loading and unloading for OC RBBC: a) OCR2; b) OCR4; c) OCR8. 238

Table 6.11: Pre-shear conditions and initial stiffness results for six tests performed to investigate the effect of the pre-shear stress path on the pre-failure behavior of OCR2 RBBC. 249

Table 6.12: Variation of the linear threshold and the coefficient of non-linearity with pre-shear consolidation path (OCR2 RBBC). 251

Table 6.13: Range of strain rates investigated. 252

Table 6.14: Tests performed to investigate strain rate dependency of NC RBBC. 253

Table 6.15: Pre-shear conditions and initial stiffness results for tests performed at $\sigma'_{vc}$~1.7 ksc employing different strain rates. 253

Table 6.16: Pre-shear conditions and initial stiffness results for tests performed on OCR2 RBBC employing different strain rates. 260

Table 6.17: Pre-shear conditions and initial stiffness results for tests performed on OCR4 RBBC employing different strain rates. 261

Table 6.18: Pre-shear conditions and initial stiffness results for tests performed on OCR8 RBBC employing different strain rates. 261

Table 6.19: Pre-shear conditions and initial stiffness results for tests performed at ~2.4 ksc ($t_{aging}$ = 1 and 11 days). 278

Table 6.20: Pre-shear conditions and initial stiffness results for tests performed at ~4.0 ksc ($t_{aging}$ = 1 and 11 days). 278

Table 7.1: Summary of parameters describing the small strain non-linearity of RBBC. 303

## List of Figures


| | | Page |
|---|---|---|
| Figure 1.1: | Stress paths around an excavation in NC Boston Blue clay derived from finite element analyses using the MIT-E3 soil model: a) q-p plane; b) q-$\tau$ plane (Hashash 1992). | 39 |
| Figure 1.2: | Surface settlement at the side of an excavation in NC Boston Blue clay determined through finite element analyses using a) elastic, MCC and b) MIT-E3 soil models (Whittle and Hashash 1994). | 40 |
| Figure 2.1: | Strain rates in the laboratory and in the field (Lo Presti 1994). | 51 |
| Figure 2.2: | Definition of Stiffness Parameters. | 53 |
| Figure 2.3: | Schematic of variation of stiffness with strain. | 54 |
| Figure 2.4: | Linear stress strain behavior of various geo-materials at small strains: a) Pisa clay (Tatsuoka et al. 1997); b) Toyoura Sand (Tatsuoka and Shibuya 1992); c) cement treated soil (Tatsuoka and Shibuya 1992); d) sedimentary soft mudstone (Tatsuoka et. al. 1997). | 55 |
| Figure 2.5: | Comparison of Pisa clay stiffness obtained from dynamic and monotonic tests (Lo Presti 1994). | 56 |
| Figure 2.6: | Use of void ratio function $F(e)=e^{-1.11}$ to normalize the initial shear stiffness of NC and OC Garigliano clay (Jamiolkowski et. al. 1994). | 61 |
| Figure 2.7: | Variation of initial shear stiffness for reconstituted and intact London clay [BE measurements in CIUC tests, $G_0=G_{MAX}$] (Viggiani and Atkinson 1995). | 62 |
| Figure 2.8: | $N_G$ coefficient versus secondary compression index from torsional shear tests (Lo Presti et. al. 1996). | 64 |
| Figure 2.9: | Linear threshold shear strain from resonant column tests (Lo Presti 1989). | 66 |
| Figure 2.10: | Effect of strain rate on Young's modulus measured in monotonic CIUC triaxial tests performed on reconstituted clay [p' = mean stress] (Shibuya et. al. 1996). | 67 |

Figure 2.11: Comparison of stiffness of hydrostatically and one dimensionally consolidated Pisa clay during drained triaxial compression loading (Lo Presti et. al. 1995). 68

Figure 2.12: Position of Y2 sub-yield surface for NC and OC Magnus Till (Jardine 1992). 70

Figure 2.13: Relationship between permanent and total strain for Magnus Till (Jardine 1992). 71

Figure 2.14: Increase of stress level exponent with strain for NC kaolin [CIUC tests, p' = mean consolidation stress, $p_r$ = reference pressure] (Viggiani and Atkinson 1995). 72

Figure 2.15: Effect of strain on stress level exponent (Jardine 1994). 72

Figure 2.16: Effect of OCR on undrained compression stiffness at 0.01% [p' = mean consolidation stress] (Jardine 1994). 73

Figure 2.17: Coefficient of strain rate, $\alpha$, versus strain (Lo Presti et. al. 1996). 74

Figure 2.18: Effect of plasticity index on stiffness at 0.01% strain (Jardine 1994). 76

Figure 3.1: Schematic of equipment used to resediment Boston Blue Clay. 89

Figure 3.2: Schematic of consolidation operations employed when preparing RBBC: a) counter balance of piston mass, b) application of dead weights, and c) use of air pressure actuator. 91

Figure 3.3: Results of grain size analyses on RBBC Series IV. 94

Figure 3.4: Plasticity chart with data from RBBC Series IV. 95

Figure 3.5: Results of $K_0$-consolidation of RBBC in the triaxial apparatus: a) compression curves; b) coefficient of consolidation (Force 1998). 98

Figure 3.6: Lateral stress ratio versus effective stress during $K_0$-consolidation of RBBC (Santagata 1994). 100

Figure 3.7: Comparison of $K_0$ and stress path consolidation (Santagata 1994). 101

Figure 3.8: Undrained strength ratio versus OCR from $CK_0U$ test in triaxial compression (Sinfield 1994, Santagata 1994), extension (Sheahan 1991), and direct simple shear (Ahmed 1990). 104

Figure 3.9: Behavior of RBBC (OCR = 1, 2, 4, 8) in undrained triaxial compression: (a) stress paths; (b) stress strain curves; (c) normalized excess pore pressures; (d) normalized shear induced pore pressures (Santagata 1994). 106

Figure 3.10: $q_f(c)$ versus $K_0$ for $CK_0UC$ tests on NC RBBC (Santagata 1994). 109

Figure 3.11: Friction angle at maximum obliquity for RBBC (Santagata 1994). 110

Figure 3.12: Strain at failure versus OCR for RBBC (Santagata 1994). 111

Figure 3.13: Undrained modulus versus axial strain (Santagata 1994). 112

Figure 3.14: Effect of strain rate on the behavior of NC RBBC: a) stress strain curves; b) shear induced pore pressure; and c) stress paths (Sheahan et. al. 1996). 113

Figure 3.15: Effect of strain rate on the behavior of OCR 4 RBBC: a) stress strain curves; b) shear induced pore pressure; and c) stress paths (Sheahan et. al. 1996). 114

Figure 3.16: Normalized shear strength in $CK_0U$ triaxial compression versus strain rate at OCR = 1, 2, 4, and 8 (Sheahan et. al. 1996). 115

Figure 3.17: Representative normalized effective stress paths for SHANSEP $CK_0UC$ triaxial tests at varying OCR: Building 68 site (Berman 1993). 118

Figure 4.1: MIT automated stress path triaxial cell – schematic (connections between transducers and PC not shown). 127

Figure 4.2: Triaxial chamber - schematic. 128

Figure 4.3: Difference between external and internal measurement of the axial load. 131

Figure 4.4: Modified piston - load cell – top cap connection. 133

Figure 4.5: Schematic of yokes. 137

Figure 4.6: Functional block diagram of signal conditioning unit. 139

Figure 4.7: LVDT stability with CSSD at 20°C (a) over 300s and (b) 24 hours. 141

Figure 4.8: LVDT stability with commercial signal conditioner at 20°C over 300s. 142

Figure 4.9: LVDT stability as a function of temperature over (a) 300 seconds and (b) 24 hours. 143

Figure 4.10: Results of proof testing on aluminum. 145

Figure 4.11: Results of proof testing on PMMA. 146

Figure 4.12: Quality of data for NC RBBC: (a), (b), (c) stress strain behavior; (d) stiffness versus logarithm of axial strain (*TX418S3* ). 147

Figure 4.13: Comparison of results from 2 LVDT's after modifications to system of load application: (a) TX418S1 (NC RBBC); (b) TX418S6 (OC RBBC). 148

Figure 4.14: Comparison of results from 2 LVDT's before modifications to load application. 148

Figure 4.15: Comparison of results from internal and external measurements of the strains (NC RBBC). 149

Figure 4.16: Comparison of results from internal and external measurements of the strains (OC RBBC). 150

Figure 4.17: Repeatability of results on NC RBBC: stiffness versus logarithm of axial strain. 150

Figure 4.18: Shear results for frozen Manchester Fine Sand. 152

Figure 4.19: Comparison of results from 2 LVDT's from a test on frozen Manchester fine sand. 152

Figure 5.1: Variation of $K_0$(NC) with stress level ( Test *TX455* ). 158

Figure 5.2: Consolidation of NC RBBC along constant K paths. 160

Figure 5.3: Hydrostatic consolidation of OCR2 RBBC. 160

Figure 5.4: Consolidation stress paths considered for NC RBBC. 161

Figure 5.5: Unloading and Loading consolidation stress paths considered for OC RBBC. 162

Figure 5.6: Additional consolidation stress paths examined for OCR2 RBBC. 163

Figure 5.7: Strain rate versus axial strain for three tests on OCR2 RBBC. 164

Figure 5.8: Example of a multi-stage test ( *TX406* ): a) e – log $\sigma'_v$, b) q - p'. 167

Figure 5.9: Multi-stage test with undrained unloading of shear stress (*TX438* ): (a) stress paths for phases 1 and 2; (b) stress strain curve for shear S2. 168

Figure 5.10: Parameters investigated using the multi-stage approach: (a) stress level, (b) OCR, (c) consolidation path, and (d) strain rate. 170

Figure 5.11: Comparison of results from first shear of test *TX362* and second shear of test *TX403* . 172

Figure 5.12: Sequence of shears in test *TX427* on OCR2 RBBC. 173

Figure 5.13: Comparison of results for shears S3 and S5 ( Test *TX427* ) on OCR2 RBBC: (a), (b) stress strain curves; (c) stiffness versus logarithm of axial strain, (d) $E_u/E_{u}MAX$ versus logarithm of axial strain. 174

Figure 5.14: Effect of multi-stage test shear sequence on behavior of OC RBBC. 175

Figure 5.15: Effect of soil storage time on the pre-failure behavior of RBBC. 176

Figure 5.16: Phases of data processing. 182

Figure 5.17: Derivation of initial stiffness from early portion (0-0.001%) of stress strain curve: a) stress strain curve; b) stiffness versus logarithm of axial strain (*TX418S3* - NC RBBC). 184

Figure 6.1: Stress strain curves for test *TX475S1* . 188

Figure 6.2: Stiffness degradation curves for test *TX475S1* : a) secant stiffness ($E_u$); b) normalized stiffness ($E_u/E_{u}MAX$). 189

Figure 6.3: Excess and shear induced pore pressures ( *TX475S1* ). 190

Figure 6.4: Stress paths for test *TX475S1* . 191

Figure 6.5: Elastic and plastic component of strain ( NC-RBBC –*TX475S1* ). 192

Figure 6.6: Stiffness degradation curves for four tests performed on NC RBBC at $\sigma'_{vc}$ equal to 1.7 ksc. 193

Figure 6.7: Stiffness results for tests performed at $\sigma'_{vc}$ equal to a-b) 2.4 ksc; c-d) 3.1 ksc; e-f) 4.0 ksc; g-h) 5.8 ksc; i-j) 7.8 ksc. 195

Figure 6.8: Stiffness of NC RBBC as a function of stress level. 197

Figure 6.9: Normalization of initial stiffness, $E_u$, by stress level. 198

Figure 6.10: Power relationship between vertical consolidation stress and initial stiffness for $K_0$-consolidated NC RBBC. 199

Figure 6.11: Relations between stress level, void ratio and initial stiffness for $K_0$-consolidated NC RBBC. 200

Figure 6.12: Stiffness vs. stress level power relationship in non linear region. 202

Figure 6.13: $E_u/E_{u}MAX$ versus axial strain for $K_0$-consolidated NC RBBC: a) 22 results obtained; b) coefficient of variation; c) average curve. 203

Figure 6.14: Independence of a) the linear threshold and b) the coefficient of non-linearity from $K_0$. 205

Figure 6.15: Plots of $E_{u}MAX/\sigma'_{vc}$ versus $\sigma'_{vc}$ for OC RBBC. 207

Figure 6.16: Relationship between stress level and initial stiffness for: OCR2; b) OCR4; c) OCR8 RBBC. 208

Figure 6.17: Relationship between stress level and initial stiffness for NC and OC RBBC. 208

Figure 6.18: Plots of void ratio versus vertical consolidation stress and of initial stiffness versus void ratio for a-b) OCR2; c-d) OCR4 and e-f) OCR8 RBBC. 209

Figure 6.19: Comparison of NC and OC behavior at the same stress level or void ratio. 211

Figure 6.20: Variation of $E_uMAX$ at $\sigma'_{vc}$ ~ 2.4 ksc as a function of OCR. 212

Figure 6.21: Comparison of stiffness degradation curves for NC and OCR4 RBBC. 212

Figure 6.22: Normalized stiffness degradation for OCR2 RBBC. 213

Figure 6.23: Normalized stiffness degradation for a) OCR4 and b) OCR8 RBBC. 214

Figure 6.24: Stiffness degradation curves for RBBC with OCR equal to 1, 2, 4, and 8. 215

Figure 6.25: a) Linear threshold and b) coefficient of non-linearity as a function of OCR. 216

Figure 6.26: Ratio of $(E_u/E_uMAX)_{OC}$ to $(E_u/E_uMAX)_{NC}$. 216

Figure 6.27: Elastic and Plastic Component of Strain ( OCR4 RBBC –*TX442S1* ). 217

Figure 6.28: Stress paths during $K_0$- and stress path consolidation at a fixed value of K of RBBC. 218

Figure 6.29: Initial stiffness of RBBC stress path consolidated at constant K: a) comparison to $K_0$-consolidated data; b) results for $\sigma'_{vc}$ equal to 6 ksc 219

Figure 6.30: Compression behavior of $K_0$-consolidated and stress path consolidated (K=constant) RBBC. 220

Figure 6.31: Relationship between void ratio, initial stiffness and mean consolidation stress for $K_0$- and stress path (K=constant) consolidated NC RBBC. 221

Figure 6.32: Behavior of $K_0$- and stress path consolidated (K=constant) NC RBBC at 6 ksc: a-b) stress strain curves; c) stiffness degradation curves. 222

Figure 6.33: Stiffness degradation curves for NC RBBC for different values of the pre-shear lateral stress ratio. 224

Figure 6.34: Variation of a) the linear threshold and b) the coefficient of non-linearity with the pre-shear lateral stress ratio. 224

Figure 6.35: Increase in stiffness produced by variation in the lateral stress ratio. 225

Figure 6.36: Relationship between void ratio, initial stiffness and mean consolidation stress for $K_0$- and hydrostatically consolidated OCR2 RBBC. 227

Figure 6.37: Behavior of $K_0$- and hydrostatically consolidated (K=constant) OCR2 RBBC at 3.9 ksc: a-b) stress strain curves. 227

Figure 6.38: Stiffness degradation curves for $K_0$- and hydrostatically consolidated OCR2 RBBC. 228

Figure 6.39: Stress paths during $K_0$-and stress path (constant $\sigma'_h$ and constant p') consolidation of NC RBBC. 229

Figure 6.40: Relationships between a) vertical consolidation stress and $E_u$MAX, b) vertical consolidation stress and void ratio, c) void ratio and $E_u$MAX, and d) mean consolidation stress and $E_u$MAX for $K_0$- and stress path consolidated (constant $\sigma'_h$ and constant p') NC RBBC. 230

Figure 6.41: Behavior of $K_0$- and stress path consolidated (constant $\sigma'_h$ and constant p') NC RBBC at 2.4 ksc: a-b) stress strain curves. 231

Figure 6.42: Normalized stiffness versus axial strain: a) constant$\sigma'_h$ and b) constant p' pre-shear consolidation paths 232

Figure 6.43: Pre-failure non-linearity for stress path (constant p' and constant$\sigma'_h$ paths) and $K_0$-consolidated NC RBBC. 232

Figure 6.44: Example of multistage test performed to investigate the effect of the pre-shear stress path: a) e-log $\sigma'_v$ space; b) q-p' space. 234

Figure 6.45: Effect of the pre-shear path on the initial stress strain behavior of OC RBBC: a-b) OCR2; c-d) OCR4; e-f) OCR8. 237

Figure 6.46: Relationship between initial stiffness and pre-shear vertical stress and void ratio for loading and unloading consolidation paths: a-b) OCR2; c-d) OCR4; e-f) OCR8. 239

Figure 6.47: Behavior of OCR2 RBBC after unloading and loading pre-shear consolidation paths. 241

Figure 6.48: Behavior of OCR4 RBBC after unloading and loading pre-shear consolidation paths. 242

Figure 6.49: Behavior of OCR8 RBBC after unloading and loading pre-shear consolidation paths. 243

Figure 6.50: Stiffness degradation behavior of OC RBBC after loading consolidation path: a) OCR2; b) OCR4; c) OCR8. 244

Figure 6.51: Effect of OCR and pre-shear stress path on non linear behavior of RBBC. 245

Figure 6.52: a) Linear threshold and b) non-linearity coefficient as a function of OCR ( $U$ and $L$ paths ). 246

Figure 6.53: Ratio of $E^*_{OC}$ to $E^*_{NC}$ for loading consolidation path. 246

Figure 6.54: Ratio of $E^*_{Unload}$ to $E^*_{Load}$ for OC RBBC. 247

Figure 6.55: Six pre-shear stress paths investigated for OCR2 RBBC. 248

Figure 6.56: Stiffness degradation curves for six tests performed to investigate the effect of the pre-shear stress path on the pre-failure behavior of OCR2 RBBC. 250

Figure 6.57: Effect of strain rate on the pre-failure stress-strain behavior of NC RBBC $\sigma'_{vc}$~1.7 ksc: a) 0-0.1%; b) 0-0.01%; c) 0-0.005%. 254

Figure 6.58: Plots of stiffness versus a) void ratio and b) vertical stress for $K_0$-consolidated NC RBBC sheared at rates in the range 0.05-4%/hr. 255

Figure 6.59: Pre-shear creep rate of NC RBBC after ~ 30 hours of aging. 256

Figure 6.60: Normalized stiffness degradation curves for NC RBBC: a) $d\varepsilon/dt$=1%/hr; b) $d\varepsilon/dt$=2%/hr; c) $d\varepsilon/dt$=4%/hr. 257

Figure 6.61: Average stiffness degradation curves for NC RBBC as a function of strain rate (0.1, 1, 2, and 4%/hr). 258

Figure 6.62: Change in normalized stiffness produced by an increase in strain rate. 259

Figure 6.63: Effect of strain rate on a) the linear threshold and b) the non-linearity coefficient. 259

Figure 6.64: Initial stiffness versus vertical consolidation stress and void ratio for tests conducted employing rates in the range 0.1%-4%/hr on a-b) OCR2; c-d) OCR4 and e-f) OCR8 RBBC. 262

Figure 6.65: Effect of strain rate on the pre-failure stress-strain behavior of OCR2 RBBC at $\sigma'_{vc}$~2.4 ksc (U-Path) : a) 0-0.1%; b) 0-0.01%; c) 0-0.005%. 265

Figure 6.66: Effect of strain rate on stiffness degradation curve of OCR2 RBBC at $\sigma'_{vc}$~2.4 ksc (U-Path). 266

Figure 6.67: Change in normalized stiffness produced by an increase in strain rate (OCR2 RBBC- U path). 266

Figure 6.68: Effect of strain rate on the pre-failure stress-strain behavior of OCR2 RBBC at $\sigma'_{vc}$~2.4 ksc (L-Path) : a) 0-0.1%; b) 0-0.01%; c) 0-0.005%. 267

Figure 6.69: Effect of strain rate on stiffness degradation curve of OCR2 RBBC at $\sigma'_{vc}$~2.4 ksc (L-Path). 268

Figure 6.70: Change in normalized stiffness produced by an increase in strain rate (OCR2 RBBC- L path). 268

Figure 6.71: Effect of strain rate on the pre-failure stress-strain behavior of OCR4 RBBC at $\sigma'_{vc}$~0.7 ksc (U-Path) : a) 0-0.1%; b) 0-0.01%; c) 0-0.005%. 270

Figure 6.72: Effect of strain rate on stiffness degradation curve of OCR4 RBBC at $\sigma'_{vc}$~0.7 ksc (U-Path). 271

Figure 6.73: Change in normalized stiffness produced by an increase in strain rate (OCR4 RBBC- U-path). 271

Figure 6.74: Effect of strain rate on the pre-failure stress-strain behavior of OCR4 RBBC at $\sigma'_{vc}$~0.7 ksc (L-Path) : a) 0-0.1%; b) 0-0.01%; c) 0-0.005%. 272

Figure 6.75: Effect of strain rate on stiffness degradation curve of OCR4 RBBC at $\sigma'_{vc}$~0.7 ksc (L-Path). 273

Figure 6.76: Change in normalized stiffness produced by an increase in strain rate (OCR4 RBBC- L-path). 273

Figure 6.77: Effect of strain rate on the pre-failure stress-strain behavior of OCR8 RBBC at $\sigma'_{vc}$~1.9 ksc (U-Path) : a) 0-0.1%; b) 0-0.01%; c) 0-0.005%. 274

Figure 6.78: Effect of strain rate on stiffness degradation curve of OCR8 RBBC at $\sigma'_{vc}$~1.9 ksc (U-Path). 275

Figure 6.79: Change in normalized stiffness produced by an increase in strain rate (OCR8 RBBC- U-path). 275

Figure 6.80: Variation in coefficient of non-linearity as a function of strain rate: a) unloading and b) loading test on OC RBBC. 276

Figure 6.81: a) Linear threshold and b) non-linearity coefficient for NC RBBC as a function of small variations in the standard duration of aging. 277

Figure 6.82: Effect of prolonged aging on the behavior of NC RBBC at $\sigma'_{vc}$~2.4 ksc: a-b) stress strain curves; c-d) stiffness degradation curves. 277

Figure 6.83: Effect of prolonged aging on the behavior of NC RBBC at $\sigma'_{vc}$ ~ 4.0 ksc: a-b) stress strain curves; c-d) stiffness degradation curves. 279

Figure 6.84: Relationship between maximum stiffness and void ratio for NC RBBC ($t_{aging}$=1 and 11 days). 280

Figure 6.85: Average stiffness degradation curves for different durations of laboratory aging. 282

Figure 6.86: Variation of the a) linear threshold and the b) coefficient of non-linearity of NC RBBC as a function of aging duration. 282

Figure 6.87: Increase in the normalized stiffness of NC RBBC produced by prolonged aging. 283

Figure 6.88: a) Modification of the stiffness degradation curve and b) increase in the normalized stiffness of hydrostatically consolidated NC RBBC, due to prolonged laboratory aging. 284

Figure 7.1: Schematic of the parameters affecting the initial stiffness and the stiffness degradation behavior of cohesive soils. 288

Figure 7.2: Relationship between initial stiffness and a) void ratio, b) vertical consolidation stress and c) mean consolidation stress (NC RBBC). 290

Figure 7.3: Relationship between initial stiffness and a) void ratio, b) vertical consolidation stress and c) mean consolidation stress (OCR2 RBBC). 291

Figure 7.4: Relationship between initial stiffness and a) void ratio, b) vertical consolidation stress and c) mean consolidation stress (OCR4 RBBC). 292

Figure 7.5: Relationship between initial stiffness and a) void ratio, b) vertical consolidation stress and c) mean consolidation stress (OCR8 RBBC). 293

Figure 7.6: Relationship between initial stiffness and void ratio (OCR 1, 2, 4, 8 RBBC). 295

Figure 7.7: Relationship between initial stiffness and mean consolidation stress (OCR 1, 2, 4, 8 RBBC). 295

Figure 7.8: Relationship linking the initial stiffness of RBBC to void ratio and consolidation stress level for OCR 1, 2, 4 and 8. 296

Figure 7.9: Effect of unloading or loading consolidation path on the initial stiffness of OCR2 RBBC. 297

Figure 7.10: Effect of "slow" strain rate and prolonged aging on the initial stiffness of NC RBBC. 298

Figure 7.11: Range in stiffness degradation behavior of RBBC produced by changes in the testing conditions. 300

Figure 7.12: Effects of changes in the testing conditions on the stiffness degradation behavior of NC RBBC: a-b) OCR; c-d) strain rate and aging; e-f) lateral stress ratio. 304

Figure 7.13: Effect of strain rate on the stiffness degradation of OC RBBC: a-b) OCR2; c-d) OCR4; e-f) OCR8. 305

Figure 7.14: Coefficient of non-linearity versus linear threshold (NC and OC RBBC). 306

Figure 7.15: Residual plastic strain after shearing to ~0.1-0.15% axial strain: a) $K_0$-consolidated NC RBBC ( *TX475S1* ); b) OCR4-L RBBC ( *TX442S1* ); c) OCR4-U RBBC ( *TX438S5* ) (all at 0.1%/hr). 306

Figure 7.16: Residual plastic strain after unloading from 0.1% axial strain versus coefficient of non-linearity for NC and OC RBBC. 307

Figure 7.17: a) Mobilization factor as a function of strain for selected tests not involving load reversal; b) mobilization factor at 0.1% axial strain versus coefficient of non-linearity. 308

Figure 7.18: Mobilization factor as a function of strain for NC and OCR2 ( *U* and *L* ) RBBC. 309

Figure 7.19: Mobilization factor at 0.1% axial strain versus coefficient of non-linearity ( *U* -tests). 309

Figure 7.20: Relationship between unloading axial strain increment before shear and non-linearity ( *U* - tests). 310

Figure 7.21: Relationship between non-linearity and axial strain since most recent stress reversal ( *L* - tests). 311

Figure 7.22: Mobilization factor f as a function of strain for tests on NC RBBC at various strain rates. 312

Figure 7.23: Mobilization factor as a function of strain for tests on NC RBBC after standard and prolonged laboratory aging. 312

Figure 7.24: Mobilization factor at 0.1% axial strain versus coefficient of non-linearity (high strain rate and prolonged aging tests on NC RBBC). 313

Figure 7.25: Example of the undrained creep deformation occurring at the end of shear: a) stress-strain curve; b) axial strain versus time. 314

# List of Symbols

| | |
|---|---|
| A/D | Analog-to-digital converter |
| BBC | Boston Blue Clay |
| BE | Bender elements |
| COV | Coefficient of variation |
| CRS | Constant rate of strain |
| CSSD | Clever small strain device |
| DCDT | Direct current displacement transducer |
| DSC | Directional shear cell |
| DSS | Direct simple shear |
| LVDT | Linear voltage displacement transducer |
| OED | Oedometer test |
| PC | Personal computer |
| PMMA | Polymethylmethacrylate |
| PSA | Perfect Sampling Approach |
| PVC | Pressure volume controller |
| RBBC | Resedimented Boston Blue Clay |
| TX | Triaxial |
| | |
| a' | Cohesion intercept |
| $C_I$ | Constant |
| *C1*, ... | Consolidation phase number |
| $C_c$ | Compression Index |
| CID | Isotropically consolidated drained shear test |
| CIUC/E | Isotropically consolidated undrained shear test, compression/extension |
| $CK_0UC/E$ | $K_0$-consolidated undrained shear test, compression/extension |
| $C_{NL}$ | Coefficient of non-linearity |
| CR | Virgin compression ratio |
| $c_u$ | Undrained strength ratio |
| $c_v$ | Coefficient of consolidation for vertical flow |
| $C_\alpha$ | Secondary compression index |
| $C_{\alpha\varepsilon}$ | Secondary compression ratio |
| E | Young's modulus |
| E | Void ratio |
| $E^*$ | Normalized stiffness ($E_u/E_uMAX$) |
| $E_{ij}$ | Stiffness in the plane i-j |
| $E_{max}$ | Maximum Young's modulus |
| $E_{xx\%}$ | Young's modulus at xx% axial strain |
| $E_{sec}$ | Secant Young's Modulus |
| $E_{tan}$ | Tangent Young's Modulus |
| $E_uMAX$ | Initial Maximum Stiffness in Undrained Compression |
| $E_v$ | Vertical Young's Modulus |

| | |
|---|---|
| $E_u$ | Undrained stiffness |
| F(e) | Void ratio function |
| f, *f* | Frequency, mobilization factor |
| G | Specific gravity |
| $G_{eq}$ | Equivalent shear modulus |
| $G_{ij}$ | Shear modulus in plane i-j |
| $G_{sec}$ | Secant shear modulus |
| $G_{tan}$ | Tangent shear modulus |
| IC | Integrated circuit |
| k | OCR exponent in $K_0$ equation or OCR exponent in initial stiffness equation |
| $k_v$ | vertical hydraulic conductivity |
| $K_0$ | Coefficient of lateral earth pressure at rest |
| $K_{0(NC)}$ | Coefficient of lateral earth pressure at rest for NC soil |
| K, $K_c$ | Lateral stress ratio at end of consolidation |
| *L* | Loading |
| *LL* | Loading, loading |
| *LU* | Loading, unloading |
| m | OCR exponent in SHANSEP equation for undrained strength ratio |
| *n* | Stress level exponent |
| *n* | Mean consolidation stress exponent |
| $N_G$ | Factor describing increase in stiffness with aging |
| NC | Normally consolidated |
| OC | Overconsolidated |
| OCR | Overconsolidation ratio |
| p' | Average effective stress ( $[\sigma'_1+\sigma'_3]/2$) |
| $p'_c$ | Average effective consolidation stress |
| $p'_m$ | Mean effective stress ( $[\sigma'_1+\sigma'_2+\sigma'_3]/3$) |
| $p'_{mc}$ | Mean effective consolidation stress |
| $p_a$ | Reference pressure |
| PI | Plasticity index |
| PL | Plastic limit |
| q | Shear stress |
| $R_0$ | Overconsolidation ratio expressed in terms of the mean effective stress |
| *S1*, ... | Shear phase number |
| $S_c$ | Undrained strength ratio in triaxial compression at OCR equal to 1 |
| SD | Standard Deviation |
| SHANSEP | Stress History and Normalized Soil Engineering Properties |
| $S_{ij}$ | Structure factor in i-j plane |
| SR | Swelling ratio |
| t | Time |
| $t_{creep}$ | Duration of creep |
| $t_p$ | Time to end of primary consolidation |
| $t_{shear}$ | Duration of shear |
| $t_{storage}$ | Duration of storage |

| | |
|---|---|
| *U* | Unloading |
| u, $\Delta u$ | Pore pressure, change in pore pressure |
| $u_e$ | Excess pore pressure |
| *UL* | Unloading, loading |
| $u_s$ | Shear induced pore pressure |
| *UU* | Unloading, unloading |
| UU | Unconsolidated undrained shear test |
| VCL | Virgin compression line |
| $v_s$ | Shear wave velocity |
| $w_n$ | Natural water content |
| | |
| $\alpha$ | Strain rate coefficient |
| $\Delta q$, $\Delta q_{max}$ | Shear stress increment, maximum shear stress increment |
| $\varepsilon_a$, $\varepsilon_{ax}$ | Axial strain |
| $\varepsilon_{aRev}$ | Axial strain since most recent load reversal |
| $\varepsilon_{aU}$ | Unloading axial strain |
| $\varepsilon_{EL}$ | Elastic strain |
| $\varepsilon_{lin}$ | Linear threshold |
| $\varepsilon_{PL}$ | Plastic strain |
| $\varepsilon_{TOT}$ | Total axial strain |
| $\varepsilon_{vol}$ | Volumetric strain |
| $\varepsilon$ dot | Strain rate |
| $\phi'$ | Friction angle based on effective stresses |
| $\gamma$ | Shear strain |
| $\gamma$ dot | Shear strain rate |
| $\gamma_t$ | Total unit weight of soil |
| $\gamma_w$ | Unit weight of water |
| $\nu$ | Poisson's ratio |
| $\rho$ | Density |
| $\sigma'_v$, $\sigma'_h$ | Vertical, horizontal effective stress |
| $\sigma'_p$ | Effective preconsolidation pressure |
| $\sigma'_{vc}$ | Effective vertical consolidation stress |
| $\sigma'_{vi}$ | Consolidation stress at which secondary compression occurred |
| $\sigma'_{vm}$ | Maximum past pressure |
| $\sigma_1$, $\sigma_2$, $\sigma_3$ | Principal stresses |
| $\sigma_{oct}$ | Mean octahedral stress |
| $\tau$, $\tau_{max}$ | Shear stress, maximum shear stress |

# CHAPTER 1

# INTRODUCTION

## 1.1 PROBLEM STATEMENT

In many civil engineering works deformation serviceability requirements, rather than system failure, establish the main design constraints. This is especially true for deep excavations constructed within deep clay deposits in highly congested urban environments. Around these structures soil movements are difficult to control even when advanced excavation techniques are used (Hashash and Whittle 1998). In these cases the prediction of movements in the surrounding soil and their effects on adjacent structures and facilities (Boscardin and Cording 1989) become crucial to the engineer.

The prediction of ground movements in cohesive soils is a complex problem, and has been extensively investigated over the years through both empirical procedures, and more recently, analytical techniques, such as the finite element method, that, combined with a soil model facilitate the study of more complex problems (complex stratigraphy and/or construction processes). This has been a major focus of research at MIT (e.g. Whittle et al. 1993, Hashash 1992, Jen 1998, etc.), and a large amount of work has been performed on the analysis of deep excavations in clay, using the finite element method in conjunction with an advanced constitutive model for cohesive soils (MIT-E3, Whittle and Kavvadas 1994).

Many factors affect the deformations induced in the ground by an engineering structure. As shown in Table 1.1, they can be classified in three main categories: 1) existing ground conditions, 2) construction details and 3) properties of geomaterials. The ability of engineers to make accurate predictions relies on their knowledge of and their ability to account for the complete list of these factors. In particular, Whittle et al. (1993) point out that uncertainties in the engineering properties of the soils stemming from inadequate characterization through laboratory tests and/or field investigations of the relevant parameters for all soil layers, and

approximate representation of the constitutive behavior used in the analysis are mostly responsible for difficulties in achieving reliable analytical predictions.

| |
|---|
| 1) **EXISTING GROUND CONDITIONS**<br>▪ Geological history<br>▪ Stratigraphy, spatial variations<br>▪ Ground water conditions<br>▪ Stress history, $K_0$ profile<br>▪ Earlier construction work |
| 2) **CONSTRUCTION DETAILS**<br>▪ Scale of work, geometry<br>▪ Sequence of operations<br>▪ Imposed loads and their timing<br>▪ Drainage boundary conditions<br>▪ Stiffness of structural members |
| 3) **PROPERTIES OF GEOMATERIALS**<br>▪ Permeability<br>▪ Shear Strength<br>▪ Pre-failure deformation properties<br>▪ Time (aging, strain rate dependency, and creep) |

**Table 1.1:** Factors affecting ground movements induced by engineering structures (adapted from Jardine 1994).

This thesis focuses on issues related to the characterization of soil properties. As indicated in Table 1.1, it is essential to have knowledge not only of the strength and flow properties of the soils, but also of the small strain or pre-failure deformation behavior. In fact, observations performed in the field indicate that in many practical problems the soil undergoes limited straining under working conditions. A variety of examples, derived from field measurements or based on analytical predictions, demonstrate the predominance of small strain deformations induced by excavations, tunnels and foundations, in different geomaterials (e.g., Burland 1989, Tatsuoka and Kohata 1994). Based on the analysis of a large number of these case histories, Jardine (1994) concludes that *"almost all of the overall ground movement seen at typical working loads is developed within regions of the ground where the major principal strain ($\varepsilon_1$) ranges between 0.001% and 0.5%"* and that *"the major part of the movement is often contributed by regions where $\varepsilon_1$ falls between 0.01 and 0.1%."* Therefore, in order to make accurate calculations of ground movements, the stress-strain response in the pre-failure region of strains must be well understood.

Laboratory characterization of the pre-failure soil deformation properties must also account for the stress paths encountered in the field, as it has been shown (e.g Atkinson et al. 1990) that the behavior of soils is affected by the pre-shear stress history. For example, a construction sequence can lead to very complex stress paths in the soil involving rotation of the principal stresses and reversals of loading. An example of this is shown in Figure 1.1 which presents the effective stress paths for soil elements located behind a retaining wall at varying depths (indicated by a particular symbol). These results were obtained by Hashash (1992) using non linear finite element analyses in conjunction with the MIT-E3 soil model.[1]

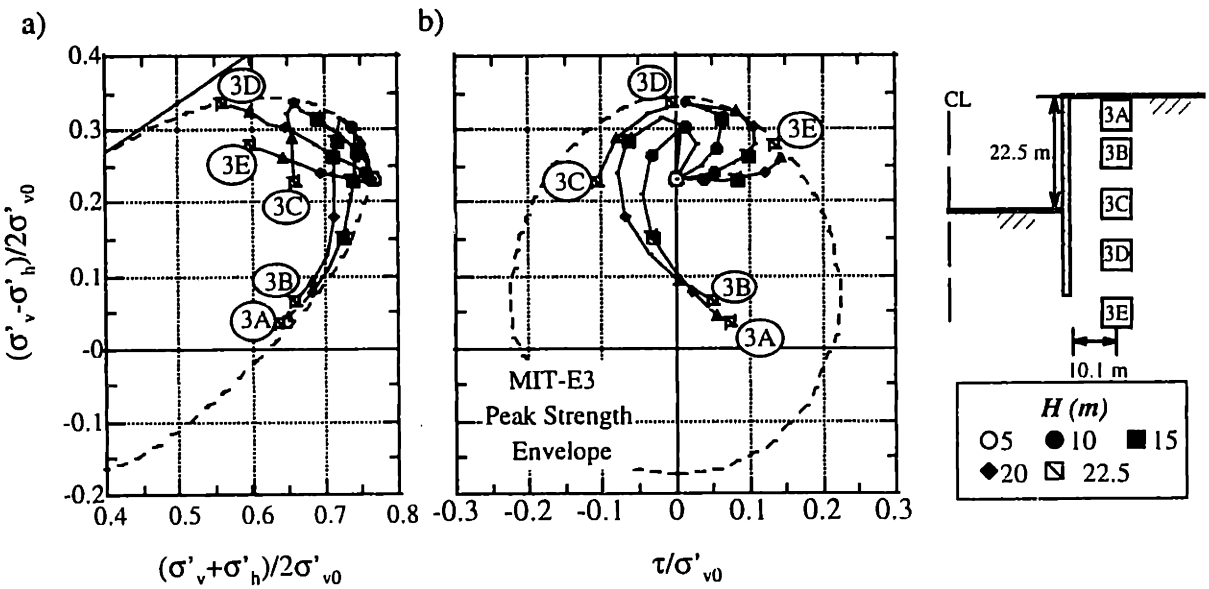


**Figure 1.1:** Stress paths around an excavation in NC Boston Blue clay derived from finite element analyses using the MIT-E3 soil model: a) q-p plane; b) q-τ plane (Hashash 1992).

Over the past 10-15 years increasing effort has focused on the laboratory characterization of the pre-failure behavior of soils. In particular, the development of new laboratory technology which allows more precise on-specimen measurements of strain has produced measurements of stiffness much closer to the values obtained in situ, and back-calculated from the field. These stiffness measurements have assisted in closing the gap between the dynamic and static measurements of the small strain modulus (e.g., Tatsuoka and Shibuya 1992). In addition, it has

[1] MIT-E3 (Whittle and Kavvadas 1994) is a generalized effective stress soil model, capable of describing the stress-strain-strength anisotropy, small strain non-linearity and path dependent behavior of normally consolidated and lightly overconsolidated soils.

become clear that most soils display significant non-linearity in the behavior even at small strains.

The comparison of the predictions made using simple soil models with those of more complex models that take into account small-strain non-linearity clearly demonstrates that the characterization and the accurate description of the pre-failure behavior in the model are essential for reliable predictions of soil deformations. For example, Figure 1.2 shows predictions of the surface settlement produced by an excavation (maximum depth = 22.5 m, width=40 m) in normally consolidated Boston Blue clay. These results were obtained by Whittle and Hashash (1994), employing the finite element method in conjunction with three different models: elastic, Modified Cam Clay (MCC, Roscoe and Burland 1968) and MIT-E3 (Whittle and Kavvadas1994).

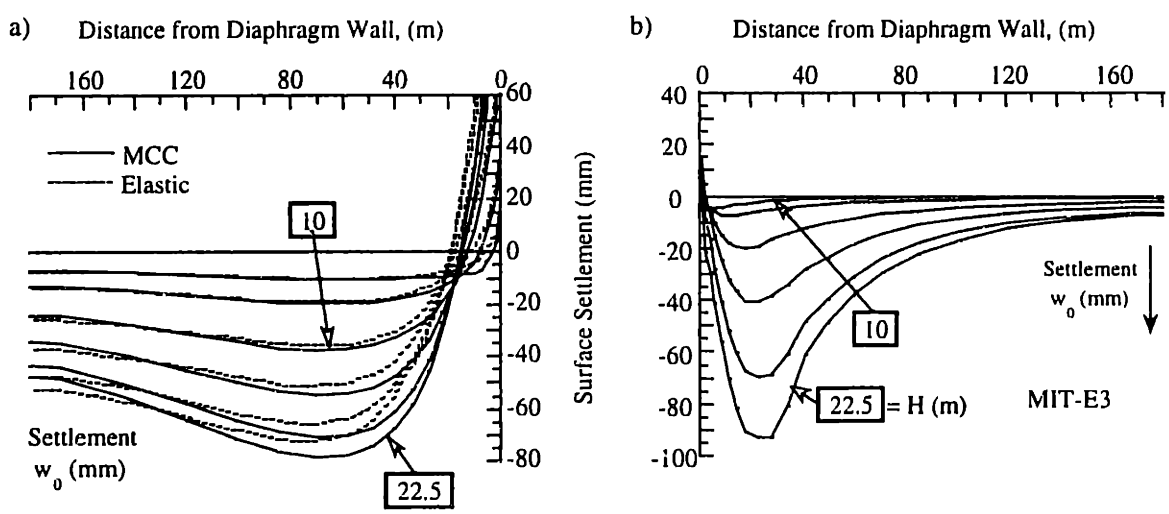


**Figure 1.2:** Surface settlement at the side of an excavation in NC Boston Blue clay determined through finite element analyses using a) elastic, MCC and b) MIT-E3 soil models (Whittle and Hashash 1994).

Figure 1.2 shows that the elastic model and the MCC model predict a marked upward movement of the wall, and significant settlements up to 200 m away from the excavation. On the other hand, the prediction obtained using the MIT-E3 model shows a different settlement pattern, characterized by minimal upward movement of the wall, and rapid decrease in the settlement with distance from the excavation. This shape of the settlement trough is more realistic and generally agrees better with field observations. The capability of this model to

predict ground movements is primarily attributable to its ability to describe the small-strain non-linearity of clays.

The discussion above outlines the relevance of the study of the pre-failure behavior of soils, and demonstrates that the improved characterization of the small strain non-linear behavior of soils can greatly enhance predictive capabilities.

In this arena much still needs to be done to establish a fundamental understanding of the effects of parameters such as OCR, recent stress history, and strain rate, on the small strain behavior of cohesive soils, particularly in the small strain non-linear region (0.001-0.1%). In fact, due to the difficulties and costs associated with obtaining undisturbed samples, to the variability of natural soils, as well as to the concerns with extrapolating results for reconstituted clays to natural soils, much of the work done over the last few years in the characterization of the pre-failure behavior of clays has addressed limited aspects of soil behavior.[2]

## 1.2 RESEARCH OBJECTIVES

The overall objective of the research presented in this thesis is to gain an improved understanding of the factors influencing the small strain behavior of cohesive soils. This goal is pursued through an extensive experimental program on Resedimented Boston Blue Clay (RBBC). RBBC has been used at MIT for research purposes for decades, and there exists an extensive database of its behavior under a variety of conditions. Therefore, it represents an ideal testing material when performing fundamental studies of soil behavior such as the one presented in this thesis.

Taking advantage of the uniformity and reproducibility in the behavior of RBBC, this research specifically investigates the role of the following factors on both the initial stiffness and the small strain non linearity (axial strain $\varepsilon_a$<0.1%) of RBBC in undrained triaxial compression: consolidation stress level, OCR, pre-shear stress path, pre-shear lateral stress ratio, rate of shear, and laboratory aging. The results of these investigations are expected to provide insight into the significance of these variables, and aid in isolating parameters that can provide a consistent and concise description of the small strain behavior of soils. Ultimately this work is aimed at

[2] An exception is represented, for example, by the work done at City University on natural and reconstituted London clay (e.g., Atkinson et al. 1990, Richardson 1988, Stallebrass 1990).

developing a qualitative framework describing the dependence of the small strain ($10^{-6}$-$10^{-3}$) behavior of soft clays on various testing conditions.

This program also seeks to enhance the technology available for the experimental determination of the small strain behavior of clays in the triaxial apparatus. Particular emphasis is placed on the development of a versatile on-specimen device that can consistently and accurately measure small axial strains, over a large range of deformation.

Finally, within the context of achieving the broader goals of this program, it is also intended that this work will extend the existing database on RBBC to include the pre-failure behavior of this material that has previously never been investigated.

## 1.3 ORGANIZATION OF THE THESIS

This thesis is organized in eight chapters, with the intention of presenting the reader with a complete picture of the problem investigated: relevant background, experimental details and finally presentation and analysis of the results.

The following four chapters (2, 3, 4 and 5) present background information on the topic, the soil used for testing, the testing equipment and the research approach and procedures employed. The second part of the thesis (Chapters 6-8) presents and analyzes the results, which represent the main contribution of this dissertation. All chapters are intended to be self-contained and, in light of this, pertinent references are summarized at the end of each chapter. Details of the contents of each chapter are summarized in the following.

Chapter 2 summarizes the state of the knowledge on the pre-failure behavior of cohesive soils. A large amount of data is available in the literature on this topic, and consequently the scope of the chapter is limited to laboratory experimental work performed on natural and reconstituted cohesive soils. The chapter is organized in two main sections: one describing the behavior of clays in the very small strain region (<~0.001%) characterized by mostly linear and rate independent stress-strain behavior; the second discussing behavior in the subsequent non-linear region. The factors influencing the magnitude of the stiffness, the transition from linear to non-linear behavior, and the stiffness degradation with strain level are discussed.

Chapter 3 presents an overview of Resedimented Boston Blue Clay (RBBC) the material used in the entire testing program. The chapter summarizes the resedimentation procedure used to prepare block samples, the index properties of the soil, and provides extensive background on

its engineering properties. In particular the current knowledge on the consolidation and undrained shear behavior of RBBC is reviewed in some detail. The intent of this effort is to summarize the reference database that this research complements and demonstrate that the behavior of RBBC is typical of that of many natural soils.

Chapter 4 describes the experimental equipment used to perform the tests presented in the thesis. As previous theses (e.g., Sheahan 1991) have extensively dealt with this topic, the chapter presents only a brief overview of the stress path automated triaxial cells developed by the MIT Geotechnical Laboratory. The primary focus of the chapter is on the innovations introduced to measure the small strain behavior of soils. In particular, the system for the on-specimen measurement of small strains, which makes use of miniature LVDT's mounted on clamp-on yokes, is described in detail. Design criteria are examined and both the mechanical and the electrical systems are described, including issues of signal stability as a function of time and temperature. The chapter also presents results of proof tests conducted on specimens of aluminum, PMMA (polymethylmethacrylate), RBBC and frozen sand to validate the equipment.

As mentioned in the previous section, this thesis investigated the role of several variables (stress level, OCR, stress path, strain rate, etc.) on the pre-failure behavior of RBBC employing an innovative testing approach. Chapter 5 elaborates on the rationale for the choice of the variables investigated and for the ranges of variation examined, and discusses the details of the multi-stage testing approach, providing a number of examples that demonstrate its validity and its usefulness for the work presented herein. Finally the chapter summarizes the experimental program and the data reduction and evaluation procedures employed in analyzing the collected data.

In this thesis the results are presented and analyzed in two separate chapters. The first one (Chapter 6) presents, one by one, the variables investigated, examining their effects on the pre-failure behavior of RBBC. In each section, the initial stiffness and the small strain non-linearity are addressed separately using as a reference the behavior of $K_0$ normally consolidated RBBC sheared in undrained triaxial compression at a standard rate of 0.1%/hr after 1 day of laboratory aging.

Chapter 7 provides the synthesis and the interpretation of the results. The chapter is organized in two main parts. Section 7.2 reviews the initial stiffness data and furnishes an expression for the derivation of $E_{uMAX}$. Section 7.3 addresses the factors that affect the stiffness

degradation behavior of RBBC. Both sections examine the relative significance of the variables investigated (OCR, rate, etc.) and provide an interpretation of the factors controlling the behavior.

A summary of the results and of the main conclusions drawn from the analysis is contained in Chapter 8, which also presents recommendations for future research.

## 1.4 REFERENCES


1. Atkinson, J.H., Richardson, D. and Stallebrass, S.E. (1990), "Effect of Recent Stress History on the Stiffness of Overconsolidated Soil," ***Géotechnique***, 40 (4), pp. 531-540.

2. Boscardin, M.D. and Cording, E.J. (1989), "Building Response to Excavation Induced Settlement," ***Journal of Geotechnical Engineering***, ASCE, 115 (1), pp. 1-21.

3. Burland, J.B. (1989), "Ninth Laurits Bjerrum Memorial Lecture: 'Small is Beautiful' – the Stiffness of Soils at Small Strains," ***Canadian Geotechnical Journal***, 26, pp. 499-516.

4. Hashash, Y. M. A. (1992), "Analysis of Deep Excavations in Clay," Ph.D. Thesis, Department of Civil and Environmental Engineering, MIT, Cambridge, MA, 337 p.

5. Hashash, Y.M.A. and Whittle, A.J. (1996), "Ground Movement Prediction for Deep Excavations in Soft Clay," ***Journal of Geotechnical Engineering***, ASCE, 122 (6), pp. 474-486.

6. Hight, D.W. and Higgins, K.G. (1994), "An Approach to the Prediction of Ground Movements in Engineering Practice: Background and Application," *Proc. Int. Symp. Pre-Failure Deformation Characteristics of Geomaterials* ( Hokkaido'94), Vol. 2, pp. 909-945.

7. Jardine, R.J., Potts, D.M., Fourie, A.B., and Burland, J.B. (1986), "Studies of the Influence of Non-Linear Stress-Strain Characteristics in Soil Structures Interaction," ***Géotechnique***, 36 (3), pp. 377-396.

8. Jardine, R.J., Potts, D.M., St.John, H.D., and Hight D.W. (1991), Some Practical Applications of a Non-linear Ground Model," *Proc. 11th European Conference on Soil Mechanics and Foundation Engineering*, Florence, Vol.2, pp.223-228.

9. Jardine, R.J. (1994), "One Perspective of the Pre-Failure Deformation Characteristics of Geomaterials," *Proc. Int. Symp. Pre-Failure Deformation Characteristics of Geomaterials (IS-Hokkaido'94),* Vol. 2, pp. 855-885.

10. Jen, L.C. (1998), "The Design and Performance of Deep Excavations in Clay," Ph.D. Thesis, Department of Civil and Environmental Engineering, MIT, Cambridge, MA, 698 p.

11. Richardson, D. (1988), *Investigations of Threshold Effects in Soil Deformations*, Ph.D. Thesis, The City University, London, UK, 302 p.

12. Roscoe, K.H. and Burland, J.B. (1968), "On the Generalized Stress-Strain Behavior of 'Wet' Clay," ***Engineering Plasticity***, pp. 535-609.

13. Sheahan, T.C. (1991), "An Experimental Study of the Time-Dependent Undrained shear Behavior of Resedimented Clay Using Automated Stress-Path Triaxial Equipment," Sc.D. Thesis, Department of Civil Engineering, MIT, Cambridge, 955 p.

14. Stallebrass, S.E. (1990), "Modeling the Effect of Recent Stress History on the Behaviour of Overconsolidated Soil," Ph.D. Thesis, The City University, London, UK, 156 p.

15. Tatsuoka, F. and Shibuya, S. (1992), "Deformation Characteristics of Soils and Rocks from Field Laboratory Tests," Report of the Institute of industrial Science, The University of Tokyo, 37 (1), March 1992.

16. Tastuoka, F. and Kohata, Y. (1994), "Stiffness of Hard Soils and Soft Rocks in Engineering Applications," *Proc. Int. Symp. Pre-Failure Deformation Characteristics of Geomaterials (IS-Hokkaido'94),* Vol. 1, pp. 947-1063.

17. Whittle, A.J., Hashash, Y.M.A., and Whitman, R.V. (1993), "Analysis of Deep Excavation in Boston," ***Journal of Geotechnical Engineering***, ASCE, 119 (1), pp. 69-91.

18. Whittle, A.J. and Hashash, Y.M.A. (1994), "Soil Modeling and Prediction of Deep Excavation Behavior," *Proc. Int. Symp. Pre-Failure Deformation Characteristics of Geomaterials (IS-Hokkaido'94),* Vol. 1, pp. 589-595.

19. Whittle, A.J. and Kavvadas, M.J. (1994), "Formulation of the MIT-E3 Constitutive Model for Overconsolidated Soils," ***Journal of Geotechnical Engineering***, ASCE, 120 (1), pp. 173-1981.

# CHAPTER 2

## PRE-FAILURE BEHAVIOR OF COHESIVE SOILS

### 2.1 INTRODUCTION

As discussed in Chapter 1, there is ample evidence in the literature that knowledge of the small strain behavior of soils is essential for the prediction of ground movements and the interpretation of field data. However, for a long time, the stiffness values obtained in the laboratory were consistently smaller than the values measured in situ or back calculated from the field. This discrepancy was traditionally attributed to the effects of sampling disturbance (e.g., Lambe and Whitman 1967, Burland 1989) and it was accepted that the true static stiffness of soils could only be measured by field methods.

The early 1980's witnessed a major development in laboratory stiffness measurement with the implementation of the first techniques for on specimen measurement of the strains (e.g., Brown et al. 1980, Burland and Symes 1982, Costa Filho 1985) in the triaxial apparatus. The measurements showed that bedding errors occurring at the end platens were in great part responsible for the low stiffness values measured externally on laboratory specimens and that soils displayed marked non linearity even at small strains.

Over the following years the technology for the measurement of small strains progressed incredibly and various devices (electrolevel displacement gages [e.g., Jardine et al. 1984], Hall effect semiconductors [e.g., Clayton and Khatrush 1986], miniature LVDT's [e.g., Andersen et al. 1995, Cuccovillo and Coop 1997], proximity sensors [e.g., Hird and Yung 1989], local deformation transducers [Goto et al. 1991]) have been employed to measure strains on the order of $10^{-5}$-$10^{-6}$ in the triaxial apparatus. These devices can be divided into two categories: those that make direct strain measurements through contact with the specimen and those that require no contact with the specimen and are therefore referred to as proximity devices.

It is therefore now well established that the small strain behavior of soils can be reliably assessed in the laboratory. Concurrently, other major developments in laboratory testing (automation, stress path testing, development of hollow cylinder torsional devices capable of running monotonic, cyclic and dynamic tests on one specimen, incorporation of instrumentation for measuring shear wave velocities in various devices, etc.) have occurred, contributing to the understanding of the pre-failure behavior of soils under a variety of conditions, and aiding in closing the gap between the dynamic and the static measurements of the very small strain modulus (<0.001%).

The availability of this technology along with considerable research that lead to a renewed interest in the small strain behavior of soils culminated with the organization of the first international conference on pre-failure deformation of soils in September of 1994 in Sapporo, Japan. Since then a Géotechnique symposium in print was organized on this same topic (Vol.47, 3) and a second international conference is planned for October 1999 in Torino, Italy.

It must be pointed out that much research on the small strain properties of soils has been carried out for a number of years in the soil dynamics arena, particularly due to the development of the resonant column device. These investigations were aimed at estimating strain dependent moduli and damping properties of soils for the analysis of soil-structure interaction and earthquake response of soils. These results, together with those obtained from wave propagation measurements, have contributed to an increased understanding of the factors affecting the initial stiffness, which is today known to be quasi-independent of the rate and type of loading application. Further, while it is clear that the stiffnesses measured at higher strains in dynamic tests are not applicable to static problems (due to the effects of rate and pre-straining in the case of repeated loading), the extensive existing database provides a comparative framework through which the role of influential factors can be estimated.

This chapter presents a summary of the state of knowledge of the small strain behavior of cohesive soils. Examination of the abundant small strain literature indicates that much of the research has concentrated on the investigation of the properties of sands reconstituted in the laboratory, while the availability of data and the knowledge of the factors affecting the pre-failure behavior of clays is much more scarce. This is due to the difficulties of obtaining undisturbed

samples and the problems associated with extrapolating the results for reconstituted clays to natural soils.

The bulk of this chapter is devoted to the presentation of the state of knowledge on the pre-failure deformation of cohesive soils. Section 2.2 presents a very concise summary of the apparatuses employed to measure the small strain stiffness of soils in the laboratory in order to clarify the presentation and interpretation of the data presented in the rest of the chapter.

Section 2.3 discusses the pre-failure behavior of cohesive soils and attempts to isolate the role of the influential factors based on the most significant experimental results available in the literature. Finally, section 2.4 reports the relevant references from the literature.

## 2.2 MEASUREMENT OF SMALL STRAIN BEHAVIOR IN THE LABORATORY

This section is aimed at briefly reviewing the basic characteristics (method of loading, applied strain rate, range of strain investigated, stiffness parameters measured) of the tests employed in the laboratory to investigate the pre-failure behavior of soils. Frequent reference is made to the results obtained from these devices in the rest of the chapter. Details on the specifics of the test apparatuses and abundant experimental data can be found in various state of the art papers dealing with this topic (e.g., Lo Presti 1994, Woods 1994, Tatsuoka and Shibuya 1992, Tatsuoka et al. 1997), as well as in papers on specific topics.

It is useful to start with a classification of the tests performed in the laboratory to measure the stiffness of soils (Table 2.1). A first distinction is between static and dynamic tests.
Dynamic tests involve fast, cyclic loading conditions in which the mass forces (inertia) of the soil element cannot be neglected and acceleration of the soil mass is a major controlling factor. Static tests are defined as those (e.g., Woods 1991) in which monotonic or cyclic loading is applied at a rate slow enough that the effects of inertia can be ignored.

Dynamic tests for the assessment of the small strain behavior of soils, include the resonant column test and seismic tests. In these tests the stiffness of the soil is determined by the dynamic properties of the specimen (i.e. shear wave velocity within the specimen in seismic tests employing bender elements), or of the system including the specimen (i.e. resonant frequency of specimen and driving apparatus in resonant column tests). Both the resonant

a)

| | Static | | |
|---|---|---|---|
| | Triaxial TX | Torsional Shear | |
| | | TS (ML) | TS (CL) |
| **Method of Loading** | Monotonic | Monotonic | Cyclic |
| **Strain Rate** | 0.1%-10%/hr | 0.1%-10%/hr | Proport to f(0.01-1Hz) |
| | | | Variable linearly with $\gamma$ |
| **Strains Investigated** | >0.05% external | >0.0001% | >0.0001% |
| | >0.0001% on specimen | | |
| **Stiffness Parameters** | $E_v$ | $G_{vh}$ | $G_{vh}$ |

b)

| | Dynamic | |
|---|---|---|
| | Resonant Column (RC) | Bender Element (BE) |
| **Method of Loading** | Cyclic | Cyclic |
| **Strain Rate** | Variable with strain | - |
| | ($10^2$-$10^5$%/hr) | |
| **Strains Investigated** | 0.0001-0.1% | <0.001% |
| | | |
| **Stiffness Parameters** | $G_{vh}$ | $G_{vh}$, $G_{hh}$ f(position) |

**Table 2.1:** Apparatuses employed in the laboratory to measure stiffness: a) static, b.) dynamic.

column tests and the wave propagation measurements involve cyclic loading of the soil at strain rates that are significantly higher than those employed in static tests, and also higher than those occurring in the field, as is shown in Figure 2.1. In the resonant column test neither the number of cycles (on the order of thousands) nor the strain rate can be controlled. The strain rate is forced to vary according to the dynamic response of the material to the applied frequency of vibration and increases by several orders of magnitude with strain. The strain range probed in dynamic tests is limited compared to the static tests. Bender element tests involve sub-micron deformations corresponding to strains smaller than 0.001%, which, as will be discussed later in the chapter, are within the initial pseudo-elastic region of behavior for all soils. The resonant column device is used to evaluate the stiffness for a strain range from less than 0.001% to a maximum of about 0.1% (Tatsuoka et al. 1997). Along with the high and variable strain rate and the limitation on the range of strains explored, the difficulties in obtaining the soil stiffness from the measured quantities represent the major weaknesses of dynamic tests. In particular in the resonant column test the data interpretation relies on the assumption of a particular

constitutive model (usually visco-elastic) for the soil. In addition in all torsional shear devices the strain is a function of the radius and is therefore not uniform across the specimen.

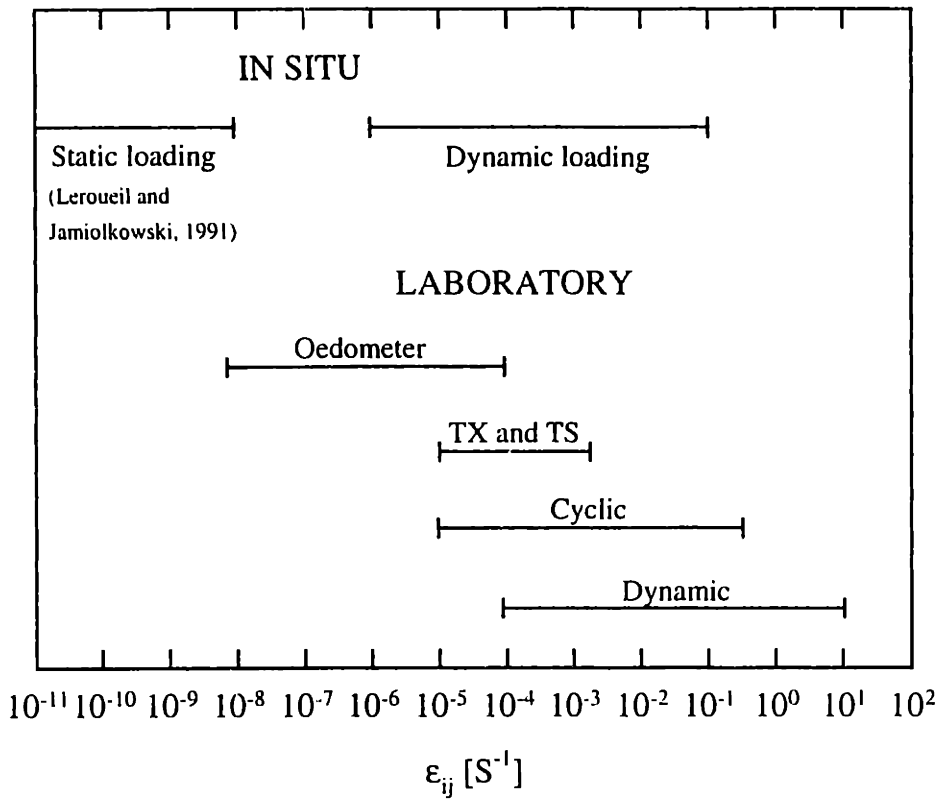


**Figure 2.1:** Strain rates in the laboratory and in the field (Lo Presti 1994).

The static tests most commonly used to investigate the small strain stiffness of soils are the triaxial test and the torsional shear test (monotonic and cyclic), although some results obtained using a plane strain apparatus (e.g., Park and Tatsuoka 1994) the hollow cylinder device (e.g., Zdravkovic and Jardine 1997) and the direct simple shear device (e.g., Douroudian and Vucetic 1995, Lanzo et al. 1997) are also in the literature. Strain rates imposed in the triaxial and in the monotonic torsional shear tests are of the same order of magnitude, and at the low end of those imposed in the laboratory. In the cyclic torsional shear tests, soil specimens are generally strained at much higher strain rates. Further, even in strain controlled torsional shear tests, the strain rate varies significantly with strain level ($d\gamma/dt=4\gamma f$) unless the cycling frequency (f) is adjusted during the test.

As indicated in Table 2.1 torsional shear tests represent a powerful tool for investigating the small strain behavior of soils under static loading. In fact, since the tangential shear strain is free from the effects of bedding errors, strains as small as 0.0001-0.00001% have been measured (e.g., Kim and Stokoe 1994, Hight et al. 1997) by instrumenting the cap. In addition, many apparatuses permit the performance of both resonant column and torsional shear tests on the same specimen (e.g., Lo Presti et al. 1993, Ampadu and Tatsuoka 1993).

Investigation of the pre-failure behavior of soils in the triaxial apparatus requires on-specimen measurement of the strains. While traditional systems that make use of external measuring devices can provide reliable estimates of the stiffness, at best, for strains larger than 0.01-0.05%, significant advances have been made by using devices such as proximity sensors, miniature LVDT's, local deformation transducers etc. mounted directly on the specimen. Accurate strain measurements can be made from strains on the order of 0.001% to failure using a single specimen. An extensive review of the different types of instrumentation employed to measure small strains in the triaxial apparatus is presented by Scholey et al. (1994).

The last row in Table 2.1 summarizes the stiffness parameters that are obtained with the various devices[1]. All the torsional based devices (i.e., resonant column and static and cyclic torsional shear) furnish a measure of the shear stiffness $G_{vh}$. Among the seismic methods, the most common one used in the laboratory involves the use of bender elements which provide, through the measurement of the shear wave velocity, the initial shear stiffness $G_{MAX}$ in the plane of wave propagation ($G_{MAX}=\rho v_s^2$, where $\rho$ = material density and $v_s$ = shear wave velocity). They have been successfully used in conjunction with oedometer (e.g., Jamiolkowski et al. 1994), triaxial (e.g., Viggiani and Atkinson 1995), and torsional shear apparatuses. Bender elements can be used, depending on their position within the soil specimen, to measure $G_{vhMAX}$ or $G_{hhMAX}$ and represent a very suitable tool to investigate the small strain anisotropy of soil (e.g., Jamiolkowski et al. 1994). In the triaxial apparatus only the vertical Young's modulus, $E_v$ is routinely measured, although systems equipped with on specimen radial measurements can also provide the Poisson ratio. Note that, in presenting results of monotonic tests, secant stiffness or, less commonly, tangent stiffness data are generally reported, while in the case of tests involving

[1] Five elastic constants can be used to describe soil as a cross-anisotropic medium: the vertical and horizontal Young's moduli, $E_v$, $E_h$, the Poisson ratios $\nu_{vh}$, $\nu_{hh}$, and the shear modulus $G_{vh}$. [$E_h=2(1+\nu_{hh})G_{hh}$]

cycling, results are presented in terms of equivalent stiffness. Figure 2.2 shows the significance of these terms for the case of a triaxial compression test. The corresponding shear stiffness parameters $G_{MAX}$, $G_{sec}$, $G_{tan}$, and $G_{eq}$ obtained from a torsional shear test can be defined in a similar way.

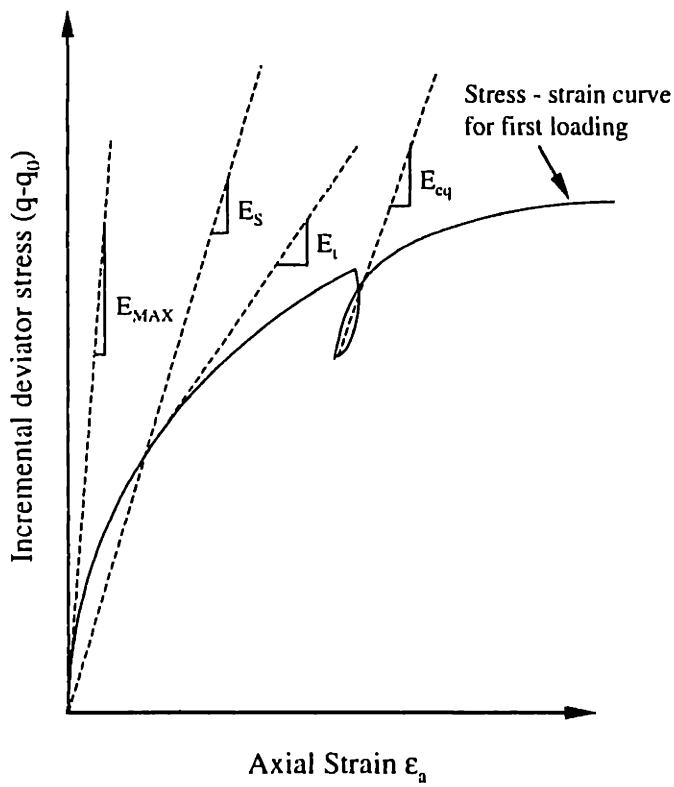


**Figure 2.2:** Definition of Stiffness Parameters.

## 2.3 PRE-FAILURE BEHAVIOR OF COHESIVE SOILS

### 2.3.1 Introduction

The stress-strain behavior of soils is influenced by a variety of factors that can be grouped in three primary categories: a) soil composition and physical state, b) stress history and current stress state and c) mode and rate of loading. The variability of these influences inevitably makes interpretation of soil stiffness complex.

The main features of soil stiffness are illustrated in a plot of G or E versus logarithm of strain (Figure 2.3). Three regions can be isolated in this idealized curve which is representative of the behavior of many geomaterials: *a)* an early portion of behavior characterized by

approximately constant stiffness; *b)* a region characterized by marked non-linearity in which the stiffness of the soil decreases significantly as the soil is strained; and *c)* a region characterized by slowly decreasing stiffness, approximately one order of magnitude smaller than the maximum value. The first two regions encompass the pre-failure behavior of the soil while, once the soil enters the third region, large scale yielding develops.

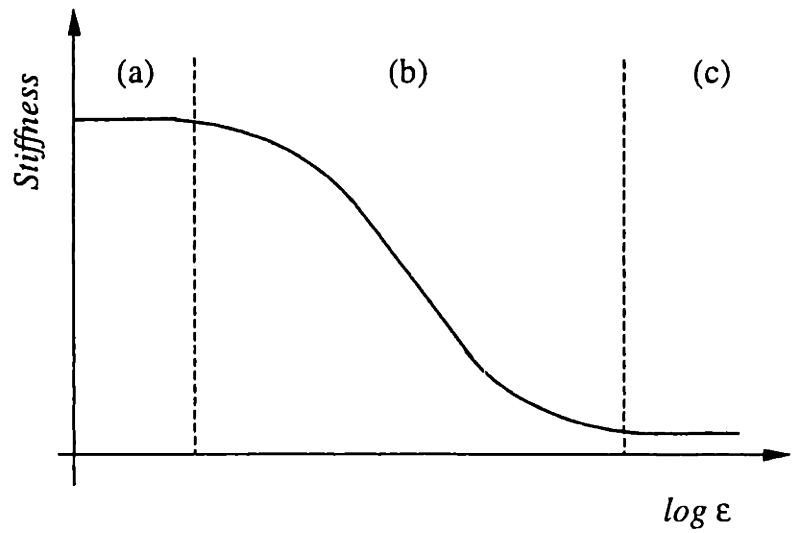


**Figure 2.3:** Schematic of variation of stiffness with strain.

As discussed in the following section, in the initial region (a), which extends to strains on the order of 0.001%, the behavior is very close to being "elastic." On the other hand, in the pre-failure non-linear region (b) the behavior is much more complex with the onset of local yielding and significant time-dependence of the stiffness. Within this region the behavior varies significantly and one researcher's framework (Jardine 1992, 1994) identifies two subregions: one (Zone II) characterized by negligible permanent strains and pore pressure build up; the second (Zone III) characterized by increasingly important plastic component of the deformation. According to this same researcher there are kinematic sub-yield surfaces bounding the linear region and the early portion of the non linear region (zone II in Jardine's framework) which move and evolve in stress space as the soil is subjected to drained (e.g., swelling or aging) or undrained (e.g., disturbance) stress changes. These sub-yield surfaces also depend on many of the factors that affect the stiffness (e.g., composition, stress state and stress history). On the other hand, the boundary between the pre-failure region and the large strain region, where plastic

strains dominate, is hypothesized to remain comparatively immobile and is affected only by relatively large strain events.

The following two sections present a summary of the most recent findings on the behavior of cohesive soils within the initial linear portion (Section 2.3.2) and the region of non linear behavior (Section 2.3.3).

### 2.3.2 The Small Strain Linear Region

This section summarizes the current knowledge of the behavior of soils at very small strains where there is evidence that the stress-strain curve is linear, i.e., the stiffness is constant. Figure 2.4 shows stress strain curves for a variety of geo-materials supporting this statement.

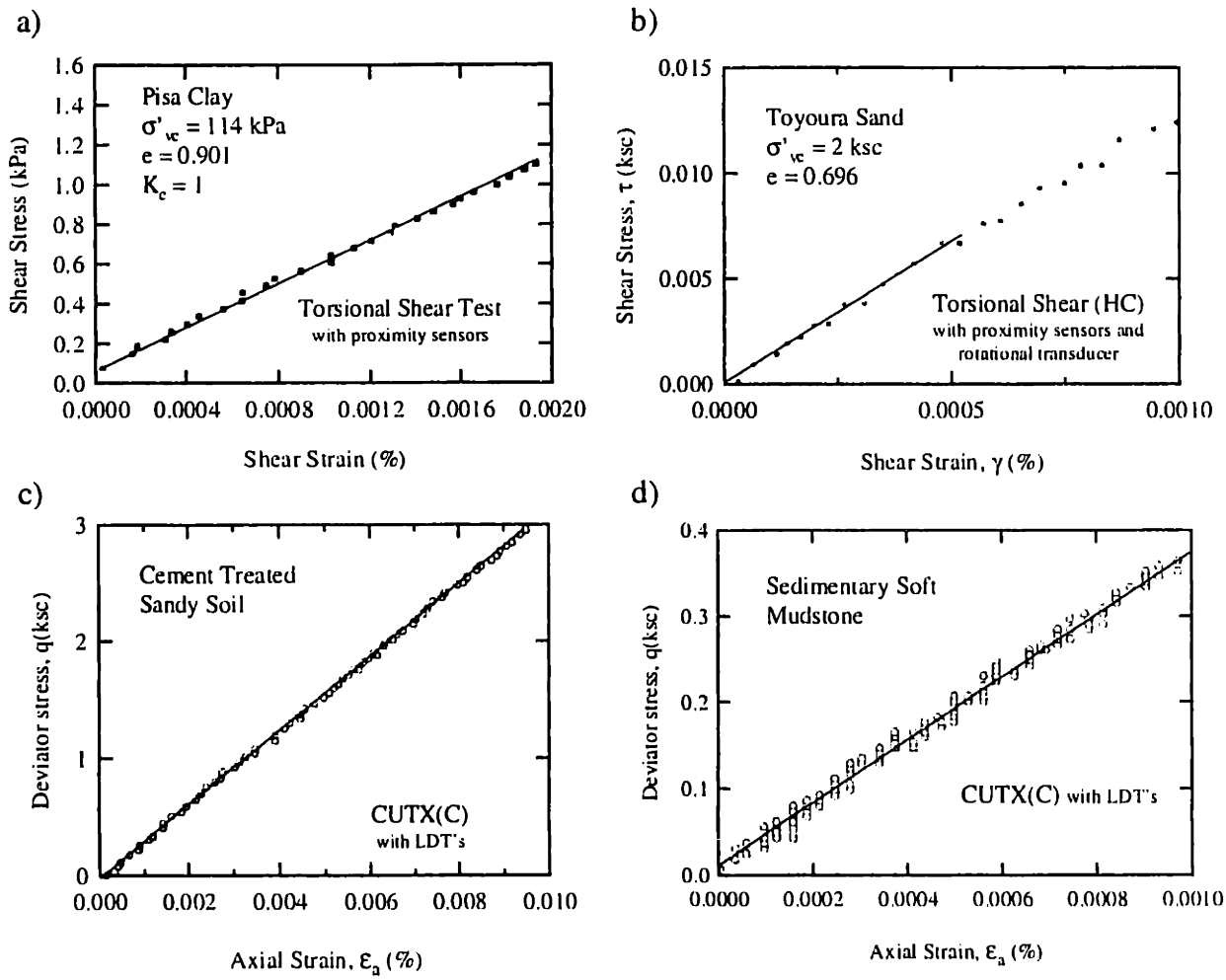


**Figure 2.4:** Linear stress strain behavior of various geo-materials at small strains: a) Pisa clay (Tatsuoka et. al. 1997); b) Toyoura Sand (Tatsuoka and Shibuya 1992); c) cement treated soil (Tatsuoka and Shibuya 1992); d) sedimentary soft mudstone (Tatsuoka et. al. 1997).

In the past this portion of the stress-strain curve has very often been referred to as elastic. However, more recent findings suggest that, while from a practical point of view this assumption may be acceptable, under more rigorous scrutiny it may not hold true. As it is well known, a material is said to behave elastically when the deformations are completely recovered upon unloading. For soils, this condition is very hard to verify in the laboratory due to the difficulties in applying very small unload reload cycles. For this reason, most researchers have relied on the observation that the initial stiffness is independent of strain rate to support presumed elastic behavior (see for example Figure 2.5).

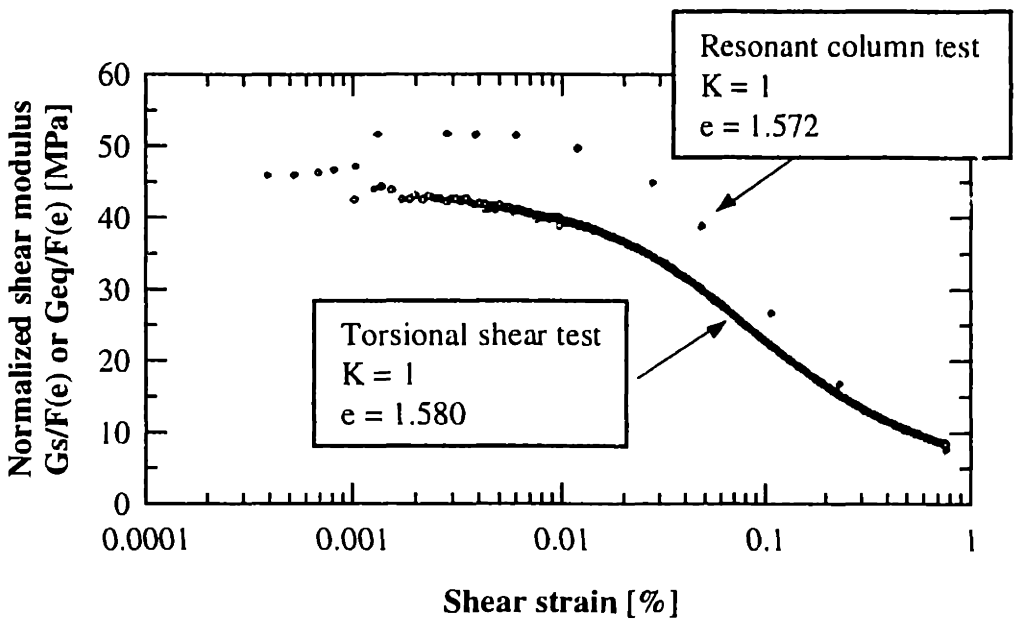


**Figure 2.5:** Comparison of Pisa clay stiffness obtained from dynamic and monotonic tests (Lo Presti 1994).

Thanks to the improvement of measurement techniques, recently several researchers (e.g., Stokoe et al. 1994, Lo Presti et al. 1996) have been able to observe small differences between monotonic and cyclic behavior which indicate that, even at very small strains, the behavior of soil is not perfectly elastic. As a result, the behavior of soils at very small strains is now more commonly termed pseudo-elastic. In the present discussion this type of behavior will be referred to simply as linear.

The subsequent two sections examine in some detail the behavior of cohesive soils in the linear zone of behavior. The following two aspects are discussed:

a) factors affecting the magnitude of the initial stiffness;

b) factors affecting the size of the linear zone.

### *2.3.2.1 Factors Affecting the Magnitude of the Stiffness in the Linear Region*

In discussing the factors that affect the value of the initial stiffness of cohesive soils, it is useful to start by recalling the relationship proposed by Hardin and Blandford (1989) to express the dependence of the maximum stiffness on the current state of a clay:

$$E_{ij} = S_{ij} \cdot F(e) \cdot \sigma_i^{n_i} \sigma_j^{n_j} \cdot OCR^k \cdot p_a^{1-n_i-n_j} \qquad \textit{Equation 2.1}$$

where:

$E_{ij}$ is the stiffness measured in the i-j plane,

$S_{ij}$ is a non dimensional material constant reflecting the anisotropy of the "reference fabric" (Hardin 1989),

F(e) is a void ratio function,

$\sigma'_i$ and $\sigma'_j$ are the pre-shear effective stresses acting in the plane in which $E_{ij}$ is measured,

$n_i$, $n_j$ and k are non dimensional material constants, and

$p_a$ is a reference pressure that is used so that all the constants may be non-dimensional.

Similar, but less general, versions of this equation have been proposed starting with Hardin's work in the mid 1960's with the resonant column device (Hardin and Black 1966, Hardin and Black 1968, Hardin 1978). This type of expression derives from contact mechanics theory. The analyses of particle assemblages (e.g., Duffy and Mindlin 1957) indicate, in fact, that fabric, stress history, state of stress and particle properties are essential elements in the constitutive equations for elasticity of particulate materials. Experimental data collected over the past 30 years (e.g., Jamiolkowski et al. 1994, Stokoe et al. 1994) for a variety of geomaterials indicate that this type of semi-empirical relationship describes quite accurately the initial stiffness of soils.

The role of initial effective stress level, void ratio, and overconsolidation ratio is discussed in the following in the context of Equation 2.1. Soil composition and time effects are also addressed.

*Stress Level*

Keypoints regarding the effect of the initial effective stress level on the maximum stiffness can be summarized as follows:

i) the Young's modulus E in the x direction ($E_{xx}$) is a function of the normal stress $\sigma'_x$ acting in the direction x;

ii) the shear modulus $G_{xy}$ depends on the two orthogonal normal stresses $\sigma'_x$ and $\sigma'_y$ acting in the plane of shear deformation;

iii) the dependence of stiffness on the relevant stresses is described by an exponential relationship.

These conclusions, which are theoretically founded on classical contact mechanics principles developed for completely elastic particles, are supported by shear wave and static measurements in sand (e.g., Roesler 1979, Stokoe et al. 1994, Bellotti et al. 1994).

Generally the stress exponents $n_i$ and $n_j$ are assumed to be equal. This has been demonstrated by Ni (Viggiani and Atkinson, 1995) for dry sand through resonant column tests on hollow cylindrical samples. Bender elements (BE) measurements on Kaolin performed by Viggiani and Atkinson (1995) in a triaxial cell varying the axial and the radial stresses support the validity of this assumption also for cohesive soils.

The value of the stress level exponent varies with type of soil. Table 2.2 summarizes data for a variety of cohesive soils. For comparison purposes data for other geomaterials are presented. The values of the stress level exponent presented in the table refer were obtained after normalizing the stiffness using an appropriate void ratio function. If the stiffness were not normalized much higher values of $n$ would be obtained (e.g., Viggiani and Atkinson 1995).

It can be seen from Table 2.2 that, for clays, $n$ varies over a fairly wide range (0.20 to 0.34), that can only in part be explained by the use of different void ratio functions. The variability of natural soils, demonstrated by the range in index properties presented in column

three of the table, further complicates the interpretation of the *n* values for these soils. Data from other researchers indicate trends of increasing *n* with plasticity index (Viggiani and Atkinson 1995) and liquid limit (Hicher 1994) for reconstituted clays. These trends do not appear to be supported by other data available in the literature.

| Clays | Test Type | Void Ratio | Stiffness Measured | *n* | *PI* (%) | *F(e)* | Reference |
|---|---|---|---|---|---|---|---|
| Panigaglia (N) | BE | 1.1-1.8 | $G_{vh}$ | 0.25 | 44 | $e^{-x}$ (x=1.30) | Jamiolkowski et al. 1994 |
| Pisa (N) | BE | 0.8-1.4 | $G_{vh}$ | 0.22 | 23-46 | $e^{-x}$ (x=1.43) | Jamiolkowski et al. 1994 |
| Garigliano (N) | BE | 0.6-0.9 | $G_{vh}$ | 0.29 | 10-40 | $e^{-x}$ (x=1.11) | Jamiolkowski et al. 1994 |
| Fucino (N) | BE | 0.9-1.8 | $G_{vh}$ | 0.20 | 45-75 | $e^{-x}$ (x=1.52) | Jamiolkowski et al. 1994 |
| Montalto di Castro (N) | BE | 0.6-0.8 | $G_{vh}$ | 0.20 | 15-34 | $e^{-x}$ (x=1.33) | Jamiolkowski et al. 1994 |
| Avezzano (N) | BE | 0.7-1.3 | $G_{vh}$ | 0.23 | 10-30 | $e^{-x}$ (x=1.27) | Jamiolkowski et al. 1994 |
| Ariake (R) | BE | 1.3-1.9 | $G_{vh}$ | 0.34 | 37 | $(1+e)^{-2.4}$ | Shibuya et al. 1997 |
| Drammen (R) | BE | 0.7-1.0 | $G_{vh}$ | 0.32 | 52 | $(1+e)^{-2.4}$ | Shibuya et al. 1997 |
| Higashi-Ohgishima (R) | BE | 1.0-1.4 | $G_{vh}$ | 0.31 | 25 | $(1+e)^{-2.4}$ | Shibuya et al. 1997 |
| Kiyohoro (R) | BE | 0.6-0.8 | $G_{vh}$ | 0.27 | 19 | $(1+e)^{-2.4}$ | Shibuya et al. 1997 |
| Kurihama (R) | BE | 1.3-1.8 | $G_{vh}$ | 0.27 | 59 | $(1+e)^{-2.4}$ | Shibuya et al. 1997 |
| Hachirougata (R) | BE | 1.1-1.9 | $G_{vh}$ | 0.34 | 54 | $(1+e)^{-2.4}$ | Shibuya et al. 1997 |
| MC - Commercial Clay | BE | 1.0-1.4 | $G_{vh}$ | 0.20 | 49 | $(1+e)^{-2.4}$ | Shibuya et al. 1997 |
| NSF - Commercial Clay | BE | 0.9-1.2 | $G_{vh}$ | 0.30 | 26 | $(1+e)^{-2.4}$ | Shibuya et al. 1997 |
| **Other Soils** | | | | | | | |
| Nagoya Gravel | TX-C | - | $E_v$ | 0.29 | - | $(2.17-e)^2/(1+e)$ | Flora et al. 1994 |
| Ticino Sand | RC | 0.58-0.93 | $G_{vh}$ | 0.22 | - | $(2.27-e)^2/(1+e)$ | Lo Presti et al. 1993 |
| Toyoura Sand | TX-C | - | $E_v$ | 0.21 | - | $(2.17-e)^2/(1+e)$ | Kohata et al. 1994 |

Notes:
N = Natural Clay BE = Bender Elements TX-C = Triaxial Compression
R = Reconstituted Clay RC = Resonant Column

**Table 2.2:** Summary of data for the stress level exponent, n.

Recent research suggests that, at least for reconstituted clays, the stress level exponent does not depend on the overconsolidation ratio (Viggiani and Atkinson 1995). These same authors as well as Shibuya et al. (1997) also hypothesize a negligible effect of structure and aging on the exponent.

Finally, although it has been shown that the shear stiffness $G_{ij}$ is independent of the stress $\sigma_k'$, in the third direction *k*, it is common practice (e.g., Porovic and Jardine 1994, Viggiani and Atkinson 1995) to present initial stiffness data as a function of $p_m'$ $(=1/3(\sigma_i'+\sigma_j'+\sigma_k')$ rather

than of the product $\sigma'_i\sigma'_j$. The stress exponent $n = (G \propto p_m'^{n})$ obtained in this case cannot be compared to those presented in Table 2.2.

### *Void Ratio*

It is well established that the linear stiffness of geo-materials increases systematically as porosity reduces. The dependence of the maximum stiffness on the void ratio is expressed by means of the void ratio function F(e). It is implicitly assumed that both Young's modulus and the shear modulus are affected in the same way by changes in the void ratio. Basically two types of void ratio functions are used in the literature. The first one is of the type $F(e)=(C_1-e)^2/(1+e)$. Hardin first proposed a function of this sort in 1966 having observed the linear relationship between shear wave velocity and void ratio for dry sands. Subsequently (Hardin and Drnevich 1972b), after having performed tests on a variety of different soils, Hardin suggested that this type of equation with a value of $C_1$ equal to 2.97 was applicable to both sands and clays. Void ratio functions of this type and a modified version $F(e)= 1/(0.3+0.7e^2)$ (Hardin 1978) have been extensively used in the literature to normalize the stiffness of clays (e.g., Vucetic and Dobry 1991, Kim and Novak 1981).

More recently Lo Presti (1989) has proposed a different expression for the void ratio function: $F(e) = e^{-x}$ . This function has been found to be applicable to a great variety of soils. (e.g., Jamiolkowski et al. 1994, Lo Presti et al. 1997). In particular, based on RC tests and shear wave propagation measurements performed in an instrumented oedometer, Jamiolkowski et al. (1994) found that $x$ varied between 1.11 and 1.52 for six Italian clays. Although the trend is not pronounced, higher values of $x$ appear to be typical of the clays with higher plasticity index.

It should be kept in mind that for clays it is not as simple as for sands to isolate the effect of void ratio changes. Variations in void ratio are, in fact, accompanied either by changes in stress level, OCR, or by changes in the initial fabric (e.g., natural or reconstituted).

### *Overconsolidation Ratio*

The effect of OCR on the initial stiffness of clays is not clearly defined. Some data in the literature indicate that, as for sands, the stress history plays only a limited role in determining the magnitude of the stiffness of cohesive soils. This is shown for example in Figure 2.6 from

Jamiolkowski et al. (1994): once the stiffness values obtained from shear wave propagation measurements are normalized for differences in void ratio using an appropriate void ratio function, the effect of OCR on the relationship between stress level and $G_{MAX}$ becomes insignificant.

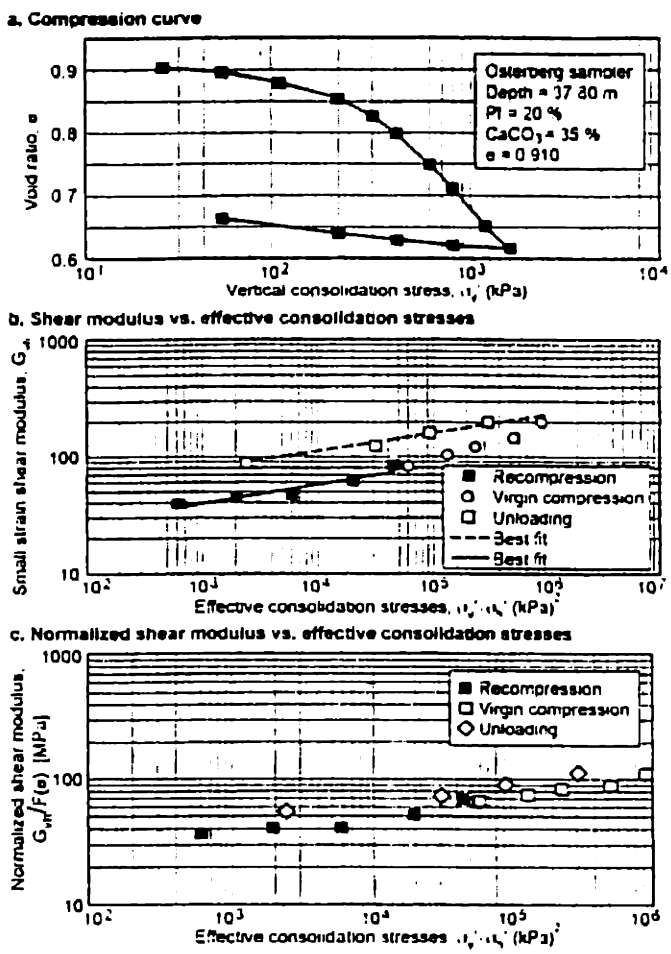


**Figure 2.6:** Use of a void ratio function ($F(e)=e^{-1.11}$) to normalize the initial shear stiffness of NC and OC Garigliano clay (Jamiolkowski et. al. 1994).

Viggiani and Atkinson (1995) offer a slightly different interpretation and compare results obtained at various values of $R_0$ (overconsolidation ratio expressed in terms of mean effective stress $p_m'$). They observe that, if no void ratio function is introduced, the dependence of the initial shear stiffness on $R_0$ is described by the following relation: $G_{MAX(OC)}=G_{MAX(NC)}(R_0)^k$

(Figure 2.7), where $G_{MAX(NC)}$ is the value of the initial stiffness measured on a NC specimen having the same mean effective stress; and $k$ is an exponent which, for the four reconstituted clays investigated by the authors, varies between 0.20 and 0.25 with a tendency to increase with increasing plasticity. Viggiani and Atkinson (1995) compare the BE results obtained for reconstituted London clay with those for the intact material and find that $k$ does not vary.

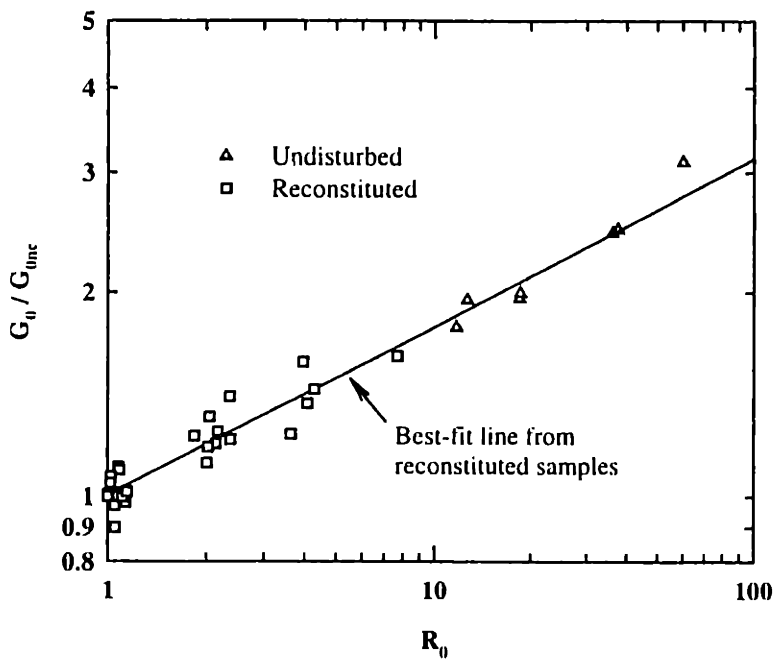


**Figure 2.7:** Variation of initial shear stiffness for reconstituted and intact London clay [BE measurements in CIUC tests, $G_0$=$G_{MAX}$] (Viggiani and Atkinson 1995).

### *Aging Effects*

In discussing time effects two topics are generally addressed: the effect of strain rate and the effect of aging. As mentioned in Section 2.3.1, strain rate appears to have a negligible influence on the initial stiffness. Regarding the effect of aging, it has been observed (e.g., Anderson and Stokoe 1978) that prolonged secondary compression causes the stiffness to increase in an approximately linear manner with the logarithm of time. As seen with the increase in preconsolidation pressure and undrained strength caused by prolonged aging, the increase in stiffness cannot be explained solely by the reduction in void ratio that occurs during secondary compression, but stems mainly from the evolution of the soil's microstructure (Anderson and

Stokoe 1978, Anderson and Woods 1976) due, for cohesive soils, to the rearrangement of the soil structure and strengthening of physical-chemical bonds. The parameter $N_G$ quantifies the increase in $G_{MAX}$ produced by aging:

$$N_G = \frac{\Delta G_{max}}{G_{max}(t = t_p) \cdot \log \frac{t}{t_p}} \qquad \textit{Equation 2.2}$$

Table 2.3 from Lo Presti et al. (1996) summarizes data for a variety of soils. For clays, an average increase in the initial stiffness of about 10% per cycle of secondary is observed. Different authors have proposed empirical correlations between $N_G$ and simple soil properties such as $D_{50}$ (Afifi and Richart 1973), PI (Kokusho et al. 1982), and the ratio of the secondary compression index $C_\alpha$ to the compression index $C_c$ (Mesri and Choi 1983). This last type of correlation has the form $N_G=10^{C_\alpha/C_c}-1$ (where $C_c$ is the compression index and $C_\alpha$ the secondary compression index) and appears the most consistent for both cohesive and cohesionless soils. Lo Presti et al (1996) suggest that there is a consistent correlation between $N_G$ and the secondary compression index $C_\alpha$ (Figure 2.8).

| Soil | $D_{50}$ [mm] | $N_G$ [%] | PI [%] | $C_\alpha$ | Notes |
|---|---|---|---|---|---|
| Quiou sand | 0.71 | 5.3 | - | 0.002 to 0.003 | Carbonate |
| Kenya sand | 0.13 | 12 | - | 0.004 | Carbonate |
| Ticino sand | 0.54 | 1.2 | - | 0.00015 | Silicate |
| Hokksund sand | 0.45 | 1.1 | - | 0.00015 | Silicate |
| Messina sand and gravel | 2.1 | 2.2 to 3.5 | - | 0.0007 to 0.0008 | Silicate |
| Messina sand and gravel | 4 | 2.2 to 3.5 | - | 0.0007 to 0.0008 | Silicate |
| Glauconite sand | 0.22 | 3.9 | - | 0.0025 | 50% quartz/50% glauconite |
| Fucino silty clay | - | 7 to 11 | 60 | 0.022 to 0.035 | - |
| Taranto clay | - | 9 to 13 | 14 to 15 | 0.01 to 0.015 | - |
| Pisa clay | - | 13 to 19 | 23 to 38 | 0.013 to 0.05 | - |
| Augusta clay | - | 8 | 35 | 0.01 to 0.02 | - |

**Table 2.3:** Values of the $N_G$ coefficient for sands and clays (Lo Presti et. al. 1996).

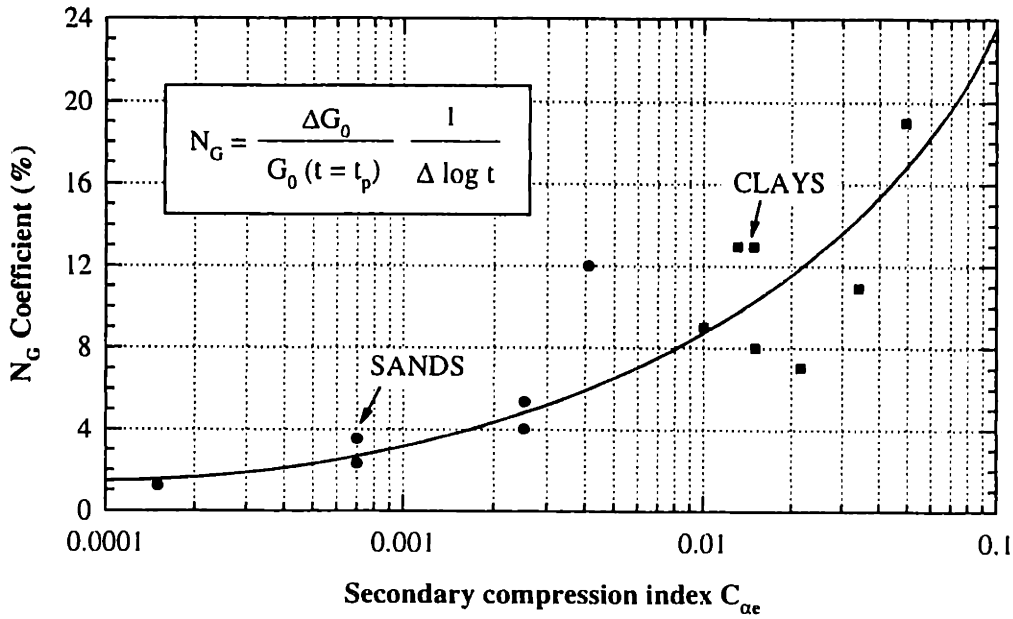


**Figure 2.8:** $N_G$ coefficient versus secondary compression index from torsional shear tests (Lo Presti et. al. 1996).

***Soil Composition***

The overall effect of soil composition on the pre-failure behavior of clays appears to be a decrease of stiffness with increasing clay content and mineral activity of the clays.

As discussed above, the parameters that appear in the relationships linking $G_{MAX}$ to stress level, void ratio and OCR are all, to a more or less degree, dependent on the composition of the clay and in particular on the plasticity of the clay. Several researchers (Hardin and Black 1968, Hardin 1978, Vucetic and Dobry 1991) suggest that as the plasticity of the soil decreases, the OCR exponent *k* tends to zero rendering the behavior of the soil increasingly less sensitive to the stress history. When PI reaches zero, i.e. for sands, the effect of OCR becomes negligible. The data available in the literature also suggest that the stress level exponent *n* and possibly the void ratio function depend on the plasticity of the soil. Viggiani and Atkinson (1995) report data indicating that, at least for reconstituted soils, the structure factor is also influenced by the plasticity of the soil: $S_{ij}$ appears to decrease quite markedly with increasing PI. Most likely, for intact materials, other aspects such as fabric and cementation will play a major role in determining $S_{ij}$.

Not surprisingly an increase in plasticity, which is associated with an increase of the ratio $C_\alpha/C_c$, is also often accompanied by a greater susceptibility to aging effects. It has been shown that the dependence of $G_{MAX}$ on both strain rate and aging (Anderson and Stokoe 1978, Kokusho et al. 1982) increases with PI.

#### *2.3.2.2 Factors Affecting the Size of the Linear Region*

Fewer data are available in the literature regarding the factors affecting the size of the linear region. The definition of the linear threshold is quite arbitrary and various assumptions are made by different researchers (e.g., strain corresponding to $G = 0.98G_{MAX}$, Georgiannou et al. 1991) to obtain numerical values. Experimental determination of linear threshold strain, which for most cohesive soils is on the order of 0.001-0.005%, is somewhat difficult as it is dramatically affected by strain rate and prestraining, and is generally overestimated by dynamic and cyclic tests. Consequently only triaxial or monotonic torsional shear tests can be employed to define its position under static loading conditions.

The following factors appear to affect to some degree the magnitude of the linear threshold: soil plasticity, strain rate, aging, OCR, pre-shear stress path and lateral stress ratio. Except for one case, relative to the effect of strain rate (Shibuya et al. 1996) the data available in the literature provide only qualitative information on the role of these parameters and no analytical relationships are available. These qualitative trends are summarized below.

***Soil Plasticity***

There is evidence in the literature (e.g., Vucetic 1994, Vucetic and Dobry 1991, Georgiannou et al. 1991) that increases in plasticity index lead to a marked increase in the linear threshold strain. Figure 2.9 summarizes the values for the linear threshold strain obtained from resonant column tests performed on a variety of soils with different values of the plasticity index.[2] Vucetic and Dobry (1991) explain this result hypothesizing that "the microstructural bonds and repulsion forces in higher plasticity soils act like a system of flexible linear springs that have the ability to take relatively larger shear strains before stiffness degradation effects appear."

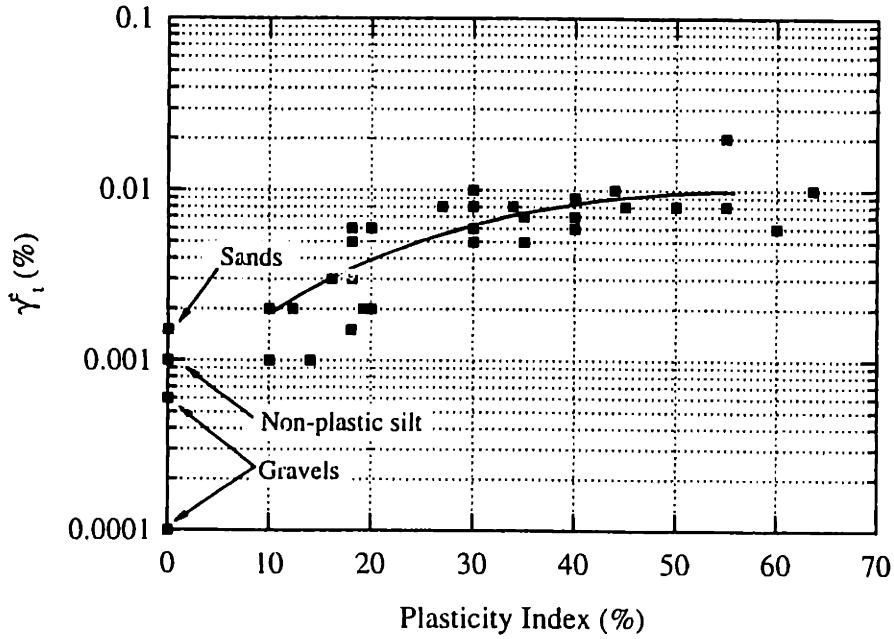


**Figure 2.9:** Linear threshold shear strain from resonant column tests (Lo Presti 1989).

***Strain Rate***

A comparison of the results of dynamic tests and static tests such as that shown in Figure 2.5 indicates that as strain rate increases so does the size of the linear region. An even clearer picture is furnished in Figure 2.10 which shows results presented by Shibuya et al. (1996). For the rather limited strain rate range considered (0.01%/min – 1.40%/min), these researchers found that, in undrained triaxial, compression the linear threshold $\varepsilon_{lin}$ of a reconstituted clay (PI=26) increased proportionally to the square root of the strain rate.

[2] As discussed above, higher strain rates such as those employed in the resonant column device, lead to overestimates of the linear threshold. This effect is expected to be increasingly significant for higher values of the plasticity index.

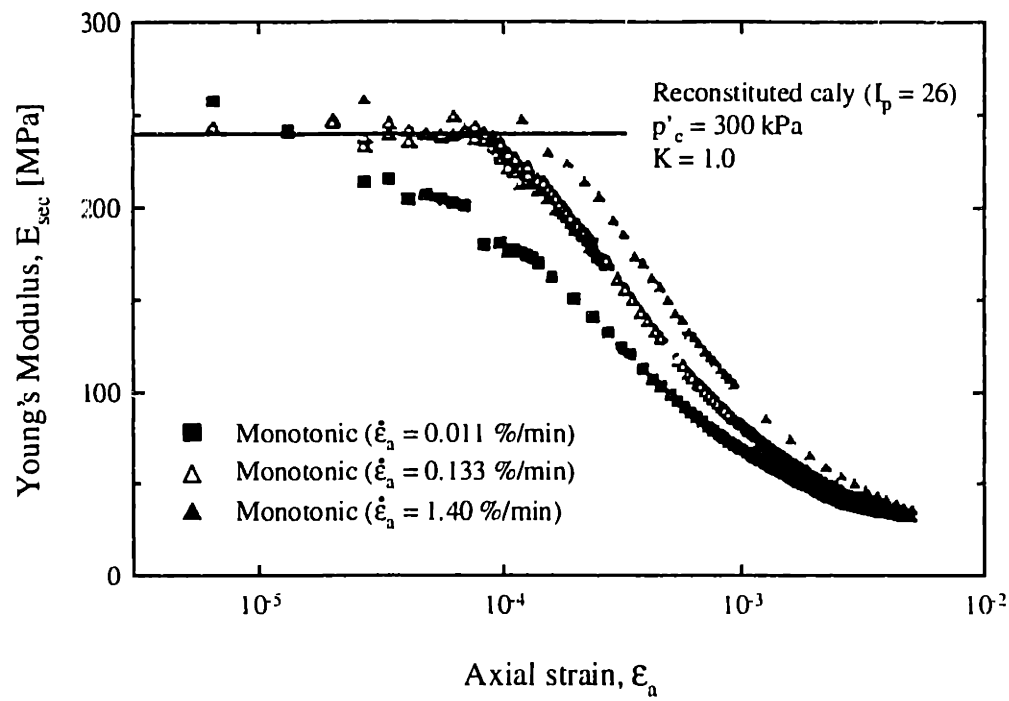


**Figure 2.10:** Effect of strain rate on Young's modulus measured in monotonic CIUC triaxial tests performed on reconstituted clay [p'=mean stress] (Shibuya et. al. 1996).

### *Aging*

Although limited comparisons of the stress-strain behavior of intact and reconstituted soils found in the literature suggest that prolonged aging causes the linear threshold to extend, no quantitative correlation linking $\Delta\varepsilon_{lin}$ to $t/t_p$ as seen above for the maximum stiffness is presented.

### *Overconsolidation Ratio*

While it appears well established (Jardine 1994) that over-consolidation makes the response of the soil increasingly linear with increasing OCR, no quantitative correlation between OCR and the size of the linear region exists in the literature.

### *Pre-shear Lateral Stress Ratio*

There is conflicting data in the literature regarding the effect of the pre-shear stress ratio on the linear threshold. Shibuya et al. (1996) propose that the linear threshold is insensitive to the pre-shear K. This conclusion however appears to be based on quite limited data. On the other hand a comparison of hydrostatically and $K_0$-consolidated specimens (Figure 2.11) indicates that the stiffness degradation is delayed for K equal to 1.

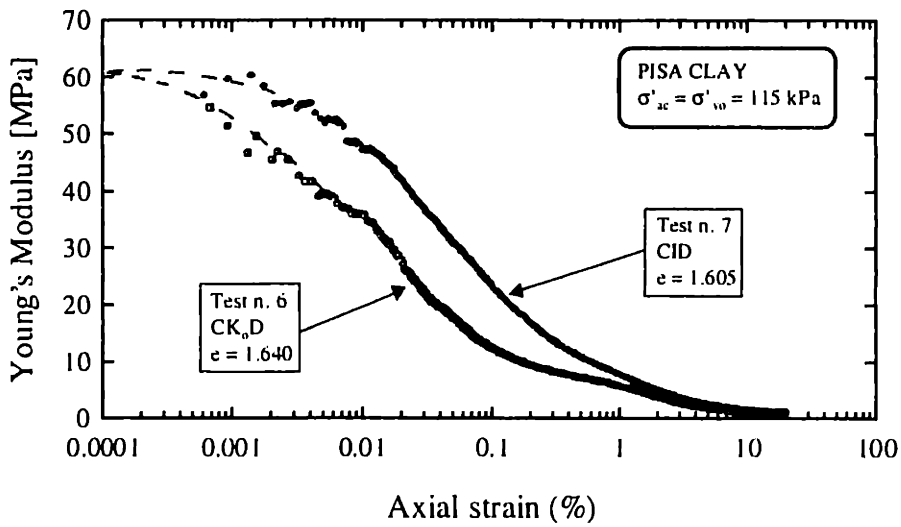


**Figure 2.11:** Comparison of stiffness of hydrostatically and one dimensionally consolidated Pisa clay during drained triaxial compression loading (Lo Presti et. al. 1995).

### *Pre-Shear Stress Path*

When the aging period experienced by the soil at the current stress state is short, the effects of recent stress history become important (Tatsuoka et al. 1997). In particular the small strain stiffness becomes dependent on the pre-shear stress path. Regarding the initial linear behavior of soils it has been found that the linear threshold extends as the relative angle between the recent effective stress path trajectory and the direction of the perturbing path decreases (Atkinson et al. 1990, Jardine et al. 1991).

## 2.3.3 The Pre-Failure Non-Linear Region

### *2.3.3.1 Overview*

As shown in Figures 2.3, 2.5, and 2.11 once the soil is sheared past its linear threshold, its stress-strain response becomes highly non-linear and the stiffness rapidly degrades with strain. Description of the behavior within this region is quite complex since factors in addition to those discussed in 2.3.2.1 influence the behavior of the soil, and the dependence of the soil stiffness on such factors varies with strain level. Most importantly, creep and strain rate phenomena have greater influence on the behavior of the soil as is shown in Figures 2.5 and 2.10, and plastic deformations become increasingly important.

Different types of behavior can be observed within this region. In the early part of the non-linear region, up to a critical value of the strain, the behavior of the soil can, on first approximation, be considered non-linear elastic as static unload-reload tests (e.g., Jardine 1992) indicate minimal irrecoverable strains. An additional behavioral threshold corresponding to the onset of significant plastic strains can therefore be identified. The surface defined in stress space by this threshold is commonly referred to as $Y_2$ in the simplified framework proposed by Jardine (1992). This boundary is conceptually analogous to the cyclic threshold that, in cyclic tests, defines the strain amplitude above which permanent pore-water pressure changes occur in the soil (e.g., Vucetic 1994). According to Vucetic (1994) this point is reached, regardless of the type of soil, when the modulus is reduced by about 35%. Tatsuoka et al. 1997 hypothesize that when the boundary of the linear region is engaged, local yielding develops at a large number of particle contacts, but that significant plastic straining, associated with interparticle slippage, is delayed until the stress point crosses the $Y_2$ surface. For most geomaterials the strain values that define the position of $Y_2$ vary between 0.007% and 0.06% depending on, among other factors, soil type, age and stress history. Figure 2.12 shows the position of $Y_2$ (here assumed, as commonly done, to be coincident with the 0.01% major principal strain contour) for Magnus Till with OCR varying between 1 and 17 and provides an illustration of its kinematic nature: as an effect of overconsolidation, the dimension, the shape and the position of $Y_2$ with respect to the pre-shear stress state are modified.

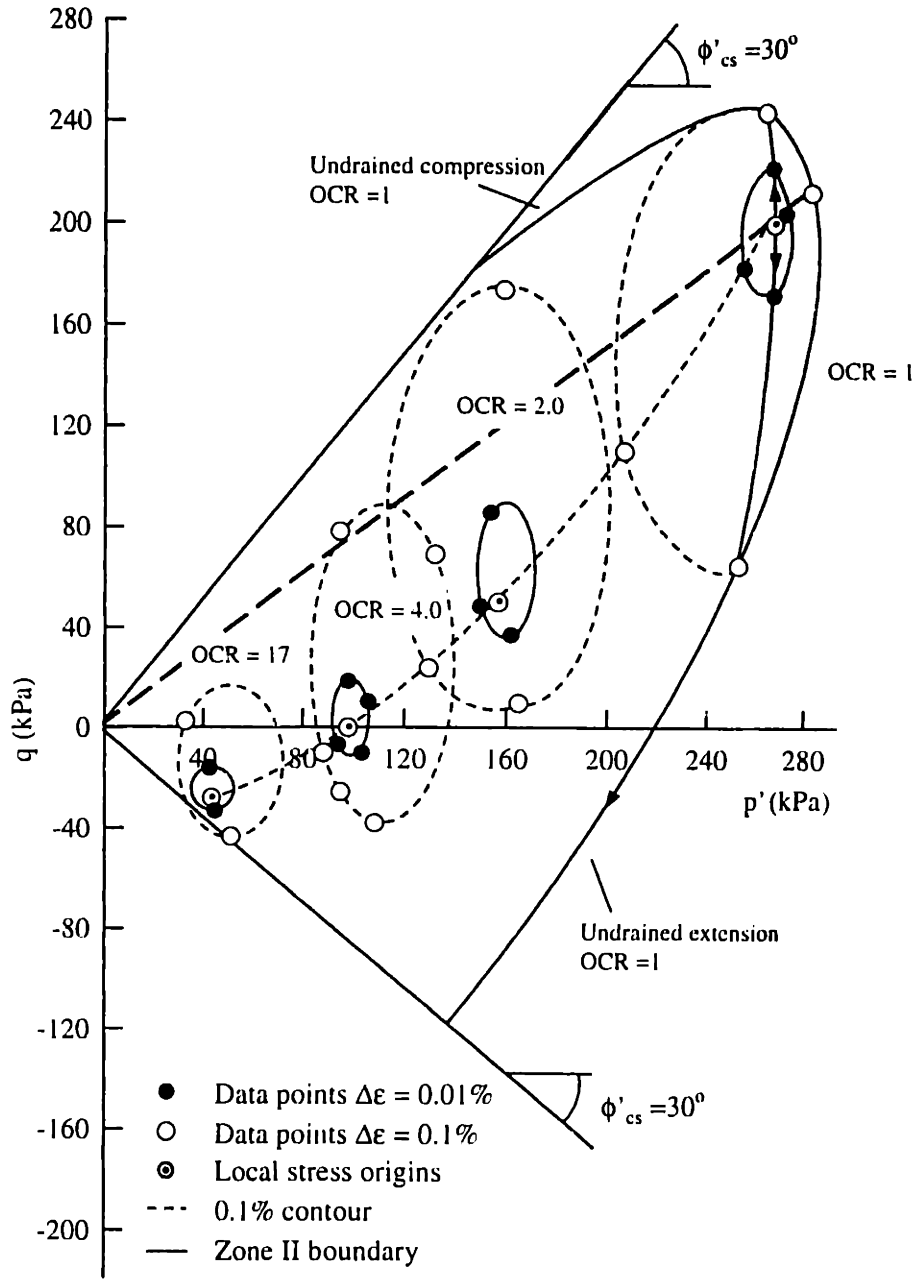


**Figure 2.12:** Position of $Y_2$ sub-yield surface for NC and OC Magnus Till (Jardine 1992).

Within the early part of the non-linear region the behavior of the soil also appears to be markedly influenced by the consolidation path followed in approaching the pre-shear stress state. In the second part of the non-linear region, the non-linearity of the soil gradually increases as plastic deformation of the soil becomes increasingly important. Results obtained by Jardine (1992) for Magnus Till indicate that deformations are still far from being purely plastic

($\varepsilon_{plastic}/\varepsilon_{total}$<<1) and that it is only when the soil enters the large strain region (Figure 2.13) that plastic strains become dominant.

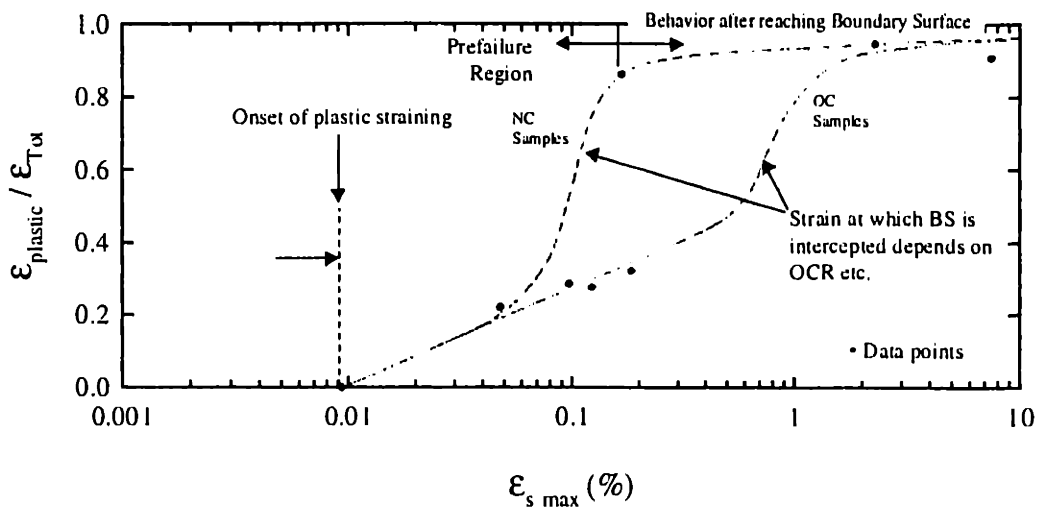


**Figure 2.13:** Relationship between permanent and total strain for Magnus Till (Jardine 1992).

### *2.3.3.2 Factors affecting the stiffness in the non-linear region*

***Stress Level***

As for the initial modulus, the stiffness in the non-linear region is also dependent on the stress level through an exponential type function. However, as the soil is sheared past the linear threshold, the stiffness $E_{ij}$ ceases to be dependent solely on the stress components in the *i* and *j* direction. In particular, the vertical Young's modulus is found to be controlled not only by the axial stress but also by the stress acting in the horizontal direction and, therefore, by the lateral stress ratio as is shown in Figure 2.11. The stress level dependence is commonly written in the form : $E(\varepsilon)= p_m'^{\,n(\varepsilon)}$ with $p_m'$ being the mean effective stress. The exponent is a function of strain level. It has been found that for reconstituted kaolin *n* increases with strain (Figure 2.14, Viggiani and Atkinson 1995)[3]. As shown in Figure 2.15 (Jardine 1994), the same type of trend is reported for a variety of other soils. The data presented by Jardine (1994) and by Viggiani and Atkinson (1995) indicate that with strain level the stiffness tends to become linearly dependent upon $p_m'$ and the stress level exponent approaches a limit value equal to one. Higher values of the exponent are reported by Lo Presti (1994) for Toyoura sand.

[3] Note that this exponent is different from that presented in Section 2.3.2.1, and should be more appropriately indicated with a different symbol (e.g., $\mathfrak{n}$)

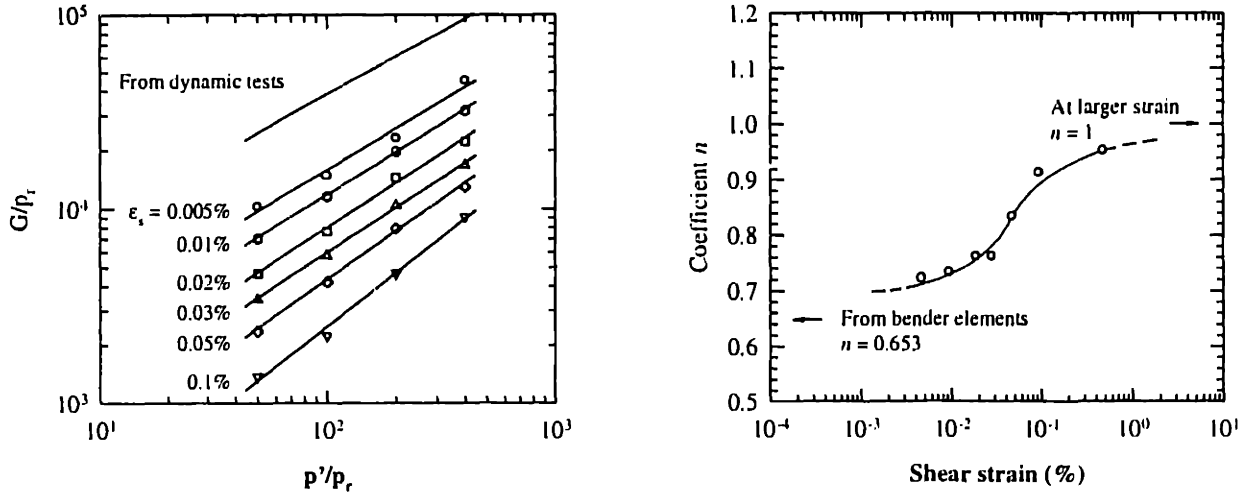


**Figure 2.14:** Increase of stress level exponent with strain for NC kaolin [CIUC tests, p'= mean consolidation stress, $p_r$= reference pressure] (Viggiani and Atkinson 1995).

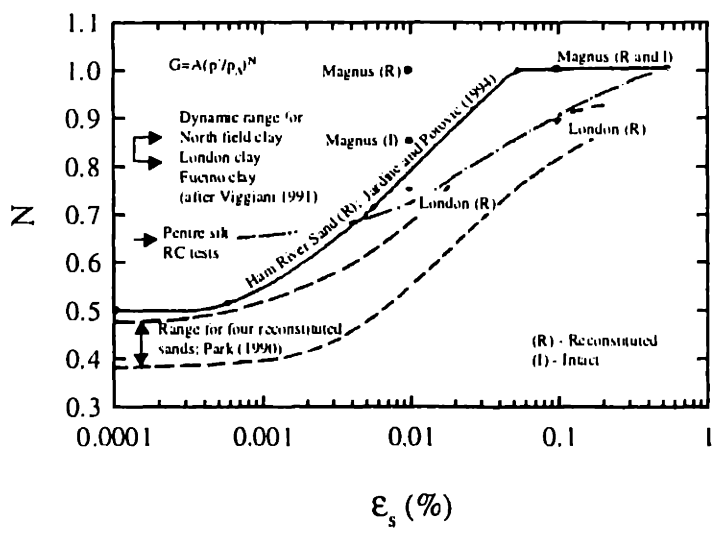


**Figure 2.15:** Effect of strain on stress level exponent (Jardine 1994).

### *Void ratio*

Very little information is available regarding the influence of void ratio on soil stiffness once the strain exceeds the linear threshold. However, there is some speculation (Porovic and Jardine 1994) that, at least for sands, the void ratio becomes less important as the strain level increases.

### *OCR*

As the soil enters the region of non-linear behavior, the effects of overconsolidation become more marked. Overconsolidation affects both the magnitude of the stiffness at any strain level, as well as the stiffness non-linearity. Although, for the same consolidation stress, the stiffness of overconsolidated clays is always higher than that of NC clays, there is no clear trend with OCR. As shown in Figure 2.16 for a variety of soils, the ratio $E_u/p_m'$ at 0.01% may rise or fall as the OCR increases from 2 to 10, depending on the soil.

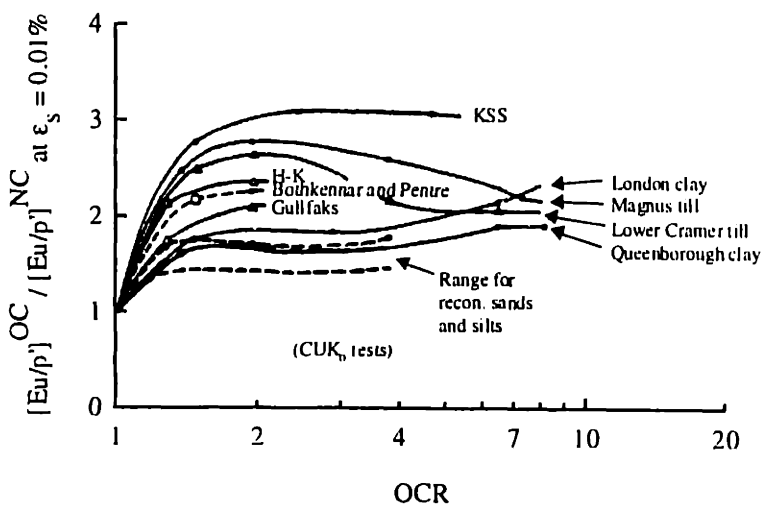


**Figure 2.16:** Effect of OCR on undrained compression stiffness at 0.01% [p'= mean consolidation stress] (Jardine 1994).

In general an increase in OCR is associated with a decreased strain level dependency of the secant stiffness which makes the response progressively more linear as the OCR increases and delays the development of large scale yielding (Figure 2.13).

### *Strain Rate*

Unlike granular soils (Lo Presti et al. 1997), the stress-strain behavior of cohesive soils is significantly influenced by strain rate once the soil has been strained beyond the linear threshold. As was shown earlier in Figure 2.10, higher strain rates lead to higher values of the stiffness at a given strain level. The effect of strain rate on soil stiffness can be quantified through the coefficient of strain rate $\alpha$ (Lo Presti 1989) which is defined, at any strain level, as the increase in

shear stiffness over one logarithmic cycle of strain rate, normalized by the shear modulus obtained employing the reference rate:

$$\alpha(\gamma) = \frac{\Delta G(\gamma)}{\Delta(\log \dot{\gamma}) \cdot G(\gamma, \dot{\gamma}_{ref})} \qquad \textit{Equation 2.3}$$

Figure 2.17 shows the coefficient of strain rate versus the axial strain as obtained from tests on various intact and reconstituted clays and indicates that α increases with strain level and plasticity index.

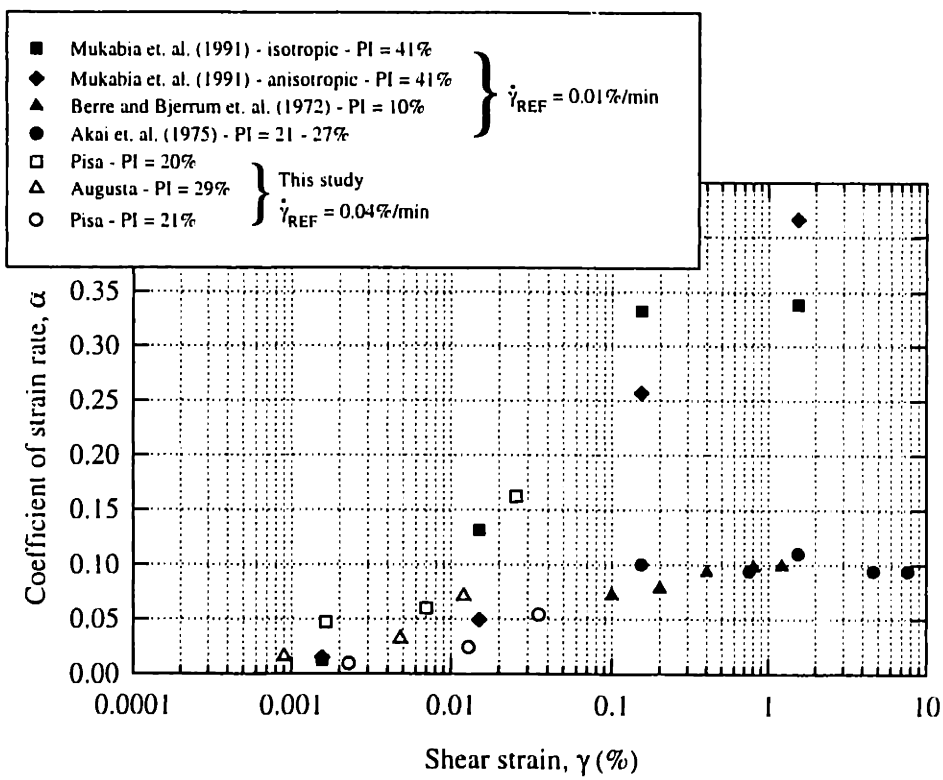


**Figure 2.17:** Coefficient of strain rate, α, versus strain (Lo Presti et. al. 1996).

Conflicting results are reported in the literature regarding the effect of the loading mode on the stress-strain behavior of cohesive soils. Monotonic tests generally show a stress response softer than that resulting from cyclic loading. According to some (e.g., Lo Presti et al. 1996, 1997) this behavior cannot be solely explained by the different strain rates characteristic of these tests, and must be therefore attributed to the different loading conditions. On the other hand, data

presented by Shibuya et al (1996) indicates no significant differences between cyclic and monotonic tests performed employing similar strain rates.

### *Pre-Shear Stress Path*

Work by Atkinson et al. (1990), Jardine et al. (1991), Smith (1992) and others indicate that the behavior of clays in the non-linear region is markedly affected by the pre-shear stress path. According to Atkinson et al. (1990), there is a general trend for the stiffness of reconstituted clays to increase when the effective stress path turns through a sharp corner. The stiffness varies systematically according to the angle $\theta$ between the recent stress path trajectory and the direction of the perturbing path: the maximum and minimum stiffness values are reached respectively for values of $\theta$ equal to 180 ° and 0 °. Similar features are observed by Jardine et al. (1991) in the behavior of intact overconsolidated London clay.

Sensitivity to the pre-shear stress path seems to be particularly marked in the early part of the non-linear region, and is more pronounced in higher plasticity soils (Atkinson et al. 1990).

### *Soil Composition*

In the non linear region there appears to be a general trend of decreasing stiffness with increasing plasticity (e.g., Vucetic 1994). This is shown in Figure 2.18 which summarizes data from undrained triaxial compression tests performed on 20 different cohesive soils all with OCR~1.5 and consolidation stress varying within a fairly limited range (100-250kPa). The Young's modulus at 0.01% is used in this figure as a measure of the stiffness in the early part of the non linear region. The spread in the results reflects partly the different stress levels and the fabrics of the various soils.

Composition also influences the degree of non-linearity exhibited by soils. A trend exists for low plasticity clays to show a steeper reduction in stiffness with strain than more plastic soils. This has been shown very clearly by Vucetic and Dobry (1991) who present an extensive review of the effects of soil plasticity on the cyclic response of soils. These researchers propose that soil plasticity is the main factor controlling the modulus reduction curve ($G/G_{MAX}$ versus $\gamma$) during cyclic loading.

As seen for the linear threshold, the second threshold, which defines the position of the $Y_2$ surface, also increases with increasing soil plasticity (Vucetic 1994).

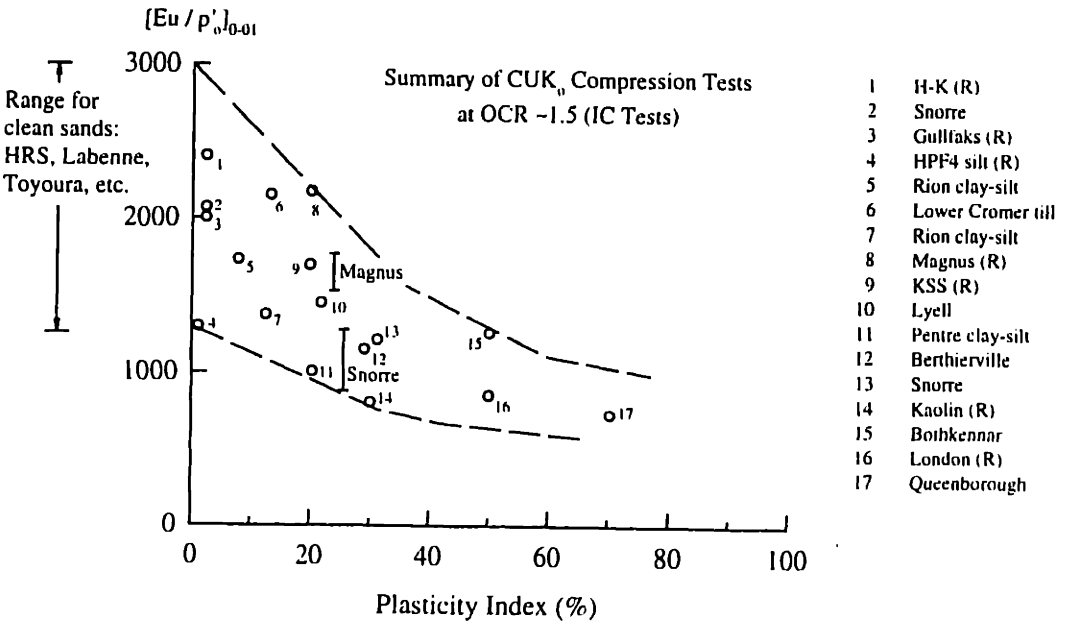


**Figure 2.18:** Effect of plasticity index on stiffness at 0.01% strain (Jardine 1994).

## 2.4 REFERENCES


1. Afifi, S.S. and Richart, F.E. (1973), "Stress History Effects on Shear Modulus of Soils," ***Soils and Foundations***, 13 (1), pp. 77-95.

2. Ampadu, S.K. and Tatsuoka, F. (1993), "A Hollow Cylinder Torsional Simple Shear Apparatus Capable of a Wide Range of Shear Strain Measurement," ***Geotechnical Testing Journal***, 16 (1), pp. 3-17.

3. Andersen, G.R., Swan, C.W., Ladd, C.C. and Germaine, J.T. (1995), "Small-Strain Behavior of Frozen Sand in Triaxial Compression," ***Canadian Geotechnical Journal***, 32, pp. 428-451.

4. Anderson, D.G. and Woods, R.D. (1976), "Time-Dependent Increase in Shear Modulus of Clay," ***Journal of the Geotechnical Engineering Division***, ASCE, 102 (GT5), pp. 525-537.

5. Anderson, D.G. and Stokoe, K.H. (1978), "Shear Modulus: A Time Dependent Soil Property," **Dynamic Geotechnical Testing**, ASTM STP 654, pp. 66-90.

6. Atkinson, J.H., Richardson, D., and Stallebrass, S.E. (1990), "Effect of Recent Stress History on the Stiffness of Overconsolidated Soil," ***Géotechnique***, 40 (4), pp. 531-540.

7. Bellotti, R. Jamiolkowski, M., Lo Presti, D.C.F. and O'Neill, D.A. (1996), "Anisotropy of Small Strain Stiffness in Ticino Sand," ***Géotechnique, 46 (1)***pp. 115-131.

8. Brown, S.F. Austin, G., and Overy, R.F. (1980), "An Instrumented Triaxial Cell for Cyclic Loading of Clays," ***Geotechnical Testing Journal***, 3 (4), pp. 145-152.

9. Burland, J.B. (1989), "'Small is Beautiful' – The Stiffness of Soils at Small Strains," 9th Laurits Bjerrum Memorial Lecture, Canadian Geotechnical Journal, 26, pp. 499-516.

10. Burland, J.B. and Symes, M. (1982), "A Simple Axial Displacement Gauge for Use in the Trixial Apparatus," ***Géotechnique***, 32 (1), pp. 62-65.

11. Clayton and Khatrush (1987), "A New Device for Measuring Local axial Strains on Triaxial Specimens," ***Géotechnique***, 36 (4), pp. 593-597.

12. Costa-Filho, L. (1985), "Measurement of Axial Strains in Triaxial Tests on London Clay," ***Geotechnical Testing Journal***, 8 (1), pp. 3-13.

13. Cuccovillo, T. and Coop, M.R. (1997b), "The Measurement of Local Axial Strains in Triaxial Tests Using LVDT's," ***Géotechnique***, 47 (1), pp. 167-171.

14. Douroudian, M. and Vucetic, M. (1995), "A Direct Simple Shear Device for Measuring Small-Strain Behavior," ***Geotechnical Testing Journal***, 18 (1), March, pp. 69-85.

15. Duffy, J. and Midlin, R.D. (1957), "Stress Strain Relations and Vibrations of a Granular Medium," ***Journal of Applied Mechanics***, 24, pp. 585-593.

16. Georgiannou, V.N., Rampello, S. and Silvestri, F. (1991), "Static and Dynamic Measurements of Undrained Stiffness on Natural Overconsolidated Clays," *Proc. Xth European Conference on Soil Mechanics and Foundation Engineering*, Vol. 1, pp. 91-96.

17. Goto S., Tatsuoka, F., Shibuya, S., Kim, Y-S, and Sato, T. (1991), "A Simple Gauge for Local Small Strain Measurements in the Laboratory," ***Soils and Foundations***, 31 (1), pp. 169-180.

18. Hardin, B.O. and Black, W.L. (1966), "Sand Stiffness under Various Triaxial," ***Journal of the Soil Mechanics and Foundation Division***, ASCE, 92 (SM2), March, pp. 27-42.

19. Hardin, B.O. and Black, W.L. (1968), "Vibration Modulus of Normally Consolidated Clay," ***Journal of the Soil Mechanics and Foundation Division***, ASCE, 94 (SM2), March, pp. 353-369.

20. Hardin, B.O. and Black, W.L. (1978), "The Nature of Stress-Strain Behavior of Soils," *Proc. ASCE Specialty Conference on Earthquake Engineering and Soil Dynamics*, Pasadena, California, Vol.1, pp.3-90.

21. Hardin, B.O. and Drnevich V.P., (1972), "Shear Modulus and Damping in Soils: Measurement and Parameter Effects," ***Journal of the Soil Mechanics and Foundation Division***, ASCE, 98 (SM6), June, pp. 603-624.

22. Hicher, P.Y. (1996), "Elastic Properties of Soils," ***Journal of Geotechnical Engineering***, 122, 8, pp.641-648.

23. Hight, D.W., Bennell, J.D., Chana, B., Davis, P.D., Jardine, R.J., and Porovic, E. (1997), "Wave Velocity and Stiffness Measurements of the Crag and Lower London Tertiaries at Sizewell," ***Géotechnique***, 47 (3), pp. 451-474.

24. Hird, C.C. and Yung, P.C.Y. (1989), "The Use of Proximity Transducers for Local Strain Measurements in Triaxial Cells," ***Geotechnical Testing Journal***, 12 (1), pp. 292-296.

25. Jamiolkowski, M., Lancellotta, R., and Lo Presti, D.C.F. (1994), "Remarks on the Stiffness at Small Strains of Six Italian Clays," *Proc. Int. Symp. Pre-Failure Deformation Characteristics of Geomaterials*, Hokkaido'94, Vol. 2, pp. 817-854.

26. Jardine, R.J. (1992), "Some Observations on the Kinematic Nature of Soil Stiffness," ***Soils and Foundations***, 32 (2), pp. 111-124.

27. Jardine, R.J. (1994), "One Perspective of the Pre-Failure Deformation Characteristics of Some Geomaterials," *Proc. Int. Symp. Pre-Failure Deformation Characteristics of Geomaterials (IS-Hokkaido'94)*, Vol. 2, pp. 855-885.

28. Jardine, R.J., St. John, H.D. Hight, D.W. and Potts, D.M., (1991), "Some Practical Applications of a Non-Linear Ground Model," *Proc. X$^{th}$ European Conference on Soil Mechanics and Foundation Engineering*, Vol. 1, pp. 223-228.

29. Jardine, R.J., Symes, M.J. and Burland, J. B. (1984), "The Measurement of Soil Stiffness in the Triaxial Apparatus," ***Géotechnique***, 34 (3), pp. 323-340.

30. Kim, D.S. and Stokoe, K.H. (1994), "Torsional Motion Monitoring System for Small Strain ($10^{-5}$% to $10^{-3}$%) Soil Testing," ***Geotechnical Testing Journal***, 17 (1), pp. 17-26.

31. Kim, T.C. and Novak, M. (1981), "Dynamic Properties of Some Cohesive Soils of Ontario," ***Canadian Geotechnical Journal***, 18, pp. 371-389.

32. Kohata, Y., Tasuoka, F., Dong, J., Teachavorasinskun, S., and Mizumoto, K. (1994), "Stress States Affecting Elastic Deformation Moduli of Geomaterials," *Proc. Int. Symp. Pre-Failure Deformation Characteristics of Geomaterials (IS-Hokkaido'94)*, Vol. 1, pp. 3-9.

33. Kokusho, T. Yoshida, Y. and Esashi, Y. (1982), "Dynamic Properties of Soft Clay for Wide Strain Range," ***Soils and Foundations***, 22 (4), pp. 1-18.

34. Lambe, T.W. and Whitman, R.V. (1969), **Soil Mechanics**, John Wiley and Sons, New York, 553 p.

35. Lanzo, G., Vucetic, M. and Douroudian, M. (1995), "Reduction of Shear Modulus at Small Strain in Simple Shear," ***Journal of Geotechnical and Geoenvironmental Engineering***, 123 (11), November, pp. 1035-1042.

36. Leroueil, S. and Jamiolkowski, M. (1991), "Exploration of Soft Soil and Determination of Design Parameters," *Proc. Geo-Coast '91*, Yokohama, Japan.

37. Lo Presti, D. C. F., Pallara, O., Lancellotta, R., Armandi, M., and Maniscalo, R. (1993), "Monotonic and Cyclic Loading Behavior of Two Sands at Small Strains," ***Geotechnical Testing Journal***, 16 (4), pp. 409- 424.

38. Lo Presti, D.C.F. (1989), "Proprieta' Dinamiche dei Terreni," XIV Conferenza Geotecnica di Torino, Politecnico di Torino (in Italian).

39. Lo Presti, D.C.F. (1994), "General Report: Measurement of Shear Deformation of Geomaterials," *Proc. Int. Symp. Pre-Failure Deformation Characteristics of Geomaterials*, Hokkaido'94, Vol. 2, pp. 1067-1088.

40. Lo Presti, D.C.F., Jamiolkowski, M., Pallara, O. and Cavallaro, A. (1996), "Rate and Creep Effect on the Stiffness of Soils," ASCE Convention, Washington, 10-14 Nov. 1996, ***Geotechnical Special Publication No.61***, pp.166-180.

41. Lo Presti, D.C.F., Jamiolkowski, M., Pallara, O., Cavallaro, A. and Pedroni, S. (1997), "Shear Modulus and Damping of Soil," ***Géotechnique***, 47 (3), pp. 603-617.

42. Lo Presti, D.C.F., Pallara, O. Costanzo, D. and Impavido, M. (1994), "Small Strain Measurements during Triaxial Tests: Many Problems, Some Solutions," *Proc. Int. Symp. Pre-Failure Deformation Characteristics of Geomaterials (IS-Hokkaido'94)*, 1, pp. 11-16.

43. Lo Presti, D.C.F., Pallara, O., and Puci, I. (1995), "Modified Commercial Triaxial Testing System for Small Strain Measurements: Preliminary Results on Pisa Clay," ***Geotechnical Testing Journal***, 18 (1), March, pp. 15-31.

44. Mesri, G. and Choi, Y.K. (1983), "Discussion - Dynamic Properties of Soft Clays for Wide Strain Range," ***Soils and Foundations***, 23 (1), pp. 125-127.

45. Mukabi, J.N., Tatsuoka, F., Kohata, Y., Tsuchida, T., and Akino, N. (1994), "Small Strain Stiffness of Pleistocene Clays in Triaxial Compression," *Proc. Int. Symp. Pre-Failure Deformation Characteristics of Geomaterials (IS-Hokkaido'94)*, Vol. 1, pp. 189-195.

46. Park, C.S. and Tatsuoka, F. (1994), "Aniusotropic Strength and Deformation of Sands in Plane Strain Compression," *Proc. 13th Int. Conf. On Soil Mechanics and Foundation Engineering*, New Delhi, Vol.1, pp.1-6.

47. Porovic, E. and Jardine, R.J. (1994), "Some Observations on the Static and the Dynamic Shear Stiffness of Ham River Sand," *Proc. Int. Symp. Pre-Failure Deformation Characteristics of Geomaterials (IS-Hokkaido'94)*, Vol. 1, pp. 25-30.

48. Roesler, S.K. (1979), "Anisotropic Shear Modulus due to Stress-Anisotropy," ***Journal of the Geotechnical Engineering Division***, ASCE, 105 (GT7), pp. 871-880.

49. Scholey, G.K., Frost, D.J., Lo Presti, D.C.F., and Jamiolkowski, M. (1995), "A Review of Instrumentation for Measuring Small Strains During Triaxial Testing of Soil Specimens," ***Geotechnical Testing Journal***, 18 (2), June, pp. 137-156.

50. Sheahan, T.C. and Germaine, J.T. (1992), "Computer Automation of Conventional Triaxial Equipment," ***Geotechnical Testing Journal***, 15 (4), pp. 311-322.

51. Sheahan, T.C., Ladd, C.C., and Germaine, J.T. (1996), "Rate-Dependent Undrained Shear Behavior of Saturated Clay," ***Journal of Geotechnical Engineering***, ASCE, 122 (2), February, pp. 99-108.

52. Shibuya, S., Hwang, S.C., and Mitachi, T. (1997), "Elastic Shear Modulus of Soft Clays from Shear Wave Velocity Measurement," ***Géotechnique***, 47 (3), pp. 593-601.

53. Shibuya, S., Mitachi, T., Hosomi, A. and Hwang, S.C. (1996), "Strain Rate Effects on Stress-Strain Behavior of Clay as Observed in Monotonic and Cyclic Triaxial Tests," ASCE Convention, Washington, 10-14 Nov. 1996, ***Geotechnical Special Publication No.61***, pp.214-227.

54. Smith, P.R. (1992), "Properties of High Compressibility Clays with reference to Construction on Soft Ground," Phd. Thesis, University of London.

55. Stokoe, K.H., Hwang, S.K., Lee, J.N.-k. and Andrus, R.D. (1994), "Effects of Various Parameters on the Stiffness and Damping of Soils at Small to Medium Strains," *Proc. Int. Symp. Pre-Failure Deformation Characteristics of Geomaterials, (IS-Hokkaido'94)*, Vol. 2, pp. 785-816.

56. Tatsuoka, F., Jardine, R.J., Lo Presti, D.C.F., Di Benedetto, H. and Kohata, Y. (1997), "Characterising the Pre-Failure Deformation Properties of Geomaterials," *Hamburg Keynote Lecture.*

57. Tatsuoka, F. and Kohata, Y. (1994), "One Perspective of the Pre-Failure Deformation Characteristics of Some Geomaterials," *Proc. Int. Symp. Pre-Failure Deformation Characteristics of Geomaterials, (IS-Hokkaido'94)*, Vol. 2, pp. 947-1053.

58. Tatsuoka, F. and Shibuya, S. (1992), "Deformation Characteristics of Soil and Rocks from Field and Laboratory," Keynote Lecture, *Proc. IX Asian Conference on Soil Mechanics and Foundation Engineering, Bangkok*, 1991 2, pp.101-170.

59. Viggiani, G. and Atkinson, J.H. (1995), "Stiffness of Fine-Grained Soil at Very Small Strains," ***Géotechnique,*** 45 (2), pp.249-265.

60. Vucetic M. and Dobry R. (1991), "Effect of Soil Plasticity on Cyclic Response," ***Journal of Geotechnical Engineering***, ASCE, 117 (1), pp. 89-107.

61. Vucetic, M. (1994), "Cyclic Threshold Shear Strain in Soils," ***Journal of Geotechnical Engineering***, ASCE, 120 (12), pp. 2208-2228.

62. Woods, R. D. (1994), "Laboratory Measurement of Dynamic Soil Properties," **Dynamic Geotechnical Testing II**, ASTM, STP 1213, pp. 165-190.

63. Woods, R.D. (1991), "Field and Laboratory Determination of Soil Properties at Low and High Strains," *Proc. 2nd Int. Conf. On Recent Advances in Geotechnical Earthquake Engineering and Soil Dynamics*, St. Louis, Vol. II, pp. 1727-1743.

64. Zdravkovic, L. and Jardine, R.J. (1997), "Some Anisotropy Stiffness Characteristics of a Silt under General Stress Conditions," ***Géotechnique***, 47 (3), pp. 407-437.

# CHAPTER 3

## RESEDIMENTED BOSTON BLUE CLAY

### 3.1 INTRODUCTION

This chapter presents an overview of Resedimented Boston Blue Clay (RBBC), the material employed for the experimental program performed for this thesis. RBBC is a soil resedimented in the laboratory from natural Boston Blue Clay, an illitic CL clay consisting of glacial outwash deposited in a marine environment 14000 to 12000 years ago, in the period immediately following deglaciation of the Boston basin (Kenney 1964).

RBBC exhibits characteristics very similar to those of the original material, and to many natural cohesive soils, including stress-strain-strength anisotropy, low to medium sensitivity, and significant strain rate dependency. Along with its local relevance, its reproducible behavior, complete saturation and virtually infinite supply represent the key characteristics which have made this soil an ideal research material to investigate fundamental aspects of soil behavior without having to take into account the variability of natural soils.

Table 3.1 summarizes the research performed on Resedimented Boston Blue Clay since 1961, and also provides most of the history of geotechnical research at MIT during the last 40 years in the area of clay behavior. In fact, while many natural materials have been investigated at MIT during this period (e.g. Boston Blue Clay, Arctic soils, Venezuela Clay, Mexico City Clay, Taipei Clay etc.) most of the research on the fundamental aspects of clay behavior has been carried out on RBBC. The extensive study of the behavior of RBBC is also strongly linked to the development of soil models at MIT. The three generalized constitutive models formulated at MIT (MIT-E1 Kavvadas 1982, MIT-E3 Whittle 1987, MIT-S1 Pestana 1994) have all been validated using the extensive database for RBBC, which provides an unmatched source of information on soil behavior under a variety of testing conditions.

| YEAR | Researcher | Series | Batch | Topic | Tests Performed |
|---|---|---|---|---|---|
| 1961 | Bailey | Ia | MIT 1139 | Effect of salt concentration on undrained strength | - |
| 1963 | Jackson | | - | Thixotropy | CIU, CID on OCR 1 |
| 1964 | Varallyay | | S4, S5, S6 | Influence of stress system on undrained strength | TX CIUC/E $CK_0UC/E$ (NC) |
| 1965 | Ladd R.S. | Ib | - | Use of pressure transducer to measure soil pressure | - |
| 1965 | Preston | | S1 | Sample disturbance | Triaxial |
| 1966 | Braathen | | S2 | Disturbance effects on undrained strength | Triaxial |
| 1967 | Dickey | | 150, 160 | Development of plane strain device | Plane Strain Device |
| | Rixner | | 300, 400, 700 | Behavior in plane strain at OCR 1, 2, 4 | $CK_0U$-PSA and $CK_0U$-PSP OCR 1, 2, 4 |
| 1968 | Bovee | | 1000, 1100, 1200, 1300 | Behavior in plane strain at OCR 1, 2, 4 | $CK_0U$-PSA and $CK_0U$-PSP OCR 1, 2, 4 |
| 1970 | Kinner | | 100,150, 200, 300, 400, 800, 900, 1000, 1100, 1200, M101, M104, M107, M200, M400 | Behavior of strip footings during undrained loading | Model footing tests OCR 1, 2, 4 |
| 1971 | Ladd et al. | | 160, 1300, 1500 | Plane strain tests | Plane Strain Device |
| 1982 | Germaine | II | 101-104 | Cross-anisotropic behavior at OCR 4 | DSC, CIUCTX(rec), CIUETX(rec) all on OCR4 |
| 1984 | Bensari | | 105, 111 | Stress-strain and yielding behavior | $CK_0UC$, $CK_0UE$, $CK_0DC$, $CK_0DE$ OCR 1 and 4 |
| 1985 | O'Neill | | 105-112 | Anisotropy of thixotropic clay | DSC, TX(rec) |
| 1986 | Fayad | | 113 | Volumetric and undrained behavior | $CK_0UC$ on OCR 1, 2, 4, 8 OED |
| 1987 | Malek | | 111, 112 | Behavior under cyclic loading | $CK_0U$-DSS(Cyc) OCR 1,1.4,2,4 Monotonic OCR1 |
| 1988 | Walbaum | III | 200-202 | Investigation of sample disturbance | DSS (both incremental and CRS consolidation) |
| | Sheahan | | 107, 112, 202 | Modification of computer controlled triaxial apparatus | $CK_0UC$, $CK_0UE$ OCR 1 and 3.3 |
| 1989 | DeGroot | | 200-203 | Behavior in undrained multidirectional DSS at OCR1 | Multidirectional DSS OCR 1 |
| 1990 | Ahmed | | 204-205,207 | Normalized Behavior in DSS | DSS |
| | Seah | | 200-207 | Anisotropy at OCR1 | DSC |
| 1991 | Ting | | 211-213 | Performance of sand drains | - |
| 1991 | Sheahan | | 210, 214, 216 | Time dependent behavior | TX: $CK_0UC$, $CK_0UE$ OCR 1, 2, 4, 8 |
| 1992 | Ortega | | - | Computer automation of DSS | DSS |
| 1993 | Cauble | | 217-218 | Cyclic and post-cyclic behavior in simple shear | Monotonic (OCR 1, 2, 4) Cyclic (OCR4) $CK_0UDSS$ |
| 1994 | Santagata | | 216, 217, 218 219-220 | Effects of tube sampling disturbance and reconsolidation procedures OCR 1, 2, 4, 8 | $CK_0UTX$-standard and with simulation of disturbance and reconsolidation |
| 1994 | Sinfield | IV | 402-403 | Simulation of sampling and effects on compression and shear | Sampling from batch; CRS TX-UU on sampled soil |
| 1996 | Cauble | | 401, 404-411, 413-417 | Behavior of a model suction caisson | Installation and tensile loading of model caisson |
| 1998 | Santagata | | 418, 419 | Pre-failure behavior | $CK_0UC$-TX, CKUC-TX OCR 1, 2, 4, 8 |
| 1998 | Force | | 420 | Strain rate selection in triaxial tests | CRS testing (Wissa consolidometer, modified triaxial) |

**Table 3.1:** Overview of studies performed employing RBBC.

In addition, as apparent from Table 3.1, the well defined and repeatable behavior of RBBC has also made it an asset in the development and proofing of new laboratory apparatuses (Dickey 1967, Wissa and Heiberg 1969, Sheahan 1988), as well as in the modification or automation of existing devices (e.g., Germaine 1982, DeGroot 1989, Ortega 1992).

The use of laboratory resedimentation at MIT was pioneered by Wissa (1961) who designed the first apparatus for the production of large batches of clay. Resedimentation of Boston Blue Clay initiated in 1961 with the work performed by Bailey, under the direction of Professor C.C. Ladd, on the effect of salt concentration on the triaxial undrained strength of clays. More research on the triaxial behavior of clays and in particular on sample disturbance was performed in the following years culminating with the development of the simple clay concept (Ladd 1964) and the classical work on the Perfect Sampling Approach (Ladd and Lambe, 1963).

With the development by Dickey of the plane strain device, much effort went into understanding the behavior of RBBC in this mode of loading over the following years (e.g. Bovee and Ladd 1970, Ladd et al. 1971).

While limited work was performed using RBBC during the following decade, the 1980's and the 1990's have been punctuated almost yearly by investigations using this soil. This has been due primarily to the improvements in the resedimentation procedure introduced by Germaine in 1982 and the availability of new devices such as the Directional Shear Cell for which RBBC represented an ideal proof testing material. Significant advances in the understanding of the undrained anisotropy of clays were made in the following years, making use of this apparatus (Germaine 1982, O'Neill 1985, Seah 1990).

Starting in the mid 1980's, and thanks also to the establishment of the Center for Scientific Excellence in Offshore Engineering, much of the experimental research at MIT was driven by the design of offshore structures. In particular the DSS apparatus was extensively used to investigate the cyclic behavior of both natural soils (e.g., Arctic silt) and, because of the high costs of obtaining high quality samples from the field, of RBBC (Malek 1987, Cauble 1993).

The interest in the triaxial behavior of RBBC has remained a constant throughout the years (Varallyay 1966, Bensari 1983, Fayad 1985, Sheahan 1988, 1991, Santagata 1994, Sinfield

1994, Force 1998) and thanks to these data much has been learned about the factors affecting the undrained stress-strain-strength behavior of clays.

As seen in Table 3.1, in addition to providing material for laboratory element tests, entire batches of RBBC have been utilized to carry out model tests within the resedimentation consolidometer. These studies include work performed by Kinner (1970) on the behavior of strip footings, investigations on the performance of sand drains by Ting (1990), the analysis of tube sample disturbance by Sinfield (1994), and most recently an in depth evaluation of the performance of suction caissons (Cauble 1996).

Finally, note that Table 3.1 does not include research performed using RBBC slurry, in particular the work by Zreik (1994) on the erosional and low stress shear strength of clays.

The natural soil employed as source material for RBBC is present throughout the Boston area. Typical land deposits vary in thickness from 20 to 40 meters, and are overlain by a sand and gravel layer (0 to 15 m thick), a layer of organic silt (0 to 7 m) and about 3 meters of fill. A stiff overconsolidated (OCR=2-5) crust forms the upper 12 to 20 meters of the BBC deposit, while underneath the soil is often near normally consolidated. While the depositional and general characteristics of BBC are fairly similar throughout most of the Boston basin, variability in the soil retrieved from different locations, and thus in the resedimented BBC made from the different natural sources, should be expected. The index properties of the clay depend on many factors, including the particle size distribution, the mineralogy of the material, and the pore fluid chemistry. These may also vary at a given location as a function of depth.

The origin of the natural material employed to manufacture RBBC defines the batch series (Table 3.1), and when BBC from a new location is employed, the series number of the clay is incremented. To this day BBC has been obtained for resedimentation from four different locations and thus four series of RBBC exist. No exact record of the origin of Series I and II BBC is available. Series III made use of clay collected from pile augers at a depth of approximately 23 m at the construction site of a parking garage in Kendall Square, Cambridge. The natural soil for series IV, employed to prepare all the soil used in this thesis, was obtained from the base of an excavation for MIT's Biology Building (Building #68) at a depth of about 12 m, where the OCR of the soil varied between 1.3 and 3.4 (Berman 1993).

Resedimented Boston Blue Clay is produced, as discussed in the following section, in the form of batches. Throughout this chapter both index and engineering properties are always

referenced to the batch number. Unfortunately, the convention for numbering batches has varied over time. For series I RBBC the batches were numbered following no consistent method and often on a project by project basis. Starting from Series II all batches have been recorded. For Series II and III RBBC, the batches were numbered sequentially starting respectively from 100 and 200. For series IV it was decided that the first number of the batch should coincide with that of the series, and, consequently, batches were numbered from 400 up.

The resedimentation procedure, first developed in the early 1960's, has undergone considerable modifications through the years. The most significant improvements were introduced by Germaine (1982), who developed a method to produce fully saturated specimens. The equipment and the procedure presently used to manufacture RBBC are discussed in Section 3.2.

The following two sections (3.3 and 3.4) summarize the properties of RBBC. Because RBBC has been studied at MIT for over 40 years, its behavior as a function of stress history and stress system is well documented. Thus a database exists that permits comparison with any new experimental results. Section 3.3 presents the material index properties: grain size distribution, Atterberg limits, specific gravity and salt concentration data. These data are essential in verifying that the material from a new source exhibits characteristics similar to that of the soil previously used and in assuring batch to batch consistency.

Section 3.4 provides a summary of the knowledge of the mechanical behavior of RBBC. As apparent from Table 3.1, the database for RBBC is quite extensive and extends to a large number of devices and shearing modes. Section 3.4 analyzes in some detail the behavior during $K_0$-consolidation and during undrained triaxial compression, which are most relevant to the current research. Other aspects such as strain rate sensitivity and anisotropy are also briefly discussed in this section. In both Sections 3.3 and 3.4 the discussion is limited for the most part to the properties measured on the most recent batches of RBBC (series III and IV). When employing a laboratory manufactured soil to pursue fundamental research, the question is often raised as to whether the behavior of this material is representative of that of natural soils. A brief comparison of key properties of RBBC with those of a natural BBC is presented in Section 3.4.5.

Finally, Section 3.5 lists the most relevant references on the behavior of RBBC and natural Boston Blue Clay.

## 3.2 RESEDIMENTATION PROCEDURE

As mentioned above, the procedure for preparing Resedimented Boston Blue clay has been modified over its more than 35 years of use.

The early method (e.g. Ladd and Varallyay 1965) employed to manufacture RBBC consisted of mixing dry Boston Blue Clay powder and tap water at a water content of about 400%. The slurry was then passed through #100 and # 200 sieves and caused to flocculate by adding a small amount of a NaCl. After siphoning off the excess water, the resulting slurry with water content of approximately 140% was heated to 70°C under continuous stirring and poured under vacuum into an evacuated consolidometer and then consolidated in most cases to 1.5 ksc.

This procedure produced partially saturated samples that could only be saturated using a 2 ksc back pressure. This became a critical issue when RBBC was used for testing with the Directional Shear Cell (Germaine 1982) in which the soil specimens could not be back-pressure saturated. Therefore, Germaine substantially revised the technology for producing RBBC. Further modifications were introduced by Seah (1990) who improved the layout of the system to increase productivity, modified the technique for extrusion of the soil cake from the consolidometer and implemented remote data acquisition to provide continuous monitoring of the consolidation process.

The more than 50 batches used since 1982, including those employed for this research, have been manufactured using the following procedure[1] which can be divided into four main steps: powdering, resedimentation, consolidation and storage.

*a) Powdering*

After retrieving Boston Blue Clay from the ground, the soil is cleaned and powdered. Soil particles larger than medium sand and foreign objects such as wood and shells are removed by wet sieving the natural soil through a U.S. standard #40 sieve. The soil is then oven-dried, pre-crushed and pulverized into powder, to pass a #100 sieve. For the clay used in this research (series IV) this operation was performed by the Strurtevant Company using a roller mill. Prior to storage in sealed containers, the powder is manually randomized by several blending operations.

[1] Exceptions to this are the batches produced by Sinfield (1994) and Cauble (1996) for which a different consolidation procedure was followed.

*b) Resedimentation*

This operation takes place using the equipment shown schematically in Figure 3.1. The resedimentation apparatus consists of three major components: an upper mixing chamber, a lower free-fall chamber and the stainless steel consolidometer. These three elements are mounted one on top of the other inside a steel frame. Two vacuum pumps are used to evacuate the chambers. Plastic tubing and valves connect the various components.

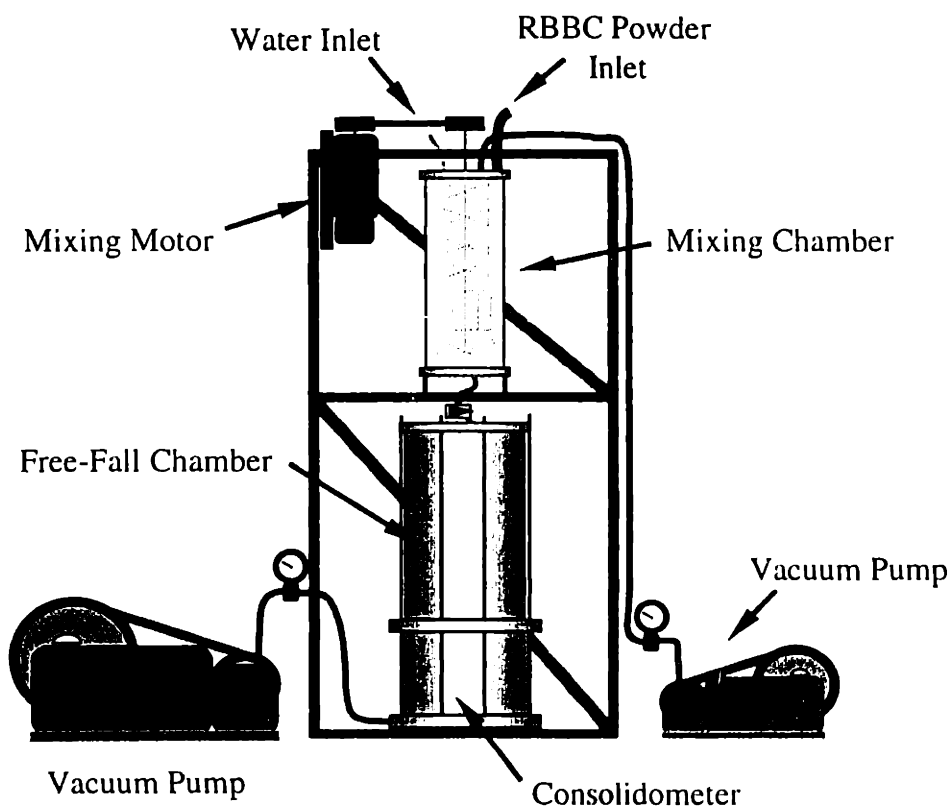


**Figure 3.1:** Schematic of equipment used to resediment Boston Blue Clay.

Fifteen kg of oven-dried soil are mixed with 15 kg of de-aired water under a vacuum to create a slurry. This operation is performed introducing alternatively 1 kg of water and 1 kg of soil inside the mixing chamber until the entire quantities are mixed. About 100 g of sodium chloride and 2ml of phenol are also added to the slurry. The salt, sufficient to produce a final slurry concentration of 16g/liter, is used as a flocculant to minimize segregation of the soil particles and achieve a structure similar to that of natural BBC, a marine illitic clay. The phénol is a bacterial growth inhibitor.

The components of the slurry are combined using blades rotating at ~60 rpm in the upper chamber while maintaining a constant water content of 100% (compared to a liquid limit of about 40 to 45%). The slurry is then mixed at 120 rpm for about 30 minutes and finally sprayed over a period of about 5 minutes through the lower free-fall chamber into the consolidometer by opening the valve between the two chambers. The vacuum in the upper chamber is reduced during this spraying operation to facilitate slurry flow. Note that the walls of the consolidometer are greased at the time the apparatus is assembled to minimize friction during consolidation and extraction of the soil from the consolidometer.

*c) Consolidation*

After releasing the vacuum and removing the free fall chamber, the consolidometer is fitted with a piston and the slurry is incrementally loaded, with a load increment ratio ($\Delta\sigma_v/\sigma_v$) of 1, from 0.016 ksc to a maximum vertical stress of 1 ksc and then unloaded to 0.25 ksc to produce an OCR of 4. The consolidation operations are illustrated in Figure 2. As the weight of the piston produces a stress of about 0.017 ksc, a counter balance system is required to achieve the lowest stress increment (Figure 2a). The next two increments, up to a stress of 0.0625 ksc, are applied using dead weights (Figure 2b). The consolidometer is then placed under an air pressure actuator that applies the higher consolidation stresses (Figure 2c). Except for the initial low stress increments, each load increment is maintained at least until the end of primary consolidation, while the maximum stress is held for one cycle of secondary compression. The consolidation process in the consolidometer, which has double drainage, is completed in about 19 days. At OCR=4 the soil is close to hydrostatic conditions (i.e., $K_0$ is near unity) and the shear strains due to the removal of the soil cake from the consolidometer are minimal, as confirmed by the work performed by Santagata (1994) on sample disturbance. Hence RBBC batches have essentially no sample disturbance.

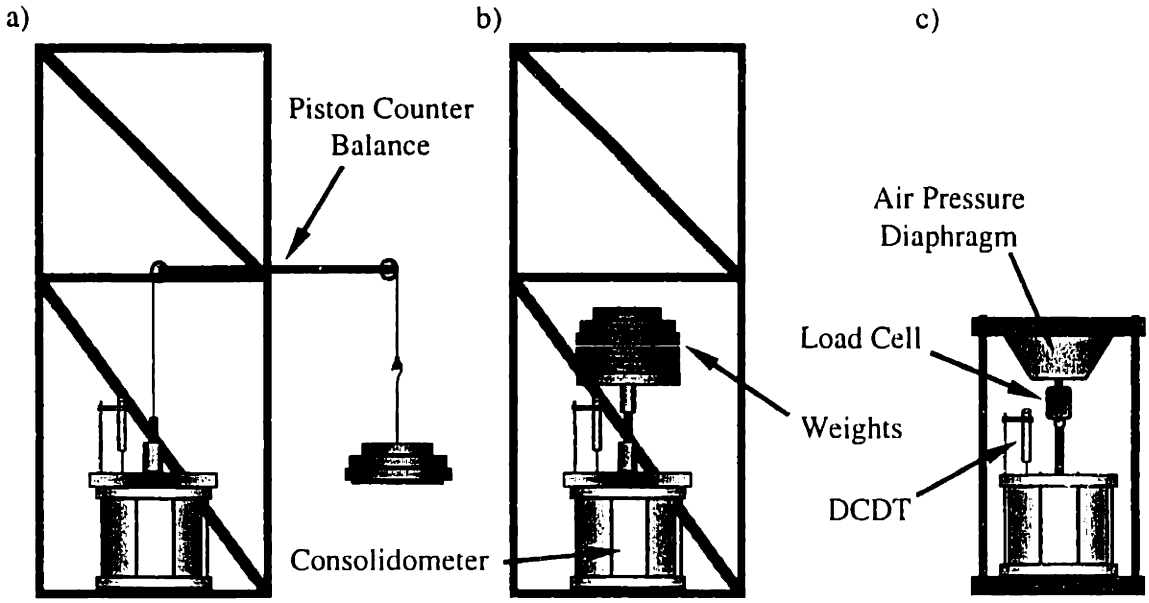


**Figure 3.2:** Schematic of consolidation operations employed when preparing RBBC: a) counter balance of piston mass, b) application of dead weights, and c) use of air pressure actuator.

*d) Storage*

After consolidation is completed, the soil cake, 30.5 cm in diameter and about 12.5 cm tall, is removed from the consolidometer and prepared for storage. The soil cake is extracted from the consolidometer by separating the consolidometer wall from the consolidometer base. The wall is then lifted vertically, taking advantage of the grease on its interior, and removed from the soil cake. The soil cake is then briefly inverted so that it can be separated from the consolidometer base. After righting the cake on a sheet of Plexiglas, the cake is cut into smaller pieces (depending on project requirements) making use of a wire saw and a miter box. Each piece is stored with a four-layer protection: a layer of cellophane, a layer of a 50/50 mixture of paraffin wax and petroleum jelly, a second layer of cellophane, and a second layer of the wax-jelly mixture. The pieces are stored in a room maintained at 90-100% relative humidity until they are used for testing.

Additional details on the resedimentation procedure and apparatus are provided by Seah (1990).

## 3.3 INDEX PROPERTIES

### 3.3.1 Introduction

The index properties of natural Boston Blue clay can vary widely over the Boston area even though the mineralogy of the clay is thought to be quite similar. Therefore, each time a new source of material is obtained for resedimentation, a battery of index and engineering tests is performed after processing to verify that the soil is sufficiently similar to prior batched materials. In addition, Atterberg limits are performed on soil from each batch to verify consistency between batches. As discussed above, resedimentation of BBC at MIT has produced more than 50 recorded batches of testing material for a variety of projects. Table 3.2 summarizes the specific gravity, Atterberg limits, clay fraction and salt concentration values reported for batches belonging to Series I, II, III and IV. The variability in the index properties reflects differences in the source material as well in the techniques of resedimentation employed by the different researchers. In addition, reprocessing of RBBC, particularly that which had been oven dried, may have lead to some variation in the properties, although Cauble (1993) was not able to isolate any effect of this sort.

In general, except for series Ia RBBC, all the index properties are quite consistent. Specific gravity shows negligible variation in the range 2.75-2.785. Larger variation is observed for the Atterberg limits particularly in the older batches. The plasticity index (excluding data from Ia) for example varies from 14.9% to 25.5%. This variation is related mainly to changes in the liquid limit, from 34.5 to 47.6%, as the plastic limit data reported for all batches are fairly consistent (17.8-24.9%). The range in the limits can be partially explained by the variation in the clay fraction, which varies between 35% and 58%. Although these ranges in the Atterberg may seem large, the resulting soil classification for all RBBC, including the Series Ia material, is CL, which corresponds to a low-to medium plasticity clay (Figure 3.4).

Except for the soil used by Bailey, who investigated the effects of salt concentration on the engineering properties of RBBC, salt concentration varies from 8 to 24 g/l for Series I-III RBBC.

The following subsections summarize the index properties for the series IV RBBC used throughout the experimental program presented in this thesis.

| Series | Batch | Wn (%) | LL (%) | PL (%) | PI (%) | $G_s$ | Salt g/L | Clay Fraction | Reference |
|---|---|---|---|---|---|---|---|---|---|
| Ia | MIT1139 | - | 30 | 17.5 | 12.5 | 2.77 | 2-3 | 40 | Fayad (1986) |
| | MIT1139 | - | 34.7 | 17.7 | 17 | 2.77 | 35 | 40 | Fayad (1986) |
| | S4 | - | 32.6 | 19.5 | 13.1 | - | - | - | Varallyay (1964) |
| | S5 | 31.2 | 33.3 | 20.4 | 12.9 | 2.78 | 16.8 | 35.5 | Varallyay (1964) |
| | S6 | 30.3 | 32.8 | 20.3 | 12.5 | - | 16 | - | Varallyay (1964) |
| Ib | S1 | 42 | 45.6 | 23.4 | 22.2 | 2.77 | 24 | 35 | Preston (1965) |
| | S2 | 41.5 | 45.4 | 23.1 | 22.3 | 2.77 | 22 | - | Preston (1965) |
| | 100 | - | 43.5 | 19.6 | 23.9 | - | - | - | Kinner (1970) |
| | 150 | 34.1 | 43.5 | 23.9 | 19.6 | 2.78 | 7 | - | Kinner (1970) |
| | 160 | 34.4 | 38.1 | 17.8 | 20.3 | - | 8 | - | Bovee (1968) |
| | 200 | - | 38.1 | 17.8 | 20.3 | - | 8 | - | Kinner (1970) |
| | 300 | 35.9 | 39.7 | 21.6 | 18.1 | - | 10 | - | Kinner (1970) |
| | 400 | 36.7 | 39.4 | 21.3 | 18.1 | - | 10 | - | Kinner (1970) |
| | 800 | - | 41.5 | 19.5 | 22 | - | 16 | - | Kinner (1970) |
| | 900 | - | 41.2 | 18.7 | 22.5 | - | 16 | - | Kinner (1970) |
| | 1000 | 37.3 | 41.1 | 19.5 | 21.6 | - | 16 | - | Kinner (1970) |
| | 1100 | 43.4 | 42 | 20.6 | 21.4 | - | 16 | - | Kinner (1970) |
| | 1200 | 38.1 | 40.2 | 18.6 | 21.6 | - | 16 | 48 | Kinner (1970) |
| | 1300 | 35.6 | 42.1 | 22.1 | 20 | - | 16 | - | Kinner (1970) |
| | 1500 | - | 43.8 | 20.6 | 23.2 | 2.78 | 16 | - | Ladd et al. (1971) |
| | M101 | - | 40.7 | 19.6 | 21.1 | - | - | 52 | Kinner (1970) |
| | M104 | - | 40.3 | 19.6 | 20.7 | - | - | - | Kinner (1970) |
| | M107 | - | 41.3 | 19.6 | 21.7 | - | - | - | Kinner (1970) |
| | M200 | - | 42.3 | 18.5 | 23.8 | - | - | 52 | Kinner (1970) |
| | M400 | - | 39.8 | 18.9 | 20.9 | - | - | 47 | Kinner (1970) |
| II | Powder | - | 41.8 | 21.6 | 20.2 | 2.779 | 3.5 g/kg | - | O'Neill (1985) |
| | 101-104 | 40.72+0.77 | 41.8 | 21.6 | 20.2 | 2.782 | 15.9 | - | Germaine (1982) |
| | 105-112 | - | 41.3 | 22.1 | 19.2 | 2.78 | 16 | 52 | O'Neill (1985) |
| III | Source | - | 44.9+0.14 | 22.45+0.07 | 22.45 | 2.785 | 1.98g/kg+0.1 | 52.1+4.1 | Seah (1990) |
| | 200 | 41.1+0.80 | 45.90 | 21.95+0.35 | 23.95 | - | 22.13+2.02 | - | Seah (1990) |
| | 201 | 39.42+1.9 | 44.82 | 21.19+0.35 | 23.63 | - | 14.53+1.43 | 57.6+1.1 | Seah (1990) |
| | 202 | 40.67+0.40 | 45.46 | 22.27+0.62 | 23.19 | - | 15.05+0.95 | - | Seah (1990) |
| | 203 | 40.70+0.5 | 44.50 | 21.18+0.58 | 23.32 | - | 15.90+3.20 | - | Seah (1990) |
| | 204 | 40.19+0.40 | 45.60 | 21.47+0.58 | 24.13 | - | 13.63+3.02 | - | Seah (1990) |
| | 205 | 40.66+0.27 | 45.01 | 21.62+0.63 | 23.39 | - | 15.69+3.65 | - | Seah (1990) |
| | 206 | 41.24+0.30 | 45.17 | 22.10+0.64 | 23.07 | - | 17.38+2.52 | - | Seah (1990) |
| | 207 | 40.75+0.10 | 45.12 | 22.15+0.57 | 22.97 | - | 16.25+1.73 | - | Seah (1990) |
| | 210 | 39.92+1.21 | 45.39+1.77 | 21.93+0.15 | 23.46 | - | - | - | Sheahan 91 |
| | 214 | 38.71+0.38 | 45.62+0.49 | 20.11+4.71 | 25.51 | - | - | - | Sheahan 91 |
| | 216 | 37.78+0.10 | 45.79+0.00 | 22.25 | 23.54 | - | 19.30+1.26 | - | Sheahan 91 |
| | 217 | 38.89+0.55 | 36.46+1.64 | 20.05+0.78 | 16.41 | 2.78 | 22.94+0.08 | - | Cauble (1993) |
| | 218 | 39.11+0.55 | 37.50+3.25 | 22.59+1.22 | 14.91 | 2.775 | - | - | Cauble (1993) |
| | 219 | 36.8 | 41.4 | 20.0 | 21.4 | - | - | - | Santagata (1994) |
| | 220 | 37.5 | 39.2 | 21.5 | 17.7 | - | - | - | Santagata (1994) |
| IV | Powder | - | 47.0+0.4 | 23.8+0.9 | 23.2 | 2.79 | - | - | Sinfield (1998) |
| | 401 | - | 46.7 | 21.8 | 24.9 | - | - | - | Cauble (1996) |
| | 402 | - | 46.8 | 22.4 | 24.4 | - | - | - | Sinfield (1994) |
| | 403 | - | 47.2 | 23.3 | 23.9 | - | - | - | Sinfield (1994) |
| | 404 | - | 47.4 | 21.9 | 25.5 | - | 10.4 | - | Cauble (1996) |
| | 405 | - | 45.2 | 22.1 | 23.1 | - | 10.0 | - | Cauble (1996) |
| | 406 | - | 45.0 | 22.6 | 22.4 | - | 12.5 | 57.6 | Cauble (1996) |
| | 407 | - | 44.6 | 23.0 | 21.6 | - | 13.1 | 57.8 | Cauble (1996) |
| | 408 | - | 44.7 | 23.9 | 20.8 | - | 10.1 | 58.7 | Cauble (1996) |
| | 409 | - | 45.4 | 24.0 | 21.4 | - | 13.0 | 56.8 | Cauble (1996) |
| | 410 | - | 46.6 | 25.0 | 21.6 | - | 13.4 | - | Cauble (1996) |
| | 411 | - | 46.7 | 24.5 | 22.2 | - | 10.2 | 56.9 | Cauble (1996) |
| | 413 | - | 45.5 | 24.3 | 21.2 | - | 9.7 | - | Cauble (1996) |
| | 414 | - | 46.3 | 24.3 | 22.0 | - | 12.0 | - | Cauble (1996) |
| | 415 | - | 46.1 | 24.7 | 21.4 | - | 10.5 | - | Cauble (1996) |
| | 416 | - | 46.7 | 24.0 | 22.7 | - | 12.9 | - | Cauble (1996) |
| | 417 | - | 47.2 | 24.5 | 22.7 | - | 13.2 | | Cauble (1996) |
| | 418 | 42.6+1.1 | - | - | - | - | - | - | Santagata (1998) |
| | 419 | 42.5+0.6 | 47.8 | 23.3 | 24.5 | - | - | - | Santagata (1998) |
| | 420 | 44.02 | 45.2 | 22.6 | 22.6 | - | - | - | Force (1998) |

**Table 3.2:** Index properties of RBBC.

### 3.3.2 Series IV RBBC

Figure 3.3 shows the grain size distribution for series IV powder and RBBC. The tests on RBBC batches 406-409, 411 were performed after the batching operations and the addition of salts and phenol. The distributions show that the soil has a fine fraction (%passing #200 sieve) greater than 98% and an average clay fraction (% less than 2μm) of 58±1.2%. Both values are slightly higher than those reported for Series III RBBC (90-95% and 46-56% respectively).

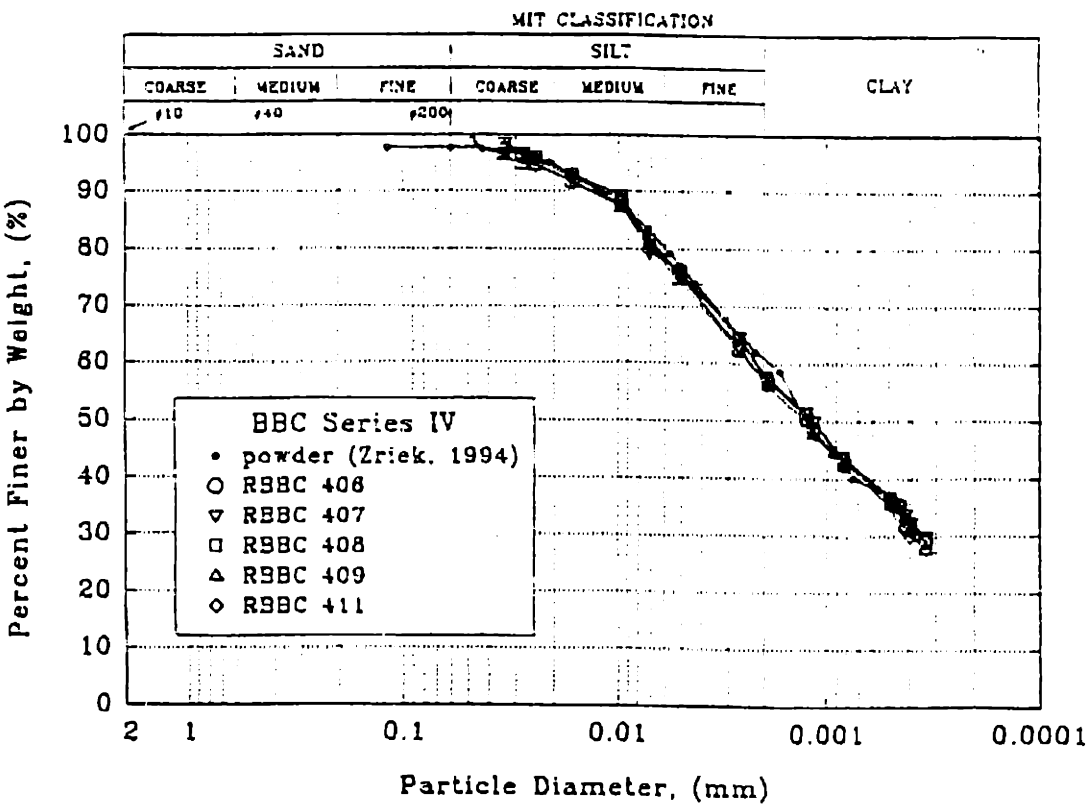


**Figure 3.3:** Results of grain size analyses on RBBC Series IV (Cauble 1996).

Data from Atterberg limit tests, performed on all batches, with the exception of Batch 412 and 418, obtained from RBBC IV are shown in Figure 3.4 and reveal exceptional batch to batch consistency. The average plastic limit, liquid limit and plasticity index are respectively 23.5±1.1%, 46.1±0.9% and 22.7±1.2%. For batches 418-419 the average water content values are 42.6±1.1% and 42.5±0.6 %, respectively.[2] The liquid limit and plasticity index data for

[2] For batches 401-417 no water contents are available as the soil was either consolidated following a different procedure and/or tested inside the consolidometer.

series IV RBBC are plotted on the plasticity chart in Figure 3.4 confirming that RBBC is a CL clay.

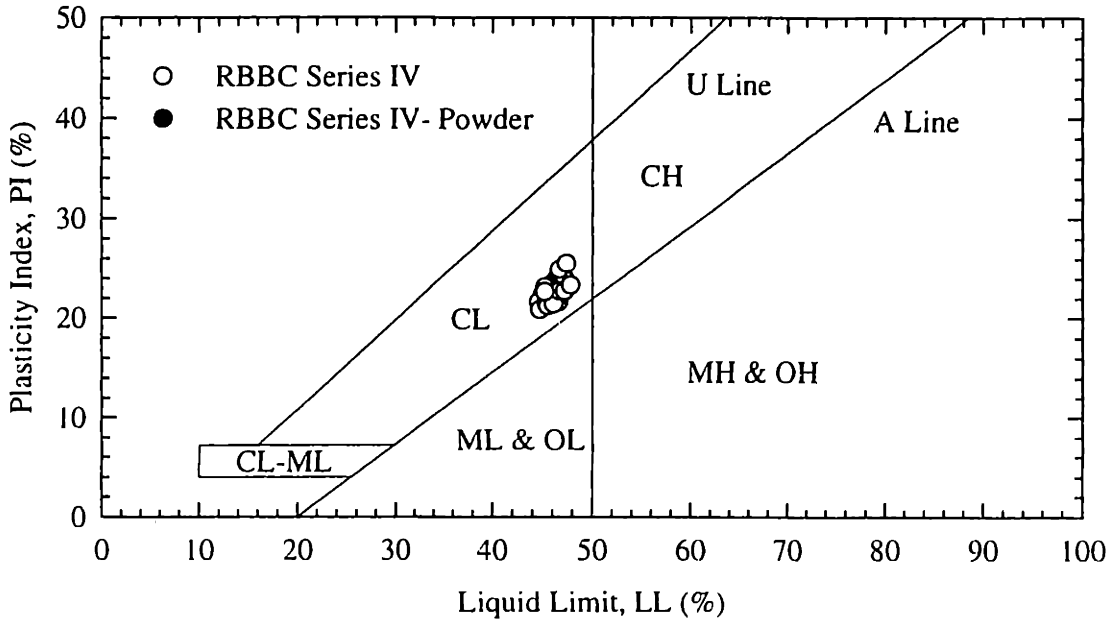


**Figure 3.4:** Plasticity chart with data from RBBC Series IV.

Measurements of the specific gravity $G_S$ for series IV RBBC performed by Cauble (1996) yielded a value of 2.81, slightly higher than that measured in previous research.

Salt content[3] was measured using a conductivity method recommended by Martin (1970) and calibrated against a KCl standard. The average value determined for batches manufactured from Series IV RBBC was 11.6±1.5 g/l. This value is slightly lower than that determined for most previous batches of RBBC, and is a result of modifications in the processing procedure.

The series IV RBBC organic content is 4.4% as determined by combustion. Similar data are not available for previous series of RBBC.

[3] As discussed in section 3.2, sodium chloride is added to the soil slurry during resedimentation.

## 3.4 BEHAVIOR OF RBBC

### 3.4.1 Introduction

This section summarizes the key features of the behavior of RBBC during one-dimensional consolidation (Section 3.4.2) and in undrained shear (sections 3.4.3 and 3.4.4). The first of these last two sections presents a brief overview of the most important aspects of the general undrained behavior of RBBC (normalized behavior, anisotropy, strain rate dependency). Section 3.4.4 provides a more detailed description of the behavior of RBBC in undrained triaxial compression which is most relevant to the work presented in this thesis.

The focus of these sections is to provide a clear picture of the behavior of RBBC to be used as reference in discussing the results presented in the following chapters.

As limited engineering element tests have been performed on RBBC IV (cf. Table 3.1), throughout the following sections reference is made, unless otherwise noted, exclusively to tests performed on RBBC III, which resembles quite closely RBBC IV (see Section 3.3). Batches from this series were prepared following repeatable and rigorous procedures with control of the origin material, and the soil was free from the effects of thixotropy which hampered much of the interpretation of tests performed on RBBC II (O' Neill 1985). Finally, with respect to previous batches, testing of RBBC III has benefited from developments in laboratory capabilities including equipment automation that have led to improved quality of the tests as well as to increased productivity.

### 3.4.2 Compression Behavior

#### *3.4.2.1 Introduction*

There is a large amount of data on the compression behavior of RBBC as derived from oedometer and CRS tests and from the one-dimensional consolidation phase of triaxial and DSS tests. Table 3.3 summarizes the sources of information for the compression behavior of RBBC for Series III and IV RBBC. The table also summarizes relevant 1-D compression parameters reported in these references. Corresponding index properties can be derived from Table 3.2

| Test Type (#) | Batch | $\sigma'_p$ (ksc) | CR | SR @ OCR=4 | $K_{0(NC)}$ | Reference |
|---|---|---|---|---|---|---|
| OED (3) | 200 | 1.04 | 0.163 | - | - | Seah (1990) |
| OED (1) | 201 | 0.98 | 0.165 | - | - | |
| OED (2) | 202 | 0.99 | 0.177 | - | - | |
| OED (1) | 203 | 1.00 | 0.183 | - | - | |
| OED (2) | 204 | 0.97 | 0.156 | - | - | |
| OED (2) | 205 | 1.00 | 0.162 | 0.013 | - | |
| OED (2) | 206 | 0.98 | 0.153 | 0.016 | - | |
| OED (1) | 207 | 1.00 | 0.159 | 0.017 | - | |
| CRS (3) | 204-207 | 1.05±0.05 | 0.169±0.003 | 0.013±0.001 | - | Ahmed (1990) |
| DSS (5) | 204 | 0.99±0.05 | 0.186±0.002 | 0.017±0.002 | - | |
| DSS (2) | 205 | 1.03 | 0.185 | 0.015 | - | |
| DSS (4) | 207 | 1.01±0.03 | 0.159±0.003 | - | - | |
| TX (2) | 205 | 0.975±0.035 | 0.179±0.015 | 0.016 | 0.495±0.019 | Sheahan (1991) |
| TX (5) | 206 | 0.904±0.043 | 0.157±0.005 | 0.013 | 0.489±0.016 | |
| TX (3) | 207 | 0.920±0.061 | 0.161±0.008 | 0.014 | 0.482±0.017 | |
| TX (12) | 210 | 1.132±0.038 | 0.153±0.013 | 0.015 | 0.487±0.016 | |
| TX (16) | 214 | 1.079±0.059 | 0.151±0.006 | 0.013 | 0.487±0.016 | |
| TX (5) | 216 | 1.068±0.054 | 0.154±0.002 | 0.014 | 0.487±0.016 | |
| DSS (2) | 214 | 1.105 | 0.155 | 0.016 | - | |
| DSS (21) | 217 | 1.45±0.07 | 0.173±0.004 | 0.016±0.003 | - | Cauble (1993) |
| DSS (20) | 218 | 1.35±0.15 | 0.157±0.010 | 0.012±0.002 | - | |
| TX (7) | 216 | 1.11±0.08 | 0.180±0.015 | - | 0.490±0.016 | Santagata (1994) |
| TX (5) | 217 | 1.19±0.10 | 0.168±0.016 | - | 0.469±0.013 | |
| TX (4) | 218 | 1.27±0.08 | 0.164±0.012 | - | 0.463±0.028 | |
| TX (9) | 219 | 1.27±0.09 | 0.165±0.008 | - | 0.506±0.022 | |
| TX (6) | 220 | 1.16±0.13 | 0.143±0.011 | - | 0.492±0.019 | |
| CRS (7) | 420 | 1.18±0.10 | 0.168±0.005 | - | - | Force (1998) |
| TX (14) | 420 | 1.05±0.06 | 0.170±0.006 | - | - | |

**Table 3.3:** Overview of database on one-dimensional compression behavior of RBBC Series III and IV.

### *3.4.2.2 Compression Curves and Compressibility Parameters*

Figure 3.5a presents an example of a set of compression curves obtained from the $K_0$-consolidation phase at constant rate of strain of several triaxial tests performed on RBBC specimens obtained from the same batch (RBBC 420, Force 1998). The figure provides an example of the exceptional repeatability in the behavior of RBBC. It can be seen that the shape of the compression curve is characterized by a well defined break corresponding to the batch preconsolidation pressure and by an approximately constant slope of the virgin compression line in the range of stresses 2-5 ksc. At higher stresses the curve displays more of an S-shape. In the unloading portion, the curve is much flatter, but becomes steeper with increasing OCR. Similar behavior is observed from oedometer and CRS tests (Seah 1990, Ahmed 1990).

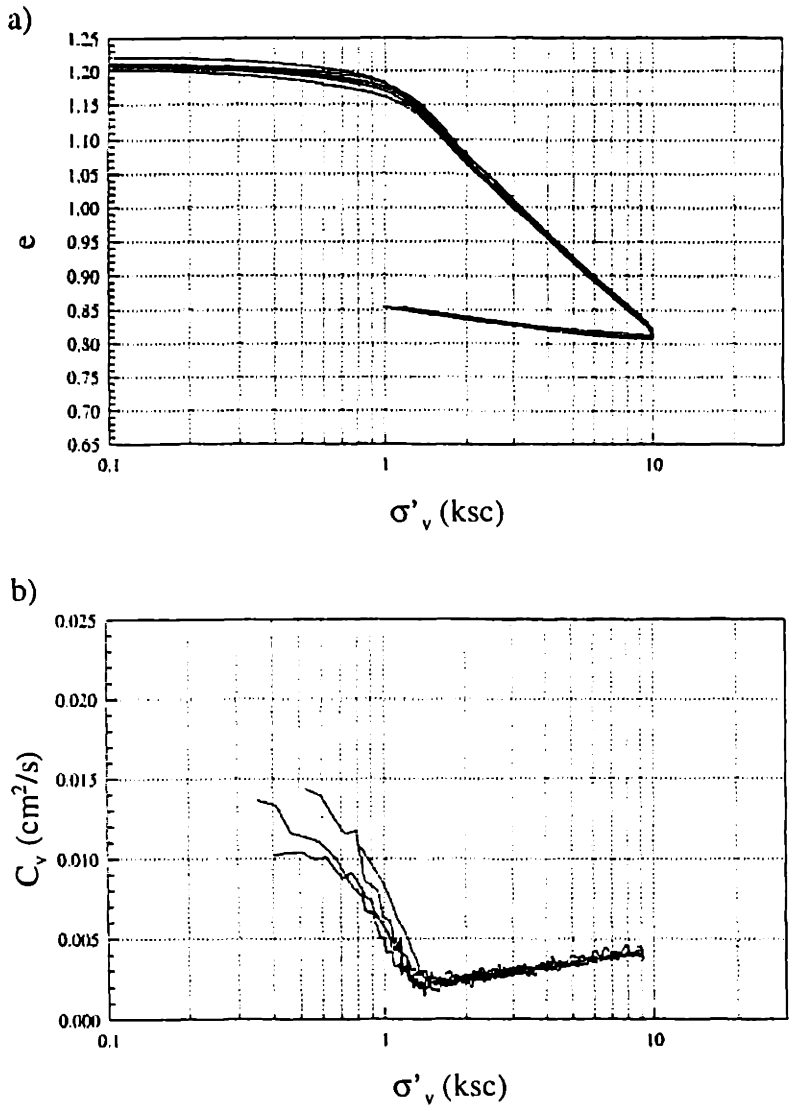


**Figure 3.5:** Results of $K_0$-consolidation of RBBC in the triaxial apparatus: a) compression curves; b) coefficient of consolidation (Force 1998).

Determination of the preconsolidation pressure (i.e., the maximum pressure applied to the batch plus the influence of one cycle of secondary compression) using the Strain Energy Method (Becker et al. 1987) yields values generally in the range 0.95 to 1.20 ksc, with fairly consistent results for specimens obtained from the same batch. As seen in Table 3.3, in some cases the preconsolidation pressure values are significantly higher than the nominal maximum pressure of 1 ksc applied during batch consolidation. This remains true even when increases in $\sigma'_p$ resulting from secondary compression at $\sigma'_{vm}$ are accounted for employing the method proposed by Mesri

and Castro (1987).[4] This is the case, for example of batches 217, 218 and 219. It is suspected (Cauble 1993) that for these batches the maximum stress applied during consolidation was higher than 1 ksc.

As shown in Table 3.3, the compression ratio [$CR=\Delta\varepsilon_a/\Delta\log\sigma'_v$)][5] of RBBC generally varies in the range 0.155-0.180. No clear trend of CR with the index properties is evident.

Figure 3.5a shows that the slope of the swelling curve increases as the soil is unloaded to higher OCR's. The swelling ratio (SR), defined by the slope of the line drawn through the points corresponding to the start an the end of the unloading phase, is approximately an order of magnitude smaller than CR. To evaluate batch to batch consistency, Table 3.3 summarizes the data of SR for RBBC with OCR of 4, which varies in the range 0.012-0.017. Note that the higher values of SR are generally measured on the specimens characterized by higher values of CR. Ahmed (1990) and Sheahan (1991) provide SR data at different OCR's: for OCR of 2 and 8 SR is equal respectively to approximately 0.011 and 0.019. Concurrently with the increase in SR with OCR, the ratio CR/SR decreases with OCR from approximately 14 for OCR of 2, to 10 and 8 respectively for OCR of 4 and 8.

Note that the data reported by Cauble (1993) and Ahmed (1990) are derived from the consolidation phase of DSS tests in which specimens are swelled under truly oedometric conditions. On the other hand in the triaxial tests reported by Sheahan (1991) the specimens were unloaded following stress path consolidation to the desired OCR based on an estimate of $K_0$ at that OCR (cf. Section 3.4.2.3).

### *3.4.2.3 Lateral Stress Ratio*

Data on the coefficient of earth pressure at rest can be obtained from $K_0$-consolidated triaxial tests. Figure 3.6 shows the typical trend of $K_0$ with vertical stress during consolidation, as observed in all the tests performed by Santagata (1994). $K_0$ decreases during the initial loading within the overconsolidated region until approximately 1 ksc (batch maximum stress), and then increases. Once the soil is consolidated well into the virgin compression region $K_0$

[4] According to this method the increase in $\sigma'_p$ is a function of the duration of secondary compression, and the properties of the soil (CR, RR, $c_{\alpha\varepsilon}$). For RBBC an additional cycle of secondary compression translates into an increase in preconsolidation pressure of 5-8%.

[5] The value of CR is generally calculated as the slope of the compression line in the stress range 2-4 ksc.

remains approximately constant. The value of $K_0$ in the virgin compression region is referred to as the normally consolidated value $K_{0(NC)}$.

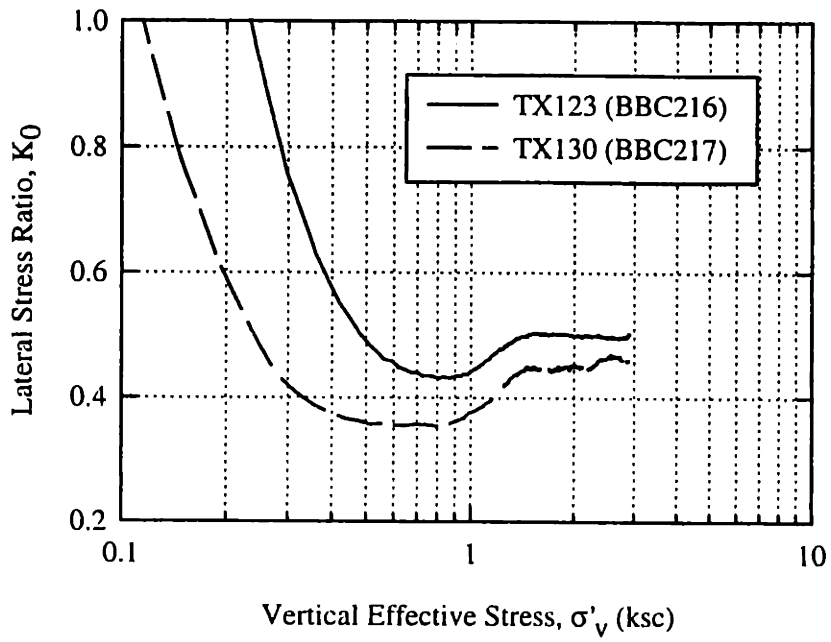


**Figure 3.6:** Lateral stress ratio versus effective stress during $K_0$-consolidation of RBBC (Santagata 1994).

For NC RBBC Santagata (1994) observed a limited variability in the results for $K_{0(NC)}$ between 0.44 and 0.52, even for specimens obtained from the same batch. The reasons of this scatter have not been determined. In an effort to control the pre-shear stress state more precisely, Santagata (1994) performed stress path consolidation. In this procedure the desired vertical and horizontal effective stresses were targeted by first reaching the desired K value at constant radial stress and then achieving the final stress state following a constant K path. This procedure shifted the compression curve toward lower effective stresses, causing its slope to decrease. This is shown in Figure 3.7, which compares the stress-paths and the compression curves of two specimens reaching the same consolidation stresses, respectively after $K_0$-consolidation and stress path consolidation.

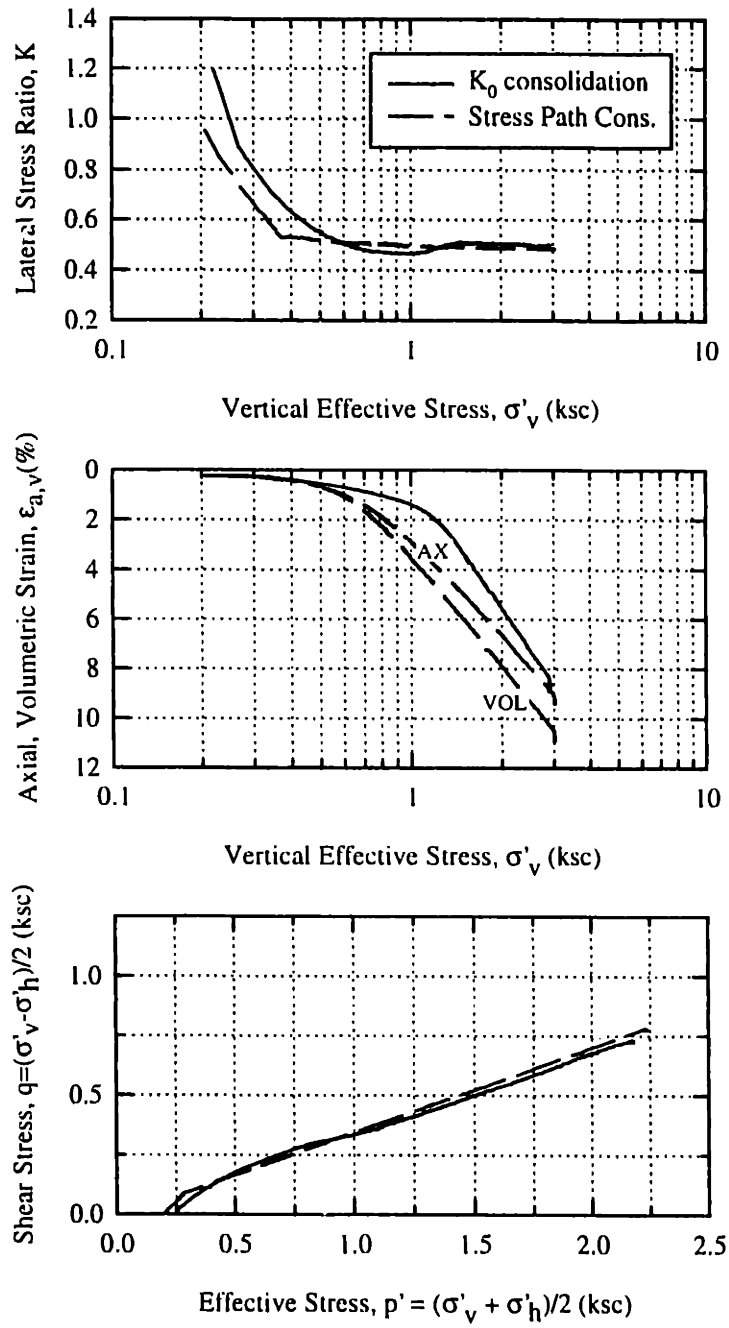


**Figure 3.7:** Comparison of $K_0$ and stress path consolidation (Santagata 1994).

The coefficient of earth pressure at rest, $K_0$, increases with increasing OCR. $CK_0U$ triaxial tests and lateral stress oedometer tests (O'Neill 1985), indicate that for RBBC the increase in $K_0$ with OCR is well described by an empirical equation of the type proposed by Schmidt (1966):

$$K_o = K_{0(NC)}(OCR)^n \qquad \textit{Equation 3.1}$$

For RBBC it is generally assumed (Sheahan 1991, Santagata 1994) that the average value of the normally consolidated $K_{0(NC)}$ equals 0.48 and that the exponent $n$ is equal to 0.426 (1-sin 35°). This equation is used routinely at MIT to obtain the pre-shear K for all overconsolidated shear tests on RBBC.

#### *3.4.2.4 Secondary Compression*

The largest sets of data on the secondary compression behavior of RBBC are provided by Cauble (1993) and by Sheahan (1991), based on DSS (incremental consolidation only) and $K_0$-consolidated triaxial tests respectively.[6]

For NC RBBC both Cauble and Sheahan present data for $C_{\alpha\varepsilon} = d\,\varepsilon_a / d \log t$ in the range 0.28±0.05%. The $C_{\alpha\varepsilon}$/CR ratio reported by these authors is 0.0173±0.0042. A slightly higher value (0.02) was obtained by Seah (1990) from a series of incremental oedometer tests. All these data are well below the range observed by Mesri and Castro (1987) for a variety of inorganic soft clays (0.04±0.01) and are also on the low side of $C_{\alpha\varepsilon}$/CR data previously reported for RBBC II (0.036±0.004, O'Neill 1985).

In accordance with the constant $c_\alpha/c_c$ concept developed by Mesri and Castro (1987) the secondary compression rate of OC RBBC is about an order of magnitude smaller than that of the NC soil.

#### *3.4.2.5 Coefficient of Consolidation*

Figure 3.5b shows the variation in $c_v$ during a CRS[7] test on RBBC IV (Force 1998) performed in a modified triaxial apparatus. In general, $c_v$ decreases with $\sigma'_v$ in the recompression range until $\sigma'_p$ (~1ksc) is reached, drops abruptly, and then begins to rise with increasing stress level in the normally consolidated region.

---

[6] Sheahan (1991) developed a method to evaluate the rate of secondary compression at constant stresses after constant strain rate loading. The method consists of defining an artificial time to end of primary through an iterative procedure based on the selection of the time scale that provides the most linear $\varepsilon_{ax}$-log time relationship.

### 3.4.3 Overview of Behavior in Undrained Shear

This section briefly reviews the key general features of the undrained shear behavior of RBBC for $CK_0U$ testing: the normalized behavior and the validity of the SHANSEP (Stress History and Normalized Soil Engineering Properties) method (Ladd and Foott 1974, Ladd 1991), the anisotropy and strain rate sensitivity. Additional details on the behavior of RBBC in triaxial compression are provided in Section 3.4.4.

Extensive testing performed at MIT on RBBC has indicated that this soil exhibits normalized behavior. This means that clay specimens having the same overconsolidation ratio, but different consolidation stresses, and therefore different preconsolidation pressures, exhibit similar properties (i.e. strength, stress-strain, pore pressure parameters, etc.) when normalized with respect to the consolidation stress (Ladd and Foott 1974). This concept applies to a large range of natural clays, mostly mechanically overconsolidated, which maintain the same basic structure during loading beyond the in situ stresses and that are characterized by a generally constant virgin compression index. It has significant practical value as it provides a useful framework for comparing and relating the behavioral characteristics of different cohesive soils and has led to the development of the SHANSEP method. SHANSEP testing programs[8] carried out at MIT on RBBC, both in triaxial compression (Sheahan 1991, Santagata 1994), extension (Sheahan 1991) and in direct simple shear (Ahmed 1990), have resulted in a solid database of the normalized behavior of this soil at various values of the OCR. In particular, a large amount of data on the normalized parameter most significant for undrained stability analyses, the undrained strength ratio, is available.

As shown in Figure 3.8, for a given shear mode (TC, TE or DSS), the variation of the undrained strength ratio versus the overconsolidation ratio is closely approximated by the relationship

$$\frac{c_u}{\sigma'_{vc}} = S \cdot (OCR)^m \qquad \textit{Equation 3.2}$$

---

[7] The value of $c_v$ is calculated from the following equation: $c_v=k_v/m_v\gamma_w$ where $k_v$ is the vertical hydraulic conductivity; $m_v=\Delta\varepsilon/\Delta\sigma'_v$; and $\gamma_w$ is the unit weight of water.

[8] These tests involve $K_0$-consolidation to a stress level greater than 1.5 times the batch preconsolidation pressure (1ksc) and then 24 hours of aging. For the OC tests these operations are followed by unloading to the desired OCR and another 24 hours of aging.

where S is the undrained strength ratio for the normally consolidated clay, and m is the slope of the regression line. This equation is commonly referred to as the SHANSEP equation. Figure 3.8 summarizes the triaxial compression, triaxial extension and direct simple shear SHANSEP parameters (S and m), determined from tests on RBBC III. These values are typical of those reported for CL sedimentary clays (Jamiolkowski et al. 1985, Ladd 1991). The dependency of S on the mode of shear is indicative of the anisotropic behavior of RBBC.

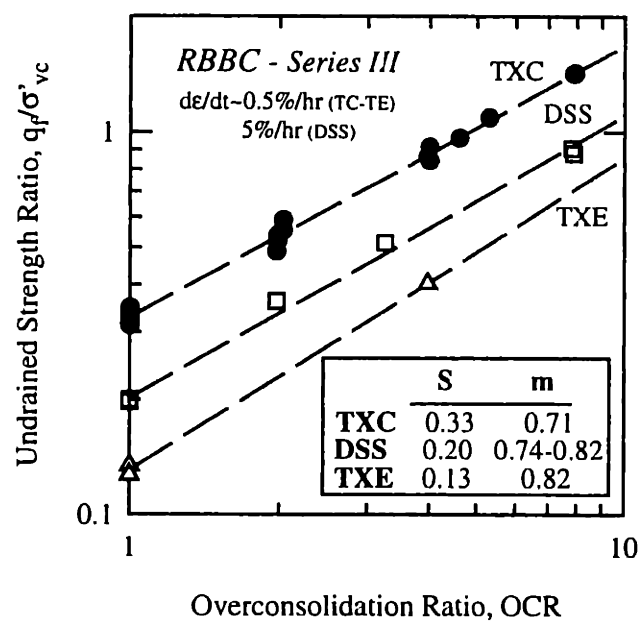


**Figure 3.8:** Undrained strength ratio versus OCR from $CK_0U$ test in triaxial compression (Sinfield 1994, Santagata 1994), extension (Sheahan 1991), and direct simple shear (Ahmed 1990).

Deviation from perfect normalized behavior is observed when analyzing the stress strain curves and the pore pressure behavior. This is most notable for direct simple shear in which case the strain at failure, and the $\Delta u/\sigma'_{vc}$ versus strain, are found to increase and decrease respectively with increasing consolidation stress (Ahmed 1990). Overall, in all three modes of shear the same behavioral trends with OCR are observed. Increasing OCR produces an increase in the normalized strength, an increase in the strain at peak, and increasingly dilatant behavior.

The large differences in the behavior as a function of shear mode show that RBBC exhibits significant anisotropic behavior. The rotation of the principal stresses (from $\delta$=0 ° for

TC to ~50 ° and 90 ° for DSS and TE respectively)[9] is associated with a significant decrease in strength, and an increase in the strain at failure. These observations are confirmed by the results obtained in the direction shear cell (DSC) by Seah (1990) who also observes an increase in the shear induced pore pressures and in the shear modulus at a given strain level with increasing $\delta$. As shown in Figure 3.8, the strength anisotropy decreases slightly with increasing OCR.

Another distinctive feature of the undrained behavior of RBBC is its strain rate dependency, which was extensively investigated by Sheahan (1991) for triaxial compression. In this shear mode increasing strain rate is associated with increasing shear stress at all strain levels and with a suppression of the shear induced pore pressures, while the envelope formed by the stress states at maximum obliquity is independent of strain rate. This rate dependence decreases with increasing OCR at lower strain rates.

More details on the rate sensitivity of RBBC in triaxial compression are provided in Section 3.4.4.7.

### 3.4.4 Behavior in Undrained Triaxial Compression

#### *3.4.4.1 Introduction*

As seen in Table 3.1, undrained triaxial compression tests on RBBC have been performed by a large number of researchers at MIT. In this section, however, the discussion focuses exclusively on the results presented by Sheahan (1991) and Santagata (1994), as their work is not only the most comprehensive, but also was performed on more recent batches of RBBC III employing *automated stress path cells* which provide the best quality results. Note that the analysis of the undrained behavior in triaxial compression presented in Sections 3.4.4.2-3.4.4.6 is limited to the results of tests conducted at a standard rate of 0.5%/hour. An overview of the behavior at lower and higher strain rates is presented in Subsection 3.4.4.7 with the discussion of the strain rate sensitivity of RBBC.

#### *3.4.4.2 General Behavior*

Figures 3.9a-d illustrate the typical undrained triaxial compression behavior of RBBC at nominal OCR's of 1, 2, 4, and 8. Figure 3.9a presents the effective stress paths normalized to the

[9] Note that in these tests also b ($=(\sigma_2-\sigma_3)/(\sigma_1-\sigma_3)$) varies. It is equal to 0, 1 and about 0.4 for TC, TE and DSS respectively.

maximum vertical consolidation stress $\sigma'_{vm}$. Figure 3.9b shows the stress-strain curves ($q/\sigma'_{vm}$ vs. $\varepsilon_a$) and Figures 3.9c and 3.9d plot respectively the excess ($u_e = \Delta u - \Delta\sigma_3$) and the shear induced pore pressures ($u_s = \Delta u - \Delta\sigma_{oct}$) generated during shear.

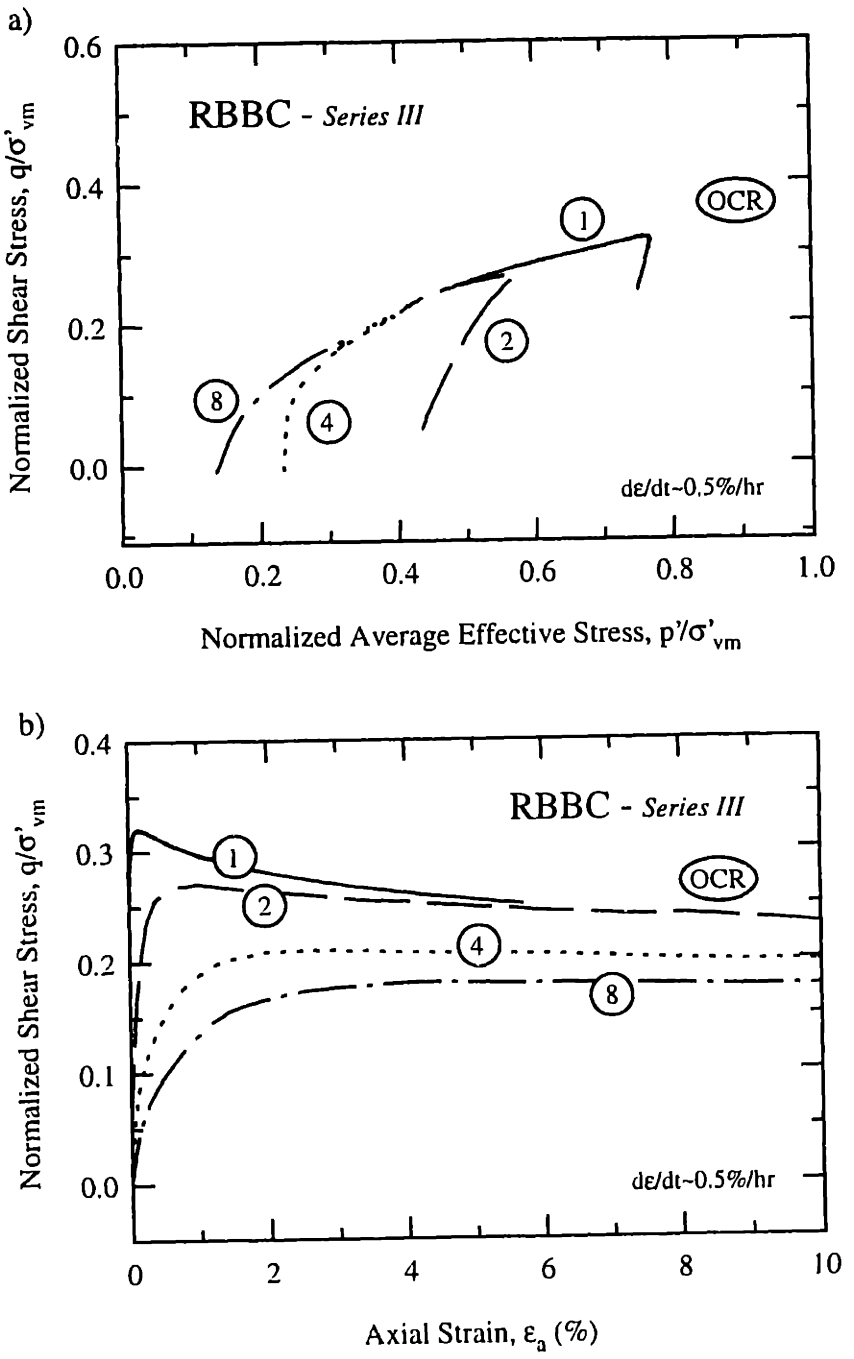


**Figure 3.9:** Behavior of RBBC (OCR = 1, 2, 4, 8) in undrained triaxial compression: (a) stress paths; (b) stress strain curves (Santagata 1994).

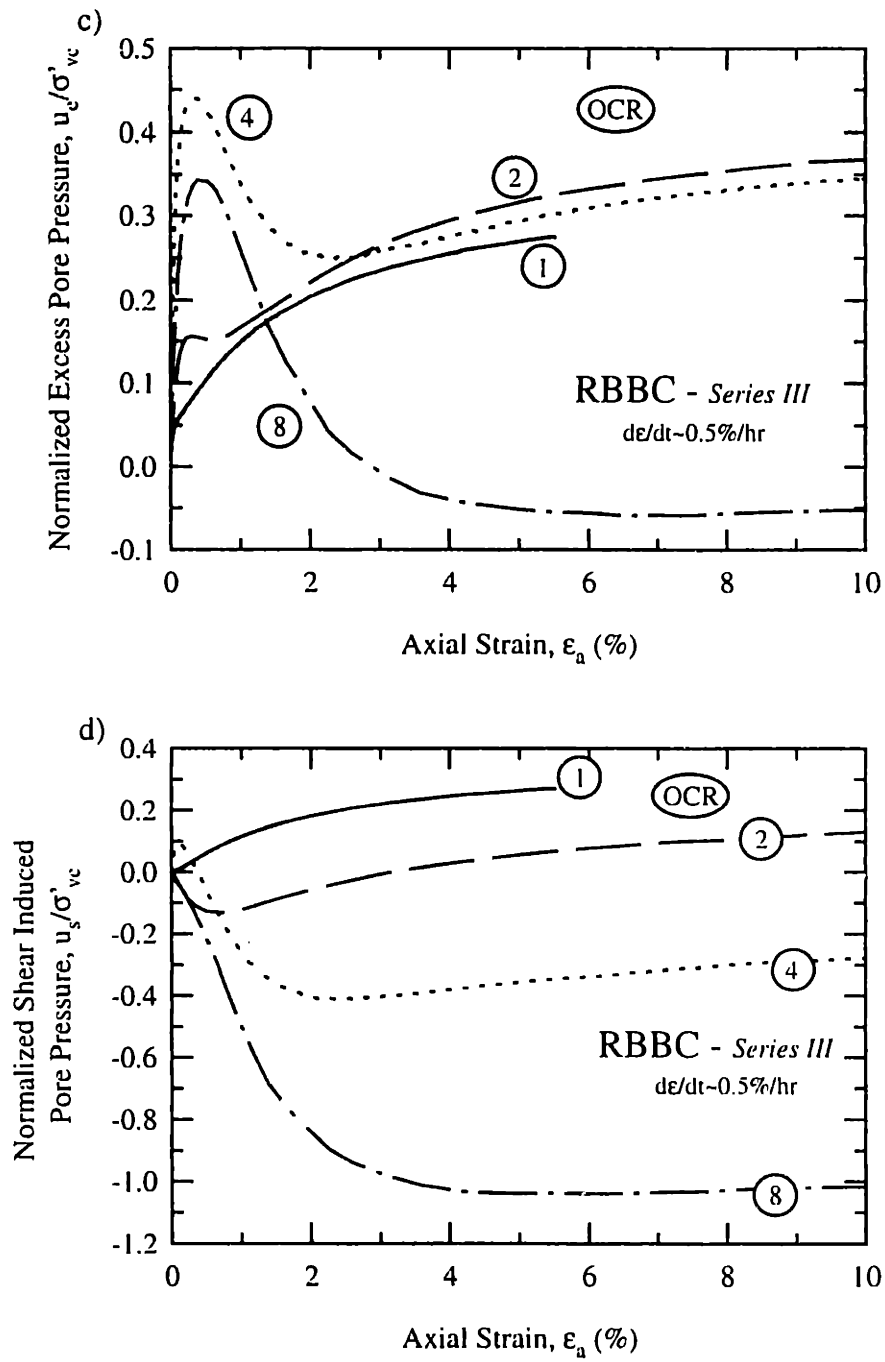


**Figure 3.9:** (continued) Behavior of RBBC (OCR = 1, 2, 4, 8) in undrained triaxial compression: (c) normalized excess pore pressures; (d) normalized shear induced pore pressures (Santagata 1994).

The following can be observed:

a) the effective stress-paths approach a common failure envelope at large strains;

b) the NC behavior is characterized by a peak at a small strain followed by development of large positive pore pressures that cause a significant decrease in p' and significant post-peak softening.

c) increasing OCR causes:

- a decrease in the peak value of the strength normalized to the maximum vertical stress;
- a decrease in strain softening;
- an increase in the axial strain at failure;
- a decrease of the shear induced pore pressure beyond 0.5 to 1.0% strain;
- a decrease in the development of excess pore pressure which becomes increasingly negative, causing a transition from a fully contractive behavior for OCR1 to entirely dilatant undrained shear behavior at OCR 8

#### *3.4.4.3 Undrained Strength Ratio*

Data collected by Sheahan (1991) and Santagata (1994) show some scatter in the values of the undrained strength ratio of normally consolidated RBBC around a mean peak value of 0.33. The scatter has been found to be linked to the variation in the values of the pre-shear lateral stress ratio K (cf. Section 3.4.2.3). As illustrated in Figure 3.10, an increase of the pre-shear value of K is associated with a decrease of the undrained strength ratio. The data are quite consistent and the equation of the regression through the data points can be used to describe the relation between $K_0$ and $q_f(c)/\sigma'_{vc}$ (i.e., $S_c$):

$$S_C = 0.55 - 0.47 \cdot K_{0(NC)} \qquad \textit{Equation 3.3}$$

Note that Figure 3.10 plots data not only from $K_0$-consolidated tests, but also from stress path tests conducted especially to check the validity of this relationship outside the range of experimental variability of $K_0$.

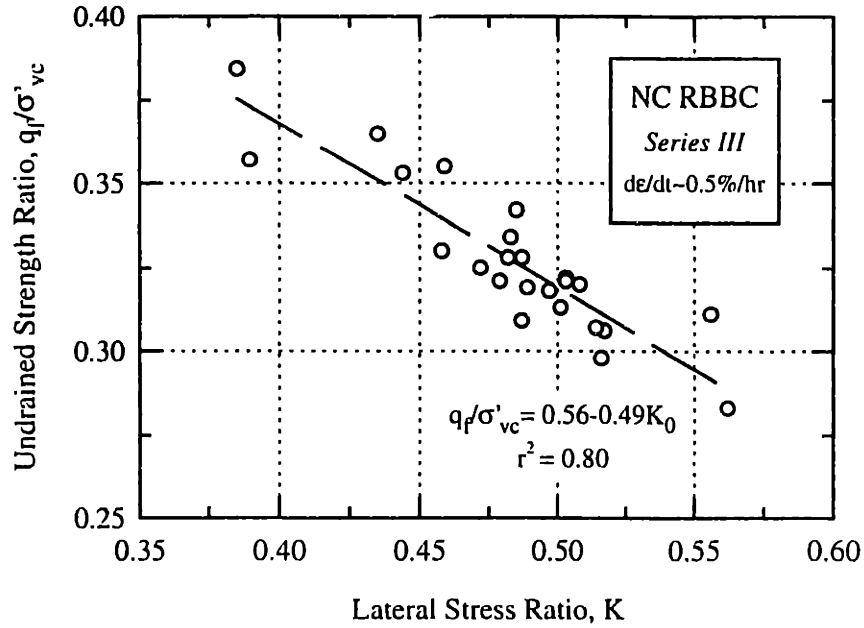


**Figure 3.10:** $q_f$(c) versus $K_0$ for $CK_0UC$ tests on NC RBBC (Santagata 1994).

As discussed in Section 3.4.3, RBBC exhibits normalized behavior. The relationship between normalized strength ($c_u/\sigma'_{vc}$) and overconsolidation ratio is well described by the SHANSEP equation:

$$\frac{c_u}{\sigma'_{vc}} = S \cdot (OCR)^m \qquad \textit{Equation 3.4}$$

Based on the data obtained by Sheahan (1991) and Santagata, (1994) for triaxial compression S=0.33±0.01 and m=0.71 (n=21, $r^2$ = 0.99 – see Figure 3.8).

### *3.4.4.4 Effective Stress Failure Envelope*

Values of shear stress versus average effective stress at maximum obliquity for triaxial compression tests performed on NC and OC RBBC are plotted in Figure 3.11, both normalized by the maximum past pressure. A linear regression through these data is used to define the q-p' effective stress failure envelope at maximum obliquity:

$$\frac{q}{\sigma'_{vm}} = \frac{a'}{\sigma'_{vm}} + \frac{p'}{\sigma'_{vm}} \cdot \sin(\varphi') \qquad \textit{Equation 3.5}$$

The linear regression through the data yields the following:

$$\frac{q}{\sigma'_{vm}} = 0.009 + \frac{p'}{\sigma'_{vm}} \cdot \sin(31.06^{\circ}) \qquad \textit{Equation 3.6}$$

Note that the lower the OCR, the higher the strain at which the maximum obliquity failure envelope is mobilized ($\varepsilon_a$>10% for NC RBBC) and that only for OCR of 8 does the soil reach the maximum obliquity envelope before reaching the peak undrained strength.

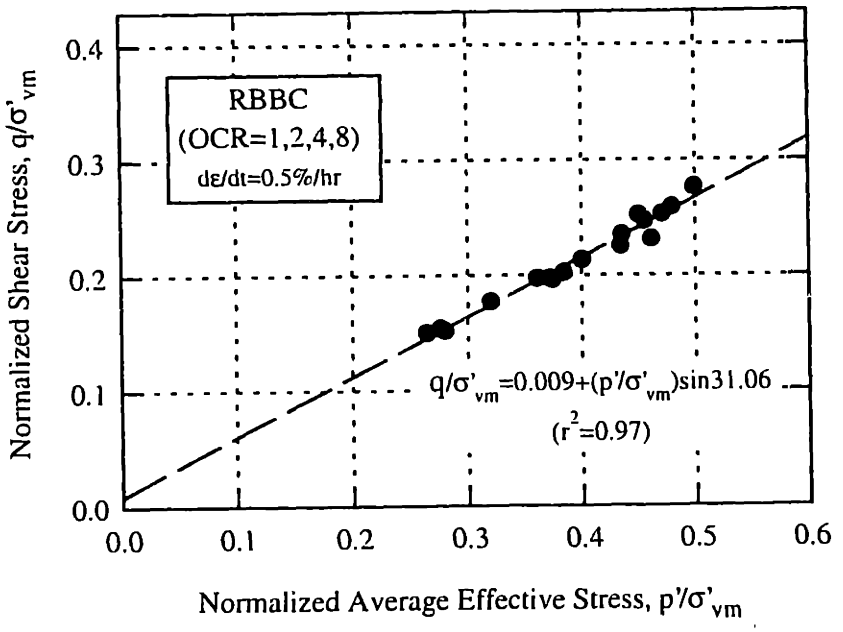


**Figure 3.11:** Friction angle at maximum obliquity for RBBC (Santagata 1994).

### *3.4.4.5 Strain at Failure*

As shown in Figure 3.9a NC RBBC reaches the peak strength at a small axial strain of about 0.1%. The measured data vary between 0.09% and 0.26%. Some of the scatter is undoubtedly due to the strain measurement technique that, in both Sheahan's and Santagata's

work, relied only on an external LVDT'[10]. Although no clear trend is apparent, the higher values of $\varepsilon_{peak}$ appear to be mostly associated with the higher values of K.

As shown in Figures 3.9b and 3.12, the strain at failure increases with OCR from about 1% for OCR of 2, to approximately 3.5% and 6% for OCR equal to 4 and 8, respectively.

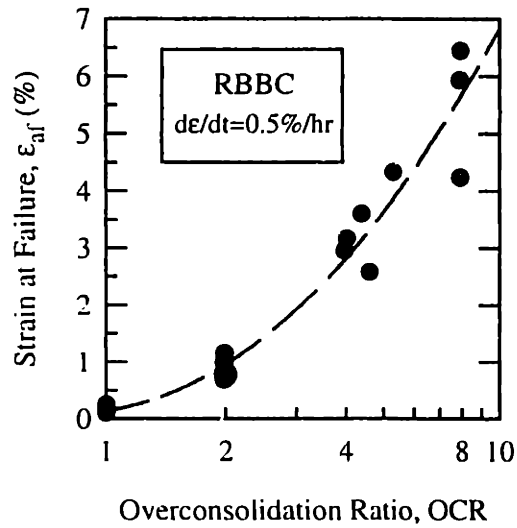


**Figure 3.12:** Strain at failure versus OCR for RBBC (Santagata 1994).

### *3.4.4.6 Stiffness*

Figure 3.13 shows curves of the secant Young's modulus normalized to the vertical consolidation stress ($E_u/\sigma'_{vc}$) versus axial strain on a log-log plot for NC and OC RBBC. As the measurements were performed employing external LVDT's the estimates of the stiffness are considered reliable only above 0.01-0.05%.

The figure illustrates how the behavior of NC RBBC differs significantly from that of the OC soil. The curves for RBBC with OCR in the range 2 –8 fall within a narrow band and display a trend of increasing normalized stiffness with increasing OCR at any given axial strain. The NC soil shows consistently smaller normalized stiffness than the OC clay at all strain levels and exhibits the strongest non-linearity from the very beginning. The decrease in stiffness is particularly marked once the soil reaches failure due to the large amount of post peak strain softening.

[10] In addition, Sheahan (1991) made use of lubricated ends.

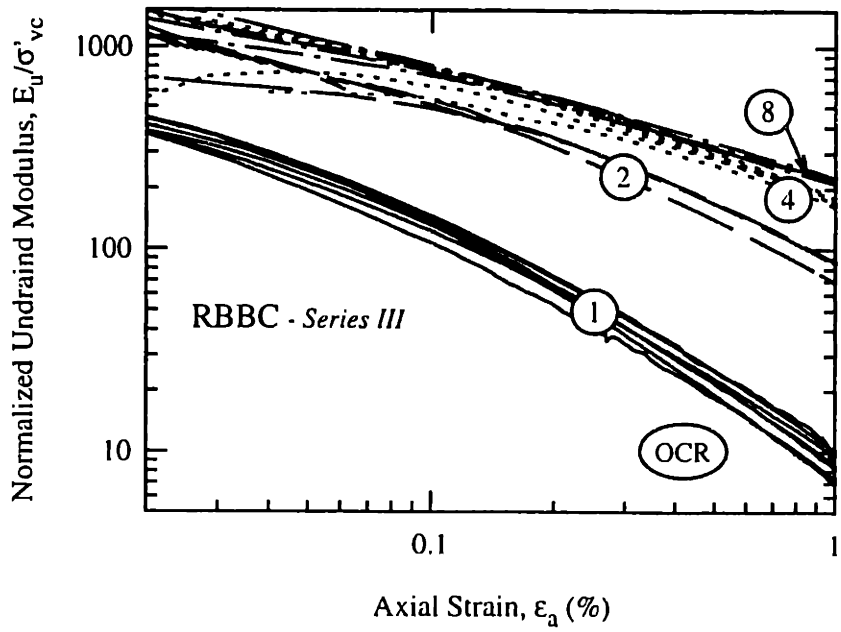


**Figure 3.13:** Undrained modulus versus axial strain (Santagata 1994).

### *3.4.4.7 Strain Rate Sensitivity*

The time dependent behavior of RBBC in undrained triaxial compression was investigated by Sheahan (Sheahan et al. 1996). Sheahan explored the effects of four strain rates (0.05%/hr to 50%/hr) on the undrained stress-strain behavior and the strength of RBBC at OCR 1, 2, 4, and 8. The triaxial apparatus used in Sheahan's study made use of lubricated end platens and had the ability to measure pore pressures at the mid-height of the test specimen. No analysis of the small strain behavior of the soil was performed, as the apparatus was not equipped with on-specimen measurements of the strain. The main findings of this work are described in the following.

Figures 3.14 and 3.15 summarize the results obtained for RBBC at OCR=1 and 4. It can be seen that strain rate affects the strength of the soil, the development of the shear induced pore pressure and the stress path during shear.

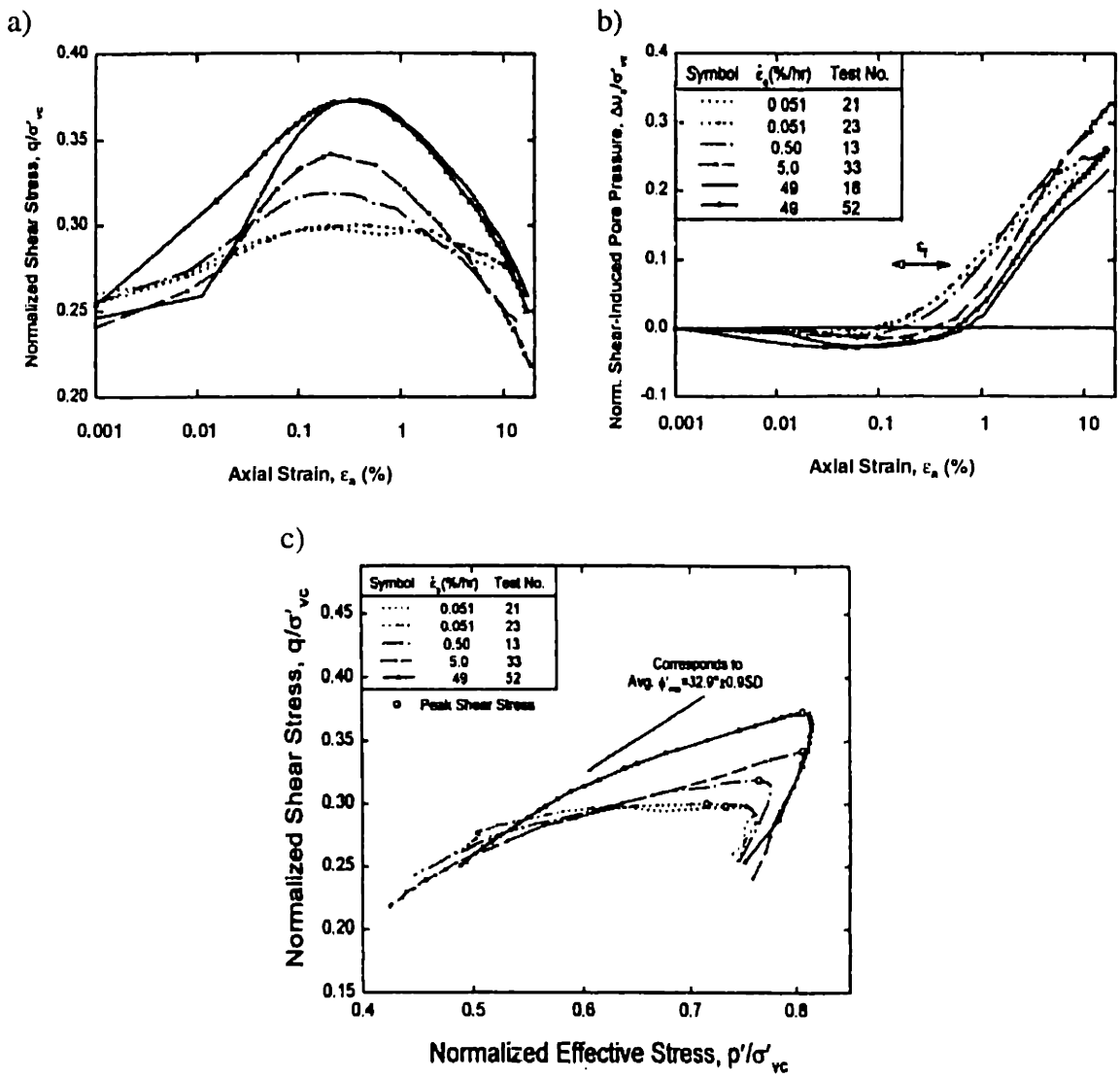


**Figure 3.14:** Effect of strain rate on the behavior of NC RBBC: a) stress strain curves; b) shear induced pore pressure; and c) stress paths (Sheahan et. al. 1996).

The strain rate sensitivity of RBBC is dependent on OCR and the strain rate range examined. This is shown in Figure 3.16 which summarizes the effect of strain rate on the normalized undrained shear strength of RBBC as a function of OCR. The numbers in parenthesis refer to $\rho_{0.5}$, the change in normalized strength ($s_u/\sigma'_{vc}$) across one log cycle, expressed as a percentage of the value measured at a reference rate of 0.5%/hr. For the two log-cycles from a strain rate of 0.05%/hr to 5%/hr, the figure shows that the average value of $\rho_{0.5}$

drops from 6.5% for NC RBBC, to 4.5% for OCR=2 and finally to zero for OCR of 8. In the region from 5 to 50%/hr strain rate, all OCR's display a relatively constant increase in strength of about 9.5%±2.0 SD. The data also show that the strain rate below which the strength of the clay becomes rate insensitive decreases with OCR (at least for OCR 2-8).

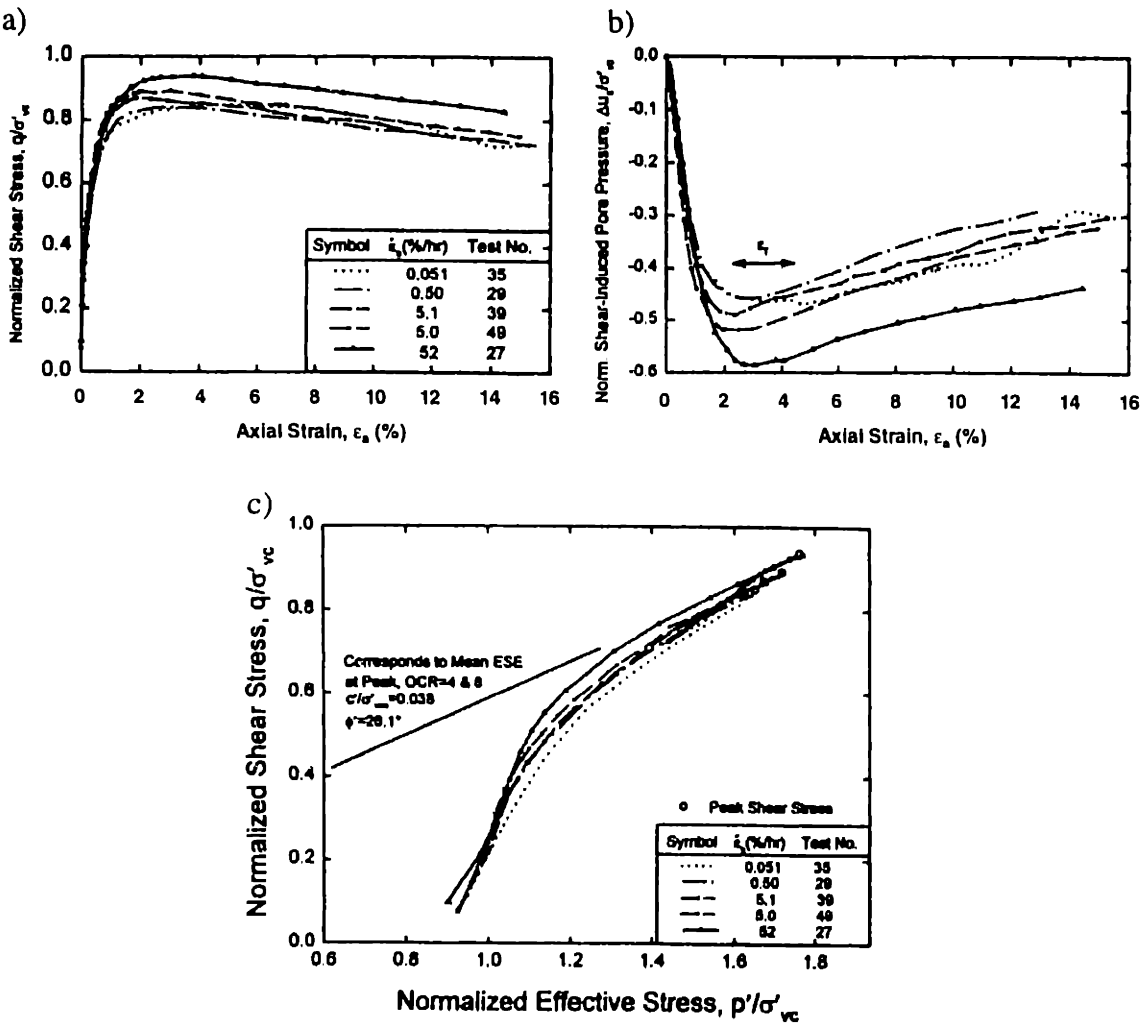


**Figure 3.15:** Effect of strain rate on the behavior of OCR 4 RBBC: a) stress strain curves; b) shear induced pore pressure; and c) stress paths (Sheahan et. al. 1996).

In RBBC, increasing undrained strength with increasing strain rate results from a combination of two factors: a higher mobilized friction angle at peak and the suppression of shear induced pore pressures. Both mechanisms of strength increase act for NC and OCR=2

RBBC, whereas lower shear induced pore pressures (i.e. higher values of p') are solely responsible for any rate dependence at higher OCR's.

Analysis of the data at high strains corresponding to the effective stress envelope at maximum obliquity shows that this envelope is independent of strain rate and can be defined by $c'/\sigma'_{vm}$=0.01 and $\phi'$=31.3 °.

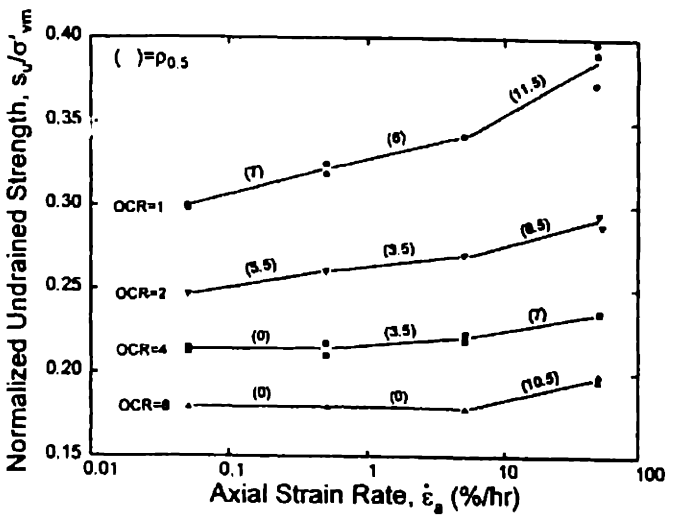


**Figure 3.16:** Normalized shear strength in $CK_0U$ triaxial compression versus strain rate at OCR = 1, 2, 4, and 8 (Sheahan et. al. 1996).

As shown in Table 3.4, the SHANSEP parameters *S* and *m* vary as a function of strain rate: due to the increase in the NC undrained strength with strain rate, and the decreased strain rate sensitivity with OCR, an increase in strain rate causes an increase in *S* and a decrease in *m*.

| Strain Rate (%/hr) | *S* | *m* | $r^2$ | Number of Observations n |
|---|---|---|---|---|
| 0.05 | 0.298 | 0.757 | 0.9997 | 6 |
| 0.5 | 0.320 | 0.714 | 0.9993 | 6 |
| 5 | 0.340 | 0.689 | 0.9997 | 5 |
| 50 | 0.373 | 0.686 | 0.9984 | 8 |

**Table 3.4:** Effect of strain rate on SHANSEP parameters for $CK_0U$ triaxial compression (Sheahan et al. 1996).

Figure 3.14 shows that increasing strain rate leads to significant change in the stress strain behavior of NC RBBC. In particular, the degree of post peak strain softening and the initial stiffness of the soil both increase quite markedly with strain rate. On the other hand no consistent trend is observed between strain at peak and rate. Similar changes in stiffness apply to OC RBBC, but the post-peak strain softening is virtually identical for all tests (Figure 3.15). For all OCR's the rate dependence decreases with strain level.

Finally, except for OCR of 1, for a given stress history, the curves of applied stress level ($\Delta q/\Delta q_{max}$) versus strain are found to be essentially rate independent. This result can represent the basis for modeling rate dependent stress-strain behavior based on q and $\varepsilon$ at failure.

### 3.4.5 Comparison with Natural Boston Blue Clay

#### *3.4.5.1 Introduction*

This section presents a brief comparison of the behavior of RBBC described above with that of natural Boston Blue Clay. The database provided by Berman (1993) is used as reference for the behavior of the natural soil. This study involved triaxial compression and extension, DSS and CRS testing. In addition, the site investigated by Berman, which is located on the MIT campus (referred to in the following as the Building 68 site), is the same site at which the origin material for RBBC series IV was excavated. It is also fairly close to the location from which the soil for RBBC III was retrieved.

#### *3.4.5.2 Index Properties*

The index properties of natural Boston Blue clay can vary greatly throughout the Boston basin, and also with depth at a particular site. For the Building 68 site Berman (1993) cites the following average index properties: LL =36.8$\pm$8.6, PL 24.7$\pm$3.2, PI 15.5$\pm$6.2. Futher, the soil's salt concentration is observed to vary between 5 and 20 g/l, with a decrease in salt content with increasing depth, and the clay fraction of the soil ranges from 40 to 53%. The specific gravity is equal to 2.79. All of these values were obtained by averaging results from a 20 m deposit, having a crust of 10-12 m. The values for the liquid limit, and therefore for the plasticity index, quoted by Berman (1993) are significantly lower compared to those cited for other sites on both the MIT campus (Ladd and Luscher 1965) and the greater Boston area (e.g., Ladd et al. 1998),

Comparison with the data presented in Section 3.3.2 for RBBC IV indicates considerable agreement between the index properties of natural and resedimented Boston Blue clay.

#### *3.4.5.3 Compression Behavior*

As for RBBC, the compression behavior of natural BBC at the Building 68 site is characterized, in the majority of cases, by a fairly constant slope of the virgin compression curve. Berman reports values of CR of 0.179±0.038 for BBC obtained from the crust of the deposit, very close to the values determined for RBBC. Similar trends of swelling ratio with OCR are also reported for both soils. However, significantly higher values of CR (up to 0.4-0.7) have been reported by other authors, particularly for soil below the upper crust at other sites in the Boston area (e.g. de La Beaumelle 1991). Hence the compression behavior of RBBC more closely resembles that of the upper crust of natural BBC, rather than that of the deposit as a whole.

Natural BBC at the Building 68 site is generally characterized by higher values of the normally consolidated $K_0$ (0.51-0.60 vs. 0.48-0.52 for RBBC). The same type of relationship ($K_0=K_{0NC}OCR^n$) linking the increase in $K_0$ to OCR observed for RBBC is found to apply for BBC. For the Building 68 site the value of n suggested by Berman (1993) is equal to 0.45, compared to 0.426 determined for RBBC.[11]

#### *3.4.5.4 Triaxial Compression Undrained Shear Behavior*

Many of the features of the behavior of NC and OC RBBC in undrained triaxial compression described in Section 3.4.4 are also observed in SHANSEP tests on natural BBC. As an example, Figure 3.17 shows the stress paths for four SHANSEP tests performed on BBC with nominal OCR's of 1, 2, 4 and 6 which can be compared to those shown in Figure 3.9a for RBBC. For both soils similar stress paths, and also stress-strain curves, are observed as a function of OCR. Minor differences can be noticed in the behavior of the normally consolidated natural soil, which exhibits a slightly higher strain at peak and reduced post-peak softening. Excellent agreement in the data of the strain at peak is obtained for OC BBC and RBBC.

[11] Similar values of $K_0$ and n are reported for other sites in the Boston area. Based on testing at locations in South and East Boston, Ladd et al. (1998) suggest using $K_0$=0.53, and n=0.40.

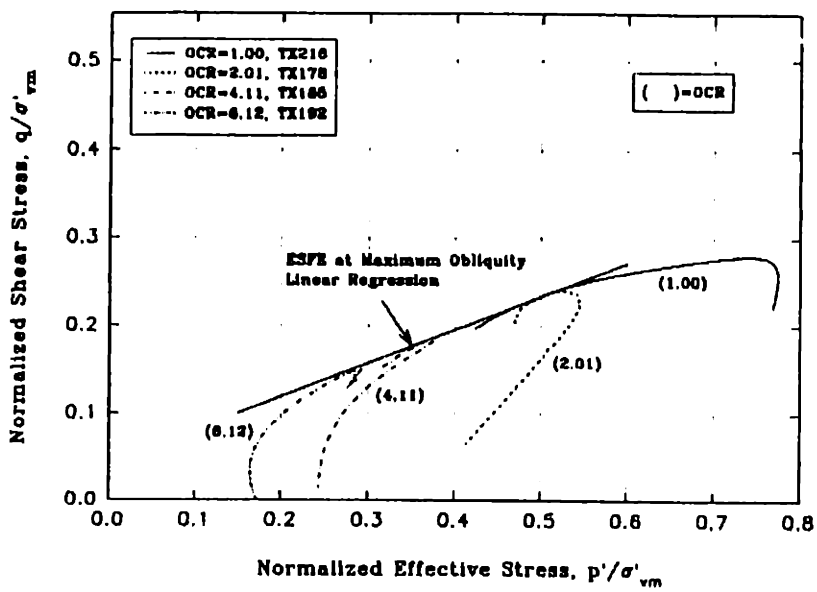


**Figure 3.17:** Representative normalized effective stress paths for SHANSEP $CK_0UC$ triaxial tests at varying OCR: Building 68 site (Berman 1993).

As seen for RBBC, the normalized undrained strength of BBC can be related to the stress history of the soil via the SHANSEP equation. The SHANSEP parameters quoted by Berman (1993) for BBC in triaxial compression are $S_c$=0.279 and m=0.696. Almost identical values are reported for the South Boston site ($S_c$=0.280 and m=0.681, de La Beaumelle 1991). The value of the normalized undrained strength for NC BBC is smaller by about 15% than that typical of RBBC. The difference is due primarily to the higher value of $K_0$ which characterizes BBC. The same relation observed to link the NC undrained strength ratio of RBBC to the pre-shear value of the lateral stress ratio, is found to be valid also for the natural soil.

The maximum obliquity envelope for natural BBC at Building 68 is characterized by a higher value of cohesion intercept ($a'/\sigma'_{vm}$=0.043) and a lower friction angle ($\phi'$=22.5°) compared to RBBC. Note that values of friction angle closer to those determined for RBBC are reported at other sites in Boston (e.g. South Boston: $a'/\sigma'_{vm}$=0.015, $\phi'$ = 29.0°, de La Beaumelle 1991).

Finally comparison with the results obtained by Berman for triaxial extension and direct simple shear suggests that the two soils display similar degree of strength anisotropy, which decreases slightly with increasing OCR.

The discussion presented above, finalized at showing that the undrained shear behavior of RBBC is typical of that exhibited by natural non structured clays, was based on the results of SHANSEP tests on natural BBC. More appropriately, perhaps, it should have relied on the results of Recompression tests as this reconsolidation procedure does not cause destructuring of the clay. However, extensive testing performed by Berman (1993) on BBC from the Building 68 site shows, at least for undrained triaxial compression, excellent agreement between the results performed on natural BBC with the SHANSEP method and those performed with the Recompression method, particularly in terms of the undrained strength ratio $S_c$, the relationship between $q_f(c)/\sigma'_{vc}$ and OCR, and the effective stress failure envelope. The trend between strain at failure $\varepsilon_{af}$ and OCR is also similar, although the Recompression tests present a larger increase in $\varepsilon_{af}$ with increasing OCR.

## 3.5 REFERENCES


1. Ahmed, I. (1990), "Investigation of Normalized Behavior of Resedimented Boston Blue Clay using Geonor Direct Simple Shear," S.M. Thesis, Department of Civil Engineering, MIT, Cambridge, MA, 372 p.

2. Bailey, W.A. (1961), "Effects of Salt on the Shear Strength of Boston Blue Clay," S.B. Thesis, Department of Civil and Sanitary Engineering, MIT, Cambridge, MA, 83 p.

3. Becker, D.E., Crooks, J.H.A., Been, K. and Jefferies, M.G. (1987), "Work as a Criterion for Determining In-Situ and Yield Stresses in Clays," ***Canadian Geotechnical Journal***, 24 (1), pp. 549-564.

4. Bensari, J.E. (1984), "Stress-Strain Characteristics from Undrained and Drained Triaxial tests on Resedimented Boston Blue Clay," S.M. Thesis, Department of Civil Engineering, MIT, Cambridge, MA, 193 p.

5. Berman, D.R. (1993), "Characterization of the Engineering Properties of Boston Blue Clay at the MIT Campus," S.M. Thesis, Department of Civil and Environmental Engineering, MIT, Cambridge, MA, 429 p.

6. Bovee, R. B. (1970), "Analysis of Undrained Plane Strain Shear of Boston Blue Clay," S. M. Thesis, Department of Civil Engineering, MIT, Cambridge, MA, 177 p.

7. Bovee, R. and Ladd, C.C. (1970), "MIT Plane Strain Device," Research In Earth Physics, Phase Rep. 12, Department of Civil Engineering, MIT, Cambridge, MA.

8. Braathen, N.F. (1966), "Investigation of Effects of Disturbance on Undrained Shear Strength of Boston Blue Clay," S.M. Thesis, Department of Civil Engineering, MIT, Cambridge, MA, 159 p.

9. Cauble, D.F. (1993), "The Behavior of Resedimented Boston Blue Clay at OCR4 in Cyclic and Post-Cyclic Undrained Direct Simple Shear," S.M. Thesis, Department of Civil and Environmental Engineering, MIT, 819 p.

10. Cauble, D.F. (1996), "An Experimental Investigation of the Behavior of a Model Suction Caisson in a Cohesive Soil," Ph.D. Thesis, Department of Civil and Environmental Engineering, Department of Civil and Environmental Engineering, MIT, Cambridge, MA, 626 p.

11. De Groot, D.J. (1989), "The Multidirectional Direct Simple Shear Apparatus with Application to Design of Offshore Arctic Structures," Ph.D. Thesis, Department of Civil Engineering, MIT, Cambridge, MA, 699 p.

12. de La Beaumelle, A.C.L.A. (1993), "Evaluation of SHANSEP Strength-Deformation Properties of Undisturbed Boston Blue Clay from Automated Triaxial Testing," S.M. Thesis, Department of Civil Engineering, MIT, Cambridge, MA, 499 p.

13. Dickey, J.W. (1967), "A Plane Strain Shearing Device for Testing Clays," S.M. Thesis, Department of Civil Engineering, MIT, Cambridge, MA, 159 p.

14. Fayad, P.H. (1986), "Aspects of the Volumetric and Undrained Behavior of Boston Blue Clay," M.S. Thesis, Department of Civil Engineering, MIT, Cambridge, MA, 273 p.

15. Force, E. A. (1998), Factors Controlling Pore-Pressure Generation during $K_0$-Consolidation of Laboratory Tests," S.M. Thesis, Department of Civil and Environmental Engineering, MIT, Cambridge, MA, 166 p.

16. Germaine, J.T. (1982), "Development of the Directional Shear Cell for Measuring Cross-Anisotropic Clay Properties," Sc.D. Thesis, Department of Civil Engineering, MIT, Cambridge, MA, 530 p.

17. Jackson, W.T. (1963), "Stress Paths and Strain in a Saturated Clay," S.M. Thesis, Department of Civil Engineering, MIT, Cambridge, MA, 101 p.

18. Jamiolkowski, M., Ladd, C.C., Lancellotta, R., and Germaine, J.T. (1985), "New Developments in Filed and Laboratory testing of Soils," ***Proc. XI International Conference on Soil Mechanics and Foundation Engineering***, San Francisco, August 1985.

19. Kavvadas, M. (1982), "Non-Linear Consolidation around Driven Piles in Clays," Sc.D. Thesis, Department of Civil Engineering, MIT, Cambridge, MA, 666 p.

20. Kenney, T.C. (1964), "Sea-Level Movements and the Geologic Histories of the Postglacial Marine Soils at Boston, Nicolet, Ottawa and Oslo," ***Géotechnique***, 14 (3), pp. 203-230.

21. Kinner, E.B. (1970), "Load-Deformation Behavior of Saturated Clay during Undrained Shear," Sc.D., Department of Civil and Environmental Engineering, MIT, Cambridge, MA, 303 p.

22. Ladd, C.C. (1964), "Stress-Strain Behavior of Saturated Clay and Basic Strength Principles," Research Report R64-17, Research on Earth Physics, Department of Civil Engineering, MIT, Cambridge, 112 p.

23. Ladd, C.C. (1991), "Stability Evaluation during Staged Construction," ASCE, ***Journal of Geotechnical Engineering***, 117 (4), April.

24. Ladd, C.C., Bovee, R.B., Edgers, L., and Rixner, J.J. (1971), "Consolidated-Undrained Plane Strain Shear Tests on Boston Blue Clay," Research Report R71-13, No.273, Department of Civil Engineering, MIT, Cambridge, MA, 243 p.

25. Ladd, C.C. and Foott, R. (1974), "New Design Procedure for Stability of Soft Clays," ***Journal of the Geotechnical Engineering Division***, ASCE, 100 (7), 763-786.

26. Ladd, C.C. and Lambe, T.W. (1963),"The Strength of Undisturbed Clay Determined from Undrained Tests," Symposium on Laboratory Shear Testing of Soils, ***ASTM STP. 361***, pp.342-371.

27. Ladd, C.C. and Luscher, U. (1965), "Engineering Properties of the Soils Underlying the MIT Campus," Research Report R65-58, Department of Civil Engineering, MIT, Cambridge, MA, December.

28. Ladd, C.C. and Varallyay, J. (1965), "The Influence of Stress system on the Behavior of Saturated Clays during Undrained Shear," Research Report R65-11, Soil Publication No. 177, Department of Civil Engineering, MIT, Cambridge, MA, 263 p.

29. Ladd, C.C., Young, G.A., Kraemer, S.R., and Burke, D.M. (1998), "Engineering Properties of Boston Blue Clay from Special Testing Program," Geo-Congress 1998, ASCE National Convention, Boston, October.

30. Ladd, R.S. (1965), "Use of Electrical Pressure Transducers to Measure Soil Pressure," Research Report R65-48, No.80, Department of Civil Engineering, MIT, Cambridge, MA.

31. Malek, A.M. (1987), "Cyclic Behavior of Clay in Undrained Simple Shearing and Application to Offshore Tension Piles," Ph.D. Thesis, Department of Civil Engineering, MIT, Cambridge, MA, 381 p.

32. Martin, R.T. (1970), "Suggested Method of Test for Determination of Soluble Salts in Soil," ***ASTM STP 479***, pp. 288-290.

33. Mesri, G. and Castro, A. (1987), "$C_\alpha/C_c$ Concept and $K_0$ during Secondary Compression," ***Journal of the Geotechnical Engineering Division***, ASCE, 113 (3), pp. 230-247.

34. O'Neill, D. (1985), "Undrained Strength Anisotropy of an Overconsolidated Tixotropic Clay," S.M. Thesis, Department of Civil Engineering, MIT, Cambridge, MA, 360 p.

35. Ortega, O.J. (1992), "Computer Automation of the Consolidated-Undrained Direct Simple Shear Test," S.M. Thesis, Department of Civil and Environmental Engineering, MIT, Cambridge, MA, 172 p.

36. Pestana, J.M. (1994), "A Unified Constitutive Model for Clays and Sands," Sc.D. Thesis, Department of Civil and Environmental Engineering, MIT, Cambridge, MA, 473 p.

37. Preston, W.B. (1965), "The Effects of Sample Disturbance on the Undrained Strength Behavior of Boston Blue Clay," S.M. Thesis, Department of Civil Engineering, MIT, Cambridge, MA, 193 p.

38. Rixner, J. J. (1967), "The Influence of Plane Strain Conditions on the Strength Behavior of Saturated Clay," S. M. Thesis, Department of Civil Engineering, MIT, Cambridge, MA, 113 p.

39. Santagata, M.C. (1994), "Investigation of Sample Disturbance in Soft Clays Using Triaxial Element Tests," S.M. Thesis, Department of Civil and Environmental Engineering, MIT, Cambridge, MA, 289 p.

40. Schmidt, B. (1966), Discussion of "Earth Pressure at Rest Related to Stress History," ***Canadian Geotechnical Journal***, 3 (4), pp.239-242.

41. Seah, T.H. (1990), "Anisotropy of Resedimented Boston Blue Clay," Sc.D. Thesis Department of Civil and Environmental Engineering, MIT, Cambridge, MA, 1061 p.

42. Sheahan, T.C. (1988), "Modification and Implementation of a Computer Controlled Triaxial Apparatus," S.M. Thesis, Department of Civil and Environmental Engineering, MIT, Cambridge, MA, 266 p.

43. Sheahan, T.C. (1991), "An Experimental Study of the Time-Dependent Undrained Shear Behavior of Resedimented Clay Using Automated Stress-Path Triaxial Equipment," Sc.D. Thesis, Department of Civil and Environmental Engineering, MIT, Cambridge, MA, 955 p.

44. Sheahan, T.C., Ladd, C.C., and Germaine, J.T. (1996), "Rate-Dependent Undrained Shear Behavior of Saturated Clay," ***Journal of Geotechnical Engineering***, ASCE, 122 (2)m February, pp. 99-108.

45. Sinfield, J.V. (1994), "An Experimental Investigation of Sampling Disturbance Effects in Resedimented Boston Blue Clay," S.M. Thesis, Department of Civil and Environmental Engineering, MIT, Cambridge, MA, 413 p.

46. Ting, N.A. (1990), "Effects of Disturbance on Consolidation with Vertical Drains," S.M. Thesis, Department of Civil Engineering, MIT, Cambridge, MA, 406 p.

47. Varallyay, J. (1964), "The Influence of Stress System Variables on the Undrained Strength of Boston Blue Clay," S.M. Thesis, Department of Civil Engineering, MIT, Cambridge, MA, 179 p.

48. Walbaum, M. (1988), "Procedure for Investigation of Sample Disturbance using the Direct Shear Apparatus," S.M. Thesis, Department of Civil Engineering, MIT, Cambridge, MA, 367 p.

49. Whittle, A.J. (1987), "A Constitutive Model for Overconsolidated Clays with Application to the Cyclic Loading of Friction Piles," Sc.D. Thesis, Department of Civil and Environmental Engineering, MIT, Cambridge, MA, 641 p.

50. Wissa, A.E.Z. (1961), "A Study of the Effects of Environmental Changes on the Stress-Strain Properties of Kaolinite," S.M. Thesis, MIT, Cambridge, MA, 179 p.

51. Wissa, A.E.Z. and Heiberg S. (1969), "New One-Dimensional Consolidation Test," Research Report n. 69-9, Soils Publication No. 229, Department of Civil Engineering, MIT, Cambridge, MA.

52. Zreik, D.A. (1994), "Behavior of Cohesive Soils and their Drained, Undrained, and Erosional Strengths at Ultra-low Stresses," Ph.D. Thesis, Department of Civil and Environmental Engineering, MIT, Cambridge, MA, 533 p.

# CHAPTER 4

# EQUIPMENT

## 4.1 INTRODUCTION

This chapter describes the triaxial equipment used to perform the experimental program. The current system has extended the capabilities of the automated triaxial apparatus originally developed in the MIT geotechnical laboratory by Sheahan (1991). Substantial innovations have been introduced to induce and observe the micron-level displacements corresponding to the pre-failure behavior of geomaterials, with a particular emphasis on cohesive soils. This chapter highlights these innovations.

The most significant improvement to the existing equipment was the development of a system for the on-specimen measurement of small strains, based on the use of LVDT's. Successful investigation of the small strain behavior of soils in the triaxial apparatus relies, however, not only on the availability of effective technology for the measurement of small strains, but also on several other details of the testing system. Internal force measurement, stress path control, precise axial alignment tolerances, and the availability of a high-resolution data acquisition system represent other essential characteristics.

Prior to discussing the characteristics and the performance of the system for measuring local strains, a brief overview of the triaxial system employed in the MIT Geotechnical Laboratory for testing cohesive soils is presented in Section 4.2. Particular emphasis is placed on the description of the chamber and on the axial load application system, which was recently modified to improve investigation of the pre-failure behavior. Since the level at which displacements can be resolved is also governed by the precision of the data acquisition system, a brief discussion of the data acquisition system is also provided. A more complete description of the equipment can be found in Sheahan (1991).

The second part of the chapter (Section 4.3) focuses on the system developed over the past two years in the MIT Geotechnical Laboratory for the measurement of small strains. As

discussed in more detail in Section 4.3.1, the design of this new system was based on various requirements. These requirements included a need to accommodate a wide variety of geomaterials of varying stiffnesses, and the desire to test specimens after prolonged consolidation and under a variety of stress and temperature conditions. The resulting system was developed in a joint effort between the author and other researchers in the MIT Geotechnical laboratory, in particular Greg Da Re (Da Re 1999), a doctoral candidate who is investigating the small strain behavior of frozen Manchester Fine Sand. It involves the use of two miniature LVDT's mounted on a pair of lucite yokes, which clamp onto a standard triaxial specimen (10 $cm^2$ x 8 cm). Although similar to the system developed by Andersen (1991), who initiated small strain measurements at MIT, a number of substantial innovations have been made to the original system. These include a more refined mechanical design as well as a completely new MIT-developed signal-conditioning system. Both the mechanical and the electrical systems are discussed in some detail in Sections 4.3.2 and 4.3.3, while section 4.3.4 describes the mounting procedures. Signal stability is established as a function of time, temperature and confining pressure in Section 4.3.5. The performance of this device is then discussed based on proof tests conducted on aluminum and PMMA [polymethylmethacrylate] (section 4.3.6) and on RBBC and frozen Manchester fine sand (Section 4.3.7) the soils for which the apparatus has been developed.

## 4.2 MIT AUTOMATED STRESS PATH TRIAXIAL CELLS

### 4.2.1 General Overview

A large effort has been invested at MIT over the past 10 years into automating the existing conventional testing equipment. This process has occurred following the approach of *adaptable automation* (Sheahan and Germaine 1992) whereby each component of an existing manual system is examined and modified to permit automation, and additional innovative components are added to complete the system automation. This approach offers the potential advantages of preserving customized technology, lowering costs, and increasing flexibility. The first application of this concept, which resulted in the development of the MIT Automated Stress Path Triaxial Cells, is described in detail by Sheahan (1991) and Sheahan and Germaine (1992). A similar philosophy has since been employed successfully for the automation of other laboratory testing devices, for example the triaxial apparatus for testing sands (Andersen 1991),

the direct simple shear device (Ortega 1992) and two MIT designed apparatuses: the plane strain reinforcement (APSR) cell (Chauhan 1995) and the caisson element test (CET) cell (Cauble 1996). In all cases the resulting technology is characterized by increased versatility, dramatic labor reduction and exceptional quality control.

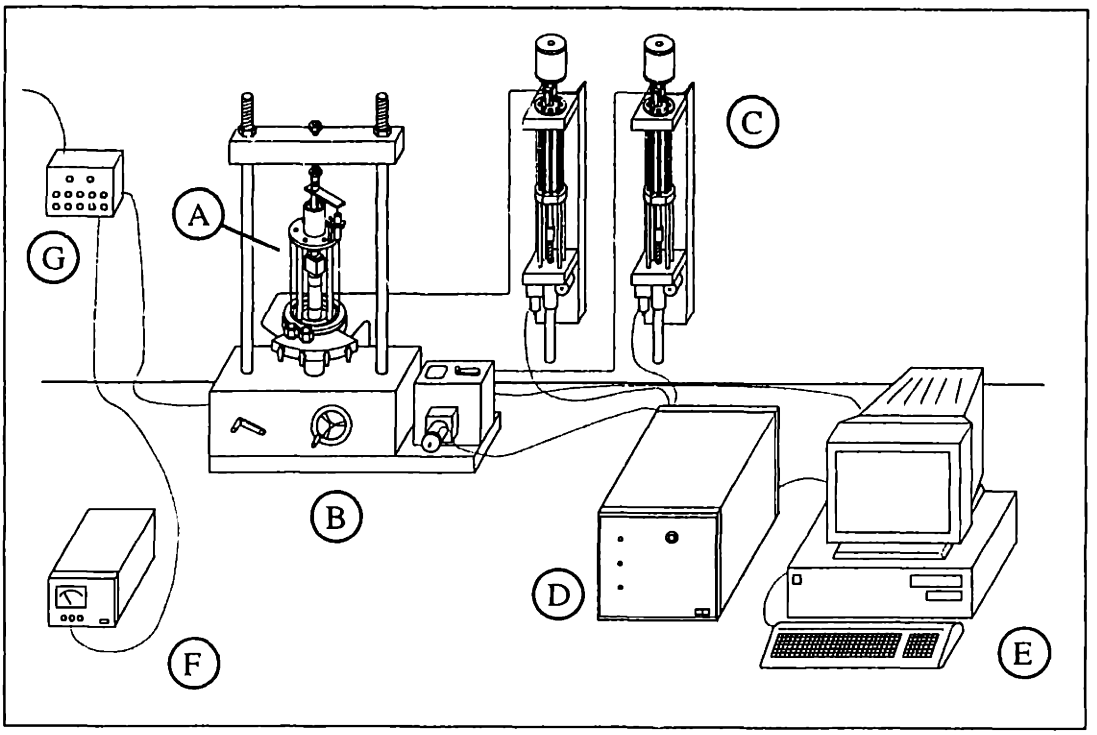


A - Triaxial Cell
B - Load Frame
C - Pressure/Volume Controllers
D - Motor Control Box
E - Personal Computer
F - DC Power Supply
G - Data Acquisition Channels

**Figure 4.1:** MIT automated stress path triaxial cell – schematic (connections between transducers and PC not shown).

Figure 4.1 shows a schematic of a computer controlled triaxial testing apparatus used in the MIT geotechnical laboratory for testing cohesive soils. In line with the concept described above, the system combines existing MIT testing equipment (e.g. load frame, triaxial cell, etc.) with some innovative components (e.g. analog-to-digital converter, electronic motor control system, etc.). The apparatus includes six basic components: 1) the triaxial chamber; 2) the system for load application comprising the pressure-volume controllers and the loading frame; 3) the motors, motor controllers and drivers; 4) the instrumentation package including the power

supply and all transducers; 5) the personal computer based control system; and 6) the central data acquisition system (not shown in the figure).

The triaxial chamber (Figure 4.2) contains the specimen and sets the boundary conditions. It incorporates internal posts, top and bottom drainage, a fixed top cap and a compact shear-beam load cell located within a Plexiglas chamber for direct measurement of the axial deviator stress. The load cell is connected to the loading piston that rides through a low friction linear bearing. Piston movement is monitored with an externally mounted DCDT. Cell fluid leakage is prevented through the use of a rolling diaphragm seal. The system is filled using Dow-Corning "200 fluid", 20 centistokes silicone oil. This particular silicone oil exhibits extremely low viscosity under a wide range of temperatures, is optically transparent and does not degrade the seals or the latex membranes used in testing. This oil was initially selected to limit leakage over the course of a test, but also offers the added benefit of being nonconductive which is essential when locating electronic devices such as the load cell and the on-specimen small strain measurement system within the triaxial chamber.

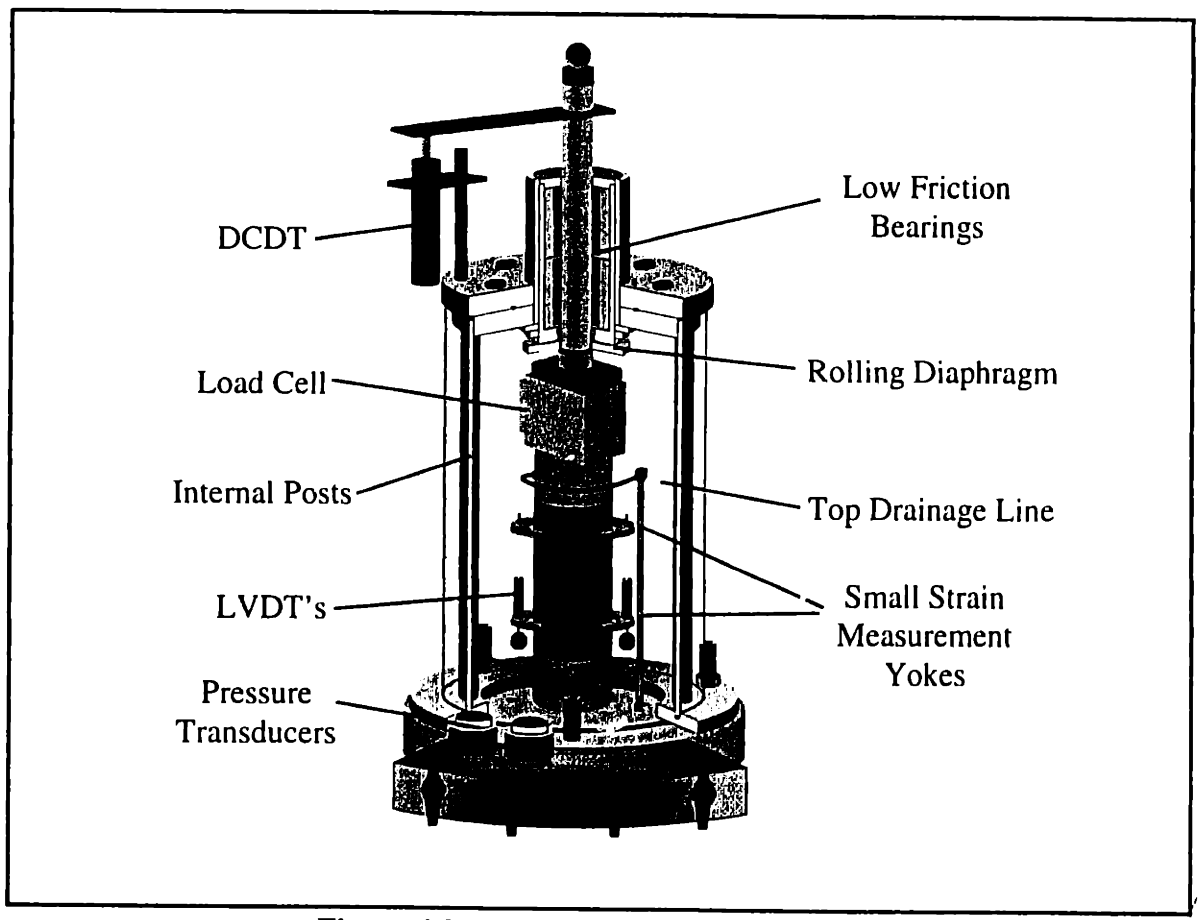


**Figure 4.2:** Triaxial chamber – schematic.

The entire system is axially loaded through the use of a 1060 kg capacity bench-top Wykeham Farrance screw driven loading frame with adjustable gear ratios. Pressure-volume controllers (PVC) are used to control both the cell and back (pore water) pressures. These devices consist of a motor driven ball-screw jack that converts the rotary motion of the motor into the linear motion of a piston that displaces fluid from a cylinder. A DCDT monitors piston displacement on the back pressure PVC to measure volume changes in the specimen. Both the chamber and back pressures are monitored with high-performance diaphragm type pressure transducers that have a range of 0-14 ksc and are located on the base of the cell to reduce system compliance. All transducers are powered by a DC current regulated power supply. Copper tubing and ball valves are employed to minimize compliance and limit pressure loss in the loading system.

The triaxial chamber, the load frame and the two pressure volume controllers are housed in a temperature-regulated enclosure maintained at 25$\pm$0.2 °C using an air circulating unit activated by a regulating thermostat thermometer. The enclosure and the rest of the apparatus are located inside an air conditioned laboratory.

Automated control is carried out using a PC and a control program written in BASIC. The program is task specific and able to perform all phases of a triaxial test including initial pressure up, back pressure saturation, B-value check, consolidation along any stress path or $K_0$ consolidation and (un)drained shear in compression and in extension.

During each phase of the test, signals from the pressure and displacement transducers and the load cell are converted from analog to digital by an MIT designed (Sheahan 1991) 22 bit A/D integration card. The software in the PC processes the digital information. The current values of the stresses and the displacements in engineering units are determined and compared with the target values. A closed loop proportional gain control algorithm is used to calculate, based upon the estimated system stiffness, the control signals that are sent via a Strawberrytree 12 bit digital to analog converter to the MIT-designed motor control box. (Note that when shearing at a constant strain rate the system operates in an open loop configuration). Finally, extensive use of cable shielding and grounding is employed to reduce the impact of electromagnetic noise on small changes in output signal.

The triaxial apparatus described above includes two data acquisition systems: a central system used to collect all the data in the MIT Geotechnical Laboratory and a local one used by the personal computer for control purposes.

The central system is based on a 486 microprocessor PC interfaced with an expanded channel Hewlett Packard HP3497A data acquisition unit. The system is capable of analog to digital conversion and storage of data at a trigger rate of up to 1Hz. The system, which can presently monitor up to 140 channels, is driven by Windows based software. Since small displacements during shear correspond to extremely small changes in the LVDT's output, the sensitivity of this system has been instrumental in observing levels of strain down to $10^{-6}$. This high quality, low noise system also makes it possible to directly measure, without any signal amplification, the output from the load cell and pressure transducers whose full-scale output is on the order of 200 mV. The resolutions and the stability of transducer signals as measured by the central data acquisition are summarized in Table 4.1.

| Device | Range | Resolution | Stability |
|---|---|---|---|
| Axial Strain LVDT | 1.4 cm (~17.5%) | ±0.0005% (0.1 mV) | ±0.005% (1 mV) |
| Volumetric Strain LVDT | 10 $cm^3$ (~12.5%) | ±0.0002% (0.1 mV) | ±0.005% (1 mV) |
| Cell Pressure Transducer | 25 ksc | 0.0001 ksc (0.001 mV) | 0.001 ksc (0.01 mV) |
| Pore Pressure Transducer | 25 ksc | 0.0001 ksc (0.001 mV) | 0.001 ksc (0.01 mV) |
| Load Cell | 45 kg | 0.3 g (0.001 mV) | 3 g (0.01 mV) |
| Load Cell | 90 kg | 0.6 g (0.001 mV) | 6 g (0.01 mV) |

Calculations based on standard triaxial specimen size (H = 8 cm, D = 3.8 cm).

**Table 4.1:** Resolution and stability of transducer signals as measured by the central data acquisition system (adapted from Sheahan 1991).

Local data acquisition is achieved by the PC running the test, through the use of a 22 bit A/D converter that is primarily used for control purposes. This high quality system can be programmed to integrate the signal over a time span of 16ms to 300 ms. In this research it was

used for data collection during the undrained shear phase of tests that involved strain rates higher than 0.1% to facilitate data collection at up to 40 Hz, and thus obtain better definition of the stress-strain behavior at very small strains.

The readings collected by both of the data acquisition units can be stored into data files. A Quick-BASIC reduction program modified for the analysis of tests with on-specimen measurement of the strains is used to calculate stresses and strains during all phases of the test.

### 4.2.2 Recent Modifications for Small Strain Measurements

The most recent modifications to the triaxial apparatus were introduced to improve the determination of soil stiffness in the pre-failure region. Along with the development of a system for measurement of the small strains (discussed separately in Section 4.3), additional modifications included the introduction of the internal measurement of the axial load, the design of the connection between the piston, load cell and top cap, as well as additional improvements to the load application system and loading procedure.

The use of an internal load cell eliminates the effects of load system friction on the load measurement. In particular, it is essential for the accurate determination of the small strain behavior of soft clays for which the increments in axial load associated with initial nonlinearity may be as small as a few hundred grams.

A comparison of stress strain curves determined using both internal and external measurements of the axial load performed on the same specimen is shown in Figure 4.3 for the

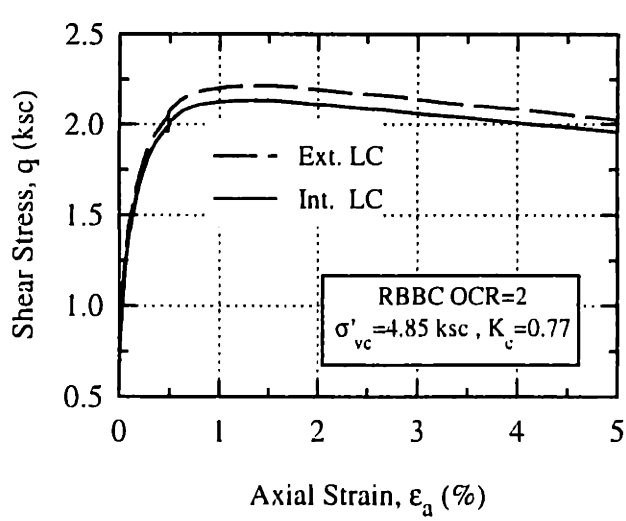


**Figure 4.3:** Difference between external and internal measurement of the axial load.

undrained shear phase of a standard triaxial test with external measurement of the axial strain performed on a specimen of RBBC with an OCR of 2. The results indicate that even with the low friction ball bearings used in the MIT triaxial apparatus, there is a significant difference in the measured shear stress at all levels of strain. External measurement of the axial load overestimates the load acting on the specimen by about 1000g. Note that the insensitivity of the shear beam load cells to cell pressure was also verified, thus eliminating concerns of using these devices within the test chamber.

Measurement of the axial load inside the triaxial chamber also has a second advantage. Since the load cell measures only the deviator stress acting on the specimen, a much lower capacity load cell can be employed. As a consequence the resolution in the load measurement is enhanced. This results in more accurate measurements of small strain behavior, particularly in soft soils, such as RBBC, for which, as said above, small strain shearing is associated with limited increases in the axial load. A 45 kg (100 lbs.) load cell was employed for the majority of the tests presented in this thesis. A 90 kg (200 lbs.) cell was used in a limited number of tests that explored behavior at higher confining stresses.

With the relocation of the load cell inside the triaxial chamber between the top cap and the piston, the connection between these components had to be redesigned. This operation went through two phases, as it became apparent, through preliminary tests on aluminum, PMMA and soil, that minor eccentricities in load application led to significant differences in the strains measured by the LVDT's on opposite sides of the specimen, and thus limited the reproducibility of very small strain measurements. In fact, following the development of the on-specimen strain measurement system, the difficulty in applying the load to the specimen in a "perfect" manner, i.e. uniformly and coaxially, was identified as the major limitation in the investigation of the very small strain behavior (<0.001%) of RBBC. Cuccovillo and Coop (1997a) reported similar findings in measuring the small strain behavior of structured sands and had to resort to the design of a new connection between specimen and top cap.

Rather than pursue the strategy followed by Cuccovillo and Coop (1997b), who created a fairly "flexible" structure that would accommodate the effects of minor eccentricities in the load application, all efforts were taken to minimize any lateral play in the system and to guarantee perfect alignment of the loading axis with the center of the specimen, and parallelism of the top cap surface to the specimen base.

To achieve these goals, the design of the piston-top cap assembly followed the following guidelines:

a) The components in the piston assembly were minimized. In particular, the top cap was modified to connect directly to the load cell without any intermediate components.

b) The connections between the top cap and load cell and the piston and load cell have flat bearing surfaces to ensure tight contact between components and thus eliminate the play characteristic of bearing on screw threads (Figure 4.4).

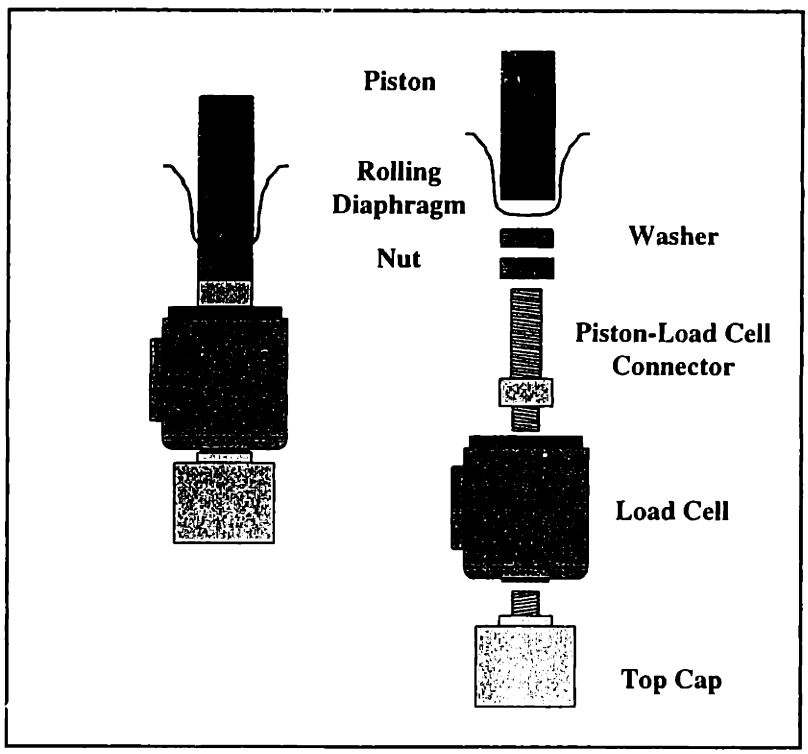


**Figure 4.4:** Modified piston - load cell – top cap connection.

c) All connecting components of the piston-load cell-top cap assembly were machined and assembled in a single session on the lathe to ensure concentricity.

d) A large nut was added to secure the adjustable height piston to the top structural ring of the triaxial chamber.

e) The alignment of the assembly was checked regularly particularly if the results of a test showed evidence of tilting of the specimen.

In addition the following actions were taken:

a) Tighter tolerance bearings were employed to eliminate instability of the piston (Figure 4.2).
b) The moment break between the loading piston and the upper crossbar, which originally consisted of ball seats on both components, was modified to a hardened steel ball in a ball seat on the piston bearing against a flat surface on the crossbar, to ensure point loading of the specimen through its central axis.
c) The load frame uprights were pre-tensioned to increase stability and reduce the amount of flexure upon loading.
d) The load frame was shimmed with the aid of a high precision level to ensure that the cell was level.

To accommodate the presence of the load cell inside the triaxial cell new extended posts and a taller plexiglass cylinder were also manufactured. In addition, holes were driven through the base of the cell to provide electrical connections for the load cell, as well as for the LVDT's employed for the on-specimen strain measurements.

## 4.3 SMALL STRAIN MEASURING SYSTEM

### 4.3.1 Design Criteria

The system for the measurement of small strains was designed to meet several requirements. These requirements were based on three primary issues: the capabilities necessary to meet the objectives of this study (measure strains as small as $5 \times 10^{-6}$ or better), the need to integrate the system with existing equipment, and the versatility of the final design. In general the system had to possess the following properties:

- high resolution
- virtually unlimited range in strain
- DC output
- pressure insensitivity
- relative insensitivity to temperature
- no influence on specimen loading as a result of displacement
- compact design
- no interference with the pressure seals on the test specimen

- ability to be integrated into existing triaxial technology
- and limited cost.

While investigation of soil behavior at strains on the order of $5 \times 10^{-6}$ is necessarily associated with high resolution on-specimen measurements, many possibilities exist regarding the choice of instrumentation and setup configuration. Since the triaxial apparatus is the device most commonly used in the investigation of the stress-strain behavior of soils, substantial efforts have gone into implementing techniques for the measurement of the small strain behavior in this apparatus. Various devices including electrolevel displacement gages (e.g., Burland and Symes, 1982, Jardine et al. 1984), Hall effect semiconductors (e.g. Clayton and Khatrush 1987, Clayton et al. 1989), miniature LVDT's (e.g. Brown et al. 1980, Costa Filho 1985, Andersen et al. 1995, Cuccovillo and Coop 1997b), proximity sensors (e.g. Hird and Yung 1989, Lo Presti et al. 1994) and local deformation transducers (e.g. Goto et al. 1991) have been employed to consistently measure strains on the order of $10^{-5}$.[1] Scholey et al. (1995) present a review of these methods, summarizing their capabilities and limitations.

Throughout this program the compatibility of the small strain measurement system with the triaxial apparatuses available in the MIT Geotechnical Laboratory was of primary concern. Thus the measurement system had to accommodate a 3.56 cm diameter specimen surrounded by a rubber membrane and fit within the confined space of the existing triaxial chamber. It was also desirable for the same device to measure, without major modifications, the small strain stiffness of a wide range of geomaterials. In particular, the final design had to meet the immediate requirements posed by two research projects: one dealing with a fundamental investigation of the small strain behavior of Resedimented Boston Blue Clay, which is presented in this thesis; the second focusing on the pre-failure behavior of frozen Manchester Fine Sand (Da Re 1999). These two materials differ in their initial stiffness by more than two orders of magnitude thus establishing a range in behavior that encompasses that of most soils.

Investigation of such different materials posed problems not only of a practical nature related to the connection between specimen and instrumentation, but also related to different testing needs. The testing program for RBBC required performing SHANSEP type tests at a variety of stress levels and overconsolidation ratios. In these tests shear would occur in all cases

[1] Note that the smallest strain measurable is also a function of the specimen size.

after at least 5% consolidation strain. Clearly the need for such tests ruled out devices such as the LDT (Goto et al., 1991) which have an axial strain limit of about 2%, beyond which they cease to function. The testing program on RBBC also included multi-stage tests in which various small amplitude ($\varepsilon_a$<0.1%) shears, separated by consolidation phases with 1.5-2% axial strain, would be performed on one specimen. In this case it was necessary to employ a device characterized by a large enough linear range to accommodate measurement of strains over a range of 0.5 cm, or to provide a means to adjust the position of the devices prior to each shear phase.

Specific to the investigation of frozen MFS was the need to run tests to very high strains (25-30%) at fairly high confining pressures, up to 10 MPa, and at temperatures as low as -25°C. The system had to be robust enough to withstand these conditions and yet still be able to resolve the displacements necessary to characterize the pre-failure deformations. The first two requirement influenced the selection of the type of measuring device, and its connection to the soil specimen. The last posed issues related to the electronics employed and in particular to the performance of the signal conditioning system.

Finally, the desire to make the measurement of pre-failure deformations a standard procedure in the MIT Geotechnical Laboratory, required implementation of the technology in the six stress path cells employed to test clays and in two high pressure stress path cells used to test frozen and unfrozen sands. This requirement established the need for a low cost system which, if necessary, could be easily moved from one triaxial apparatus to another.

### 4.3.2 Mechanical Configuration

The current system used in the MIT Geotechnical Laboratory to measure the small strain response of geomaterials has resulted from years of continuous development of the mechanical and electrical design. The system is based on two LVDT's set diametrically opposite to each other on two yokes, as shown schematically in Figure 4.5. The yokes are fabricated out of Lucite, chosen for its strength and light weight. They are hinged, and clamp onto the specimen at three points, each 120 degrees from the other. Due to the lightweight design, the clamping force needed to maintain stability is very small and can be varied by proper selection of a small spring placed across the hinge of each yoke. This type of clamping mechanism avoids insertion of pins in the specimen, as done by several researchers, thus preserving the integrity of the

membrane and eliminating the possibility of leakage, particularly during the long duration multi-stage tests[2] performed in this research on Resedimented Boston Blue Clay. In addition, the "open" clamping mechanism accommodates radial deformation of the specimen while maintaining the alignment of the transducers. Barreling of the specimen at large strains is also not impeded. The yokes currently employed are designed for a standard sized triaxial specimen (3.56cm in diameter), yet the design can easily be scaled up for larger sized specimens.

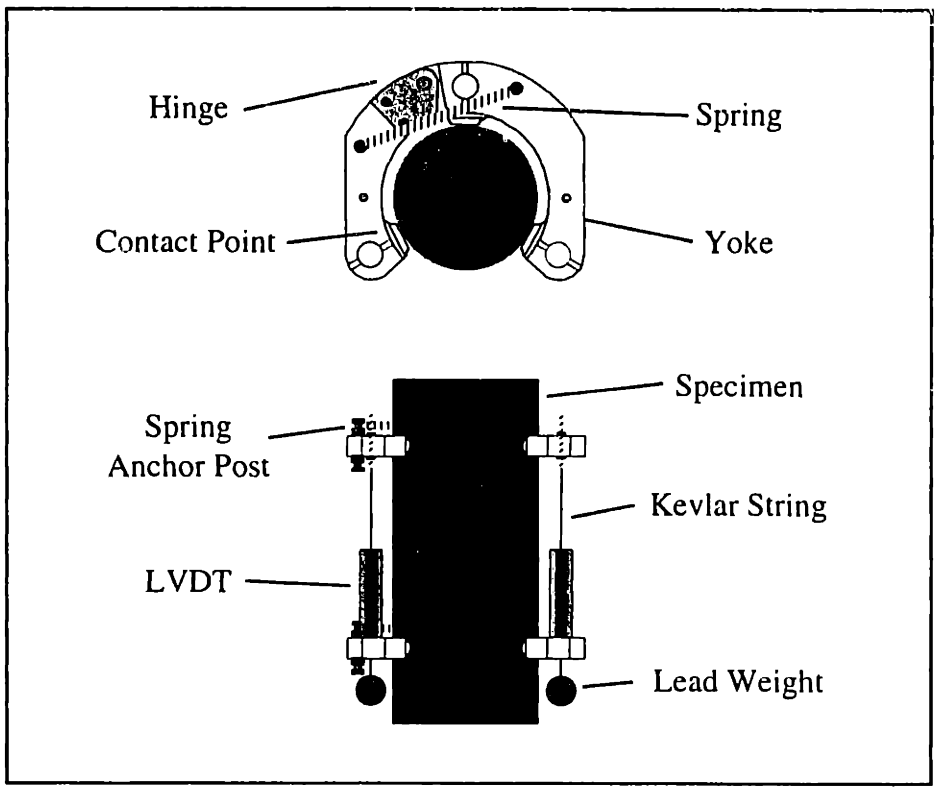


**Figure 4.5:** Schematic of yokes.

As shown in Figure 4.5, the LVDT body is mounted on the lower yoke while the core assembly is suspended from the upper yoke using an adjustable screw. To allow for free movement of the core in the transducer body and to limit friction, the LVDT core was extended using stainless steel rods such that the actual core length was longer than the transducer body. This was found to reduce stick-slip problems at extremely small displacements. To further reduce friction, particularly at higher strains as the specimen undergoes some barreling, the

[2] Details on the multi-stage testing approach employed are provided in Chapter 5.

extended core was connected to the upper yoke screw assembly with a small length of woven Kevlar string thus allowing the core to find its center within the LVDT body. A small lead weight (6-10g) was attached to the other end of the core with another small length of Kevlar string to provide a small tensile force on the core assembly.

Extensive proof testing on aluminum, PMMA and soil indicates that the mechanical design described, in particular the connection between the transducer cores and the upper yoke, eliminates the mounting, alignment and friction problems traditionally associated with on specimen measurements of strains using LVDT's (Scholey et al. 1995). Further, the yoke system appears to have no influence on the integrity of the membrane surrounding the specimen.

The transducers chosen for this application are Schaevitz's XS-B Series subminiature LVDT's. These transducers, 22.4 mm in length and only 4.77 mm in diameter, have a mass of 4.0 grams each. In addition to their small size, they offer a number of additional features which make them particularly attractive for this type of application. They are energized by an external AC source and have a relatively large linear range of $\pm$0.254 cm ($\pm$0.1 in.). They also have an outstanding range in environmental compatibility. Typical operating temperatures range from -55 °C to 150 °C. This makes these devices ideal for the low temperature measurements on frozen sand. They can also operate continuously in fluids pressurized to 3000 psi (21 MPa).

The induction principle by which the LVDT operates gives this device two outstanding characteristics. The first is truly infinite resolution. This means that the LVDT can respond to even the most minute motion of the core. Thus, the primary limitation on the resolution is the capability of the data acquisition system. The inherent symmetry of the LVDT construction produces the other feature, null repeatability. The null position of an LVDT is extremely stable and repeatable.

### 4.3.3 Signal Conditioning Unit

The operation of the type of LVDT described above requires the use of signal conditioning on both the input and output of the transducer. The standard signal conditioning units available for these transducers performed according to the manufacturer's specifications; however, the resulting levels of stability and noise reduction did not permit resolution of the strains ($10^{-6}$) required for this program. For this reason a new signal conditioning system, referred to in the following as the CSSD (Clever Small Strain Device) unit was developed in

house to meet the required criteria. This new signal conditioner performs three tasks: 1) it provides the appropriate amplitude-regulated AC voltage to the transducer at the appropriate frequency, 2) it amplifies the LVDT's AC output since it is usually too low level to be sensed accurately, and 3) it converts the output signal to filtered DC such that it can be read by the data acquisition system.

The CSSD signal conditioning unit was designed around the Analog Devices AD698 IC chip (Analog Devices Inc. 1994) which has an internal circuit that can be optimized for use with any LVDT, including half-bridge and series opposed (4 wire) configurations, and the AD826 operational amplifier. The AD698 integrated circuit provides a complete monolithic LVDT subsystem in a ceramic dipped package. It is powered by 30 V (+/- 15V) and has an operating temperature range of -55°C to +125°C, similar to that of the LVDT's employed. A functional block diagram of the circuit developed is provided in Figure 4.6.

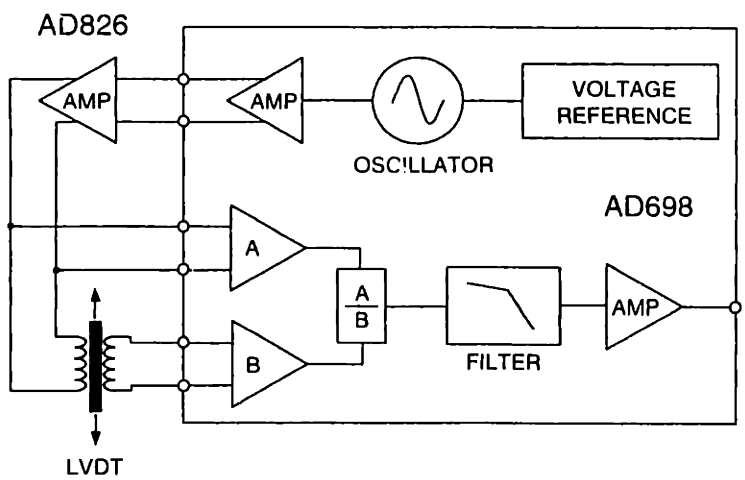


**Figure 4.6:** Functional block diagram of signal conditioning unit.

The AD698 energizes the LVDT primary coil through the use of a low distortion sine wave oscillator and power amplifier. A single external resistor and capacitor determine frequency and amplitude. Output frequency can range from 20 Hz to 20 kHz and amplitude from 2V to 24 V. For the LVDT's described above, best performance was achieved through excitation at 2V rms at 2.5 kHz. A high-speed low power unity gain amplifier was used on the output of the AD698 due to the extremely low impedance of this particular type of LVDT. The AD698 decodes the LVDT's by synchronously demodulating the amplitude-modulated input and a fixed input reference. The ratio of the LVDT output to its input excitation is then calculated

and multiplied by a scale factor. This eliminates scale factor errors due to drift in the amplitude of the primary drive, improving temperature performance and stability. The AD698 also includes a phase compensation network to add phase lead or lag to the LVDT output to compensate for the LVDT primary to secondary phase shift. Once both channels are demodulated and filtered, an output amplifier scales a reference current (by the ratio of LVDT output to input) converting it to a voltage. This voltage can then be measured to determine the LVDT core displacement. This output ranges from -10 V to +10 V over the linear range of the transducer (0.508 centimeters).

### 4.3.4 Mounting of the Small Strain System on the Triaxial Specimen

Mounting of the yokes on the specimen occurs once the specimen is setup on the triaxial cell base. Alignment of the top and bottom yokes is ensured through the use of 3 alignment posts that also set the desired gage length (usually equal to 5.08 cm). Once the yokes are clamped onto the specimen the posts are removed by extracting, with a pair of tweezers, six small brass pins, thus allowing the yokes to move freely as the specimen strains. A schematic of an instrumented specimen is shown in Figure 4.5. Prior to set-up, the position of the threaded rod holding the core in the top yoke is adjusted to ensure that the devices will come into range at the appropriate strain. This is a particularly crucial step in the SHANSEP tests performed on RBBC as the transducers are out of the linear range at the time of set-up. To ease positioning of the cores additional holes were made in the vertical alignment posts and a dummy aluminum specimen having the same diameter as the standard triaxial specimen was fabricated with a series of grooves cut into it every 0.127 cm (0.05"). The yokes are placed on the grooves corresponding to the expected pre-shear height[3] and the position of the threaded rod is adjusted to achieve the desired output. The initial gage length is reset prior to clamping the yokes around the soil specimen.

[3] As the compression behavior of RBBC is well known, the strain, and therefore the displacement, corresponding to the targeted axial stress can be predicted with some confidence.

### 4.3.5 Electrical Performance

#### *4.3.5.1 Stability Characteristics*

One of the most important characteristics of the LVDT-signal conditioning system is the stability of its output over both the short term and the long term. Short-term stability is necessary in order to accurately measure the stress-strain behavior of soils, whereas long term stability is essential for accurate measurements of creep behavior.

The electrical stability of the newly developed LVDT-signal conditioning system was evaluated by monitoring the transducer output using the central data acquisition system in MIT's Geotechnical Laboratory. Figures 4.7a and 4.7b present the results obtained at room temperature (20° C) over periods of 5 minutes and 24 hours respectively. For these tests the LVDT was placed horizontally inside the triaxial chamber to avoid the possible influence of creep in the

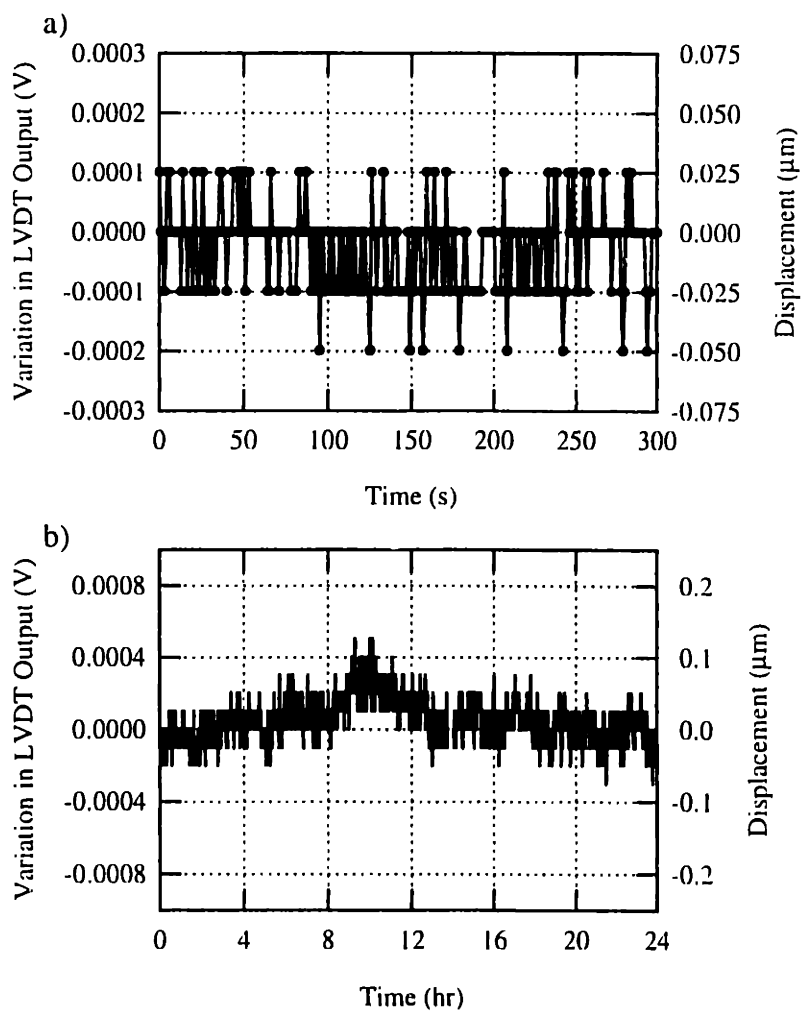


**Figure 4.7:** LVDT stability with CSSD at 20 °C (a) over 300s and (b) 24 hours.

Kevlar string, over the longer period of time. Both the triaxial apparatus and the signal conditioning electronics were also located inside an environmental enclosure to ensure proper temperature control. As shown in Figure 4.7a, over a period of 300 seconds the signal of the LVDT fluctuated by only ±0.15mV, corresponding to 3 bits of digital noise[4]. Based on the transducer's calibration factor this noise band corresponds to a displacement of 0.075 μm and translates into a strain of about 0.00015%, for a gage length of 5.08 cm. Note that even at the slowest strain rate employed (0.1%/hr), the entire small strain region is crossed during the first 5 minutes of shear. Figure 4.7b shows that over 24 hours the output signal of the LVDT fluctuated by approximately ±0.3mV without any appreciable signal drift.

It is interesting to compare the performance of the LVDT's used in conjunction with the newly developed signal conditioning units to that obtained using a commercial signal conditioning system provided by the manufacturer of the LVDT's. Figures 4.8 presents a plot of the LVDT stability over 300 seconds similar to that shown in Figure 4.7a, but obtained employing the commercial system. The data in Figure 4.8a indicate that over 300 seconds the signal noise band is about 0.8 mV. This performance is within the manufacturer's specifications and is generally satisfactory for commercial applications. However, comparison with the data presented in Figure 4.7 shows that the new conditioning system leads to a significant improvement in the electrical performance of the LVDT that is very valuable in research investigations.

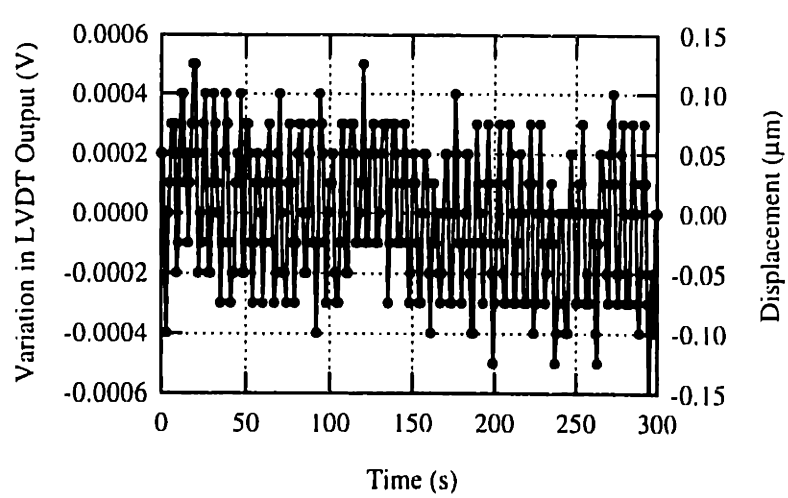


**Figure 4.8:** LVDT stability with commercial signal conditioner at 20 °C over 300s.

[4] This is true when the absolute value of the measured voltage exceeds 1V. For smaller values of |V|, the noise band is still equal to ± 0.1 mV but the bit size decreases.

#### *4.3.5.2 Effect of Temperature on LVDT Output*

As the instrumentation was also designed to measure the pre-failure behavior of frozen sands, its electrical performance was evaluated below room temperature. Figures 4.9a and 4.9b compare stability data over 300 seconds and 24 hours respectively for three different temperatures: 20°C, -10°C (only over 300 seconds) and -20°C. No significant difference in the stability over 300 seconds is observed as a function of temperature. On the other hand, over 24 hours the data obtained indicate that at lower temperatures the signal is characterized by a much greater noise band, of about 2mV, and minor drift on the order of 1mV over 24 hours at -20° C. Note that this drift (1mV corresponds to 0.25 μm) is insignificant when compared to the strains occurring, for example, during secondary compression, indicating that overall, temperature has a negligible effect on the small strain measurement capabilities of the LVDT system.

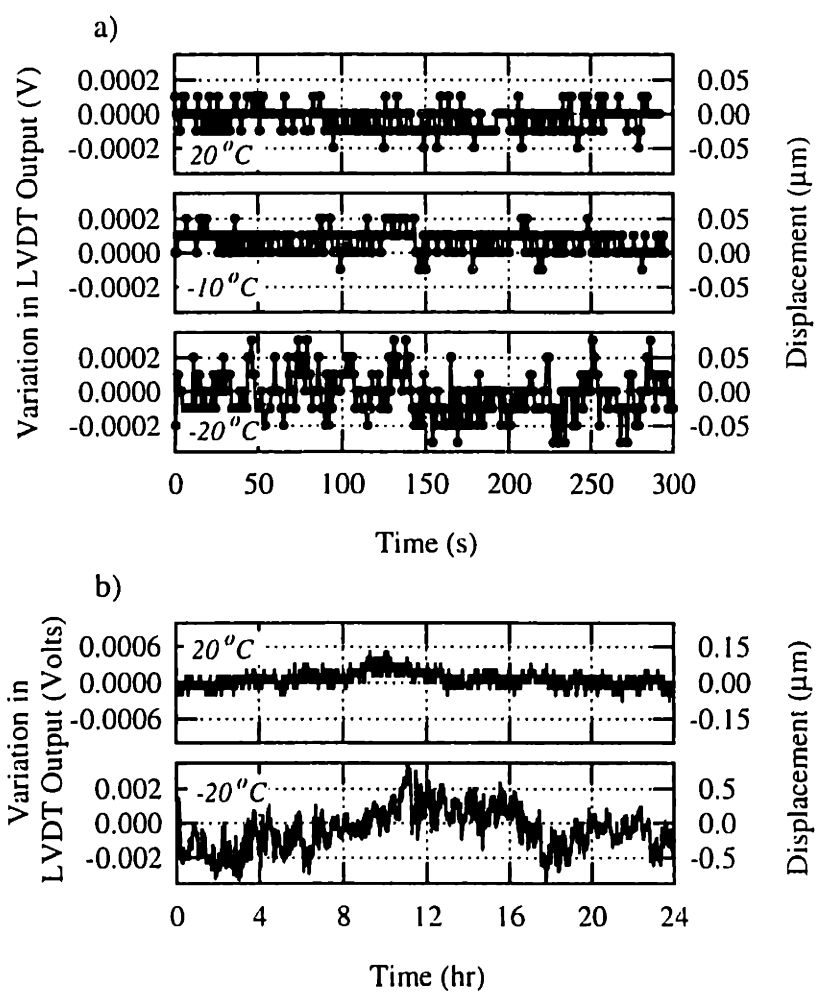


**Figure 4.9:** LVDT stability as a function of temperature over (a) 300 seconds and (b) 24 hours.

It is important to note that the magnitude of the output from the LVDT changes significantly with temperature (approximately 5-10mV/°C). This is due to changes in the resistance of the LVDT coils and signal conditioning circuitry, which is maintained at the same temperature as the soil specimen. However, in the range of temperatures investigated (-20°C to +20°C), the LVDT still calibrates linearly and its calibration factor remains unchanged. Since testing is conducted at a constant temperature, the variation in the signal magnitude with temperature does not represent a limit of the device. It must, however, be accounted for in some specific cases, such as during set-up of the frozen sand specimens (Da Re 1999). In this case, due to the fact that the testing room is always kept at a temperature lower than the actual test temperature, part of the strain measured as the temperature equilibrates is due to temperature induced changes in the LVDT output, and not to actual straining of the specimen.

Tests were also performed to verify the sensitivity of the miniature LVDT's to variations in the chamber pressure. Some authors (e.g. Cuccovillo and Coop, 1997a) have in fact reported the necessity of drilling a small pressure-relieving hole in the LVDT casing to allow the oil to flow freely in and out and potentially eliminate such effects. However, due to the particular construction of the miniature LVDT's used, it was not possible to drill such a hole in its casing without causing the transducer to malfunction. Note that, in the experiments performed, this factor is not a concern since the on-specimen LVDT's are employed to measure the deformation of the soil specimen only during undrained shear, and in some cases, during secondary compression. Both of these processes occur at constant confining stress. During the other phases of the test (saturation, consolidation, swelling) evaluation of the specimen's axial strain relies exclusively on the external LVDT. The results of the tests exploring the pressure dependency of the LVDT signald are discussed by Da Re (1999), as pressure sensitivity is a greater concern for high pressure (~125 ksc) tests.

### 4.3.6 Proof Testing on Aluminum and PMMA

A series of tests were carried out using the new axial strain measurement system in order to quantify its performance characteristics. This was done by substituting various materials of known moduli in place of the regular soil specimen and measuring the strains that resulted from cycles of loading. The materials that were chosen were standard 6061 aluminum and PMMA (polymethylmethacrylate) since they are both extremely homogenous, readily available, and have

well-known material properties. The quoted values of the Young's modulus in compression are 69 GPa for the aluminum and 3.3 GPa for the PMMA specimen (Ashby 1992). The difference in Young's modulus in compression for these two materials is greater than two orders of magnitude and therefore allows for performance evaluation over a significant range. All of the proof tests presented herein were performed using two thin latex rubber membranes placed over each specimen to simulate actual soil-testing conditions.

Figure 4.10 shows the stress-strain curve obtained by applying two cycles of load on the aluminum specimen in the high pressure triaxial cell used to test frozen sand. The Young's modulus for this specimen calculated from the slope of the regression through the data is 71.6 GPa.

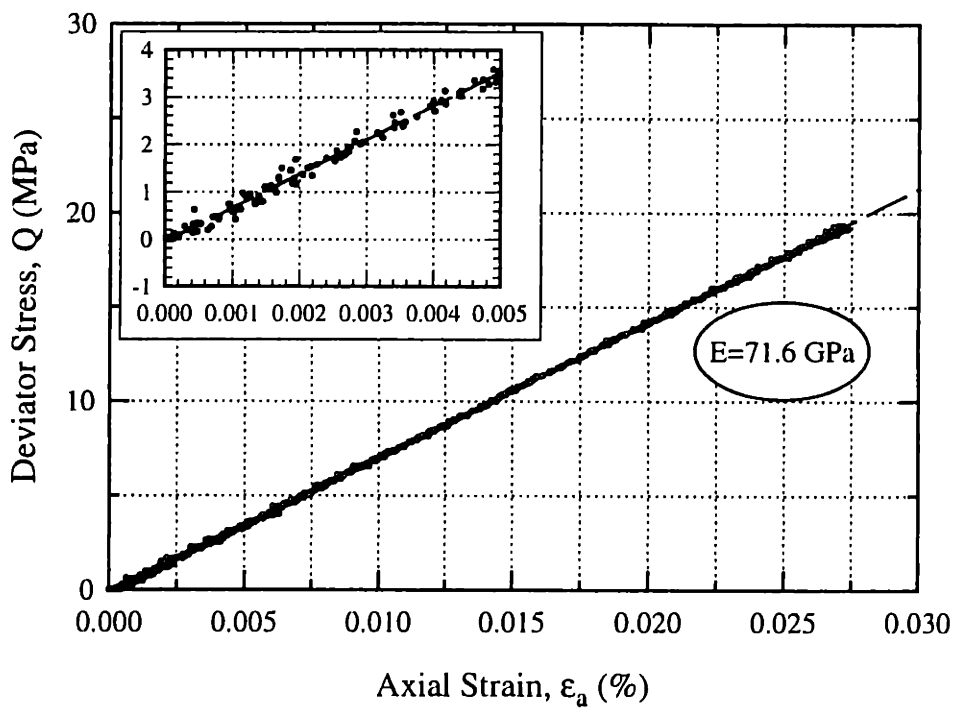


**Figure 4.10:** Results of proof testing on aluminum.

The data for the PMMA obtained in the triaxial cell used to test cohesive soils are presented in Figure 4.11. In this case the curves obtained from both LVDT's are shown. As seen for aluminum, the stiffness of the PMMA specimen (3.3 GPa) is also in excellent agreement with the reference values available in the literature, thus indicating that the axial strain measuring system can be used effectively to investigate the small strain stiffness of various materials in compression.

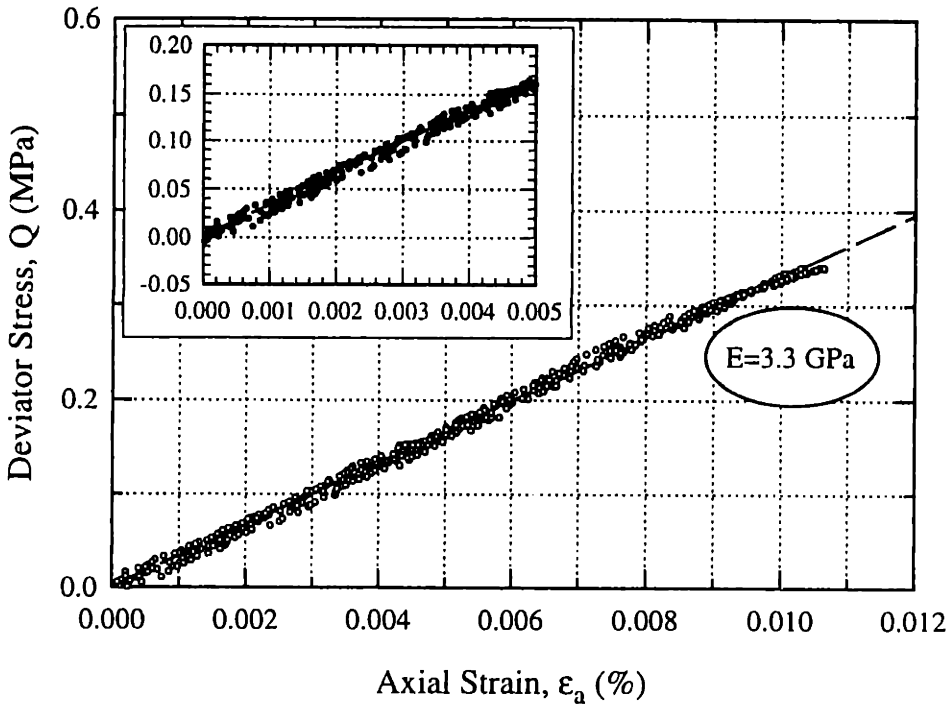


**Figure 4.11:** Results of proof testing on PMMA.

### 4.3.7 Validation/Evaluation of Technology

#### *4.3.7.1 Tests on Resedimented Boston Blue Clay*

The first soil employed to evaluate the performance of the small strain measurement system is Resedimented Boston Blue Clay (RBBC), the soil used for this thesis and described in detail in Chapter 3.

Particularly in the normally consolidated (NC) state, RBBC exhibits a fairly soft behavior and rapid softening in undrained triaxial compression. Investigation of its small strain behavior poses challenges due to the expected low linear threshold and low stiffness. These aspects require extraordinary resolution in both the axial strain and load measurements.

Figure 4.12 shows an example of the quality of the small strain measurements obtained employing the system described in the previous sections. The data are for a specimen of normally consolidated RBBC $K_0$-consolidated to a vertical stress of 3.05 ksc ($K_0$=0.48) and sheared at a rate of 0.1%/hour after about 24 hours of laboratory aging. Stress strain curves in the range of strains 0-0.0005%, 0-0.005% and 0-0.05% are presented in Figures 4.12a, b, and c respectively. Figure 4.12d shows the curve of secant stiffness versus logarithm of axial strain. As indicated in these figures the measuring system accurately captures the initial linear behavior

(Figure 4.12a), and the onset of non-linearity at about 0.002% axial strain (Figure 4.12b). The large amount of high quality data collected allows precise description of the S-shaped curve of secant stiffness versus logarithm of axial strain (Figure 4.12d). Shearing of this specimen was actually halted at 0.1% axial strain due to particular requirements of the testing program.

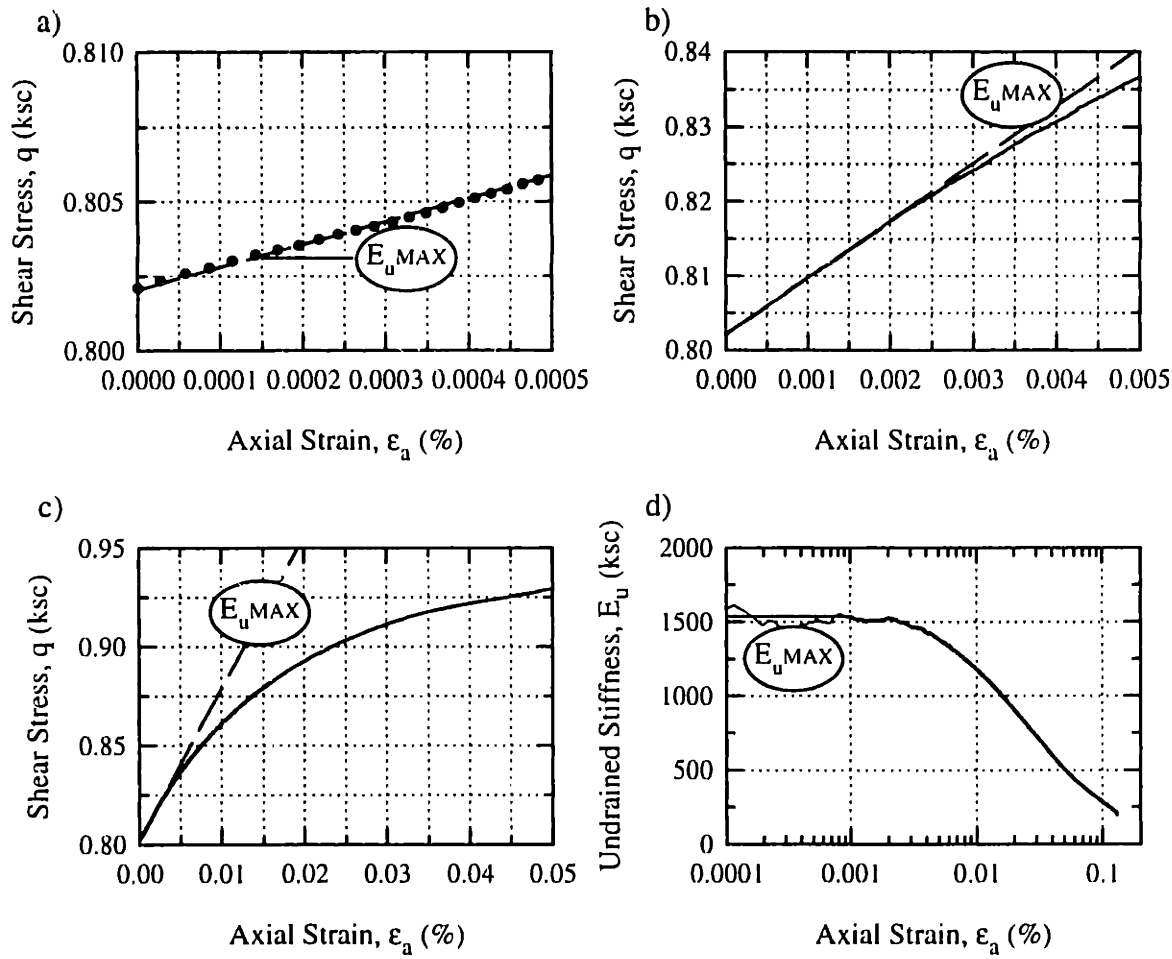


**Figure 4.12:** Quality of data for NC RBBC: (a), (b), (c) stress strain behavior; (d) stiffness versus logarithm of axial strain *(TX418S3)*.

The on-specimen data presented in Figure 4.12 are obtained by averaging the displacements measured by the two LVDT's. A measure of the reliability of the results, particularly for a homogeneous material such as RBBC, is provided by the agreement between the two transducers. Figures 4.13a and 4.13b show a comparison of the stress–strain curves in the intermediate (0-0.05%) strain range obtained by individually analyzing the data from the two

LVDT's for two tests: one on NC RBBC and one on RBBC with OCR of about 9. In both cases the difference in the initial stiffness $E_{max}$, measured with the two transducers is less than 5%.

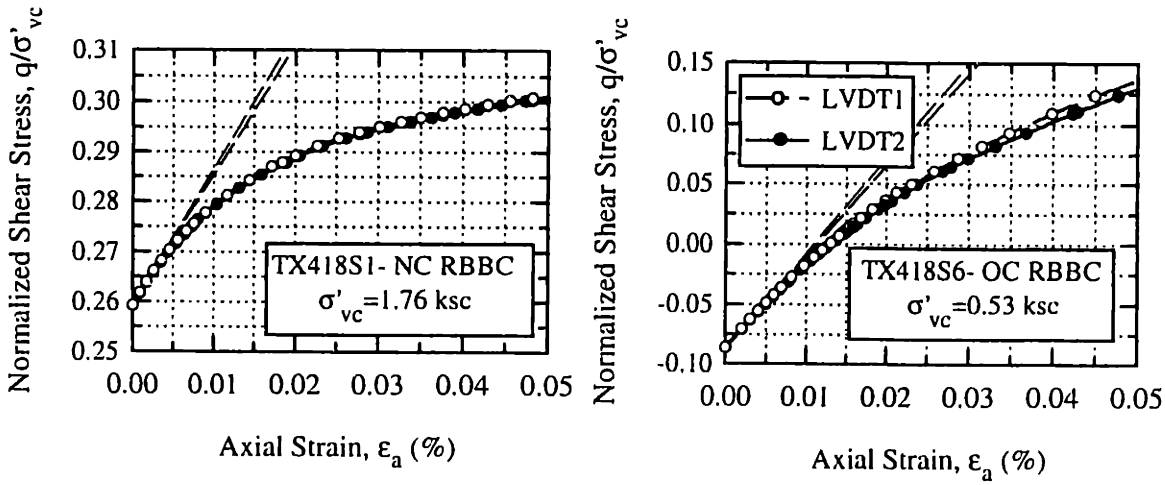


**Figure 4.13:** Comparison of results from 2 LVDT's after modifications to system of load application: (a) TX418S1 (NC RBBC); (b) TX418S6 (OC RBBC).

It should be pointed out that the modifications to the piston-top cap connection and the moment break (cf. Section 4.2.2) were instrumental in achieving such high quality results. This is illustrated in Figure 4.14 which presents an example of the typical results that were obtained prior to the introduction of these improvements. Here the difference ($\Delta E_{MAX}/E_{MAX_{ave}}$) in the value of the initial stiffness estimated with two LVDT's is closer to 40%.

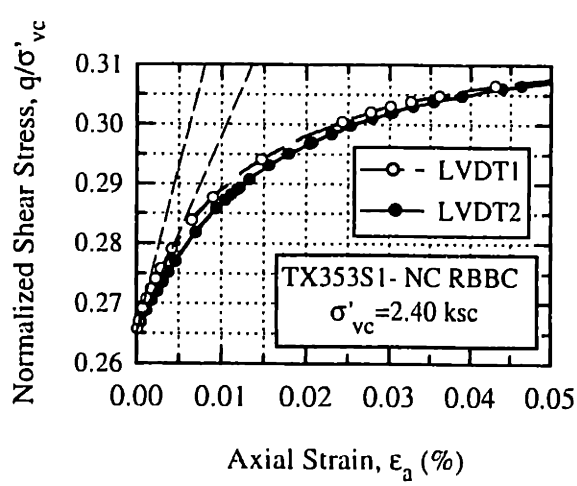


**Figure 4.14:** Comparison of results from 2 LVDT's before modifications to load application.

The main advantage of using on-specimen strain measurement lies in avoiding bedding errors, end effects, and overall system compliance, which reduce the value of the stiffness measured. This is shown in Figure 4.15 that compares the results obtained by employing internal and external measurements of the strains in the reduction of the data from the same test on NC RBBC (*TX418S3*- see Figure 4.12). As expected, a marked difference in the stress-strain behavior is observed. Except for the early part of the shear during which the external measurements display erratic results, over most of the shear much larger displacements are recorded by the external device, leading to lower estimates of the stiffness. It is observed that the external measurements provide reliable estimates of the stiffness above 0.02-0.03% axial strain.

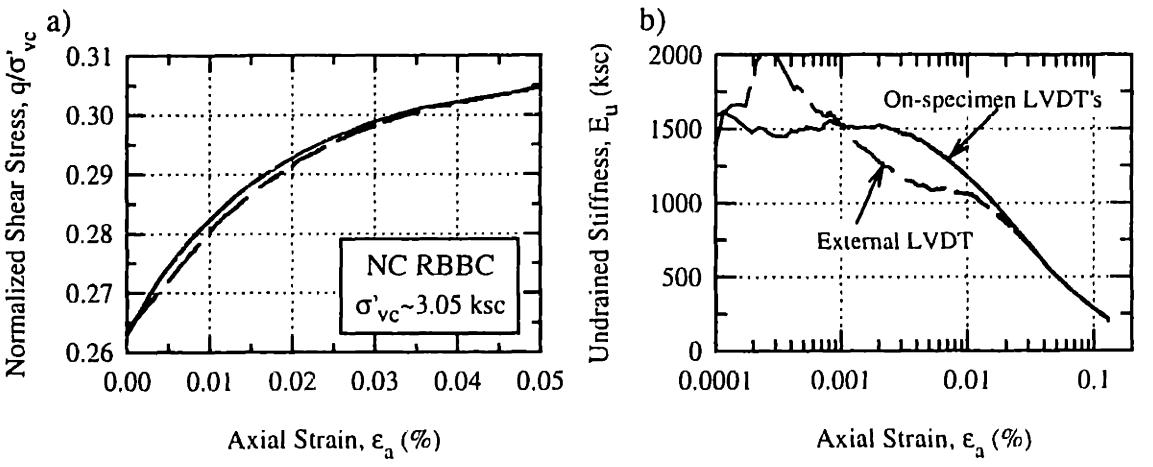


**Figure 4.15:** Comparison of results from internal and external measurements of the strains (NC RBBC).

Figures 4.16a-b present a similar comparison for a test performed on OC RBBC (*TX418S5*) after unloading from the virgin compression line. In this case a more significant discrepancy is observed between the two measurements, and the two curves do not converge until the axial strain reaches about 0.08%.

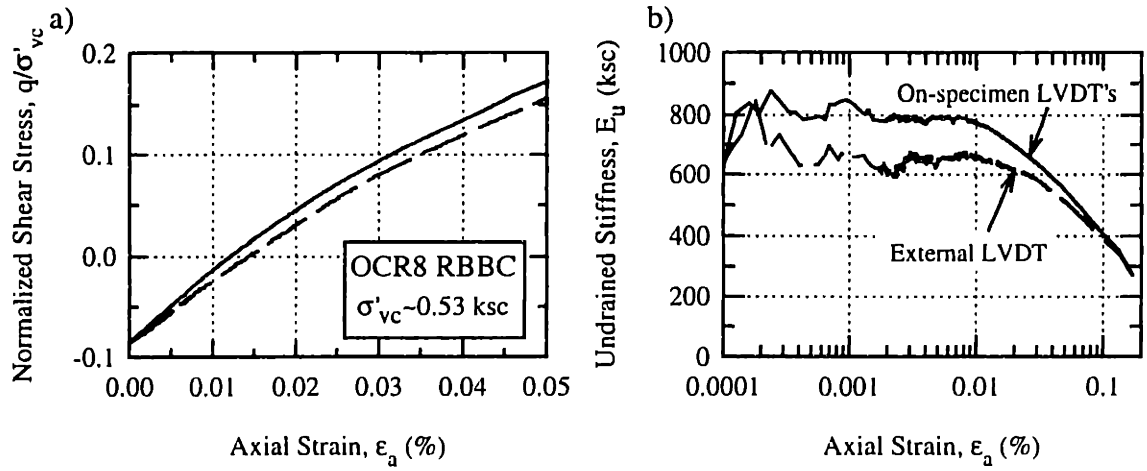


**Figure 4.16:** Comparison of results from internal and external measurements of the strains (OC RBBC).

As shown in Figure 4.17, the method for measuring the small strain behavior of soils in the triaxial apparatus described in this thesis produces extremely repeatable results. The figure presents four curves of secant stiffness versus axial strain during undrained shear (at 0.1%/hr, after 24 hours of secondary compression) of four different specimens all $K_0$-consolidated to the same stress level (~2.4 ksc). The data show excellent agreement over the entire range of strain investigated.

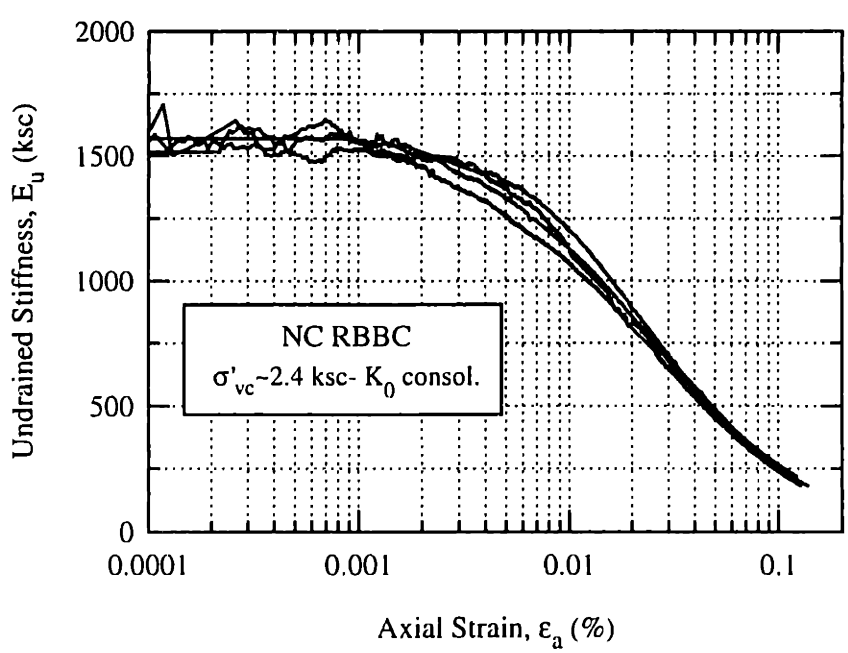


**Figure 4.17:** Repeatability of results on NC RBBC: stiffness versus logarithm of axial strain.

#### *4.3.7.2 Tests on Frozen Manchester Fine Sand*

Further evaluation of the performance of the small strain measurement system was obtained on frozen specimens of saturated Manchester fine sand, a natural sand obtained from the banks of the Merrimack River in Manchester, New Hampshire and processed to remove a portion of the fines.

This particular sand has been well studied in both its frozen and unfrozen states (Andersen 1991, Swan 1994, Andersen et al. 1995). Frozen sands exhibit complex stress-strain-time-temperature behavior due to interactions between the soil skeleton and the pore matrix, which is composed of ice and unfrozen water. The current research program (Da Re 1999) involves assessing the small strain behavior over a wide range of confining pressures, relative densities, strain rates, and temperatures. The major problems encountered in testing this soil stem from its high stiffness (~25GPa) and the particular design of the top cap in the testing apparatus, which contributes to seating errors. In addition, as the soil is sheared immediately after pressure-up (i.e. UU type testing), the possible advantages of the consolidation phase, which reduces the effects of bedding errors, are lost.

Despite the fact that previous programs on frozen Manchester fine sand represented the state of the art at their time, the results of these efforts displayed in general unsatisfactory repeatability (Andersen et al. 1995). This appears to have stemmed primarily from inadequate control in the load application leading to non-uniformities in the strain field, poor control of the strain rate imposed during shear (particularly for $\varepsilon_a$<1%), as well as problems in the design of the yoke, in particular its excessive rigidity

The stress-strain data shown in Figure 4.18 were obtained from a specimen of frozen MFS sheared at a constant rate of strain (0.5 %/hr) in triaxial compression using lubricated end conditions. Figure 4.18 shows that the measuring system is capable of resolving the strains necessary to capture the initial linear behavior, which for this soil extends to approximately 0.005% strain. The device is also able to resolve the upper yield stress which represents the onset of very significant plastic deformations in frozen soils due to ice-matrix cracking and shearing of ice crystals. This point typically occurs at around 0.3-0.5% axial strain. Systems which use the external LVDT for axial strain measurement often fail to capture this point in the stress-strain curve.

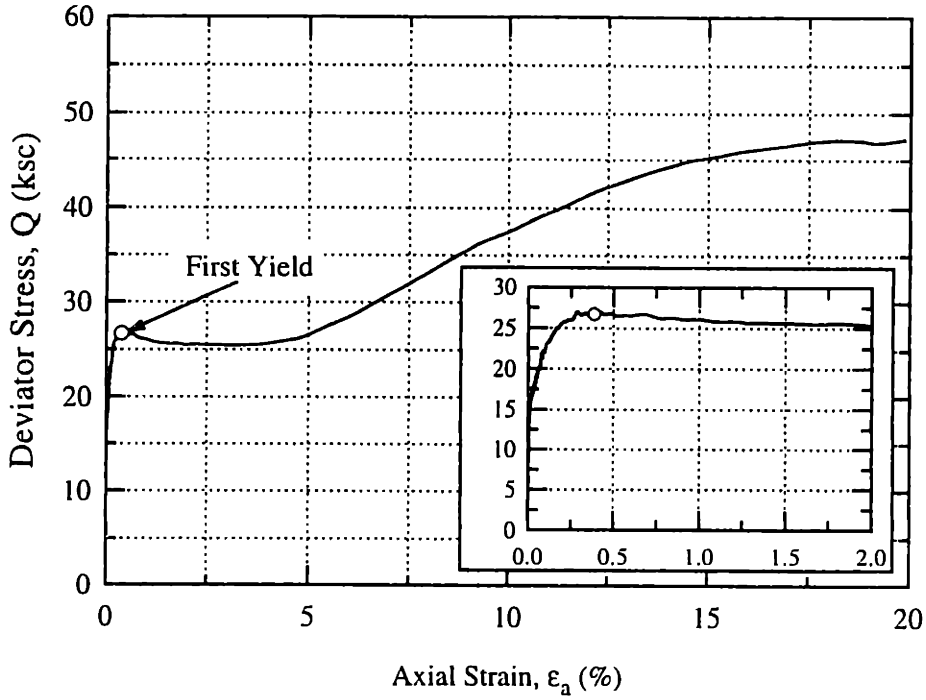


**Figure 4.18:** Shear results for frozen Manchester fine sand.

As with the data presented on RBBC, the data in Figure 4.18 represent the average strain of the two LVDT's. Figure 4.19 shows that the agreement between the two transducers for the same test specimen is very good since measurements of the initial stiffness differ by less than 5% for axial strains of less than 0.005%. As the strain level is increased the two transducers tend to deviate but their average is generally accurate up until 2% strain at which point the external LVDT is used to compute the strain of the specimen.

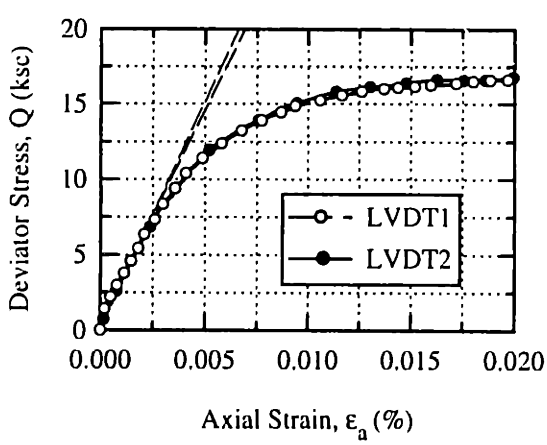


**Figure 4.19:** Comparison of results from 2 LVDT's from a test on frozen Manchester fine sand.

## 4.4 REFERENCES


1. Analog Devices Inc. (1994), **Design–In Reference Manual**, pp. 16-67 – 16-77.

2. Andersen, G.R. (1991), "Physical Mechanisms Controlling the Strength and Deformation Behavior of Frozen Sand," Sc.D Thesis, Department of Civil and Environmental Engineering, MIT, Cambridge, MA, p. 560.

3. Andersen, G.R., Swan, C.W., Ladd, C.C. and Germaine, J.T. (1995), "Small-Strain Behavior of Frozen Sand in Triaxial Compression", ***Canadian Geotechnical Journal***, 32, pp. 428-451.

4. Ashby M.F. (1992), **Materials Selection in Mechanical Design**, Pergamon Press, Oxford.

5. Brown, S.F. Austin, G., and Overy, R.F. (1980), "An Instrumented Triaxial Cell for Cyclic Loading of Clays", ***Geotechnical Testing Journal***, 3 (4), pp. 145-152.

6. Burland, J.B. and Symes, M. (1982), "A Simple Axial Displacement Gauge for Use in the Trixial Apparatus", ***Géotechnique***, 32 (1), pp. 62-65.

7. Cauble, D.F. (1996), "An Experimental Investigation of the Behavior of a Model Suction Caisson in a Cohesive Soil," Ph.D. Thesis, Department of Civil and Environmental Engineering, MIT, Cambridge, MA, 626 p.

8. Chauhan, S. (1995), "Laboratory Measurements of Load-Transfer in Geosynthetic Reinforced Soils," Ph.D. Thesis, Department of Civil and Environmental Engineering, MIT, Cambridge, MA, 520 p.

9. Clayton and Khatrush (1987), "A New Device for Measuring Local Axial Strains on Triaxial Specimens", ***Géotechnique***, 36 (4), pp. 593-597.

10. Clayton, C.R.I., Khatrush, S.A., Bica, A.V.D., and Siddique, A. (1989), "The Use of Hall Effect Semiconductors in Geotechnical Instrumentation", ***Geotechnical Testing Journal***, 12 (1), pp. 69-76.

11. Costa-Filho, L. (1985), "Measurement of Axial Strains in Triaxial Tests on London Clay", ***Geotechnical Testing Journal***, 8 (1), pp. 3-13.

12. Cuccovillo, T. and Coop, M.R. (1997a), "Yielding and Pre-Failure Deformation of Structured Sands", ***Géotechnique***, 47 (3), pp. 491-508.

13. Cuccovillo, T. and Coop, M.R. (1997b), "The Measurement of Local Axial Strains in Triaxial Tests Using LVDT's," ***Géotechnique***, 47 (1), pp. 167-171.

14. Da Re, G. (1999), "Constitutive Modeling of Frozen Sand," Ph.D Thesis in progress, Department of Civil and Environmental Engineering, MIT, Cambridge, MA.

15. Goto S., Tatsuoka, F., Shibuya, S., Kim, Y-S, and Sato, T. (1991), "A Simple Gauge for Local Small Strain Measurements in the Laboratory," ***Soils and Foundations***, 31 (1), pp. 169-180.

16. Hird, C.C. and Yung, P.C.Y. (1989), "The Use of Proximity Transducers for Local Strain Measurements in Triaxial Cells", ***Geotechnical Testing Journal***, 12 (1), pp. 292-296.

17. Jardine, R.J., Symes, M.J. and Burland, J. B. (1984), "The Measurement of Soil Stiffness in the Triaxial Apparatus," ***Géotechnique***, 34 (3), pp. 323-340.

18. Lo Presti, D.C.F., Pallara, O. Costanzo, D. and Impavido, M. (1994), "Small Strain Measurements during Triaxial Tests: Many Problems, Some Solutions," *Proc. Int. Symp. Pre-Failure Deformation Characteristics of Geomaterials (IS-Hokkaido'94)*, 1, pp. 11-16.

19. Ortega, O.J. (1992), "Computer Automation of the Conoslidated-Undrained Direct Simple Shear Tests," S.M. Thesis, Department of Civil and Environmental Engineering, MIT, Cambridge, MA, 290 p.

20. Scholey, G.K., Frost, D.J., Lo Presti, D.C.F., and Jamiolkowski, M. (1995), "A Review of Instrumentation for Measuring Small Strains During Triaxial Testing of Soil Specimens," ***Geotechnical Testing Journal***, 18 (2), June, pp. 137-156.

21. Sheahan, T.C. (1991), "An Experimental Study of the Time-Dependent Undrained Shear Behavior of Resedimented Clay Using Automated Stress-Path Triaxial Equipment," Sc.D. Thesis, Department of Civil and Environmental Engineering, MIT, Cambridge, MA, 955 p.

22. Sheahan, T.C. and Germaine, J.T. (1992), "Computer Automation of Conventional Triaxial Equipment," ***Geotechnical Testing Journal***, 15 (4), pp. 311-322.

23. Swan, C. (1994), "Physical Mechanisms Controlling the Deformation and Strength Behavior of Unfrozen and Frozen Manchester Fine Sand," Sc.D Thesis, Department of Civil and Environmental Engineering, MIT, Cambridge, MA, 1044 p.

# CHAPTER 5

# RESEARCH METHODOLOGY

## 5.1 INTRODUCTION

The experimental program presented in this thesis is designed to investigate the small strain behavior of RBBC under a variety of conditions. This chapter discusses the research methodology employed to design the extensive testing program and describes the novel testing approach followed in testing RBBC in the MIT stress path triaxial cells.

Section 5.2 discusses the variables investigated in the experimental program, thereby providing the rationale for their selection and for the range of variation examined.

The following section discusses in detail the *multi-stage testing approach* developed to reduce testing time, soil use and minimize specimen to specimen variability while investigating the small strain behavior of RBBC. The procedures and the advantages of this approach are described first, followed by data that verify its applicability.

Section 5.4 summarizes the experimental program. A description of the data reduction and evaluation procedures follows in Section 5.5. Finally, Section 5.6 lists the references pertinent to the material presented in this chapter.

## 5.2 VARIABLES INVESTIGATED

### 5.2.1 Introduction

The overall focus of this experimental program was to study the nature of soil behavior. However, the scope of the investigation was inevitably biased by experimental capabilities, engineering interest, and, of course, time. Therefore, efforts targeted a limited number of variables, and in particular, their effects on the undrained behavior of RBBC at small strains ($\varepsilon_a$<0.1%). These variables included:

a) Consolidation Stress Level

b) OCR

c) Lateral Stress Ratio (K)

d) Pre-Shear Stress Path

e) Strain Rate ($\dot{\varepsilon}_a$)

f) Duration of Pre-Shear Secondary Compression

The following sections explain the significance of these variables and discuss the rationale for the selection of their ranges of study.

### 5.2.2 OCR

As indicated in Table 5.1, the majority of the tests[1] presented in this thesis were performed on normally consolidated RBBC. Particularly in the initial phase of development of the system for small strain measurement, most of the testing made use of NC soil, as it is characterized by the smallest linear threshold and the most marked small strain non-linearity, thus establishing the most stringent conditions for validation of the technology.

As in previous experimental programs on RBBC (Sheahan 1991, Santagata 1994), additional tests were conducted on RBBC with OCR of 2, 4, and 8. Such a range in OCR reflects the typical variation observed in deposits of Boston Blue Clay in the Boston area (e.g., Ladd et al. 1998). Such tests were aimed at addressing the role of OCR on the small strain stiffness of cohesive soils, and, in particular at quantifying its effects on the small strain non linearity.

| | ***OCR*** | | | |
|---|---|---|---|---|
| | **1** | **2** | **4** | **8** |
| ***Number of Shears*** | 52 | 22 | 11 | 10 |

**Table 5.1**: Number of tests conducted on RBBC at each investigated OCR.[2]

[1] The word test in this case is used to mean shear. As will become more clear in Section 5.3, each test included more than one shear phase.

[2] Table includes only tests rated satisfactorily according to criteria discussed in Section 5.4.

Note that the values in Table 5.1 actually refer to tests conducted at the same *nominal* OCR. In reality, due to a lack of precision in targeting the stress conditions during the consolidation and swelling phases, the real OCR may actually differ slightly from the nominal targeted OCR. Such inaccuracies occurred almost exclusively during the early testing phase as the test control did not account for the effect of membranes and the filter paper strips[3] on the stresses imposed on the test specimen.

### 5.2.3 Consolidation Stress Level

It is well known that the stiffness of soils is stress-level dependent. As discussed in Chapter 2, a large amount of research, particularly making use of wave propagation techniques, has shown that the relationship between initial stiffness and stress level is of exponential form. On the other hand the dependence of stiffness on stress level at intermediate strains is less well understood. Among the goals of this research was the definition of the parameters for the exponential function describing the stress level dependence of the initial stiffness of RBBC, and the investigation of the relationships applicable at higher strain levels (up to 0.1%).

This research has investigated the variation of the undrained Young's modulus with vertical consolidation stress for both NC and OC RBBC. Table 5.2 summarizes the ranges in stress level and the number of stress levels investigated for each OCR. Tests were performed at a minimum of three different stress levels for each value of OCR.

| *Stress* | *OCR* | | | |
|---|---|---|---|---|
| | **1** | **2** | **4** | **8** |
| ***Range (ksc)*** | 1.7-13.0 | 1.1-4.0 | 0.7-2.3 | 0.5-1.9 |
| ***# Levels*** | 8 | 4 | 3 | 3 |

**Table 5.2:** Ranges in stress level investigated.

[3] Two thin membranes are used to separate the specimen from the cell fluid. Eight filter papers, each 0.5 cm wide are positioned vertically around the specimen for radial drainage.

The lower limit in the ranges indicated in Table 5.2 stemmed from the need to ensure that, prior to shear or swelling, the soil reached the virgin compression line. This is generally assumed to be true (e.g., O'Neill 1985) when the vertical stress exceeds 1.3-1.5 times the maximum pressure applied during batching (1 ksc). Limitations in the maximum cell pressure sustainable by the Plexiglas chamber (14 ksc) and in the capacity of the load cell[4] employed to measure the axial load dictated the upper limit.

### 5.2.4 Lateral Stress Ratio

The third parameter investigated in this experimental program was the lateral stress ratio, an intrinsic part of soil behavior. Investigation of this parameter is relevant to understand how the stiffness of a soil may vary as K changes due to construction and/or excavation procedures. In addition, understanding the effects of this parameter on the small strain behavior can aid in interpreting the results obtained employing devices that allow only hydrostatic consolidation.

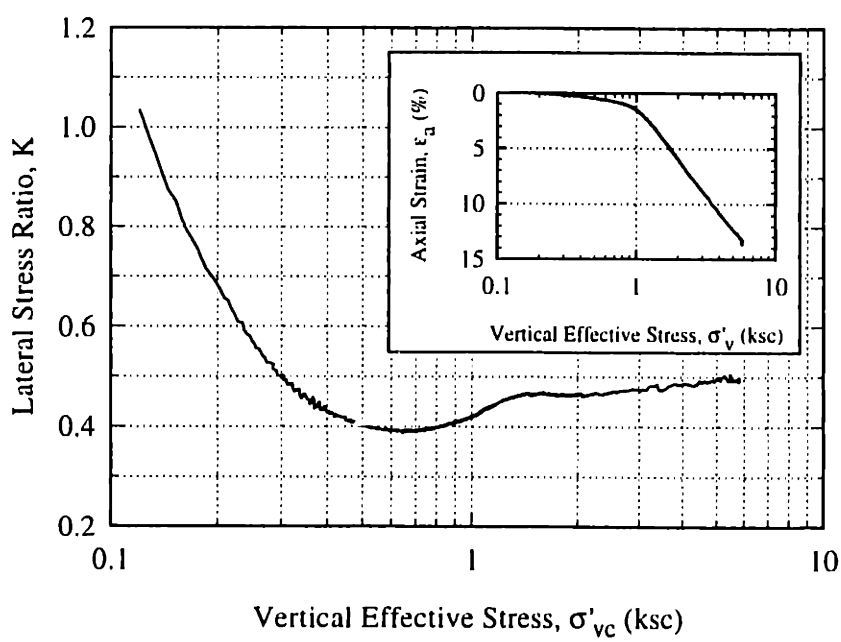


**Figure 5.1:** Variation of $K_{0(NC)}$ with stress level (Test *TX455*).

[4] As the load cell is positioned inside the triaxial chamber it measures only the deviator stress ($\sigma_1$-$\sigma_3$) applied to the specimen. Two different load cells, with capacity of 45 and 90 kg respectively, were employed in the experimental program.

For NC RBBC the vast majority of the tests were performed after $K_0$-consolidation to the desired vertical stress. Some scatter in the measured $K_{0(NC)}$ values, between 0.46 and 0.52, was observed. This reflects some specimen to specimen variability but also differences in stress level. As shown in Figure 5.1, $K_0$ is found, in fact, to increase slightly once the soil reaches the virgin compression line. Results by Force (1998) confirm this trend up to 10 ksc.

Additional tests on NC RBBC included consolidation at constant K, for comparison to the $K_0$-consolidated tests. As shown in Figure 5.2 and Table 5.3, tests were performed for K equal to 0.7, 0.9 and 1. The scope of such tests was to verify the independence of the initial Young's modulus in undrained compression on the horizontal confining stress, and to quantify changes in the non-linear behavior as a function of variations in K. Note that the *hydrostatically* consolidated tests were actually performed employing a slightly lower K value equal to 0.99 to ensure that a small deviator stress was always acting on the specimen. This was done to improve control during the hold stress phase preceding shear due to the difficulties in maintaining zero load.

| | ***OCR*** | | | |
|---|---|---|---|---|
| $K_c$ | **1** | **2** | **4** | **8** |
| $K_0$ | 0.47-0.51 | 0.62-0.66$^+$ | 0.86-0.93$^+$ | 1.13-1.26$^+$ |
| **0.7** | x | - | - | - |
| **0.90** | x | - | - | - |
| **1.0** | x | x | - | - |

\+ In the OC tests the specimen is $K_0$ consolidated in the NC range and then stress-path rebounded to the $K_0$ estimated using equation 5.1.

**Table 5.3:** Values of K investigated for each OCR.

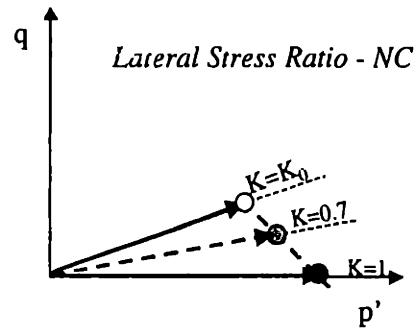


**Figure 5.2:** Consolidation of NC RBBC along constant *K* paths.

The sensitivity analysis for K was extended to OC RBBC only with OCR = 2, and K~1. Figure 5.3 shows that, in this test, the soil specimen was both loaded to the maximum stress and unloaded to OCR = 2 along the q = 0 line.

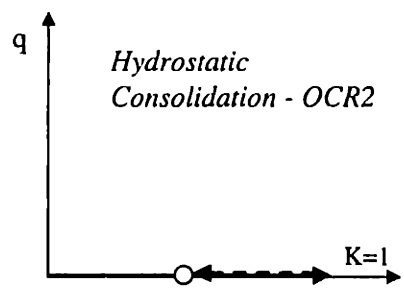


**Figure 5.3:** Hydrostatic consolidation of OCR2 RBBC.

In all the other tests on OC RBBC, the soil was swelled *under stress-path consolidation*[5] mode to the desired vertical and radial stresses, having estimated the value of $K_0$ appropriate for that OCR from the relationship discussed in Section 3.4.2.3:

$$K_o = K_{0(NC)}(OCR)^n \qquad \textit{Equation 5.1}$$

with $K_{0(NC)}$ equal to 0.485 and n equal to 0.426. The resulting $K_0$ values for OCR's of 2, 4 and 8 are summarized in Table 5.3. As shown later in the chapter in the summary of all the tests

[5] Two options for consolidation/swelling are available in the menu of the control program. In the first one (*$K_0$-Consolidation*) only the vertical target stress is inputed, while the radial stress is adjusted to maintain equal axial and volumetric strains, thus allowing one to measure the true $K_0$ of the soil. In the second option (*Stress Path Consolidation*) both the vertical and radial stress are inputed and the stress path follows a straight line to the final stress point.

performed, slight differences from these nominal values of $K_0$ may occur due to slight inaccuracies in the stress applied during consolidation.

### 5.2.5 Pre-Shear Stress Path

As discussed in Chapter 2, there is evidence that within a certain range of strains the stiffness behavior of soils depends not only on the point in the stress space from which shearing takes place, but also on the path followed by the soil in approaching the pre-shear stress state (e.g., Atkinson et al. 1990, Hight and Higgins 1994, Mukabi et al. 1994). This phenomenon has both practical and fundamental consequences: if the stiffness is strongly dependent on the pre-shear stress path, this factor must be accounted for in laboratory measurements, as well as in soil models.

To investigate this aspect of soil behavior specimens of RBBC were sheared in undrained compression following different consolidation procedures. For the NC soil, a series of tests investigated the differences between one-dimensional consolidation and stress-path consolidation, and the consequences of approaching the desired point in stress space from different directions. Figure 5.4 shows the three different consolidation paths considered. In case (a) the soil is consolidated to the desired stress level under constant area conditions; in the other two cases the soil specimen reaches the pre-shear stress state through a combination of hydrostatic consolidation and stress path consolidation at constant $\sigma'_h$ (b) or p' (c).

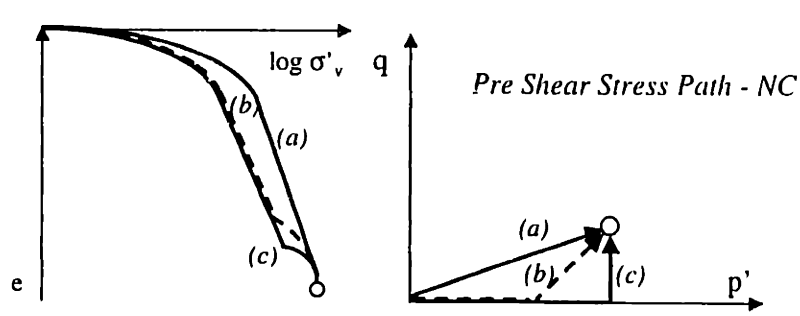


**Figure 5.4:** Consolidation stress paths considered for NC RBBC.

In the case of OC RBBC, the primary focus was to determine, for all three values of OCR investigated, how the small strain behavior varied if the desired stresses were reached by

unloading from the virgin compression line or upon reloading from higher OCR's (Figure 5.5). These two situations reflect common field conditions in which a stress state has been reached either by erosion of a deposit, or after reloading due to deposition. Throughout this thesis the letters *U* (for unloading) and *L* (for loading) are used to indicate these two stress paths followed prior to shear.

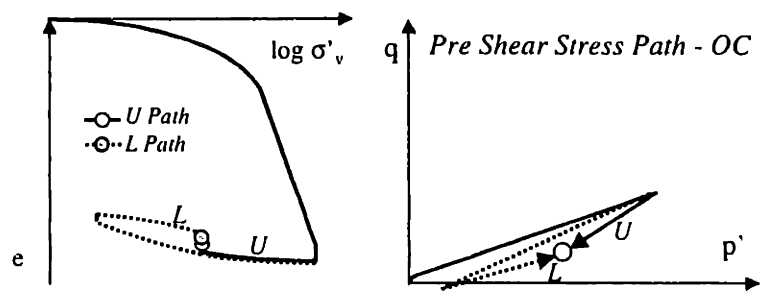


**Figure 5.5:** *Unloading* and *Loading* consolidation stress paths considered for OC RBBC.

Additional tests were performed on OCR 2 RBBC to explore this aspect further, approaching the pre-shear stress point at constant p', both from the hydrostatic compression line, and from higher shear stress level (Figure 5.6). In addition, for OCR2 RBBC, the influence of the second to last direction in stress path was also investigated. For example, the illustration on the left in Figure 5.6 shows two tests in which the pre-shear stress state was reached following a drained shear loading at constant $p' = p'_c$ from the hydrostatic state after the $[p'=p'_c, q=0]$ point in stress space had been reached either by unloading from higher values of p', or by loading from lower values of p'. These pre-shear paths that involve changes in direction are indicated with two letters corresponding to the axial load direction in each of the phases that comprise the consolidation process (e.g., *UL* corresponds to a consolidation path in which the axial load acting on the specimen first decreases and then increases).

As discussed in Section 5.2.4 in the tests on OC RBBC, the soil specimens were swelled/consolidated directly to the desired OCR employing the *stress path consolidation* option available in the control program menu, calculating $K_0$ from equation 5.1. The same value of $K_0$ was targeted for both the *U* and the *L* stress paths. This ignores the variation in $K_0$ with the

direction of loading (unloading or loading, respectively from lower or higher values of OCR) in order to better isolate the sole effect of the direction of the consolidation path.

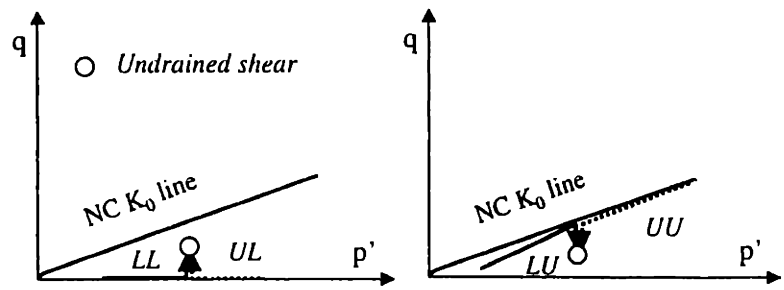


**Figure 5.6:** Additional consolidation stress paths examined for OCR2 RBBC.

### 5.2.6 Strain Rate

This research has investigated the effects of strain rate on the pre-failure behavior of RBBC. The main goal of this portion of the experimental program was to determine the variation in strain rate sensitivity in a continuous manner as a function of strain level for the four OCR's examined. Existing data on strain rate sensitivity as a function of strain level, for example through the use of the coefficient of strain rate $\alpha$ (e.g., Lo Presti et al. 1996), is unfortunately quite scarce below 0.1% axial strain, and the effect of OCR on this parameter has not been quantified (see also Section 2.3.3.2).

The range of rates examined in this experimental program encompassed about three orders of magnitude from 0.005%/hr to 4%/hr. Table 5.4 summarizes the rates examined for each OCR. The most extensive investigation was performed for NC RBBC (5 different rates). For OC RBBC the analysis was limited to three rates for OCR's of 2 and 4, and to only two rates for OCR 8. Research by Sheahan et al. (1996) shows that the strain rate sensitivity of RBBC decreases with overconsolidation ratio. Note that for OC RBBC the effect of strain rate was investigated for both the *U* and the *L* pre-shear consolidation paths.

In the case of NC RBBC, investigation of the effect of strain rate was performed for at least two consolidation stress levels at each strain rate. For OC RBBC only one stress level, for each OCR, was examined at varying strain rates.

The rates quoted in Table 5.4 should be interpreted as nominal rates as the strain rate is not strictly constant during shear. Figure 5.7 illustrates this fact for three shears performed on OCR2 RBBC at strain rates of 0.1, 1 and 4%/hr. In all three cases the strain rate gradually rises

| | OCR | | | | | | |
|---|---|---|---|---|---|---|---|
| ***Rate*** | **1** | **2** | | **4** | | **8** | |
| ***(%/hr)*** | | ***U*** | ***L*** | ***U*** | ***L*** | ***U*** | ***L*** |
| **0.05** | x | x | x | - | - | - | - |
| **0.1** | x | x | x | x | x | x | x |
| **1** | x | x | x | x | x | - | - |
| **2** | x | - | - | - | - | - | - |
| **4** | x | x | x | x | x | x | x |

**Table 5.4:** Strain rates examined for NC and OC RBBC.

between the start of shear and about 0.03% axial strain. The rate then attains a constant value that is used to define the nominal strain rate for that shear. This strain variation stems from the fact that the target strain rate is used by the computer simply to send a constant control signal to the axial motor, and, inevitably, there is some rise time required to bring the motor from a stand still up to the proper rate. Note that the shearing operation does not make use of any feedback from the on-specimen LVDT's to compare the actual strain rate with the target rate.

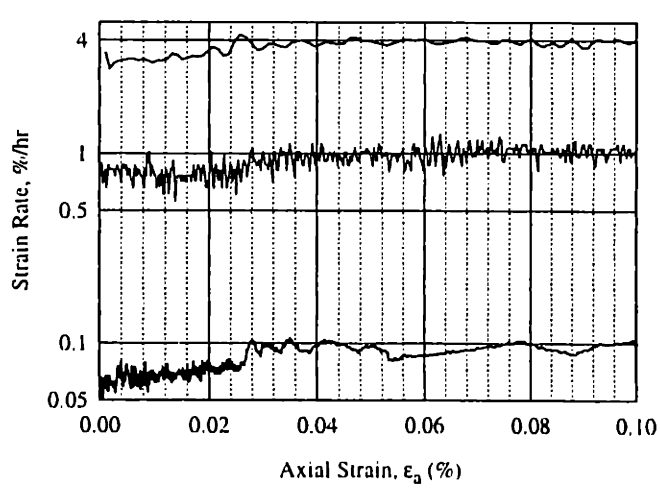


**Figure 5.7:** Strain rate versus axial strain for three tests on OCR2 RBBC.

As discussed in Section 4.2.1, the local data acquisition system was employed in addition to the central unit for the test strain rates in excess of 0.1%/hr, to collect more data at the very

small strains. In an effort to collect the highest quality data as frequently as possible, an integration time of 133 ms was selected and it was decided that only the channels for the load cell and the two LVDT's would be read locally. Note that, due to the maximum input voltage limitation in the A/D card, the local data acquisition system can be used to collect data only if the absolute value of the signals is less than 5V. In the case of the LVDT's this limitation results in the loss of half the range of the devices. As a consequence, extra care must be put in the mounting operations during setup (see Section 4.3.4) to ensure that the transducers will be in the right position at the end of consolidation.

### 5.2.7 Duration of Pre-Shear Aging

The vast majority of the tests presented in this thesis were performed allowing for the standard 24 hours of secondary compression prior to shear advocated for example by Ladd et al. (1998). However, the effects of more prolonged aging were investigated on a limited basis for $K_0$-consolidated NC RBBC to complement the data regarding the effects of the pre-shear stress history on the small strain behavior of RBBC. Due to time limitations the duration of secondary compression was varied within a limited range: from a minimum of 22 hours to a maximum of 11 days.

As discussed for the other variables, reference is made to a nominal duration of aging. Due to time constraints, the standard 1 day aging period actually lasted between 22 and 40 hours. As shown in Chapter 6, this limited variation in the pre-shear hold stress phase has no impact on the subsequent shear behavior.

## 5.3 MULTI-STAGE TESTING APPROACH

### 5.3.1 Description and Procedures

A multi-stage testing approach was developed for the experimental program to reduce testing time, conserve soil, and minimize specimen variability in the investigation of the small strain behavior of RBBC.

The basic idea of such an approach is that of performing more than one test on the same specimen in order to gather information at different stress levels, OCR's, etc. in a manner similar to what is done in tests involving measurements of the shear modulus with bender elements (e.g., Jamiolkowski et al. 1994, Viggiani and Atkinson 1995). In bender element tests, however, only

elastic deformations are imposed. Thus the effects of each shear phase are completely recoverable.

In this program the behavior of soil at strains smaller than 0.1% is of interest, and, as discussed in Chapter 2, this range includes non-elastic behavior. Therefore, following each undrained shear phase, which need not proceed further than 0.1% strain, the effects of previous shears must be "erased" through reconsolidation procedures (as outlined in Section 5.3.2 below) before additional small strain shears can be performed on the same specimen. This approach has been extensively evaluated in this program and proof of its validity is provided in Section 5.3.3.

An example of a multistage test is shown in Figures 5.8 a (e - log $\sigma'_v$ space) and b ( q - p' space). In this test (*TX406*) a total of six small strain shears (*S1-S6*) were performed on the same specimen. On both graphs a hollow symbol indicates the pre-shear stress state, while a full symbol is used to mark the end of shear. As shown in Figures 5.8a-b, all shear phases were separated by a consolidation and/or swelling phase (*C1-C6*). The first four shears (*S1-S4*) were performed at four different stress levels, all on RBBC in the normally consolidated state. The last two shears were performed on OC RBBC with OCR 4, in one case (*S5*) after swelling from the virgin compression line, in the second case (*S6*) after reloading from a higher value of OCR.

All of the tests performed for this research included several shear phases, ranging from a minimum of two to a maximum of eight.

The procedure employed to perform multi-stage tests was developed to ensure repeatability of the tests and eliminate any effects of previous shears. For a typical test, like the one shown in Figure 5.8, it can be summarized as follows:

*a)* After the standard phase of pressure up and back-pressure saturation, the soil specimen is consolidated, employing a rate of 0.1%/hr, to the desired stresses corresponding to the pre-shear conditions for the first shear of the test (*S1*). The soil is maintained at constant stresses for a minimum of 24 hours. The first shear phase always occurs after the specimen has been consolidated to at least 1.5 ksc.

*b)* Undrained shearing is performed employing the appropriate rate (0.1%/hr in the majority of the tests) until 0.1% axial strain is reached.

*c)* Unlike what is shown in Figure 5.8 for *TX406*, in a large number of tests after undrained shearing to ~0.1% axial strain, the soil was unloaded to the pre-shear deviator stress in

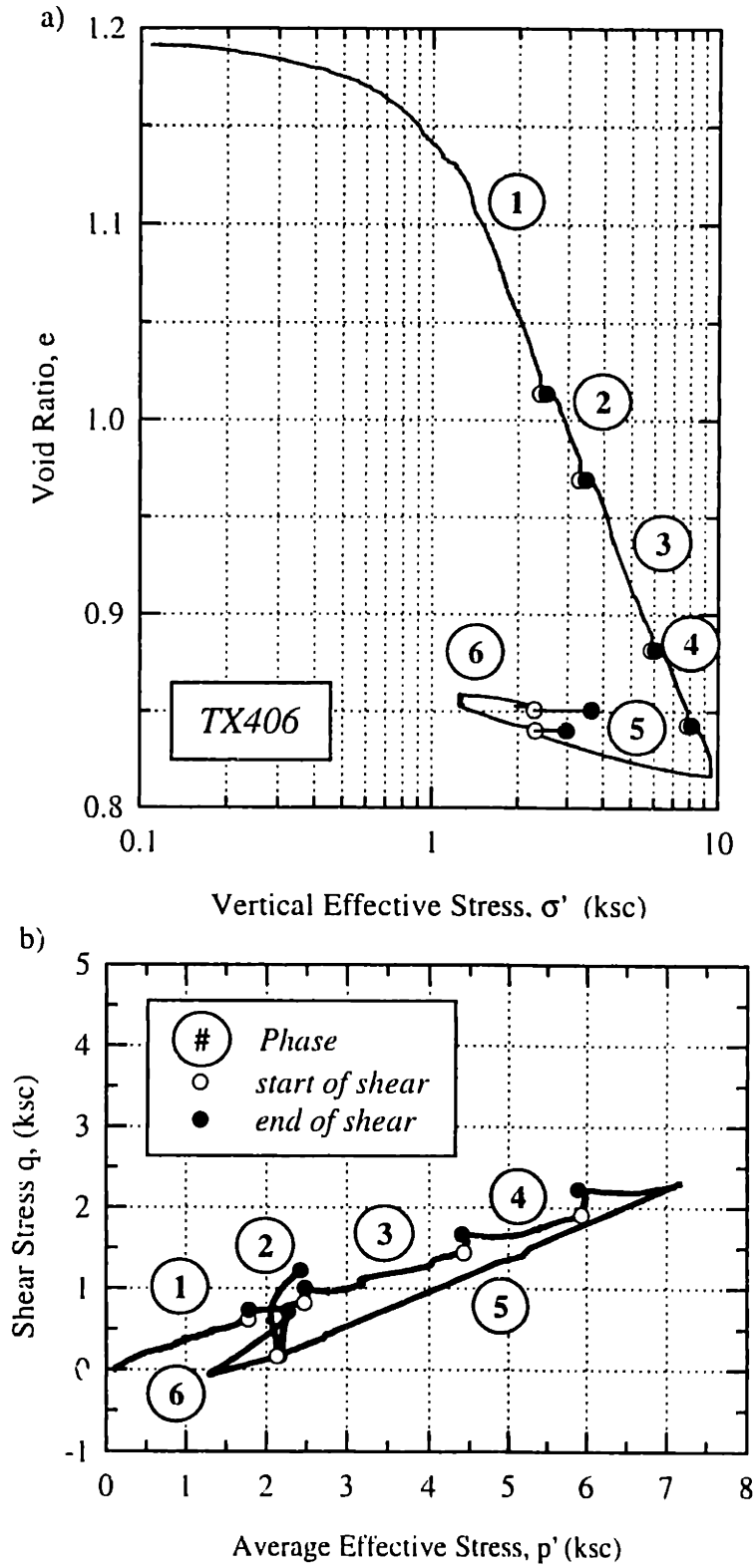


**Figure 5.8:** Example of a multi-stage test (*TX406*): a) e – log $\sigma'_v$, b) q - p'.

undrained conditions to determine the permanent axial strain. An example of such a test is presented in Figure 5.9.

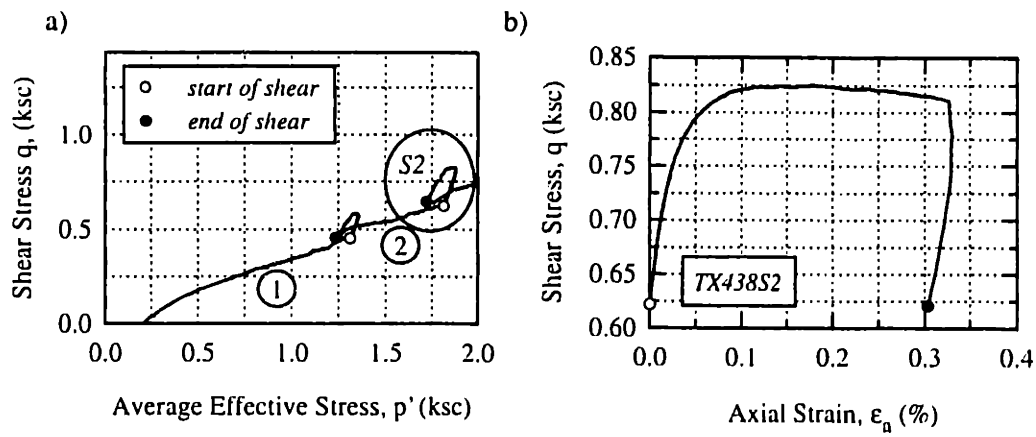


**Figure 5.9:** Multi-stage test with undrained unloading of shear stress (*TX438*): (a) stress paths for phases 1 and 2; (b) stress strain curve for shear S2.

*d)* At the end of the shear phase, the back pressure is re-equilibrated to the pore pressure value inside the specimen, and, in the case of subsequent $K_0$-consolidation, the volumetric zero is changed in the control program input data file to obtain $\varepsilon_{vol} = \varepsilon_{ax}$.

*e)* A new phase of the test is initiated as the specimen is consolidated to the stress state corresponding to the pre-shear conditions for the subsequent shear. It is maintained on hold stress at these stresses for 24 hours.

*f)* Steps *(b)*, *(c)*, *(d)* and *(e)* are repeated for all shears performed on NC RBBC.

*g)* When a shear on OC RBBC follows one on NC RBBC, prior to swelling to the desired OCR, the soil is always first consolidated further along the virgin compression line (see Figure 5.8) so that a positive consolidation strain (generally greater than 1%) is obtained to eliminate the effects of the previous shear. The specimen is maintained at this maximum stress for 24 hours.

*h)* Unloading to the OC state occurs at a rate of 0.1%/hr employing the stress path consolidation option available in the control program menu. At the end of swelling, 24 hours of hold stress precede the shear of the OC soil.

*i)* Shear to 0.1% axial strain, unloading (when applicable) and re-equilibration of the back pressure are performed as described above in *(b)*, *(c)* and *(d)*.

*j)* When a second test at the same OCR is to be performed after a loading (*L*) stress path (see 5.2.5) the soil is swelled to a higher OCR (generally 4 times higher) and left to rest at this stress level for 24 hours. It is then reloaded to the desired OCR where, again, it undergoes 24 hours of secondary compression. Undrained shearing follows.

*k)* In the final shear the soil is sheared in compression to at least 1% strain.

Slightly modified procedures were employed for special tests. Details are furnished when these special tests are discussed.

Much work was done to perfect the procedure described above, which evolved significantly during the first phase of testing. For example, in the early tests, the soil was swelled to OCR2 directly after completion of the last undrained shear on the NC soil. After shearing at OCR2 the soil was swelled to OCR4, sheared, then swelled to OCR 8 and sheared again. While this procedure significantly shortened the testing duration required for the same number of shears, overall it did not yield repeatable OC results (e.g., $\sigma'_{vm}$ was not precisely controlled). The OC data presented in this thesis refer, unless otherwise noted, exclusively to tests performed in accord with the final procedure detailed above.[6]

During the process of refining the procedure for multi-stage testing it was recognized that the following factors in particular were instrumental in guaranteeing that the small strain undrained shear behavior of RBBC was not influenced by previous shears:

i) the presence of a consolidation phase involving axial straining greater than 1.5% between shears on NC RBBC;

ii) at least 24 hours of aging prior to each shear;

iii) a phase of compression or recompression involving positive straining prior to each shear on OC RBBC.

### 5.3.2 Applications and Advantages

The multi-stage approach described above was successfully employed in this experimental program to investigate the small strain behavior of RBBC at different stress levels

[6] As the procedure for testing NC RBBC was not modified, data from the first testing phase on this soil is used throughout the thesis.

(Figure 5.10a) and values of OCR (Figure 5.10b), after different consolidation paths (Figure 5.10c), and at different strain rates (Figure 5.10d).

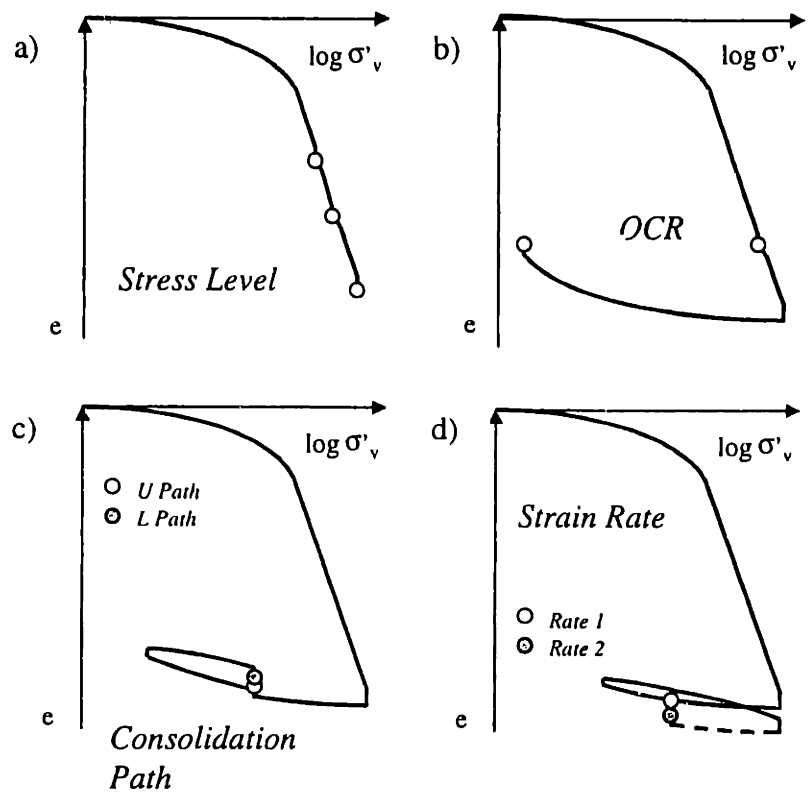


**Figure 5.10:** Parameters investigated using the multi-stage approach: (a) Stress level, (b) OCR, (c) consolidation path, and (d) strain rate.

The advantages of the multi-stage approach are numerous. Using this method it is possible to gather a large amount of information from one test specimen, resulting in great savings of time and soil, and limiting the effects of specimen to specimen variability. The use of RBBC as a research tool is thus exploited to a maximum. Table 5.5 summarizes the duration of a typical multi-stage test such as the one shown in Figure 5.8. This particular test involved six shears and had a total duration of 21 days. In general it is observed that after the initial six days required for set-up, pressure-up, saturation and consolidation to the virgin compression line every additional shear increases the overall test duration by about 2 days for NC and 4.5 days for OC RBBC. If each of the shears performed in test *TX406* had used a separate test specimen more than 40 days would have been necessary to collect the same information. Further six specimens would have been required. Thus, not only does the multistage approach limit soil use,

but it also reduces variability in the test results by providing the potential to compare several shears on the same specimen. Overall, as discussed in Chapter 3, concerns over soil variability were even further reduced since this research made use of only two batches of RBBC (418 and 419).

| *Phase* | *Duration* |
|---|---|
| *Setup + Press. Up+ Sat.* | *1.5 days* |
| *Consol. + Second. + Shear* | ① *4.5 days* |
| *Reconsol. + Second. + Shear* | ② *2 days* |
| *Reconsol. + Second. + Shear* | ③ *2 days* |
| *Reconsol. + Second. + Shear* | ④ *2 days* |
| *Reconsol. + Secon. + Swelling + + Second. + Shear* | ⑤ *4.5 days* |
| *Swelling + Second. + Recons.+ + Second. + Shear* | ⑥ *4.5 days* |
| *TOTAL* | *21 days* |

**Table 5.5:** Duration of a multi-stage test (*TX406*) (numbers in circles refer to Figure 5.8).

### 5.3.3 Validation

While the multi-stage approach described is very appealing for the reasons explained above, it is important to show that it does not introduce any bias in the results, i.e., that the results of any shear are not influenced by the previous phases of the same test.

Observation of Figure 5.8b indicates that after each shear on NC RBBC, the subsequent consolidation phase is successful in bringing the soil back to the same $K_0$ line. The slight decrease in the slope of the stress path after shears *S2* and *S3* is explained by the higher stress level achieved (see Section 5.2.4). Similarly, Figure 5.8a shows that sufficient post shear consolidation returns the NC soil to the same virgin compression line, uninfluenced by the prior shearing.

The validity of the multi-stage approach can be examined even more effectively by comparing results of shears on "virgin" specimens and on specimens subjected to previous shears. Figure 5.11 compares the stiffness versus logarithm of axial strain curves for three NC shears performed after 1 day of secondary compression on specimens $K_0$-consolidated to 2.4 ksc. Two curves are for the first shear in tests *TX362 and TX406*; the third curve is for the second

shear in test *TX403*. Although the specimens were obtained from two different batches (*TX362* from RBBC 418, *TX403* and *TX406* from RBBC 419), the three curves differ by less than 5% and indicate no added variability due to the effects of previous shears. This aspect is discussed in more detail in Chapter 6.

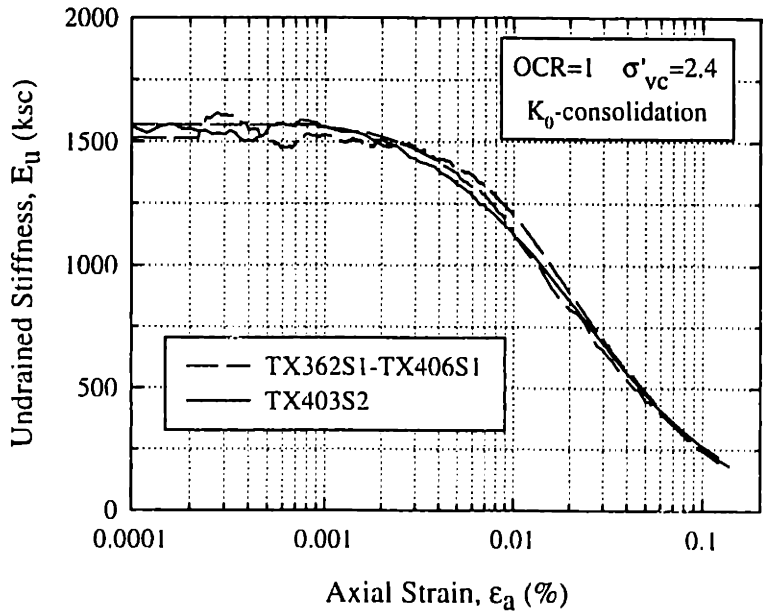


**Figure 5.11:** Comparison of results from first shear of test *TX362* and second shear of test *TX403*.

The multi-stage approach has also been extensively used to investigate the behavior of OC RBBC. The last illustration in Figure 5.10 shows schematically how, for example, the strain rate dependency of RBBC at a given OCR and stress level can be investigated by performing successive shears at two different strain rates, on the same specimen using this concept. As shown in the figure, after the first test on OC RBBC performed as described in Section 5.3.1, the specimen can be re-consolidated to the maximum pressure experienced prior to swelling, held at constant stresses for 24 hours and then re-tested at a different strain rate at the same OCR[7]. The same "philosophy" can be applied to investigate the behavior at different values of OCR.

Prior to running these types of tests it was necessary to verify that under the same conditions, the same behavior would be measured in each pair of tests. To prove this, an experiment was carried out in test *TX427*. This test included seven shears all performed on hydrostatically consolidated soil: two on NC RBBC (*S1-S2*) and five (*S3-S7*) on OCR2 RBBC.

[7] Note that the OCR is actually slightly greater in the second swelling phase, due to the higher effective preconsolidation pressure.

A blow-up of the e-log$\sigma'_v$ plot for the phases of interest (*S3–S5*) is shown in Figure 5.12a. As seen in Figure 5.12a, shears *S3* and *S5* were performed under almost identical conditions, i.e., at the same stress level and OCR, after unloading from the same maximum pressure, although at slightly different values of void ratio. An additional shear (*S4*) was performed in between the two. Comparison of the behavior observed in shears *S3* and *S5* is expected to confirm the validity of the multi-stage approach. Figure 5.12b shows the stress paths relative to phases 3 and 5 of the tests and indicates that the stress paths of the two undrained shear phases are virtually coincident.

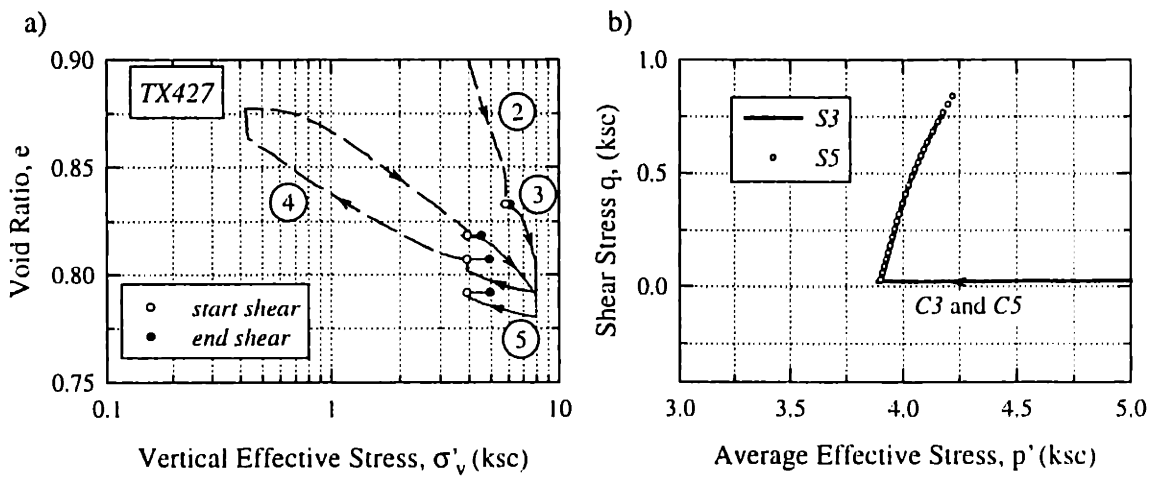


**Figure 5.12:** Sequence of shears in test *TX427* on OCR2 RBBC.[8]

The results for shears *S3* and *S5* from test *TX427* are compared in Figures 5.13a-d. Figures 5.13 a and b show the stress strain curves respectively at small strains (0-0.005%) and up to 0.1% axial strain. The corresponding stiffness versus axial strain curves are shown in Figure 5.13c. At all strain levels the difference between the two curves is less than 5%. In fact, the slightly lower value of e for shear *S5* may account for the marginally higher values of stiffness. Note that if the stiffness is normalized by the initial maximum value (Figure 5.13 d) the curves for the two shears become indistinguishable. This exceptional consistency in the results indicates that the behavior of the soil was not affected by the intermediate shear (*S4*). Note that the level of reproducibility shown here is, of course, enhanced because both measurements were performed on the same specimen.

[8] For S5 only a few data points are shown for clarity.

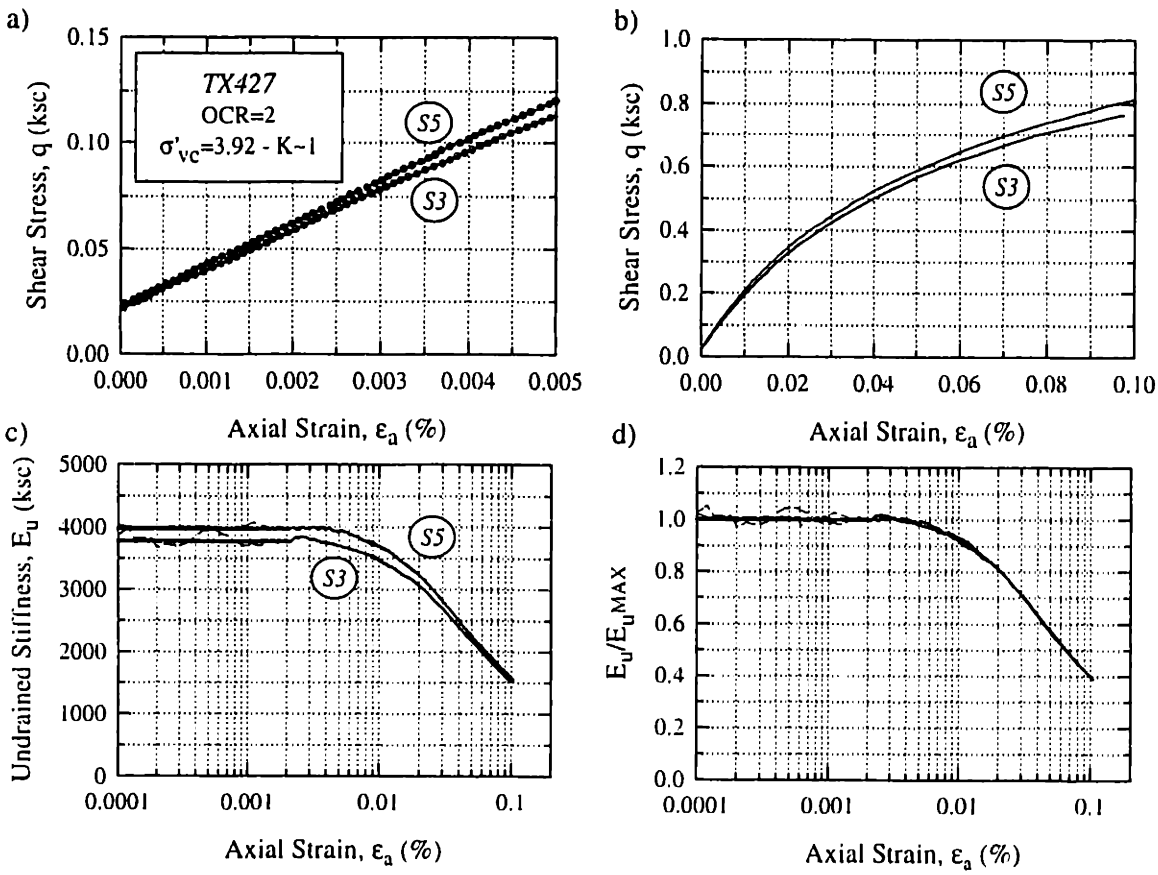


**Figure 5.13:** Comparison of results for shears *S3* and *S5* (Test *TX427*) on OCR2 RBBC: (a), (b) stress strain curves; (c) stiffness versus logarithm of axial strain, (d) $E_u/E_{uMAX}$ versus logarithm of axial strain.

The multistage approach has also been used extensively to investigate how the pre-shear stress path (unloading from the virgin compression line or reloading from higher values of OCR) influences the undrained behavior of OC RBBC (see Figure 5.10c). An example of a test (*TX406*) performed for this purpose was presented in Figure 5.8 (shears *S5* and *S6*). A blow-up of the e-log $\sigma'_v$ plot for shears *S5* and *S6* is shown in Figure 5.14a. Here an initial shear (*S5*) was performed after unloading from the virgin compression line and a subsequent shear (*S6*) was carried out after reloading back to the same point in stress space. This was the shear sequence followed in most of the tests conducted to investigate this aspect of behavior. However, it was also necessary to ensure that the sequence of the shear phases did not affect the results. To prove this point, in test *TX438* the shears on OCR4 RBBC were performed in reverse order (Figure 5.14b): the specimen was unloaded from the virgin compression line to OCR 8 without any shear

at OCR 4; it was then reloaded to OCR 4 where it was sheared, as usual, after 24 hours of secondary compression; at the end of shear *S5* the soil was once again consolidated to the maximum past pressure and re-swelled to OCR 4 prior to shearing again (*S6*). A final shear (*S7*) after a second unloading-reloading consolidation path concluded the test.

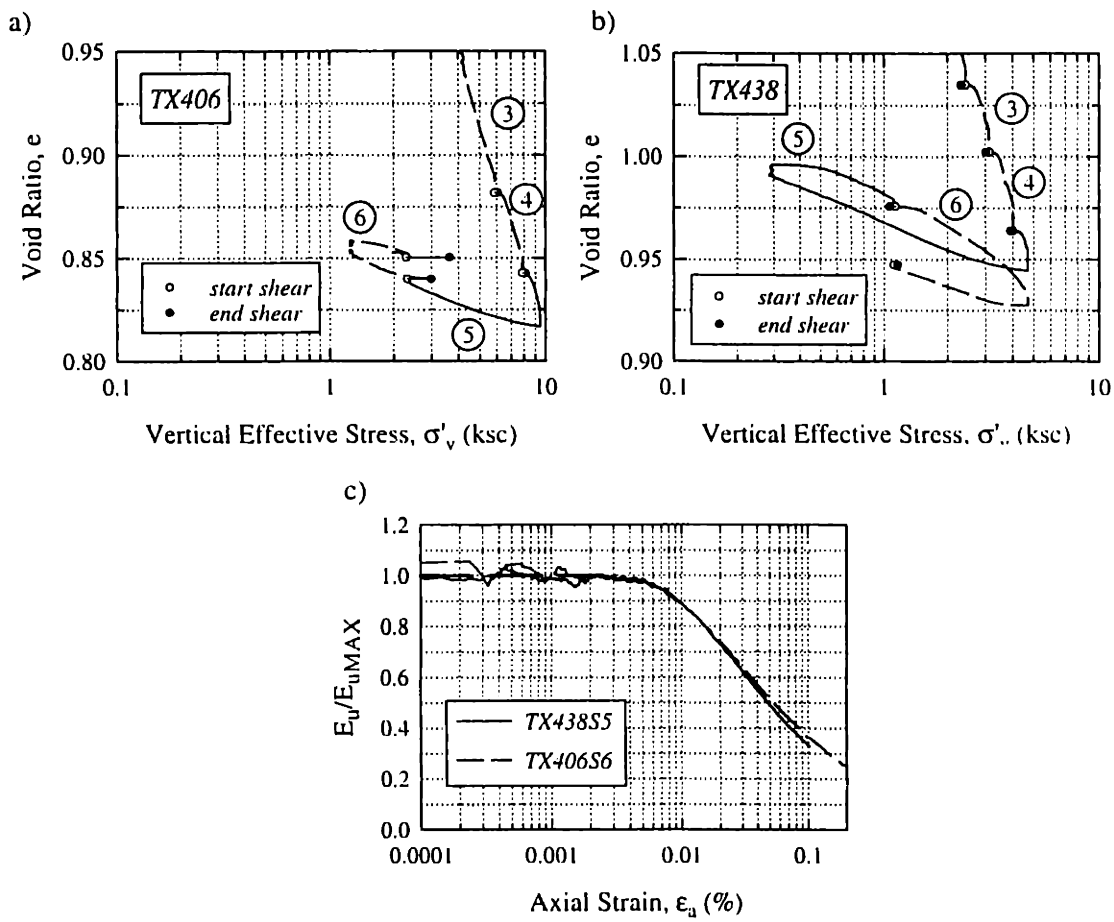


**Figure 5.14**: Effect of multi-stage test shear sequence on behavior of OC RBBC.

The stiffness degradation curves for shears *TX438S5* and *TX406S6* are compared in Figure 5.14c. Due to the fact that the two tests differ in the consolidation stress (1.1 and 2.3 ksc respectively), the comparison is done in terms of normalized stiffness ($E_u/E_{uMAX}$) versus axial strain. Comparison in this manner was justified since extensive testing performed as part of this research indicates that at any OCR the stiffness degradation with axial strain is independent of stress level. Although deviating slightly at strains greater than 0.02%, the two curves shown in

Figure 5.14c show remarkable similarity confirming the independence of the behavior of OC RBBC from the shear sequence.

Finally, an issue arises regarding soil selection because of the multi-stage approach followed in this research. Due to the great savings in soil, and to the duration of each test, each batch of soil lasted several months, resulting in large differences in the storage times for the various specimens (between five days and more than a year). This was potentially a concern as one series of previous batches of RBBC exhibited thixotropic behavior (O'Neill, 1985) resulting in increased preconsolidation pressure with time. The estimates of the preconsolidation pressure $\sigma'_p$ derived from the first $K_0$-consolidation phase of each test employing the strain energy method (Becker et al. 1987) are quite consistent ($\sigma'_p$=1.09±0.08 S.D.) and display no trend with storage time. Also the shear behavior is not affected, as shown in Figure 5.15 a and b. These figures compare the results of two tests performed on specimens differing in storage time (~5 days versus ~14 months). The curves of stiffness versus axial strain indicate exceptional consistency. In conclusion, at least within the range examined, differences in storage time did not lead to any significant variation in the 1-D compression or in the undrained small strain behavior of the Series IV RBBC.

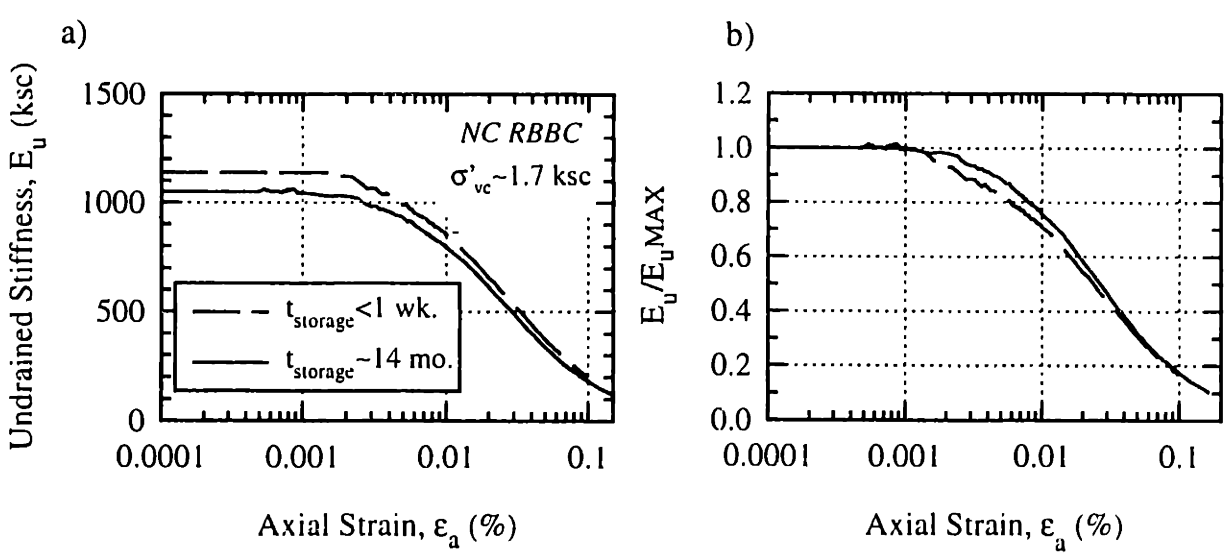


**Figure 5.15:** Effect of soil storage time on the pre-failure behavior of RBBC.

## 5.4 SUMMARY OF EXPERIMENTAL PROGRAM

More than 115 shears were performed as part of this experimental program. Of these, based on considerations discussed in the following section, 95 were employed for the analysis. These are summarized in Table 5.6 in the order in which they were performed. For each shear phase the table provides the most relevant information: OCR, vertical consolidation stress, pre-shear lateral stress ratio, pre-shear consolidation path, strain rate employed during shear, duration of aging, and void ratio. The shaded cells in Table 5.6 refer to those shears performed before the final guidelines for multi-stage testing of OC RBBC had been established (see end of Section 5.3.1, including footnote 5 for details).

## 5.5 DATA REDUCTION AND EVALUATION

As mentioned in Chapter 3, the readings recorded by the central data acquisition system are stored in data files which are then used in the test calculation program to obtain the test information in terms of engineering units.

During consolidation, measurements are obtained of the axial load, pore pressure and cell pressure acting on the specimen. In addition, vertical displacement (external) and pore fluid volume-change are also monitored. These values are used to compute volumetric strain, axial strain, vertical effective stress and radial effective stress. These calculations are based on the initial specimen dimensions and incorporate corrections for the area of the specimen and the stiffness of the membranes and vertical drains on the specimen. This procedure is standard practice for all triaxial tests run at MIT and is reported in detail by Sheahan (1991).

During the shear phase of testing, axial load, cell pressure, excess pore pressure, and (external) displacement are measured. Two LVDT's are also used to provide an internal measure of displacement. From these measurements, engineering values are again determined for axial strain, pore pressure, and vertical and radial effective stresses. However, in this case these calculations are based on the pre-shear specimen dimensions while the membrane and drain corrections are still based on the setup dimensions of the specimen. In addition, the LVDT measurements require some manipulation to eliminate the effects of electronic noise and mechanical problems. Figure 5.16 summarizes the steps involved in the process of reducing the data from the shear phases.

| # | Test Batch Cell | Phase | OCR | $\sigma'_{vc}$ (ksc) | K | Preshear Path | Rate (%/hr) | Aging (days) | e | Rating |
|---|---|---|---|---|---|---|---|---|---|---|
| *1* | **TX353** | **S1** | 1 | 2.40 | 0.47 | $K_0$ | 0.1 | 22 | 1.023 | ***Fair*** |
| | *418* | | | | | | | | | |
| | *MIT05* | | | | | | | | | |
| *2* | **TX359** | **S1** | 1 | 1.72 | 0.48 | $K_0$ | 0.1 | 25 | 1.081 | ***Good*** |
| | *418* | | | | | | | | | |
| | *MIT05* | | | | | | | | | |
| *3* | **TX361** | **S3** | 1 | 3.12 | 0.50 | $K_0$ | 0.1 | 21 | 0.948 | ***Fair*** |
| *4* | *418* | **S4** | 2.10 | 1.52 | 0.63 | *U* | 0.1 | 30 | 0.933 | ***Good*** |
| | *MIT05* | | | | | | | | | |
| *5* | **TX362** | **S1** | 1 | 2.42 | 0.46 | $K_0$ | 0.1 | 32 | 1.023 | ***Good*** |
| *6* | *MIT04* | **S3** | 1 | 3.91 | 0.47 | $K_0$ | 0.1 | 28 | 0.950 | ***Excellent*** |
| *7* | **TX363** | **S1** | 1 | 3.13 | 1.00 | const. K | 0.1 | 62 | 0.928 | ***Fair*** |
| *8* | *418* | **S2** | 1 | 5.92 | 1.00 | const. K | 0.1 | 93 | 0.900 | ***Fair*** |
| | *MIT04* | | | | | | | | | |
| *9* | **TX403** | **S1** | 1 | 1.70 | 0.47 | $K_0$ | 0.1 | 36 | 1.096 | ***Excellent*** |
| *10* | *418* | **S2** | 1 | 2.42 | 0.50 | $K_0$ | 0.1 | 29 | 1.043 | ***Good*** |
| | *MIT05* | | | | | | | | | |
| *11* | **TX406** | **S1** | 1 | 2.39 | 0.49 | $K_0$ | 0.1 | 43 | 1.017 | ***Excellent*** |
| *12* | *419* | **S2** | 1 | 3.30 | 0.50 | $K_0$ | 0.1 | 57 | 0.973 | ***Excellent*** |
| *13* | *MIT05* | **S3** | 1 | 5.89 | 0.51 | $K_0$ | 0.1 | 28 | 0.885 | ***Excellent*** |
| *14* | | **S4** | 1 | 7.87 | 0.52 | $K_0$ | 0.1 | 40 | 0.845 | ***Excellent*** |
| *15* | | **S5** | 4.11 | 2.30 | 0.86 | *U* | 0.1 | 21 | 0.843 | ***Excellent*** |
| *16* | | **S6** | 4.13 | 2.29 | 0.86 | *L* | 0.1 | 27 | 0.853 | ***Excellent*** |
| *17* | **TX418** | **S1** | 1 | 1.76 | 0.48 | $K_0$ | 0.1 | 27 | 1.069 | ***Excellent*** |
| *18* | *419* | **S2** | 1 | 2.42 | 0.47 | $K_0$ | 0.1 | 38 | 1.016 | ***Good*** |
| *19* | *MIT04* | **S3** | 1 | 3.05 | 0.48 | $K_0$ | 0.1 | 32 | 0.982 | ***Excellent*** |
| *20* | | **S4** | 1 | 4.04 | 0.48 | $K_0$ | 0.1 | 30 | 0.938 | ***Excellent*** |
| *21* | | **S5** | 8.94 | 0.53 | 1.17 | *U* | 0.1 | 45 | 0.949 | ***Good*** |
| *22* | | **S6** | 8.94 | 0.53 | 1.17 | *L* | 0.1 | 41 | 0.960 | ***Excellent*** |
| *23* | **TX422** | **S1** | 1 | 3.07 | 0.48 | $K_0$ | 0.1 | 25 | 0.968 | ***Excellent*** |
| *24* | *419* | **S2** | 1 | 4.14 | 0.49 | $K_0$ | 0.1 | 28 | 0.925 | ***Excellent*** |
| *25* | *MIT04* | **S3** | 1 | 5.81 | 0.49 | $K_0$ | 0.1 | 30 | 0.876 | ***Good*** |
| *26* | | **S4** | 1 | 7.86 | 0.50 | $K_0$ | 0.1 | 30 | 0.832 | ***Excellent*** |

**Table 5.6:** Summary of Tests Performed.

| # | Test Batch Cell | Phase | OCR | $\sigma'_{vc}$ (ksc) | K | Preshear Path | Rate (%/hr) | Aging (days) | e | Rating |
|---|---|---|---|---|---|---|---|---|---|---|
| *27* | **TX424** | **S1** | 1 | 2.44 | 0.71 | const. K | 0.1 | 32 | 0.992 | ***Good*** |
| *28* | *419* | **S2** | 1 | 6.09 | 0.67 | const. K | 0.1 | 30 | 0.865 | ***Excellent*** |
| *29* | *MIT04* | **S3** | 1 | 8.43 | 0.45 | const p' | 0.1 | 33 | 0.811 | ***Excellent*** |
| *30* | | **S4** | 8.82 | 1.06 | 1.13 | *U* | 0.1 | 27 | 0.847 | ***Good*** |
| *31* | | **S5** | 8.82 | 1.05 | 1.13 | *L* | 0.1 | 38 | 0.857 | ***Excellent*** |
| *32* | **TX427** | **S1** | 1 | 3.12 | 0.99 | const. K | 0.1 | 25 | 0.908 | ***Fair*** |
| *33* | *419* | **S2** | 1 | 5.82 | 0.99 | const. K | 0.1 | 32 | 0.829 | ***Fair*** |
| *34* | *MIT04* | **S3** | 2 | 3.92 | 0.99 | *U* | 0.1 | 34 | 0.803 | ***Fair*** |
| *35* | | **S4** | 2 | 3.92 | 0.99 | *L* | 0.1 | 33 | 0.814 | ***Fair*** |
| *36* | | **S5** | 2 | 3.92 | 0.99 | *U* | 0.1 | 35 | 0.788 | ***Fair*** |
| *37* | | **S6** | 2 | 3.92 | 0.99 | *L* | 0.1 | 37 | 0.800 | ***Fair*** |
| *38* | | **S7** | 2.20 | 3.63 | 0.99 | *post-shear* | 0.1 | 46 | 0.800 | ***Fair*** |
| *39* | **TX432** | **S1** | 1 | 2.44 | 0.48 | const p' | 0.1 | 35 | 0.967 | ***Good*** |
| *40* | *419* | **S2** | 1 | 3.13 | 0.48 | const p' | 0.1 | 31 | 0.941 | ***Good*** |
| *41* | *MIT04* | **S3** | 2.03 | 2.32 | 0.63 | *U* | 0.1 | 25 | 0.906 | ***Excellent*** |
| *42* | | **S4** | 2.04 | 2.32 | 0.63 | *L* | 0.1 | 24 | 0.913 | ***Fair*** |
| *43* | **TX438** | **S1** | 1 | 1.76 | 0.49 | $K_0$ | 1 | 33 | 1.071 | ***Excellent*** |
| *44* | *419* | **S2** | 1 | 2.43 | 0.49 | $K_0$ | 1 | 57 | 1.023 | ***Excellent*** |
| *45* | *MIT04* | **S3** | 1 | 3.12 | 0.50 | $K_0$ | 1 | 31 | 0.990 | ***Excellent*** |
| *46* | | **S4** | 1 | 4.01 | 0.50 | $K_0$ | 1 | 34 | 0.952 | ***Excellent*** |
| *47* | | **S5** | 4.19 | 1.13 | 0.89 | *L* | 0.1 | 32 | 0.964 | ***Good*** |
| *48* | | **S6** | 4.20 | 1.12 | 0.88 | *U* | 0.1 | 39 | 0.936 | ***Excellent*** |
| *49* | | **S7** | 4.17 | 1.13 | 0.88 | *post-shear* | 0.1 | 33 | 0.946 | ***Excellent*** |
| *50* | **TX442** | **S1** | 4.27 | 0.73 | 0.92 | *U* | 0.1 | 32 | 0.995 | ***Good*** |
| *51* | *419* | **S2** | 4.23 | 0.74 | 0.93 | *L* | 0.1 | 28 | 1.006 | ***Good*** |
| *52* | *MIT04* | **S3** | 2.02 | 2.42 | 0.65 | *U* | 4 | 57 | 0.920 | ***Good*** |
| *53* | | **S4** | 1.94 | 2.53 | 0.63 | *L* | 4 | 63 | 0.929 | ***Fair*** |
| *54* | | **S5** | 2.03 | 2.42 | 0.65 | *U* | 1 | 37 | 0.910 | ***Excellent*** |
| *55* | | **S6** | 2.03 | 2.42 | 0.65 | *L* | 1 | 36 | 0.916 | ***Good*** |
| *56* | | **S7** | 2.03 | 2.42 | 0.65 | *U* | 0.05 | 41 | 0.908 | ***Fair*** |
| *57* | | **S8** | 2.03 | 2.42 | 0.65 | *L* | 0.05 | 29 | 0.915 | ***Good*** |
| *58* | **TX445** | **S1** | 1 | 1.67 | 0.48 | $K_0$ | 2 | 33 | 1.086 | ***Excellent*** |
| *59* | *419* | **S2** | 2.09 | 1.08 | 0.66 | *U* | 0.1 | 41 | 1.047 | ***Excellent*** |
| *60* | *MIT05* | **S3** | 2.08 | 1.08 | 0.66 | *L* | 0.1 | 43 | 1.033 | ***Excellent*** |

**Table 5.6:** (continued) Summary of Tests Performed.

| # | Test Batch Cell | Phase | OCR | $\sigma'_{vc}$ (ksc) | K | Preshear Path | Rate (%/hr) | Aging (days) | e | Rating |
|---|---|---|---|---|---|---|---|---|---|---|
| *61* | **TX455** | **S1** | 1 | 5.75 | 0.49 | $K_0$ | 4 | 37 | 0.885 | ***Good*** |
| *62* | *419* | **S2** | 2.03 | 3.95 | 0.65 | *U* | 0.1 | 26 | 0.848 | ***Fair*** |
| *63* | *MIT05* | **S3** | 2.03 | 3.95 | 0.65 | *L* | 0.1 | 32 | 0.851 | ***Fair*** |
| *64* | | **S4** | 2.03 | 3.96 | 0.64 | *UL* | 0.1 | 34 | 0.822 | ***Fair*** |
| *65* | | **S5** | 2.03 | 3.97 | 0.64 | *LL* | 0.1 | 35 | 0.828 | ***Excellent*** |
| *66* | **TX459** | **S1** | 1 | 1.76 | 0.50 | $K_0$ | 4 | 27 | 1.057 | ***Fair*** |
| *67* | *419* | **S2** | 1 | 2.38 | 0.51 | $K_0$ | 2 | 46 | 1.009 | ***Excellent*** |
| *68* | *MIT04* | **S3** | 4.33 | 0.77 | 0.91 | *U* | 4 | 33 | 0.986 | ***Excellent*** |
| *69* | | **S4** | 4.42 | 0.76 | 0.91 | *L* | 4 | 35 | 1.000 | ***Excellent*** |
| *70* | | **S5** | 4.41 | 0.76 | 0.90 | *U* | 1 | 34 | 0.973 | ***Fair*** |
| *71* | | **S6** | 4.40 | 0.76 | 0.91 | *L* | 1 | 30 | 0.988 | ***Excellent*** |
| *72* | **TX468** | **S1** | 1 | 2.39 | 0.48 | const $\sigma'_h$ | 0.1 | 35 | 1.003 | ***Excellent*** |
| *73* | *419* | **S2** | 1 | 4.08 | 0.48 | const $\sigma'_h$ | 0.1 | 34 | 0.927 | ***Good*** |
| *74* | *MIT05* | **S3** | 1 | 5.87 | 0.48 | const $p'$ | 0.1 | 28 | 0.864 | ***Good*** |
| *75* | **TX470** | **S1** | 1 | 1.72 | 0.49 | $K_0$ | 0.05 | 35 | 1.056 | ***Excellent*** |
| *76* | *419* | **S2** | 1 | 2.42 | 0.49 | $K_0$ | 0.05 | 31 | 1.006 | ***Good*** |
| *77* | *MIT04* | **S3** | 1 | 3.12 | 0.51 | $K_0$ | 4% | 25 | 0.973 | ***Excellent*** |
| *78* | **TX471** | **S2** | 1 | 9.87 | 0.50 | $K_0$ | 0.1 | 29 | 0.814 | ***Excellent*** |
| *79* | *419* | **S3** | 1 | 12.58 | 0.50 | $K_0$ | 0.1 | 30 | 0.781 | ***Excellent*** |
| *80* | *MIT05* | **S4** | 8.57 | 1.85 | 1.22 | *U* | 4 | 27 | 0.795 | ***Good*** |
| *81* | | **S5** | 8.55 | 1.85 | 1.22 | *L* | 4 | 30 | 0.809 | ***Excellent*** |
| *82* | | **S6** | 8.56 | 1.85 | 1.21 | *U* | 0.1 | 24 | 0.772 | ***Fair*** |
| *83* | | **S7** | 8.56 | 1.85 | 1.22 | *L* | 0.1 | 32 | 0.787 | ***Excellent*** |
| *84* | **TX473** | **S1** | 1 | 3.10 | 0.90 | const.K | 0.1 | 30 | 0.960 | ***Fair*** |
| *85* | *419* | **S2** | 1 | 5.87 | 0.91 | const.K | 0.1 | 26 | 0.885 | ***Good*** |
| | *MIT04* | | | | | | | | | |
| *86* | **TX474** | **S1** | 1 | 1.72 | 0.48 | $K_0$ | 0.05 | 38 | 1.073 | ***Good*** |
| *87* | *419* | **S2** | 1 | 2.37 | 0.49 | $K_0$ | 0.05 | 33 | 1.024 | ***Excellent*** |
| *88* | *MIT04* | **S3** | 1 | 3.10 | 0.48 | $K_0$ | 0.1 | 25 | 0.985 | ***Excellent*** |
| *89* | **TX475** | **S1** | 1 | 1.70 | 0.49 | $K_0$ | 0.1 | 33 | 1.081 | ***Excellent*** |
| *90* | *419* | **S2** | 1 | 2.40 | 0.49 | $K_0$ | 0.1 | 268 | 1.032 | ***Good*** |
| *91* | *MIT04* | **S3** | 1 | 3.87 | 0.51 | $K_0$ | 0.1 | 276 | 0.961 | ***Excellent*** |
| *92* | **TX476** | **S1** | 9.12 | 0.64 | 1.26 | *U* | 0.1 | 39 | 0.938 | ***Excellent*** |
| *93* | *419* | **S2** | 9.04 | 0.65 | 1.26 | *L* | 0.1 | 39 | 0.946 | ***Good*** |
| *94* | *MIT04* | **S3** | 2.03 | 3.98 | 0.66 | *UU* | 0.1 | 64 | 0.856 | ***Good*** |
| *95* | | **S4** | 2.03 | 3.99 | 0.66 | *LU* | 0.1 | 35 | 0.862 | ***Good*** |

**Table 5.6:** (continued) Summary of Tests Performed.

The first operation is to define the beginning of loading. Due to the backlash in the axial loading gear system, some time may go by between the instant that the motors are turned on (which is when the acquisition system is timed to start acquiring data) and when the load actually starts to pick up. An example of this is shown in Figure 5.16a. This problem was eventually completely eliminated for shear phases in which the pre-shear stress state is reached by loading from lower vertical stresses (i.e., all shears on NC RBBC and shears on OC RBBC after reloading from higher OCR) by not allowing the motor to unload in the 24 hours of hold stress preceding shear. During this time, the motor can move only in the direction of loading, while the soil's natural tendency to relax takes care of unloading when the motor overshoots. Therefore the load frame's gears remain engaged in the loading direction. To minimize this problem in the case of shears following an unloading consolidation path, the beginning of shear was delayed until visual observation indicated that the load frame gears were properly engaged.

The second operation in the reduction procedure entails *smoothing* the LVDT data. When the rate at which readings are acquired is large compared to the strain rate, the smoothing operation helps to eliminate high frequency artifacts of electrical noise in the data. Thus, when experiments were performed in this program at strain rates $\leq 0.1\%/hr$ the first ten minutes of the data set (which corresponds to the 0 – 0.02% axial strain range) were typically smoothed. This process is carried out by averaging data within a finite strain window that is moved through the data set. For a given data collection rate, this averaging window corresponds to n data points, where n is generally a positive odd integer. In this procedure, for the first (n-1)/2 data points, each data point, all the data points behind it, and an equal number of data points ahead of it, are averaged. After reaching data point number (n-1)/2, the data within a window of dimension n centered on each subsequent point is averaged. This operation was typically performed twice on any given data set using a nine point moving window.

The results of such an operation are shown in Figure 5.16b in which the load cell raw data is plotted versus both the *unsmoothed* (symbols) and the smoothed LVDT output (no symbols). The figure shows that the smoothing operation introduces no distortion in the data maintaining the trend exhibited by the original raw data. Note that no "smoothing" was performed on the data obtained during the tests performed at rates greater than 0.1%/hr.

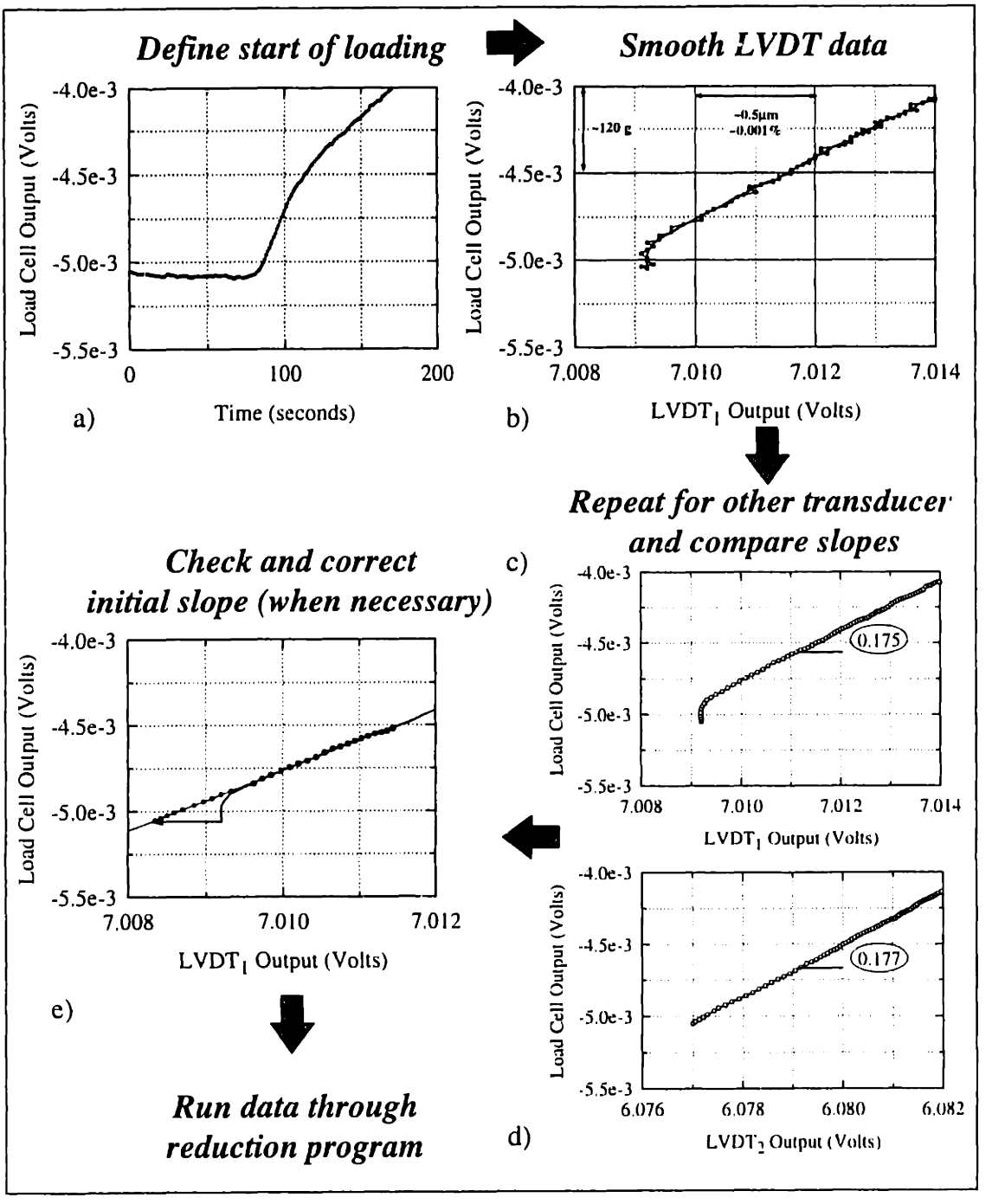


**Figure 5.16:** Phases of data processing.

Once the "smoothing" operation is completed, the load versus displacement curves, in volts, are plotted for both LVDT's (Figures 5.16c-d). Two types of information are gathered in this stage: comparison of the slopes for the two transducers (number inside the ellipse) provides a measure of consistency and observation of the behavior at the beginning of shear indicates if the specimen was loaded in a perfectly axial manner. As discussed later in this section, both of

these aspects are taken into account in judging the quality of the results from each shear phase. As fairly linear behavior is expected below 0.0005% axial strain, load-displacement behavior as that observed in Figure 5.16c for $LVDT_1$ at the beginning of shear is an indication of the fact that the specimen was not loaded in perfect coaxial manner.[9] Comparison with the general behavior and slope of the curve obtained with $LVDT_2$ (Figure 5.16d) appears to confirm this. In such an occurrence a correction is made to the data as shown in Figure 5.16e. Note that the modifications to the piston - load cell - top cap connection described in Section 4.2.2 have for the most part eliminated this problem.

With the improvements to the signal conditioning unit and the system of load application, data handling has been dramatically reduced and generally involves only the smoothing operation.

At this point the data is imported in the reduction program. The program, written in Quick Basic is an updated version of the original program (Sheahan 1991) used to reduce standard triaxial tests. The only significant change introduced in the current version is the calculation of the axial strain from the average of the displacements measured by the two LVDT's[10]. In addition, the conversion to Quick Basic allows handling of the much larger data sets. A simple interpolation routine was also added to the program to calculate all the parameters (shear stress, pore pressures, stiffness, etc.) at specific strain levels. Organization of the data in such a form aids comparison of results from different tests, as will be shown in later chapters.

After reduction, the data, in the form of engineering values are used to produce the plots presented throughout this thesis. Only one further data processing phase occurs after this stage, and exclusively for the sake of presentation. As shown in Figure 5.17, even for shears in which the stress strain behavior at very small strains is actually very close to a straight line (Figure 5.17a), the stiffness values derived in this same range show some variation (Figure 5.17b). This is due to the fact that at this strain level small inaccuracies in the strain measurement, stemming in most cases from electronic noise, can impact the calculated stiffness ($E_{sec}=2\Delta q/\varepsilon_a$) quite significantly. As shown in Figure 5.17b, in shear *TX418S3* the stiffness calculated point by point

[9] In the early phases of testing this behavior was also attributed to a stick-slip phenomenon between LVDT core and coil. The use of extended cores seems to have completely eliminated this contribution to the problem.

for the range 0.0001-0.001% axial strain varies by ±5%. Therefore, in the following chapters, when presenting the stiffness data, in the early portion of shear, where there is clear indication that the behavior is linear, rather than plot the individual data points, the straight line corresponding to the slope of the regression through these points is shown.

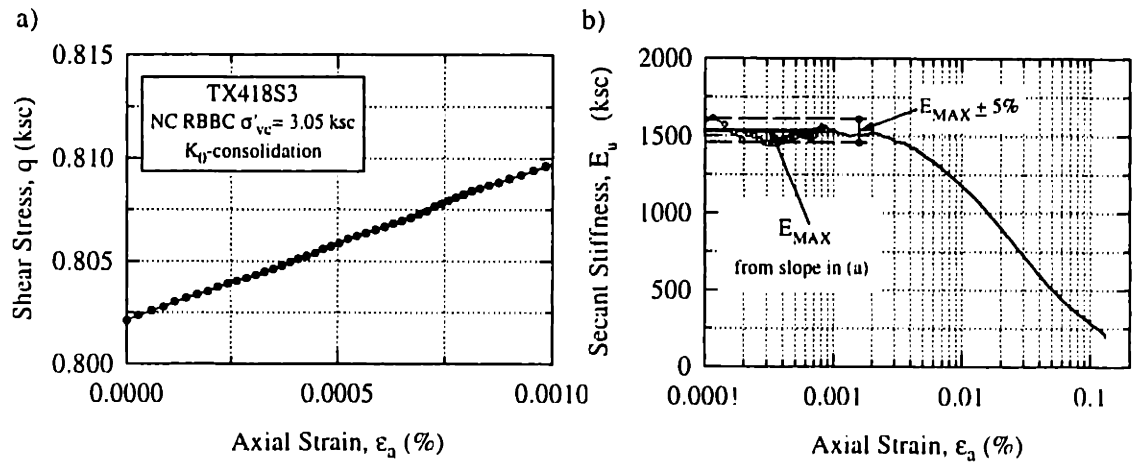


**Figure 5.17:** Derivation of initial stiffness from early portion (0-0.001%) of stress strain curve: a) stress strain curve; b) stiffness versus logarithm of axial strain (TX418S3- NC RBBC).

Finally, a simple rating system was established to provide an indication of the repeatability of shear results.[11] Each shear phase was assigned one of four ratings from *excellent* to *poor*. This rating was based on two criteria:

- the difference in slopes between the two transducers for the linear portions of the load cell versus LVDT curve (e.g., Figure 5.16 c and d);
- the presence and extent of the initial steeper portion in the load cell versus LVDT curve (Figure 5.16 b);

For a shear phase to be considered *excellent* the following had to apply:

i) the difference in slope between the two transducers in the very early linear portion of the stress-strain curve had to be less than 15%;

[10] The program switches to use the external LVDT for strain calculation either at a given axial strain threshold imputed by the user or when one of the two on specimen LVDT's goes out of the linear range.
[11] A similar procedure was adapted by Andersen (1991) and Swan (1994) for small strain testing of frozen Manchester Fine Sand

ii) correction of the initial steep portion of the curve could not affect strain greater than 0.0008%.

If only one of these conditions were satisfied, the test was considered *good*, while failure to meet both categories resulted in a rating of *fair*. Finally, if the difference between the two slopes of the initial linear portions of the curves was greater than 40% and/or great difficulties were encountered in defining the initial stiffness due to mechanical or electrical problems, the tests were classified as *poor*, and are therefore not included in this thesis. Ratings for all the shears employed in the analysis are summarized in the last column of Table 5.6.

## 5.6 REFERENCES


1. Andersen, G. (1991), "Physical Mechanisms Controlling the Strength and Deformation Behavior of Frozen Sand," Sc.D. Thesis, Department of Civil and Environmental Engineering, MIT, Cambridge, MA, 560 p.

2. Atkinson, J.H., Richardson, D., and Stallebrass, S.E. (1990), "Effect of Recent Stress History on the Stiffness of Overconsolidated Soil", ***Géotechnique***, 40 (4), pp. 531-540.

3. Becker, D.E., Crooks, J.H.A., Been, K. and Jefferies, M.G. (1987), "Work as a Criterion for Determining In-Situ and Yield Stresses in Clays," ***Canadian Geotechnical Journal***, 24 (1), 549-564.

4. Force, E. (1998), "Factors Controlling Pore Pressure Generation during $K_0$-consolidation of Laboratory Tests," S.M. Thesis, Department of Civil and Environmental Engineering, MIT, Cambridge, MA, 166 p.

5. Hight, D.W. and Higgins, K.G. (1994), "An Approach to the Prediction of Ground Movements in Engineering Practice: Background and Application," *Proc. Int. Symp. Pre-Failure Deformation Characteristics of Geomaterials*, Hokkaido'94, Vol. 2, pp. 909-946.

6. Jamiolkowski, M., Lancellotta, R., and Lo Presti, D.C.F. (1994), "Remarks on the Stiffness at Small Strains of Six Italian Clays", *Proc. Int. Symp. Pre-Failure Deformation Characteristics of Geomaterials*, Hokkaido'94, Vol. 2, pp. 817-854.

7. Ladd, C.C., Young, G.A., Kraemer, S.R., and Burke, D.M. (1998), "Engineering Properties of Boston Blue Clay from Special Testing Program," *Proc. Geo-Congress 1998*, ASCE National Convention, Boston, October.

8. Lo Presti, D.C.F., Jamiolkowski, M., Pallara, O. and Cavallaro, A. (1996), "Rate and Creep Effect on the Stiffness of Soils," ASCE Convention, Washington, 10-14 Nov. 1996, ***Geotechnical Special Publication No.61***, pp.166-180.

9. Mukabi, J.N., Tatsuoka, F., Kohata, Y., Tsuchida, T., and Akino, N. (1994), "Small Strain Stiffness of Pleistocene Clays in Triaxial Compression", *Proc. Int. Symp. Pre-Failure Deformation Characteristics of Geomaterials*, Hokkaido'94, Vol. 1, pp. 189-195.

10. O'Neill, D. (1985), "Undrained Strength Anisotropy of an Overconsolidated Tixotropic Clay," S.M. Thesis, Department of Civil Engineering, MIT, Cambridge, MA, p.360.

11. Santagata, M.C. (1994a), "Investigation of Sample Disturbance in Soft Clays Using Triaxial Element Tests," S.M. Thesis, Department of Civil and Environmental Engineering, MIT, Cambridge, MA, p. 289.

12. Sheahan, T.C. (1991), "An Experimental Study of the Time-Dependent Undrained shear Behavior of Resedimented Clay Using Automated Stress-Path Triaxial Equipment," Sc.D. Thesis, Department of Civil and Environmental Engineering, MIT, Cambridge, MA, 955 p.

13. Sheahan, T.C., Ladd, C.C., and Germaine, J.T. (1996), "Rate-Dependent Undrained Shear Behavior of Saturated Clay," ***Journal of Geotechnical Engineering***, ASCE, 122 (2), February, pp. 99-108.

14. Swan, C. W. (1994), "Physical Mechanisms Controlling the Deformation and Strength Behavior of Unfrozen and Frozen Manchester Fine Sand," Sc.D. Thesis, Department of Civil and Environmental Engineering, MIT, Cambridge, MA, 1044 p.

15. Viggiani, G. and Atkinson, J.H. (1995), "Stiffness of Fine-Grained Soil at Very Small Strains," ***Géotechnique***, 45 (2), pp.249-265.

# CHAPTER 6

# RESULTS

## 6.1 INTRODUCTION

The objective of this chapter is to present the results of the triaxial experimental program highlighting the role of the variables investigated (e.g. stress level, OCR, lateral stress ratio, pre-shear path, strain rate, and laboratory aging) on the pre-failure behavior of RBBC. The chapter is organized in the following manner: in the next section the results for the conditions which represent the base case (i.e. NC RBBC, $K_0$ consolidation, standard rate of shear (0.1%/hr), 1 day laboratory aging) are discussed, and the basic criteria used for the interpretation of the results are introduced. The subsequent sections discuss one by one the variables considered pointing out their role on both the initial stiffness and the behavior in the non-linear region. In general the results for NC and OC RBBC are examined separately. The chapter provides no discussion of the relative importance of the parameters under investigation, as this type of analysis is presented in the following chapter.

## 6.2 OVERVIEW OF BEHAVIOR FOR $K_0$-CONSOLIDATED NC RBBC

As discussed in Chapter 5, the majority of the tests performed for this experimental program involved shearing of NC RBBC at 0.1%/hr after $K_0$-consolidation and 24 hour laboratory aging. Figures 6.1a-d present the results of one of these tests, showing the typical features of the pre-failure behavior of NC RBBC. This particular test (*TX475S1*) was conducted on a soil specimen $K_0$-consolidated to 1.70 ksc, with a void ratio of 1.055 and $K_0$ equal to 0.49. Another example of the behavior of NC RBBC was presented in Chapter 4 (Figure 4.12 - Test *TX418S3*: $\sigma'_{vc}$=3.05 ksc, e= 0.982, $K_0$=0.487).

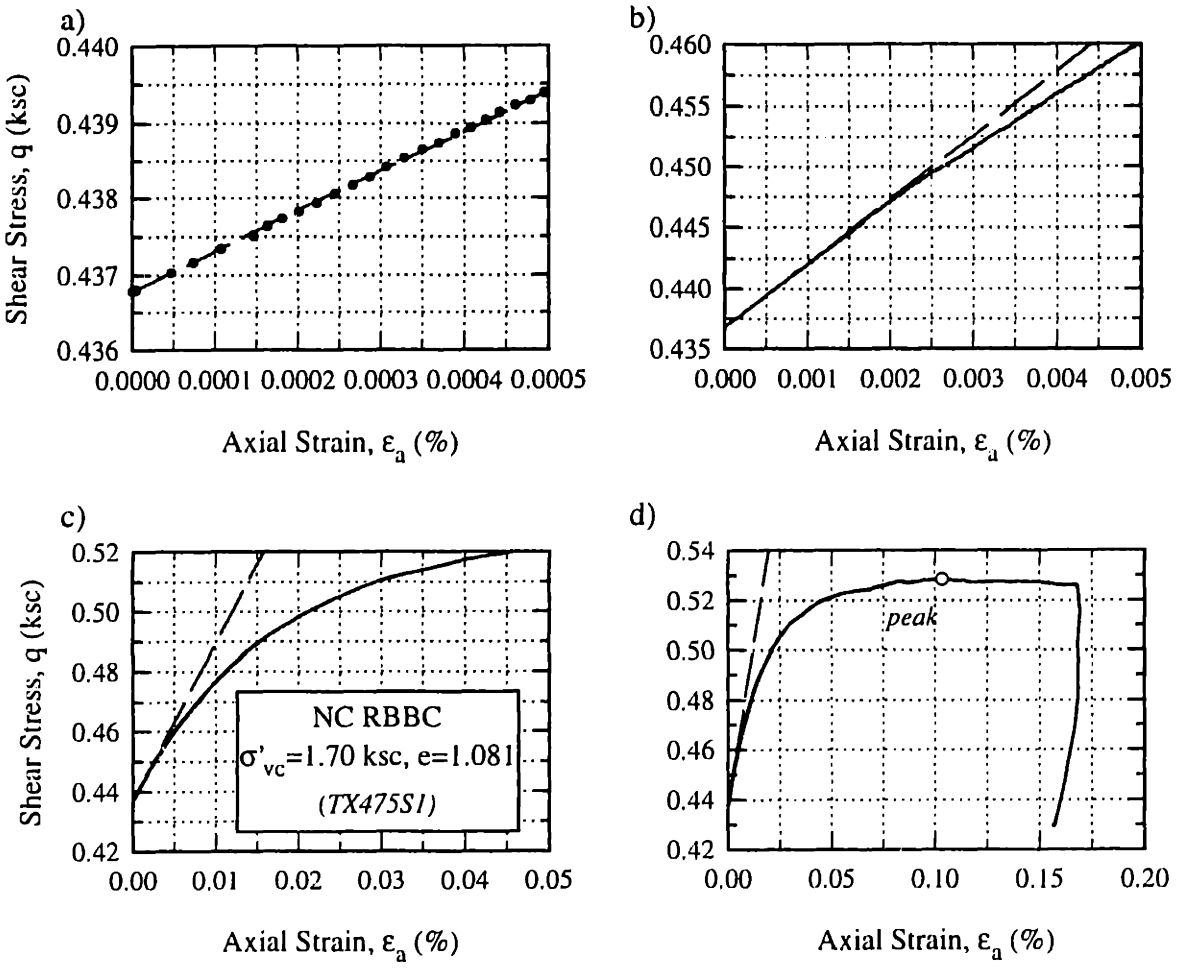


**Figure 6.1:** Stress strain curves for test *TX475S1*.

The four graphs in Figures 6.1a-d present the stress strain curves for different ranges of the axial strain (0.0005%, 0.005%, 0.05%, 0.2%). Figure 6.1a shows that at very small strains the behavior of the soil is practically linear. The figure displays the points corresponding to each of the measurements made, as well as the regression through this early portion of the stress strain curve. The slope of this line represents the maximum value of $E_u/\sigma'_{vc}$ equal here to 619, and corresponding to a maximum initial undrained stiffness of 1051 ksc. This value is referred to as $E_{uMAX}$. As shown in the following figure (6.1b), the linear behavior extends further in the stress-strain curve to approximately 0.001%-0.0015% axial strain, after which the stress strain curve becomes increasingly non linear (Figure 6.1b and c). The line indicating the initial stiffness is included in all the figures for reference. As shown in Figure 6.1d, NC RBBC reaches the peak strength at approximately 0.1% axial strain. The normalized strength measured in this test (0.311) is lower than the value normally cited for NC RBBC (0.33 - see Chapter 3, Section

3.4.4.3) due to the lower strain rate employed in this testing program (0.1%/hr compared to the standard rate of 0.5%/hr). This value is consistent with the trend of strength with strain rate proposed by Sheahan et al. (1996- see Section 3.4.4.7).

Figure 6.2a shows the calculated secant stiffness as a function of strain level. This representation allows one to better determine both the onset and the degree of non-linearity in the stress-strain behavior. The curve displays a reversed S-shape, with an initial constant stiffness portion (corresponding to the linear region observed in Figures 6.1a-b) extending slightly beyond 0.001% axial strain; it is followed by a region characterized by increasingly rapid decrease of the stiffness up to the peak strength. For test *TX475S1*, no data are available beyond 0.15% strain. However other tests show that the curve becomes increasingly flatter.

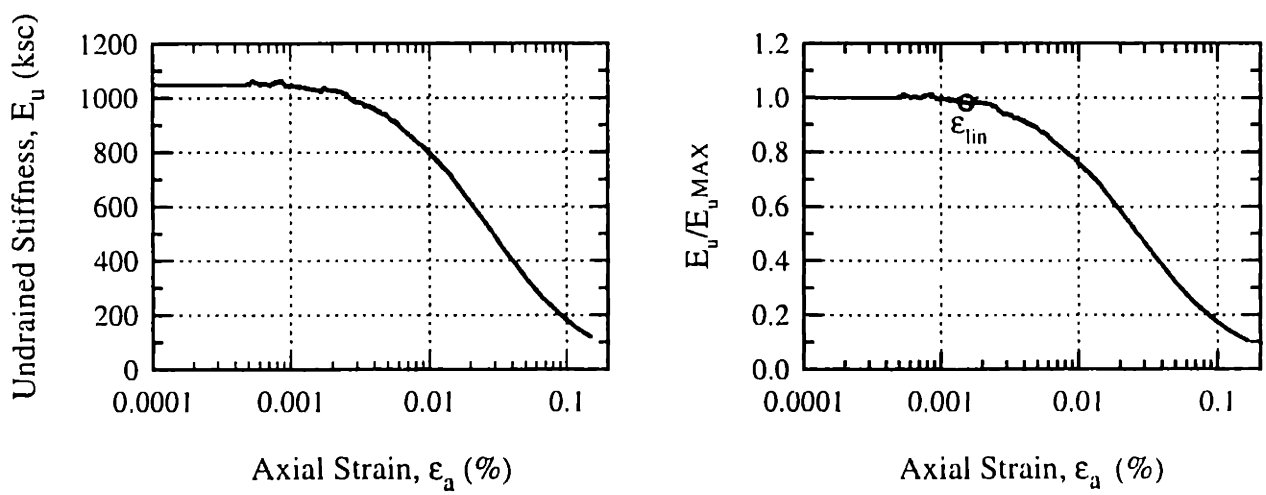


**Figure 6.2:** Stiffness degradation curves for test *TX475S1*: a) Secant stiffness ($E_u$); b) Normalized stiffness ($E_u/E_{uMAX}$).

It is beneficial to report the stiffness data in normalized form, i.e. divided by the initial stiffness, as shown in Figure 6.2b. This type of representation is useful to quantify the degree of non-linearity and the stiffness degradation with strain level when comparing results for tests performed under different conditions (different stress, OCR, etc.). The values of the strain at selected values of $E_u/E_{uMAX}$ ( e.g. 0.98, 0.80, 0.50, etc.) can be employed to quantify modifications in the stress strain behavior induced by over-consolidation, changes in shearing rate, laboratory aging, etc. In particular, in this thesis the value of the axial strain at $E_u/E_{uMAX}$=0.98, is used as an arbitrary definition of the linear threshold, $\varepsilon_{lin}$, corresponding to

the end of the linear region and the onset of non linearity. This point, which for test *TX475S1* is equal to 0.0015%, is depicted in Figure 6.2b with an open symbol.

To provide a simple measure of the degree of non-linearity in the pre-failure region the parameter $C_{NL}$ (coefficient of non-linearity) is introduced. $C_{NL}$ is defined as the ratio between the stiffness at 0.001% and that at 0.1% axial strain. $C_{NL}$ has a minimum value of 1 corresponding to the condition in which the linear threshold extends past 0.1% (i.e. $E_{0.001\%}=E_{0.1\%}$) and increases as the soil exhibits more significant non-linearity in the pre-failure region. For test *TX475S1* $C_{NL}$ equals 5.7.

Plots of the excess and the shear pore induced pore pressures for test *TX475S1* are shown in Figures 6.3a and b. It should be noted that in this testing program pore pressures were measured through a porous stone located at the base of the specimen. This measurement can be biased by end effects and therefore may not be representative of the mid-specimen region where the axial strains are measured, particularly in the case of OC soils. However, Figure 6.3b indicates that the pore pressure data is in fair agreement with the stiffness degradation curves, i.e. negligible shear induced pore pressure is measured as long as the soil remains inside the linear region. In fact, the development of shear induced pore pressure is delayed until the axial strain reaches 0.002-0.003%, indicating that up to that strain the behavior of the soil may be predominantly elastic.

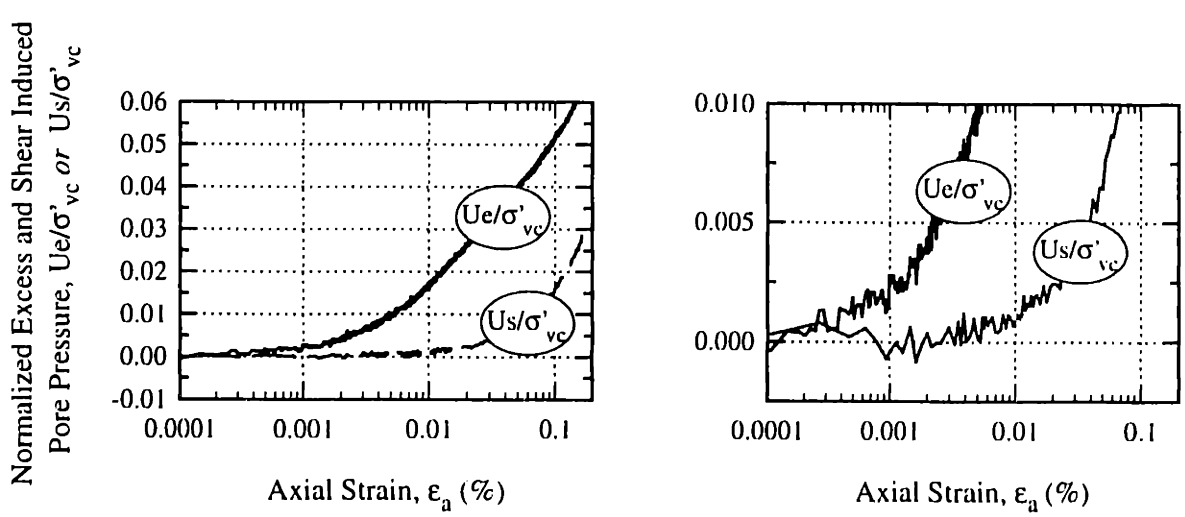


**Figure 6.3:** Excess and shear induced pore pressures (*TX475S1*).

Stress paths for test *TX475S1* are shown in Figure 6.4a and b. The first figure presents the stress path for the complete shear phase, while Figure 6.4b shows a close-up of the early portion of the shear ($\varepsilon_a$<~0.005%). In both figures the points corresponding to selected values of the axial strain are also clearly marked.

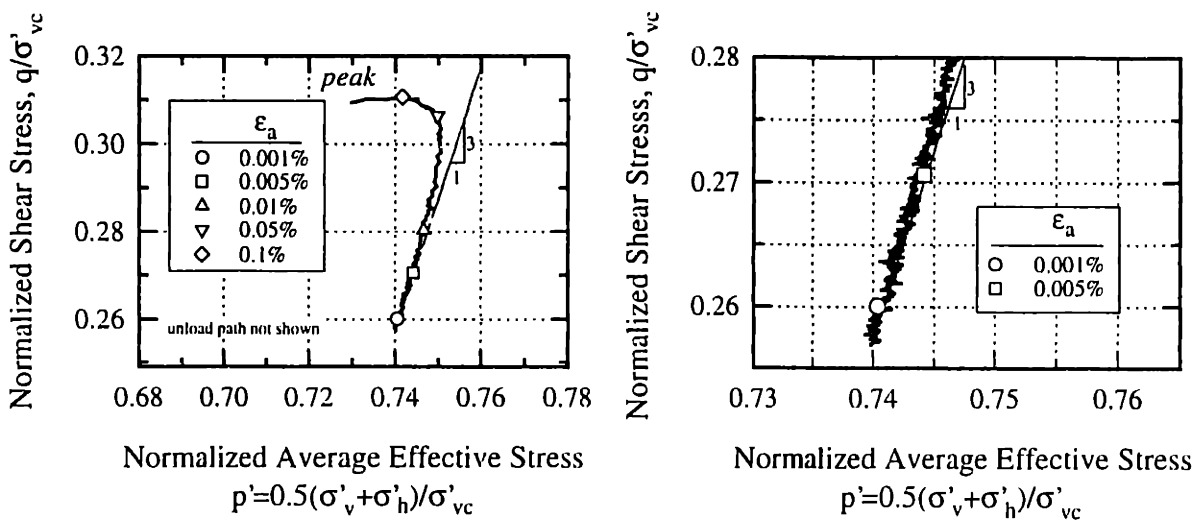


**Figure 6.4:** Stress paths for test *TX475S1*.

As in most of the tests conducted in this experimental program, shearing was prolonged to a maximum axial strain of 0.1-0.15%, after which the soil was unloaded in undrained conditions[1] to the pre-shear stress state (Figure 6.1d). As indicated more clearly in Figure 6.5, this final unloading, is associated, in the case of NC RBBC, with very limited straining, i.e. at this strain level, which corresponds approximately to the strain at peak, the deformation is predominantly plastic. In test *TX471S5* the ratio $\varepsilon_{PL}/\varepsilon_{TOT}$ equals 94%.

Note that due to the back-lash in the axial loading system there is a delay between the reversal in the direction of the axial motor and the actual unloading of the specimen. During this time the soil is free to creep/relax. In fact, even as unloading starts to occur, positive increments of the strain produced by creeping of the soil are still observed.[2] Although not too apparent in Figure 6.4a, this effect was observed to be quite significant in other tests, making the

[1] As discussed in Chapter 5 (Section 5.3.1) the practice of unloading the specimen in undrained conditions prior to initiating a new consolidation phase was initiated only in the second half of the experimental program. The unload information is therefore not available for most of the standard (rate=0.1%/hr, 1 day aging) $K_0$-consolidated tests, which were mostly performed in the first testing phase.

[2] This effect can be minimized by using a higher strain rate at the beginning the unloading phase.

quantification of the $\varepsilon_{PL}/\varepsilon_{TOT}$ ratio somewhat arbitrary, and definitely hampering the possibility of gaining information on the slope of the unload portion of the stress strain curve.

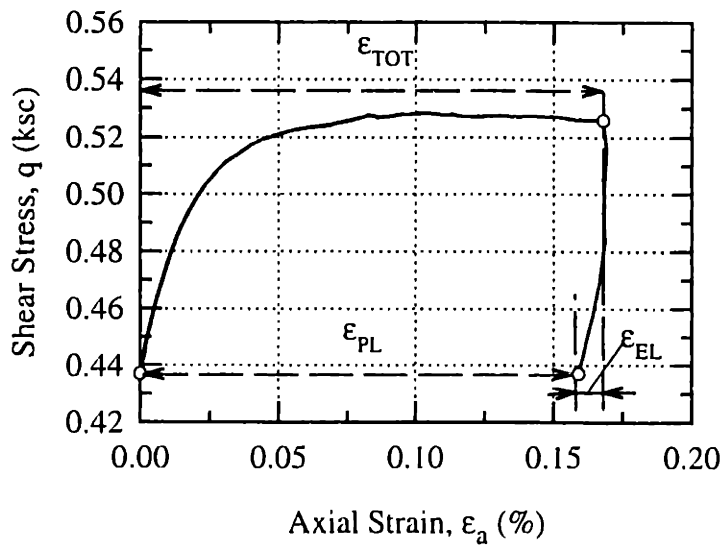


**Figure 6.5:** Elastic and plastic component of strain (NC-RBBC – *TX475S1*).

Three other tests were performed with stress conditions similar to those described for test *TX475S1*. Exact pre-shear conditions for these tests are summarized in Table 6.1, along with the batch and cell[3] information and the initial stiffness results. Comparison of these data furnishes an indication of the consistency of the results.

| Test (Batch-Cell) | $\sigma'_{vc}$ (ksc) | K | e | $t_{aging}$ (h) | $E_{uMAX}$ (ksc) | $\Delta E_{MAX}/E_{AVE}$ (%) |
|---|---|---|---|---|---|---|
| **TX359S1** (418-MIT05) | 1.72 | 0.48 | 1.070 | 25 | 1031 | -1.2 |
| **TX403S1** (419-MIT05) | 1.70 | 0.47 | 1.096 | 36 | 1138 | +9.0 |
| **TX418S1** (419-MIT04) | 1.76 | 0.48 | 1.069 | 27 | 958 | -8.2 |
| **TX475S1** (419-MIT04) | 1.70 | 0.49 | 1.081 | 33 | 1049 | +0.5 |

Statistics: E=1044±24 S.D. (COV=7%)

**Table 6.1:** Tests performed on NC RBBC at $\sigma'_{vc}$ equal to 1.7 ksc.

Figure 6.6a shows the stiffness degradation curves for the four tests presented in Table 6.1. The curves for the individual tests are plotted with dashed lines, while a solid line denotes the average curve. The bracket around the average maximum stiffness indicates a range of ±5%. Comparison of the non-linear behavior can be best performed by plotting the normalized stiffness data, as shown in Figure 6.6b, and by looking at the linear threshold and coefficient of non-linearity data summarized in Table 6.2. The data demonstrate great consistency in the shape of the normalized stiffness curve, and also emphasizes that factors affecting the variability of the initial stiffness (e.g. small variations in the stress level and in the void ratio stemming from specimen to specimen variability) influence the curve as a whole. Thus the shape of the normalized stiffness curve can be considered unique.

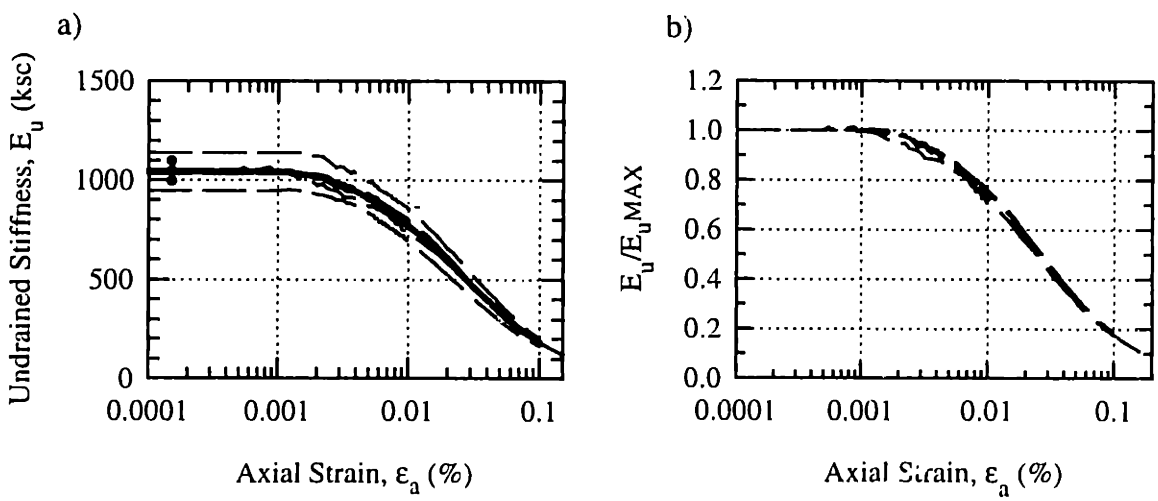


**Figure 6.6:** Stiffness degradation curves for four tests performed on NC RBBC at $\sigma'_{vc}$ equal to 1.7 ksc.

[3] The two stress path automated cells employed for this experimental program are referred to as *MIT04* and *MIT05*.

| Test | $\varepsilon_{lin}$ (%) | $C_{NL}$ |
|---|---|---|
| **TX359S1** | 0.0013 | 5.7 |
| **TX418S1** | 0.0019 | 5.9 |
| **TX475S1** | 0.0015 | 5.7 |
| **TX403S1** | 0.0014 | 5.9 |

Statistics: $\varepsilon_{lin}$=0.0015±0.0003 S.D. (COV=15%)
$C_{NL}$=5.8±0.1 S.D. (COV=2%)

**Table 6.2:** Linear threshold and coefficient of non-linearity for four tests performed on NC RBBC at $\sigma'_{vc}$ equal to 1.7 ksc.

## 6.3 EFFECT OF STRESS LEVEL

### 6.3.1 Introduction

Investigation of the pre-failure behavior of NC RBBC after $K_0$-consolidation was performed at a variety of stress levels, between 1.7 and 12.6 ksc. Of the thirty-one total tests performed on $K_0$-consolidated NC RBBC, twenty-two meeting the requirements for excellent, good or fair (see Chapter 5 – Section 5.5) are here employed to show the behavior of NC RBBC as a function of stress level (Table 6.3).

| *Stress Level (ksc)* | *Number of Shears* | *Test and shear #* |
|---|---|---|
| 1.7 | 4 | 359S1, 403S1, 418S1, 475S1 |
| 2.4 | 5 | 353S1, 362S1, 403S2, 406S1, 418S2 |
| 3.1 | 4 | 361S3, 418S3, 422S1, 474S3 |
| 4.0 | 3 | 362S3, 418S4, 422S2 |
| 5.8 | 2 | 406S3, 422S3 |
| 7.9 | 2 | 406S4, 422S4 |
| 9.9 | 1 | 471S2 |
| 12.6 | 1 | 471S3 |

**Table 6.3:** Tests performed at each of the stress levels examined.

As shown in Figure 6.6 and Table 6.1 for $\sigma'_{vc}$ equal to 1.7 ksc, even for tests performed at the same stress level, variability in the results is observed. Figures 6.7 a, c, e, g, and i present the curves of secant stiffness versus strain for the tests performed at the other stress levels

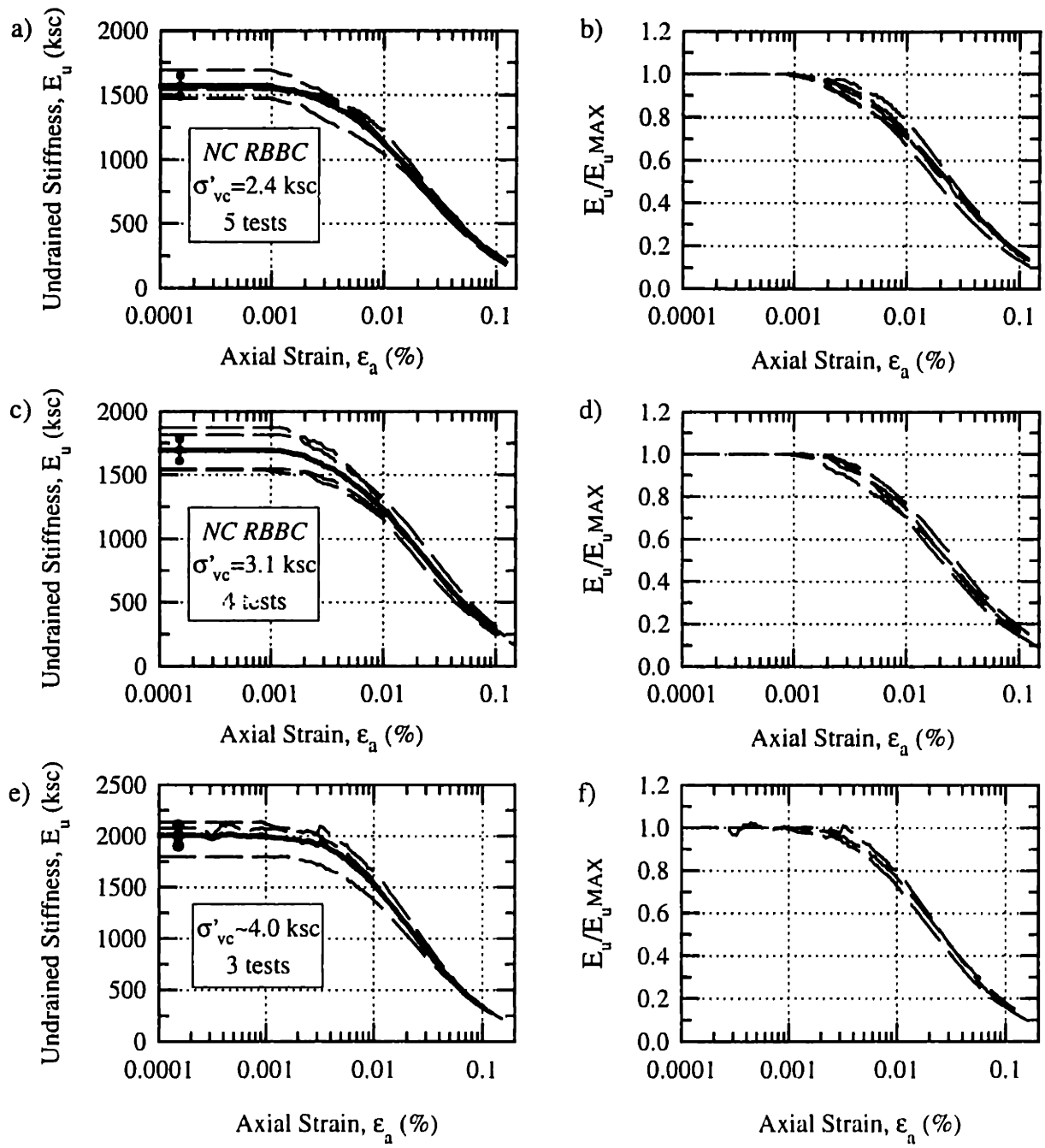


**Figure 6.7:** Stiffness results for tests performed at $\sigma'_{vc}$ equal to a-b) 2.4 ksc; c-d) 3.1 ksc; e-f) 4.0 ksc.

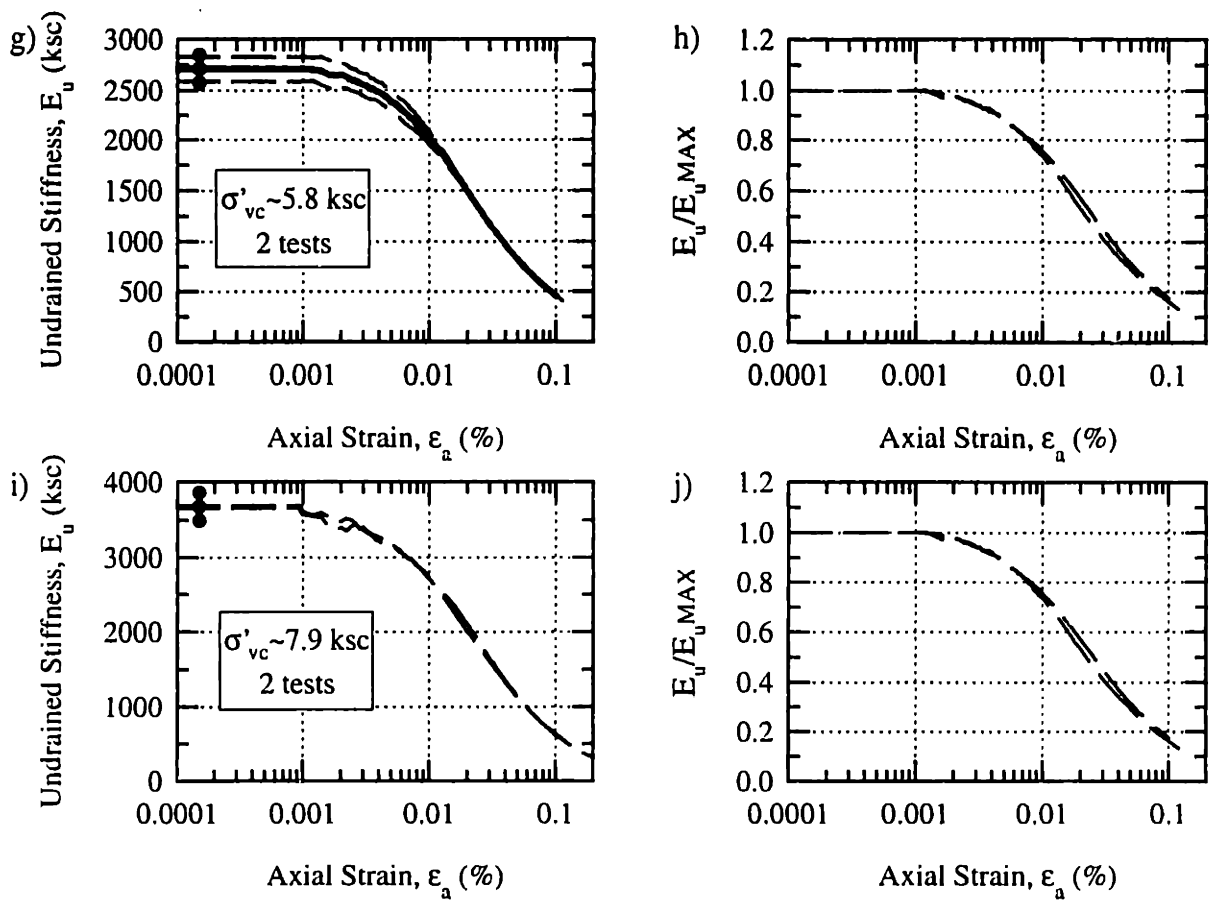


**Figure 6.7:** (continued) Stiffness results for tests performed at $\sigma'_{vc}$ equal to: g-h) 5.8 ksc; i-j) 7.8 ksc.

investigated having more than one test. As in Figure 6.5, dashed lines are used to indicate the results from the individual tests, while a solid line defines the curve obtained by averaging all the data. In addition, a bracket indicating a $\pm 5\%$ range around the average $E_{uMAX}$ is also shown. Overall the results display good repeatability. A considerable effort was invested in trying to isolate the source of this variability, and it was verified that in most cases it stemmed from variations in the pre-shear void ratio: the lower the void ratio, the higher the value of the stiffness measured at the same vertical consolidation stress. This is the case, for example, in Figure 6.7c which summarizes the results for $\sigma'_{vc}$ equal to 3.1 ksc, where the two bottom curves correspond to values of the void ratio (0.982 and 0.985) higher than those for the two upper curves (0.968 and 0.948).

In the five companion graphs (Figures 6.7 b, d, f, h, and j) appearing on the right the data are normalized by the maximum stiffness (for clarity only the results for the individual tests are shown). These results confirm again that, following normalization by the initial stiffness, much of the variability in the curves is eliminated.

The average curves for seven of the eight stress levels examined are summarized in Figure 6.8. Note that in the case of $\sigma'_{vc}$ equal to 12.6 where only test was performed, the results for this test are used in place of the average curve. The figure shows that increasing values of the vertical consolidation stress cause increased values of the stiffness at all strain levels.

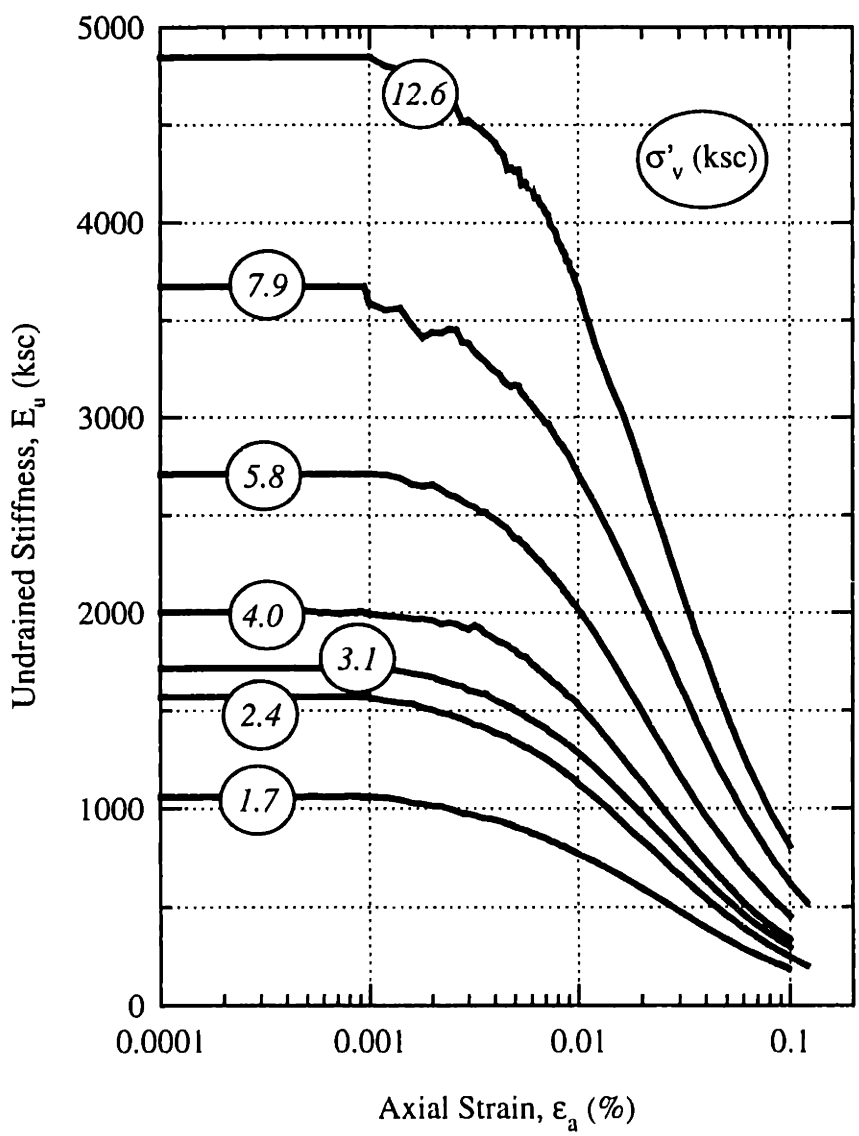


**Figure 6.8:** Stiffness of NC RBBC as a function of stress level.

### 6.3.2 Initial Stiffness

Having observed that the initial undrained stiffness increases with stress level, it is of interest to determine the form of this relationship. Contrary to what has been observed for other properties (e.g. the NC undrained strength), the variation of the initial stiffness is not linear with stress level. This is shown in Figure 6.9a which plots the same average curves presented in Figure 6.8, normalized in this case by the (average) vertical consolidation stress. For the range of stress levels examined, the maximum value of the normalized stiffness $E_{uMAX}/\sigma'_{vc}$ varies quite significantly (546±94), and, as shown in Figure 6.9b, tends to decrease with increasing stress level.

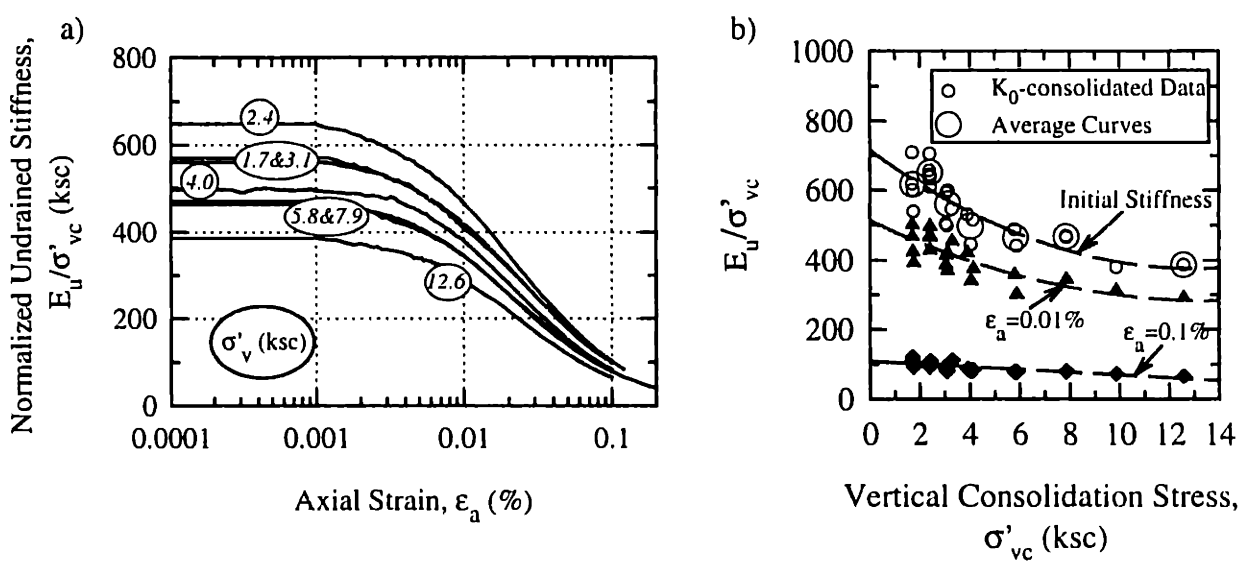


**Figure 6.9:** Normalization of the initial stiffness, $E_u$, by stress level.

Instead, as shown in Figure 6.10, the variation of $E_{uMAX}$ with stress level is better described by an exponential function of the type $E_{uMAX} \propto \sigma'^{n}_{vc}$. The exponent $n$ represents the slope of the regression line through the data points in the $\log E_{uMAX}$-$\log\sigma'_{vc}$ space (Figure 6.10). For the NC data consolidated under $K_0$ conditions examined here, $n$ is found to be about 0.74. As all tests are characterized by similar values of the lateral stress ratio, the same relationship applies also between mean consolidation stress ($p'_{mc}=(\sigma'_{vc}+2\sigma'_{hc})/3$) and initial stiffness, i.e. $E_{uMAX} \propto p'^{0.74}_{mc}$.

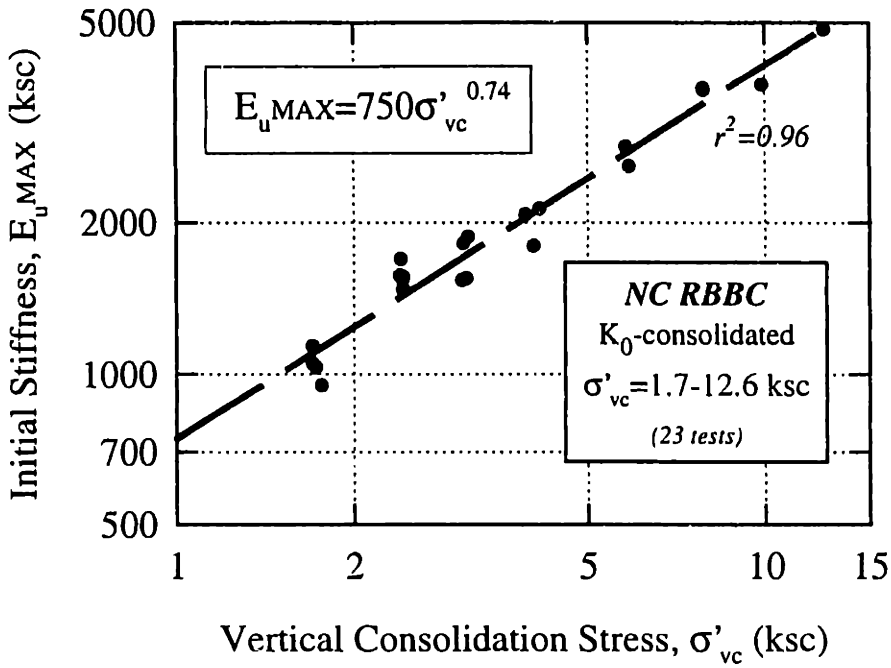


**Figure 6.10:** Power relationship between vertical consolidation stress and initial stiffness for $K_0$-consolidated NC RBBC

Variations in stress level always cause changes in the void ratio of the soil, and the relation between $e$ and $\sigma'_v$ should be unique for a given consolidation procedure (for specimens taken from identical, homogeneous batches). This is shown in Figure 6.11c which plots in the log$e$-log $\sigma'_v$ space the pre-shear conditions for all the tests examined so far (in full symbols) along with points derived from a variety of other tests also consolidated one-dimensionally. All the points lie near a line with slope of 0.165 showing a relationship between void ratio and stress level of the type $\Delta(\log e) \propto \Delta(\log \sigma'_v)$. This representation is preferred to the more conventional $\Delta e \propto \Delta(\log \sigma'_v)$ as it holds true over larger ranges of variation of the void ratio (Pestana 1994).

As a consequence, the relationship shown in Figure 6.10 and 6.11 b linking stress level to maximum stiffness can be written also in terms of void ratio, i.e. $E_{uMAX} \propto e^{-x}$. As shown in Figure 6.11a, for $K_0$-consolidated NC RBBC $x$ is equal to 4.5. Note that while this void ratio function has the same exponential form of that proposed by Lo Presti (1989) and used by several other authors, the exponent is much greater than the values reported for a variety of other clays (see Chapter 2). This is because these authors in general consider *both* a stress level and a void ratio function (i.e . $E_{uMAX} \propto e^{-x}\sigma'_{vc}{}^{n}$). In fact, also for the data presented so far for NC RBBC it

is possible to write the initial stiffness in terms of both stress level and void ratio by optimizing the curve-fitting process to determine the exponents that best fit the data. In the case of $K_0$-consolidated NC RBBC, however, the use of two parameters ($\sigma'_{vc}$ and e) is redundant because they are uniquely related.

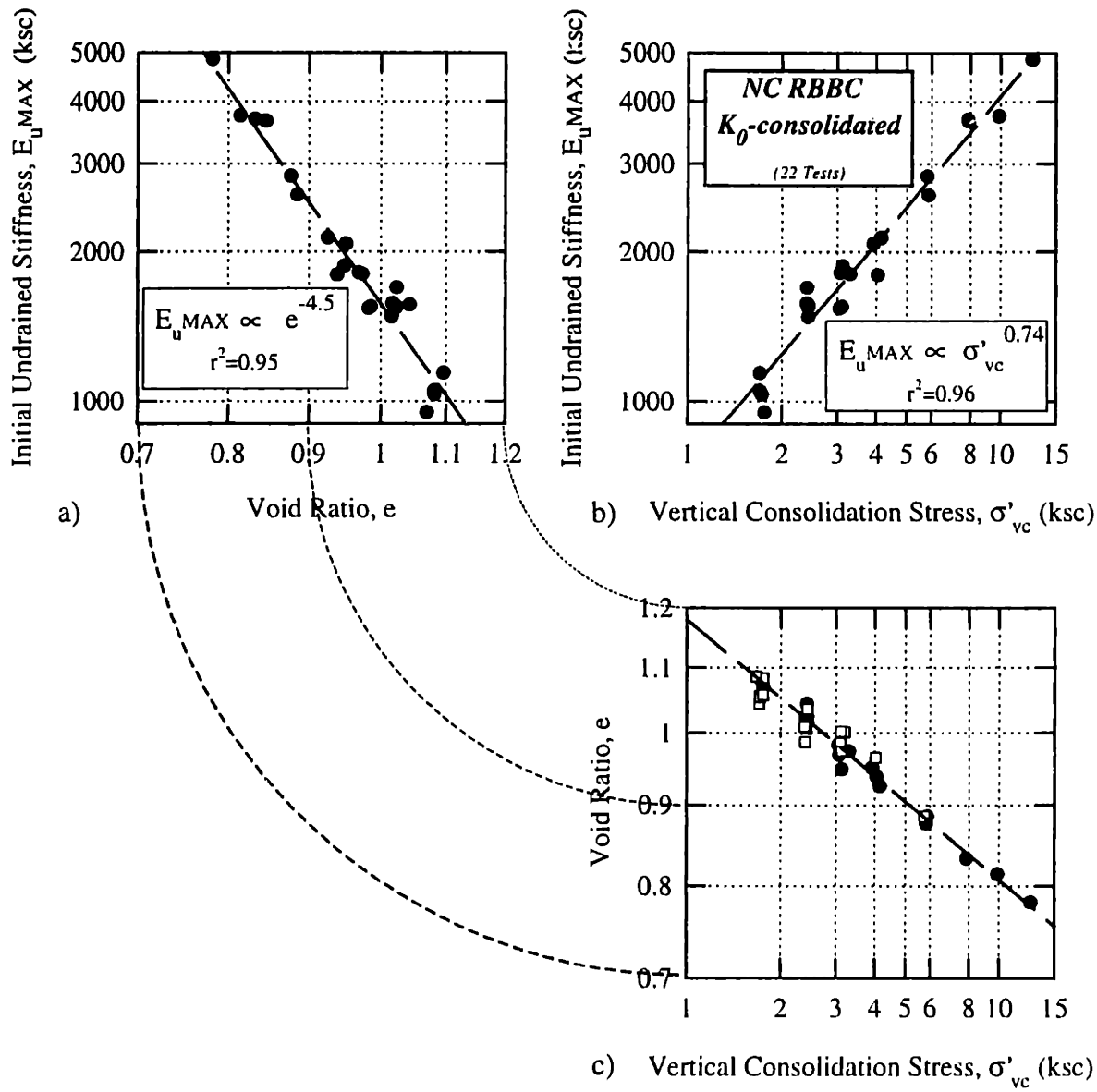


**Figure 6.11:** Relations between stress level, void ratio and initial stiffness for $K_0$-consolidated NC RBBC.

It should be noted that the measurement of the stresses is, in general, more consistent than that of the void ratio, particularly in the case of the multi-stage tests performed in this experimental program. Appendix A contains the phase relations for all the tests performed.

### 6.3.3 Non-Linear Region

As discussed above for $E_u$MAX, the relationship between stiffness and stress level continues to be non-linear at higher strain levels. The two lower curves in Figure 6.9b indicate that at 0.01% and 0.1% axial strain there is a trend of decreasing $E_u/\sigma'_{vc}$ with stress level.

Figure 6.12a presents data of $E_u$ calculated at specific values of the axial strain (0.001%, 0.005%, 0.01%, 0.05% and 0.1%) versus $\sigma'_{vc}$, in the same format used in Figure 6.10 for $E_u$MAX. The same type of exponential equation derived in Figure 6.10 for the initial stiffness, is observed to describe the relationship between stiffness and stress level also at higher strains, i.e. $E_u(\varepsilon)=\propto\sigma'_{vc}{}^{n(\varepsilon)}$. In fact, the regression lines through the data appear parallel, indicating no significant variation in the exponent ($n(\varepsilon)=n$). The individual values of the stress level exponent at the selected strain levels are summarized in the right hand bottom of the figure, while Figure 6.11b plots $n(\varepsilon)$ as a function of strain level. The exponent increases slightly between 0.001 and 0.01% axial strain, after which it decreases and finally reaches what appears to be a constant value, up to 0.1% axial strain.

Note that similar plots linking the stiffness to the pre-shear void ratio can also be generated. However, they provide the same type of information, i.e. that the exponent of the void ratio function is essentially the same for all strains, up to 0.1%.

The fact that at all strains up to 0.1% the stiffness of the soil shows the same dependence on the vertical consolidation stress means that the shape of the $E_u/E_u$MAX versus strain curve is independent of stress level. In fact, as shown in Figure 6.13a, when the curves of normalized stiffness for the twenty-two results available at the eight stress levels examined, are plotted on the same graph they fall in a relatively tight band. Figure 6.13b shows the coefficient of variation (COV= standard deviation/mean) derived for this data set. Note that the fact that the coefficient of variation is equal to zero at small strains results from having used the slope through the early portion of the curve in place of the actual calculated secant stiffness (see Section 5.5), and having normalized the data by the initial stiffness. The average normalized stiffness versus axial strain curve is shown with a solid line in Figure 6.13c. This curve is used throughout the thesis to represent the reference behavior of $K_0$-consolidated NC RBBC.

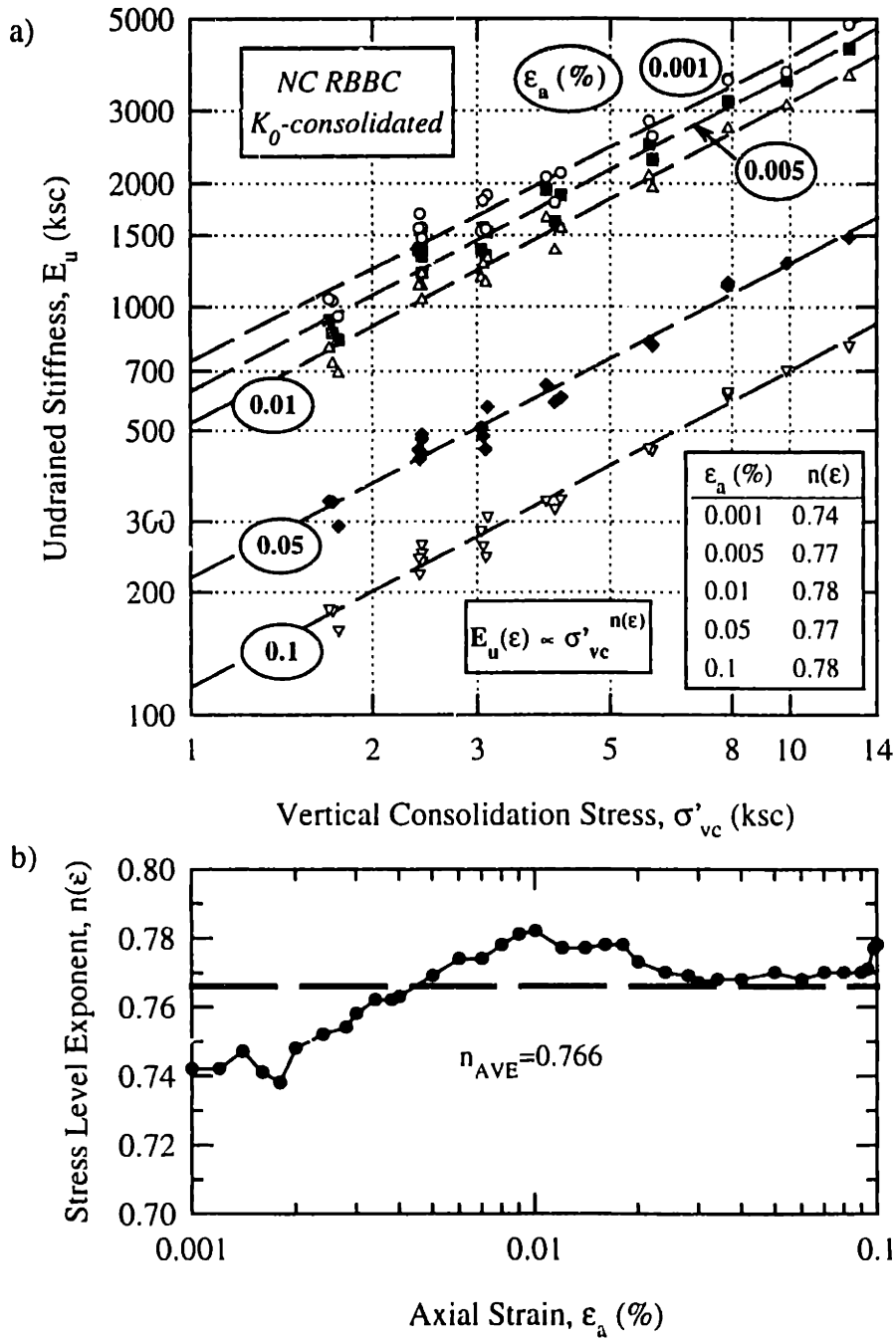


**Figure 6.12:** Stiffness vs. stress level power relationship in non linear region.

Figure 6.13c also presents the two lines corresponding to the average plus or minus the standard deviation calculated, as a function of strain level, from the 22 results available. The reference curve is characterized by a linear threshold of 0.0015% axial strain and $C_{NL}$ equal to

6.0. Also shown in Figure 6.13, for scaling purposes, is a shaded region corresponding to a ±5% band around the "reference" curve.

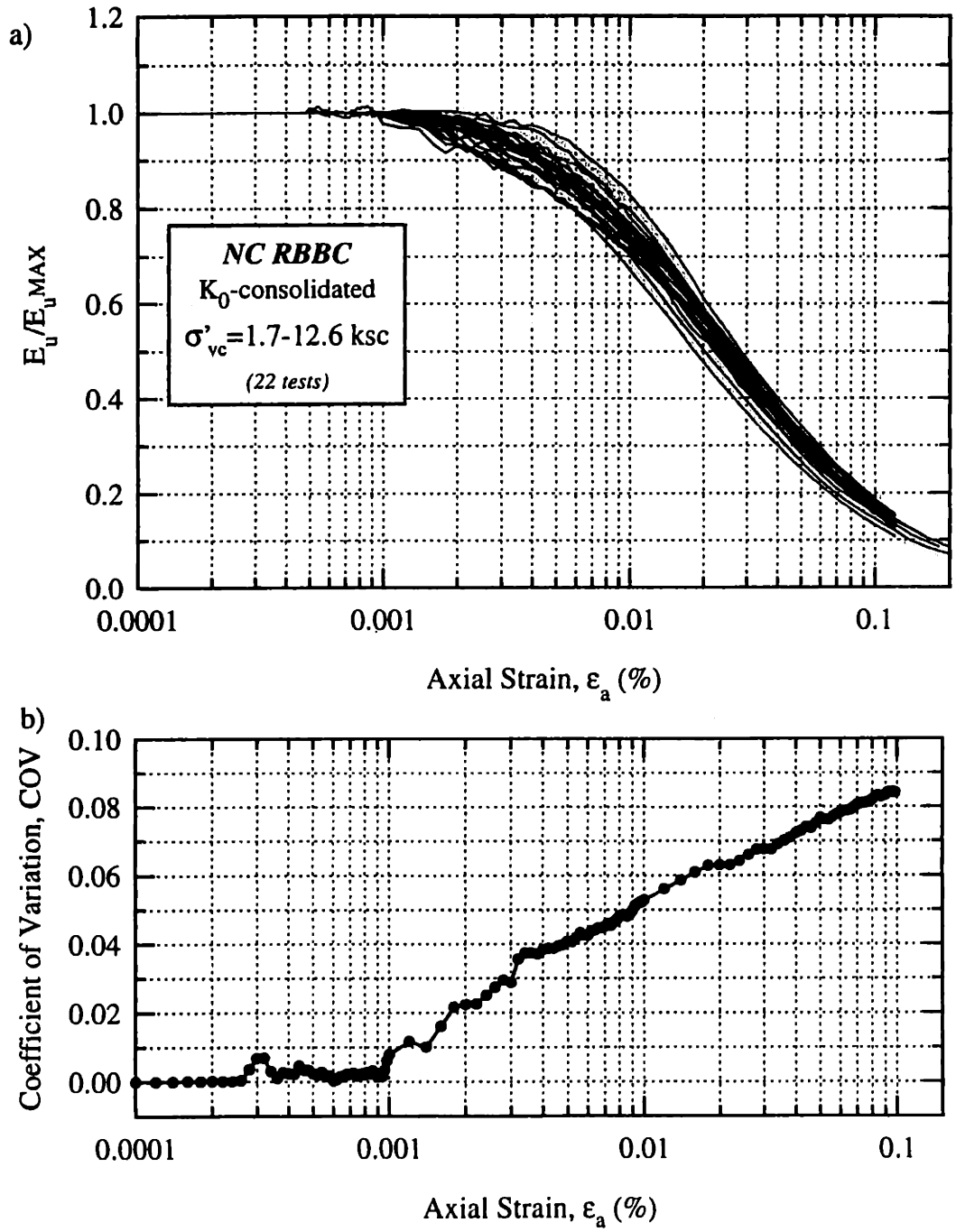


**Figure 6.13:** $E_u/E_{uMAX}$ versus axial strain for $K_0$-consolidated NC RBBC: a) 22 results obtained; b) coefficient of variation.

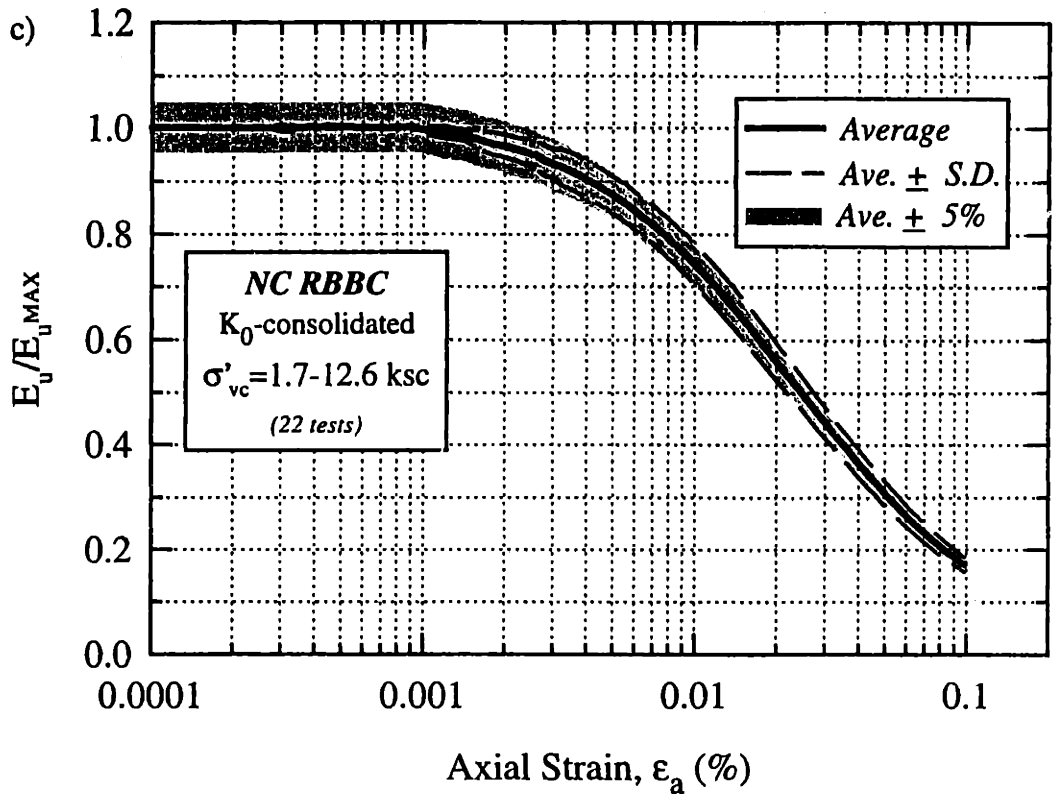


**Figure 6.13:** $E_u/E_{uMAX}$ versus axial strain for $K_0$-consolidate NC RBBC: c) average curve.

Considerable effort was invested to evaluate the source of the variability in the curve. It is clear that it is not caused by variations in the value of $\sigma'_{vc}$ (e.g. Figure 6.7), $K_0$ or duration of aging. Figures 6.14 a-b, show for example that there is no trend between the pre-shear value of $K_0$, which in fact presents some scatter (between 0.46 and 0.51), and both the linear threshold and the coefficient of non-linearity. Similar figures demonstrating the insensitivity of the stiffness degradation curve to modest changes in the duration of the pre-shear aging phase are presented and discussed later in the chapter (Figure 6.81).

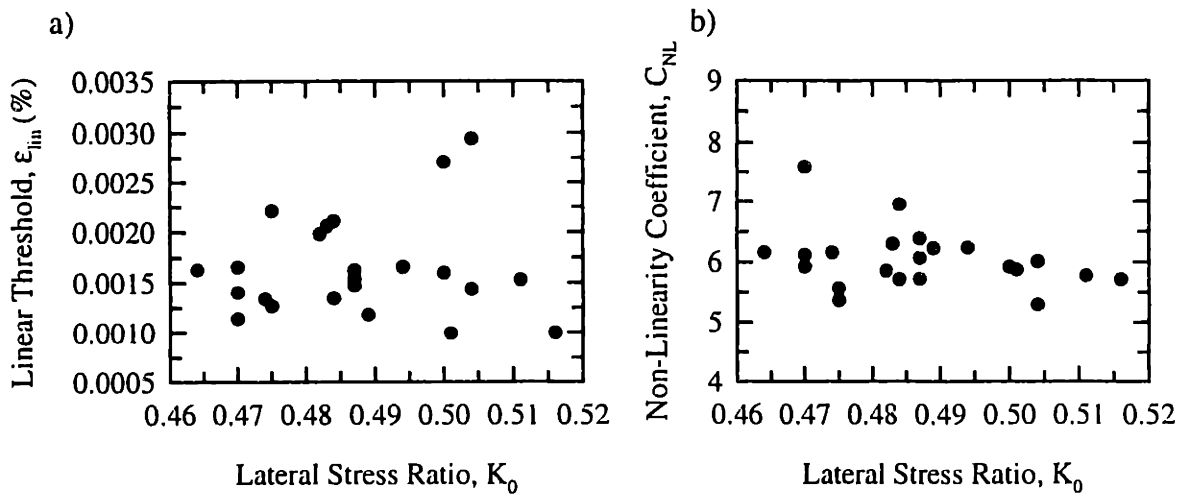


**Figure 6.14:** Independence of a) the linear threshold and b) the coefficient of non-linearity from $K_0$.

In four of the tests on $K_0$-consolidated NC RBBC, at the end of the shear phase the soil specimen was unloaded to the pre-shear value of shear stress in undrained conditions as described in Section 5.2.1, and as shown in Figure 6.5 (see also footnote 1).

The values of total and plastic strains, as well as of the $\varepsilon_{PL}/\varepsilon_{TOT}$ ratio for these tests are summarized in Table 6.4. These results show exceptional consistency, with $\varepsilon_{PL}/\varepsilon_{TOT}$ equal to 94.1±0.6%. They confirm that independently of stress level, the deformation of NC RBBC at 0.1-0.15% axial strain is almost exclusively plastic.

| Test | $\sigma'_{vc}$ (ksc) | $\varepsilon_{TOT}$ (%) | $\varepsilon_{PL}$ (%) | $\varepsilon_{PL}/\varepsilon_{TOT}$ (%) |
|---|---|---|---|---|
| TX471S2 | 9.87 | 0.116 | 0.109 | 94.0 |
| TX471S3 | 12.58 | 0.111 | 0.105 | 94.9 |
| TX474S3 | 3.10 | 0.102 | 0.095 | 93.3 |
| TX475S1 | 1.70 | 0.168 | 0.158 | 94.1 |
| | | | Average = 94.1±0.6 | |

**Table 6.4:** Total and residual strains measured in NC RBBC after unloading from 0.1% axial strain.

## 6.4 EFFECT OF OVERCONSOLIDATION RATIO

### 6.4.1 Introduction

Investigation of the OC behavior of RBBC included three nominal values of OCR: 2, 4, and 8. Stress levels examined for each OCR are summarized in Table 6.5 with the numbers for the corresponding tests. Additional information on the tests is provided in Table 5.6. In this section the discussion is limited to the tests in which the overconsolidated state was reached, as is most commonly done in SHANSEP type testing programs, by unloading from the virgin compression line after $K_0$-consolidation to the maximum stress. In addition, undrained shear was performed at a rate 0.1%/hr after 1 day of laboratory aging. These conditions are referred to as "standard" conditions. Results for different pre-shear consolidation paths and higher strain rates are presented in Section 6.7 and 6.8 respectively.

| | OCR2 | OCR4 | OCR8 |
|---|---|---|---|
| **Stress Level (ksc)** (Test and Shear #) | 1.08 (TX445S2) | 0.73 (TX442S1) | 0.53 (TX418S5) |
| | 1.52[4] (TX361S4) | 1.12 (TX438S6) | 1.06 (TX424S4) |
| | 2.32 (TX432S3) | 2.30 (TX406S5) | 1.85 (TX471S6) |
| | 3.98 (TX455S2) | - | - |

**Table 6.5:** Tests performed on OC RBBC ("standard" conditions only).

### 6.4.2 Initial Stiffness

Before addressing the relationship between $E_{uMAX}$ and OCR, it is appropriate to verify that the concepts discussed for OCR of 1, i.e. the exponential type relationship between initial stiffness and stress level (or void ratio) apply also to OC RBBC. Note that in this case the data set is rather limited, and, as indicated in Table 6.5, at most four data points are available for each OCR.

[4] *TX361S4* is the only overconsolidated test performed in the early part of the experimental program used in the analysis. It was performed following procedures different from those used for the other tests. For example in the early tests the soil was swelled to OCR2 directly after completion of the last undrained shear on the NC soil. Additional details are provided in Section 5.3.1.

As for the NC soil, the initial stiffness is not linearly related to the vertical confining stress. This is shown in Figure 6.15, which plots the values of $E_{uMAX}/\sigma'_{vc}$ versus stress level for the four OCR's examined. For all values of OCR, despite the much more limited data set, there is a trend of decreasing normalized modulus with stress level. Note that the lines drawn through the points are not regressions but simply represent trends.

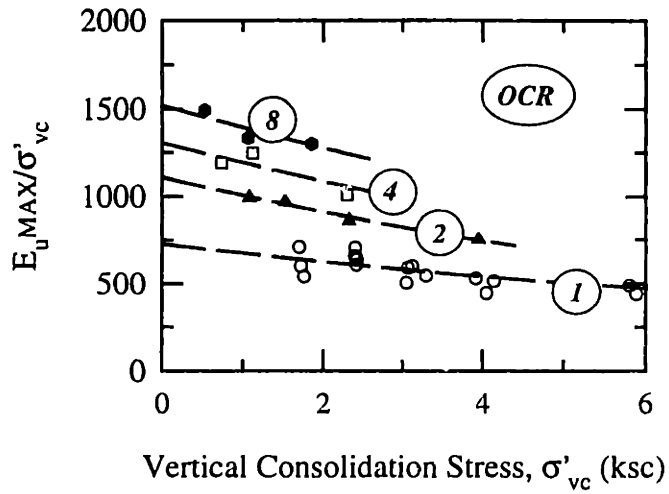


**Figure 6.15:** Plots of $E_{uMAX}/\sigma'_{vc}$ versus $\sigma'_{vc}$ for OC RBBC.

As seen in Figures 6.16a-c, that plot the initial stiffness versus the vertical consolidation stress for each of the three OCR's on a double logarithmic plot, there exists a log-linear relationship between initial stiffness and consolidation stress. Therefore, it is found that the same type of power law relationship ($E_{uMAX} \propto \sigma'^{n}_{vc}$ ) between stress level and initial stiffness, observed to fit the data for the NC soil, describes quite accurately the stiffness-stress level relationship for all values of OCR. The values of the stress level exponent derived for the OC soil are slightly greater than that obtained from the NC data (0.74), and there appears to be a trend of increasing *n* with OCR. However, the limited data available increases the uncertainty in the measured relationship between *n* and OCR. The data for both NC and OC RBBC is compiled in a unique plot in Figure 6.17. Although the slopes of the regression lines through the four sets of data are fairly close, the data for the different OCR's lie on distinct bands.

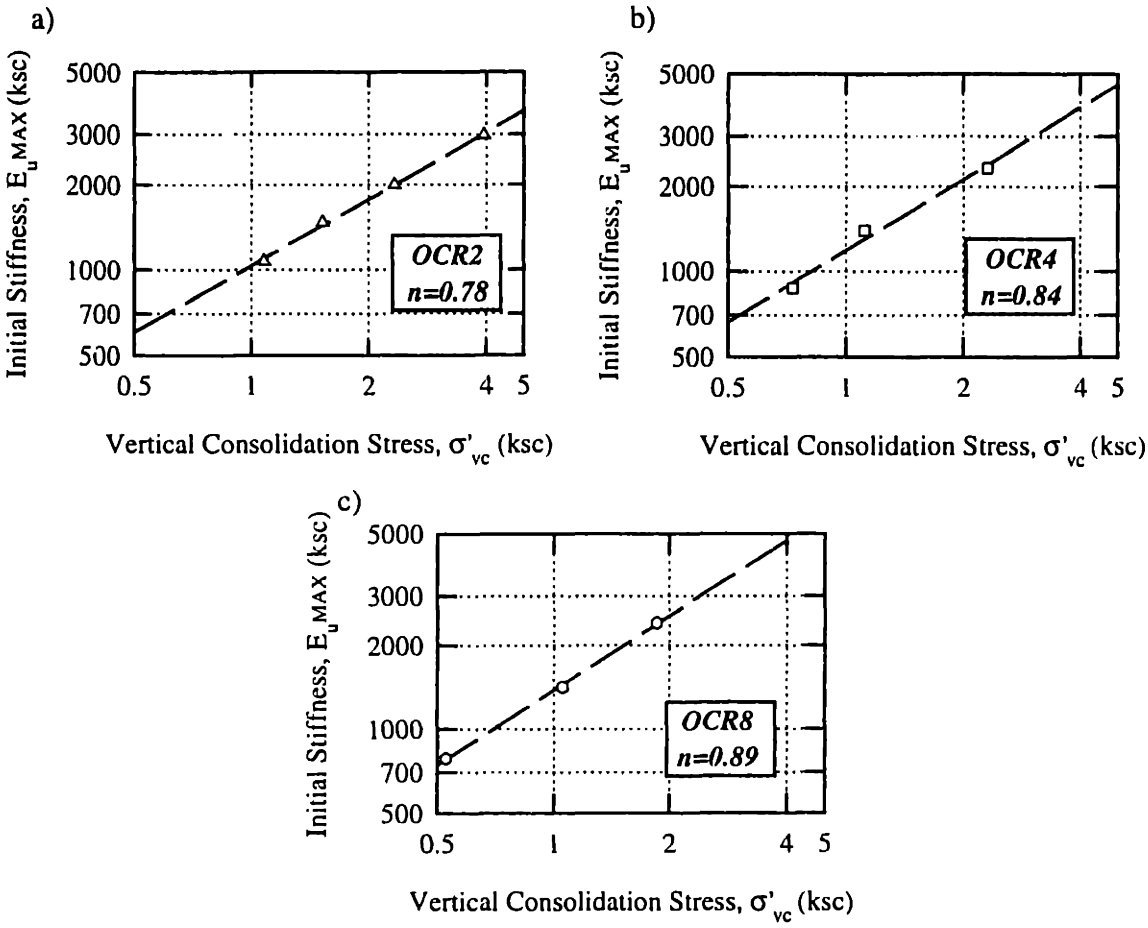


**Figure 6.16:** Relationship between stress level and initial stiffness for: OCR2; b) OCR4; c) OCR8 RBBC.

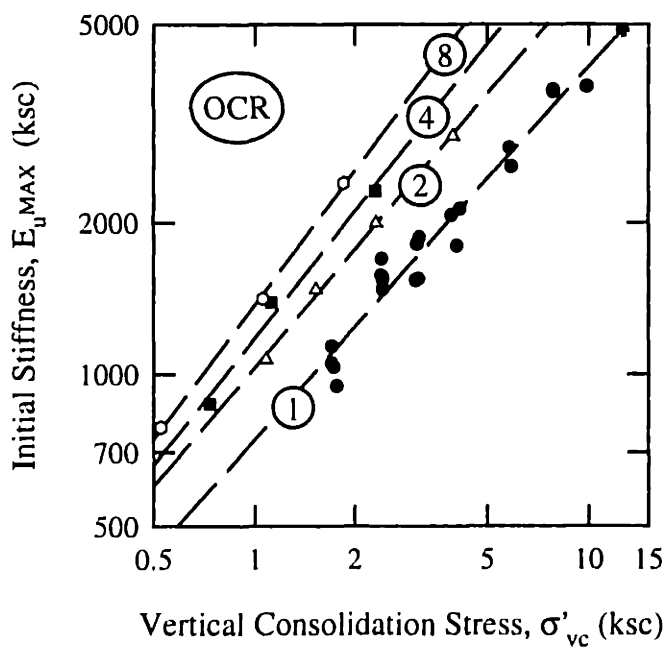


**Figure 6.17:** Relationship between stress level and initial stiffness for NC and OC RBBC.

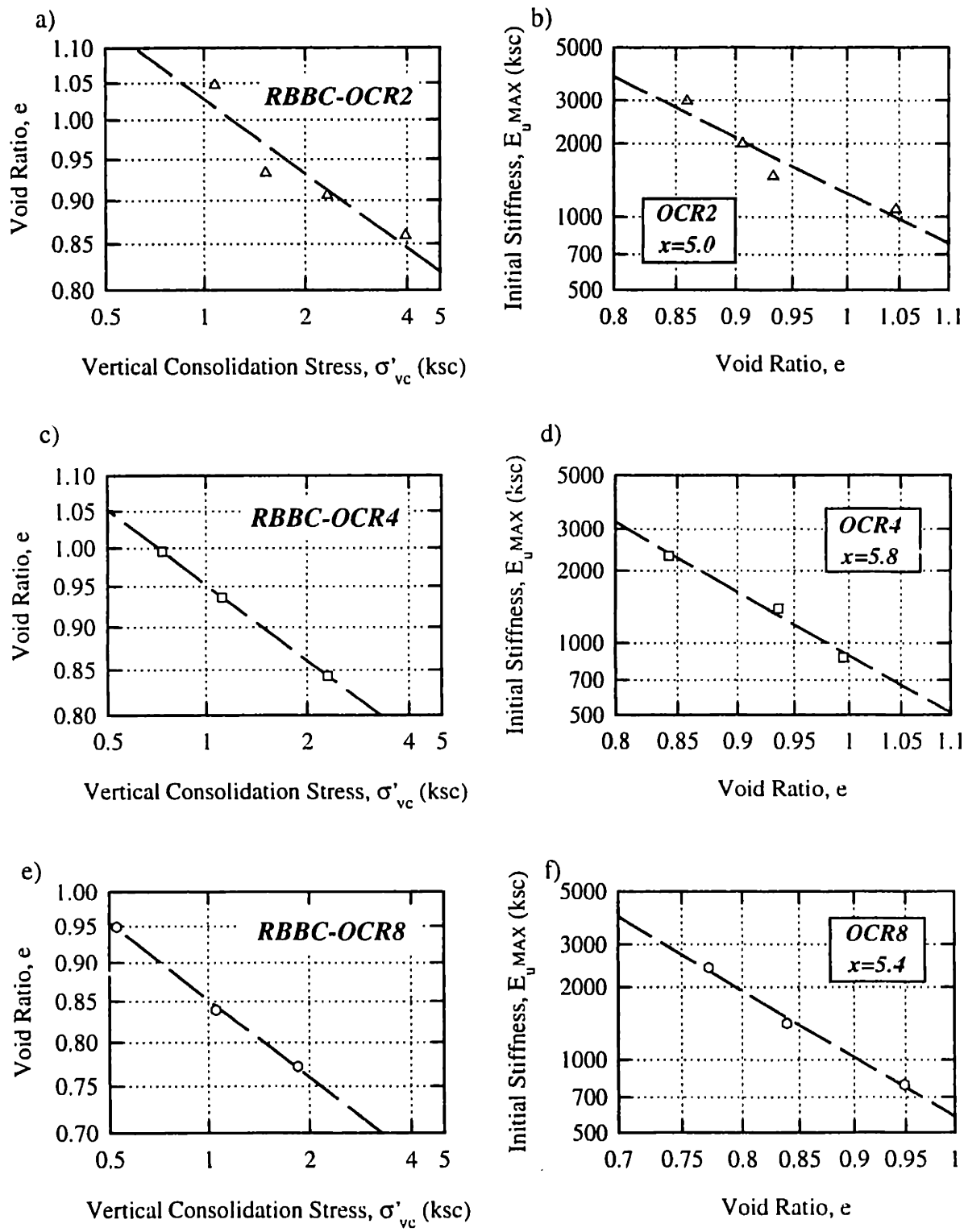


**Figure 6.18:** Plots of void ratio versus vertical consolidation stress and of initial stiffness versus void ratio for a-b) OCR2; c-d) OCR4 and e-f) OCR8 RBBC.

As for NC RBBC, at each value of OCR, there exists a unique relationship between the logarithm of the stress level and the logarithm of the void ratio (Figures 6.18 a, c and e). As a consequence the initial stiffness can be written as a function of the void ratio. This function has the form $E_uMAX \propto e^{-x}$. Plots of $E_uMAX$ versus void ratio for OC RBBC with OCR of 2, 4, and 8 are shown in Figures 6.18b, d, and f.

With the dependence between $E_uMAX$ and $\sigma'_{vc}$ (or *e*) illustrated at all OCR's , it is now important to investigate the manner in which the initial stiffness changes as a function of OCR. When comparing the behavior of OC clay to that of the same soil in the normally consolidated state, it has to be established whether the comparison is performed at the same stress level, or at the same void ratio. This is illustrated in Figure 6.19 that presents the stiffness degradation curves for three different tests. Curve (*a*) is for RBBC with OCR of about 4 sheared after swelling to 2.30 ksc at a void ratio of 0.839. The other two curves are for shears on NC RBBC: one (*b*) performed at approximately the same void ratio, and consequently at a higher effective stress; the second (*c*) on soil at the same vertical consolidation stress as the OC test, but at higher void ratio.

Overconsolidation leads to a marked modification in the pre-failure stress-strain behavior of cohesive soils. With regards to the initial maximum stiffness, Figure 6.19 shows that at equal consolidation stress, the OC soil is stiffer due to the much lower void ratio. On the other hand under conditions of equal void ratio, the NC soil is stiffer, due to the higher stress level. This is the same trend observed for the variation of the undrained strength with OCR. Note that it is generally easier to compare results at the same stress level.

Similar comparisons can be performed for the other OCR's. Unfortunately, the data base from this experimental program does not allow comparison of all OCRs at a given stress level. However, for $\sigma'_{vc}$ equal to 2.3-2.4 ksc, data are available for OCR 1, 2, and 4. The initial stiffness results for these tests are shown in Figure 6.20. This plot also includes a data point for OCR8 RBBC that does not represent the result of a test but was determined from the relationship between stress level and initial stiffness shown in Figure 6.16c.

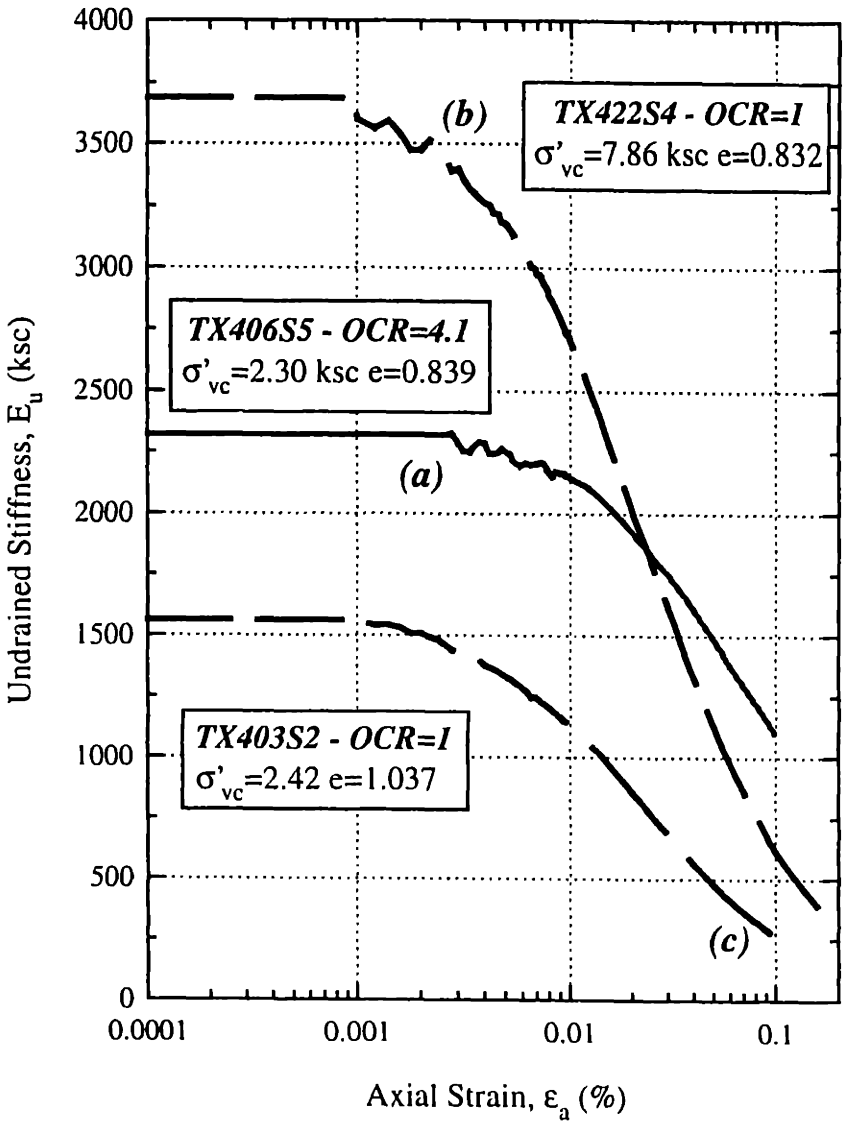


**Figure 6.19:** Comparison of NC and OC behavior at the same stress level or void ratio.

As seen in Figure 6.20, at a stress level of 2.4 ksc, the relationship between initial stiffness and OCR is of the type $E_{(OC)}=E_{(NC)}OCR^k$, with the exponent k equal to 0.28 ($E_{(NC)}$ is the stiffness of the NC soil at the same vertical consolidation stress). Unfortunately the data for OC RBBC are too limited to allow generalization of this expression to other stress levels. One could use the equations for the regression lines appearing in Figure 6.17 to generate data at all stress levels for all OCR's. In such a case one would find that the OCR exponent increases with stress level.

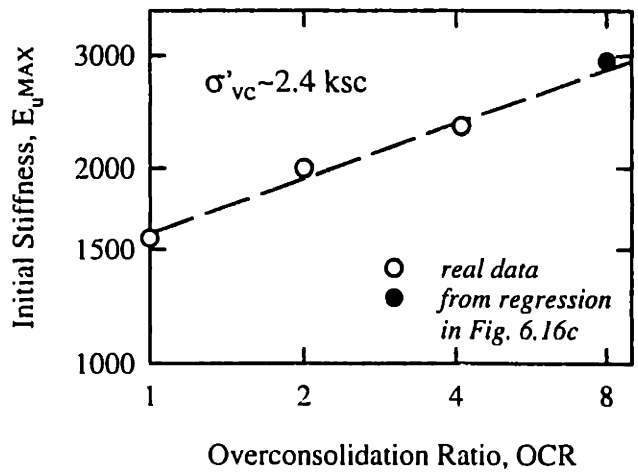


**Figure 6.20:** Variation of $E_{uMAX}$ at $\sigma'_{vc}$ ~ 2.4 ksc as a function of OCR.

### 6.4.3 Non-Linear Region

Increasing OCR leads to dramatic differences in the pre-failure behavior of RBBC. As shown in Figure 6.19, under conditions of equal vertical consolidation stress (curves *a* and *c*) , the behavior of the OC soil is characterized by higher values of stiffness at all strain levels. The figure also indicates that the overconsolidated soil displays less significant pre-failure non-linearity. This is shown more clearly in Figure 6.21, which presents the curves of $E_u/E_{uMAX}$ for

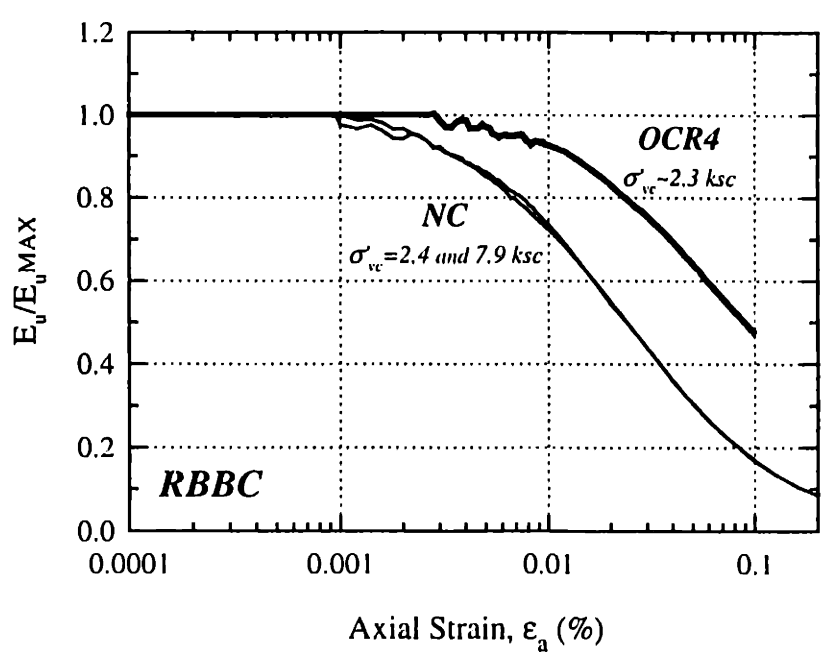


**Figure 6.21:** Comparison of stiffness degradation curves for NC and OCR4 RBBC.

the three tests shown in Figure 6.19. While the data for the two NC tests (*b* and *c*) lie virtually on top of each other, the OCR 4 curve presents a much more extended region at constant stiffness and a less rapid decrease in modulus with strain level.

Figure 6.22 presents the stiffness degradation curves normalized by the maximum stiffness for the four tests performed on OCR 2 RBBC (see Table 6.5), after unloading from the virgin compression line. The table at the bottom of the figure summarizes the pertinent pre-shear conditions for the tests presented. Note that this information is listed starting with the rightmost curve. The OCR 2 results fall within a fairly well defined band, clearly distinct from the curve representing the average behavior of NC RBBC determined in Section 6.3, and also included in Figure 6.22. Although the spread between the OCR2 curves is more significant than that observed for NC RBBC, it does not appear to be linked to the marginal variations in K, OCR or duration of laboratory aging experienced by the specimens. Moreover, it is not associated with the range in $\sigma'_{vc}$, thus indicating that, as for NC RBBC, the non-linearity in the behavior of OCR 2 RBBC is independent of stress level (or void ratio).

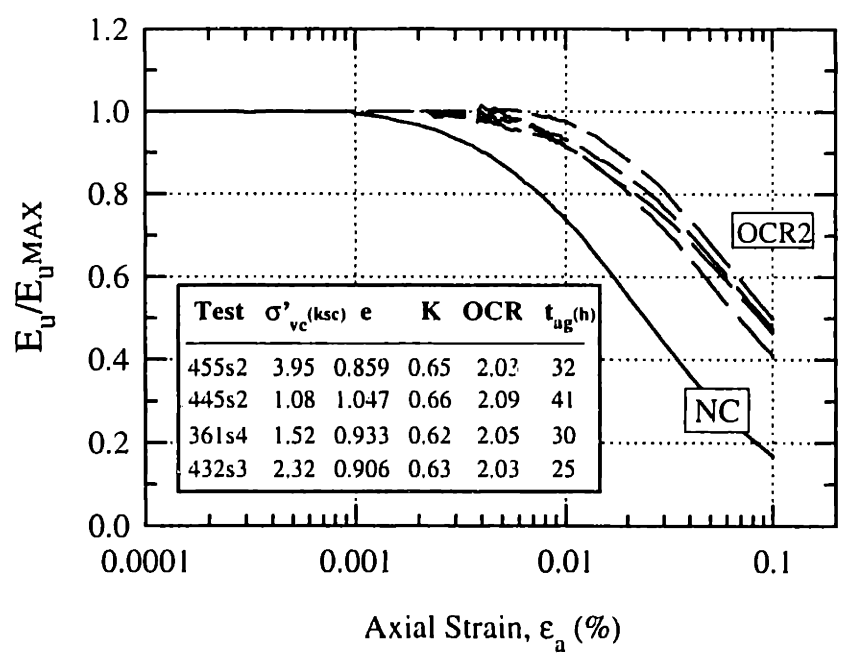


**Figure 6.22:** Normalized stiffness degradation for OCR2 RBBC.

Compared to the NC soil, OCR2 RBBC has an extended region of constant stiffness, with the average linear threshold, $\varepsilon_{lin}$, increasing from 0.0015% to 0.0054%. The soil also displays a

much less accentuated non-linearity in the stress-strain behavior below 0.1%, as the average coefficient of non-linearity goes from 6.0 to 2.2.

The following two figures (6.23 a and b) present analogous plots for OCR4 and OCR8 RBBC, along with the average behavior for NC RBBC for comparison purposes. Once again, the variation in the data is not correlated to any identifiable parameter.

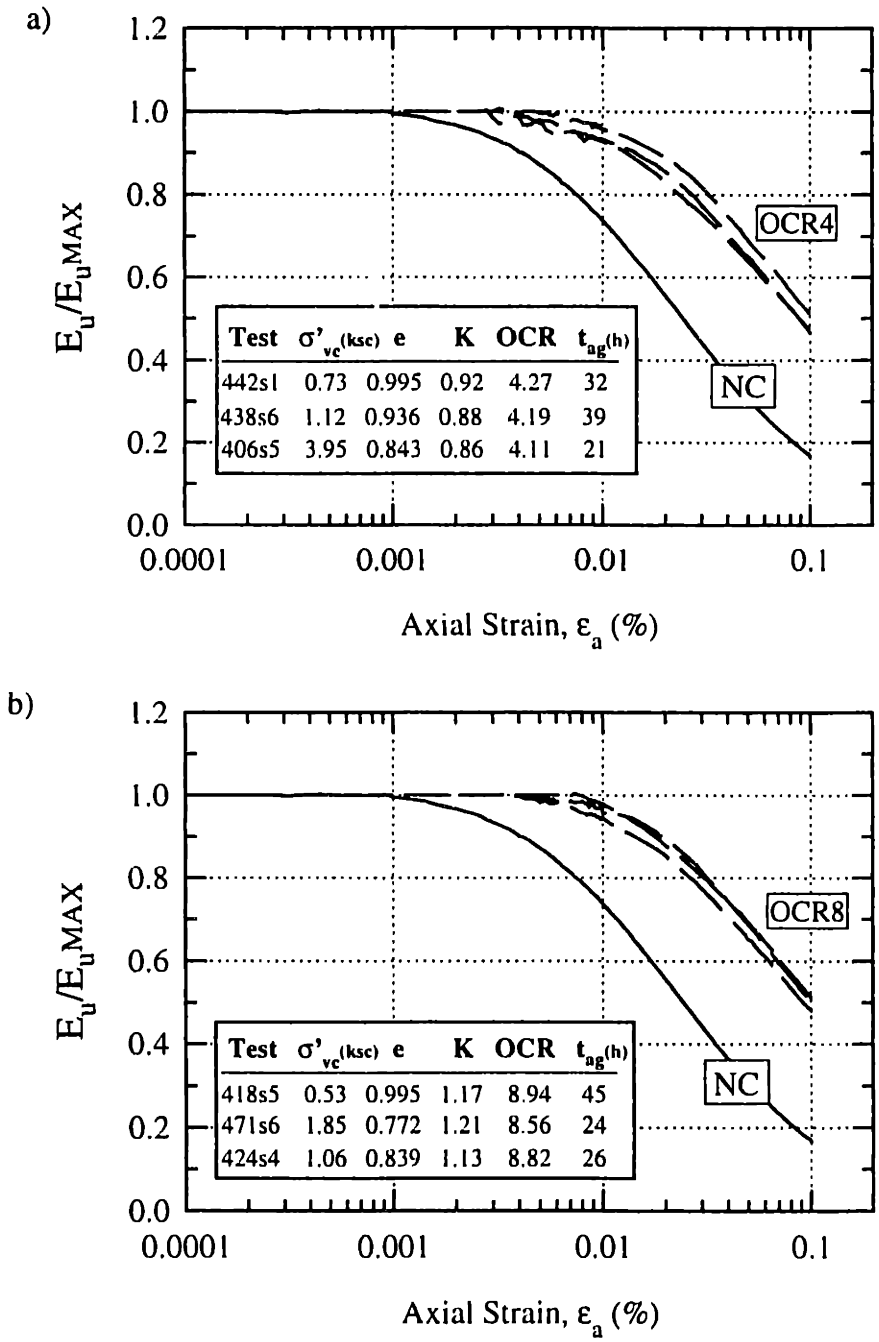


**Figure 6.23:** Normalized stiffness degradation curves for a) OCR4 and b) OCR8 RBBC.

Curves representing the mean stiffness degradation behavior at a given OCR can be determined by averaging the results for the tests performed at that OCR. Such curves for OCR equal to 2, 4 and 8 are presented in Figure 6.24 along with the reference curve for $K_0$-consolidated NC RBBC.

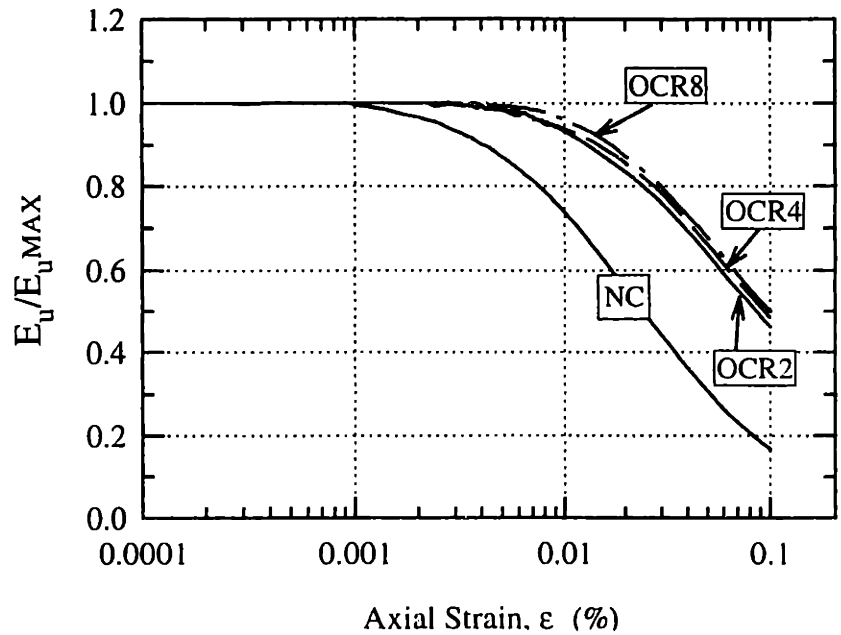


**Figure 6.24:** Stiffness degradation curves for RBBC with OCR equal to 1, 2, 4, and 8.

While NC RBBC exhibits a distinctly different behavior characterized by more pronounced non linearity, the curves for OC RBBC lie all fairly close. This indicates that at least under the conditions examined, i.e. for OCR between 2 and 8 and consolidation path involving continuous unloading from the NC state, the value of OCR plays a secondary role in determining the shape of the stiffness degradation curve. This is shown also in Figures 6.25a and b, which plot the linear threshold and the coefficient of non-linearity as a function of OCR. The figures present both the results of the individual tests and the values derived from the average curves shown in Figure 6.24. Figure 6.25a shows that, despite a general trend of $\varepsilon_{lin}$ increasing with OCR, the linear threshold data present some scatter. The data for the coefficient of non-linearity are more consistent, with $C_{NL}$ equal to $2.09 \pm 0.13$ for all OC results. The question mark in the figure reflects the fact that the behavior at low values of OCR is unknown.

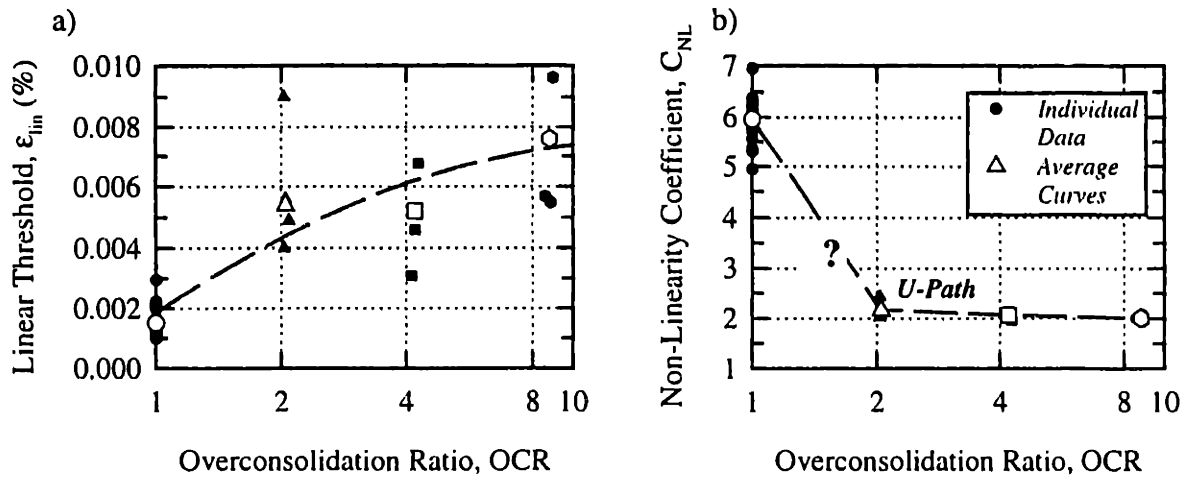


**Figure 6.25:** a) Linear threshold and b) coefficient of non-linearity as a function of OCR.

The modification to the stiffness degradation behavior produced by overconsolidation ($E_u/E_{uMAX}$) can be better visualized by plotting, for each OCR, the ratio of the normalized stiffness of the OC soil to that of NC RBBC. Note that this ratio is independent of stress level, and describes exclusively the increase in the normalized stiffness. Plots of $(E_u/E_{uMAX})_{OC}/(E_u/E_{uMAX})_{NC}$[5] for the three values of OCR examined are shown in Figure 6.26.

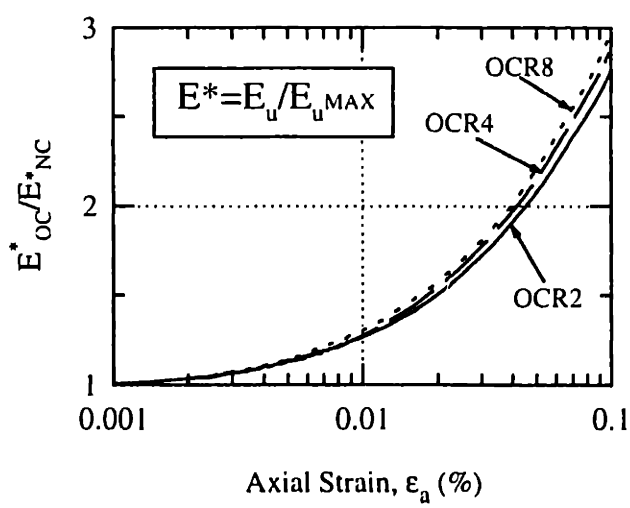


**Figure 6.26:** Ratio of $(E_u/E_{uMAX})_{OC}$ to $(E_u/E_{uMAX})_{NC}$.

This figure confirms the insensitivity of the stiffness degradation behavior to the value of OCR in the range 2-8, and indicates that the increase in normalized stiffness produced by

overconsolidation is increasingly significant with strain level. This type of representation is useful to quantify the effect of OCR on the stiffness degradation behavior of RBBC as a function of strain level (e.g., at 0.1% axial strain $E_u/E_{uMAX}$ is increased approximately by a factor of 3 for all three values of OCR) and allows easy comparison of the relative importance of different variables.

Finally, Figure 6.27 shows the complete stress-strain curve for one test performed on OCR4 RBBC at $\sigma'_{vc}$ ~0.73. The figure illustrates that after reaching a maximum strain of about 0.11%, upon undrained removal of the shear stress, most of the axial strain is recovered. The ratio $\varepsilon_{PL}/\varepsilon_{TOT}$ for this test is measured at about 21%, significantly smaller than the value (94%) obtained for NC RBBC. Identical results are obtained for the other OCR4 shear and the two OCR8 tests for which unloading data are available. Slightly greater values of $\varepsilon_{PL}/\varepsilon_{TOT}$, closer to 30%, are measured in the case of OCR equal to 2.

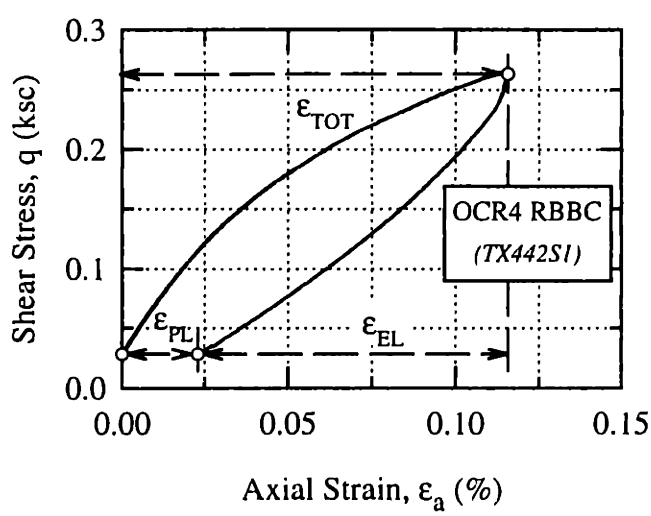


**Figure 6.27:** Elastic and plastic component of strain (OCR4 RBBC – *TX442S1*).

[5] For simplicity in the figures plotting this ratio $E_u/E_{uMAX}$ is indicated as E*.

## 6.5 EFFECT OF LATERAL STRESS RATIO

### 6.5.1. Normally Consolidated Clay

#### *6.5.1.1. Introduction*

As summarized in Section 5.2.4, in the case of NC RBBC, the pre-failure behavior was investigated as a function of variations in the pre-shear value of the lateral stress ratio K. In these tests specimens were consolidated at constant K to the desired vertical and horizontal stresses. Examples of the actual stress paths followed during such consolidation phases are presented in Figure 6.28. Table 6.6 summarizes the tests performed for each of the three values of K examined (0.70, 0.90 and 0.99), the results of which are employed in the following analysis.

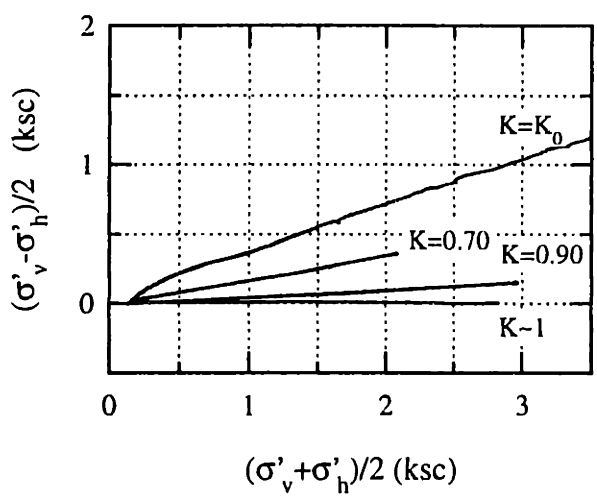


**Figure 6.28:** Stress paths during $K_0$- and stress path consolidation at a fixed value of K of RBBC.

| | *K=0.70* | *K=0.90* | *K ~1* |
|---|---|---|---|
| **Stress Level (ksc)** *(Test and Shear #)* | 2.44 *(TX424S1)* | --- | --- |
| | --- | 3.10 *(TX473S1)* | 3.12 *(TX427S1)* 3.13 *(TX363S1)* |
| | 6.09 *(TX424S2)* | 5.87 *(TX473S2)* | 5.82 (TX427S2) 5.92 *(TX363S2)* |

**Table 6.6:** Tests performed to investigate the effect of the lateral stress ratio.

### 6.5.1.2. *Initial Stiffness*

Figure 6.29a shows the values of $E_{u}MAX$ measured in these tests conducted after stress path consolidation, alongside the reference data set for $K_0$-consolidated RBBC with OCR of 1. The results for the tests performed at K greater than $K_0$ lie, for the most part, above the $K_0$ data, i.e., at a given vertical consolidation stress, the initial stiffness increases with increasing value of the lateral stress ratio. This is clearly shown at a stress level of about 6 ksc, for which data are available at all three values of K considered.

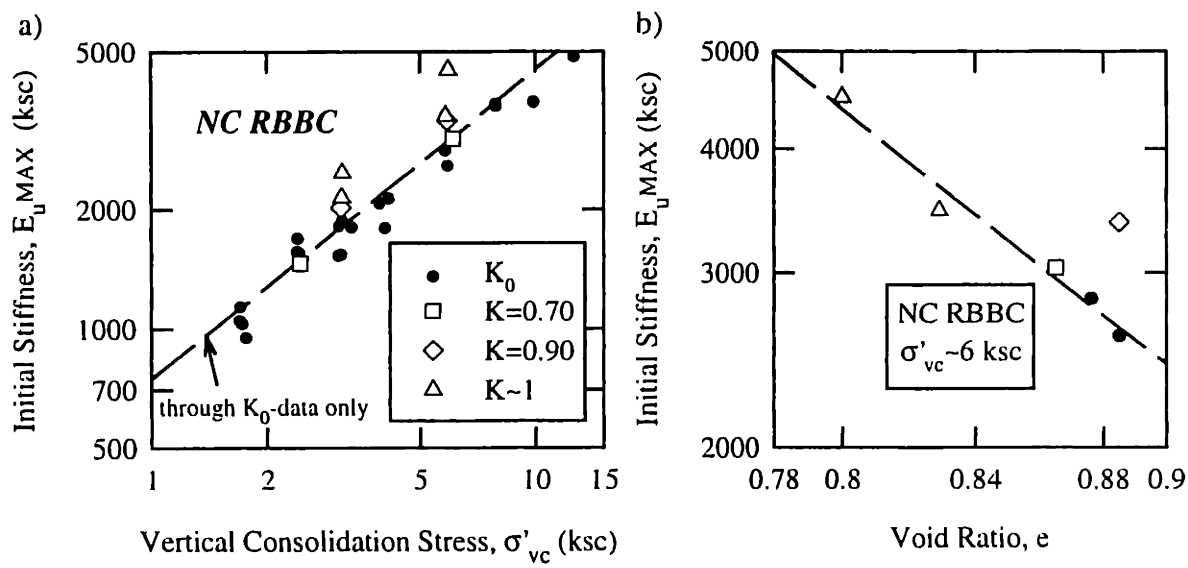


**Figure 6.29:** Initial stiffness of RBBC stress path consolidated at constant K: a) comparison to $K_0$-consolidated data; b) results for $\sigma'_{vc}$ equal to 6 ksc.

As shown in Figure 6.29b for tests conducted at $\sigma'_{vc}$ approximately equal to 6 ksc, the increase in initial stiffness with K, is linked, except for one outlier[6], to the different pre-shear values of void ratio. In fact, due to the different paths followed when approaching the pre-shear stress state, the specimens are subjected to different straining. Figure 6.30 presents the curves of axial and volumetric strain versus vertical stress for four of the stress path consolidated tests, with K equal to 0.70, 0.90, and 0.99, alongside those for a $K_0$-consolidated specimen (in this case the two curves are overlapping as the axial and volumetric strain are equal). For higher values of K,

[6] This test (*TX473S2*) displays a value of void ratio (0.885) significantly higher than expected. This is probably due to some error in the measurements used to calculate the initial void ratio. If in place of the calculated $e_{init}$, one employs the average $e_{init}$ for the batch, the void ratio at ~6ksc turns out to be about 0.861, and the result for *TX473S2* falls much closer to the line shown in the figure. However, the last group of specimens tested (starting with *TX471*), including *TX473*, all displayed values of $e_{init}$ higher than the mean. Therefore this problem remains unresolved.

a more marked difference between axial and volumetric strain is measured during consolidation: the soil is increasingly stiff in the axial direction, while larger volumetric strains are required to reach a given stress level. Ultimately, the higher the value of K, the lower the void ratio reached at a given vertical stress. Incidentally, in one of the K~1 tests displayed in Figure 6.29a (*TX363*) problems encountered during the first consolidation phase led to an additional volumetric strain which resulted in a markedly lower void ratio prior to both shears. This explains the significantly higher values of the initial stiffness measured in these two tests.

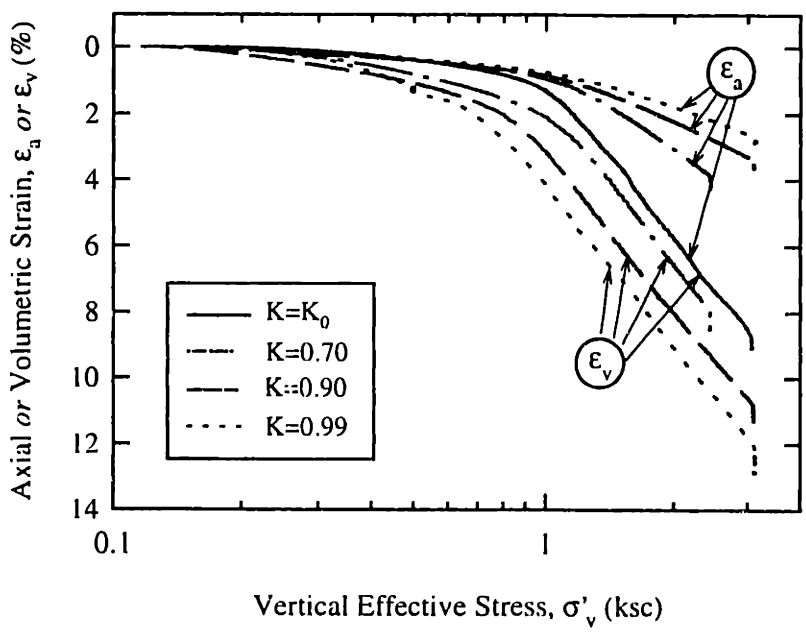


**Figure 6.30:** Compression behavior of $K_0$-consolidated and stress path consolidated (K=constant) RBBC.

Figure 6.31a plots the initial stiffness versus the pre-shear void ratio rather than versus the vertical consolidation stress. The $E_{u}MAX$ data fall on the same band, irrespective of the path followed during consolidation thus demonstrating how for NC RBBC the initial stiffness may be related solely to the pre-shear void ratio. The regression line through all the data in the figure has the same slope as the line obtained best-fitting the $K_0$-consolidated data in Figure 6.11a, i.e. the same void ratio function ($e^{-4.5}$) is found to be valid for all the data, irrespective of the path followed during consolidation.

If the data are to be normalized versus stress level, the mean consolidation stress $p'_{mc}$ ($=(\sigma'_{vc}+2\sigma'_{hc})/3$) should be used in place of the vertical consolidation stress, as shown in Figure

6.31c. In fact, for NC RBBC, unlike the relationship between void ratio and vertical consolidation stress, the one between void ratio and mean consolidation stress $p'_{mc}$ is unique and independent of the stress path followed, as shown in Figure 6.31b.

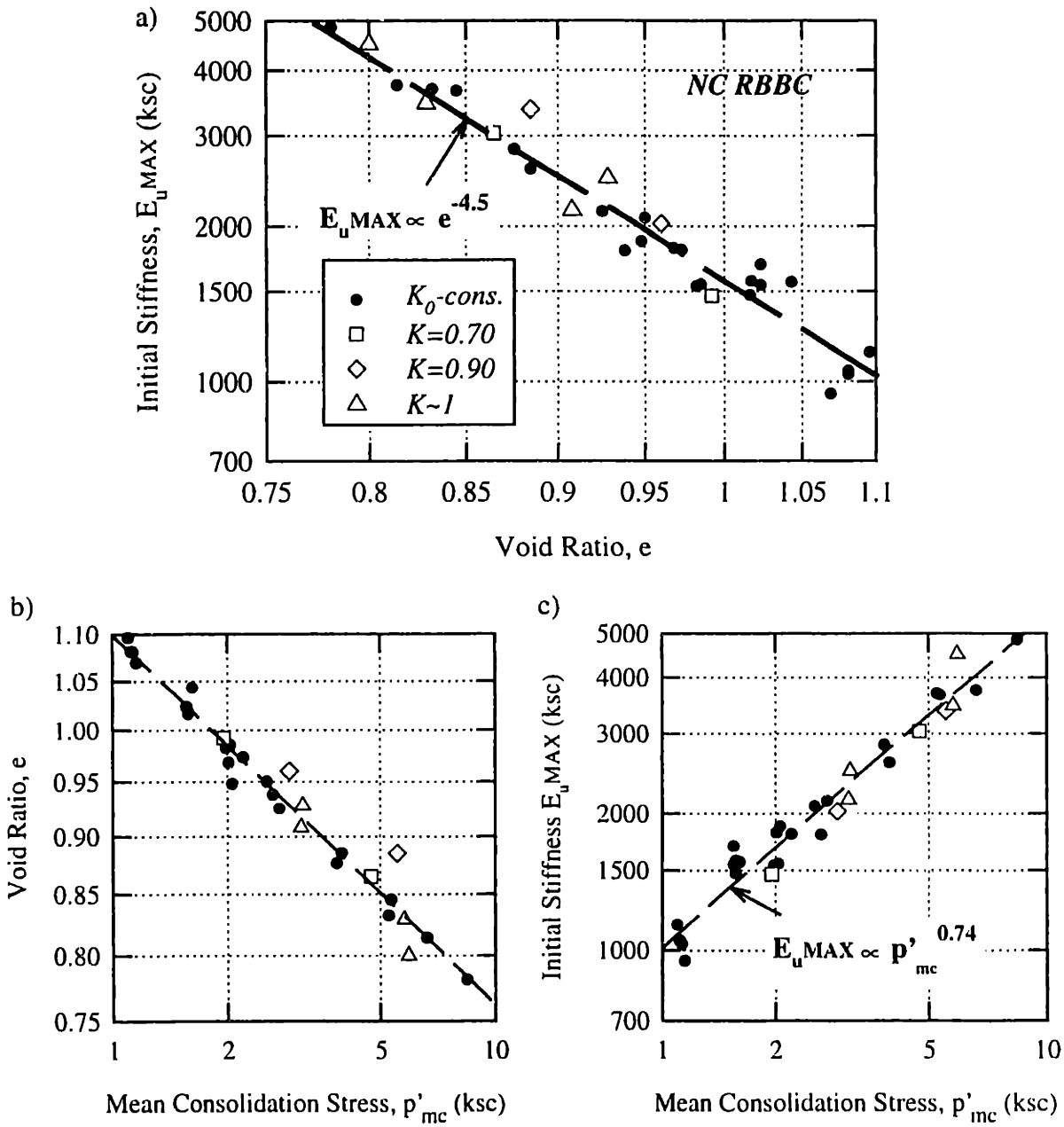


**Figure 6.31:** Relationship between void ratio, initial stiffness and mean consolidation stress for $K_0$- and stress path consolidated (K=constant) NC RBBC.

As indicated in Figure 6.31c, the slope of the regression through the data, i.e. the value of the exponent in the stress level function is basically the same as that determined in Figure 6.10 in the relationship linking vertical consolidation stress to the initial stiffness of $K_0$-consolidated NC RBBC.

### *6.5.1.3. Non-Linear Behavior*

The value of the pre-shear lateral stress ratio significantly impacts the stress strain pre-failure behavior of NC RBBC. Figures 6.32a, b and c present stress strain curves (in terms of shear stress increment versus axial strain) and the stiffness degradation curves, for tests performed at a stress level of approximately 6 ksc, after stress path consolidation at constant K equal to 0,70, 0.90, and 0.99. The curves for two tests performed at the same stress level after $K_0$-consolidation are also plotted for reference. Relevant data for all these tests, (i.e. test number, exact stress level, value of K, void ratio, and duration of laboratory aging) are summarized at the bottom of Figure 6.32c.

Figures 6.32 a, b and c indicate that increasing values of K render the response of the soil stiffer at all strain levels and cause the linear threshold to increase.

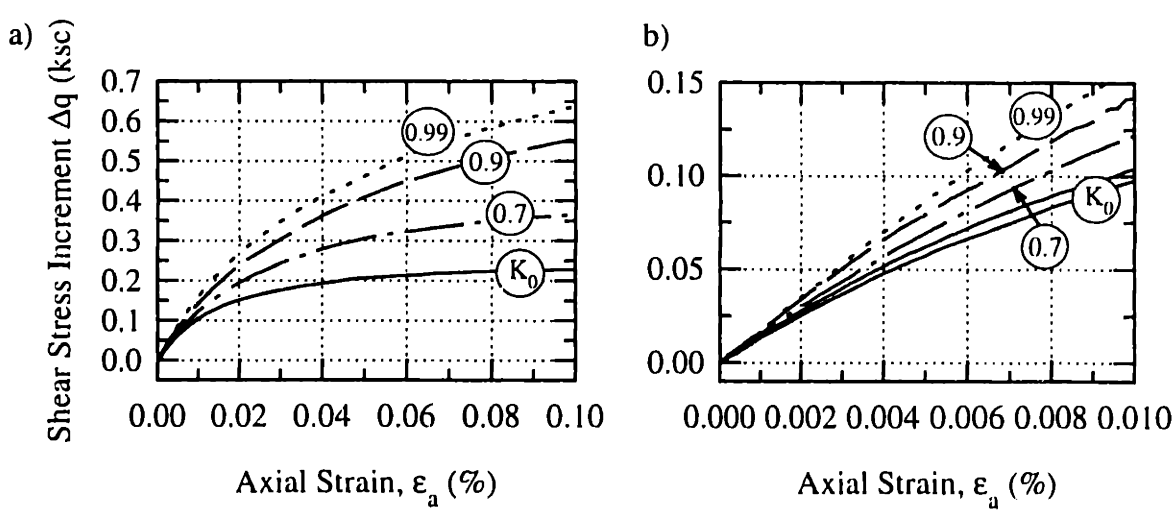


**Figure 6.32:** Behavior of $K_0$- and stress path consolidated (K=constant) NC RBBC at 6 ksc: a-b) stress strain curves; c) stiffness degradation curves.

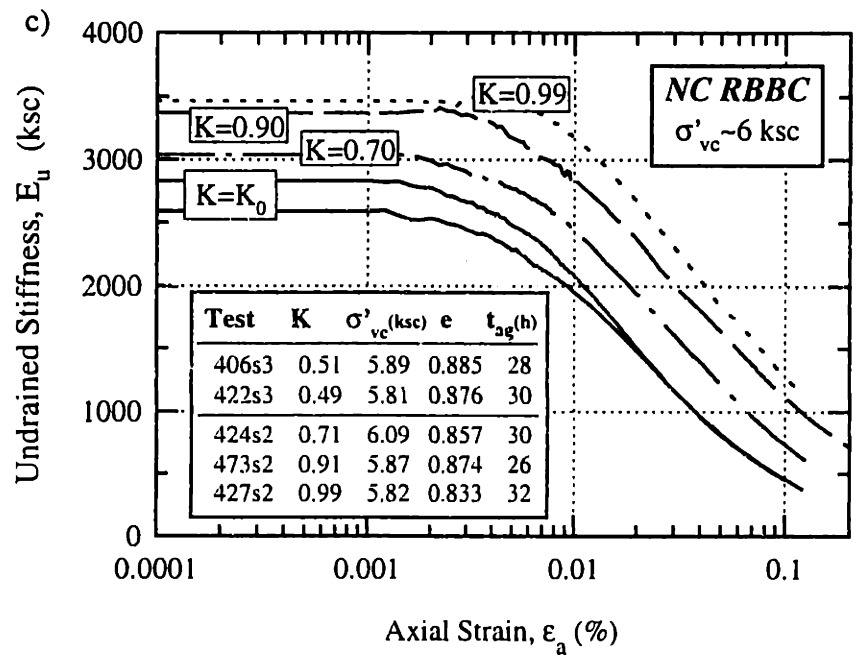


**Figure 6.32** (continued): Behavior of $K_0$- and stress path consolidated (K=constant) NC RBBC at 6 ksc: c) stiffness degradation curves.

The limited data available for each value of K as a function of stress level indicate that the degree of non-linearity is basically independent of stress level. For each value of K, the stiffness data, once normalized by $E_{uMAX}$, differ at all strain levels by less than 10%. This also indicates that the same void ratio ($e^{-4.5}$), or stress level function ($p'_m{}^{0.73}$) applies at all strain levels.

Figure 6.33 presents the average normalized stiffness degradation curves for the three values of K considered, alongside the reference plot for $K_0$-consolidated NC RBBC. Note that for K equal to 1, only two of the results (*TX427S1/S2*) were used to determine the average curve.[7] Figures 6.34 a-b present, as a function of K, the linear threshold strain and the coefficient of non-linearity for each of the stiffness degradation curves available.

Figures 6.33 and 6.34 clearly show the effects of the pre-shear lateral stress ratio K on the small strain non-linearity. Increasing values of K are associated with decreased non-linearity and a marked increase in the size of the linear region. For example, in the case of K equal to one, the

[7] In tests *TX363S1/S2* the hold-stress phase preceding shear extended past the standard 24-36 hours. While the prolonged aging does not seem to influence the initial stiffness in any significant way, it does appear to impact the stiffness degradation behavior. For this reason the results for these tests are discussed in Section 6.9, where the effects of the duration of aging are specifically addressed.

linear threshold increases by five times and the degree of non-linearity is closer to that observed for an overconsolidated soil.

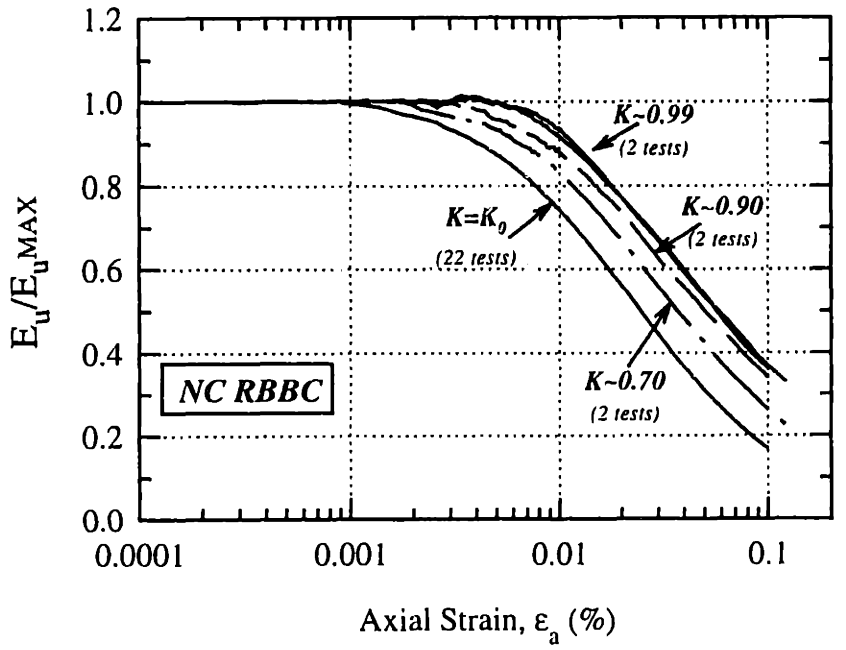


**Figure 6.33:** Stiffness degradation curves for NC RBBC for different values of the pre-shear lateral stress ratio.

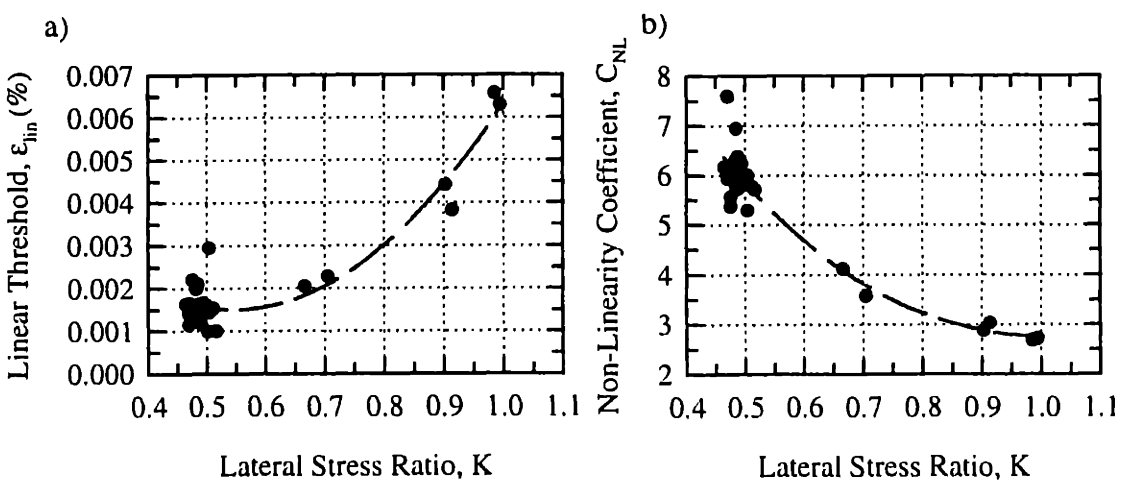


**Figure 6.34:** Variation of a) the linear threshold and b) the coefficient of non-linearity with the pre-shear lateral stress ratio.

Figure 6.35 plots, as a function of strain level, the ratio of the normalized stiffness for consolidation at constant K divided by the corresponding value of $E_u/E_{uMAX}$ for $K_0$-

consolidation. The figure quantifies the increase in normalized stiffness produced by an increase in the lateral stress ratio. For example for K equal to ~1, $E_u/E_{uMAX}$ is more than doubled at 0.1% strain. The figure also indicates a smooth transition in the behavior with increasing K (unlike what observed for the effect of OCR), and points out that, at least up to 0.1%, for a given value of K, the sensitivity to this parameter increases with strain level.

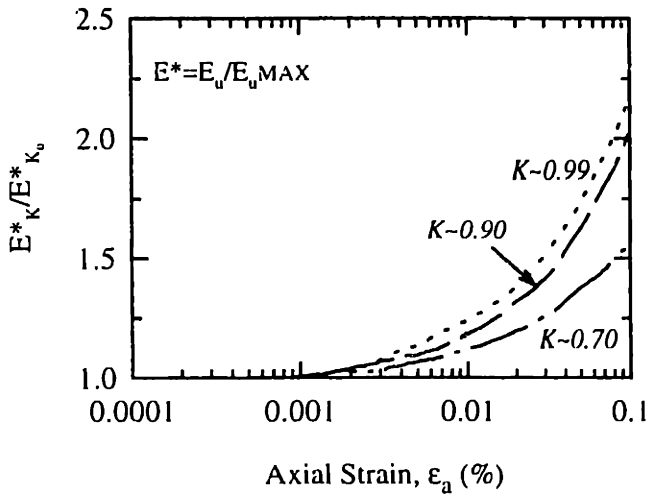


**Figure 6.35:** Increase in stiffness produced by variation in the lateral stress ratio.

One result for the residual strain after undrained unloading of the shear stress at the end of shear is available for a test performed with K equal to 0.90. In this case the $\varepsilon_{PL}/\varepsilon_{TOT}$ ratio is found to be approximately equal to 62%, compared to the average value of 94% measured in the $K_0$-consolidated tests.

### 6.5.2. Overconsolidated Clay

In the case of OC RBBC, variations in the pre-shear value of K were examined only for OCR of 2, and limited to the case of K equal to one. In the two tests (*TX427S3* and *TX427S5*) performed for this purpose the soil was both consolidated and swelled in hydrostatic conditions as discussed in Section 5.2.4 (Figure 5.3).

Table 6.7 summarizes the pre-shear conditions as well as the initial stiffness results for the two tests performed with K equal to one. The results for the $K_0$-test performed at the same stress level are also included in the table.

| Test # | K | $\sigma'_{vc}$ (ksc) | e | $E_uMAX$ (ksc) |
|---|---|---|---|---|
| TX427S3 | 0.99 | 3.92 | 0.807 | 3775 |
| TX427S5 | 0.99 | 3.92 | 0.792 | 3984 |
| TX455S2 | 0.65 | 3.95 | 0.848 | 2985 |

**Table 6.7:** Pre-shear conditions and initial stiffness results for $K_0$ and hydrostatically consolidated OCR2 RBBC.

As discussed for NC RBBC, hydrostatic consolidation results in a larger volumetric strain to reach a given stress level. Consequently, much lower values of the pre-shear void ratio are obtained. This results, as in the case of NC RBBC, in an increase of the initial stiffness.

Figures 6.36a, b and c present plots of the initial stiffness versus vertical consolidation stress, void ratio and mean consolidation stress respectively. As seen for NC RBBC, when plotted versus the void ratio and the mean consolidation stress, the hydrostatic data fall on the same line as the $K_0$ data.

Figures 6.37 a and b show stress-strain curves for these three tests. The curves for the two hydrostatic tests display exceptional consistency, differing at all strain levels by less than 2% and display marginally higher shear stress gain at any given stress level.

The average stiffness degradation curve obtained from the two hydrostatic results is shown in Figure 6.38 along with the line representing the average behavior for OCR2 RBBC after $K_0$-consolidation and swelling. The curve for $K_0$-consolidated NC RBBC is also shown for reference. The figure indicates that the average curve for hydrostatic consolidation displays similar linear threshold ($\varepsilon_{lin}$~0.0054%) and slightly greater degree of non-linearity ($C_{NL}$=2.5) compared to the results for the reference behavior ($K=K_0$) of OCR2 RBBC ($\varepsilon_{lin}$~0.0048%, $C_{NL}$=2.1)[8]. The difference between the two curves is, however, small, particularly considering the range in the stiffness degradation behavior observed at a given OCR (e.g., Figure 6.22).

[8] Note that comparison of the results for the tests in Table 6.7, rather than of the average curves for each configuration would have exacerbated differences as TX455S2 is curve displaying largest $\varepsilon_{lin}$ and smallest non-linearity in Figure 6.22.

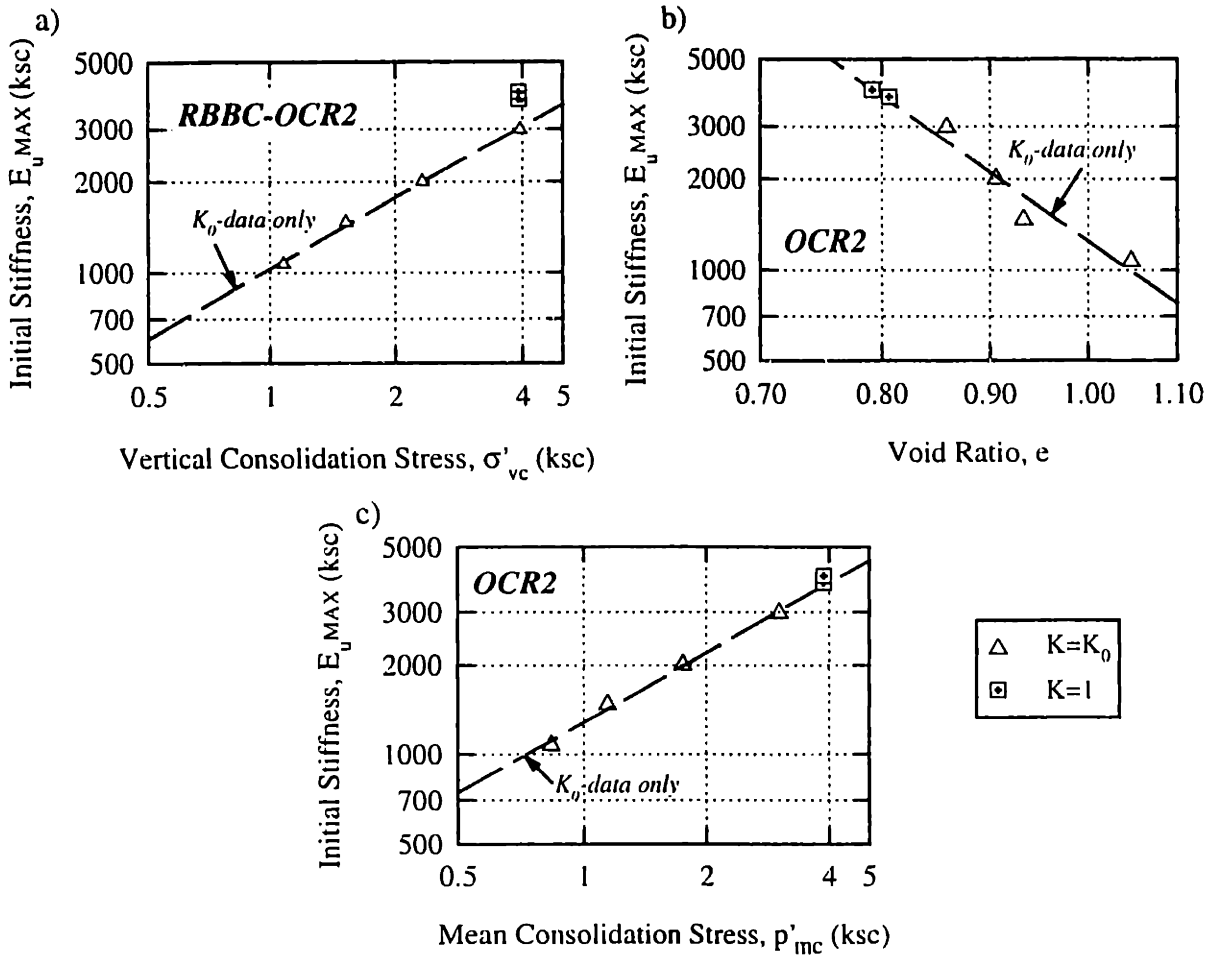


**Figure 6.36:** Relationship between void ratio, initial stiffness and mean consolidation stress for $K_0$- and hydrostatically consolidated OCR2 RBBC.

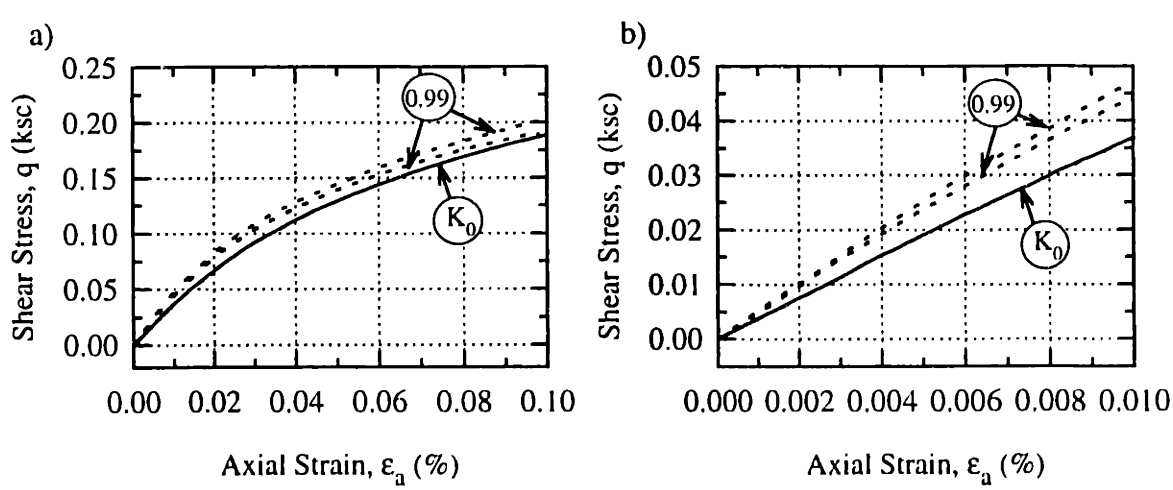


**Figure 6.37:** Behavior of $K_0$- and hydrostatically consolidated (K=constant) OCR2 RBBC at 3.9 ksc: a-b) stress strain curves.

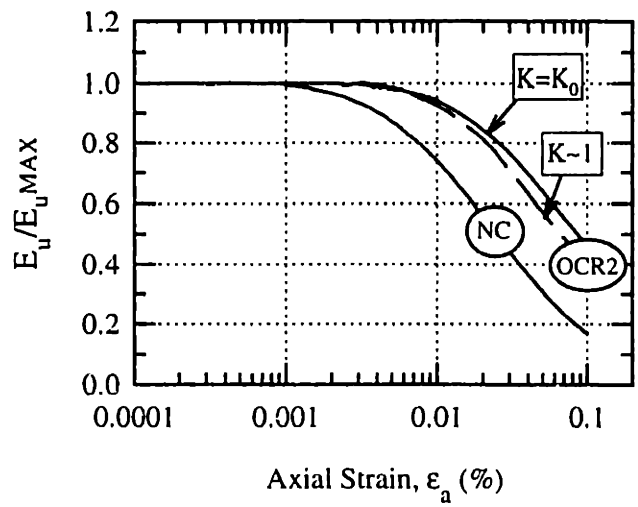


**Figure 6.38:** Stiffness degradation curves for $K_0$- and hydrostatically consolidated OCR2 RBBC.

## 6.6 EFFECT OF PRE-SHEAR STRESS PATH–NC RBBC

### 6.6.1 Introduction

In the case of NC RBBC the investigation of the effect of the pre-shear stress path extended to two stress paths besides the already discussed $K_0$-consolidation procedure.

As discussed in Chapter 5 the two additional paths investigated involved a combination of hydrostatic consolidation and stress path consolidation at constant $\sigma'_h$ or p'. They are referred to in the following as *constant* $\sigma'_h$ and *constant p'* pre-shear consolidation paths. Figure 6.39 shows stress paths followed during consolidation in these tests alongside a stress path typical for $K_0$-consolidation. Note that both stress consolidation procedures target a pre-shear value of the lateral stress ratio of about 0.48-0.49, i.e. in the range of $K_0$ values measured in the $K_0$-tests.

Table 6.8 summarizes the tests performed, specifying the test number, the vertical consolidation stress, the pre-shear values of K and of the void ratio, and also the $K_0$-consolidated tests that can be used as a reference at each stress level. Four tests at different consolidation stresses were performed following the constant p' path, to address the issue of the variability in the behavior as a function of stress level. Only two tests at different stress levels were performed for the constant $\sigma'_h$ path.

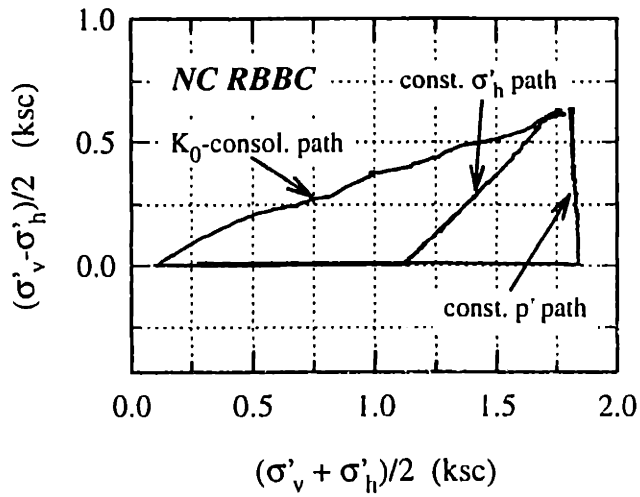


**Figure 6.39:** Stress paths during $K_0$-and stress path (constant $\sigma'_h$ and constant p') consolidation of NC RBBC.

| | *Constant $\sigma'_h$ Path* | | | | *Constant p' Path* | | | | |
|---|---|---|---|---|---|---|---|---|---|
| **Reference Stress Level (ksc)** | **Test #** | **$\sigma'_{vc}$ (ksc)** | **e** | **K** | **Test #** | **$\sigma'_{vc}$ (ksc)** | **e** | **K** | **$K_0$-Tests** |
| 2.4 | TX468S1 | 2.39 | 1.003 | 0.475 | TX432S1 | 2.44 | 0.967 | 0.481 | 353S1, 362S1, 403S2, 418S2 |
| 3.1 | - | - | - | - | TX432S2 | 3.13 | 0.941 | 0.482 | 361S3, 418S3, 422S1, 474S3 |
| 4.0 | TX468S2 | 4.08 | 0.927 | 0.475 | - | - | - | - | 362S3, 418S4, 422S2 |
| 5.8 | - | - | - | - | TX468S3 | 5.87 | 0.864 | 0.481 | 406S3, 422S3 |
| 7.8 | - | - | - | - | TX424S3 | 8.40 | 0.804 | 0.453 | 406S4, 422S4 |

**Table 6.8:** Tests conducted to investigate the effect of the pre-shear stress path on the pre-failure behavior of NC RBBC.

### 6.6.2 Initial Stiffness

The initial stiffness data for the constant $\sigma'_h$ and constant p' consolidation paths are plotted in Figure 6.40 a versus the vertical consolidation stress, alongside the reference data for $K_0$-consolidated NC RBBC. No significant effect of the pre-shear path is observed, as the results for the stress path consolidated tests fall virtually on the same band defined by the $K_0$-consolidated data.

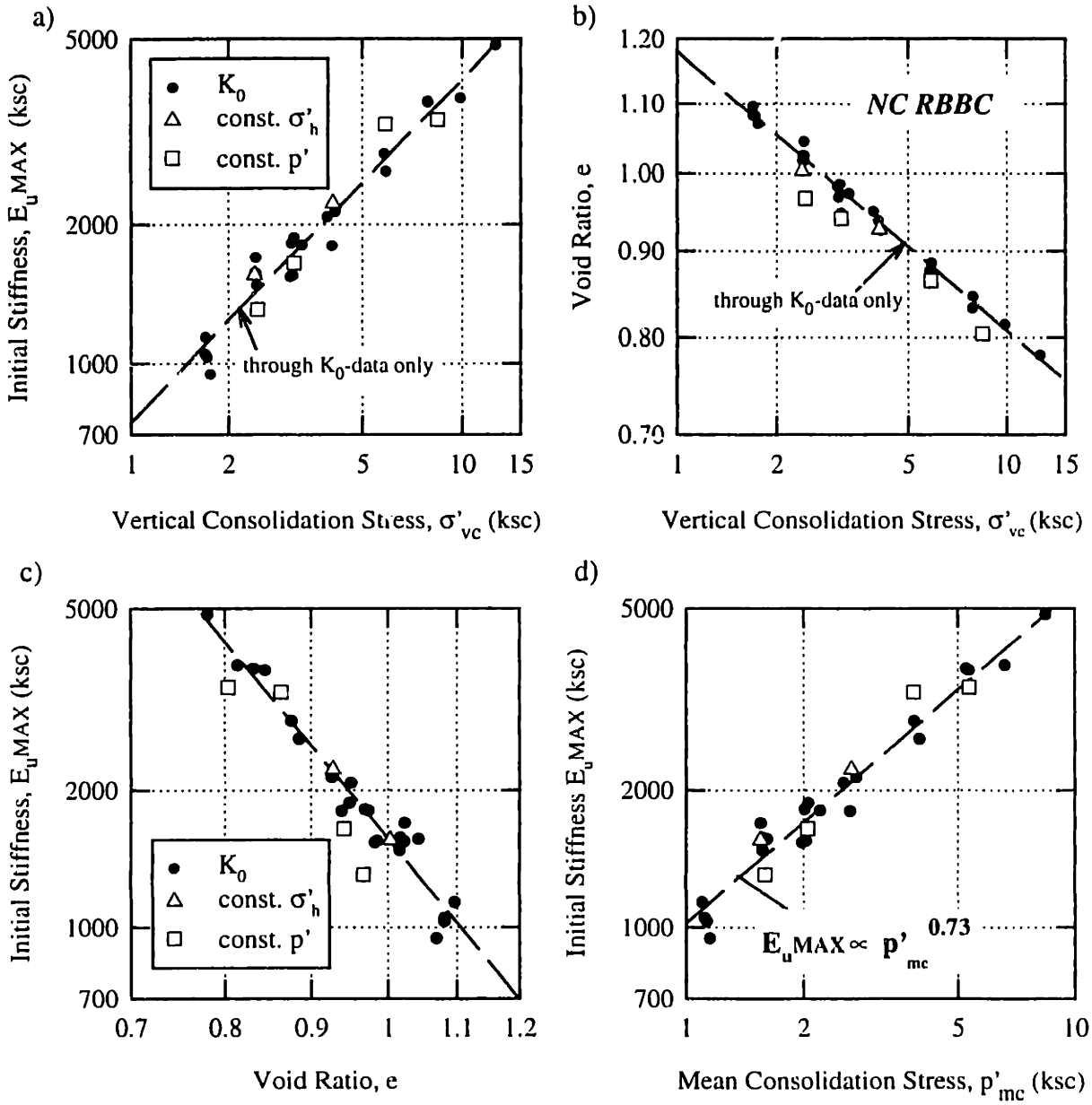


**Figure 6.40:** Relationships between a) vertical consolidation stress and $E_u$MAX, b) vertical consolidation stress and void ratio, c) void ratio and $E_u$MAX, and d) mean consolidation stress and $E_u$MAX, for $K_0$- and stress path consolidated (constant $\sigma'_h$ and constant p') NC RBBC.

As indicated in Figure 6.40b, stress path consolidation actually results in slightly lower values of the void ratio at any given stress level, particularly in the case of the constant p' path. The difference is however quite small, in most cases within the range encountered for the $K_0$-consolidated tests.

Alternatively, the initial stiffness results can be plotted versus the pre-shear void ratio or the mean consolidation stress as shown in Figures 6.40 c and d, respectively. Figure 6.40c indicates that the results for the constant p' paths yield values of the initial stiffness marginally lower than those expected for the measured values of *e*. However, this trend is not apparent in the plot of $E_{uMAX}$ versus $p'_{mc}$ in Figure 6.40d. In this plot the stress path consolidated data are shown to fall perfectly within the band formed by the results for $K_0$-consolidation. It is therefore thought that the apparent trend of lower values of stiffness displayed by the constant p' data in Figure 6.40 c is a product of inaccuracies in the measurements of e.

### 6.6.3 Non-Linear Behavior

Figures 6.41a and b show stress-strain curves for two tests sheared after stress path consolidation (constant $\sigma'_h$ and constant p') to approximately 2.4 ksc (see Table 6.8). The figure also shows the curves relative to two shears performed after $K_0$-consolidation to the same stress level (the two with $K_0$ closer to the values measured in the stress path consolidated tests). Despite a slightly lower shear stress gain observed above 0.02% strain for the constant p' test, the figures indicate that differences in the consolidation path do not impact the pre-failure behavior of NC RBBC in any significant manner.

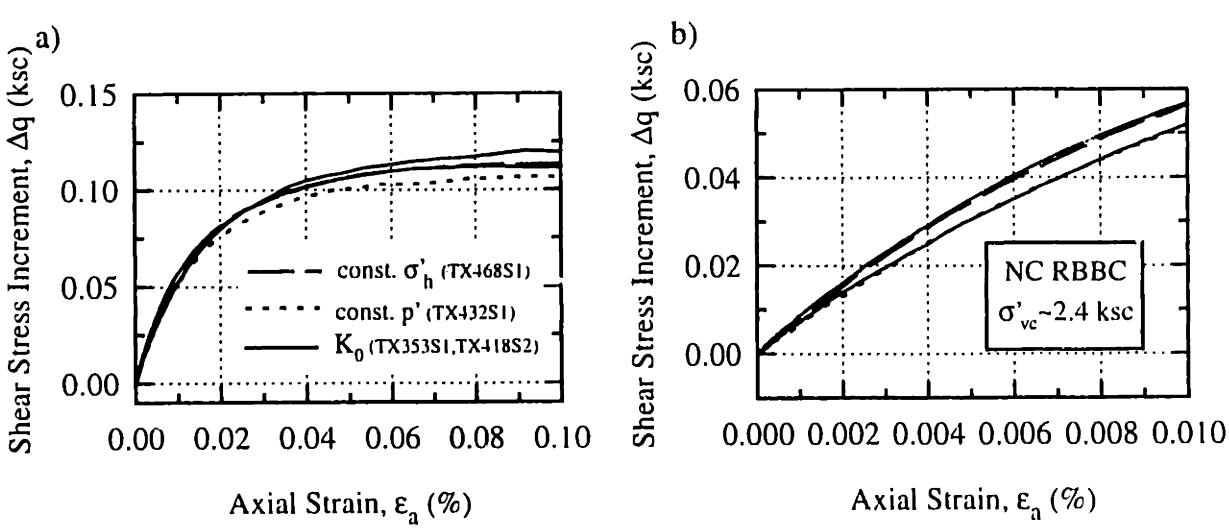


**Figure 6.41:** Behavior of $K_0$- and stress path consolidated (constant $\sigma'_h$ and constant p') NC RBBC at 2.4 ksc: a-b) stress strain curves.

Figures 6.42 a and b plot the normalized stiffness ($E_u/E_{uMAX}$) versus strain level, respectively for the two constant $\sigma'_h$ and four constant p' consolidation path results. Both figures indicate exceptional consistency in the data, confirming also in this case that the degree of non-linearity, given by the shape of the ($E_u/E_uMAX$) – $\varepsilon_a$ curve is independent of stress level.

In Figure 6.43 the average curve for each of the two pre-shear paths considered are compared with the reference curve for $K_0$-consolidated NC RBBC. The two curves for the constant $\sigma'_h$ and constant p' pre-shear paths are virtually coincident.

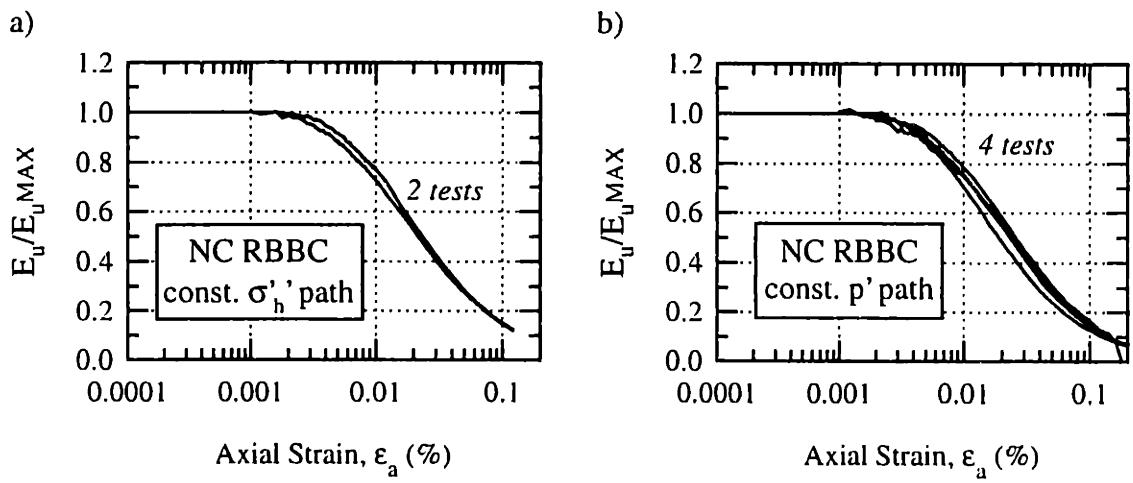


**Figure 6.42:** Normalized stiffness versus axial strain: a) constant $\sigma'_h$ and b) constant p' pre-shear consolidation paths.

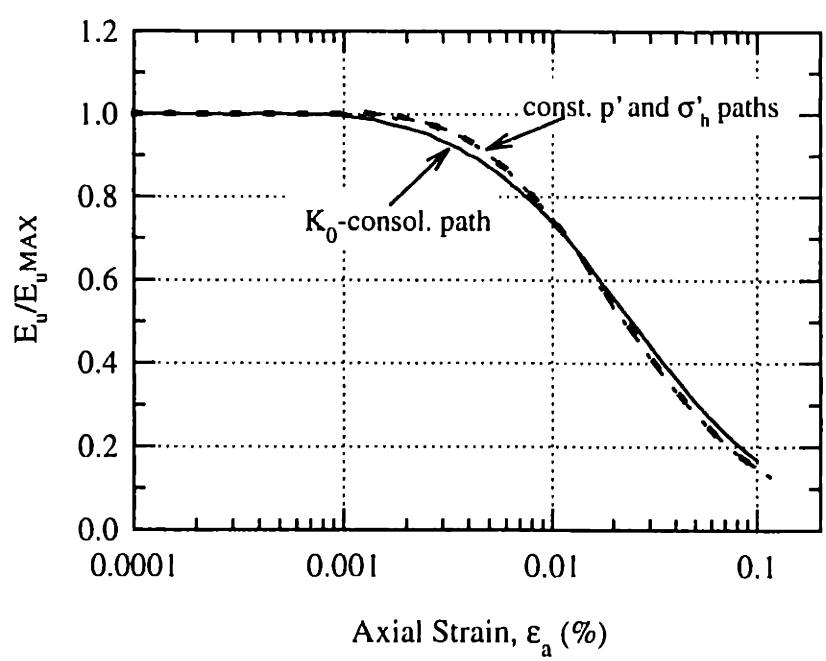


**Figure 6.43:** Pre-failure non-linearity for stress path (constant p' and constant $\sigma'_h$ paths) and $K_0$-consolidated NC RBBC.

The difference observed with respect to the $K_0$-consolidated data is small, although consistent. The stress path consolidated data present a marginally higher value of the linear threshold which increases from 0.0016±0.0004 for the $K_0$-consolidated data to 0.0021±0.0004 (~+30%) for the six stress path consolidated tests. In addition the stress path consolidated tests display a slightly more marked non-linearity in the behavior below 0.1% axial strain. This is reflected by an increase in the average value of $C_{NL}$ from 6.0 for the $K_0$ tests, to 6.81 (~+15%) for the constant p' and constant $\sigma'_h$ tests.

## 6.7 EFFECT OF PRE-SHEAR STRESS PATH: OC RBBC

### 6.7.1 Unloading and Loading Paths

#### *6.7.1.1 Introduction*

An extensive investigation of the effects of the pre-shear path was performed on OC RBBC. At almost all the stress levels examined, the behavior of the soil was evaluated both upon unloading from the virgin compression line and after reloading from higher values of OCR. These two paths are referred to in the following as *unloading path* (or *U-path*) and *loading path* (or *L-path*). Additional pre-shear stress-paths were investigated for OCR2 RBBC. Their results are discussed in Section 6.7.2.

The behavior of OC RBBC after unloading from the VCL was presented in detail in Section 6.4. In this section the discussion focuses on the results for the loading pre-shear path, and on highlighting the differences in behavior deriving from a modified consolidation path (*L* vs. *U*).

As described in Chapter 5, the multi-stage approach used in the testing proved to be extremely valuable in studying this particular aspect of soil behavior, allowing the two shears performed at a given stress after the unloading and the loading path to be performed on the same specimen. Details of this methodology and of the specific testing procedures are discussed in Section 5.3.1.

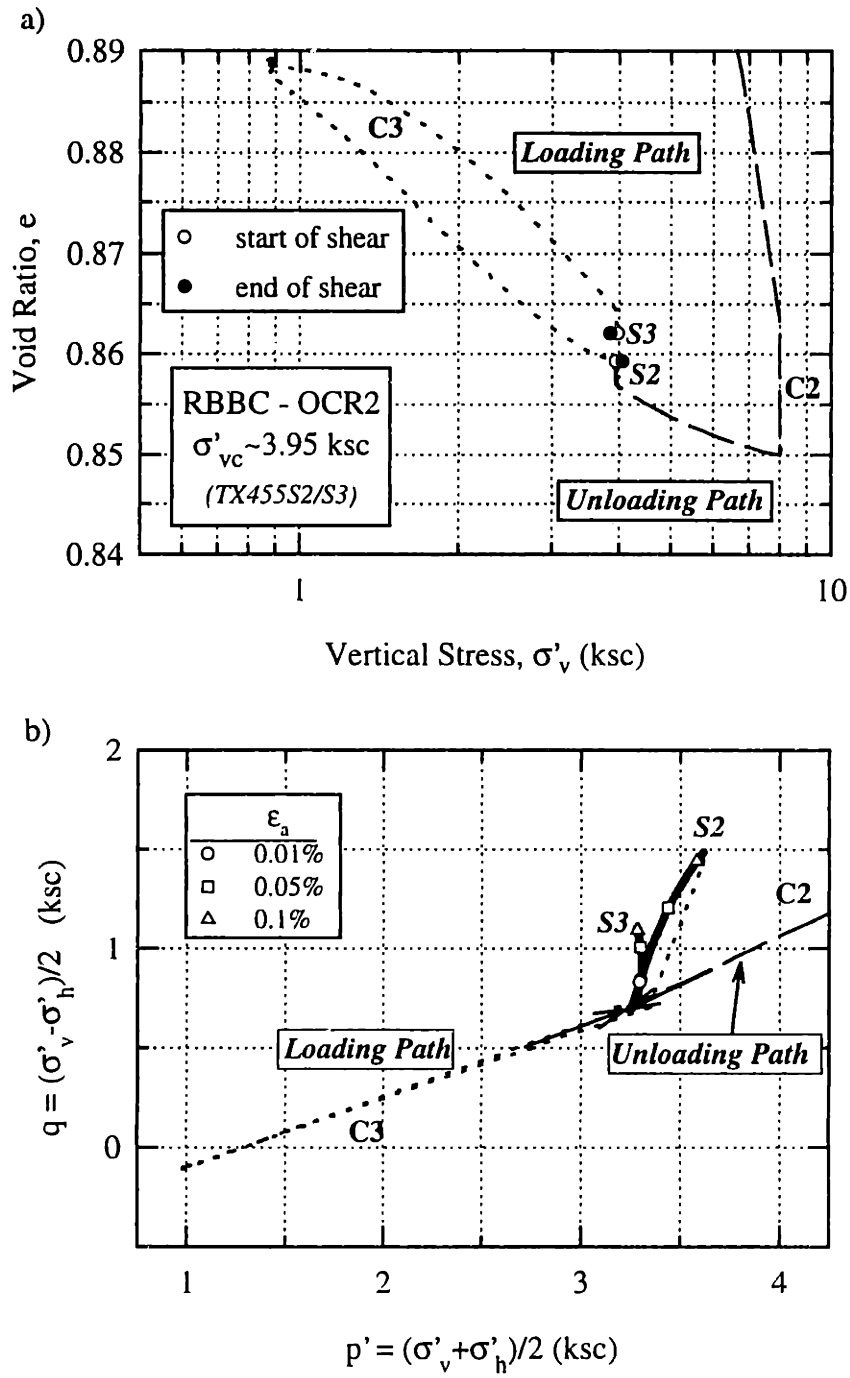


**Figure 6.44:** Example of multistage test performed to investigate the effect of the pre-shear stress path: a) e-log $\sigma'_v$ space, b) q-p' space.

Figures 6.44 a and b summarize the consolidation and the shear phases, in the *e-log*($\sigma'_v$) and the *q-p'* planes respectively, of a multi-stage test conducted to determine the effect of the pre-shear stress path on the pre-failure behavior of OCR2 RBBC at a stress level of about 4 ksc.

The figure indicates how shearing occurs in both cases from almost exactly the same point in stress space and how the two consolidation paths lie at about 180° with respect to each other. In addition it is observed (Figure 6.44a) that, due to the unload-reload "cycle", the shear after loading occurs at a void ratio which is slightly higher that that existing prior to the unloading shear.

Table 6.9 summarizes the tests performed at each OCR, specifying the stress level and the test number. For each OCR at least three tests, at different stress levels were performed. In all cases, the results for the "companion" unloading test is also available. Additional information on the pre-shear conditions (e.g. K, e, etc) for these tests is supplied in the following (Tables 6.10 a-c) . In all these tests, with the exception of test *TX438*, in which the order of the shears was reversed (the shear after loading preceded the shear after unloading), procedures similar to those shown in Figures 6.44a-b were followed. Note that the table includes only shears performed using the standard shearing rate of 0.1%/hr.

| **OCR** | **2** | | **4** | | **8** | |
|---|---|---|---|---|---|---|
| | ***U*** | ***L*** | ***U*** | ***L*** | ***U*** | ***L*** |
| **Stress Level (ksc)** Test and Shear # | 1.1 (TX445S2) | 1.1 (TX445S3) | 0.7 (TX442S1) | 0.7 (TX442S2) | 0.5 (TX418S5) | 0.5 (TX418S6) |
| | 2.3 (TX432S3) | 2.3 (TX432S4) | 1.1 (TX438S6) | 1.1 (TX438S5) | 0.65 (TX476S1)[9] | 0.65 (TX476S2)[9] |
| | 4.0 (TX455S2) | 4.0 (TX455S3) | 2.3 (TX406S5) | 2.3 (TX406S6) | 1.1 (TX424S4) | 1.1 (TX424S5) |
| | | | | | 1.8 (TX471S6) | 1.8 (TX471S7)[10] |

**Table 6.9:** Tests performed to investigate the effect of unloading versus loading pre-shear stress path on the pre-failure behavior of OC RBBC.

### *6.7.1.2 Initial Stiffness*

Figures 6.45 a, c and e compare the stress strain behavior at small strains (0-0.0015%) after unloading and loading (Figures 6.45b, d, and f) for three pairs of tests on RBBC with OCR of 2,

[9] All shears performed within TX476 yielded values of stiffness much higher than expected (see also Table 6.11-Section 6.7.2). The reason for this is not understood, but these data are not used to determine the relationship between stress level, or void ratio, and $E_uMAX$. The $E_u/E_uMAX$. curve for TX476S2 is, however, in line with the results at the other stress levels. In lack of a third valid result, it is therefore used in the following to determine the average stiffness degradation curve for OCR equal to 8.

[10] Due to the problems occurred during shear, only information on the initial stiffness could be derived from *TX471S7*. The stiffness degradation results are erratic and therefore not presented in the analysis.

4 and 8, respectively. In all three pairs of tests the pre-shear stress paths differ in direction by an angle $\alpha$, which is 175° for OCR2, 170° for OCR 4 and 165° for OCR8[11]. The figures indicate that for all three values of OCR, no significant difference in the initial slope of the stress strain curve is observed, as a result of the different pre-shear path. The small vertical offset in the curves stems from a slight difference in the pre-shear value of the lateral stress ratio.

Tables 6.10 a-c summarize both the exact pre-shear conditions and the initial stiffness results for these and other pairs of unloading and loading tests performed on RBBC with OCR of 2, 4 and 8. Plots of $E_u$MAX (both unloading and loading data) versus the vertical consolidation stress are presented in Figures 6.46a, c, and e for each of the three OCR's. These results indicate that the difference in the initial stiffness due to the pre-shear stress path (shown in the last column of the three tables for each pair of tests) is modest, and independent of OCR. However, in almost all cases the stiffness after the unloading path results marginally higher than that measured after the loading path. This is in line with the fact that the void ratio prior to the loading shear is, with one exception[12], always slightly greater than that prior to the unloading shear. In fact, the largest difference in the value of $E_u$MAX is observed in those tests which differ the most in the pre-shear void ratio (e.g. *TX438S5/S6* - see Table 6.10b). As seen in Figures 6.46 a, c and e, the results for the unloading tests display the same trend with stress level falling on a band somewhat parallel to that for the loading data. Similar plots would be obtained plotting the stiffness versus the mean effective consolidation stress.

On the other hand, when the initial stiffness is plotted versus the void ratio, both the unload and the load data fall virtually on the same line, thus suggesting that the variation in $E_u$MAX is a result of the difference in void ratio generated by the different consolidation path. Plots of initial stiffness versus pre-shear void ratio are shown in Figures 6.46 b, d and f for each of three OCR's. It should be noted that the differences in void ratio between unload and load tests are quite small and would probably not translate into a systematic trend of the stiffness, where it not for the fact that both shears are performed on the same specimen.

---

[11] Small differences in the direction of the pre-shear stress path are not an issue, as will be discussed in Section 6.7.2

[12] The exception is represented by shears *S2* and *S3* in test *TX445*. In this test, as shown in Table 6.10a, the loading shear has lower void ratio than the unloading shear. Due to an error in prescribing the target stresses for the pre-shear consolidation path, during the *C3* phase, the soil was reloaded past the desired stresses. Hence it was reloaded to the maximum stress and then unloaded and reloaded again (with no intermediate loading shear). This led to additional volumetric straining, and therefore to a lower void ratio for *TX445S3*.

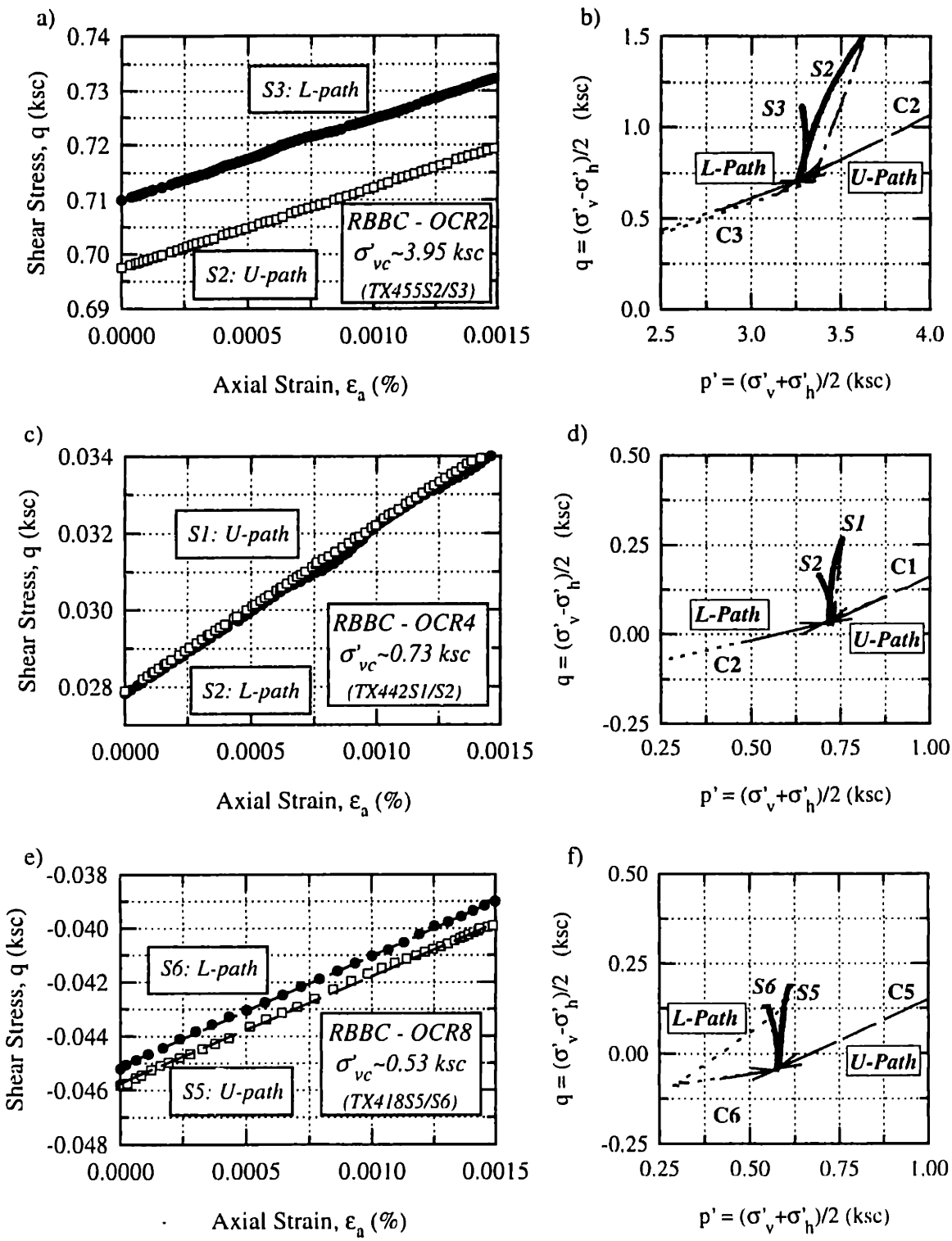


**Figure 6.45:** Effect of the pre-shear path on the initial stress strain behavior of OC RBBC:a-b) OCR2; c-d) OCR4; e-f) OCR8.

a)

| | $\sigma'_{vc}$ (ksc) | Path | OCR | e | $t_{aging}$ (h) | K | $E_uMAX$ (ksc) | $\Delta E_uMAX/(E_uMAX)_{AVE}$* (%) |
|---|---|---|---|---|---|---|---|---|
| TX445S2 | 1.08 | U | 2.09 | 1.047 | 41 | 0.66 | 1071 | 7.9 |
| TX445S3 | 1.08 | L | 2.08 | 1.033 | 43 | 0.66 | 989 | |
| TX432S3 | 2.32 | U | 2.03 | 0.906 | 25 | 0.63 | 1998 | 19.8 |
| TX432S4 | 2.32 | L | 2.04 | 0.913 | 24 | 0.63 | 1638 | |
| TX455S2 | 3.95 | U | 2.03 | 0.848 | 26 | 0.65 | 2985 | 0.7 |
| TX455S3 | 3.95 | L | 2.03 | 0.851 | 32 | 0.65 | 2965 | |

b)

| | $\sigma'_{vc}$ (ksc) | Path | OCR | e | $t_{aging}$ (h) | K | $E_uMAX$ (ksc) | $\Delta E_uMAX/(E_uMAX)_{AVE}$* (%) |
|---|---|---|---|---|---|---|---|---|
| TX442S1 | 0.73 | U | 4.27 | 0.995 | 32 | 0.92 | 872 | 1.9 |
| TX442S2 | 0.74 | L | 4.23 | 1.006 | 28 | 0.93 | 856 | |
| TX438S6 | 1.12 | U | 4.20 | 0.936 | 39 | 0.88 | 1392 | 18.1 |
| TX438S5 | 1.13 | L | 4.19 | 0.964 | 32 | 0.89 | 1161 | |
| TX406S5 | 2.30 | U | 4.11 | 0.843 | 21 | 0.86 | 2318 | 9.3 |
| TX406S6 | 2.29 | L | 4.13 | 0.853 | 27 | 0.86 | 2112 | |

c)

| | $\sigma'_{vc}$ (ksc) | Path | OCR | e | $t_{aging}$ (h) | K | $E_uMAX$ (ksc) | $\Delta E_uMAX/(E_uMAX)_{AVE}$* (%) |
|---|---|---|---|---|---|---|---|---|
| TX418S5 | 0.53 | U | 8.94 | 0.949 | 45 | 1.17 | 785.3 | -2.5 |
| TX418S6 | 0.53 | L | 8.94 | 0.960 | 41 | 1.17 | 804.8 | |
| TX476S1 | 0.64 | U | 9.12 | 0.938 | 39 | 1.26 | 1166.7 | 9.5 |
| TX476S2 | 0.65 | L | 9.12 | 0.946 | 39 | 1.26 | 1061.3 | |
| TX424S4 | 1.06 | U | 8.82 | 0.839 | 26 | 1.13 | 1413.2 | 1.7 |
| TX424S5 | 1.05 | L | 8.82 | 0.849 | 38 | 1.13 | 1390.0 | |
| TX471S6 | 1.85 | U | 8.56 | 0.772 | 24 | 1.21 | 2402.2 | 2.4 |
| TX471S7 | 1.85 | L | 8.56 | 0.787 | 32 | 1.22 | 2345.1 | |

* $\Delta E_uMAX = E_uMAX_{unload} - E_uMAX_{load}$; $(E_uMAX)_{AVE} = 0.5(E_uMAX_{unload} + E_uMAX_{load})$;

**Table 6.10:** Pre-shear conditions and initial stiffness results after loading and unloading for OC RBBC: a) OCR2; b) OCR4; c) OCR8.

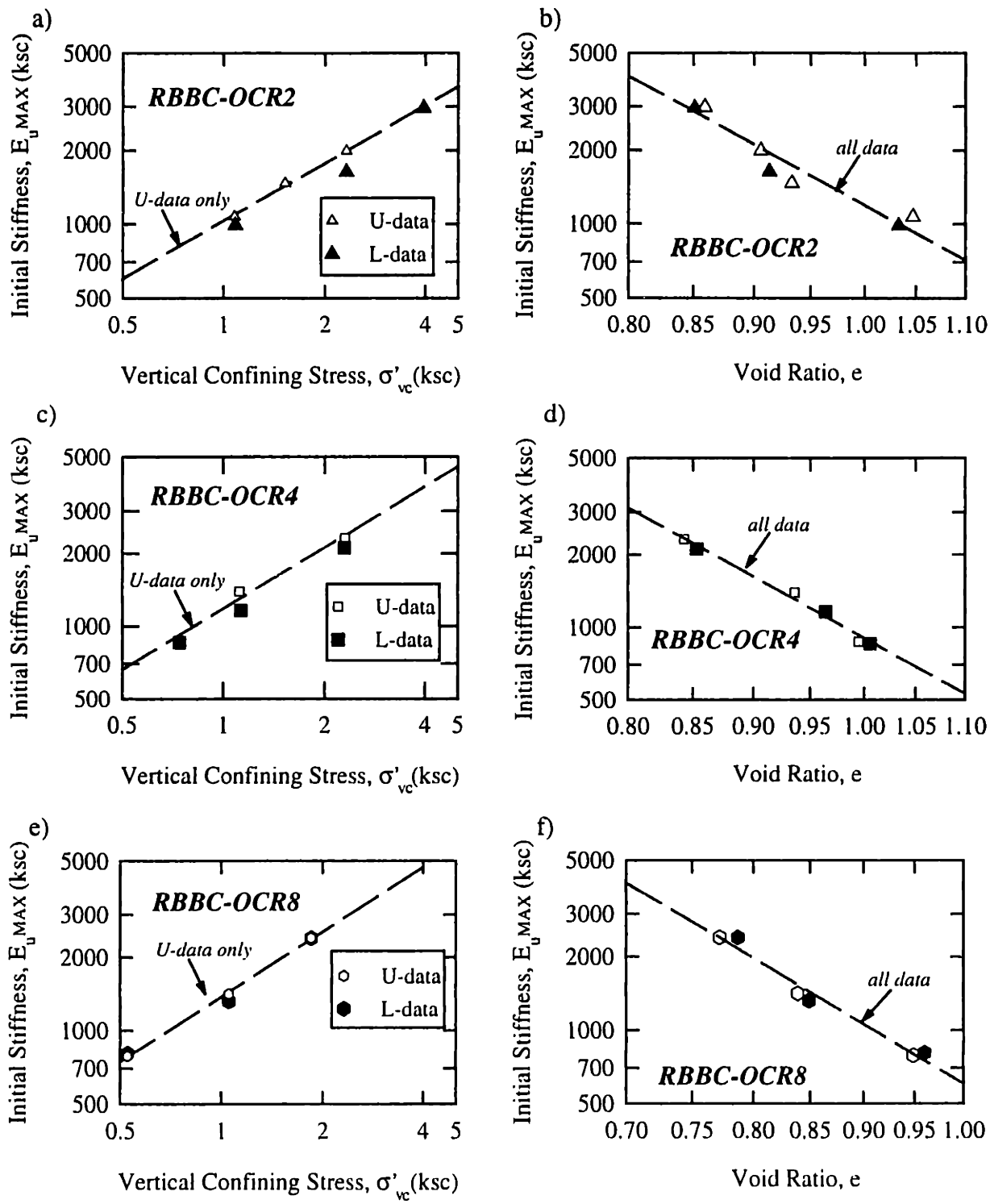


**Figure 6.46:** Relationship between initial stiffness and pre-shear vertical stress and void ratio for loading and unloading consolidation paths: a-b) OCR2; c-d) OCR4; e-f) OCR8.

#### *6.7.1.3 Non-linear Behavior*

The direction of the pre-shear path significantly affects the post-linear behavior of OC RBBC. Figures 6.47, 6.48 and 6.49 present results at one stress level to illustrate the behavior after an *unloading* and a *loading* consolidation stress path for RBBC with OCR of 2, 4 and 8, respectively. Each set of figures includes comparison of the stress-strain curves at various ranges of axial strain (Figures a-d) and a plot of the stiffness versus strain (Figure e) for pairs of tests performed at the same stress level. These figures are for the same tests displayed in Figures 6.45. Figures 6.47-6.49 indicate that, while having minimal impact on $E_uMAX$, a loading pre-shear path results, for all OCR's, in a smaller shear stress gain, and therefore a reduced stiffness, at all strains beyond the linear threshold.

In addition, upon undrained unloading of the shear stresses, at least for OCR 2 and 4, much more significant permanent strains are measured in the case of a loading pre-shear path ($\varepsilon_{PL}/\varepsilon_{TOT}$ increases from ~30 to 70% for OCR2, and from 20 to 54% for OCR4 -Figures 6.47a and 6.48a).[13]

As indicated in Table 6.9 results are available for at least three stress levels, for each OCR after a loading consolidation path. These tests provide results similar to those shown in Figures 6.47-6.49. The results, in terms of normalized stiffness $E_u/E_uMAX$ versus strain level for all tests at each of the three OCR's investigated[14] are summarized in Figures 6.50 a-c. While the results for the loading tests are all shown in dashed lines, the two solid lines in each of the graphs represent the average behavior of RBBC at that OCR (see Section 6.4) after an unloading path, and the reference behavior for $K_0$-consolidated NC RBBC (see Section 6.3). Also included at the bottom of each figure is a summary of the pre-shear conditions for each of the loading tests shown. These data are listed from the test displaying the less significant non-linearity to that showing the more marked decrease of the normalized stiffness with strain.

For each value of OCR the data appear quite consistent and no secondary trend due to slight differences in OCR, K, duration of aging, or shearing rate was isolated. However, it is observed that the degree of non-linearity is directly proportional to the magnitude of the axial reloading strain. This aspect is addressed in depth in Chapter 7. In addition, as seen for NC

---

[13] For tests on OCR 8 no data of $\varepsilon_{PL}/\varepsilon_{TOT}$ for loading tests are available.

[14] While four shears were performed on OCR8 RBBC after a loading path (Table 6.9), only three results are shown here as test *TX471S7* yielded unreliable results in the non-linear region (see footnote 10).

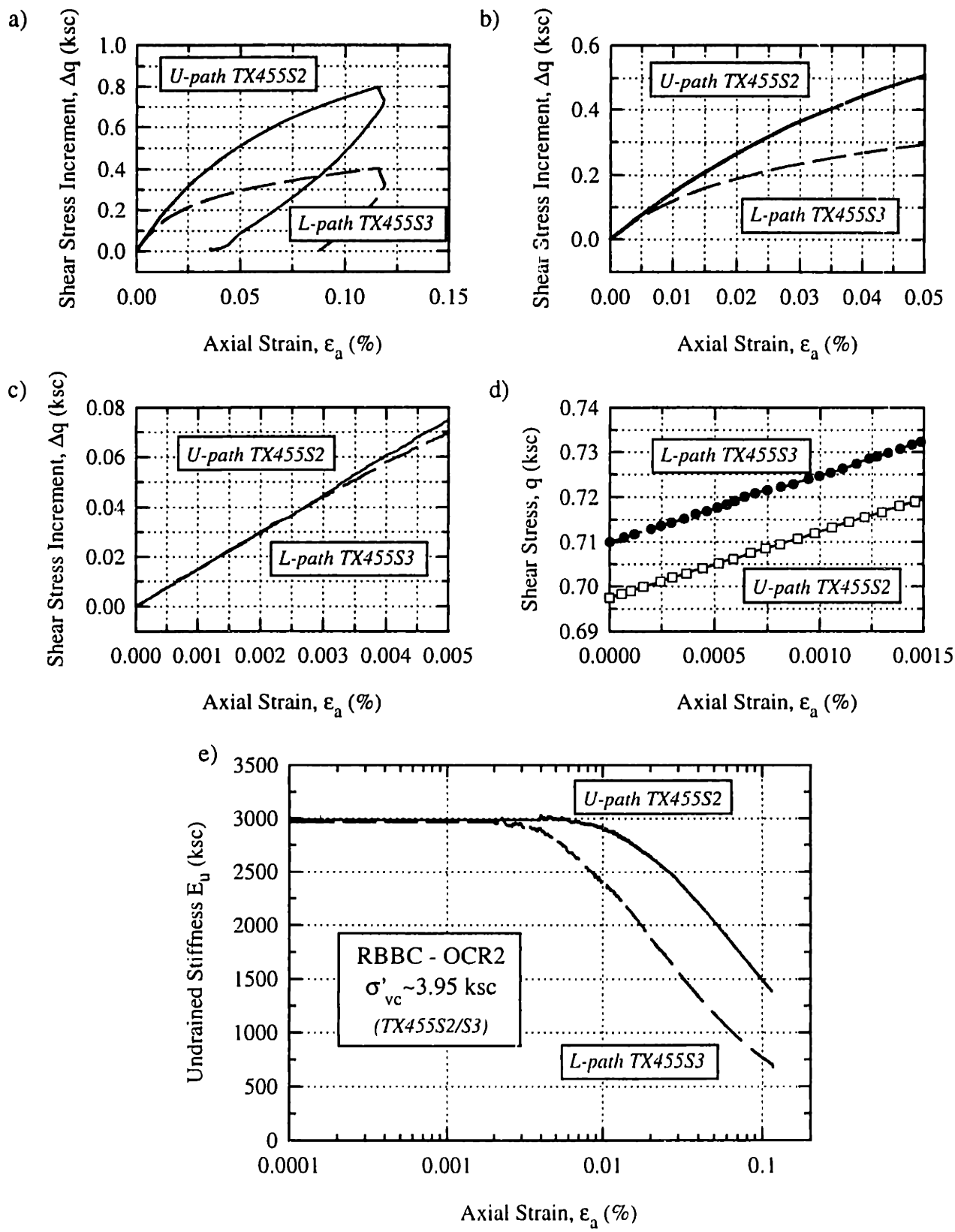


**Figure 6.47:** Behavior of OCR2 RBBC after unloading and loading pre-shear consolidation paths.

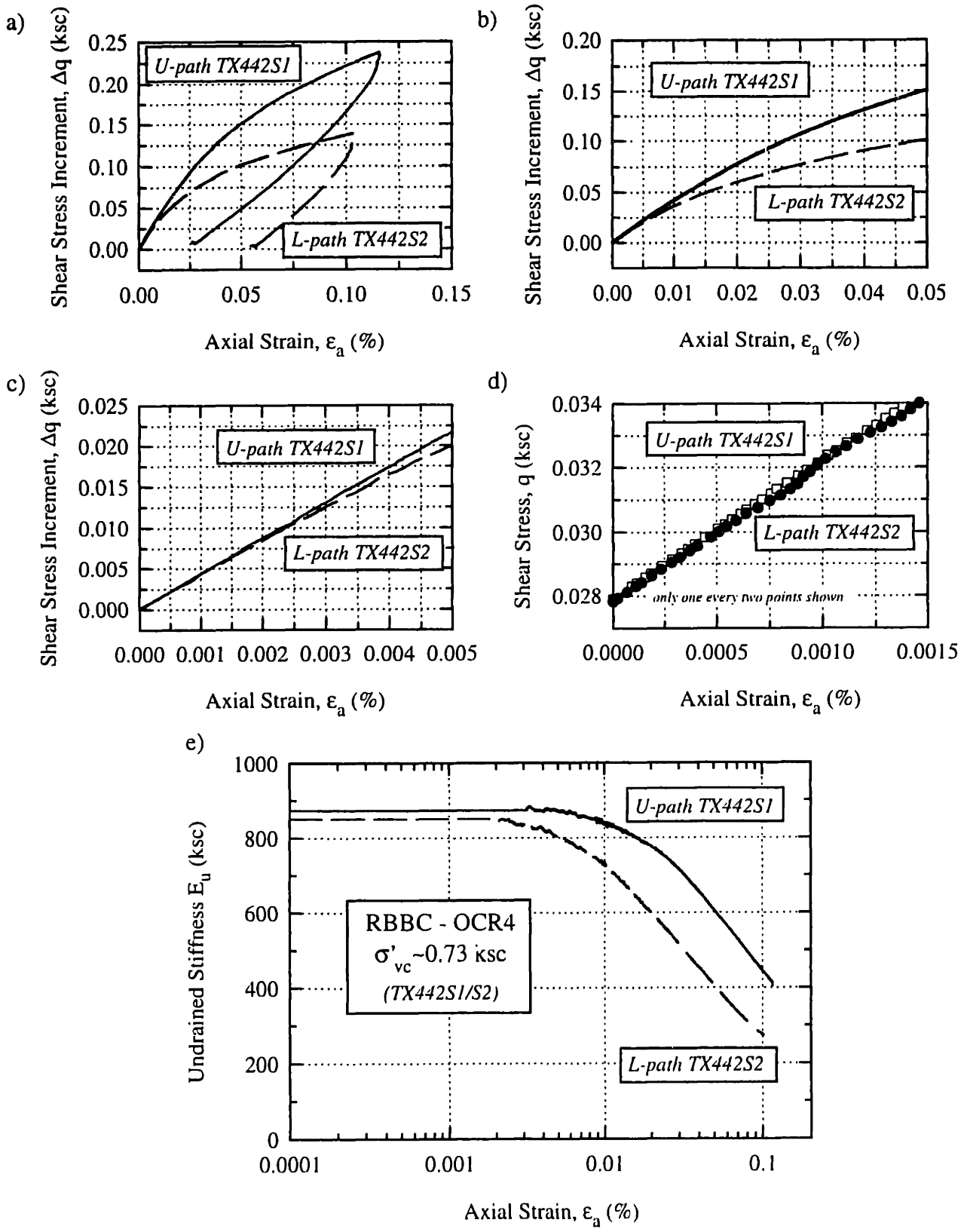


**Figure 6.48:** Behavior of OCR4 RBBC after unloading and loading pre-shear consolidation paths

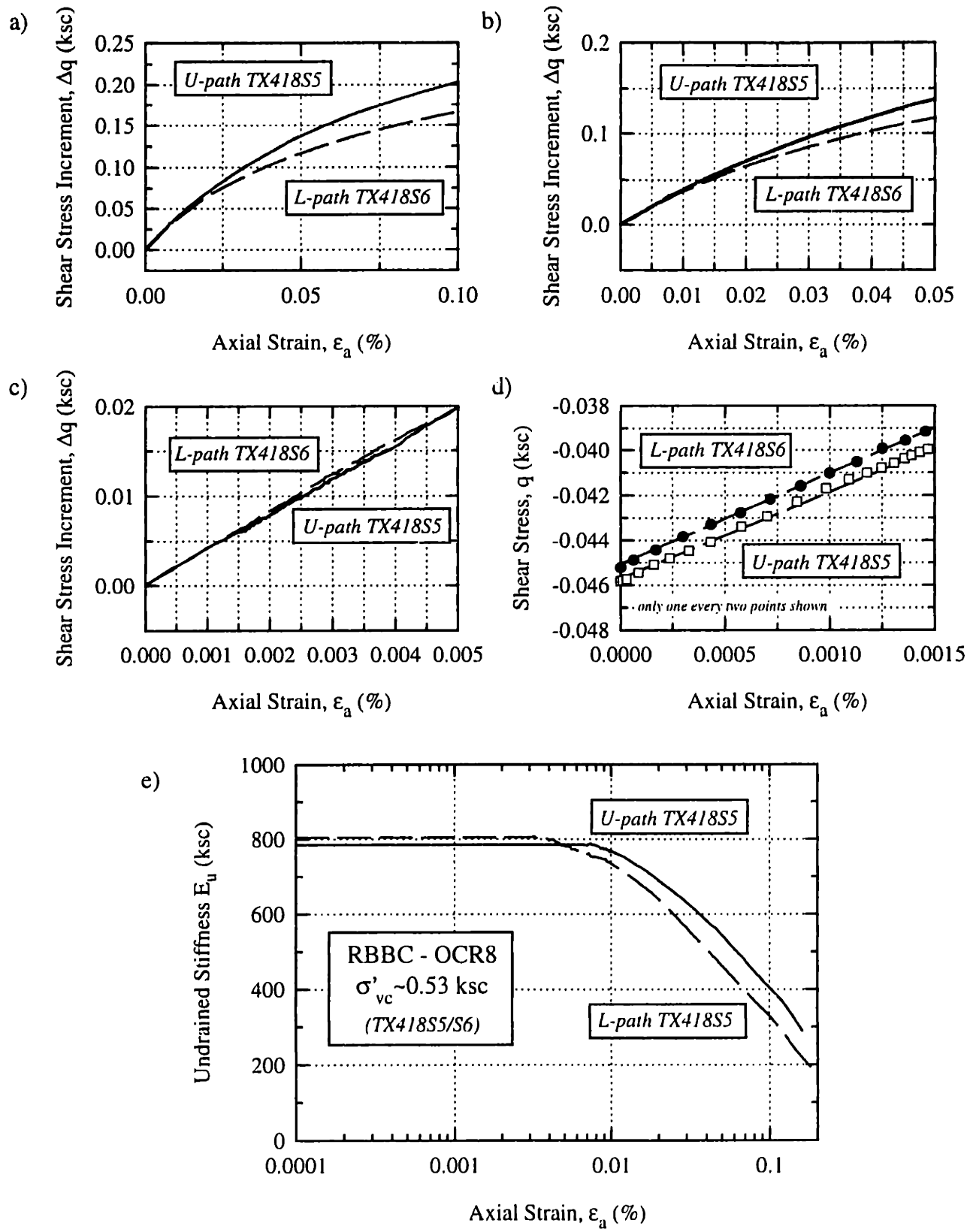


**Figure 6.49:** Behavior of OCR8 RBBC after unloading and loading pre-shear consolidation paths

RBBC, and for the tests on OC RBBC after unloading, the shape of the stiffness degradation curve appears to be independent of stress level.

The curves representing the average behavior of OCR 2, 4 and 8 RBBC after a loading pre-shear path can be obtained by averaging the three results available at each OCR. These curves are shown in Figure 6.51 alongside the corresponding plots relative to the behavior after unloading, and the reference line for $K_0$-consolidated RBBC.

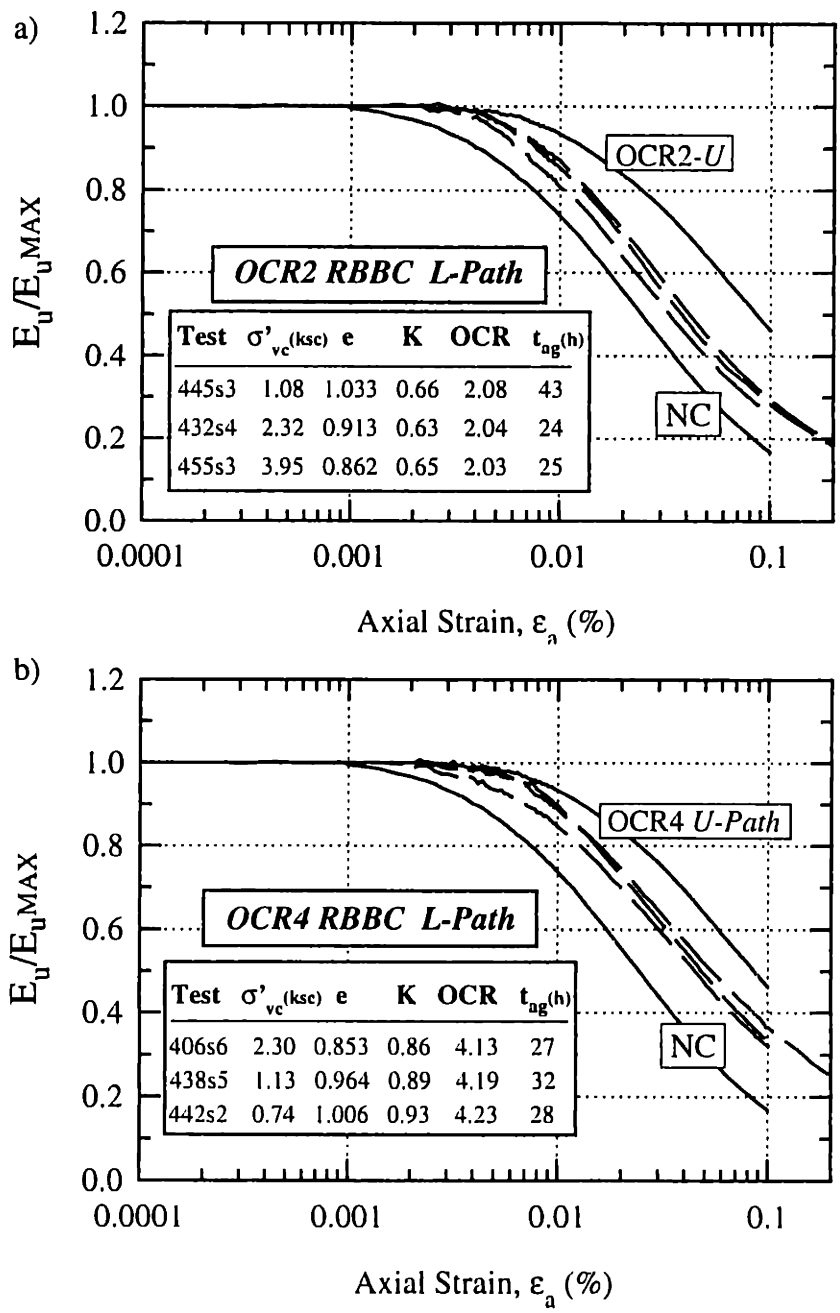


**Figure 6.50:** Stiffness degradation behavior of OC RBBC after loading consolidation path: a) OCR2; b) OCR4.

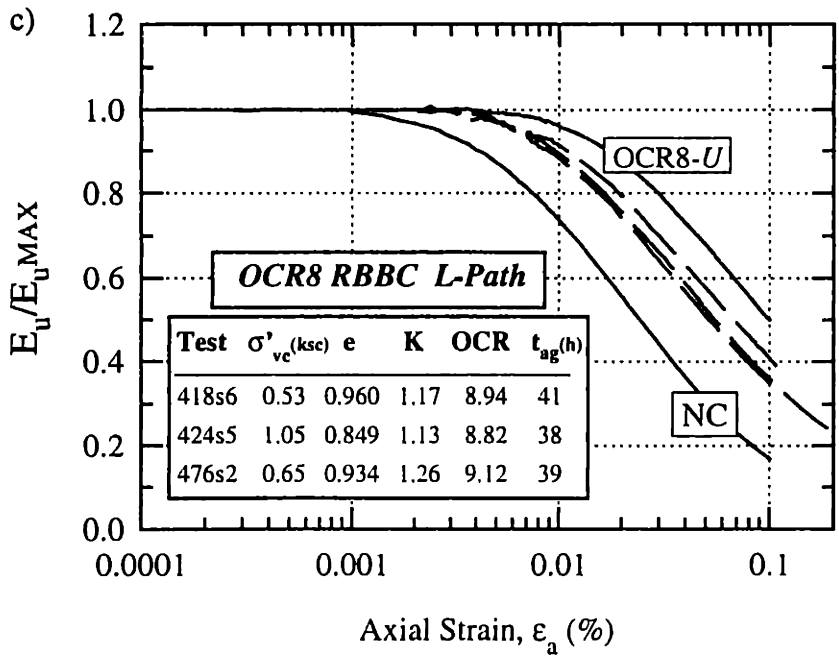


| Test | $\sigma'_{vc}$(ksc) | e | K | OCR | $t_{ag}$(h) |
|---|---|---|---|---|---|
| 418s6 | 0.53 | 0.960 | 1.17 | 8.94 | 41 |
| 424s5 | 1.05 | 0.849 | 1.13 | 8.82 | 38 |
| 476s2 | 0.65 | 0.934 | 1.26 | 9.12 | 39 |

**Figure 6.50**: (continued) Stiffness degradation behavior of OC RBBC after loading consolidation path: c) OCR8.

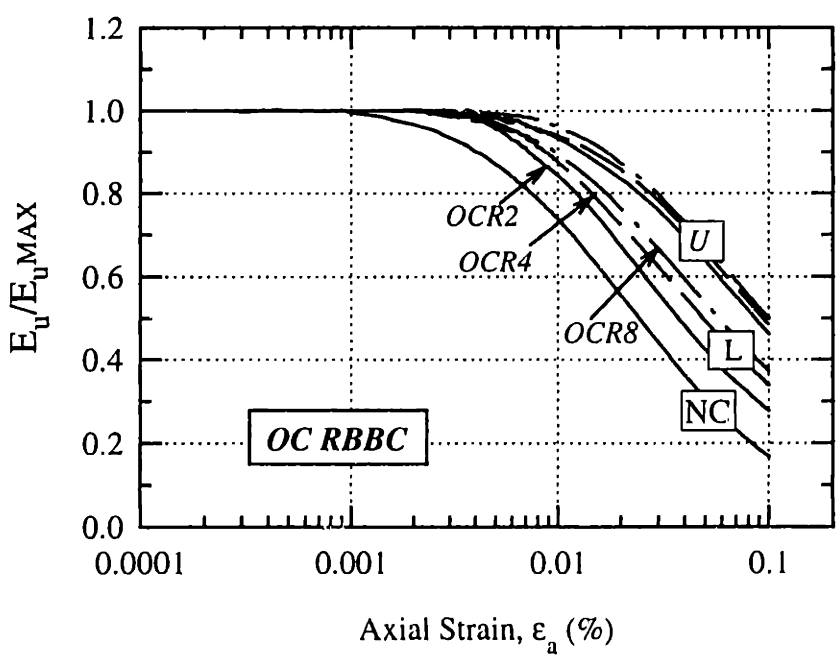


**Figure 6.51:** Effect of OCR and pre-shear stress path on non-linear behavior of RBBC.

The loading data display an increasing normalized stiffness $E_u/E_{uMAX}$ with increasing OCR. As shown in Figure 6.52a, for the loading pre-shear path, the linear threshold shows

minor variation for all values of OCR (~0.0034-0.0047%). The sensitivity to OCR, however increases with strain level. This is shown in Figure 6.53 that presents three plots, one for each OCR, of the ratio of the normalized stiffness for OC RBBC to that of the NC soil ($E^*_{OC}/E^*_{NC}$, with $E^*=E_u/E_{uMAX}$), as a function of strain level. Albeit all rising with strain, the three curves for OCR2, 4 and 8, diverge as the axial strain increases. Figure 6.53 contains also the data for the unloading tests (Figure 6.26). Comparison of these two sets of curves indicates that the behavior after loading is more sensitive to variations in the overconsolidation ratio.

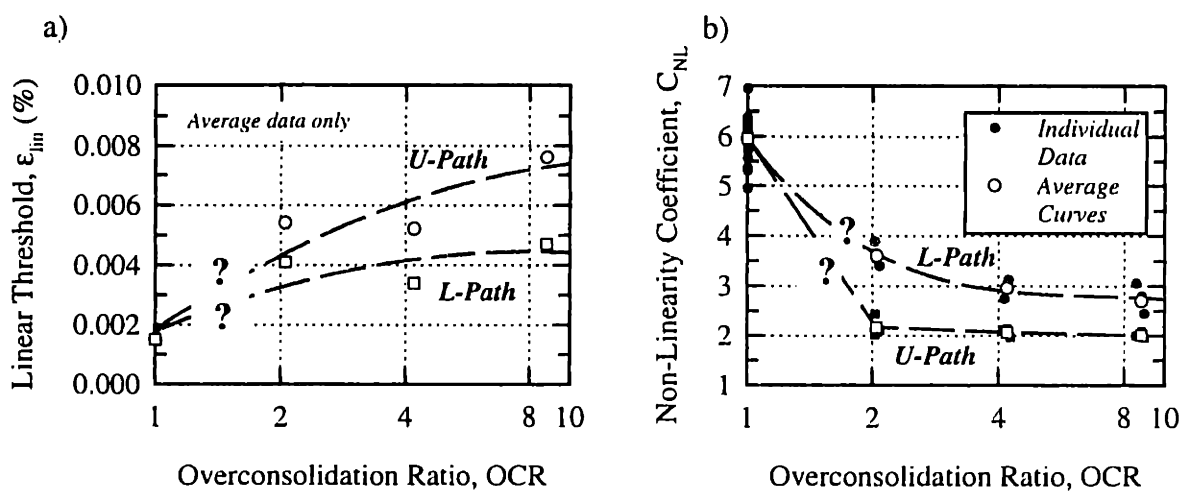


**Figure 6.52:** a) Linear threshold and b) non-linearity coefficient as a function of OCR (*U* and *L* paths).

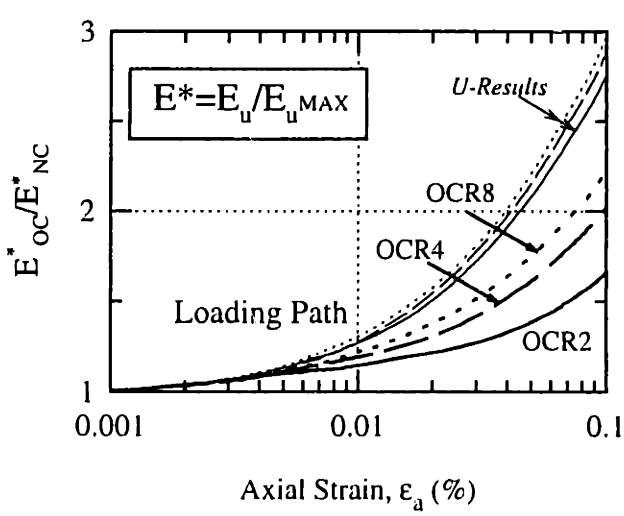


**Figure 6.53:** Ratio of $E^*_{OC}$ to $E^*_{NC}$ for loading consolidation path.

Finally Figure 6.54 presents curves of $E^*_{unload}/E^*_{load}$ ($E^*=E_u/E_{uMAX}$) versus axial strain for each of the three OCR's. The figure shows that for all OCR's, at least up to 0.1% strain, the sensitivity to the pre-shear stress path increases with strain level. The figure also demonstrates that the sensitivity of the soil to changes in the pre-shear consolidation path decreases with increasing OCR. This is also shown in Figures 6.52b in which the coefficient of non-linearity $C_{NL}$ is plotted versus OCR for both loading and unloading pre-shear paths.

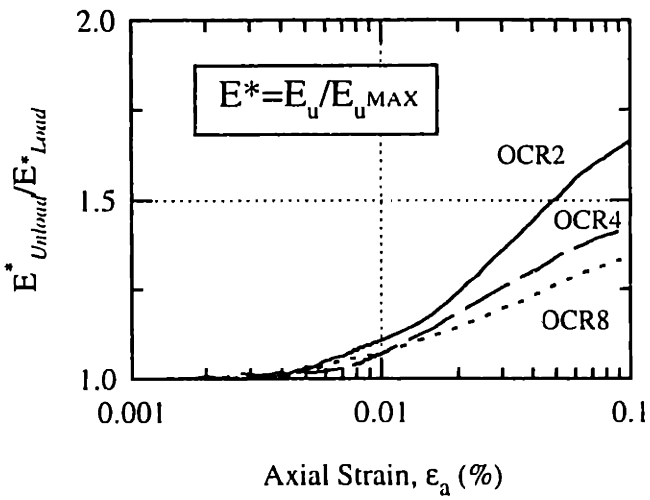


**Figure 6.54:** Ratio of $E^*_{Unload}$ to $E^*_{Load}$ for OC RBBC.

### 6.7.2 Additional Paths for OCR2 RBBC

To better understand the effects of the pre-shear stress path on the small strain undrained behavior of OC RBBC, additional tests were performed on the OCR2 soil, at approximately 4 ksc, since results from the loading and unloading paths (*L* and *U* -Figure 6.55a) at this stress level were already available. In these tests the pre-shear conditions were reached following more elaborate stress paths that involved at least one change in direction. These paths are shown in Figure 6.55 b and c.

The paths are each indicated with two letters that define the sequence of the phases of loading *(L)* or unloading *(U)* of the vertical stress that the soil undergoes during consolidation. In all cases the pre-shear state is approached by a first phase of either unloading *(U)* from the virgin compression line or loading *(L)* from higher OCR's to reach a point in stress space characterized by p' equal to $p'_c$. The final portion of the consolidation phase always follows a constant p' path ($p'=p'_c$) involving either a decrease *(U)* or an increase *(L)* of the shear stress (and therefore of the

vertical stress). For example, the designation *LU* for the path shown in Figure 6.55b shows that the consolidation path involved a first phase of loading (*L*) and a second of unloading (*U*) of the vertical stress. Note that the different phases of each of these consolidation phases follow one after the other without any intermediate hold stress phase.

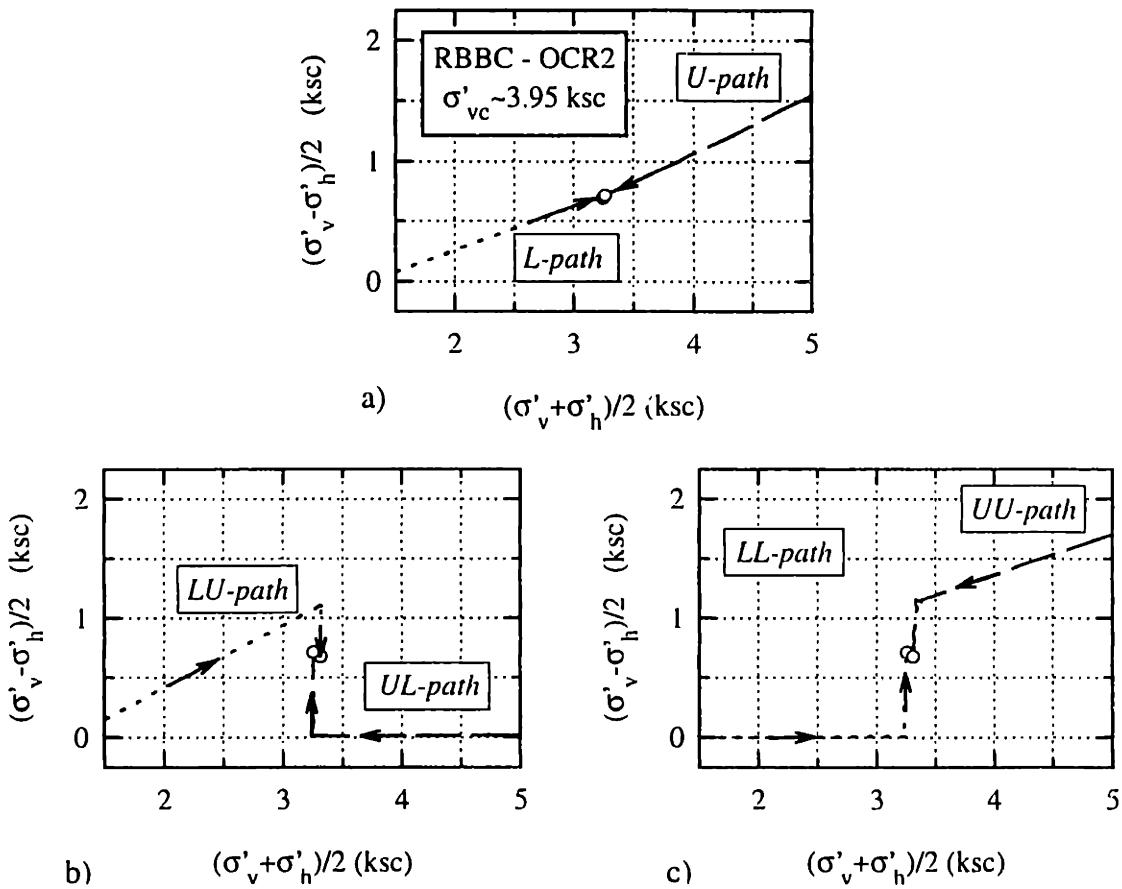


**Figure 6.55:** Six pre-shear stress paths investigated for OCR2 RBBC.

Table 6.11 summarizes the exact pre-shear conditions and the initial stiffness results for the six tests conducted on OCR2 RBBC at a stress level of approximately 4 ksc. Note that the first four shears (*U, L, UL, and LL*) were performed on the same specimen (*TX455*), while the last two (*UU* and *LU*) were carried out on another specimen (*TX476*) in the last phase of the experimental program

| | $\sigma'_{vc}$ (ksc) | Path | OCR | e | $t_{aging}$ (h) | K | $E_uMAX$ (ksc) |
|---|---|---|---|---|---|---|---|
| TX455S2 | 3.95 | U | 2.03 | 0.848 | 26 | 0.65 | 2985 |
| TX455S3 | 3.95 | L | 2.03 | 0.851 | 32 | 0.65 | 2965 |
| TX455S4 | 3.96 | UL | 2.03 | 0.822 | 34 | 0.64 | 3003 |
| TX455S5 | 3.97 | LL | 2.03 | 0.828 | 35 | 0.64 | 2914 |
| TX476S3 | 3.98 | UU | 2.03 | 0.856 | 64 | 0.66 | 3517 |
| TX476S4 | 3.99 | LU | 2.03 | 0.862 | 35 | 0.66 | 3339 |

**Table 6.11:** Pre-shear conditions and initial stiffness results for six tests performed to investigate the effect of the pre-shear stress path on the pre-failure behavior of OCR2 RBBC.

The results for the first four shears are extremely consistent (within 3%). On the other hand the values of $E_uMAX$ obtained from the last two tests (*TX476S3* and *S4*) are markedly higher (10-15%).[15] However, there are several secondary trends apparent in the initial stiffness data presented in Table 6.11. First it is clear that, as a result of differences in void ratio, tests involving unloading in the first stage of consolidation (*U, UL, UU*) are consistently stiffer than their "companion" tests (*L, LL, LU*). Secondly, tests involving a loading reversal as a result of shear (*U, UU, LU*) are consistently stiffer than those in which no reversal occurs (*L, UL, LL*).

Figure 6.56 presents the stiffness degradation curves for all six shears. The results for the *U* and the *UU* paths are basically coincident and represent the limit in the stiffness degradation behavior, characterized by the less marked non-linearity and the largest linear threshold (0.0090% and 0.0083% for *U* and *UU* test respectively[16]). This result appears to indicate that the actual stress path followed during the swelling phase is of secondary importance, in terms of its effects on the small strain behavior, as long as the entire process involves continuous unloading. This is supported by the results for the *L* and the *LL* tests. These two consolidation paths involve continuous loading following quite distinct stress paths. While displaying behavior significantly

[15] Note that the other two shears (*476S1* and *476S2*) performed on the same specimen at an OCR of 8 (see Section 6.8.2) also yielded values of $E_uMAX$ higher than expected. No clear explanation for these results has been found at this point. In the case of test *TX476S3* the specimen was left on hold stress prior to shear in excess of the usual 24-36 hours. As discussed in Section 6.9, prolonged laboratory aging results in an increase of the initial stiffness of NC RBBC. While this effect is expected to be less significant at higher OCR's, it is possible that the longer aging period is partly responsible for the higher than expected value of $E_uMAX$ measured.

[16] Note that both *TX455S2* and *TX455S4* display linear threshold significantly higher than that measured in the other *U* tests (see Figure 6.22).

softer than that observed in the unloading tests (e.g. $\varepsilon_{lin}$ is equal to 0.0033% and 0.0043 for the *L* and *LL* shears respectively), the curves for both the *L* and *LL* paths are again extremely close to each other, indicating that as long as the consolidation process involves continuous increase of the vertical stress, the subsequent undrained behavior is virtually independent of the actual consolidation path followed.

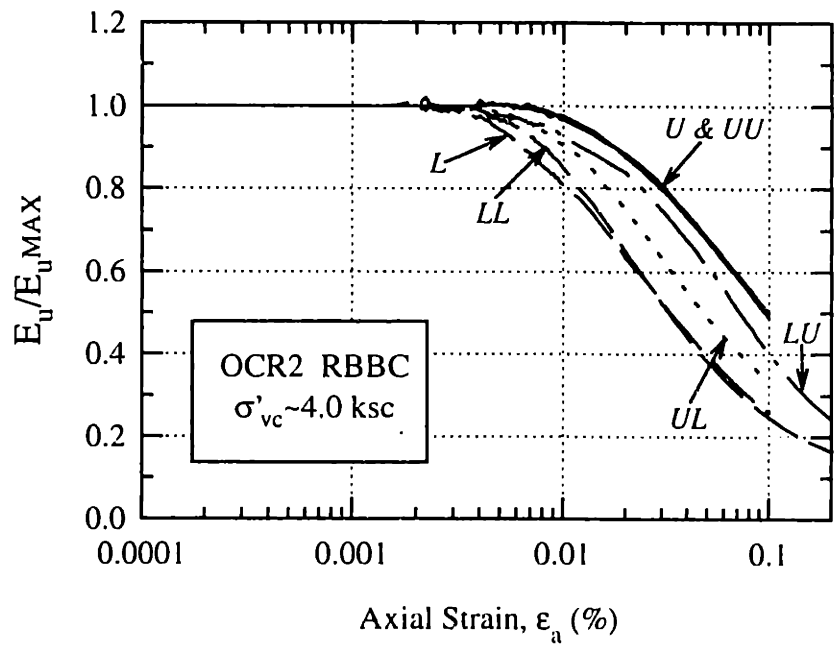


**Figure 6.56:** Stiffness degradation curves for six tests performed to investigate the effect of the pre-shear stress path on the pre-failure behavior of OCR2 RBBC.

The independence of the stiffness degradation behavior from the true *U* or *L* path, also indicates that small differences in the approach stress path are not important. This result is in agreement with the data obtained for NC RBBC. In fact, for the NC soil it was found that the stress strain behavior in the pre-failure region was the same for the three pre-shear consolidation paths examined. These all involved a continuous increase of the vertical stress.

The curves for the *UL* and *LU* paths which involve load reversal during the consolidation phase, fall in between the upper and lower envelopes formed by the pure unloading and pure loading results. It is interesting to observe that the behavior after the *UL* and the *LL* paths is quite different despite the fact that the last portions of the consolidation paths are coincident.

The same is true for the undrained shears following the *UU* and the *LU* paths, also characterized by overlapping stress paths in the last unloading phase of the consolidation process.

These results indicate that the stress-strain behavior of the soil below 0.1% is not affected simply by the direction in the last portion of the pre-shear stress path. Rather, they suggest that modest changes in the application of the axial stress (i.e., unloading associated with the last portion of consolidation) cannot override the memory of larger changes in axial stress occurring earlier in the consolidation stress path. Overall it appears that any path involving some unload in the vertical stress leads to larger linear response and less rapid stiffness degradation. Therefore the stress-strain behavior after both the *LU* and the *UL* paths involves less degradation than that following a purely loading (*L* and *LL*) consolidation path. For paths involving both loading and unloading it is the process associated with the last phase of the consolidation process that dominates, i.e. the *LU* path leads to stiffer behavior than the *UL* path.

Table 6.12 summarizes the values of the linear threshold $\varepsilon_{lin}$ and of the coefficient of non-linearity $C_{NL}$ for the tests performed on OCR 2 following different consolidation paths. For reference the values relative to the average behavior of $K_0$-consolidated NC RBBC are also included.

| Test | Path | $\varepsilon_{lin}$ (%) | $C_{NL}$ |
|---|---|---|---|
| TX455S2 | U | 0.0090[17] | 2.01 |
| TX476S3 | UU | 0.0083 | 2.05 |
| TX476S4 | LU | 0.0045 | 2.49 |
| TX455S4 | UL | 0.0050 | 2.99 |
| TX455S5 | LL | 0.0043 | 4.07 |
| TX455S3 | L | 0.0033 | 3.88 |
| NC RBBC Ref.$K_0$curve | - | 0.0015 | 5.95 |

**Table 6.12:** Variation of the linear threshold and the coefficient of non-linearity with pre-shear consolidation path (OCR2 RBBC).

[17] Note that test TX455S2 presents value of the linear threshold greater than that measured in other tests performed under similar conditions ($\varepsilon_{linave}$ for OCR2-U= 0.0054%)

## 6.8 EFFECT OF STRAIN RATE

### 6.8.1 Introduction

This research included the investigation of the effect of variations in the strain rate over approximately two orders of magnitude on the pre-failure behavior of NC and OC RBBC. Table 6.13 summarizes the rates examined for each OCR. The number in the cell indicates the number of tests performed. The shaded cells correspond to the standard rate of 0.1%/hr used for the vast majority of the tests performed in this experimental program. All tests on NC RBBC involved $K_0$-consolidation and 1 day of aging. For OCR 2 RBBC the behavior after both an unloading and a loading pre-shear path followed in both cases by the standard one day aging duration was examined.

| | Number of Tests | | | | | | |
|---|---|---|---|---|---|---|---|
| **Rate** | **NC** | **OCR2** | | **OCR4** | | **OCR8** | |
| **(%/hr)** | | ***U*** | ***L*** | ***U*** | ***L*** | ***U*** | ***L*** |
| **0.05** | 3 | 1 | 1 | - | - | - | - |
| **0.1** | 22 | 4 | 3 | 3 | 3 | 4 | 4 |
| **1** | 3 | 1 | 1 | 1 | 1 | - | - |
| **2** | 2 | - | - | - | - | - | - |
| **4** | 3 | 1 | 1 | 1 | 1 | 1 | 1 |

**Table 6.13:** Range of strain rates investigated.

### 6.8.2 NC RBBC

#### *6.8.2.1 Introduction*

As shown in Table 6.13, the investigation of the small strain rate dependency of NC RBBC involved shearing at four rates: 0.05, 1, 2 and 4 %/hr, in addition to the standard rate of 0.1%/hr. At each of these rates, tests were performed for at least two stress levels. Table 6.14 summarizes the tests performed for each shear rate.

| Rate (%/hr) | Test # | $\sigma'_{vc}$ (ksc) |
|---|---|---|
| *0.05* | TX470S1 | 1.72 |
| | TX470S2 | 2.42 |
| | TX474S2 | 2.37 |
| *1* | TX438S1 | 1.76 |
| | TX438S2 | 2.43 |
| | TX438S4 | 4.01 |
| *2* | TX445S1 | 1.67 |
| | TX459S2 | 2.38 |
| *4* | TX459S1 | 1.76 |
| | TX470S3 | 3.12 |
| | TX455S1 | 5.75 |

**Table 6.14:** Tests performed to investigate strain rate dependency of NC RBBC.

### *6.8.2.2 Initial Stiffness*

For the reference stress level (~1.7 ksc) results are available for all additional rates examined (0.05, 1, 2 and 4%/hr). The initial conditions as well as the initial stiffness results for tests with strain rates greater or equal to 1%/hr are summarized in Table 6.15. For reference the table also includes the information for one test (*TX359S1*) performed at the standard rate of 0.1%/hr (shaded row).

| Rate (%/hr) | Test # | $\sigma'_{vc}$ (ksc) | OCR | $K_c$ | e | $E_{uMAX}$ (ksc) |
|---|---|---|---|---|---|---|
| *0.1* | TX359S1 | 1.72 | 1 | 0.48 | 1.070 | 1031 |
| *1* | TX438S1 | 1.76 | 1 | 0.49 | 1.071 | 1122 |
| *2* | TX445S1 | 1.67 | 1 | 0.48 | 1.086 | 983 |
| *4* | TX459S1 | 1.76 | 1 | 0.50 | 1.057 | 949 |

Statistics: $E_{uMAX}$=1021±65 S.D. (COV=6%)

**Table 6.15:** Pre-shear conditions and initial stiffness results for tests performed at $\sigma'_{vc}$~1.7 ksc employing different strain rates.

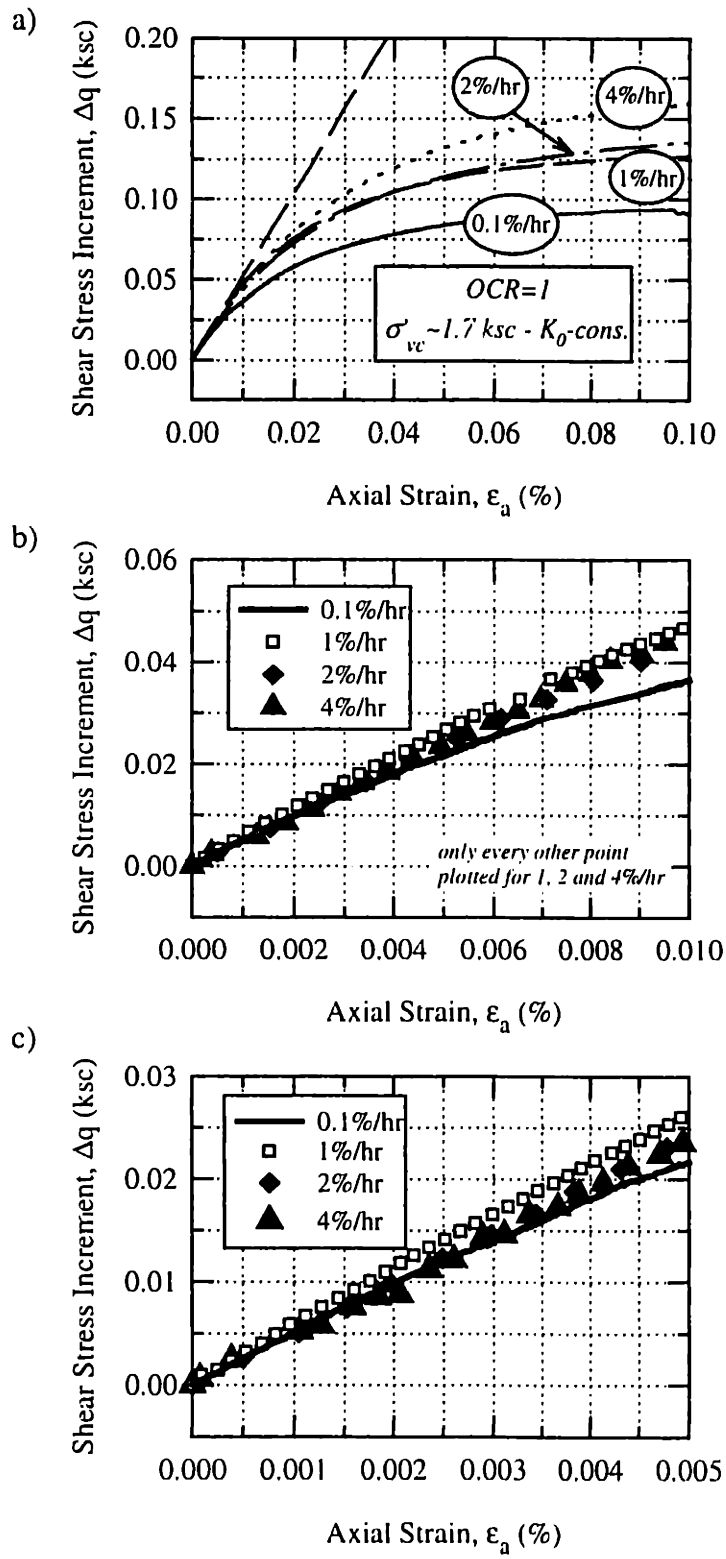


**Figure 6.57:** Effect of strain rate on the pre-failure stress-strain behavior of NC RBBC $\sigma'_{vc}$~1.7 ksc: a) 0-0.1%; b) 0-0.01%; c) 0-0.005%.

Figures 6.57a-c present the stress-strain curves at different ranges of strain (0-0.1%, 0-0.01%, 0-0.005%) relative to these tests, with the exception of the data at 0.05%/hr. For clarity, because of slight differences in the initial shear stress value, the results are presented in terms of shear stress increment ($\Delta q$) versus strain. Note that, due to limitations in the acquisition speed, as the rate increases, the amount of data collected decreases, leading to a less well defined stress-strain curve particularly at very small strains.

Figure 6.57c shows that at very small strains (<0.002%), for rates varying between 0.1 and 4%/hr, the behavior of the NC soil is independent of strain rate. In fact, the stress-strain curves are basically overlapping, and the values of initial stiffness display the same variability (COV=6% - see Table 6.15) that characterizes the results for tests performed at the same strain rate (Table 6.1). This range reflects some specimen to specimen variability particularly in terms of the pre-shear void ratio and no particular trend with strain rate is observed. Similar conclusions are derived from the analysis of the results obtained at other stress levels.

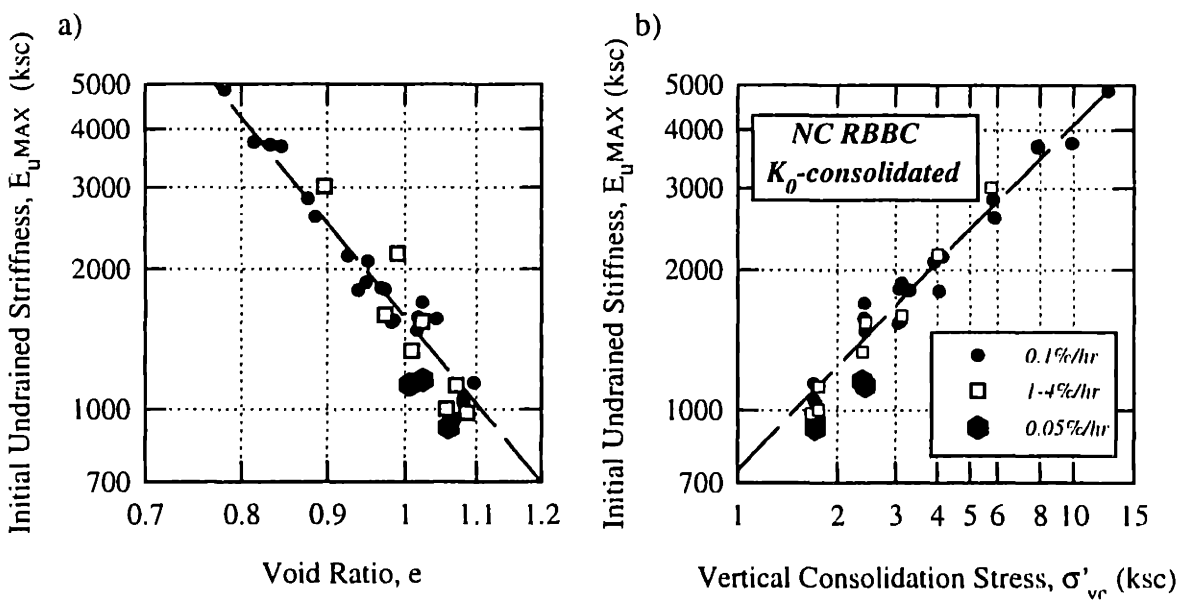


**Figure 6.58:** Plots of stiffness versus a) void ratio and b) vertical stress for $K_0$-consolidated NC RBBC sheared at rates in the range 0.05-4%/hr.
(Dashed lines are linear regressions through data at 0.1%/hr only)

In Figures 6.58 a and b the initial stiffness results for the higher rate (1, 2 and 4%/hr) tests are all plotted on the graphs of $E_{u}$MAX versus stress level and void ratio, determined for the standard rate (0.1%/hr) (Figures 6.11a-b). The higher rate results fall within the band formed by

the 0.1%/hr data confirming the independence of $E_{u}MAX$ from strain rate, at least for the 0.1-4%/hr range of rate.

As shown in Figure 6.58, the initial stiffness results derived from the tests performed at the "slow" rate (i.e. 0.05%/hr) appear to be consistently lower than the values obtained at equivalent void ratio or consolidation stress, employing all other rates. (~18-25% lower than the regression line). In both Figures 6.58 a and b, however, the "slow" data appear to fall on a line essentially parallel to the regression through all the other data, indicating the same trend with $\sigma'_{vc}$, or $e$.

These results support the hypothesis that the behavior of the soil is not purely elastic and is influenced by the pre-shear viscous straining. Figure 6.59a shows a typical curve for NC RBBC of axial strain versus time from the beginning of the hold stress phase. It shows that the drained creep rate decreases with time reaching, after 30 hours of hold stress, a value on the order of $10^{-6}$%/sec, i.e. about 0.0036-0.004%/hr. This rate of deformation is about 14 times

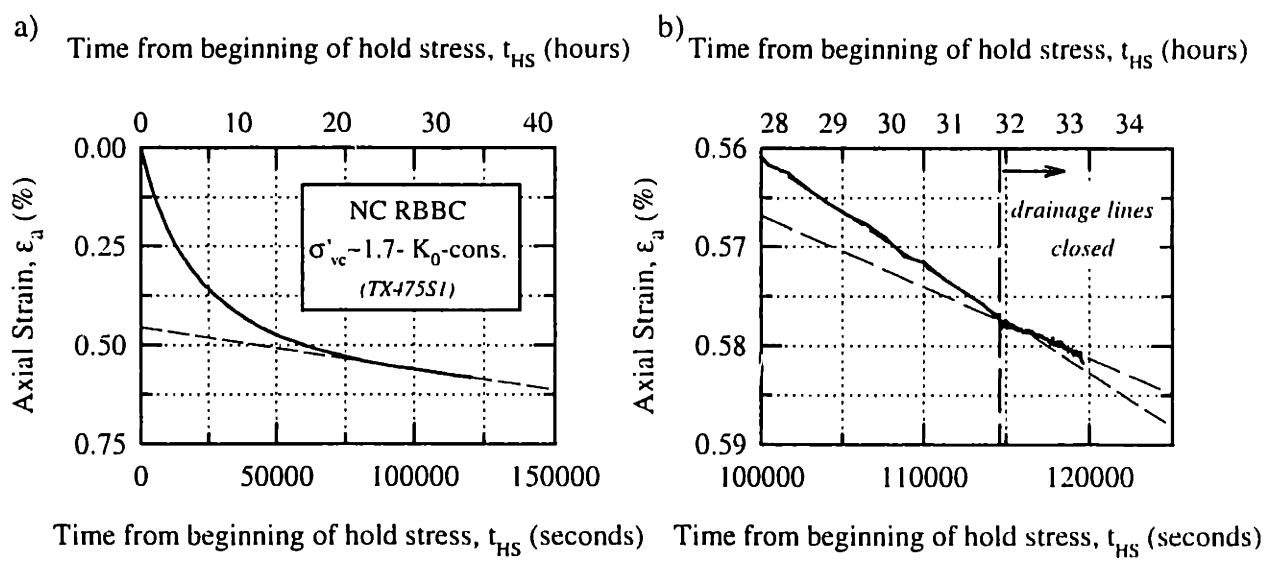


**Figure 6.59:** Pre-shear creep rate of NC RBBC after ~ 30 hours of aging.

smaller than the "slow" strain rate employed during shear. In fact, at the beginning of shear the ratio $(d\varepsilon/dt_{shear})/(d\varepsilon/dt_{creep})$ is even smaller (~8) due to the time required for the shear strain rate to reach the target value[18]. On the other hand note that once the drainage lines are closed the creep rate actually decreases approximately by a factor of 2. This is shown in Figure 6.59 b that presents a close-up view of Figure 6.59a, relative to the last portion of the hold stress phase.

[18] The value of the $(d\varepsilon/dt_{shear})/(d\varepsilon/dt_{creep})$ ratio at the beginning of shear is calculated from the strain rate measured over 0-0.002% axial strain range in three slow tests performed on NC RBBC.

Overall, regardless of the exact value of the ratio, it can be shown that increased straining due to creep accounts for the observed reduction in stiffness.

### *6.8.2.3 Non-linear Behavior*

As shown in Figure 6.57 a, beyond 0.003-0.004% strain, the behavior of NC RBBC at $\sigma'_{vc}$~ 1.7 ksc, is significantly impacted by the strain rate used. Increasing rates are associated with increased size of the linear region and larger shear stresses at all strain levels. Correspondingly the soil displays reduced non-linearity. The analysis of the results available at different stress levels demonstrates that the stiffness degradation behavior at a given strain rate is independent of stress level. This is shown in Figures 6.60 a-c which present the curves of normalized stiffness ($E_u/E_{uMAX}$) for each of the strain rates examined.

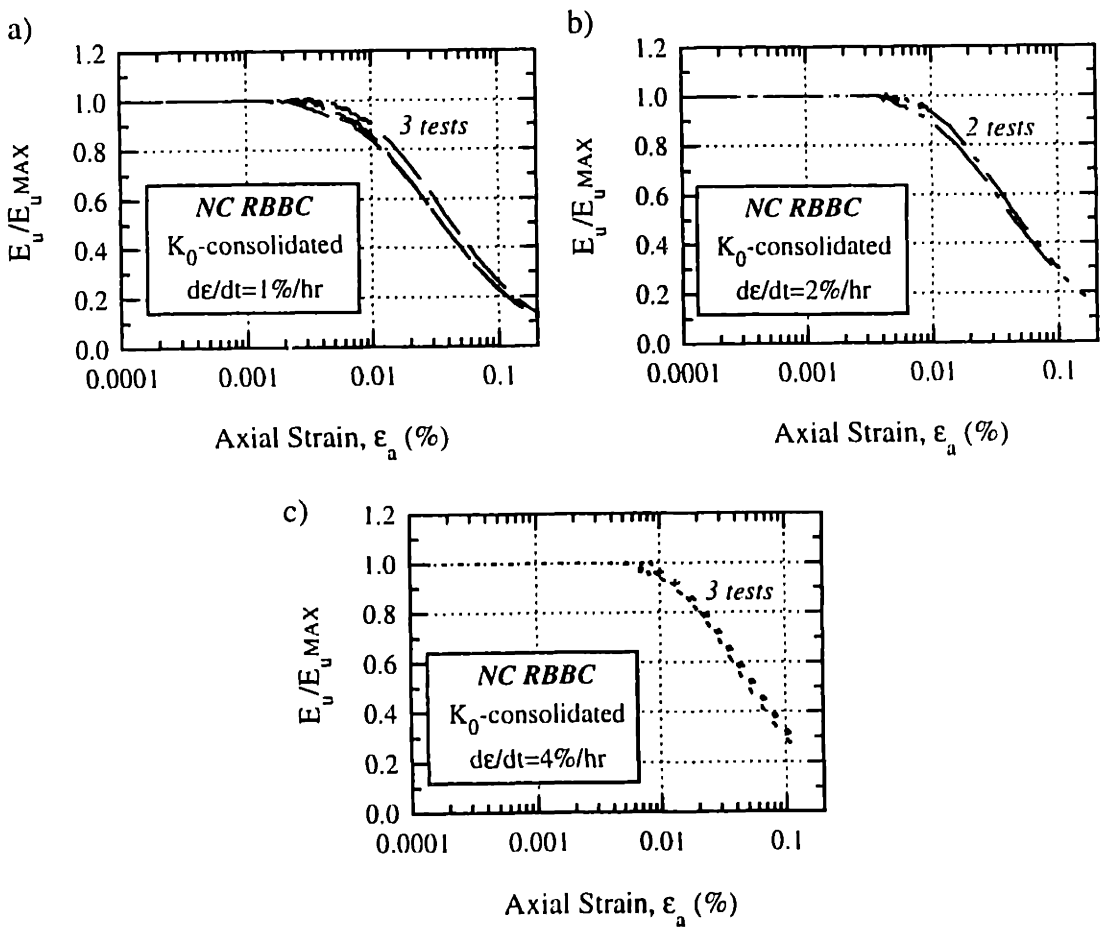


**Figure 6.60:** Normalized stiffness degradation curves for NC RBBC: a) dε/dt=1%/hr; b) dε/dt=2%/hr; c) dε/dt=4%/hr.

The average stiffness degradation curves of NC RBBC for each of the strain rates investigated are plotted in Figure 6.61 alongside the "reference" curve for the standard rate of 0.1%/hr.

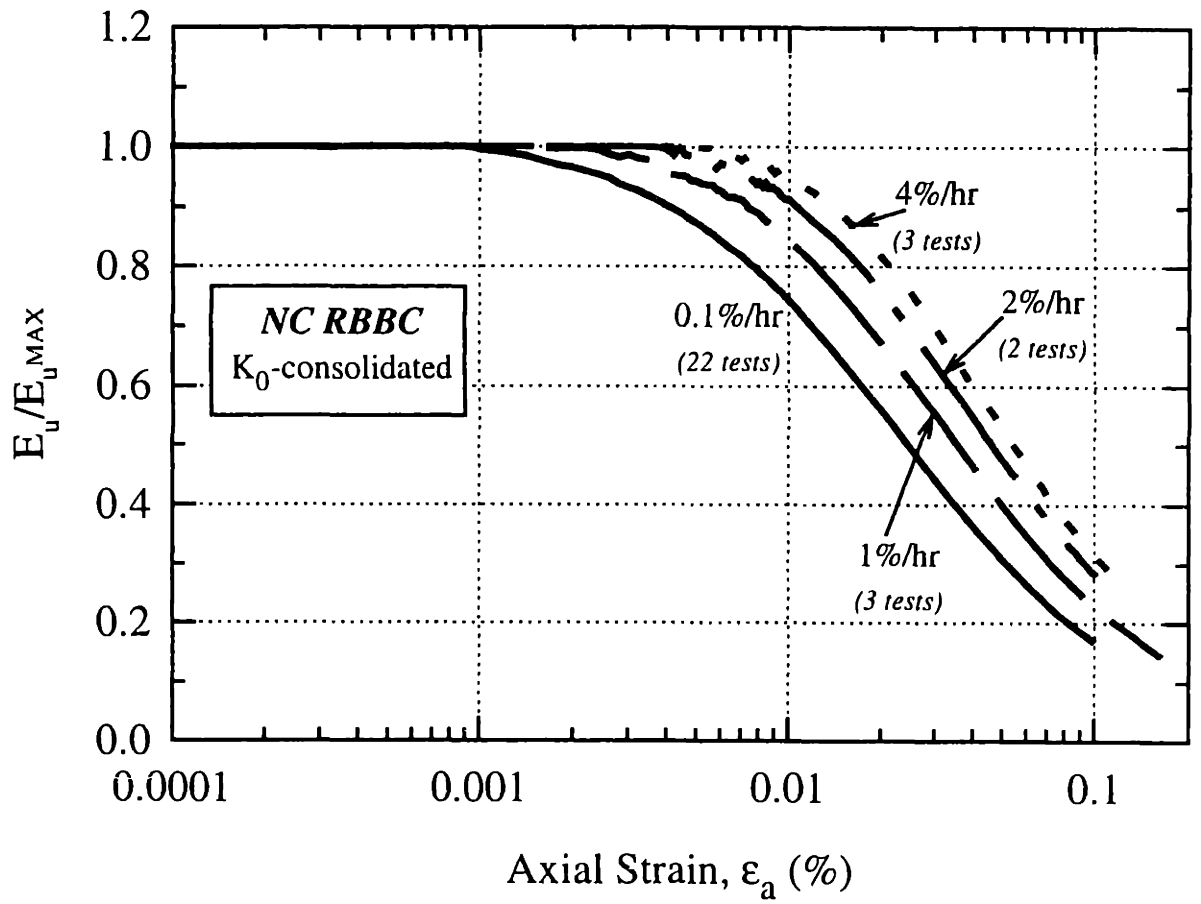


**Figure 6.61:** Average stiffness degradation curves for NC RBBC as a function of strain rate (0.1, 1, 2, and 4%/hr).

By dividing the value of the normalized stiffness at a given strain by the corresponding value from the reference curve (0.1%/hr) the effect of the increased strain rate on the non-linearity of the soil can be quantified as a function of strain level. Figure 6.62 plots this ratio as a function of strain for the three rates examined. It is shown that, at least within the strain range investigated, the susceptibility to rate increases with strain level. In the case of the fastest rate considered (4%/hr) the stiffness at 0.1% strain is almost doubled.

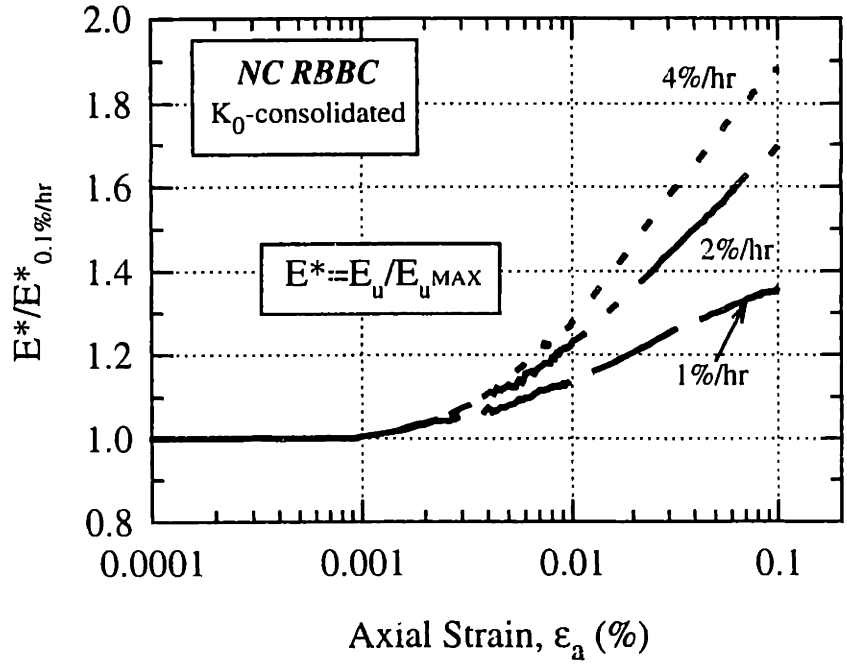


**Figure 6.62:** Change in normalized stiffness produced by an increase in strain rate.

Figures 6.63 a and b summarize the linear threshold and non-linearity coefficient data for all the tests performed at higher rates as well as for the reference data base for the $K_0$-consolidated soil. The figures indicate that an increase in strain rate results in the increase of the linear threshold and in the decrease of the non-linearity of the soil, thus confirming the observations made for the results at $\sigma'_{vc}$ ~ 1.7 ksc (Figure 6.57)

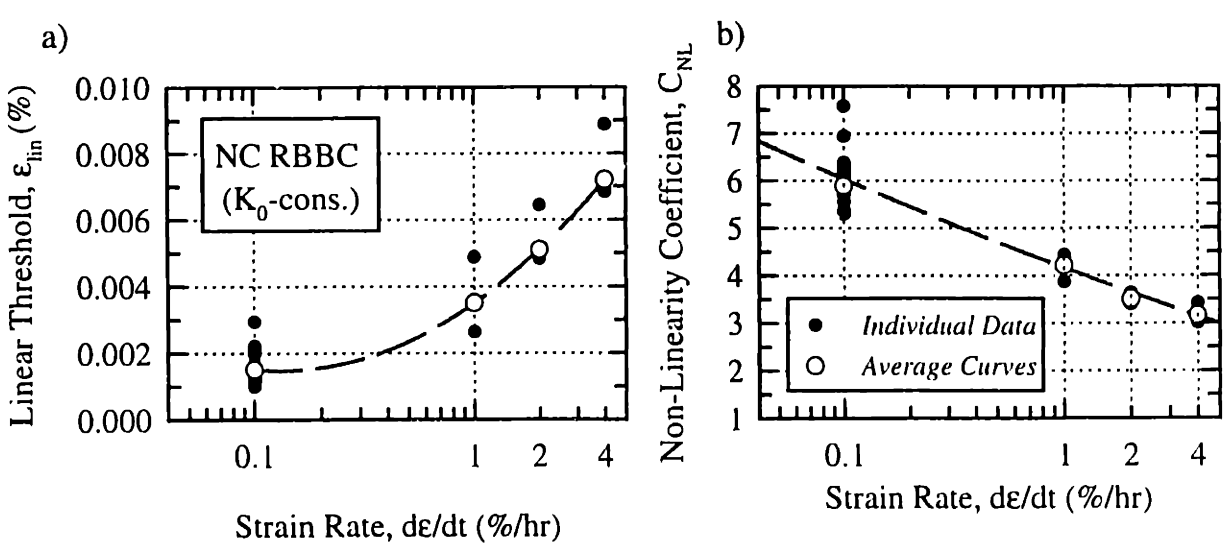


**Figure 6.63:** Effect of strain rate on a) the linear threshold and b) the non-linearity coefficient.

Finally, associated with an increase in strain rate is an increase in the strain recovered after undrained unloading at the end of shear. The value of $\varepsilon_{PL}/\varepsilon_{TOT}$ decreases from 94% (0.1%/hr) to less than 80% for the fastest strain rate (4%/hr).

The results obtained employing the slowest rate (0.05%/hr) are not included in Figures 6.61-6.63. For this rate the shape of the stiffness degradation curve is found to be very close to that determined for the standard rate tests.

### 6.8.3 OC RBBC

#### *6.8.3.1 Introduction*

In the case of OC RBBC the investigation of the effects of strain rate on the behavior of the soil focused on the rates summarized in Table 6.13 and was limited to one stress level for each OCR, for both loading and unloading consolidation paths.

#### *6.8.3.2 Initial Stiffness*

Tables 6.16-6.18 summarize the pre-shear conditions and the initial stiffness results for the tests performed on RBBC with OCR of 2, 4 and 8 respectively. The tables contain information for tests performed at rates in the range 0.1-4%/hr (0.05-4%/hr for OCR2).

| Rate (%/hr) | Test # | $\sigma'_{vc}$ (ksc) | OCR | Path | $K_c$ | $t_{aging}$ (h) | e | $E_uMAX$ (ksc) |
|---|---|---|---|---|---|---|---|---|
| *0.05* | TX442S7[19] | 2.42 | 2.03 | *U* | 0.65 | 41 | 0.908 | 2186 |
| *0.1* | TX432S3 | 2.32 | 2.03 | *U* | 0.63 | 25 | 0.906 | 1998 |
| *1* | TX442S5 | 2.42 | 2.03 | *U* | 0.65 | 37 | 0.910 | 1957 |
| *4* | TX442S3 | 2.42 | 2.02 | *U* | 0.65 | 57 | 0.920 | 1993 |
| *0.05* | TX442S8 | 2.42 | 2.03 | *L* | 0.65 | 29 | 0.915 | 1759 |
| *0.1* | TX432S4 | 2.32 | 2.04 | *L* | 0.63 | 24 | 0.913 | 1638 |
| *1* | TX442S6 | 2.42 | 2.03 | *L* | 0.65 | 36 | 0.916 | 1811 |
| *4* | TX442S4 | 2.53 | 1.94 | *L* | 0.63 | 62 | 0.929 | 1829 |

Statistics: $(E_uMAX)_U$=2034±89 S.D. (COV=4%); $(E_uMAX)_L$=1759±75 S.D. (COV=4%)

$(E_uMAX)_{ALL}$=1896±160 S.D. (COV=8%)

**Table 6.16:** Pre-shear conditions and initial stiffness results for tests performed on OCR2 RBBC employing different strain rates.

[19] In this test only the initial stiffness determination was good.

| Rate (%/hr) | Test # | $\sigma'_{vc}$ (ksc) | OCR | Path | $K_c$ | $t_{aging}$ (h) | e | $E_uMAX$ (ksc) |
|---|---|---|---|---|---|---|---|---|
| *0.1* | TX442S1 | 0.73 | 4.27 | *U* | 0.92 | 32 | 0.995 | 872 |
| *1* | TX459S5 | 0.76 | 4.41 | *U* | 0.90 | 34 | 0.973 | 986 |
| *4* | TX459S3 | 0.77 | 4.33 | *U* | 0.91 | 33 | 0.986 | 950 |
| *0.1* | TX442S2 | 0.74 | 4.23 | *L* | 0.93 | 28 | 1.006 | 850 |
| *1* | TX459S6 | 0.76 | 4.40 | *L* | 0.91 | 30 | 0.988 | 883 |
| *4* | TX459S4 | 0.76 | 4.41 | *L* | 0.91 | 35 | 1.000 | 839 |

Statistics: $(E_uMAX)_U$=936±48 S.D. (COV=5%); $(E_uMAX)_L$=857±19 S.D. (COV=2%)

$(E_uMAX)_{ALL}$=897±53 S.D. (COV=6%)

**Table 6.17:** Pre-shear conditions and initial stiffness results for tests performed on OCR4 RBBC employing different strain rates.

| Rate (%/hr) | Test # | $\sigma'_{vc}$ (ksc) | OCR | Path | $K_c$ | $t_{aging}$ (h) | e | $E_uMAX$ (ksc) |
|---|---|---|---|---|---|---|---|---|
| *0.1* | TX471S6 | 1.85 | 8.56 | *U* | 1.21 | 24 | 0.772 | 2402 |
| *4* | TX471S4 | 1.85 | 8.57 | *U* | 1.22 | 27 | 0.795 | 2639 |
| *0.1* | TX471S7 | 1.85 | 8.56 | *L* | 1.22 | 32 | 0.787 | 2397 |
| *4* | TX471S5 | 1.85 | 8.57 | *L* | 1.22 | 30 | 0.809 | 2109 |

Statistics: $(E_uMAX)_{ALL}$=2387±188 S.D. (COV=8%)

**Table 6.18:** Pre-shear conditions and initial stiffness results for tests performed on OCR8 RBBC employing different strain rates.

The initial stiffness results presented in Tables 6.16-6.18 are fairly consistent and confirm, also in the case of OC RBBC, an insensitivity of the initial stiffness to variations in strain rate, for both the unloading and loading pre-shear paths. These data also support a secondary trend in which the unloading results display marginally higher values of $E_uMAX$ than those obtained after a loading consolidation path, even once variations in void ratio are accounted for. This effect is limited, and as shown in Figures 6.64 a-f, once differences in void ratio are accounted for, the data all fall within the same band, regardless of the rate used (0.05-4%/hr). Note that, unlike what was observed for NC RBBC (Section 6.8.2), the insensitivity of the initial stiffness to rate extends also to the data obtained employing the "slow" rate of 0.05%/hr. This is explained by the fact that for OC RBBC the initial creep rate, for both *U* and *L* tests is smaller (in absolute

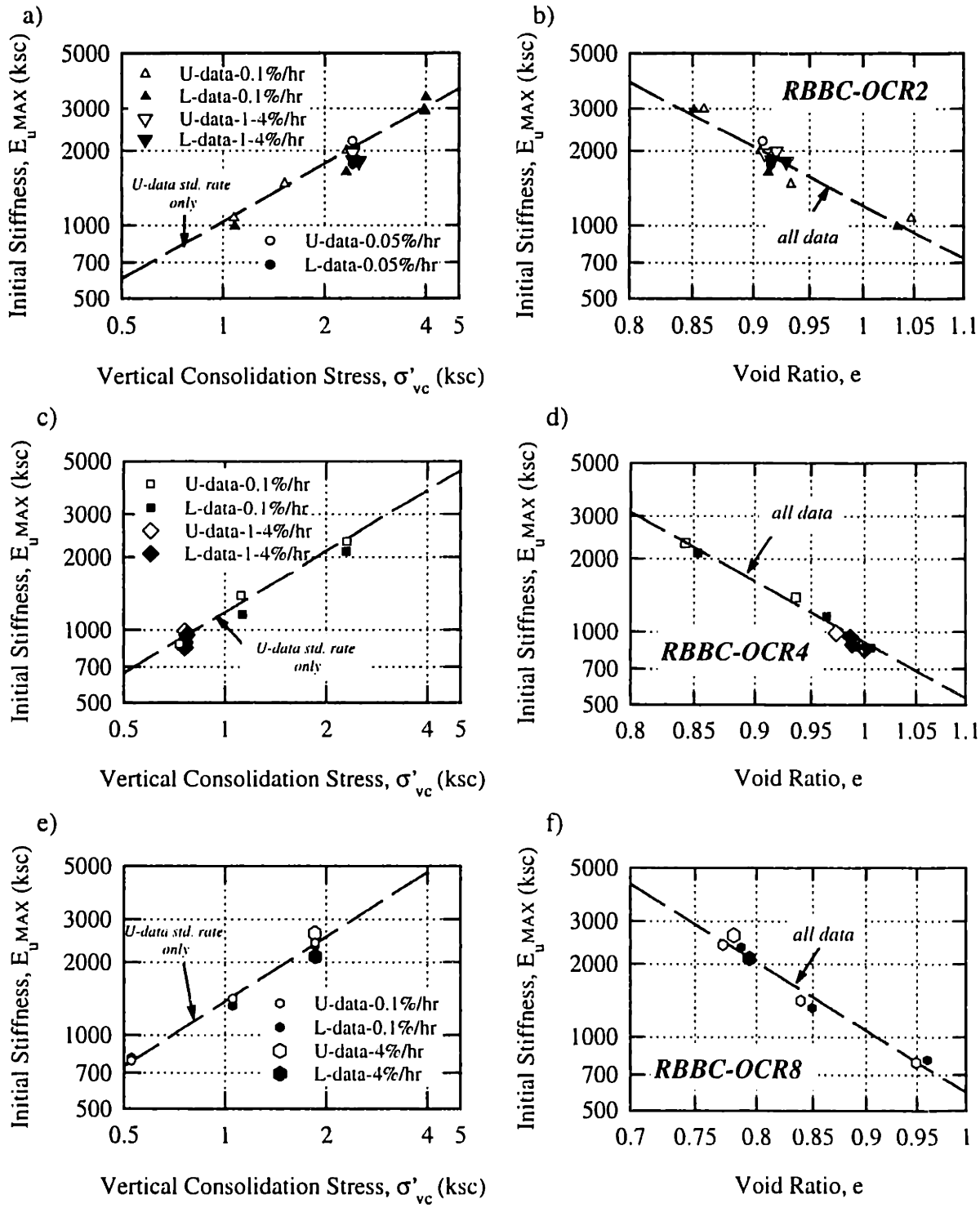


**Figure 6.64:** Initial stiffness versus vertical consolidation stress and void ratio for tests conducted employing rates in the range 0.1%-4%/hr on a-b) OCR2; c-d) OCR4 and e-f) OCR8 RBBC.

value[20]) than that measured on the NC soil by an order of magnitude. Therefore, even for the slow rate, creep strains remain negligible and do not affect the determination of the initial stiffness of the soil.

#### *6.8.3.3 Non-linear behavior*

Figures 6.65 a-c show plots of the stress-strain curves, in increasingly small ranges of strain (0-0.1%, 0-0.01% and 0.005%), for the three shears performed on OCR2 RBBC at $\sigma'_{vc}$~ 2.4 ksc employing rates of 0.1, 1 and 4%/hr, after an unloading consolidation path (see Table 6.16).[21]

Figure 6.65 shows that the initial portion of shear (0-0.01%) is uninfluenced by the strain rate. Beyond approximately 0.02% strain, however, the curves for the two higher strain rates deviate significantly from the standard rate curve, exhibiting an extended linear threshold (0.0089 and 0.0083% versus 0.0039%[22]), reduced non-linearity, and larger shear stress gain at all strains thereafter. This is reflected in a higher normalized stiffness at all strain levels beyond $\varepsilon_{lin}$, as shown in Figure 6.66.

Unlike the NC data, the OCR2 data base does not follow a continuous trend with rate, i.e. no significant difference is observed between the curves for 1 and 4%/hr. In Figure 6.67 the increase in normalized stiffness is quantified as a function of strain level by plotting the ratio of $E_u/E_{uMAX}$ for the high rate shears to that of the standard rate test. It is observed that, while the effect of strain rate increases steadily with strain level, at most a 30% increase in $E_u/E_{uMAX}$ is measured at 0.1% strain. This is significantly smaller than the effect measured on NC RBBC (Figure 6.62) and indicates a reduced strain rate sensitivity of the soil. Figure 6.67 also indicates that the effect of strain rate on the stiffness plateaus towards the end of shear.

A similar set of graphs are presented in Figures 6.68a-c, 6.69 and 6.70 for the behavior of OCR 2 RBBC after a loading pre-shear path. As seen for the unloading path results, the three stress-strain curves are virtually overlapping over the first part of shear, and then gradually diverge at higher strains (>0.005%). There is, however, a definite difference between the unloading and the loading data. In the first place for the loading data, the stiffness continues to increase with increases in strain rate, indicating a marginally higher sensitivity to strain rate than

---

[20] Following unloading from the VCL the soil presents swelling creep.

[21] The figure does not include curves for the slow strain rate (0.05%/hr) since these data were erratic beyond the linear threshold.

[22] Average value of $\varepsilon_{lin}$ for OCR2-U tests is 0.0054%, greater than the value measured for test *TX432S3*.

the unloading data. In addition, it is clear that the loading data reaches a peak sensitivity to rate at ~ 0.05% strain.

For clarity, the data for the slow rate (0.05%/hr) are not shown in Figures 6.65-6.66. At this rate the soil presents a slightly reduced linear threshold (0.0025% versus 0.0041%) and a virtually identical degree of non-linearity to that observed at the standard rate. Overall the stiffness degradation curves falls within the band formed by the results for all OCR2-*L* tests performed at 0.1%/hr (Figure 6.50a).

Associated with the increase in strain rate is also a decrease in the residual plastic strain following undrained unloading at the end of shear. In particular, it is found that $\varepsilon_{PL}/\varepsilon_{TOT}$ decreases from 29% (for $d\varepsilon/dt$=0.1%/hr) to 15-20% for the OCR2-*U* tests, and from 70% to 60% for the loading tests at the higher rates.

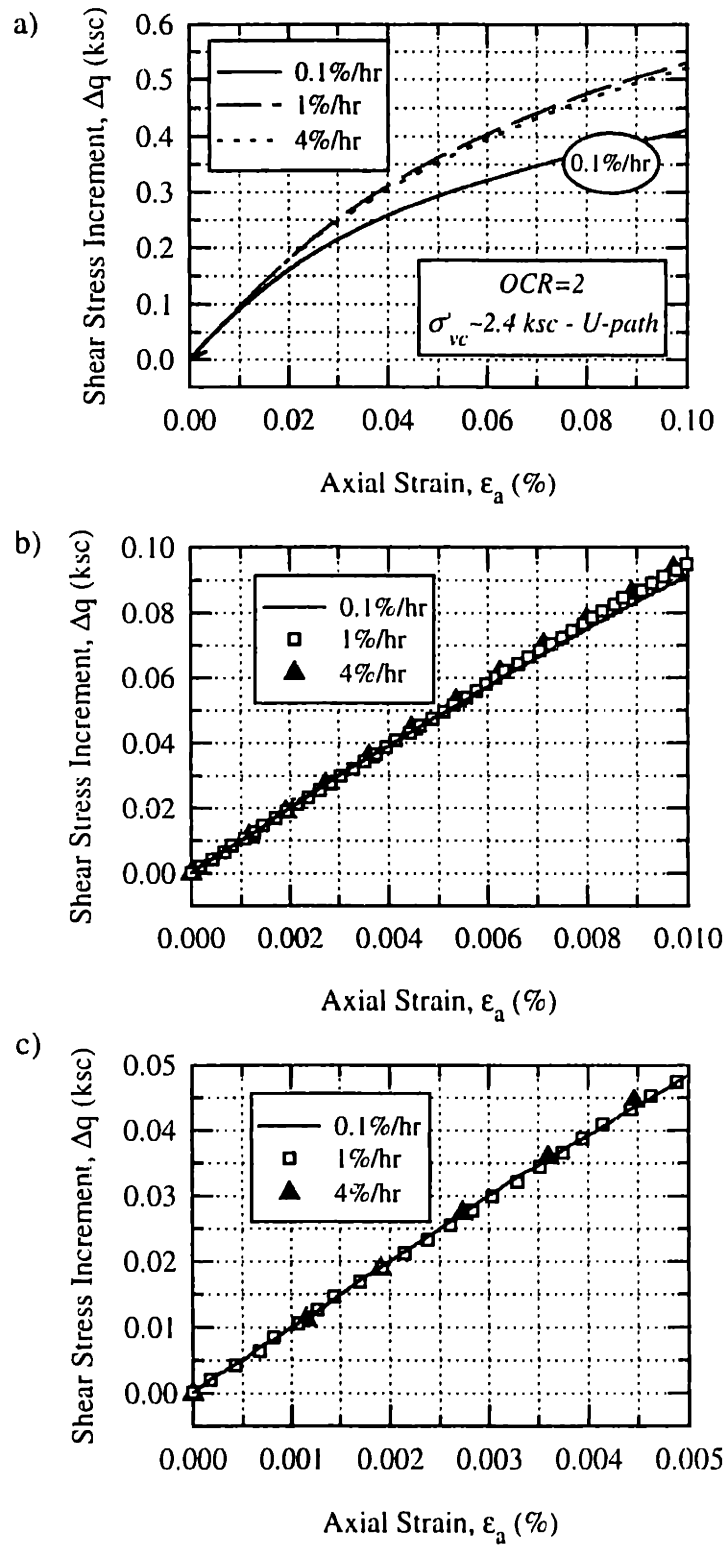


**Figure 6.65:** Effect of strain rate on the pre-failure stress-strain behavior of OCR2 RBBC at $\sigma'_{vc}$~2.4 ksc (U-Path) : a) 0-0.1%; b) 0-0.01%; c) 0-0.005%.

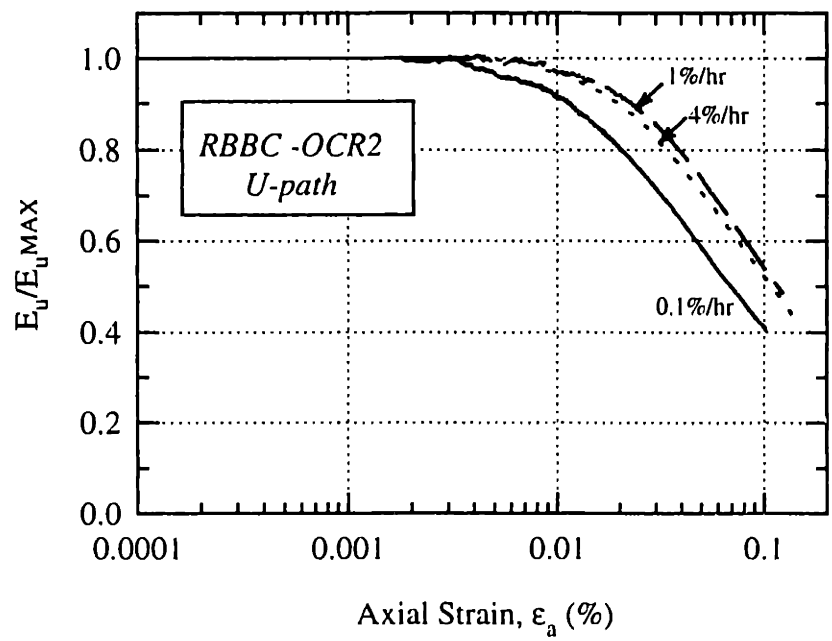


**Figure 6.66:** Effect of strain rate on stiffness degradation curve of OCR2 RBBC at $\sigma'_{vc}$~2.4 ksc (U-Path).

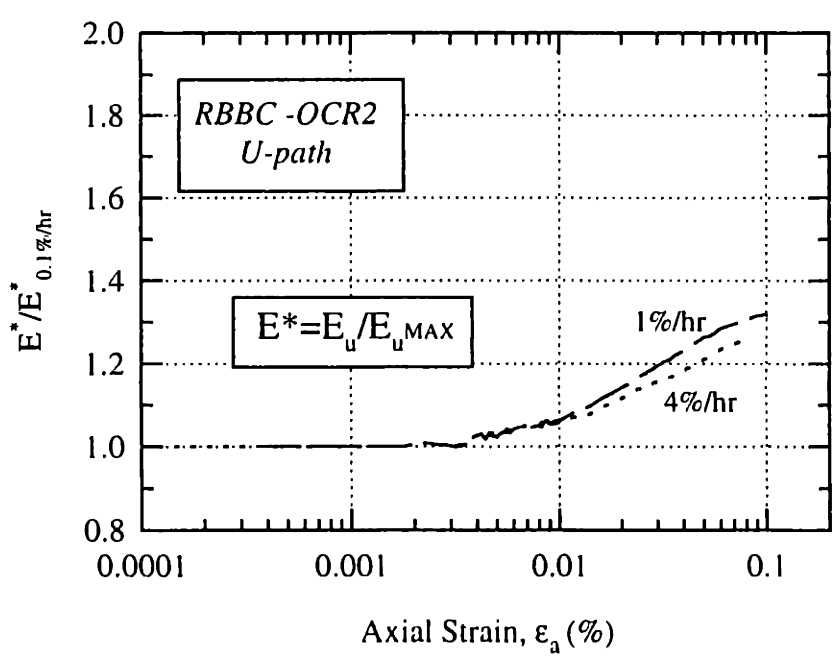


**Figure 6.67:** Change in normalized stiffness produced by an increase in strain rate (OCR2 RBBC- U path).

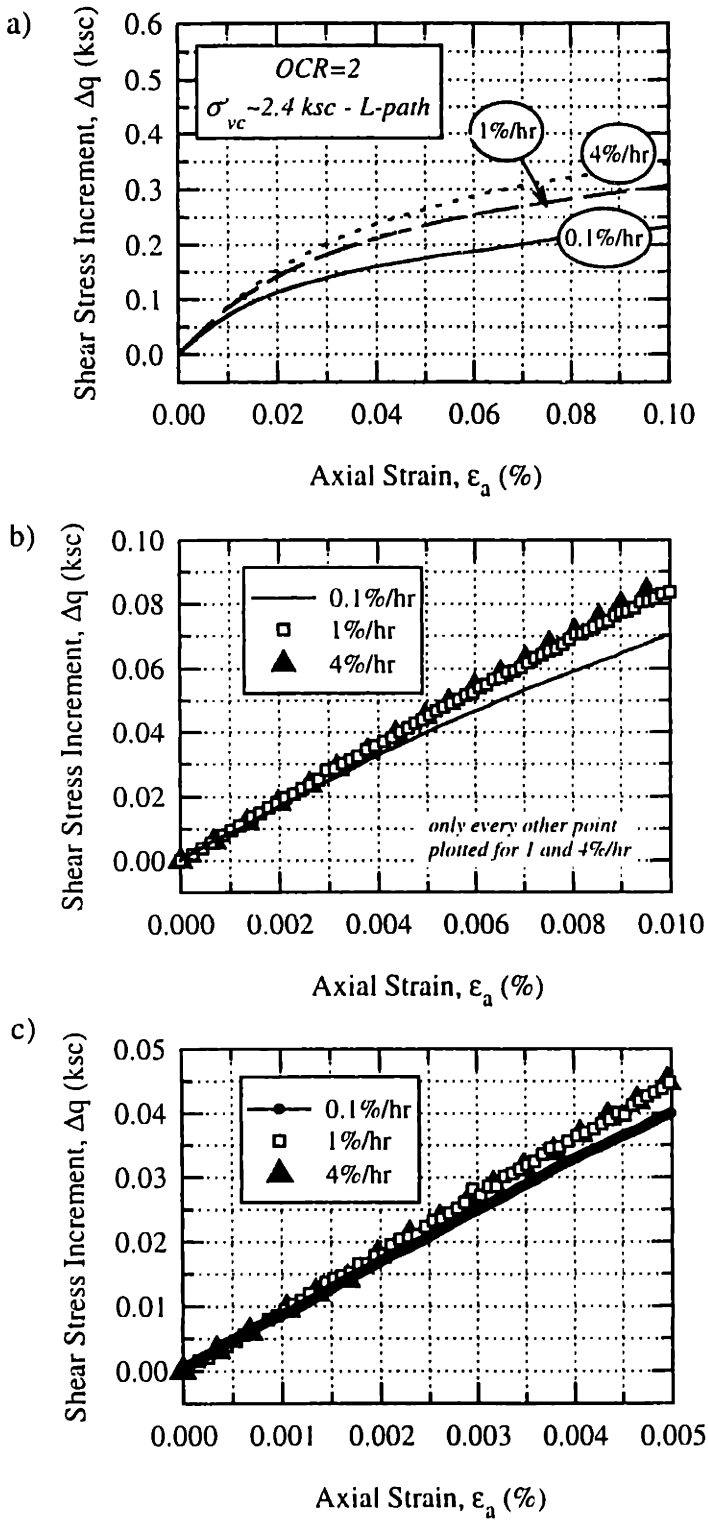


**Figure 6.68:** Effect of strain rate on the pre-failure stress-strain behavior of OCR2 RBBC at $\sigma'_{vc}$~2.4 ksc (L-Path) : a) 0-0.1%; b) 0-0.01%; c) 0-0.005%.

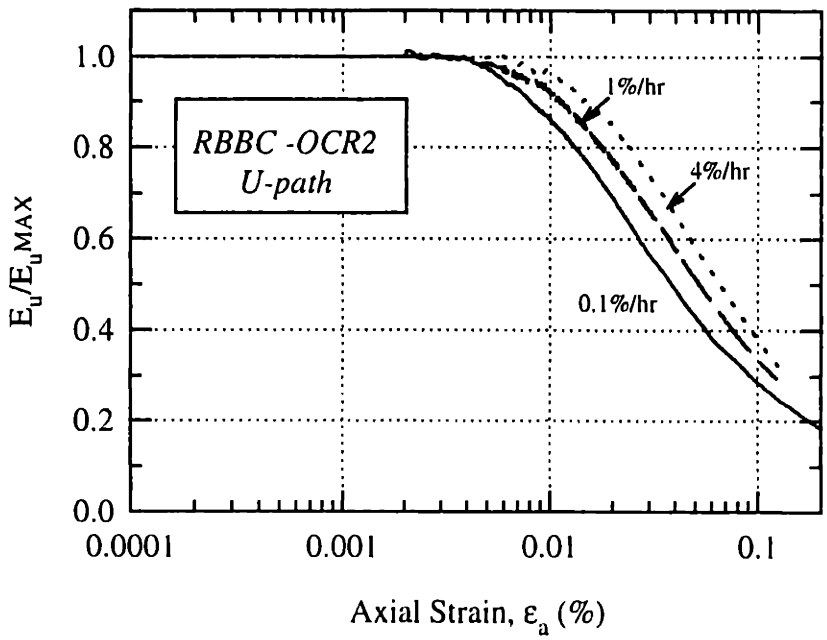


**Figure 6.69:** Effect of strain rate on stiffness degradation curve of OCR2 RBBC at $\sigma'_{vc}$~2.4 ksc (L-Path).

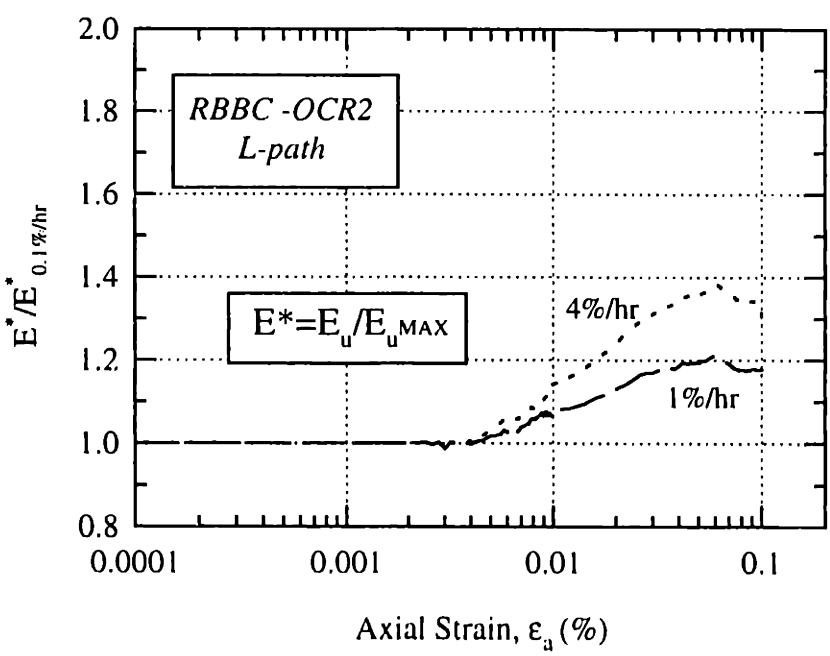


**Figure 6.70:** Change in normalized stiffness produced by an increase in strain rate (OCR2 RBBC- L path).

Figures 6.71-6.76 present plots identical to those just discussed for OCR2, for OCR equal to 4. Again, results are included for both unloading and loading pre-shear paths. The results for OCR4 RBBC are qualitatively similar to those discussed for OCR2 RBBC. The strain rate sensitivity of the soil increases with strain level, and the behavior of the soil after a loading consolidation path results more affected by the shearing rate. Comparison with the OCR2 results indicates that the strain rate sensitivity of the soil decreases with OCR.

In the case of OCR8 RBBC only two strain rates were examined (0.1 and 4%/hr). Figures 6.77-6.78 present the stress-strain and the stiffness degradation curves for shears performed at these rates after an unloading consolidation path. The difference between the curves is within the variability of the measurements, and the results indicate a negligible effect of strain rate. This is affirmed in Figure 6.79, in which the ratio of normalized stiffness at 4%/hr to the corresponding value at 0.1%/hr is found to be approximately equal to one over the entire stress-strain curve. Figure 6.79 also includes a curve for the behavior of OCR8 RBBC following a loading consolidation path. Unlike the data presented for OCR2, OCR4 and OCR8-*U* RBBC, which were derived from comparison of the curves obtained at the same stress level, this curve was obtained from the results for test *TX471* (see Table 6.18) and the average curve for OCR8 loading (Figure 6.51), as no high quality data was available at the same stress level. Figure 6.79 confirms the higher rate sensitivity of the soil following a loading, rather than an unloading consolidation path.

Figure 6.80 summarizes the coefficient of non-linearity data for both NC and OC RBBC (unloading and loading in Figure 6.80a and b, respectively), as a function of strain rate. The data are plotted normalized by the value of $C_{NL}$ derived at the standard rate of 0.1%/hr (average curve). The figures confirm that for all OCR's the strain rate sensitivity is higher in the *L*-tests rather than in the *U*-tests, and that for a given consolidation path higher reduction in non-linearity is observed at lower OCR's. This second result is in agreement with data presented by Sheahan (1991) at higher strains.

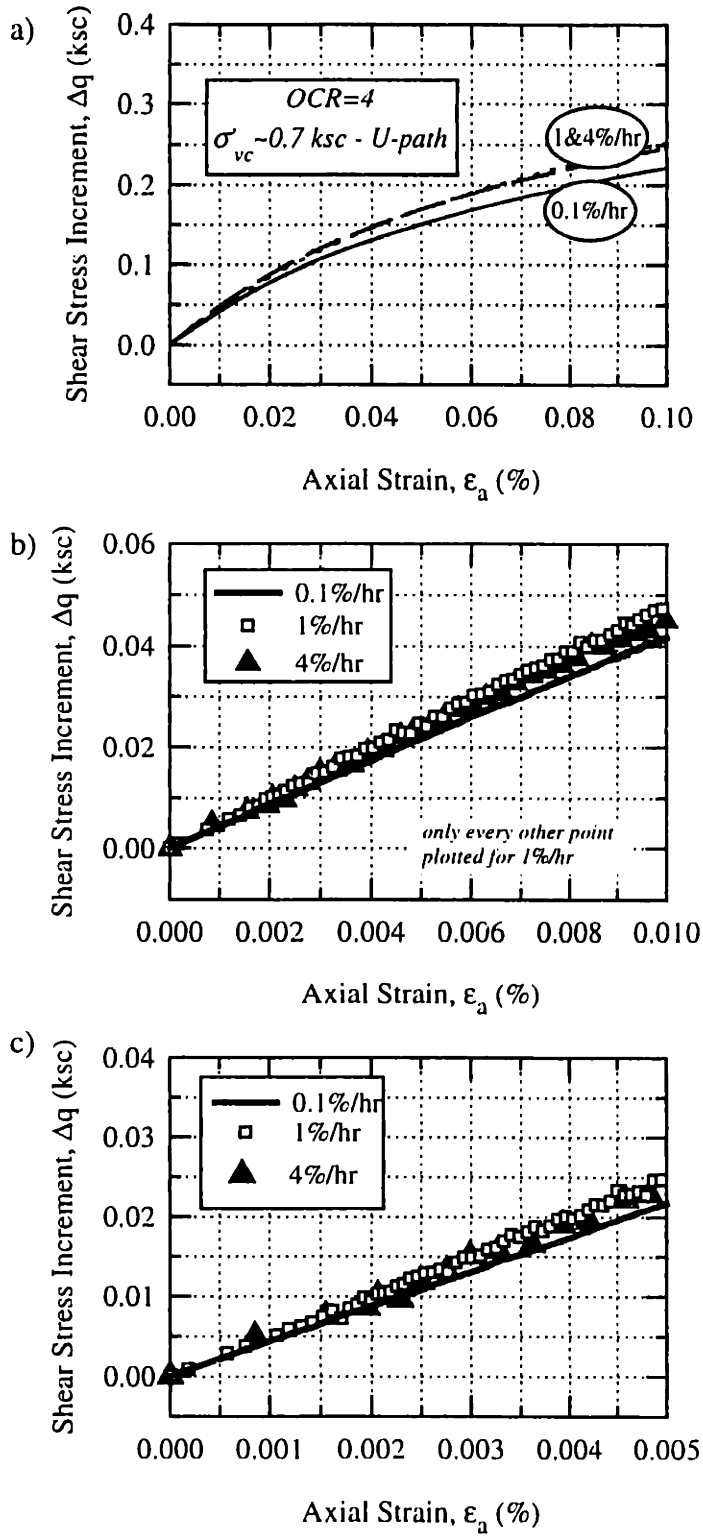


**Figure 6.71:** Effect of strain rate on the pre-failure stress-strain behavior of OCR4 RBBC at $\sigma'_{vc}$~0.7 ksc (U-Path) : a) 0-0.1%; b) 0-0.01%; c) 0-0.005%.

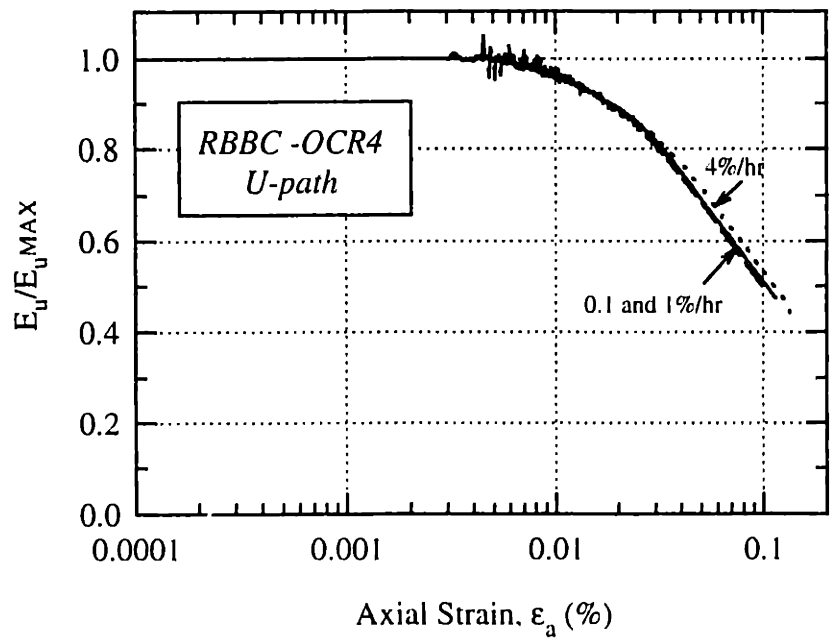


**Figure 6.72:** Effect of strain rate on stiffness degradation curve of OCR4 RBBC at $\sigma'_{vc}$~0.7 ksc (U-Path).

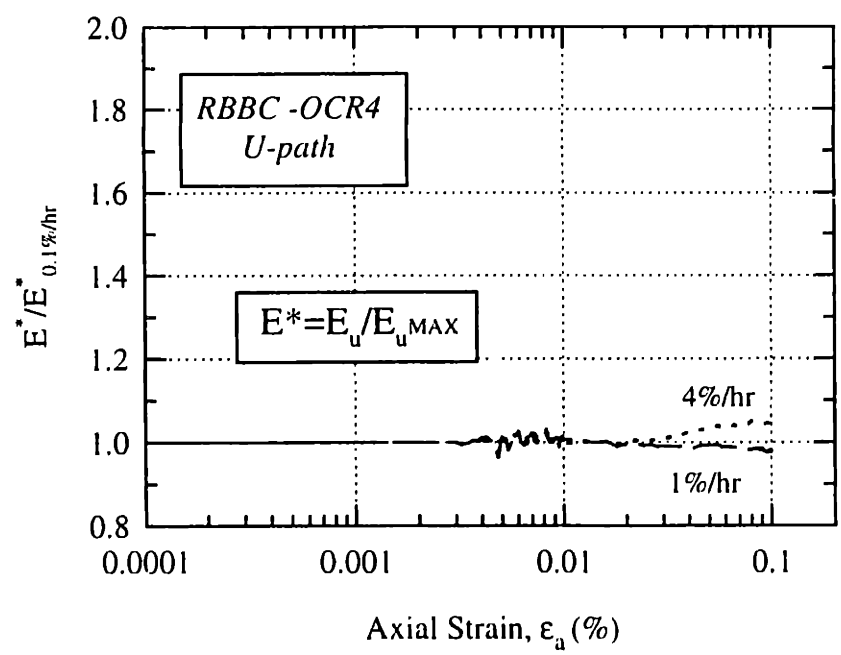


**Figure 6.73:** Change in normalized stiffness produced by an increase in strain rate (OCR4 RBBC- U-path).

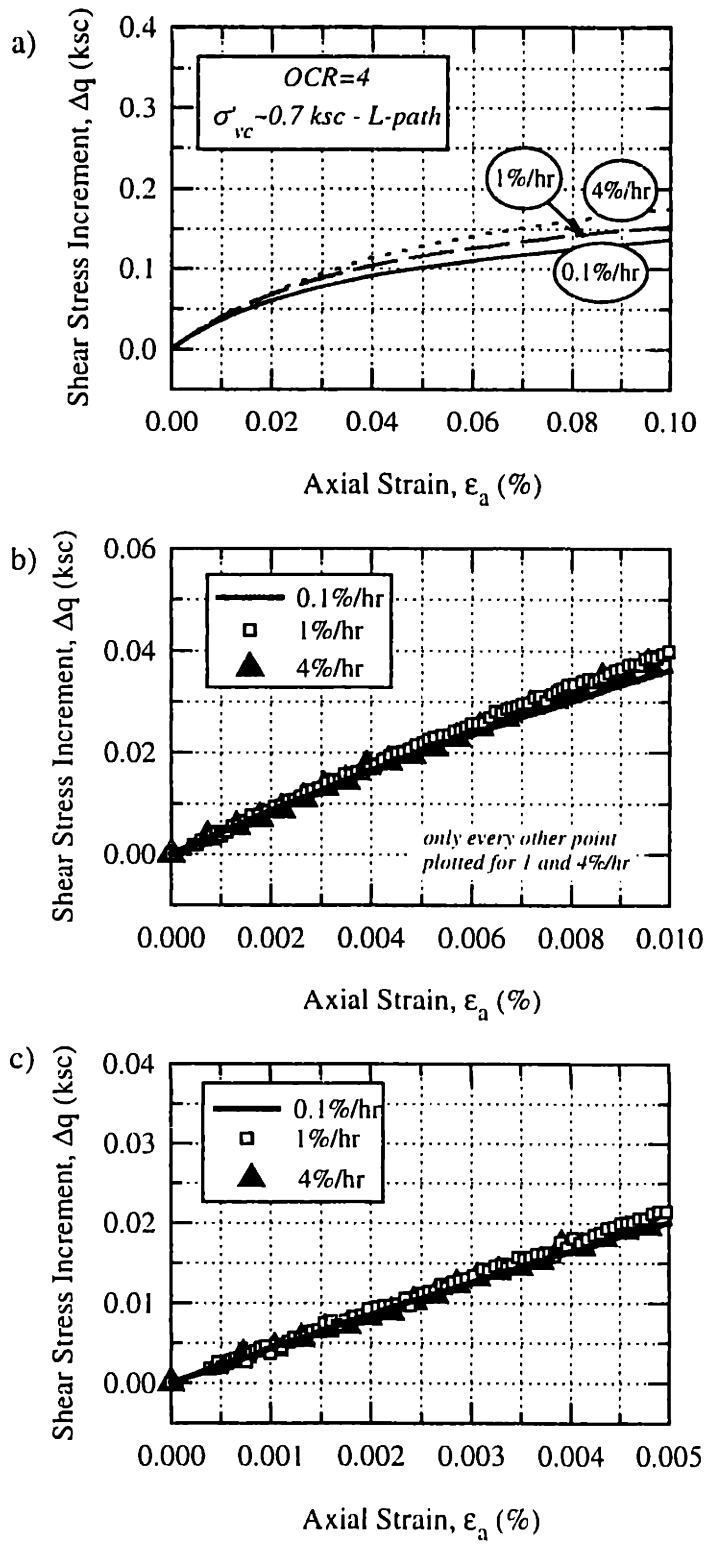


**Figure 6.74:** Effect of strain rate on the pre-failure stress-strain behavior of OCR4 RBBC at $\sigma'_{vc}$~0.7 ksc (L-Path) : a) 0-0.1%; b) 0-0.01%; c) 0-0.005%.

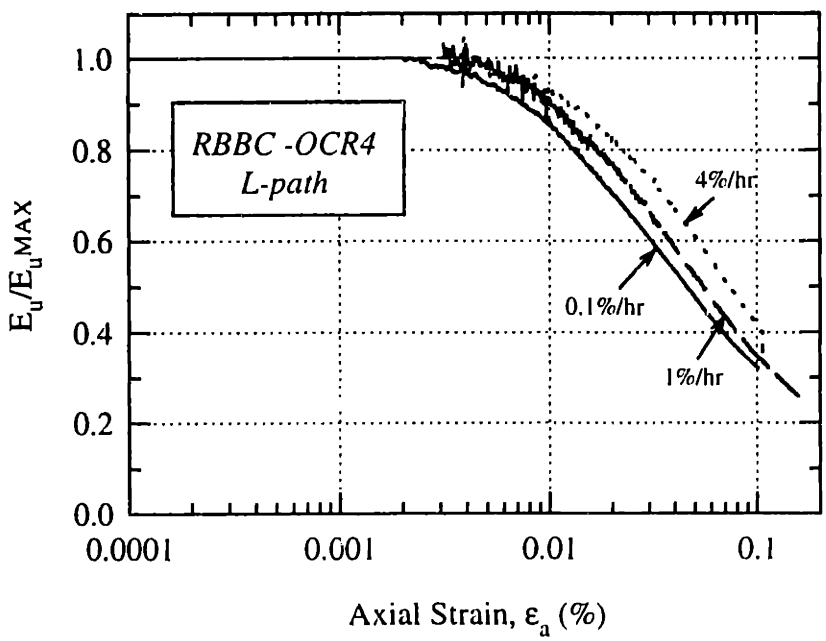


**Figure 6.75:** Effect of strain rate on stiffness degradation curve of OCR4 RBBC at $\sigma'_{vc}$~0.7 ksc (L-Path).

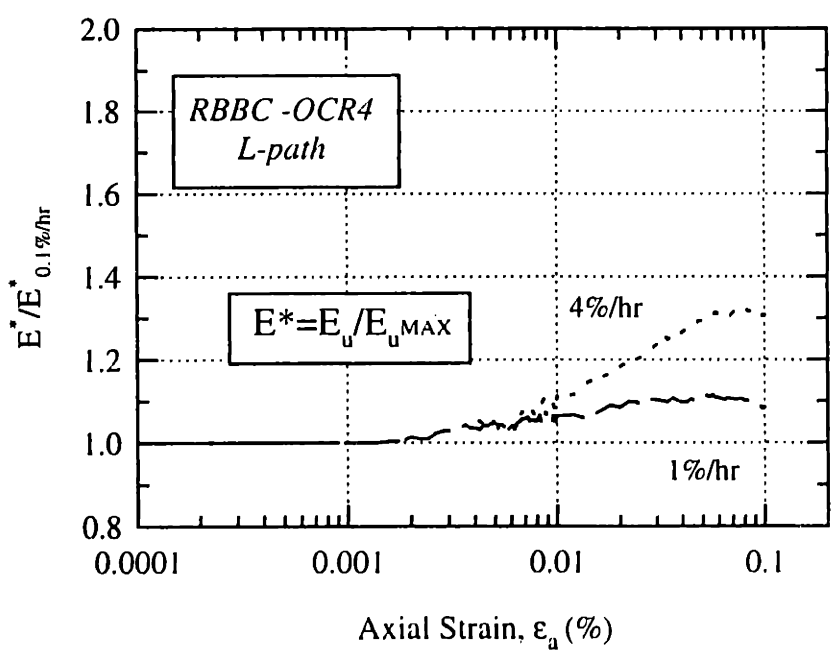


**Figure 6.76:** Change in normalized stiffness produced by an increase in strain rate (OCR4 RBBC- L-path).

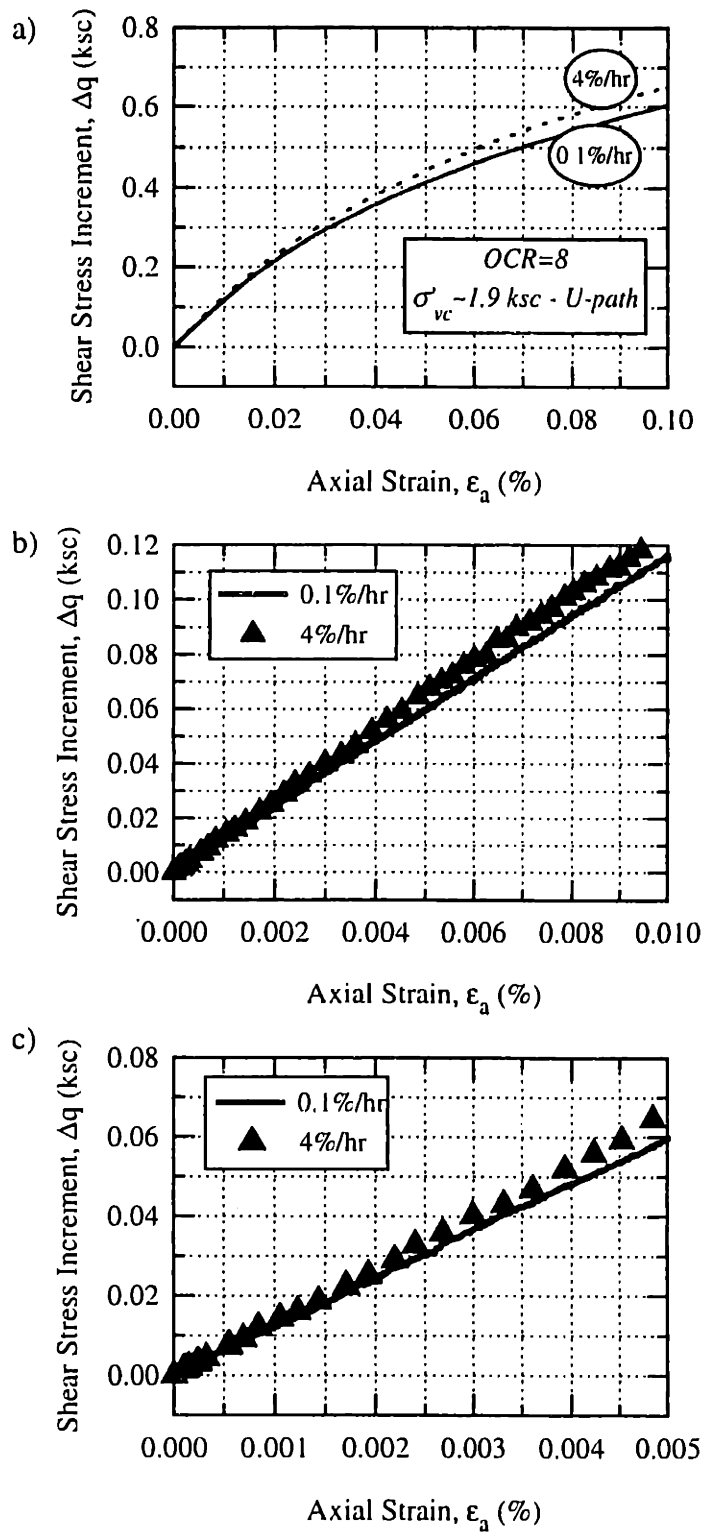


**Figure 6.77:** Effect of strain rate on the pre-failure stress-strain behavior of OCR8 RBBC at $\sigma'_{vc}$~1.9 ksc (U-Path) : a) 0-0.1%; b) 0-0.01%; c) 0-0.005%.

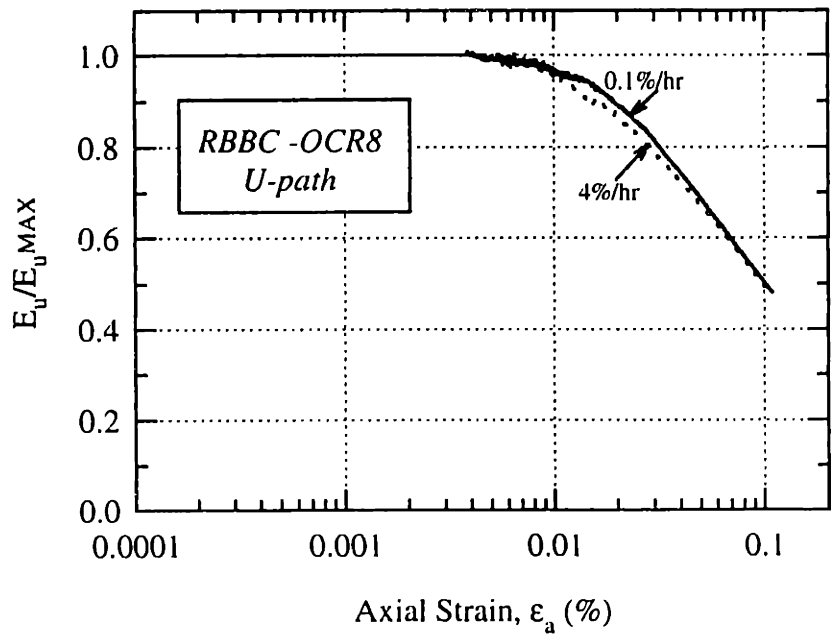


**Figure 6.78:** Effect of strain rate on stiffness degradation curve of OCR8 RBBC at $\sigma'_{vc}$~1.9 ksc (U-Path).

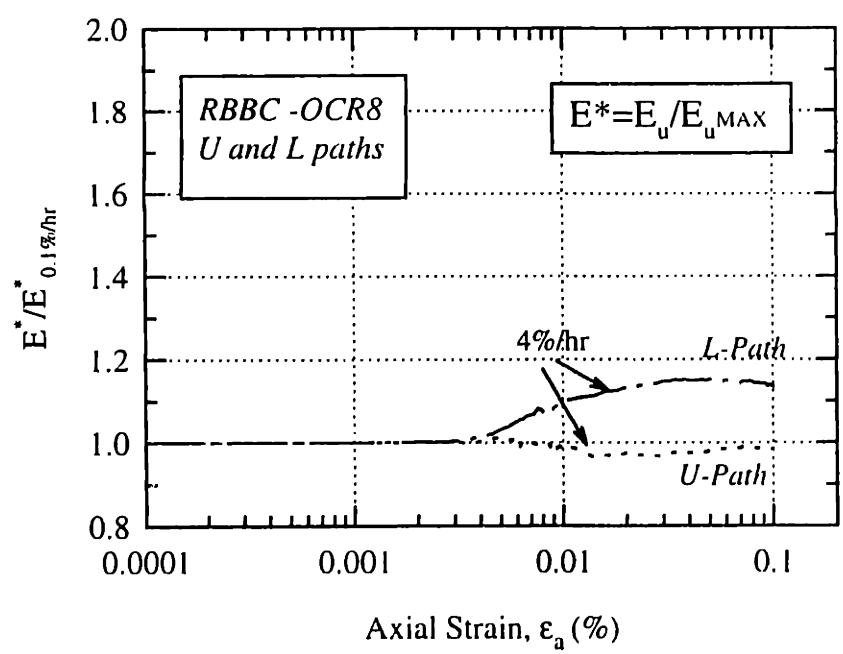


**Figure 6.79:** Change in normalized stiffness produced by an increase in strain rate (OCR8 RBBC- U-path).

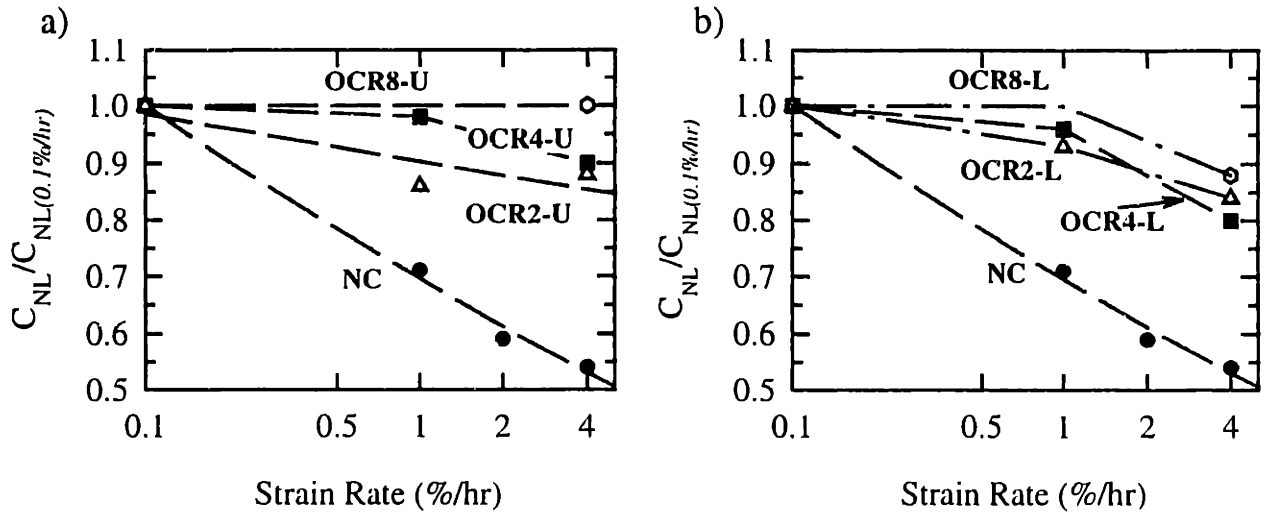


**Figure 6.80:** Variation in coefficient of non-linearity as a function of strain rate: a) unloading and b) loading tests on OC RBBC.

## 6.9 EFFECT OF LABORATORY AGING

As discussed in Chapter 5, the experimental program performed for this thesis included a limited investigation of the effects of prolonged laboratory aging on the pre-failure behavior of NC RBBC.

In the standard tests on NC RBBC the duration of laboratory aging, calculated from the time the specimen reaches the consolidation stress to the start of shear, ranged between 21 and 40 hours. Such variation in $t_{aging}$ was found to influence neither the initial stiffness nor the pre-failure non-linearity. This is demonstrated in Figures 6.81 a and b which plot the linear threshold $\varepsilon_{lin}$ and the coefficient of non-linearity $C_{NL}$ as a function of the duration of laboratory aging.

In tests *TX475S2* and *TX475S3* the pre-shear laboratory aging period was extended to approximately 11 days, corresponding to an additional cycle of secondary compression. Shear then occurred at the usual standard rate of 0.1%/hr.

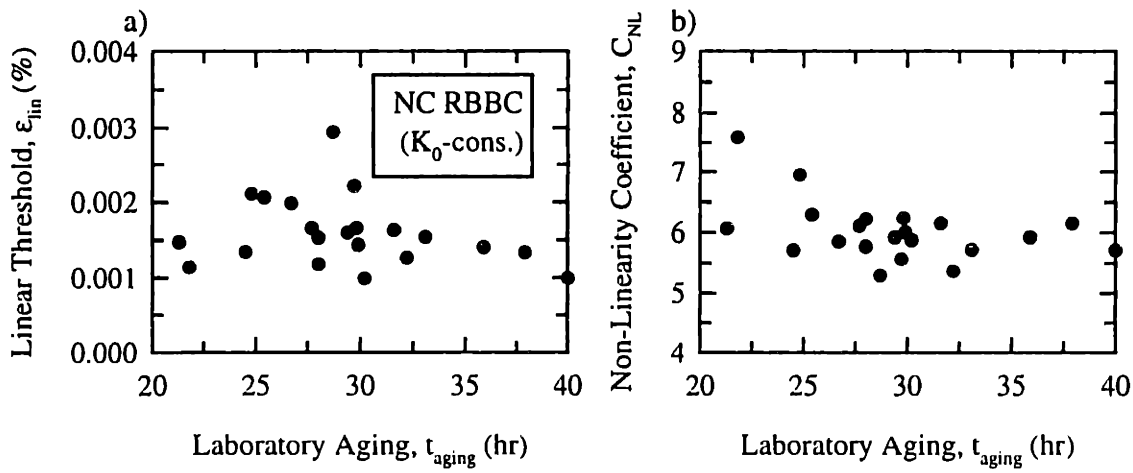


**Figure 6.81:** a) Linear threshold and b) non-linearity coefficient for NC RBBC as a function of small variations in the standard duration of aging.

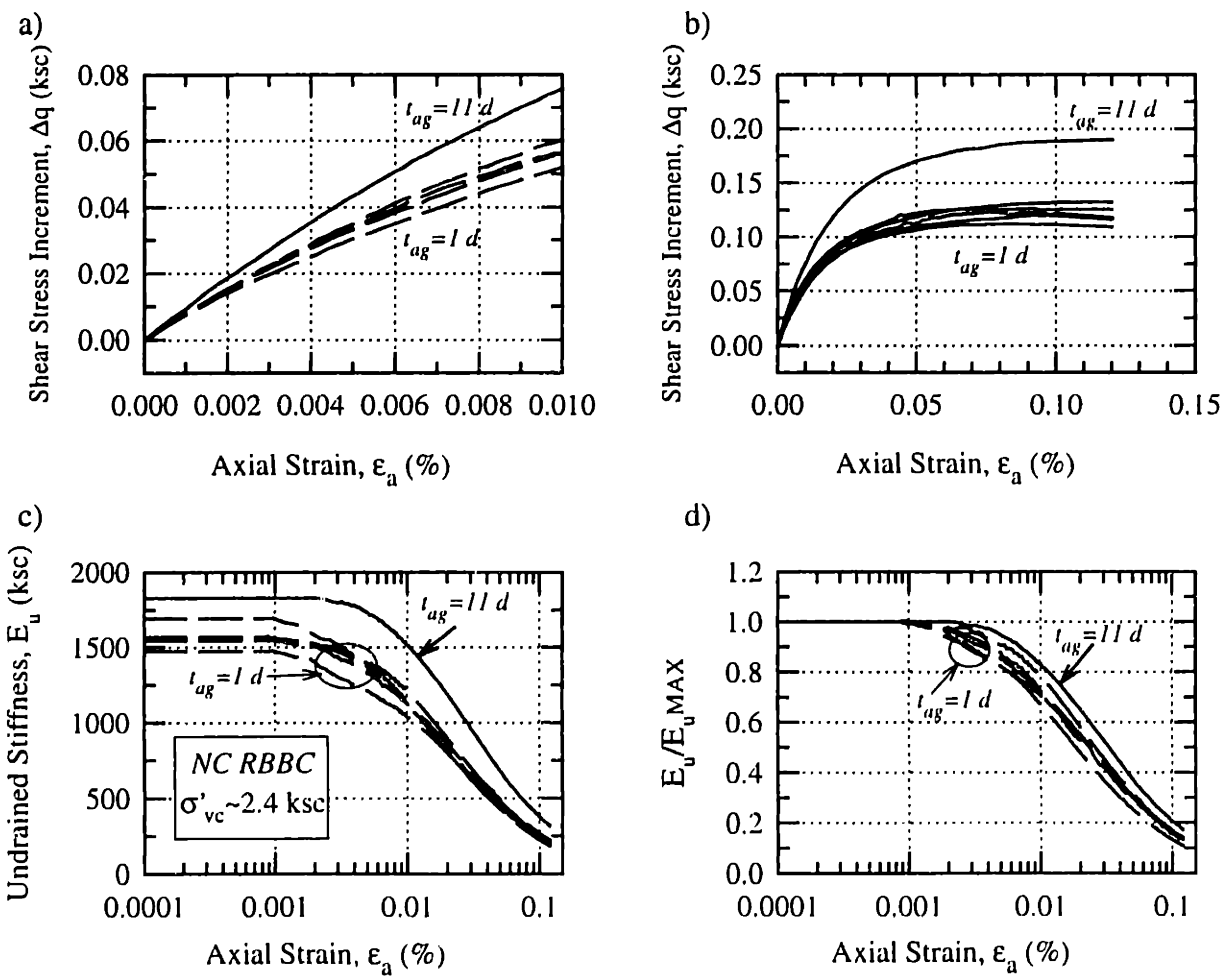


**Figure 6.82:** Effect of prolonged aging on the behavior of NC RBBC at $\sigma'_{vc}$~2.4 ksc: a-b) stress-strain curves; c-d) stiffness degradation curves.

Figures 6.82a-d show the stress-strain curves and the plots of stiffness and normalized stiffness ($E_u/E_{uMAX}$) versus axial strain for test *TX475S2*, alongside the results for five shears on NC RBBC at approximately the same vertical consolidation stress (~2.4 ksc), but with only the one day "standard" aging duration. A similar set of graphs for *TX475S3* and other three tests at a stress level of about 4 ksc are presented in Figures 6.83a-d.

Tables 6.19 and 6.20 summarize the pre-shear conditions and the initial stiffness results for these two sets of tests. The tables also include the initial void ratio of the specimens used.

| TEST | $\sigma'_{vc}$ (ksc) | K | e initial | e pre-shear | $t_{aging}$ (h) | $E_uMAX$ (ksc) | $\Delta E/E_{AVE}$ (%) |
|---|---|---|---|---|---|---|---|
| TX353S1 | 2.40 | 0.470 | 1.196 | 1.035 | 22 | 1691 | +7.9 |
| TX362S1 | 2.42 | 0.464 | 1.184 | 1.023 | 32 | 1542 | -1.6 |
| TX403S2 | 2.42 | 0.500 | 1.217 | 1.043 | 29 | 1560 | -0.5 |
| TX418S2 | 2.42 | 0.474 | 1.185 | 1.016 | 38 | 1474 | -5.9 |
| TX406S1 | 2.39 | 0.487 | 1.205 | 1.013 | 43 | 1569 | +0.1 |
| | | | | | | $E_{AVE}$=1567 | |
| **TX475S2** | **2.40** | **0.497** | **1.226** | **1.032** | **268** | **1827** | **+16.6** |

**Table 6.19:** Pre-shear conditions and initial stiffness results for tests performed at ~2.4 ksc ($t_{aging}$ = 1 and 11 days).

| TEST | $\sigma'_{vc}$ (ksc) | K | e initial | e pre-shear | $t_{aging}$ (h) | $E_uMAX$ (ksc) | $\Delta E/E_{AVE}$ (%) |
|---|---|---|---|---|---|---|---|
| TX362S3 | 3.91 | 0.470 | 1.184 | 0.950 | 28 | 2074 | +3.7 |
| TX418S4 | 4.04 | 0.475 | 1.185 | 0.938 | 30 | 1796 | -10.2 |
| TX422S2 | 4.14 | 0.489 | 1.171 | 0.925 | 28 | 2132 | -0.5 |
| | | | | | | $E_{AVE}$=2001 | 6.18a) |
| **TX475S3** | **3.87** | **0.507** | **1.226** | **0.961** | **276** | **2513** | **+25.6** |

**Table 6.20:** Pre-shear conditions and initial stiffness results for tests performed at ~4.0 ksc ($t_{aging}$ = 1 and 11 days).

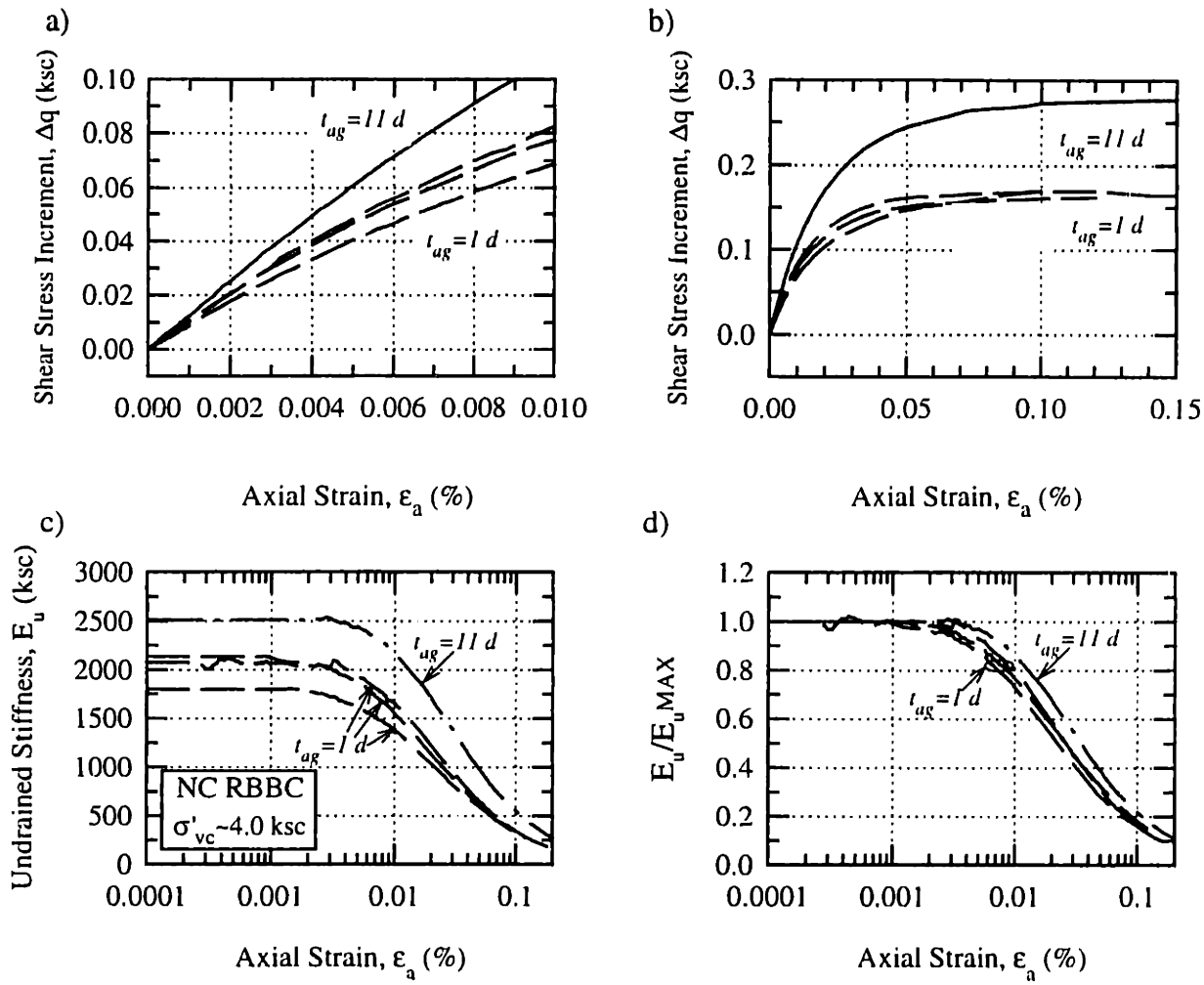


**Figure 6.83:** Effect of prolonged aging on the behavior of NC RBBC at $\sigma'_{vc}$ ~ 4.0 ksc: a-b) stress-strain curves; c-d) stiffness degradation curves.

Prolonged aging results in a significant increase in the initial stiffness compared to the standard tests at approximately the same stress level. This difference cannot be ascribed simply to a difference in void ratio. In the first place, due to differences in $e_{initial}$, there is no systematic variation of e with duration of laboratory aging.[23] In addition, Figure 6.84 shows that in the plot of $E_uMAX$ versus void ratio, the results for the "aged" specimens fall clearly above all the other data.

[23] As already mentioned, the last specimens tested, including *TX475*, all presented values of $e_{init}$ higher than those obtained from the rest of the batch.

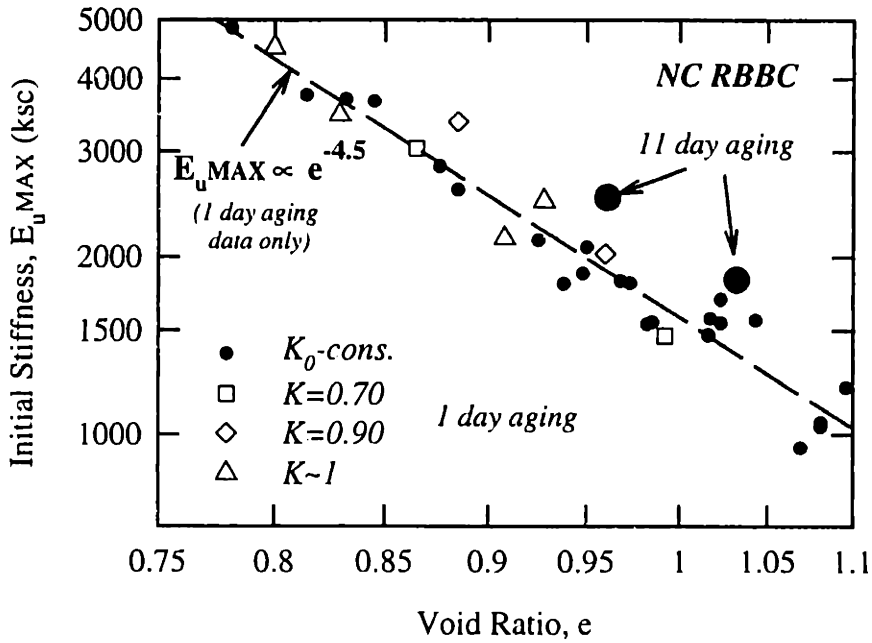


**Figure 6.84:** Relationship between maximum stiffness and void ratio for NC RBBC ($t_{aging}$=1 and 11 days).

The increase in initial stiffness caused by prolonged aging is quantified in Tables 6.19 and 6.20, using as a reference the value obtained by averaging the results at similar stress levels. More appropriately, perhaps, the variation can be determined using the regression line shown in Figure 6.84 as a reference. Using this approach, an equal increase in strength of 33% is found for both aged results. It should be mentioned that the void ratio of the specimen tested after prolonged aging (*TX475*) was significantly higher than the average value recorded for Batch 419. Thus, if instead of using the calculated value of *e* for test TX475, the average void ratio for the batch is used, the increase in strength caused by aging is reduced for both shears to 17%.

The stiffness of NC RBBC after prolonged aging is observed to be also greater than the value associated with the increased value of OCR resulting from the prolonged secondary compression phase. Based on the relationship provided by Mesri and Godlweski (1977) [24] it is

---

[24] $$\frac{\sigma'_p}{\sigma'_{vi}} = \left(\frac{t}{t_p}\right)^{\left(\frac{c_{\alpha E}}{CR}\right)\left(1-\frac{RR}{CR}\right)}$$

where $\sigma'_p$ is the preconsolidation pressure accounting for secondary compression, $\sigma'_{vi}$ is the consolidation stress at which secondary compression occurred, $t_p$ is the end of primary consolidation (here assumed to be 0.19h), $c_{\alpha E}$ is the

estimated that 11 days of aging correspond at most to an increase of the preconsolidation pressure of 1.1-1.12. However, the stiffness of NC RBBC following aging falls closer to values obtained for RBBC with OCR 1.5-2 (e.g. see Figures 6.18 a, and 6.20).

As shown in Figures 6.82 and 6.83, the prolonged time under constant stresses also leads to a modification in the shape of the stress-strain curve. The "aged soil" displays much more significant shear stress gain, and consequently stiffness, at all strain levels, and an increase in the undrained strength equal to approximately 6%. Once again, the curve of normalized stiffness is found to be independent of stress level and the two curves of ($E_u/E_{uMAX}$) versus strain for tests *TX475S2* and *TX475S3* differ, at all strain levels by less than 5%. Figure 6.85 plots the curve obtained by averaging these two results along with the reference curve for 24 hours of laboratory aging obtained in Section 6.3. The aged specimens display a large increase in the linear threshold, which goes from 0.0015% to 0.0037%, and a reduced non-linearity, as $C_{NL}$ decreases from 6.0 to 4.7.

Note that one test with intermediate value of the laboratory aging (~57 hours) was also performed (*TX406S2*: $\sigma'_{vc}$~3.30 ksc, e=0.969, $K_0$=0.50). The curve for this test is also included in Figure 6.85. Overall, it displays a shape extremely close to that of the "aged" specimens, slightly smaller $\varepsilon_{lin}$ (0.0027% vs. 0.0037) and marginally greater $C_{NL}$ (4.9 vs. 4.7). However the value of the initial stiffness ($E_{uMAX}$=1801 ksc) for this shear falls perfectly in the middle range of the values measured in other tests, at the same stress level or void ratio (e.g. see Figure 6.7c). This suggests that the shape of the stiffness degradation curve is more sensitive to the pre-shear aging, while the value of the initial stiffness is modified only for large increases in the aging period.

Figures 6.86a and b summarize the results presented so far, by plotting the linear threshold and the coefficient of non-linearity versus the duration of laboratory aging. In addition, Figure 6.87 plots the ratio of the normalized stiffness of the "aged" specimen to that obtained from the reference curve for 1 day aging, as a function of strain level. Once again it is observed that the sensitivity of the soil to the pre-shear conditions increases with strain level. Note that, as already evident in Figure 6.85, no significant difference is observed between the effect of the 2.4 day and the 11 day aging duration on the increase of the normalized stiffness. In

---

coefficient of secondary compression, CR is the compression ratio, RR is the compression ratio (for RBBC $c_{\alpha\varepsilon}$/CR =0.017, and CR/RR=0.1, based on Cauble 1993).

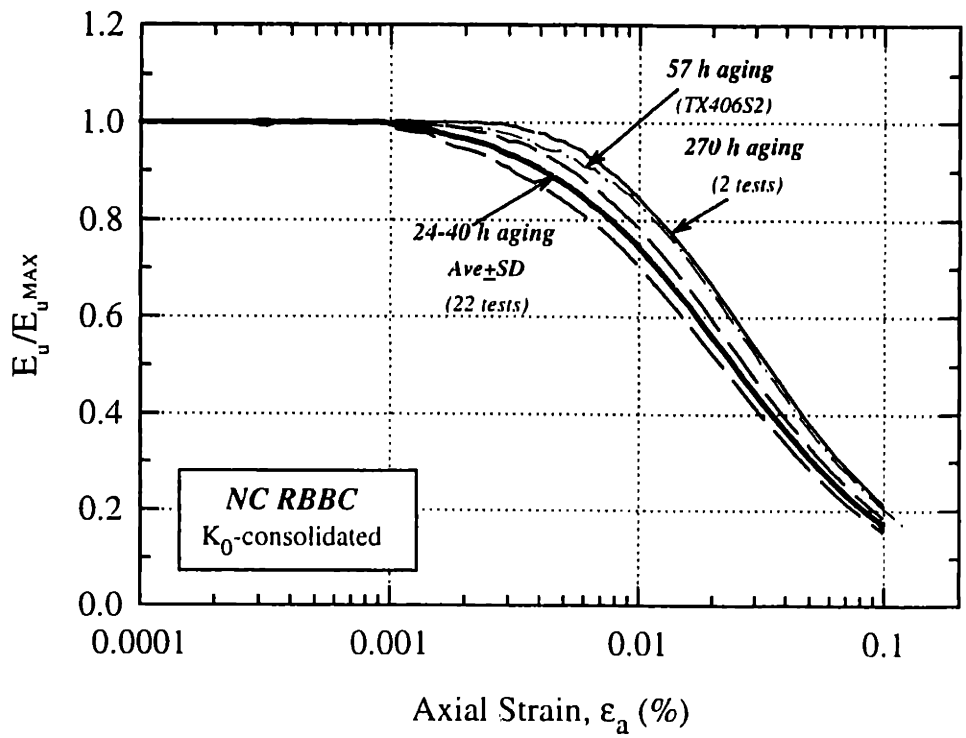


**Figure 6.85:** Average stiffness degradation curves for different durations of laboratory aging.

both cases, for example the increase is approximately 20% at 0.1% axial strain. The figure also indicates that the sensitivity of the soil to preshear aging reaches a maximum at approximately 0.05% strain, where the ratio of $E^*_{aged}/E^*_{ref}$ reaches a virtually constant value.

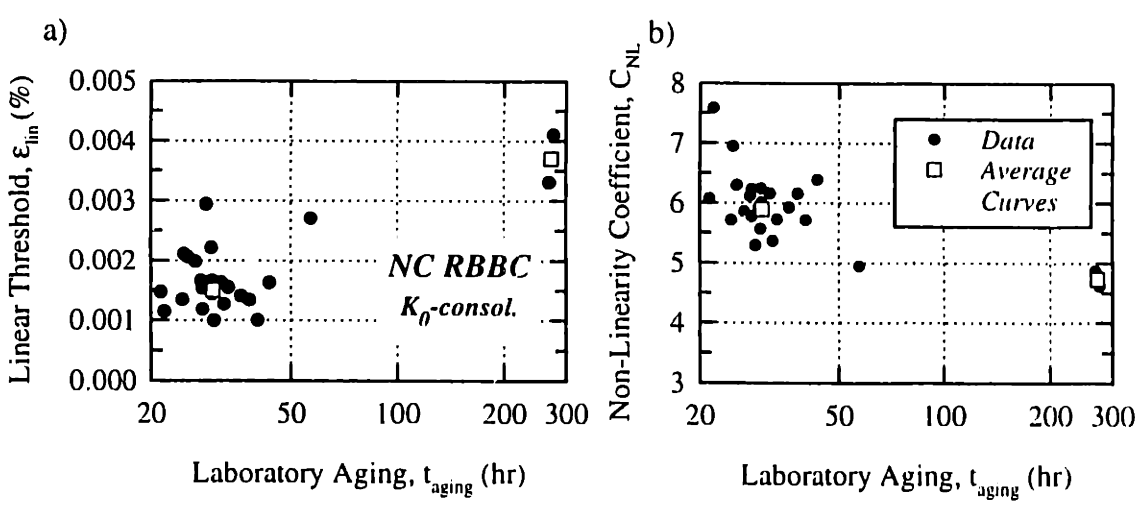


**Figure 6.86:** Variation of the a) linear threshold and the b) coefficient of non-linearity of NC RBBC as a function of aging duration.

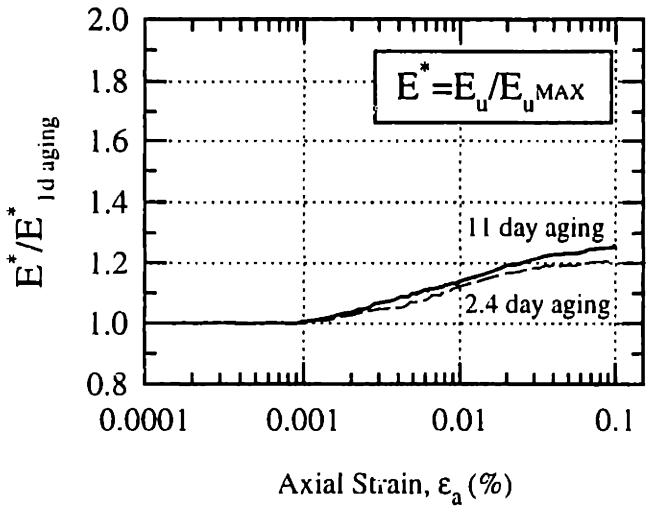


**Figure 6.87:** Increase in the normalized stiffness of NC RBBC produced by prolonged aging.

In two of the tests performed on hydrostatically consolidated specimens (*TX363S1* and *TX363S2*, see Table 6.6), the pre-shear laboratory aging period also extended past the standard "24 hours", to 62 and 93 hours respectively. Despite the difference in aging and stress level, these two tests present overlapping stiffness degradation curves. The average of these two curves is shown in Figure 6.88a, alongside the curve derived by averaging the two results (*TX427S1* and *TX427S1*) obtained after the standard aging period (*24* and *32* hours, respectively). As seen for the $K_0$-consolidated soil, also for the hydrostatically consolidated soil the increase in aging time (from 25-32 hours to 62-93 hours) results in a larger linear region ($\varepsilon_{lin}$ goes from 0.0064% to 0.0084%) and in an increase in $E_u/E_{uMAX}$ at all strains. This increase is quantified in Figure 6.88b by plotting the ratio of the normalized stiffness after prolonged aging to the value obtained from the standard aging curve. The figure indicates that for the increase in $E_u/E_{uMAX}$ is at most 10%, half of that measured in the case of the $K_0$-consolidated soil. Note that the limited increase in laboratory (up to 93 hours) does not appear to have any effect on the initial stiffness results for tests *TX363S1* and *TX363S2*. Once normalized to account for the differences in void ratio, these data fall on the same band as all the other tests on NC RBBC (see Figure 6.31a).

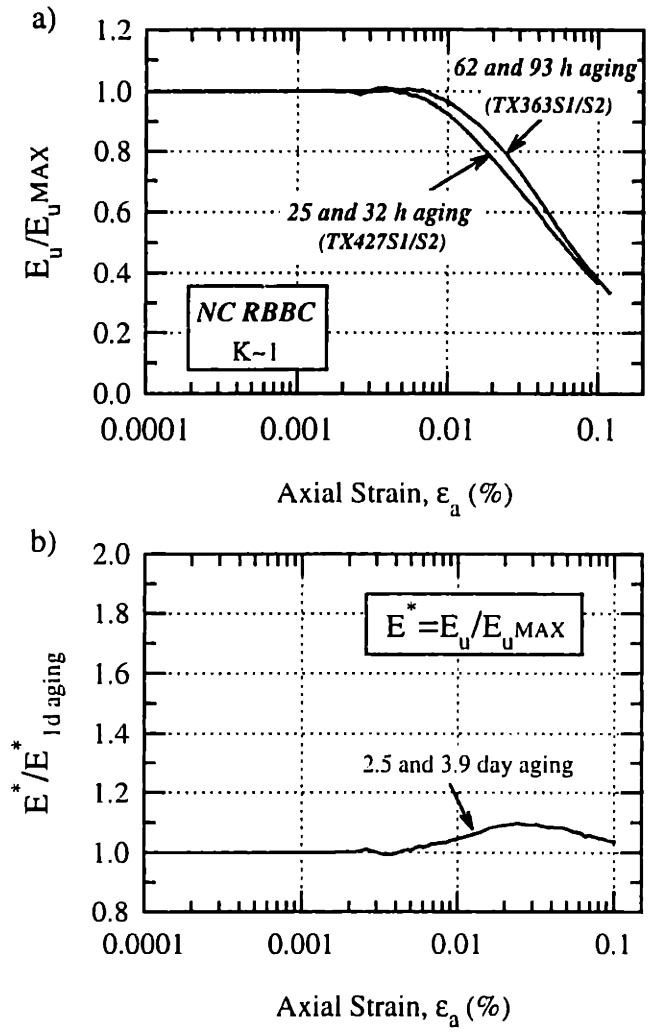


**Figure 6.88:** a) Modification of the stiffness degradation curve and b) increase in the normalized stiffness of hydrostatically consolidated NC RBBC, due to prolonged laboratory aging.

## 6.10 REFERENCES


1. Bishop, A.W. and Henkel, D.J. (1962), **The Measurement of Soil Properties in the Triaxial Test**, 2nd Ed. Edward Arnold Ltd., London.

2. Force, E.A. (1998), "Factors Affecting Pore Pressure Generation During $K_0$-Consolidation of Laboratory Tests," S.M. Thesis, Department of Civil and Environmental Engineering, MIT, Cambridge, MA, 166 p.

3. Jamiolkowski, M., Lancellotta, R., and Lo Presti, D.C.F. (1994), "Remarks on the Stiffness at Small Strains of Six Italian Clays", *Proc. Int. Symp. Pre-Failure Deformation Characteristics of Geomaterials*, Hokkaido'94, Vol. 2, pp. 817-854.

4. Lo Presti, D.C.F. (1989), "Proprieta' Dinamiche dei Terreni," *XIV Conferenza Geotecnica di Torino*, Politecnico di Torino (in Italian).

5. Mesri, G. and Golewski, P. M. (1977), "Time- and Stress-Compressibility Interrelationship," ***Journal of the Geotechnical Engineering Division***, ASCE, 103 (GT5), May, pp. 417-425.

6. Pestana, J.M. (1994), "A Unified Constitutive Model for Clays and Sands," Sc.D. Thesis, Department of Civil and Environmental Engineering, MIT, Cambridge, MA, 473 p.

7. Santagata, M.C. (1994), "Investigation of Sample Disturbance in Soft Clays Using Triaxial Element Tests," S.M. Thesis, Department of Civil and Environmental Engineering, MIT, Cambridge, MA, p. 289.

8. Schmertmann, J.H. (1991), The Mechanical Aging of Soils, (25th Terzaghi Lecture), ASCE ***Journal of Geotechnical Engineering***, 117 (9), September, pp.1288-1329.

9. Sheahan, T.C. (1991), "An Experimental Study of the Time-Dependent Undrained Shear Behavior of Resedimented Clay Using Automated Stress-Path Triaxial Equipment," Sc.D. Thesis, Department of Civil and Environmental Engineering, MIT, Cambridge, MA, 955 p.

10. Trudeau, P.J., Whitman, R.V. and Christian, J.T. (1974), "Shear wave Velocity and Modulus of a Marine Clay," ***Journal of the Boston Society of Civil Engineers***, 61 (1), pp.12-25.

# CHAPTER 7

# INTERPRETATION OF RESULTS

## 7.1 INTRODUCTION

The previous chapter presented the effects of the six variables investigated (stress level, OCR, lateral stress ratio, pre-shear stress path, strain rate and laboratory aging) on the pre-failure behavior of RBBC. The objective of this chapter is to synthesize these results, to assess the relative significance of the variables and, to build a qualitative framework that describes the stiffness of RBBC and compares the observed behavior to findings in the literature.

Overall, as done in Chapter 6, one can divide the small strain behavior into its two components: the magnitude of the initial stiffness, and the stiffness degradation behavior, i.e. the degree of non-linearity. The curve of $E_u$ versus axial strain can be thought of as the "product" of the initial stiffness, $E_{u}MAX$, times the curve of $E_u/E_{u}MAX$ versus strain. The initial stiffness provides the absolute scale, while the curve describes the decrease in stiffness with increasing strain, i.e. the stiffness degradation behavior. Any particular variable may affect one, or both of these components of the behavior. For example, it was shown in Section 6.3 that an increase in stress level, without any change in OCR, leads to an increase in stiffness but without modification of the stiffness degradation curve. On the other hand, a higher strain rate (Section 6.8) is reflected only in a different shape of the stiffness degradation curve, but in no change in the initial stiffness.

This type of interpretative framework, in which the absolute magnitude of the stiffness is examined independently of the stiffness degradation behavior, is useful for two reasons. In the first place it allows easy comparison of the effects of the various variables examined in a fairly straightforward manner. Secondly, it facilitates understanding of the mechanisms underlying the observed behavior. It should be recognized, however, that both components are complimentary and must be considered simultaneously to obtain a complete understanding of the overall stiffness behavior.

Figure 7.1 schematically summarizes the main findings obtained from the analysis of the results presented in Chapter 6. The solid line in both illustrations represents a typical curve of secant stiffness versus logarithm of strain for the reference case (OCR=1, $K_c$~$K_0$, $t_{aging}$=1day, dε/dt=0.1%/hr). The two dashed curves show the general influence of the studied parameters on the two framework components. The figure on the left illustrates that the stiffness curve is generally shifted upwards with reductions in void ratio (deriving from increased $\sigma'_{vc}$, or increased K), increasing aging, and increasing OCR (under conditions of equal consolidation stress). The figure on the right illustrates that the stiffness degradation curve is influenced by changes in the pre-shear stress path, and that the non-linearity decreases with increasing OCR, strain rate, aging, and lateral stress ratio.

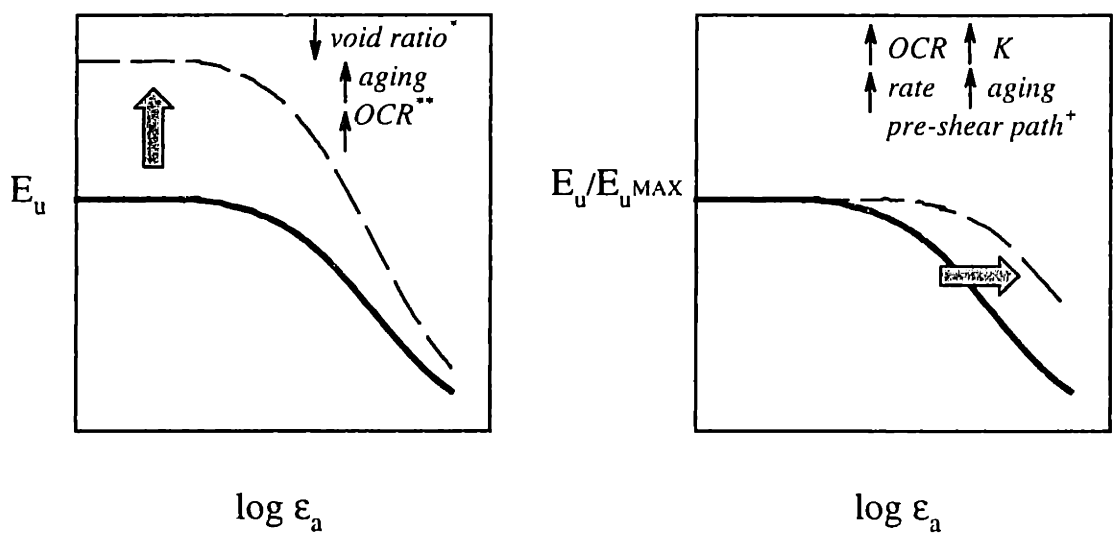


* At a given OCR, the influence of certain variables on the initial stiffness can be related to their effect on the pre-shear void ratio.

** Under conditions of equal consolidation stress.

**

\+ Paths involving unloading of the vertical stress lead to reduced non-linearity.

**Figure 7.1:** Schematic of the parameters affecting the initial stiffness and the stiffness degradation behavior of cohesive soils.

The chapter is organized in a manner that highlights the two aspects of the stiffness behavior outlined above. In Section 7.2 the analysis focuses on the initial stiffness results. The chapter then goes on to analyze the stiffness degradation behavior in Section 7.3.

## 7.2 INITIAL STIFFNESS

Figure 7.2a presents a log-log plot of the initial stiffness of NC RBBC versus the pre-shear void ratio. As shown in Chapter 6, the initial stiffness, or $E_{u}MAX$, is defined as the maximum value of secant stiffness attained in the initial linear region of the stress-strain curve. The figure includes the results of all the shears performed on the NC soil, employing strain rates equal to or greater than 0.1%/hr, after one day of pre-shear aging. The figure establishes the existence of a unique relationship between the initial stiffness of NC RBBC and the pre-shear void ratio. This relationship is independent of the initial shear stress acting on the specimen (i.e. $K_c$), of the strain rate used, at least in the range 0.1-4%/hr, and of the path followed prior to shear. It indicates that in the case of NC RBBC the variation of stiffness resulting from changes in any of the testing conditions (with the exception of laboratory aging) can be explained in terms of differences in the pre-shear void ratio. Note that the figure presents two regression lines: one (thin solid line) drawn exclusively through the data (22 tests) obtained for "standard" testing conditions ($K_0$-consolidation, 1 day aging, 0.1%/hr rate), the other (heavy dashed line) through the entire data set. The two lines are virtually coincident, indicating that the changes in test conditions associated with the non standard tests have no influence on the relationship between initial stiffness and void ratio, which has the form $E_{u}MAX \propto e^{-x}$. For NC RBBC the exponent, x, is equal to 4.6.[1]

This relationship can also be represented in terms of consolidation stress. As indicated in Figure 7.2b, normalization by the vertical consolidation stress *alone* (i.e., $E_{u}MAX \propto \sigma'_{vc}{}^{n}$) is not equally effective. In particular, the data for the specimens consolidated at constant K greater than $K_0$ display a higher stiffness for a given value of $\sigma'_{vc}$, compared to the results for $K_0$-consolidated NC RBBC. This clearly shows that the specimen void ratio or density is an important factor.

[1] The slight variation of x with respect to values reported in Chapter 6 arise from the fact that for the first time all the data for NC RBBC is compiled together in this figure.

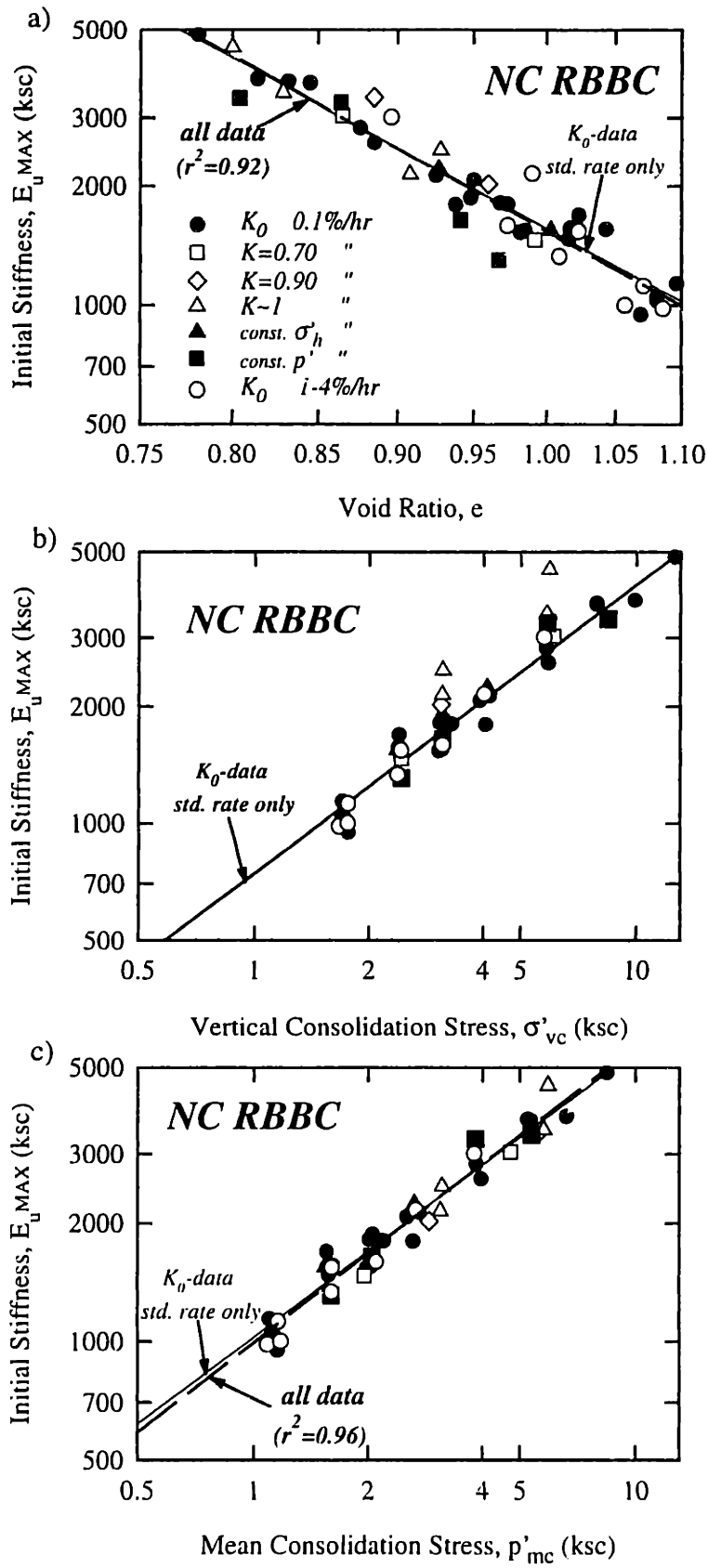


**Figure 7.2:** Relationship between initial stiffness and a) void ratio, b) vertical consolidation stress and c) mean consolidation stress (NC RBBC).

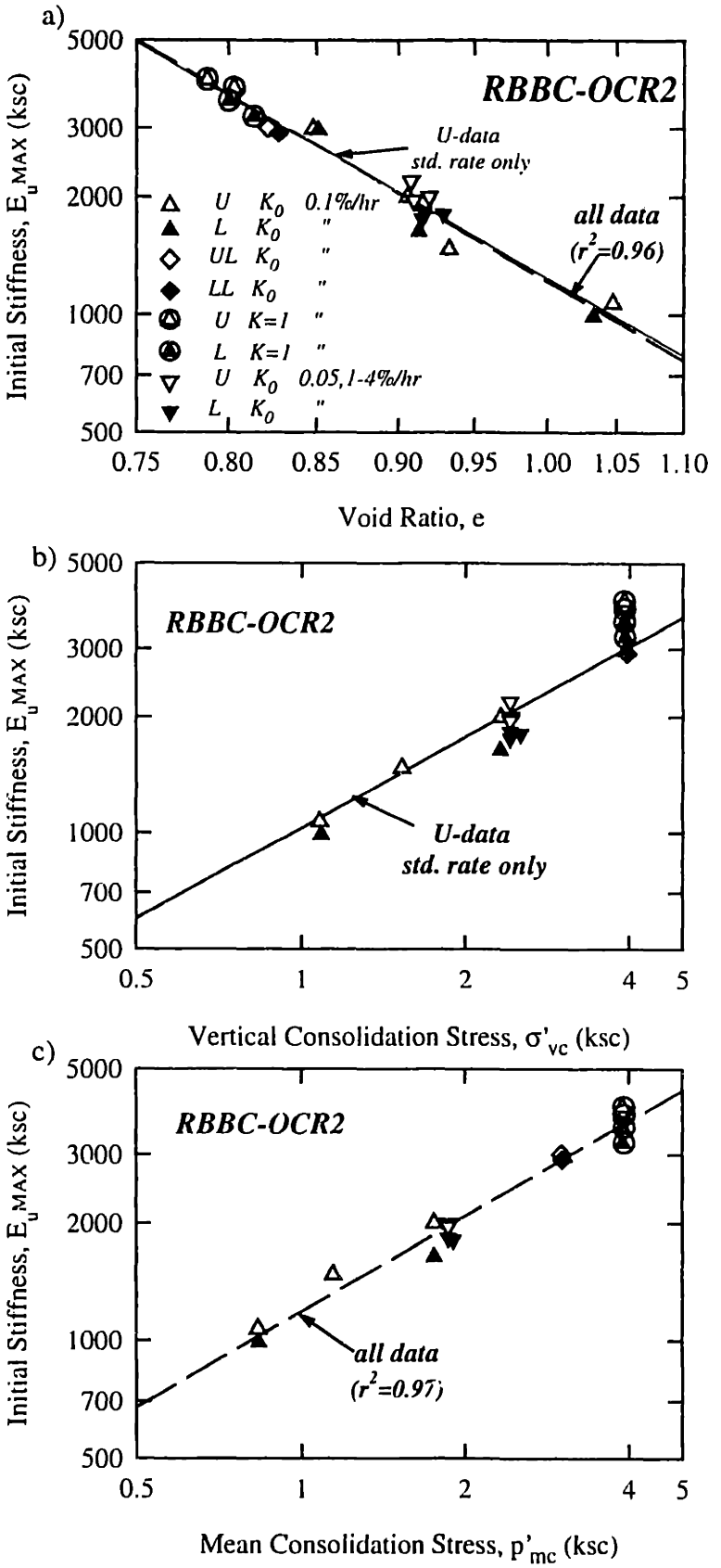


**Figure 7.3:** Relationship between initial stiffness and a) void ratio, b) vertical consolidation stress and c) mean consolidation stress (OCR2 RBBC).

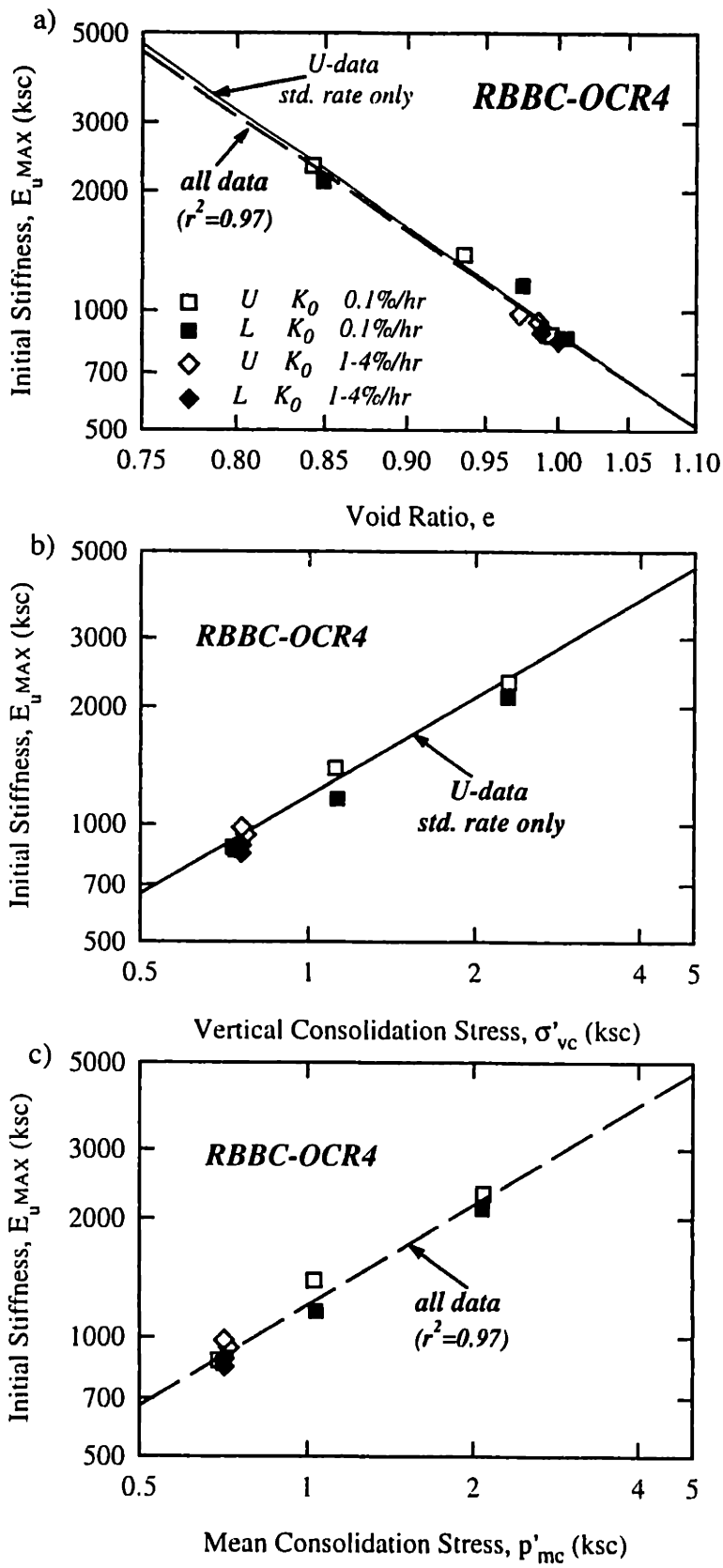


**Figure 7.4:** Relationship between initial stiffness and a) void ratio, b) vertical consolidation stress and c) mean consolidation stress (OCR4 RBBC).

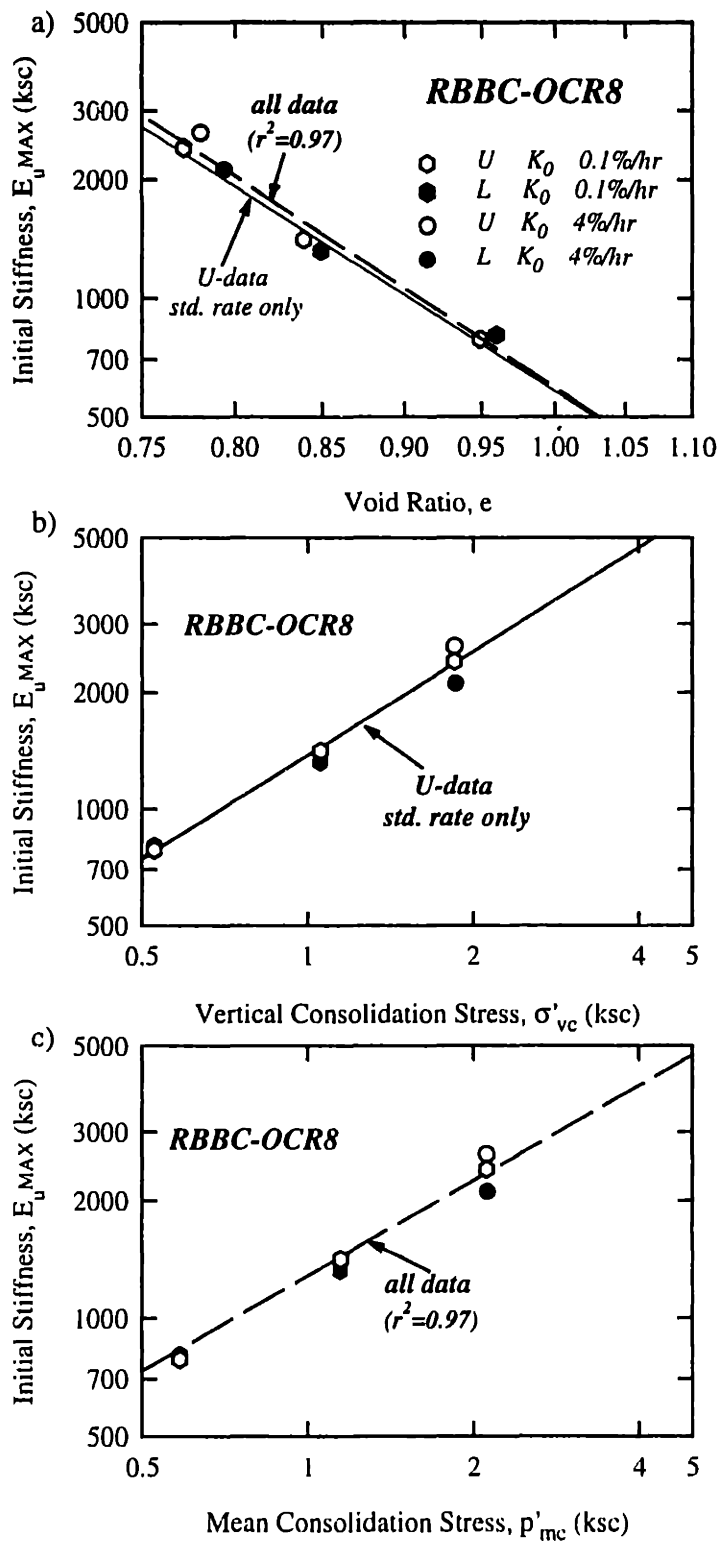


**Figure 7.5:** Relationship between initial stiffness and a) void ratio, b) vertical consolidation stress and c) mean consolidation stress (OCR8 RBBC).

For NC RBBC, the stress level dependency of the initial stiffness may be more accurately represented in terms of the mean consolidation stress, $p'_{mc}$. In fact, as there exists a unique relationship between void ratio and mean effective stress for NC RBBC (i.e. $\log p'_{mc} \propto \log e$ ) the correlation between $e$ and $E_u MAX$ translates into an analogous one between $E_u MAX$ and $p'_{mc}$ ($E_u MAX \propto p'_{mc}{}^n$ Figure 7.2c). The tighter band formed by the $E_u MAX$-$p'_{mc}$ data, compared to the $E_u MAX$-e results, stems from the greater accuracy with which stresses are measured compared to void ratios, and is thus not believed to reflect any inherently improved correlation.

Similar graphs to those examined above are presented in Figures 7.3-7.5 for RBBC with OCR of 2, 4 and 8. These also summarize the complete data set for each OCR. They indicate that the observations presented above for NC RBBC, can be extended to the overconsolidated soil (for OCR2 rate insensitivity is verified in range 0.05-4%/hr). As shown in Figures 7.3a, 7.4a and 7.5a, for a given OCR, the initial stiffness shows a consistent trend with the pre-shear void ratio. Note that a slight difference in the slopes of the regression lines through each set of data is observed, with the NC (x=4.6) and the OCR2 (x=4.9) data displaying a marginally reduced dependence compared to OCR 4 and OCR 8 RBBC (x=5.7 and 5.5, respectively).

Figure 7.6 compiles the data for all values of OCR examined on one plot of stiffness versus void ratio. The data for the different OCR's fall on distinct bands with the initial stiffness at a given void ratio increasing with decreasing OCR. The regression lines through each set of data show a trend of decreasing slope with decreasing OCR (the steeper slope of the line for OCR4 RBBC is likely a byproduct of the limited data at low void ratios). Figure 7.6 indicates that an additional variable is required to account for the variation of the stiffness at a given void ratio with OCR.

Figure 7.7 provides plots of $E_u MAX$ versus mean consolidation stress for all values of OCR. As a result of the relationships existing between e and log $p'_{mc}$, and between $K_0$ and $p'_{mc}$ for each OCR[2], all the OC data fall within a fairly narrow band, distinct from the NC results.

This figure suggests that a common trend between the initial stiffness results for all OCR's can be established if both the dependence of $E_u MAX$ on void ratio and on vertical consolidation stress are accounted for (constant values of $p'_{mc}$ involve changes in both e and $\sigma'_{vc}$).

[2] $\log e \sim 0.168 \log p'_{mc}$, for all OCR's; $(K_0)_{OC} = 0.48\ OCR^{0.43}$.

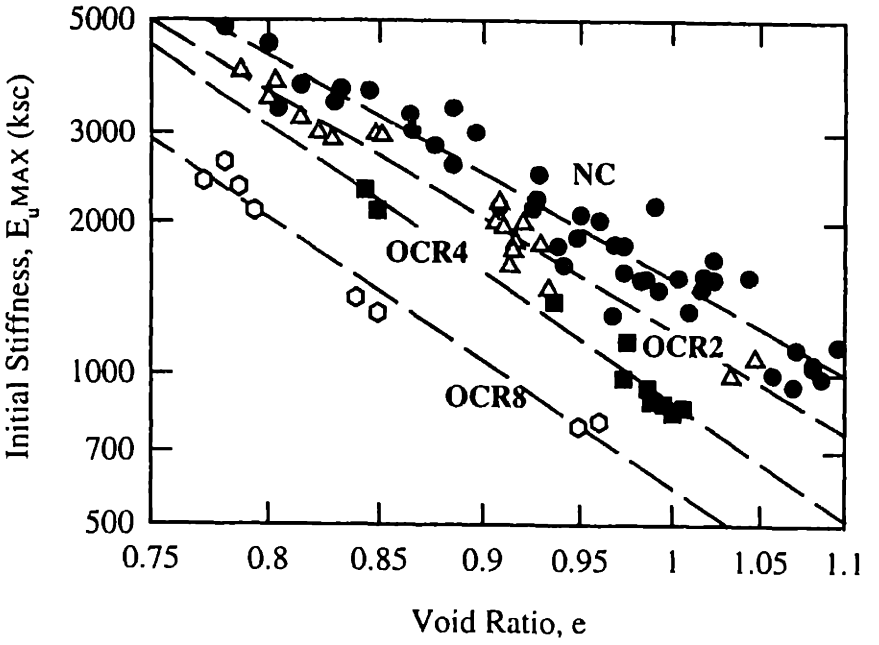


**Figure 7.6:** Relationship between initial stiffness and void ratio (OCR 1, 2, 4, 8 RBBC).

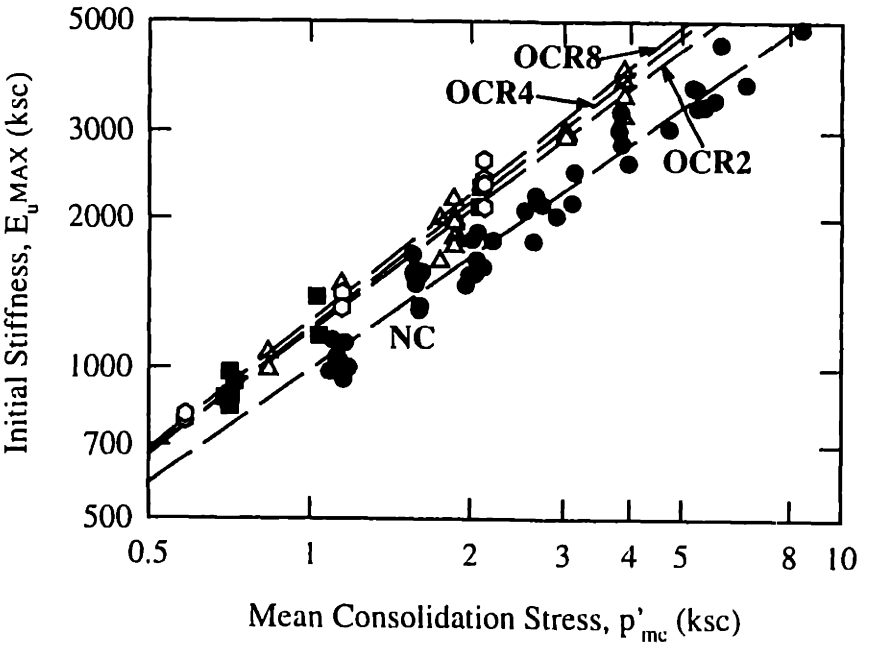


**Figure 7.7:** Relationship between initial stiffness and mean consolidation stress (OCR 1, 2, 4, 8 RBBC).

Based on the observed exponential relationships between $E_{u}MAX$ and void ratio, and $E_{u}MAX$ and vertical consolidation stress, it is hypothesized that an equation of the form $E_{u}MAX=Ae^{-x}\sigma'_{vc}{}^{n}$ can be used to link initial stiffness to e and $\sigma'_{vc}$, as observed by other researchers (e.g., Jamiokowski et al. 1994). As shown in Figure 7.8, a best fit of the data for RBBC with OCR1-8 yields the following equation:

$$E_{uMAX} = 1014 \cdot e^{-2.45} \cdot \sigma'^{0.43}_{vc} (ksc) \qquad \textit{Equation 7.1}$$

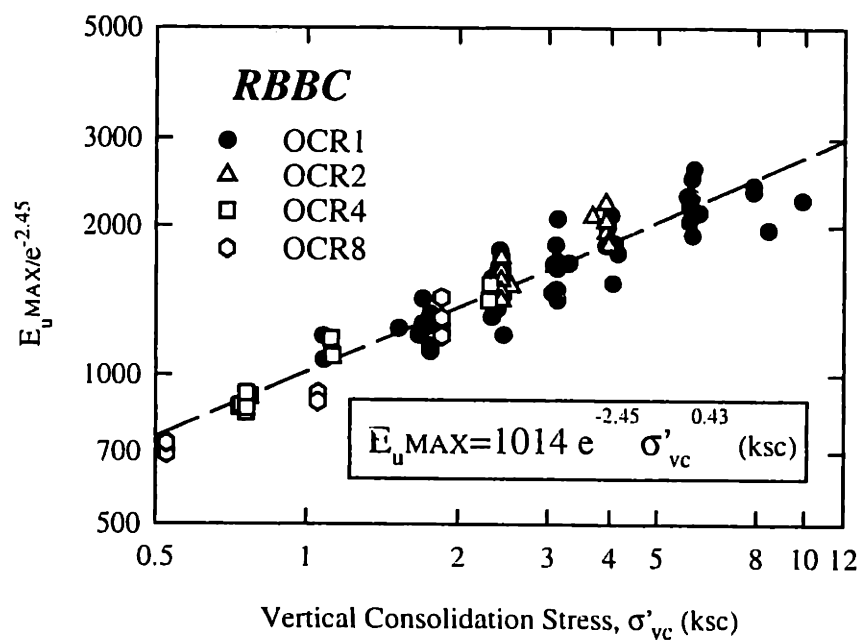


**Figure 7.8:** Relationship linking the initial stiffness of RBBC to void ratio and consolidation stress level for OCR 1, 2, 4 and 8.

While the stress level exponent determined for RBBC is in agreement with values reported for a variety of cohesive soils (see Table 2.3), the void ratio exponent is significantly higher.

Specific to OC RBBC is a small but clear influence of the pre-shear stress path on the initial stiffness. Close analysis of pairs of unloading and loading results (see for example Table 6.16) indicates a consistent trend of marginally higher values of the initial stiffness in the unloading tests, compared to the loading tests, even after accounting for differences in the pre-shear void ratio. In general this behavior is observed for all OCR's, at all strain rates and stress ratios examined. This is shown for example in Figure 7.9, which presents the regression lines

through both the unloading and the loading data for OCR2 RBBC. While the two lines are virtually parallel, the data for the unloading tests tends to plot above that for the loading tests. The increased stiffness measured in the unloading tests appears to be caused by the load reversal which accompanies the beginning of shear subsequent to an unloading phase. Even the results of the test involving more complex pre-shear stress paths (see Table 6.11) support this trend. Note that, with regards to the initial stiffness, this is a secondary trend, which would have been most likely masked by specimen to specimen variability, had the pairs of unloading and loading tests not been performed on the same specimen.

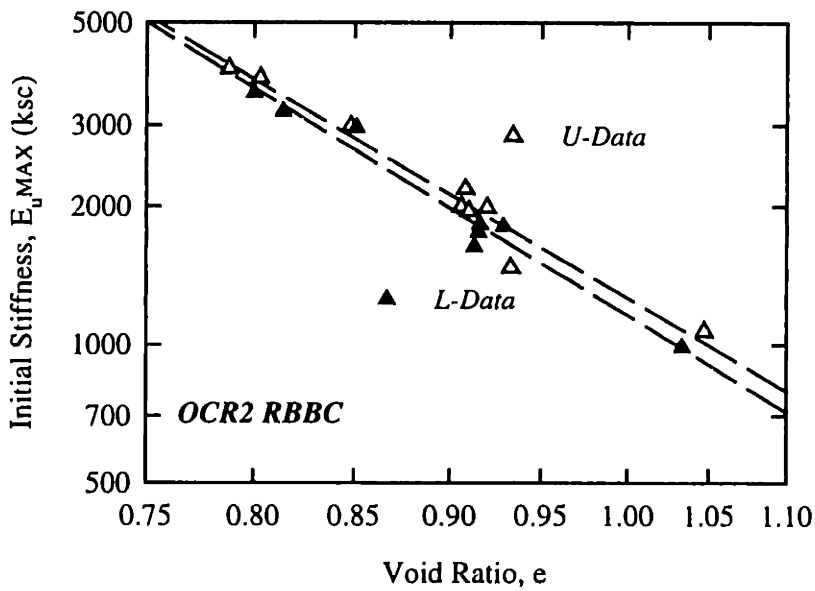


**Figure 7.9:** Effect of unloading or loading consolidation path on the initial stiffness of OCR2 RBBC.

With respect to time related effects on the initial stiffness, the discussion so far has established the insensitivity of $E_{u}MAX$ to variations in the strain rate in the range 0.1-4%/hr. Time effects do, however, come into play in affecting the initial stiffness of RBBC in two ways: through a decrease in stiffness caused by "slow" strain rates, and an increase in stiffness associated with prolonged aging. These two influences require separate discussion.

The results of the tests performed at rates slower than 0.1%/hr (i.e., 0.05) produced results that do not fall in the framework of simple dependence of $E_{u}MAX$ on the state variables (e.g., $e$ and $\sigma_v'$) outlined above. In the case of NC RBBC, for example, the stiffness decreases by about 15-20%, with respect to other tests conducted under similar conditions (e.g., equal void

ratio, see Figure 7.10). One possible explanation is to compare the applied shear strain rate with the undrained pre-shear creep rate of the soil.

As shown in Chapter 6 (Figure 6.59) the soil undergoes undrained creep even at the beginning of shear. The effect of these creep strains is negligible on the determination of the initial stiffness provided that the shear rate is sufficiently greater that the creep rate. Based on the limited experimental data obtained at slow rates, it appears that the critical value of the shear rate to creep rate ratio is on the order of 25-30.

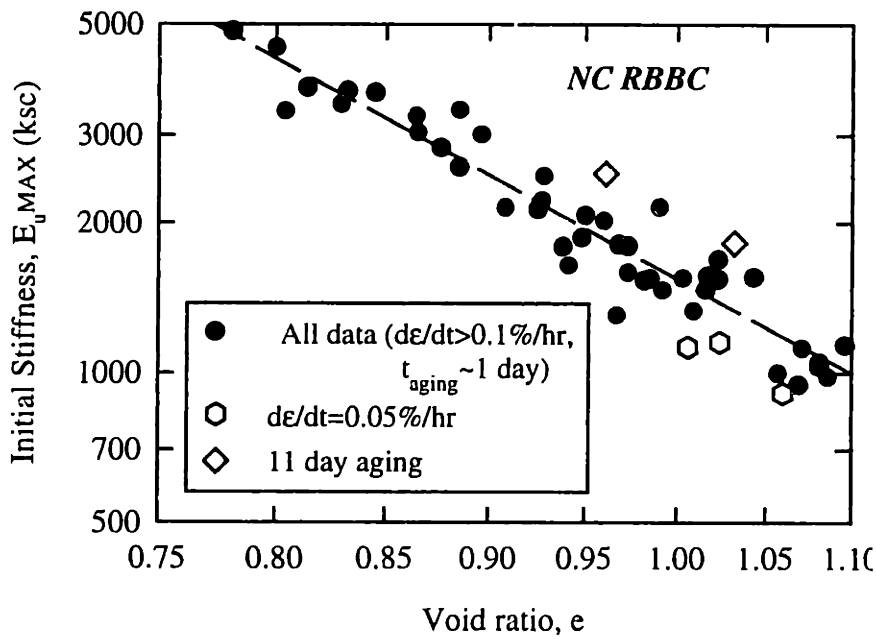


**Figure 7.10:** Effect of "slow" strain rate and prolonged aging on the initial stiffness of NC RBBC.

The second influence associated with time effects involves the issue of prolonged aging. As indicated in Section 6.9, and shown in Figure 7.10, in the case of NC RBBC, an additional cycle of secondary compression is associated with an average increase in the initial stiffness of about 25%.

This result cannot be explained solely on the basis of a reduced void ratio, nor does it stem from the reduction in the pre-shear creep rate.[3] While the data are limited, they support the hypothesis that the increase in $E_u$MAX with time is associated with the same structure forming processes that cause an increase in preconsolidation pressure and undrained strength.

[3] In this case the test performed at rates greater that 1%/hr should also display higher values of the initial stiffness.

(Schmertmann 1991). This can be represented by extending the expression of the initial stiffness to include a time dependent factor (i.e., $E_{uMAX}= E_{uMAX}*K_t$). Anderson and Stokoe (1978) propose the following expression to quantify the increase in stiffness with time:

$$N_G = \frac{\Delta G_{max}}{G_{max}(t = t_{ref}) \cdot \Delta \log(t)} \qquad \textit{Equation 7.2}$$

($K_t$ becomes equal to $1+N_G$), in which the increase in shear modulus per log cycle of time of secondary compression is normalized with respect to the stiffness at a reference time[4]. If the standard aging period (24-30 hours) is used as reference time, the data obtained lead to a value of $N_G$ of approximately 25%. This value falls at the upper end of the range of values reported in the literature for cohesive soils ($N_G$ =8-19, see Table 2.5 from Lo Presti et al. 1996) and is also slightly greater than the value determined by Trudeau et al. (1974) for Boston Blue Clay. The data on this topic are however limited to two results and additional investigation is required, particularly considering the uncertainties associated with the estimate of $\Delta E_{u}MAX/E_{u}MAX$, and therefore of $N_G$.[5]

## 7.3 NON-LINEAR BEHAVIOR

As discussed in the previous chapter, and schematized in Figure 7.1, the small strain non-linearity of RBBC is found to depend on the following factors:

- OCR,
- pre-shear stress path,
- K,
- strain rate,
- duration of aging.

In addition, this research has determined that for RBBC the stiffness degradation behavior is virtually independent of void ratio and stress level, all other conditions being equal (e.g., see Figures 6.13, 6.33, 6.60, etc.). This is a very significant result as it represents the basis

[4] Normally the end of primary is used as the reference time.

[5] Note that assuming the lower bound for the value of $\Delta E_{u}MAX/E_{u}MAX$ calculated in section 6.9, $N_G$ is reduced to 17-18.

for analyzing initial stiffness and stiffness degradation behavior separately. As discussed in the previous section, in fact, void ratio and vertical consolidation stress are the most important parameters affecting the absolute magnitude of the stiffness, yet play no part in determining the shape of the curve.

Figure 7.11 shows the modifications to the reference stiffness degradation curve ($K_0$-consolidated NC RBBC, 1 day aging, $d\varepsilon/dt$=0.1%/hr) produced by the influential parameters listed above. Note that, for clarity, the figure does not contain the curves relative to OC RBBC sheared at higher rates, nor the behavior of hydrostatically consolidated OCR2 RBBC. In addition, it does not include the curves relative to the composite pre-shear paths (*LL, UU, LU* and *UL*) investigated for OCR2.

The figure effectively depicts the wide range in behavior that is generated by variations in the testing conditions. It also permits classification of the variables in terms of their impact on the stiffness degradation behavior.

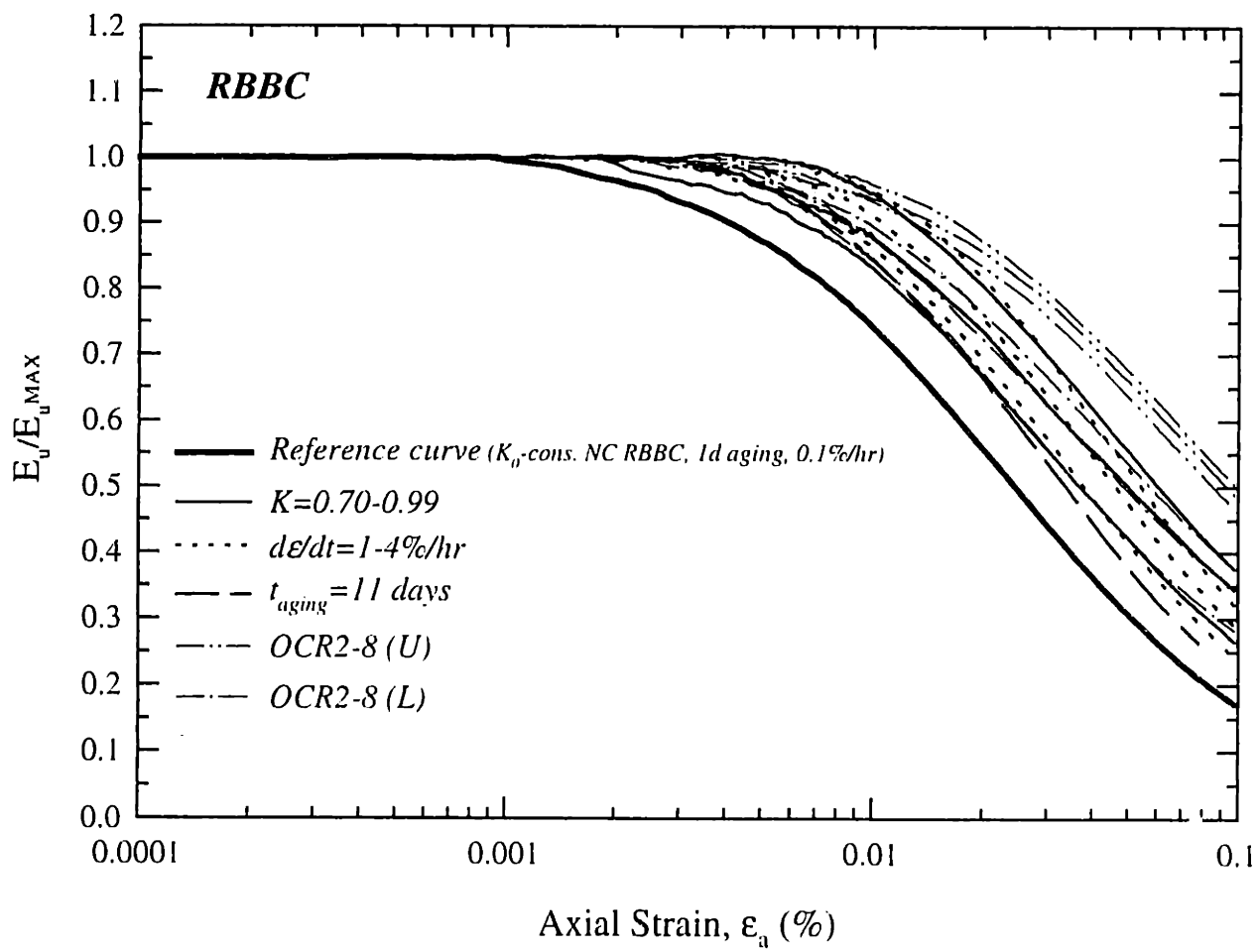


**Figure 7.11:** Range in stiffness degradation behavior of RBBC produced by changes in the testing conditions.

Figure 7.11 shows that the stiffness degradation behavior of RBBC is bound by two curves. To the left is the reference curve for $K_0$-consolidated NC RBBC that represents the behavior with the highest degree of non-linearity. The rightmost boundary is formed by the results for OC RBBC (OCR2-8) sheared after an unloading consolidation path. These data show a secondary trend of decreasing non-linearity with increasing OCR. As shown in Chapter 6 (Section 6.8) this boundary can move slightly further to the right as a result of an increase in strain rate.

Comparison of the effects of the influential variables as a function of strain level is more effectively performed by plotting the ratio of $E_u/E_{uMAX}$ for the variable of interest to that measured at the same strain level in the reference curve for $K_0$-consolidated NC RBBC. Figures 7.12a-f present these curves for all of the variables investigated in this program in two formats, i.e., with the axial strain plotted either on a logarithmic or a linear scale. This dual representation is provided to emphasize both the onset of the sensitivity to a given variable, and the general trend over the strain range examined. In plots a, c, and e, the start of the horizontal axis at 0.001% reflects the fact that below this threshold the behavior of the soil is found to be unaffected by the testing conditions. Additional plots summarizing the strain rate sensitivity of OC RBBC are presented in Figure 7.13.

Average values of the parameters used to characterize the pre-failure non-linearity of RBBC as a function of the testing conditions (the same shown in Figure 7.11) are summarized in Table 7.1. They include the linear threshold $\varepsilon_{lin}$, the coefficient of non-linearity $C_{NL}$ (equal to the stiffness at 0.001% divided by the stiffness at 0.1% axial strain), the plastic strain at 0.1% total axial strain $\varepsilon_{PL}/\varepsilon_{TOT}$, and the maximum increase in normalized stiffness $E^*/E^*_{NCMAX}$ (i.e., the maximum ordinate in the plots shown in Figure 7.12) with respect to the reference curve determined for $K_0$-consolidated NC RBBC (0.1%/hr, 1 day of laboratory aging).

As indicated in Figure 7.11 and in Table 7.1, increasing non-linearity is associated with a decreasing linear threshold. Figure 7.14 presents a plot of $C_{NL}$ versus $\varepsilon_{lin}$ (derived from the average curves). The figure indicates that the two variables are closely correlated and suggests that the increase in the linear threshold is a major contribution to the reduction in non-linearity. The figure also suggests the existence of secondary trends. For example for the same linear threshold, the behavior of NC RBBC at higher rates (1-4%/hr) appears to be characterized by more pronounced non-linearity.

Also associated with an increase in non-linearity is an increase in the plastic deformation of the soil, quantified by $\varepsilon_{PL}/\varepsilon_{TOT}$. This is clearly shown in Figures 7.15a-c which present the complete stress strain curves (undrained shear and unloading) for three tests with very different values of $C_{NL}$: 5.7, 3.0 and 2.0.[6] The figure shows that the test characterized by the highest degree of non-linearity exhibits also the most significant plastic strain upon unloading of the applied shear stresses. A decrease in the non-linearity is on the other hand associated with a decrease in the plastic strain. This trend is confirmed in Figure 7.16, in which $C_{NL}$ is plotted versus $\varepsilon_{PL}/\varepsilon_{TOT}$. The data in the figure are derived by averaging the results available for each OCR and pre-shear path. The stress strain curves in Figure 7.15 also indicate that the axial strain recovered upon unloading is significantly greater than the linear threshold (~6 times greater for NC RBBC, and approximately 12 for OCR4 *U* and *L*). This suggests that (visco)elastic behavior extends well into the non-linear region.

[6] These values may be different from those shown in Table 7.1 as they refer to the specific tests and not to the average curves.

| | $\varepsilon_{lin}$ (%) | $C_{NL}$ | $\varepsilon_{PL}/\varepsilon_{TOT}$ (%) | $E^*/E^*_{NCMAX}$ |
|---|---|---|---|---|
| NC *(Reference)* | 0.0015 | 5.95 | 94 | 1.00 |
| OCR2-U | 0.0054 | 2.16 | 29 | 2.75 |
| OCR4-U | 0.0052 | 2.06 | 20 | 2.89 |
| OCR8-U | 0.0076 | 2.00 | 20 | 2.98 |
| OCR2-L | 0.0041 | 3.60 | 70 | 1.65 |
| OCR4-L | 0.0034 | 2.95 | 53 | 2.02 |
| OCR8-L | 0.0047 | 2.69 | - | 2.21 |
| NC-K=0.70 | 0.0021 | 3.83 | - | 1.55 |
| NC-K=0.90 | 0.0041 | 2.94 | 62 | 2.02 |
| NC-K=0.99 | 0.0063 | 2.70 | - | 2.20 |
| NC-1%/hr | 0.0035 | 4.21 | 88 | 1.41 |
| NC-2%/hr | 0.0051 | 3.51 | 81 | 1.70 |
| NC-4%/hr | 0.0072 | 3.17 | 79 | 1.88 |
| NC-2.4 d aging | 0.0027 | 4.92 | - | 1.21 |
| NC-11 d aging | 0.0037 | 4.73 | 83 | 1.26 |

**Table 7.1:** Summary of parameters describing the small strain non-linearity of RBBC.

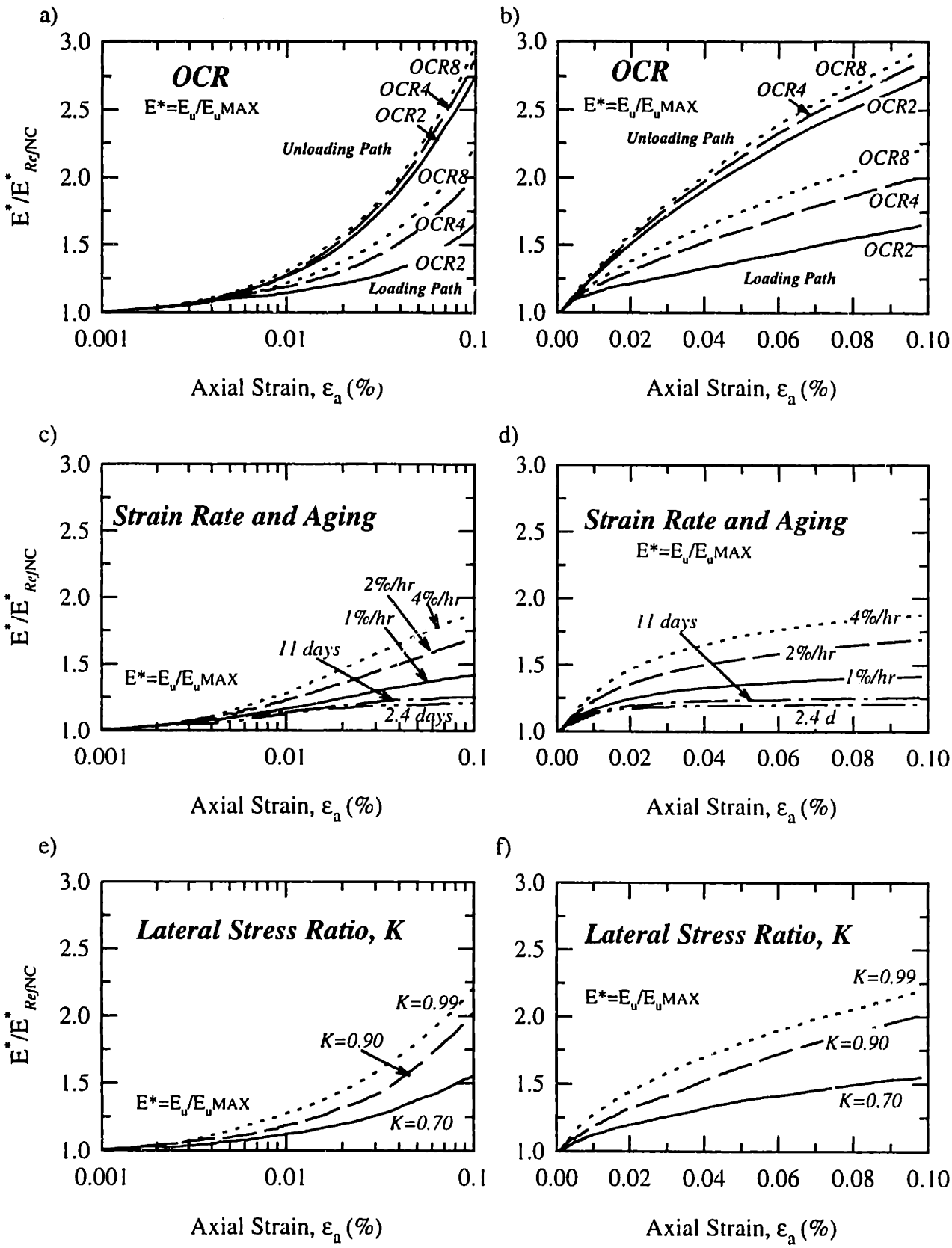


**Figure 7.12:** Effects of changes in the testing conditions on the stiffness degradation behavior of NC RBBC: a-b) OCR; c-d) strain rate and aging; e-f) lateral stress ratio.

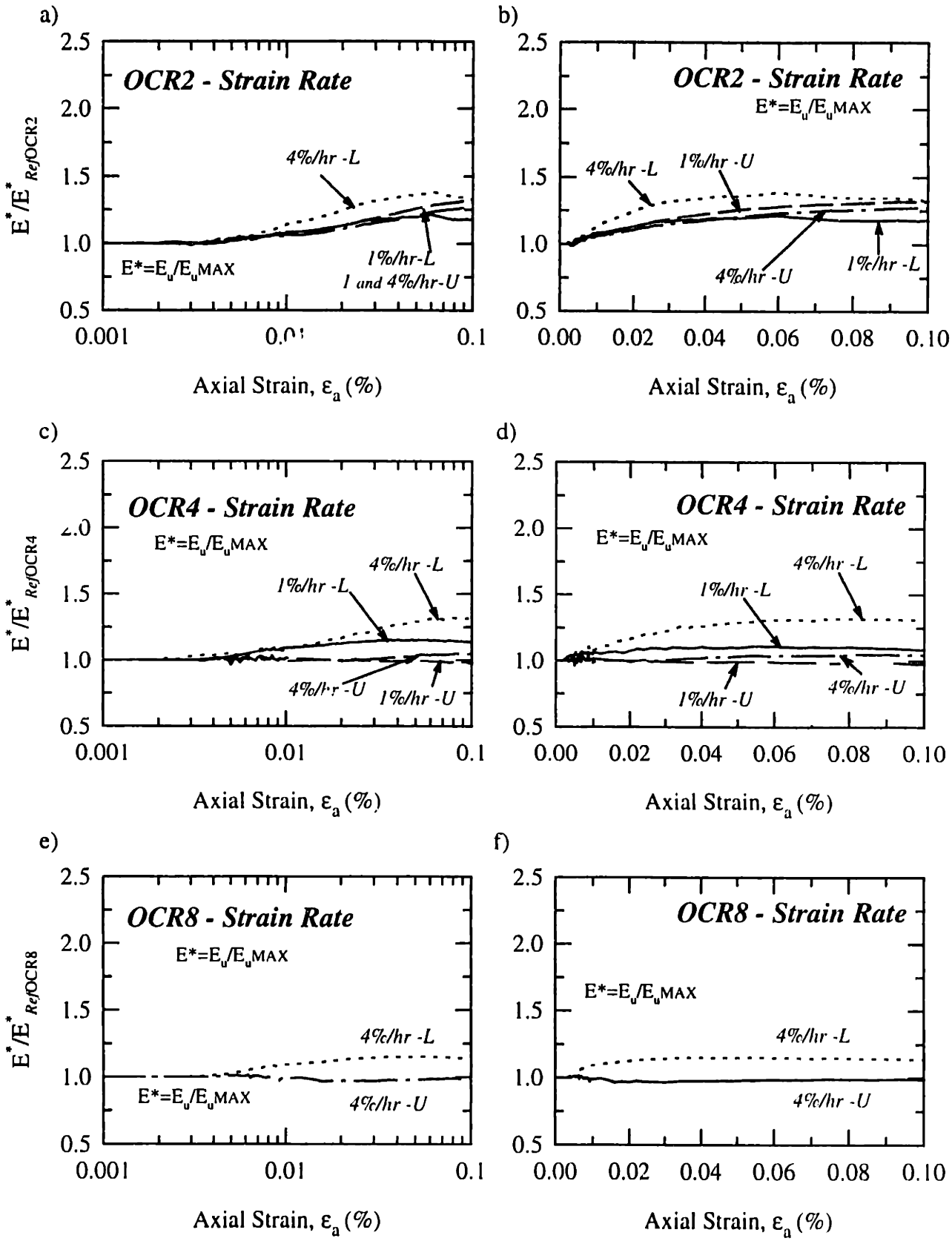


**Figure 7.13:** Effect of strain rate on the stiffness degradation of OC RBBC: a-b) OCR2; c-d) OCR4; e-f) OCR8.

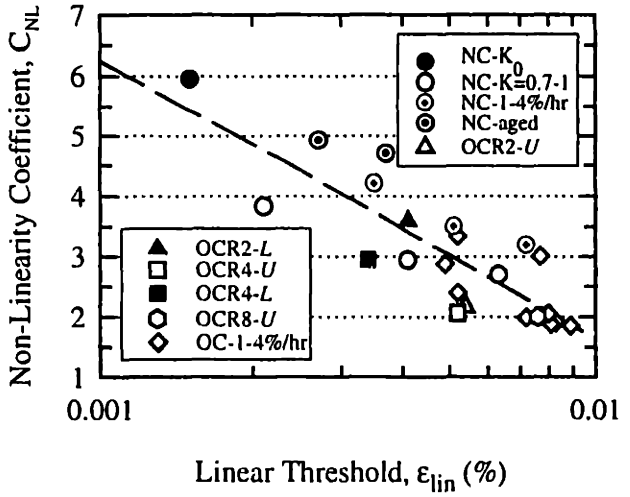


**Figure 7.14:** Coefficient of non-linearity versus linear threshold (NC and OC RBBC).

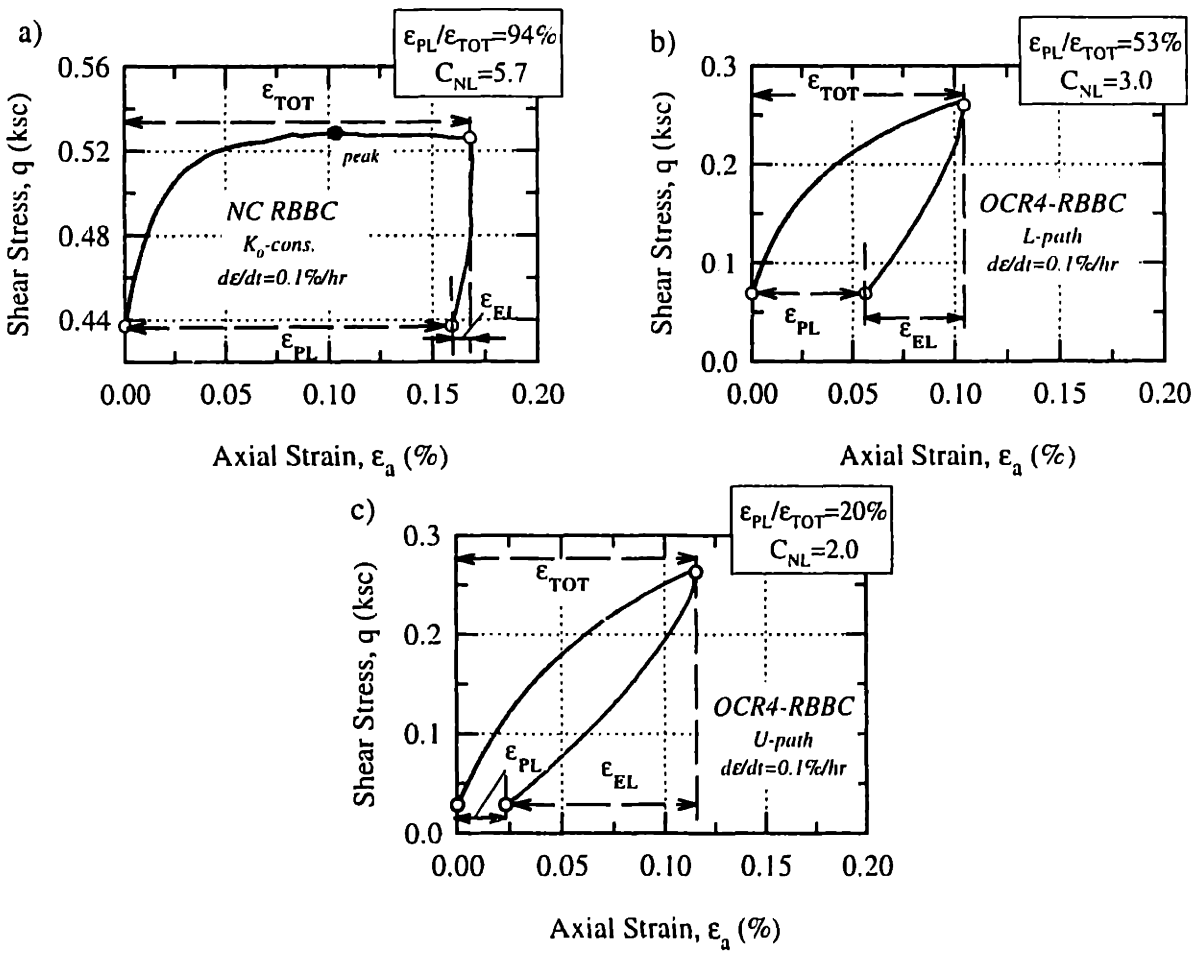


**Figure 7.15:** Residual plastic strain after shearing to ~0.1-0.15% axial strain: a) $K_0$-consolidated NC RBBC (*TX475S1*-$\sigma'_{vc}$~1.7 ksc); b) OCR4-*L* RBBC (*TX438S5*-$\sigma'_{vc}$~1.1ksc); c) OCR4-*U* RBBC (*TX442S1*-$\sigma'_{vc}$~0.7 ksc) (all at 0.1%/hr).

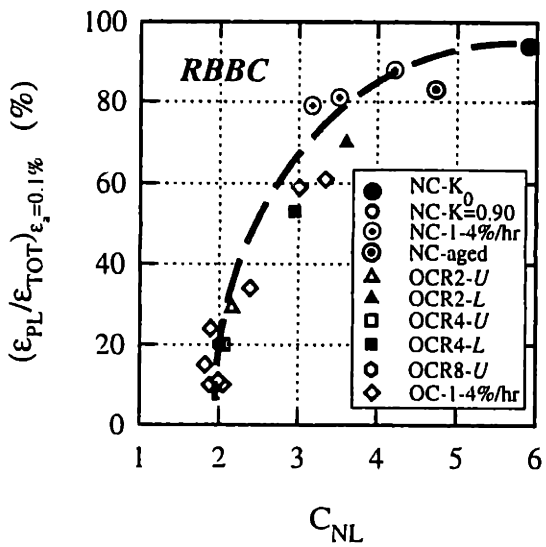


**Figure 7.16:** Residual plastic strain after unloading from 0.1% axial strain versus coefficient of non-linearity for NC and OC RBBC.

Another aspect controlling the behavior of the soil in the pre-failure region is the shear stress level reached at a given strain relative to the peak shear stress. This is quantified through the mobilization factor $f$, defined as $\Delta q/\Delta q_{MAX}$ ($f$=0 corresponds to the beginning of shear before any increment of the shear stress is imposed; $f$=1 corresponds to failure). The mobilization factor at a given strain level varies for different testing conditions. At 0.1% axial strain, for example, NC $K_0$ RBBC is very close to having reached failure (f~1), while OCR 2 $K_0$ RBBC has mobilized less than half of the maximum shear stress increment.

For all shears involving no load reversal, it is observed that the stiffness degradation at a given strain level increases with the mobilization factor $f$. This is shown in Figure 7.17a in which $f$ is plotted versus strain level for selected tests on both NC and OC RBBC. Note that determination of $f$ requires knowledge of the peak shear stress (i.e., $s_u$), which, because of the specific testing procedure followed in this program, was rarely known.[7]

[7] Exceptions are most of the tests on $K_0$-consolidated NC RBBC and most of the final shears performed on the specimens. No information can be derived from the existing database (e.g. Sheahan 1991 and Santagata 1994) as these experimental programs did not include testing of OC RBBC following loading consolidation paths. Analysis

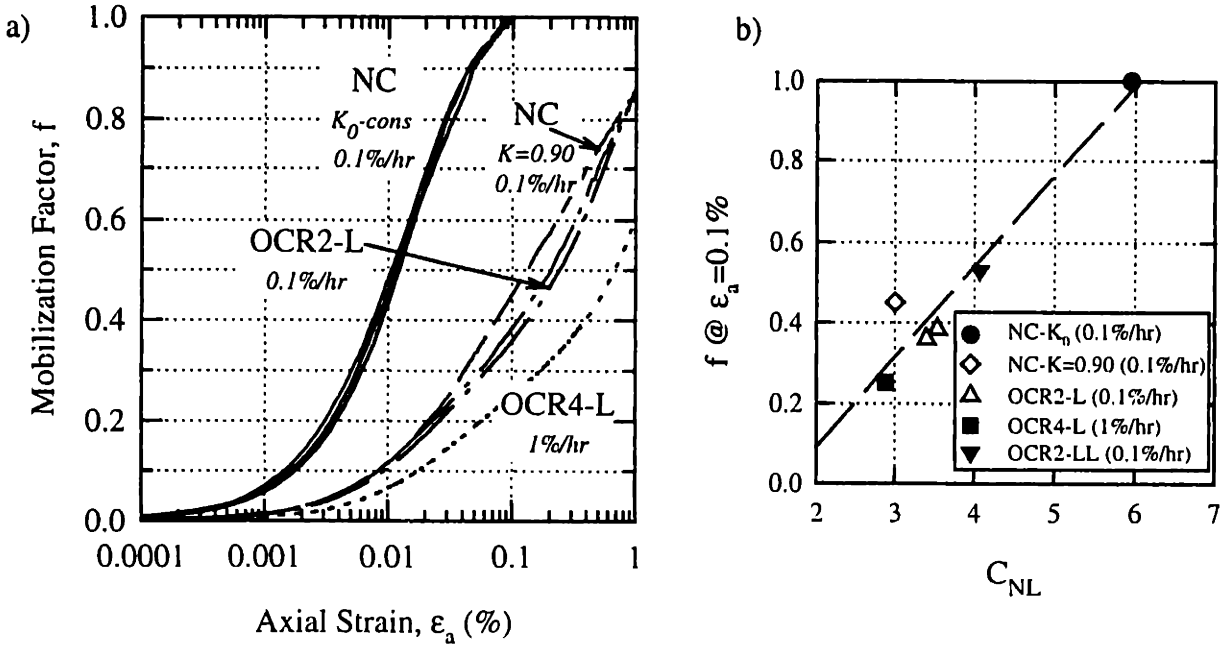


**Figure 7.17:** a) Mobilization factor as a function of strain for selected tests not involving load reversal; b) mobilization factor at 0.1% axial strain versus coefficient of non-linearity. [8]

Albeit limited, the data-set shown in Figure 7.17a presents a picture consistent with the stiffness degradation behavior shown in Figure 7.11, and explain the decrease in non linearity observed with increasing OCR (*L*-tests) and increasing lateral stress ratio. This is more compactly shown in Figure 7.17b which demonstrates the correlation between *f* at 0.1% axial strain and the coefficient of non linearity (which is a function of $E_u/E_{uMAX}$ at 0.1%).

The level of shear stresses mobilized is, however, not the only factor contributing to determine the degree of non-linearity of RBBC in the pre-failure region. Figures 7.11 and 7.12 a-b show that the most significant change in the stiffness degradation behavior occurs as OCR goes from one to two when the application of shear results in a load reversal (i.e., all OCR-*U* tests). As shown in Figure 7.18 for the case of OCR2 RBBC, however, in these tests the mobilization factor is observed to be greater than that determined for the loading tests at any strain level[9].

---

of the limited data from this experimental program indicates that OC RBBC reaches the same value of the undrained strength independently of the pre-shear path.

[8] Note that Figure 7.16b presents the result corresponding to one test (OCR2-LL) which, for clarity, is omitted from Figure 7.16a.

[9] The value of $\Delta q_{max}$ for the U test was chosen based on the relationship between undrained strength and strain rate provided by Sheahan et al. (1996) for RBBC. The curves in Figure 7.17 represent average curves.

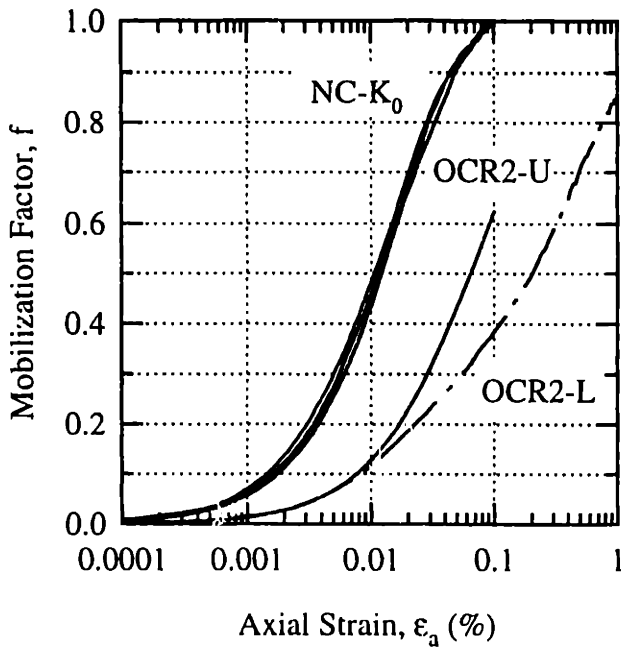


**Figure 7.18:** Mobilization factor as a function of strain for NC and OCR2 (*U* and *L*) RBBC.

This is illustrated also in Figure 7.19 that plots *f* at 0.1% axial strain versus $C_{NL}$ for the OCR2-*U* tests. It is shown that the data for these tests fall above the line obtained by best fitting the loading results presented in Figure 7.17b. Similar observations apply to the OCR4 and OCR8 data. For these two OCR's, however, the difference with respect to the loading data is reduced (reflecting the decreasing sensitivity to pre-shear path associated with increasing OCR).

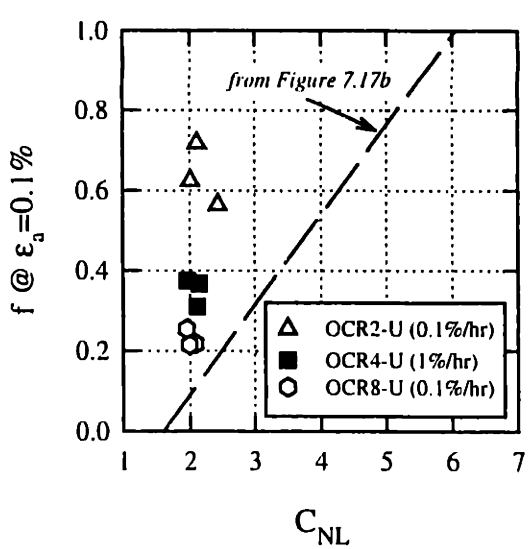


**Figure 7.19:** Mobilization factor at 0.1% axial strain versus coefficient of non-linearity (*U*-tests).

Increased reduction in the non-linearity is associated in the case of the unloading tests on OC RBBC with load reversal. This is consistent also with the results for the additional pre-shear paths examined for OCR2 RBBC. Even minimal unloading prior to shear results in a marked reduction of the small strain non-linearity. This is shown in Figure 7.20, in which the extent of unloading before shear, quantified by the magnitude of the unloading strain $\Delta\varepsilon_{aU}$ (in the case of continuous unloading during the consolidation path it coincides with the overall swelling strain), is plotted versus the coefficient of non-linearity.

The results presented in Figure 7.20 show that the degree of non-linearity is substantially insensitive to the magnitude of the unloading strain. On a test by test comparison the $\Delta\varepsilon_{aU}$ data do not correlate well with the degree of non-linearity (i.e. variations in $\Delta\varepsilon_{aU}$ do not account for the variability in the stiffness degradation behavior observed at each OCR). However, the average values calculated for each OCR and the result for the *LU* test on OCR2 RBBC show a secondary trend of decreasing non-linearity with increased unloading prior to shear.

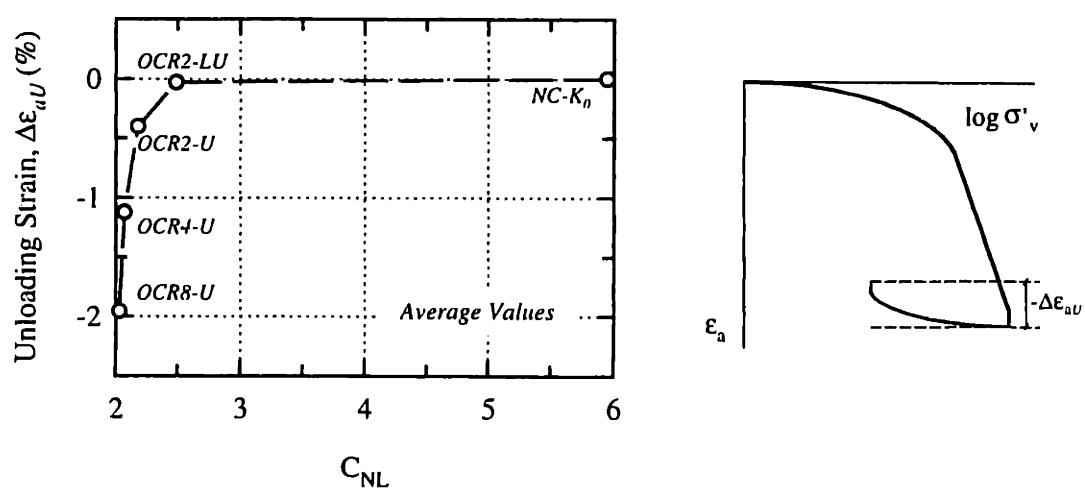


**Figure 7.20:** Relationship between unloading axial strain increment before shear and non-linearity (*U*- tests).

Reloading the soil prior to shear results in an increase in the small-strain non-linearity. Figure 7.21 plots the compressive axial strain increment occurred since the most recent stress reversal versus the coefficient of non-linearity for all tests performed on OC RBBC at 0.1%/hr (loading tests). Also shown in the lower left hand part of the figure is the range in the values of $C_{NL}$ determined (see Figure 7.20) for the U tests for which $\Delta\varepsilon_{aRev}$ is equal to zero.

The figure indicates a clear trend of increasing non-linearity with increasing axial strain increment. This suggests that more significant positive axial strain results in increased loss of memory of the previous unloading consolidation path. As seen in Figure 7.21 this effect also accounts for the variability in the results observed at a given OCR.

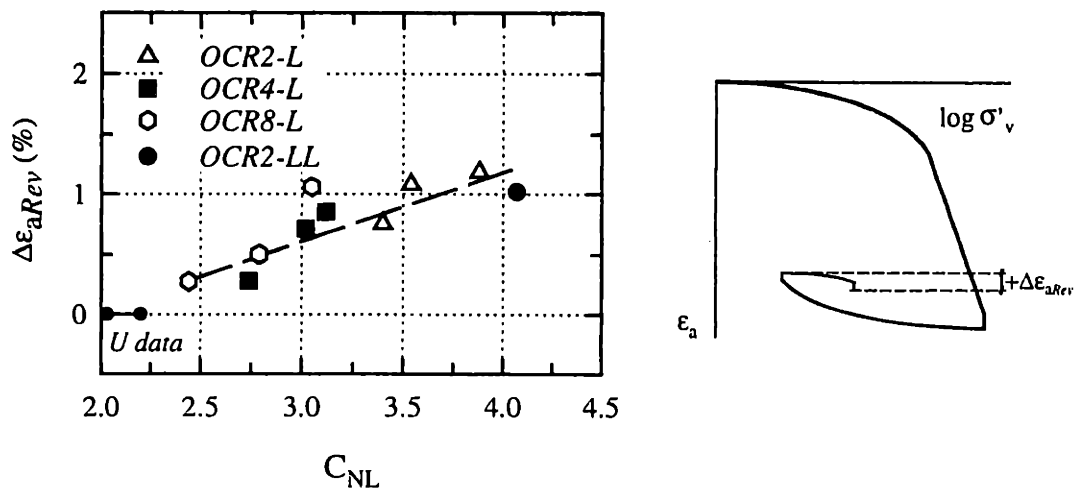


**Figure 7.21:** Relationship between non-linearity and axial strain since most recent stress reversal (*L*- tests).

Once the analysis is extended to include tests performed at different rates, it is recognized that the decrease in mobilization factor deriving from the increase in strength is not sufficient to explain the modifications in the stiffness degradation behavior (increase in $\varepsilon_{lin}$ and reduction of the non-linearity below 0.1% strain, see Figures 7.11, 7.12c-d) associated with increases in strain rate. This observation is demonstrated in Figure 7.22 for the case of NC RBBC[10], which, as discussed in Chapter 6, presents the highest rate sensitivity. The figure presents the average curves of the mobilization factor *f* versus axial strain for tests conducted at 0.1, 1, 2 and 4%/hr, all on $K_0$-consolidated NC RBBC. It is shown that the band formed by the higher rate tests lies fairly close to the curve depicting the reference behavior for NC RBBC, and is clearly distinct from the curve relative to the K=0.90 test. This curve is included in the figure for comparison purposes, as under these conditions the stiffness degradation behavior of the soil is similar to that observed for the higher rate tests (see Figures 7.11 and 7.12).

[10] Increasing strain rates are associated in the case of NC RBBC with an increase in strength of about 6.5% per log cycle of strain rate (Sheahan et al. 1996, se also Section 3.4.4.7).

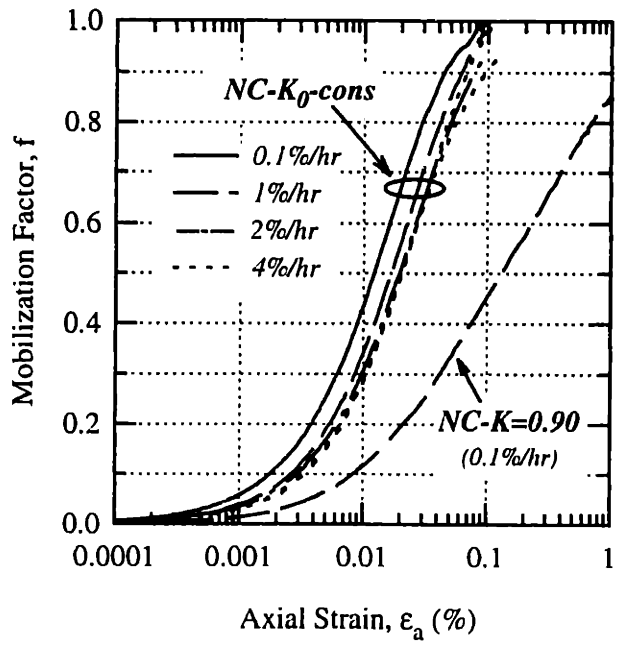


**Figure 7.22:** Mobilization factor f as a function of strain for tests on NC RBBC at various strain rates.

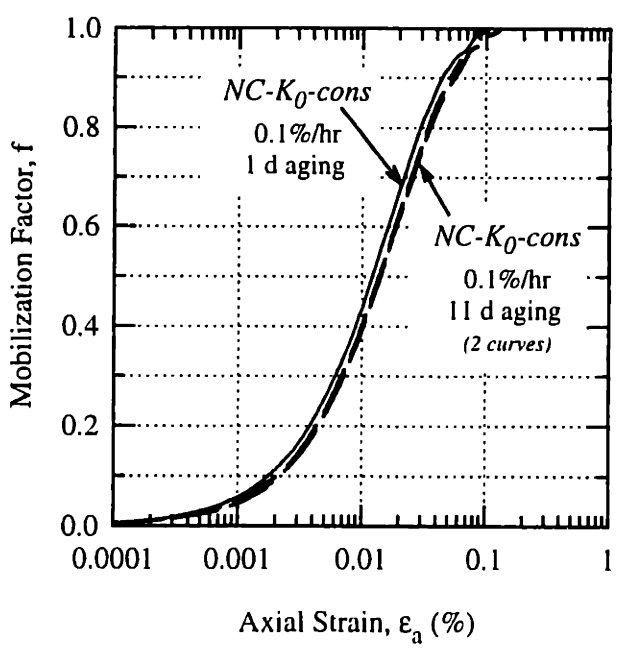


**Figure 7.23:** Mobilization factor as a function of strain for tests on NC RBBC after standard and prolonged laboratory aging

Similar observations derive from the comparison of the curves of $f$ versus axial strain for $K_0$-NC RBBC sheared under standard conditions and after prolonged aging (Figure 7.23). Also

in this case the difference in stiffness degradation behavior is not reflected in the mobilization curves.

The results for the high strain rate tests on NC RBBC, and for prolonged aging are compiled on the same plot of $f$ at 0.1% axial strain versus $C_{NL}$ in Figure 7.24. The figure shows that the results tests fall above the line derived for the NC and OC-$L$ in Figure 7.17b. This suggests that additional factors contribute to determine the behavior of the soil.

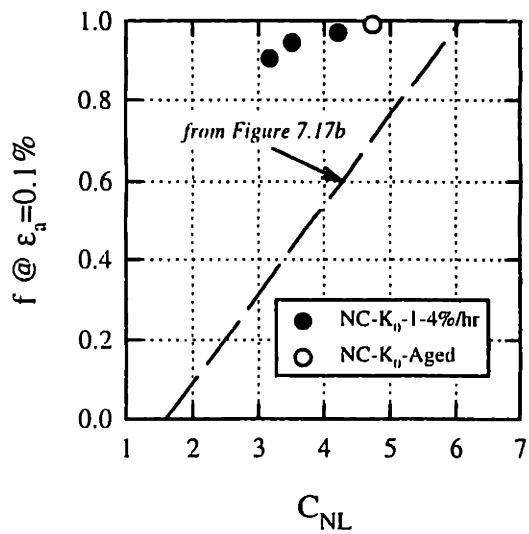


**Figure 7.24:** Mobilization factor at 0.1% axial strain versus coefficient of non-linearity (high strain rate and prolonged aging tests on NC RBBC).

Effective interpretation of these experimental observations requires consideration of the time dependent behavior of NC RBBC. The viscous nature of the behavior manifests itself through continuous deformation (i.e., creep) under conditions of constant load. Despite the fact that this research did not focus on this aspect of behavior, limited data are available from some of the tests on the rate of creep deformation occurring during the undrained hold stress phases at the beginning (see Figure 6.59) and at the end of shear[11] (e.g., Figure 7.25). Based on these data, it is found that, at the end of shear, the undrained creep rate of $K_0$-consolidated NC RBBC is approximately 0.1%/hr. The data also indicate that reduced creep rates are associated with higher values of OCR (see Figure 7.25) and with higher values of the lateral stress ratio. These data are consistent with the reduced sensitivity to strain rate manifested by the overconsolidated soil. Similarly the decrease in non-linearity observed in the aged specimens is consistent with

[11] Before undrained unloading or re-equilibration of the pore pressure for a subsequent consolidation phase occurred.

the reduction in the creep rate (by approximately an order of magnitude for an additional cycle of secondary[12]) associated with prolonged aging.

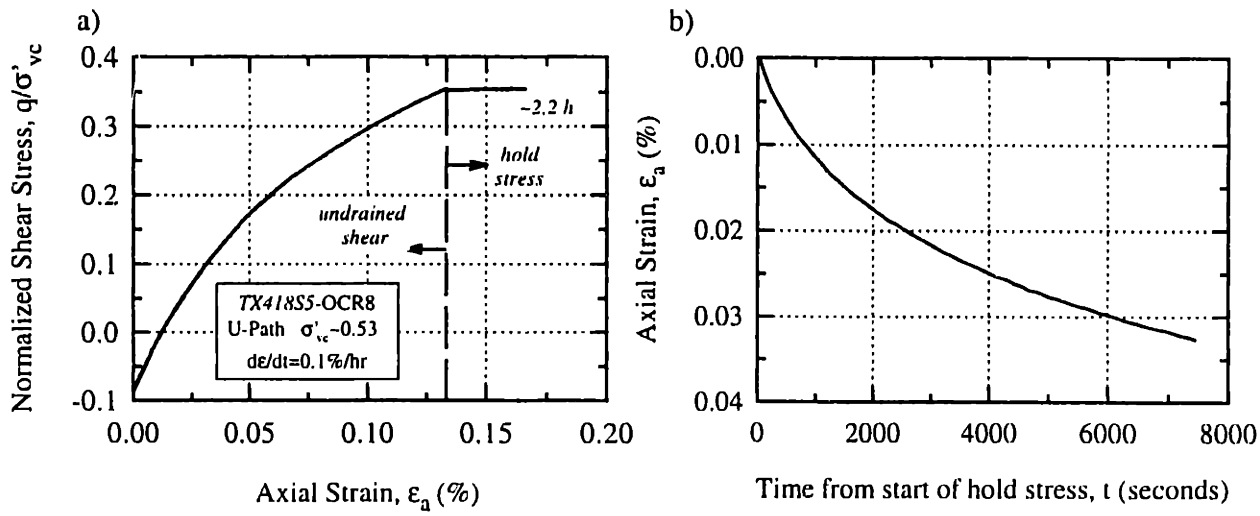


**Figure 7.25:** Example of the undrained creep deformation occurring at the end of shear: a) stress-strain curve; b) axial strain versus time.

This observation is confirmed by the similarity in the stiffness degradation behavior of NC RBBC sheared at 1.0%/hr strain rate with that of NC aged for 11 days and sheared at the standard rate (0.1%/hr) (Figures 7.12 b-c). In both cases the ratio of the shear and creep rates ($d\varepsilon/dt_{shear}/d\varepsilon/dt_{creep}$) decrease by an order of magnitude with respect to the conditions in the reference tests ($d\varepsilon/dt$=0.1%/hr, 1 day aging)

## 7.4 REFERENCES


1. Anderson D.G. and Stokoe, K.H. (1978), "Shear Modulus: A Time Dependent Soil Property," *Dynamic Geotechnical Testing, ASTM, STP 654,* ASTM, pp.66-90.

2. Jamiolkowski, M., Lancellotta, R., and Lo Presti, D.C.F. (1994), "Remarks on the Stiffness at Small Strains of Six Italian Clays," *Proc. Int. Symp. Pre-Failure Deformation Characteristics of Geomaterials*, Hokkaido'94, Vol. 2, pp. 817-854.

3. Lo Presti, D.C.F., Jamiolkowski, M., Pallara, O. and Cavallaro, A. (1996), "Rate and Creep Effect on the Stiffness of Soils," ASCE Convention, Washington, 10-14 Nov. 1996, ***Geotechnical Special Publication No.61***, pp.166-180.


[12] These creep data for aged NC RBBC refer to the beginning of shear.

4. Santagata, M.C. (1994), "Investigation of Sample Disturbance in Soft Clays Using Triaxial Element Tests," S.M. Thesis, Department of Civil and Environmental Engineering, MIT, Cambridge, MA, 289 p.

5. Sheahan, T.C. (1991), "An Experimental Study of the Time-Dependent Undrained Shear Behavior of Resedimented Clay Using Automated Stress-Path Triaxial Equipment", Sc.D. Thesis, MIT, Cambridge, 955 p.

6. Sheahan, T.C., Ladd, C.C., and Germaine, J.T. (1996), "Rate-Dependent Undrained Shear Behavior of Saturated Clay," ***Journal of Geotechnical Engineering***, ASCE, 122 (2), February, pp. 99-108.

7. Schmertmann, J.H. (1991), "The Mechanical Aging of Soils," 25th Karl Terzaghi Lecture, ***Journal of Geotechnical Engineering***, 117 (9), September, pp. 1288-1330.

8. Trudeau, P.J., Whitman, R.V. and Christian, J.T. (1974), "Shear wave Velocity and Modulus of a Marine Clay," ***Journal of the Boston Society of Civil Engineers***, 61, (1), pp.12-25.

# CHAPTER 8

## CONCLUSIONS AND RECOMMENDATIONS

### 8.1 OVERVIEW

This research performed a detailed investigation of the pre-failure behavior of cohesive soils by examining the effects of the following parameters on the pre-failure behavior of a soft clay in undrained triaxial compression: consolidation stress level (0.5-12 ksc), OCR (1-8), pre-shear stress path (loading versus unloading), pre-shear lateral stress ratio ($K_0$-1), rate of shear (0.05-4%/hr), and duration of laboratory aging (1-2 cycles). The program assessed the significance of these parameters and quantified their influence on both initial stiffness and small strain ($\varepsilon_a$ <0.1%) non-linearity.

Efforts on this study began with the enhancement of existing triaxial technology for the purpose of measuring small strains ($10^{-6}$-$10^{-3}$). This effort included both the mechanical and electrical design of a novel on-specimen axial strain measuring system. This technique makes use of two miniature LVDT's mounted on a pair of yokes which clamp onto the specimen without impeding its deformation or interfering with the pressure seals. A highly stable, low noise signal conditioning system completes the design. The device is compact, integrates with the existing equipment, and is capable of resolving displacements of less than 0.05 microns, corresponding to strains less than 0.0001%, over a range of 20% strain.

The extensive testing program was performed on Resedimented Boston Blue Clay (RBBC), a cohesive soil manufactured in the laboratory from natural BBC. The uniformity and reproducibility in the behavior of this clay, established as a result of extensive investigations at MIT over the past 30 years, permitted a detailed study of the role of the factors listed above.

Testing of RBBC was carried out employing an innovative multi-stage testing approach developed to minimize soil variability, increase testing productivity and conserve soil. This approach, which involved performing several "small strain" undrained shears, separated by

consolidation and 24 hour aging phases, on one specimen, allowed collection of a large data set, comprising more than 100 phases of undrained shear.

## 8.2 RESULTS AND CONCLUSIONS

### 8.2.1 Introduction

Prior to highlighting the main conclusions drawn from the work presented in this thesis it is important to summarize the criteria used to analyze the data gathered.

The discussion of the effects of the variables investigated on the pre-failure behavior of RBBC has been organized distinguishing between initial stiffness and small strain non-linearity. This type of interpretative framework, in which the absolute magnitude of the stiffness is examined independently of the stiffness degradation behavior, is useful as it allows easy comparison of the effects of the various variables and it facilitates understanding of the mechanisms underlying the observed behavior.

The initial stiffness is characterized exclusively through $E_{uMAX}$, the slope of the regression line through the initial portion of the stress strain curve (generally <0.001%).

Evaluation of the degree of non-linearity in the pre-failure region is based on the stiffness degradation curve, in which the normalized stiffness ($E_u/E_{uMAX}$) is plotted as a function of strain level on a logarithmic scale. The parameters used to characterize the non-linearity in the pre-failure behavior of RBBC are:

a) the linear threshold $\varepsilon_{lin}$ which indicates the onset of non-linearity and is defined as the strain corresponding to $E_u$ equal to 0.98 $E_{uMAX}$;
b) the coefficient of non-linearity $C_{NL}$, defined by the ratio of the stiffness at 0.001% strain to that at 0.1%. This value provides a simple measure of the small strain non-linearity: the greater $C_{NL}$, the greater the non-linearity in the pre-failure behavior.
c) the ratio (in %) of the permanent to total strain ($\varepsilon_{PL}/\varepsilon_{TOT}$) after undrained unloading from approximately 0.1-0.12% axial strain, at the end of shear. This ratio provides a measure of the degree of plastic straining that the soil is undergoing at that strain level.

Evaluation of effects of the variables investigated was based, whenever possible, on average curves derived from several tests performed under similar conditions.

### 8.2.2 Review of Effects of Variables

#### *8.2.2.1 Reference Behavior*

The behavior of NC RBBC consolidated one-dimensionally to the desired vertical stress, left to age for at least 1 cycle of secondary compression (~24-30 hours) and then sheared employing a rate of 0.1%/hr is used as the *reference* behavior. The effects of the various factors are evaluated by comparison to this reference behavior.

Under the conditions described, the pre-failure behavior of NC RBBC is characterized by an initial region at constant stiffness that extends to about 0.0015% strain. It is followed by a rapid decrease of the stiffness ($C_{NL}$=5.95), that reaches a value of about 20% of $E_uMAX$ at 0.1% axial strain, at which the soil has reached its peak shear stress. At this strain level the behavior of the soil is predominantly plastic, and only about 5-7% of the deformation is recovered upon removal of the applied shear stress (Figure 6.1-6.3). At any given stress level, the data for $K_0$-consolidated NC RBBC display remarkable repeatability, both in terms of the initial stiffness and of the stiffness degradation behavior (COV<8% in both cases).

#### *8.2.2.2 Effect of Stress Level – NC RBBC*

Twenty-two tests, performed at eight different values of $\sigma'_{vc}$ (1.7 to 12.6 ksc), were used to evaluate the dependence of the pre-failure behavior of $K_0$-consolidated NC RBBC on stress level. It was found that increasing values of the vertical consolidation stress were associated with increased values of the stiffness at all strain levels (Figure 6.8).

The increase in the initial stiffness produced by an increase in stress level can be described by an exponential relationship of the type $E_uMAX \propto \sigma'_{vc}{}^n$ (n=0.74). A similar relationship links $E_uMAX$ to the mean consolidation stress, $p'_{mc}$ (i.e. $E_uMAX \propto p'_{mc}{}^n$). Similarly, as changes in stress level are associated with variations in *e*, the initial stiffness can be also written as a function of the pre-shear value of the void ratio. This function has the form $E_uMAX \propto e^{-x}$ (x=-4.5) (Figure 6.11).

The shape of the $E_u/E_uMAX$ versus axial strain curve, and thus the degree of non-linearity are observed to be stress level independent (Figure 6.13). The same types of exponential relationships determined for $E_uMAX$, with virtually unchanged exponents, apply also at higher values of strain (up to 0.1%, Figure 6.12).

### 8.2.2.3 *Effect of Overconsolidation Ratio*

Investigation of the OC behavior of RBBC extended to three nominal values of OCR: 2, 4, and 8. This section reviews the results obtained exclusively after reaching the overconsolidated state by unloading from the virgin compression line. Additional results for different pre-shear stress paths are discussed in the following sections.

The same exponential type relationship between initial stiffness and stress level ($E_uMAX \propto \sigma'_v{}^n$), or void ratio ($E_uMAX \propto e^{-x}$) observed for NC RBBC, is found to apply for a given OCR. The values of both the stress level and the void ratio function exponents derived for the OC soil (Figure 6.18)are slightly greater (n=0.78-0.84, x=4.9-5.7) than those obtained from the NC results (n=0.74, x=4.6). While there appears to be a trend of increasing exponent with OCR, due to the more limited data, particularly for OCR 4 and 8, no conclusive statement can be made on this issue.

Comparison of the behavior of OC RBBC to that of NC RBBC under conditions of equal consolidation stress indicates an increase in $E_uMAX$ with OCR, which can be described by an exponential function (i.e. $E_uMAX \propto OCR^k$, k>0). A similar expression, with negative exponent (i.e. $E_uMAX \propto OCR^{k_1}$, $k_1<0$) describes the relationship under conditions of equal void ratio.

Despite displaying slightly greater variability compared to the NC data, the results for OC RBBC confirm that, for a given OCR, the shape of the stiffness degradation curve is independent of the consolidation stress level, or the pre-shear void ratio. As a consequence, the same relationship between $E_uMAX$ and $\sigma'_{vc}$ or *e* applies at all strain levels, up to 0.1%.

Compared to the NC soil, OC RBBC displays a distinctly different stiffness degradation behavior, which appears to be basically insensitive to variations in the value of OCR between 2 and 8 (Figure 6.24). The behavior of the OC soil is characterized by an increased size of the linear threshold (4-5 times the value measured for NC RBBC), a reduction in the overall degree of non-linearity below 0.1% as measured by $C_{NL}$ (from 5.7 for NC RBBC to about 2 for all tests on OC RBBC) and reduced stiffness degradation at any value of strain. This effect is observed to be increasingly significant with strain level, with $E_u/E_uMAX$ increasing by more than three times at 0.1%, compared to the NC behavior.

Finally, for OCR varying between 2 and 8, up to 0.1% axial strain the behavior of the OC soil appears to be still dominated by elastic straining, as more than 70-80% of the strain is recovered upon undrained removal of the applied shear stresses (Figure 6.27).

#### *8.2.2.4 Effect of Lateral Stress Ratio*

The pre-failure behavior of NC RBBC was investigated following stress path consolidation along a constant K line, with K equal to 0.70, 0.90 and 0.99.

In all cases the initial stiffness was higher than that obtained after $K_0$-consolidation to the same vertical stress: the higher the lateral stress ratio, the higher the value of $E_uMAX$. This increase in initial stiffness with K is found to be linked solely to the different pre-shear values of void ratio, arising from the different amount of volumetric straining which occurs during consolidation, depending on the path followed to reach the pre-shear stress state. Ultimately, the higher the value of K, the lower the void ratio reached at a given vertical stress. The same relationship between $E_uMAX$ and *e* determined for the $K_0$-consolidated NC soil, is found to apply for all values of K investigated. Rather than to $\sigma'_{vc}$, stress level dependency of the initial stiffness requires reference to the mean consolidation stress $p'_{mc}$ which, for RBBC, is uniquely linked to the void ratio (Figure 6.31).

The value of the pre-shear lateral stress ratio, K, significantly impacts the stiffness degradation behavior of NC RBBC. Increasing values of K cause the linear threshold to increase (by as much as a factor of 4 in the case of K equal to 0.99), render the response of the soil stiffer at all strain levels, reduce the small strain non-linearity (e.g. $C_{NL}$ goes from 5.95 to approximately 3.8, 2.9 and 2.7 for K equal to 0.70, 0.90 and 0.99, respectively), and increase the strain recovered upon unloading of the shear stress after shearing to 0.1% axial strain (Figure 6.33-6.34). The effects described are increasingly significant with higher values of K, but for a given value of K, they are independent of stress level. Overall, it is found that at higher values of K the behavior of NC RBBC resembles more that of an overconsolidated soil (OCR2-8).

As in the case of the overconsolidation ratio, the impact of an increase in the lateral stress ratio on the stiffness degradation behavior of RBBC, increases with strain level.

Similar although less marked effects, are observed in the case of hydrostatically consolidated OCR2 RBBC.

#### 8.2.2.5 *Effect of Pre-Shear Stress Path – NC RBBC*

The pre-failure behavior of NC RBBC was observed to be virtually insensitive to changes in the stress path followed in reaching the pre-shear stress state, provided that the final value of K was the same. The two paths examined (combination of hydrostatic consolidation and constant $\sigma'_h$ or constant p' paths) led to minimal reduction in the initial stiffness, which, as for the case of the tests performed at different values of K, was explained mostly based on the variation in the pre-shear value of *e* (Figure 6.40).

For the two paths examined the stiffness degradation behavior was observed to be virtually identical, and independent of stress level. In addition, it displayed remarkable resemblance to that observed in the $K_0$-consolidated tests, except for a marginal increase in the linear threshold (~0.0021% for both paths examined), and in the non-linearity at 0.1% axial strain (Figure 6.43).

#### 8.2.2.6 *Effect of Pre-Shear Stress Path – OC RBBC*

The effects of the direction of the pre-shear stress path on the pre-failure behavior of OC RBBC were investigated by comparing, for all values of OCR, the undrained behavior after swelling from the virgin compression line and upon reloading from higher values of OCR. These two consolidation paths which lie at approximately 180° with respect to each other in the p-q space, are referred to as *unloading path* and *loading path* (Figure 6.44).

The initial stiffness of OC RBBC was found to be marginally affected by the pre-shear stress path. Slightly larger values of $E_{uMAX}$ were measured in the unloading tests primarily due to marginally smaller values of the pre-shear void ratio generated by the different consolidation path (Figure 6.46). A secondary, yet consistent additional increase in the initial stiffness caused by load reversal, was also isolated.

The direction of the pre-shear path on the other hand significantly affects the pre-failure non-linearity of OC RBBC, for all values of OCR. The *loading* tests display a marked reduction of the linear threshold (by approximately a factor of 2), less significant non-linearity ($C_{NL}$ varies between 2.7 and 3.6, for OCR8 and OCR2, respectively) and much softer behavior at any strain level (Figure 6.52). In addition, upon undrained unloading of the shear stresses, much more significant permanent strains are measured in the case of a loading pre-shear path (e.g., for OCR2 RBBC $\varepsilon_{PL}/\varepsilon_{TOT}$ goes from ~30% to 70%). The sensitivity to the pre-shear stress path is

found to be marginally higher for the lower OCR's and increases with strain level: at 0.1% strain, for example, the unloading tests displays a secant stiffness which is 40-70% greater than the value measured in the loading tests.

As seen for the unloading data, the loading results indicate that, at a given OCR, the stiffness degradation behavior is, independent of stress level and/or void ratio

Additional undrained shears were performed on OCR 2 RBBC following consolidation phases that involved more than one change in direction of the stress path and/or reversal in loading, to shed light on this behavioral aspect (Figure 6.55). The results of these tests led to two important observations.

First it is observed that the small strain behavior of OC RBBC is affected primarily by reversals of axial load, while the actual consolidation path followed prior to shear (including changes in direction) plays a secondary sole. For example, virtually identical stiffness degradation behavior was measured for all shears following a consolidation phase that involved a continuous decrease of the vertical stress (*U* and *UU* paths), independently of the stress path followed (Figure 6.56). Similar agreement is observed in the results of the tests involving continuous increase of the axial load during consolidation (*L* and *LL* paths). This result is in agreement with the data obtained for NC RBBC.

Second, the results of the shears following "composite" consolidation paths indicate that the behavior of the OC soil is affected not only by the direction if the last portion of the pre-shear stress path, and that the "memory" of the soil extends back through the entire consolidation path, at least to the last stage of aging experienced. Overall it appears that any path involving some unload in the vertical stress leads to a larger linear response and less rapid stiffness degradation.

The curves of $E_u/E_{u}MAX$ versus axial strain derived for the purely unloading and the purely loading consolidation paths represent respectively the upper and lower bound of the stiffness degradation behavior. The results for the consolidation paths involving some reversal of the axial load fall in between these two boundaries. In such cases the behavior of the soil was stiffer or softer depending if the last segment of the consolidation path had involved unloading or loading of the specimen.

#### *8.2.2.7 Effect of Strain Rate*

The investigation of the strain rate sensitivity of the small strain behavior of NC and OC RBBC involved undrained shearing at rates varying within approximately two orders of magnitude (0.05%-4%/hr).

The initial stiffness of RBBC was found to be insensitive to variations of strain rate between 0.1 and 4%/hr for all values of OCR (0.05-4%/hr for OCR2 RBBC). For the lower rate (0.05%) the behavior of the NC soil appeared to be influenced by creep effects, resulting in a reduction of the measured initial stiffness of NC RBBC of 15-20%, compared to the values obtained at equivalent void ratio or consolidation stress (Figures 6.58, 6.64).

As the rate increase, the stiffness degradation behavior, for all values of OCR, shows the following: an increase in the size of the non-linear region, reduced non-linearity, and an increase in the strain recovered after undrained unloading at the end of shear. At least up to 0.1%, the susceptibility to rate is observed to increase with strain level. Note that at any strain rate and OCR, the stiffness degradation behavior continues, however, to be independent of stress level.

The extent of the modification to the stress-strain behavior produced by a given increase in strain rate is a function of the OCR. NC RBBC has the highest strain rate sensitivity, with the most significant increase in the size of the linear region and the most marked reduction in the non-linearity (e.g., an increase in rate from 0.1 to 4%/hr is associated with an increase in $\varepsilon_{lin}$ from 0.0015% to 0.0072%, and almost a two-fold increase of the stiffness at 0.1%, Figures 6.61-6.63). Significantly smaller effects are measured for OC RBBC, for which the sensitivity to rate decreases with increasing OCR and pre-shear consolidation path (Figures 6.80,7.13). At each OCR the behavior after a loading consolidation path is observed to be more significantly affected by strain rate compared to the results obtained after an unloading consolidation path.

#### *8.2.2.8 Effect of Laboratory Aging*

Prolonged laboratory aging affects both the initial stiffness and the stiffness degradation behavior of $K_0$-consolidated NC RBBC. An additional cycle of secondary compression ($t_{aging}$ from 1 to ~ 11 days) was found to produce an increase in $E_{uMAX}$ of about 15-25% Figure 6.84). This difference could not be accounted for solely based on the additional reduction in the pre-shear void ratio, or on the reduced pre-shear creep rate.

The stiffening of the behavior of RBBC due to aging extends to higher strains and the aged soil displays a larger linear threshold (double of that measured under standard conditions) and higher shear stress gain, by about 25%, at all strains up to 0.1%. Correspondingly a slightly reduced non-linearity ($C_{NL}$=4.7) is also observed (Figure 6.85).

The shape of the stiffness degradation curve is more sensitive to pre-shear aging than the initial stiffness. Increases in $t_{aging}$ as small a couple of days (~one third of a cycle of secondary) produce similar effects on the degree of non-linearity to those measured on the soil aged for an additional cycle of secondary (11 days).

### 8.2.3 Conclusions on Initial Stiffness

The initial stiffness of RBBC is dependent on both the pre-shear void ratio and the vertical consolidation stress through the following equation (Figure 7.8):

$$E_{u}MAX = 1014\, e^{-2.45}\, \sigma'_{vc}{}^{0.43} \quad \text{(ksc)} \qquad \textit{Equation 8.1}$$

Specific to OC RBBC is a secondary but clear influence of the pre-shear stress path on the initial stiffness, with tests involving load reversal as a result of shear having higher values of $E_{u}MAX$ (by 8-15%) even after variations in the pre-shear void ratio are accounted for (Figure 7.9). Note that both unloading and loading results are averaged to obtain Equation 8.1.

The expression presented above for the initial stiffness of RBBC (Eq.8.1) applies independently of the initial shear stress acting on the specimen and on the path followed prior to shear. It is found to be valid for strain rates varying in the range 0.1-4%/hr (0.05-4%/hr for OC RBBC), indicating that, provided the shear strain rate is greater than the creep rate by a factor of 15-30, the effects of undrained creep on the determination of the initial stiffness are negligible.

Equation 8.1 is similar in form to expressions provided by other authors (e.g., Jamiolkowski et al. 1994) to describe the dependence of the initial stiffness on the pre-shear state. While the stress level exponent is in the range of the values reported for a variety of other clays, the void ratio exponent is significantly greater.

Prolonged laboratory aging results in an increase in the initial stiffness by about 20-25% per log cycle of time, which falls at the upper end of the range reported for other cohesive soils.

This result is not due to reduction in void ratio (Figure 7.10)or the decreased pre-shear creep rate. It is hypothesized that it is related to additional modifications of the soil microstructure.

### 8.2.4 Conclusions on Stiffness Degradation Behavior

The small strain non-linearity of RBBC is observed to be virtually independent of void ratio and stress level and to depend on the following factors: OCR, pre-shear stress path, lateral stress ratio, strain rate and duration of aging.

As a result of changes in these test conditions the small strain non-linearity of RBBC presents significant variation: for example the linear threshold $\varepsilon_{lin}$ varies between 0.0015% and 0.0076%, and the stiffness degradation at 0.1% strain varies from more than 80% to about 50% (Figure 7.11).

$K_0$-consolidated NC RBBC has the highest degree of non-linearity. At the other extreme, OC RBBC has the largest linear threshold and the smallest stiffness degradation with strain, when sheared following an unloading consolidation path. Load reversal occurring as a result of shear is the most significant parameter affecting the pre-failure non-linearity: increased linear threshold and increased reduction in $C_{NL}$ are associated with larger load reversal as measured for example, by the strain increment relative to the most recent stress reversal. This observation is consistent with the data obtained for different values of OCR (2-8) and different pre-shear paths (*U, UU, LU*, Figure 7.20).

Reloading prior to shear partially erases the effects of previous unloading: the greater the reloading strain, the greater the increase in non-linearity (Figure 7.21). This effect accounts for the increased non-linearity associated with lower OCR's (OCR2-*L* vs. OCR4-*L*, for example) and the variability in the stiffness degradation results derived at a given OCR for the same loading consolidation path.

Another aspect controlling the behavior of the soil in the pre-failure region is the shear stress level reached at a given strain, relative to the peak shear stress. This is quantified through the mobilization factor $f$, ($f=\Delta q/\Delta q_{MAX}$). For all shears involving no load reversal at the onset of shear (all NC data, OC-loading results) the stiffness degradation at a given strain level increases with the mobilization factor $f$ (Figure 7.17).

Regardless of the pre-shear path, or of the mobilization factor, the degree of non-linearity is proportional to the level of plastic straining measured by the residual plastic strain ($\varepsilon_{PL}/\varepsilon_{TOT}$) at 0.1% axial strain (Figure 7.16).

Despite the increase in strength associated with increases in strain rate and with prolonged pre-shear aging, the reduction in stiffness degradation of RBBC observed under these conditions cannot be explained solely in terms of the increased value of $f$ at any given strain level (Figures 7.19,7.24). Increased reduction in the small strain non-linearity observed at higher strain rates derives instead by the increased capacity of the soil to override creep deformation. Similarly the effect of the laboratory pre-shear aging period is associated with the reduction in the creep rate of the soil.

## 8.3 RECOMMENDATIONS FOR FUTURE RESEARCH

This thesis investigated the factors affecting the pre-failure behavior of cohesive soils, based on an extensive program of triaxial tests on Resedimented Boston Blue Clay. As a by-product of this study, a great deal of experience has been gained with the specialized testing equipment used to investigate the small strain behavior of soils and several issues that must be addressed to improve the understanding of pre-failure behavior have been highlighted. Therefore recommendations for future work fall within two categories:

1) equipment enhancement,
2) additional investigations .

In addition, it is noted that the results obtained in this thesis for Resedimented Boston Blue Clay form a comprehensive data base that may provide the opportunity to test the degree to which available constitutive models are able to predict the small strain behavior of cohesive soils, under a variety of conditions.

### 8.3.1 Equipment Enhancement

Currently the main limitation of the equipment stems from the load application system. The system needs to more consistently apply a load to the test specimen that is both vertical and concentric with the specimen axis. This difficulty derives from the system compliance and imperfections in the faces of the trimmed specimens. During this program the top-cap to piston connection was redesigned, extreme care was placed in trimming the specimens, and the

alignment of the components involved in the loading process was frequently evaluated to limit the influence of this problem. These procedures, however, were time consuming, and labor intensive. It is believed that a more robust solution could be achieved by outfitting the triaxial apparatus with tighter tolerance piston bearings, and increasing the stiffness of the load frame. This issue is particularly important if the evaluation of the small strain behavior extends to routine testing.

The backlash in the gear box of the load frame was a major limitation in the testing program. This results in a delay in the load application, particularly upon reversal of the loading, as is the case when the soil is sheared after a swelling phase. This problem also limits the ability to investigate the nature of the strains through a program of unload-reload cycles, as suggested in the following section. This problem might be addressed by using a more precise gear box, for example a minimum slip worm, or possibly through the use of a hydraulic load frame.

Additional improvements to the existing triaxial equipment should include the development of a robust system for the measurements of the radial strains, so that investigation of the pre-failure behavior can be extended to drained tests, ultimately providing a mapping of different regions of behavior in the triaxial q-p' space.

Improved computer control based on feedback from the on-specimen LVDT's may also enhance the overall performance of the system as would the availability of a faster data acquisition system, particularly for the investigations at higher strain rates.

Another equipment improvement that has the potential to enhance the capabilities of the current triaxial apparatus, is the introduction of mid-specimen measurements of pore pressures. Various technologies for this purpose have been employed at MIT (e.g., Sheahan 1991, Force 1998). This capability would permit more preciase measurement of the pore pressures and provide an additional way of assessing the onset of plastic straining.

### 8.3.2 Further Investigations

The technology described in this thesis for the measurement of the small strain behavior of RBBC has proven to be quite versatile and can potentially be employed for the study of the pre-failure behavior of a variety of geomaterials. The following recommendations on future testing are however limited only to cohesive soils. Within this realm, it is recommended that additional testing should be aimed at the following goals:

1) Extending the framework to areas deemed significant by this program.
2) Gaining further understanding of the intrinsic nature of the behavior.
3) Validating the behavioral model proposed for natural soils.
4) Assessing micromechanical aspects of behavior.

With regards to the first objective the analysis of the results presented in the previous chapters indicates that the following issues are of interest:

- To understand the transition in the behavior between NC and OC soil. This requires tests at low values of OCR, in the range 1.2-1.5, to define exactly how much unloading is required to produce the dramatic reduction in the non-linearity of the soil observed in the unloading tests performed on RBBC with OCR of 2-8.
- To explore further the link between non-linearity and strain increment applied since the most recent stress reversal. This investigation should include additional tests on OC soil with *LU* consolidation path in which the load reversal stress point is varied so that the strain increment following reversal changes. Along these same lines tests on NC RBBC should be performed following reloading from higher values of OCR to assess the amount of strain required to completely erase the effects of unloading. In addition it is recommended that tests on OC soil following reloading from different stress levels also be performed, to assess the relationship between stress increment and non-linearity.
- To investigate the consequences of prolonged laboratory aging on the pre-failure behavior of OC RBBC for both *U* and *L* pre-shear paths. These tests would provide insight into the question as to if prolonged aging reduces recent stress history effects as suggested by Tatsuoka et al. (1997).
- To verify to what extent increased unloading to higher OCR's and/or the use of higher strain rates may lead to further increase in the linear threshold and reduction of the small stain non-linearity.
- To examine the behavior of RBBC following consolidation to $K_c<K_0$.
- To extend the investigation to other modes of loading, in particular undrained triaxial extension, for which no significant modifications to the equipment are necessary.

Second, it is suggested that a more in depth understanding of the intrinsic nature of the behavior in the pre-failure region may be derived by performing the following tests:

- Load-unload tests aimed at verifying the recoverability of the strains within the pre-failure region, in a manner similar to what was done in this thesis at the end of shear (at $\varepsilon_a$~0.1-0.15%). It is expected that knowledge of the degree of plastic straining as a function of strain level under different conditions (e.g. OCR and consolidation path) may further contribute to understand the development of the small strain non-linearity. It should be noted that the available technology limits the performance of such tests for very small strain increments (i.e. <0.005%, see recommendation for equipment enhancement). However, preliminary tests conducted using a screw jack to actuate the piston indicate the potential for this technology to be used to perform unload–reload cycles at least as small as $\pm$0.01% without other major modifications to the triaxial loading system.
- Small strain creep tests, as a function of strain/shear stress level to arrive at a better definition of the rate at which these processes occur, ultimately allowing to separate their effects in the analysis of the small strain behavior.

In addition it is suggested that testing of batches of RBBC prepared using different values of salt concentration, may aid in isolating the influence of soil structure and fabric on the pre-failure behavior of cohesive soils.

With regards to the validation of the behavioral model for natural soils, it is recommended that future testing programs extend the investigation of the pre-failure behavior of clays to include testing in particular of the parent material for RBBC, natural Boston Blue clay. Such an investigation should include both SHANSEP and Recompression tests on high quality (block) samples. This effort would aid in verifying the applicability of the behavioral framework presented in this thesis to natural soils, and might provide insight into the changes in behavior caused by structure forming processes occurring in the field. In addition, it would provide the first detailed laboratory investigation of the small strain behavior of Boston Blue clay. Comparison of results from the SHANSEP (this program should include tests in which the OC state is reached after reloading from higher values of OCR) and Recompression tests will also shed light into the applicability of these two reconsolidation procedures for the determination of

stiffness parameters, a question which has still not been completely resolved (e.g. Ladd et al. 1998).

Finally, despite the large amount of data available on the pre-failure behavior of cohesive soils, very little is known on the micromechanisms that form the basis of the behavior observed throughout this program. This area should therefore represent an important future research direction.

## 8.4 REFERENCES


1. Force, E.A. (1998), "Factors Affecting Pore Pressure Generation During $K_0$-Consolidation of Laboratory Tests," S.M. Thesis, Department of Civil and Environmental Engineering, MIT, Cambridge, MA, 166 p.

2. Jamiolkowski, M., Lancellotta, R., and Lo Presti, D.C.F. (1994), "Remarks on the Stiffness at Small Strains of Six Italian Clays," *Proc. Int. Symp. Pre-Failure Deformation Characteristics of Geomaterials*, Hokkaido'94, Vol. 2, pp. 817-854.

3. Ladd, C.C., Young, G.A., Kraemer, S.R., and Burke, D.M. (1998), "Engineering Properties of Boston Blue Clay from Special Testing Program," *Geo-Congress 1998*, ASCE National Convention, Boston, October 1998.

4. Sheahan, T.C. (1991), "An Experimental Study of the Time-Dependent Undrained Shear Behavior of Resedimented Clay Using Automated Stress-Path Triaxial Equipment," Sc.D. Thesis, Department of Civil and Environmental Engineering, MIT, Cambridge, MA, 955 p.

5. Tatsuoka, F., Jardine, R.J., Lo Presti, D.C.F., Di Benedetto, H. and Kohata, Y. (1997), "Characterising the Pre-Failure Deformation Properties of Geomaterials," *Hamburg Keynote Lecture.*

# APPENDIX A

# TEST PHASE RELATIONS AND TRANSDUCER CALIBRATION FACTORS

| | Test | Cell MIT# | Batch # | INITIAL CONDITIONS H cm | A $cm^2$ | V $cm^3$ | $W_{T(in)}$ g | $W_s$ g | $W_{N(in)}$ (%) | $e_{in}^1$ | $e_{in}^2$ | S | $\gamma_t$ $g/cm^3$ | FINAL CONDITIONS $W_{T(fin)}$ g | $e_{fin}$ | $e_{fin}^1$ | $e_{fin}^2$ | $W_{N(fin)}$ (%) |
|---|---|---|---|---|---|---|---|---|---|---|---|---|---|---|---|---|---|---|
| *1* | TX353 | 05 | 418 | 8.105 | 9.753 | 79.048 | 143.23 | 100.19 | 42.96 | 1.209 | 1.196 | 0.995 | 1.812 | 140.67 | 1.131 | N.A. | N.A. | 40.40 |
| *2* | TX359 | 05 | 418 | 8.113 | 9.734 | 78.972 | 143.25 | 99.79 | 43.55 | 1.216 | 1.213 | 1.003 | 1.814 | 138.63 | 1.090 | N.A. | N.A. | 38.92 |
| *3* | TX361 | 05 | 418 | 8.088 | 9.757 | 78.915 | 144.12 | 100.33 | 40.90 | 1.165 | 1.139 | 0.983 | 1.826 | 139.26 | 1.086 | N.A. | N.A. | 38.80 |
| *4* | TX362 | 04 | 418 | 7.921 | 9.792 | 77.562 | 141.36 | 99.44 | 42.16 | 1.184 | 1.174 | 0.997 | 1.823 | 133.29 | 0.953 | N.A. | N.A. | 34.04 |
| *5* | TX363 | 04 | 418 | 7.724 | 9.832 | 75.942 | 138.14 | 96.26 | 43.51 | 1.209 | 1.212 | 1.008 | 1.819 | 126.53 | 0.880 | N.A. | N.A. | 31.45 |
| *6* | TX403 | 05 | 419 | 8.098 | 9.851 | 79.768 | 144.52 | 100.74 | 43.46 | 1.217 | 1.210 | 1.000 | 1.812 | 135.10 | 0.955 | 0.95 | 0.944 | 34.11 |
| *7* | TX406 | 05 | 419 | 8.083 | 9.818 | 79.355 | 144.67 | 100.99 | 43.25 | 1.200 | 1.205 | 1.009 | 1.823 | 132.06 | 0.861 | 0.849 | 0.853 | 30.77 |
| *8* | TX418 | 04 | 419 | 8.059 | 9.861 | 79.470 | 144.68 | 101.84 | 42.07 | 1.185 | 1.178 | 0.994 | 1.821 | 137.03 | 0.968 | 0.96 | 0.954 | 34.55 |
| *9* | TX422 | 04 | 419 | 8.058 | 9.861 | 79.460 | 145.69 | 102.47 | 42.18 | 1.171 | 1.181 | 1.008 | 1.834 | 134.30 | 0.870 | 0.832 | 0.840 | 31.06 |
| *10* | TX424 | 04 | 419 | 8.058 | 9.799 | 78.960 | 143.86 | 101.46 | 41.79 | 1.179 | 1.170 | 0.992 | 1.822 | 132.10 | 0.846 | 0.857 | 0.849 | 30.20 |
| *11* | TX427 | 04 | 419 | 8.086 | 9.762 | 78.936 | 143.90 | 101.33 | 42.01 | 1.181 | 1.176 | 0.996 | 1.823 | 131.14 | 0.824 | 0.804 | 0.800 | 29.42 |
| *12* | TX432 | 04 | 419 | 8.049 | 9.762 | 78.574 | 143.82 | 101.09 | 42.28 | 1.176 | 1.184 | 1.006 | 1.830 | 135.32 | 0.948 | 0.913 | 0.919 | 33.87 |
| *13* | TX438 | 04 | 419 | 8.098 | 9.870 | 79.927 | 144.49 | 101.18 | 42.81 | 1.212 | 1.199 | 0.989 | 1.808 | 134.80 | 0.931 | 0.958 | 0.946 | 33.23 |
| *14* | TX442 | 04 | 419 | 8.073 | 9.814 | 79.228 | 145.59 | 103.12 | 41.19 | 1.151 | 1.153 | 1.002 | 1.838 | 136.40 | 0.904 | 0.908 | 0.909 | 32.27 |
| *15* | TX445 | 05 | 419 | 8.065 | 9.828 | 79.260 | 144.71 | 101.49 | 42.59 | 1.187 | 1.192 | 1.005 | 1.826 | 138.80 | 1.029 | 1.033 | 1.038 | 36.76 |
| *16* | TX455 | 05 | 419 | 8.087 | 9.724 | 78.638 | 143.87 | 100.77 | 42.77 | 1.185 | 1.198 | 1.011 | 1.830 | 131.09 | 0.842 | 0.828 | 0.838 | 30.09 |
| *17* | TX459 | 04 | 419 | 8.052 | 9.743 | 78.451 | 143.05 | 100.31 | 42.61 | 1.190 | 1.193 | 1.003 | 1.823 | 135.15 | 0.973 | 0.988 | 0.991 | 34.73 |
| *18* | TX468 | 05 | 419 | 8.058 | 9.785 | 78.848 | 143.33 | 100.02 | 43.31 | 1.207 | 1.213 | 1.004 | 1.818 | 131.79 | 0.890 | 0.864 | 0.868 | 31.77 |
| *19* | TX470 | 04 | 419 | 8.054 | 9.776 | 78.739 | 143.73 | 101.00 | 42.31 | 1.183 | 1.185 | 1.001 | 1.825 | 132.36 | 0.869 | N.A. | N.A. | 31.05 |
| *20* | TX471 | 05 | 419 | 8.064 | 9.715 | 78.342 | 143.48 | 100.28 | 43.09 | 1.188 | 1.206 | 1.016 | 1.831 | 128.47 | 0.787 | 0.773 | 0.787 | 28.12 |
| *21* | TX473 | 04 | 419 | 8.087 | 9.828 | 79.483 | 143.51 | 100.33 | 43.04 | 1.218 | 1.205 | 0.989 | 1.806 | 132.43 | 0.896 | 0.885 | 0.874 | 32.00 |
| *22* | TX474 | 04 | 419 | 8.043 | 9.729 | 78.250 | 143.56 | 100.44 | 42.93 | 1.181 | 1.202 | 1.017 | 1.835 | 134.49 | 0.949 | 0.924 | 0.943 | 33.90 |
| *23* | TX475 | 04 | 419 | 8.052 | 9.734 | 78.378 | 143.57 | 99.85 | 43.79 | 1.198 | 1.226 | 1.023 | 1.832 | 133.75 | 0.951 | 0.937 | 0.961 | 33.95 |
| *24* | TX476 | 05 | 419 | 8.038 | 9.795 | 78.732 | 143.33 | 99.72 | 43.73 | 1.211 | 1.225 | 1.011 | 1.820 | 131.36 | 0.888 | 0.850 | 0.862 | 31.73 |

| | | | | | | |
|---|---|---|---|---|---|---|
| 418 | Average | 42.614 | 1.197 | 1.187 | 0.997 | 1.819 |
| | S.D. | 1.11 | 0.02 | 0.03 | 0.01 | 0.01 |
| 419 | Average | 42.694 | 1.191 | 1.195 | 1.004 | 1.824 |
| | S.D. | 0.686 | 0.017 | 0.019 | 0.009 | 0.009 |
| All | Average | 42.678 | 1.192 | 1.193 | 1.003 | 1.823 |
| | S.D. | 0.765 | 0.018 | 0.021 | 0.010 | 0.008 |

**Note:** Shaded areas represent values not used in analysis

**Table A.1: Phase Relations**

| Definitions and Calculations: | | |
|---|---|---|
| H | Initial Height | measured at setup |
| A | Initial Area | measured at setup |
| V | Initial Volume | V=HA |
| $W_{T(in)}$ | Initial Total Weight | measured at setup |
| $W_s$ | Weight of Solids | measured at end of test |
| $W_{N(in)}(\%)$ | Initial Water Content | $W_{N(in)}(\%) = (W_{T(In)}-W_s)/W_s*100$ |
| $e_{in}^1$ | Initial Void Ratio | $e_{in}^1 = V/W_s/2.8-1$ |
| $e_{in}^2$ | Initial Void Ratio | $e_{fin}=(W_{T(in)}-W_s)/W_s/2.8$ (assuming S=1) |
| S | Initial degree of saturation | $S=(W_{T(in)}-W_s)/(V-W_s/2.8)$ |
| $\gamma_t$ | Initial unit weight | $\gamma_t=W_{T(in)}/V$ |
| $W_{T(fin)}$ | Final Total Weight | measured at end of test |
| $e_{fin}$ | Final Void Ratio | $e_{fin}=(W_{T(fin)}-W_s)/W_s/2.8$ (assuming S=1) |
| $e_{fin}^1$ | Final Void Ratio | $e_{fin}^1=e_{in}^1-\Delta e$ ($\Delta e$ from volume changes during test) |
| $e_{fin}^2$ | Final Void Ratio | $e_{fin}^2=e_{in}^2-\Delta e$ ($\Delta e$ from volume changes during test) |
| $W_{N(in)}(\%)$ | Final Water Content | $W_{N(fin)}(\%) = (W_{T(fin)}-W_s)/W_s*100$ |

**Table A.1: (continued) Phase Relations**

| | Test # | TX Cell MIT # | RBBC Batch # | Signal Conditioner | LVDT Cores[b] | CALIBRATION FACTORS | | | | | | |
|---|---|---|---|---|---|---|---|---|---|---|---|---|
| | | | | | | LVDT (1) cm/V | LVDT (2) cm/V | Load Cell kg/V/V | Cell Pressure ksc/V/V | Pore Pressure ksc/V/V | Ext.Axial LVDT cm/V/V | Volume LVDT $cm^3/V/V$ |
| 1 | TX353 | 05 | 418 | Commercial | Standard[b] | 0.019268 | 0.020023 | 1275.204 | 702.466 | 695.939 | -2.508614 | -9.343681 |
| 2 | TX359 | 05 | 418 | Commercial | Standard | 0.019268 | 0.020023 | 1275.204 | 702.466 | 695.939 | -2.508614 | -9.343681 |
| 3 | TX361 | 05 | 418 | Commercial | Standard | 0.019268 | 0.020023 | 1275.204 | 702.466 | 695.939 | -2.508614 | -9.343681 |
| 4 | TX362 | 04 | 418 | CSSD1[a] | Standard | 0.03096 | 0.02926 | 2828.74 | 703.585 | 704.958 | 2.565068 | -9.339 |
| 5 | TX363 | 04 | 418 | CSSD1 | Standard | 0.03252 | 0.03130 | 2828.74 | 703.585 | 704.958 | 2.565068 | -9.339 |
| 7 | TX403 | 05 | 419 | CSSD2[a] | Teflon[c] | -0.02527 | -0.02520 | 1275.204 | 702.466 | 695.939 | -2.508614 | -9.343681 |
| 8 | TX406 | 05 | 419 | CSSD2 | Teflon | -0.02527 | -0.02520 | 1275.204 | 702.466 | 695.939 | -2.508614 | -9.343681 |
| 9 | TX418 | 04 | 419 | CSSD1 | Extended[d] | -0.02470 | -0.02523 | 1382.221 | 703.585 | 704.958 | 2.5976 | -9.339 |
| 10 | TX422 | 04 | 419 | CSSD1 | Extended | -0.02470 | -0.02523 | 1382.221 | 703.585 | 704.958 | 2.5976 | -9.339 |
| 11 | TX424 | 04 | 419 | CSSD1 | Extended | -0.02470 | -0.02523 | 1382.221 | 703.585 | 704.958 | 2.5976 | -9.339 |
| 12 | TX427 | 04 | 419 | CSSD1 | Extended | -0.02470 | -0.02523 | 1316.449 | 703.585 | 704.958 | 2.5976 | -9.339 |
| 13 | TX432 | 04 | 419 | CSSD1 | Extended | -0.02470 | -0.02523 | 1316.449 | 703.585 | 704.958 | 2.5976 | -9.339 |
| 14 | TX438 | 04 | 419 | CSSD1 | Extended | -0.02470 | -0.02523 | 1316.449 | 703.585 | 704.958 | 2.5976 | -9.339 |
| 15 | TX442 | 04 | 419 | CSSD1 | Extended | -0.02470 | -0.02523 | 1316.449 | 703.585 | 704.958 | 2.5976 | -9.339 |
| 16 | TX445 | 05 | 419 | CSSD2 | Extended | -0.025418 | -0.023514 | 2718.57 | 702.466 | -698.737 | -2.13266 | -9.343681 |
| 17 | TX455 | 05 | 419 | CSSD2 | Extended | -0.02470 | -0.02523 | 1316.449 | 703.585 | 704.958 | 2.5976 | -9.339 |
| 18 | TX459 | 04 | 419 | CSSD1 | Extended | -0.02470 | -0.02523 | 1316.449 | 703.585 | -704.504 | 2.5976 | -9.339 |
| 19 | TX468 | 05 | 419 | CSSD2 | Extended | -0.025418 | -0.023514 | 2718.57 | 702.466 | -698.737 | -2.13266 | -9.343681 |
| 20 | TX470 | 04 | 419 | CSSD1 | Extended | -0.02470 | -0.02523 | 1316.449 | 703.585 | -704.504 | 2.5976 | -9.339 |
| 21 | TX471 | 05 | 419 | CSSD2 | Extended | -0.025418 | -0.023514 | 2718.57 | 702.466 | -698.737 | -2.13266 | -9.343681 |
| 22 | TX473 | 04 | 419 | CSSD1 | Extended | -0.02470 | -0.02523 | 1316.387 | 703.585 | -704.504 | 2.5976 | -9.339 |
| 23 | TX474 | 04 | 419 | CSSD1 | Extended | -0.02470 | -0.02523 | 1316.387 | 703.585 | -704.504 | 2.5976 | -9.339 |
| 24 | TX475 | 04 | 419 | CSSD1 | Extended | -0.02470 | -0.02523 | 1316.387 | 703.585 | -704.504 | 2.5976 | -9.339 |
| 25 | TX476 | 05 | 419 | CSSD2 | Extended | -0.025418 | -0.023514 | 2718.57 | 702.466 | -698.737 | -2.13266 | -9.343681 |

a CSSD1 and CSSD2 refer to two identical signal conditioning units

b provided by the producer (1.3 cm long)

c Teflon coated standard cores (1.3 cm long)

d Standard cores with stainless steel extensions (2.8 cm long)

**Table A.2: Equipment Details**